Report Title

"Integrated Geologic-Engineering Model for Reef and Carbonate Shoal Reservoirs Associated with Paleohighs: Upper Jurassic Smackover Formation, Northeastern Gulf of Mexico"

Type of Report

Final Project Report

Reporting Period Start Date

September 1, 2000

Reporting Period End Date

December 31, 2003

Principal Author

Ernest A. Mancini (205/348-4319)
Department of Geological Sciences
Box 870338
202 Bevill Building
University of Alabama
Tuscaloosa, AL 35487-0338

Date Report was Issued

February 25, 2004

DOE Award Number

DE-FC26-00BC15303

Name and Address of Participants

Ernest A. Mancini Dept. of Geological Sciences Box 870338 Tuscaloosa, AL 35487-0338	Bruce S. Hart Earth & Planetary Sciences McGill University 3450 University St. Montreal, Quebec H3A 2A7 CANADA	Thomas Blasingame Dept. of Petroleum Engineering Texas A&M University College Station, TX 77843-3116
Robert D. Schneeflock, Jr. Paramount Petroleum Co., Inc. 230 Christopher Cove Ridgeland, MS 39157	Richard K. Strahan Strago Petroleum Corporation 811 Dallas St., Suite 1407 Houston, TX 77002	Roger M. Chapman Longleaf Energy Group, Inc. 319 Belleville Ave. Brewton, AL 36427

Disclaimer

Integrated Geologic-Engineering Model for Reef and Carbonate Shoal Reservoirs Associated with Paleohighs: Upper Jurassic Smackover Formation, Northeastern Gulf of Mexico

Final Report
February 25, 2004

By:
Ernest A. Mancini
Joe Benson
Thomas Blasingame
Wayne Ahr
Rosalind Archer
Bruce Hart
Juan Carlos Llinas
William Parcell
Brian Panetta
Dylan Morgan
Juliana Tebo
Roger Chapman
Robert Schneeflock
Richard Strahan

Work Performed Under Contract No. DE-FC26-00BC15303

University of Alabama
Tuscaloosa, Alabama

National Energy Technology Laboratory
National Petroleum Technology Office
U.S. DEPARTMENT OF ENERGY
Tulsa, Oklahoma

ABSTRACT

The University of Alabama, in cooperation with Texas A&M University, McGill University, Longleaf Energy Group, Strago Petroleum Corporation, and Paramount Petroleum Company, has undertaken an integrated, interdisciplinary geoscientific and engineering research project. The project is designed to characterize and model reservoir architecture, pore systems and rock-fluid interactions at the pore to field scale in Upper Jurassic Smackover reef and carbonate shoal reservoirs associated with varying degrees of relief on pre-Mesozoic basement paleohighs in the northeastern Gulf of Mexico. The project effort includes the prediction of fluid flow in carbonate reservoirs through reservoir simulation modeling which utilizes geologic reservoir characterization and modeling and the prediction of carbonate reservoir architecture, heterogeneity and quality through seismic imaging.

The primary goal of the project is to increase the profitability, producibility and efficiency of recovery of oil from existing and undiscovered Upper Jurassic fields characterized by reef and carbonate shoals associated with pre-Mesozoic basement paleohighs.

Geoscientific reservoir property, geophysical seismic attribute, petrophysical property, and engineering property characterization has shown that reef (thrombolite) and shoal reservoir lithofacies developed on the flanks of high-relief crystalline basement paleohighs (Vocation Field example) and on the crest and flanks of low-relief crystalline basement paleohighs (Appleton Field example). The reef thrombolite lithofacies have higher reservoir quality than the shoal lithofacies due to overall higher permeabilities and greater interconnectivity. Thrombolite dolostone flow units, which are dominated by dolomite intercrystalline and vuggy pores, are characterized by a pore system comprised of a higher percentage of large-sized pores and larger pore throats.

Rock-fluid interactions (diagenesis) studies have shown that although the primary control on reservoir architecture and geographic distribution of Smackover reservoirs is the fabric and texture of the depositional lithofacies, diagenesis (chiefly dolomitization) is a significant factor that preserves and enhances reservoir quality. The evaporative pumping mechanism is favored to explain the dolomitization of the thrombolite doloboundstone and dolostone reservoir flow units at Appleton and Vocation Fields.

Geologic modeling, reservoir simulation, and the testing and applying the resulting integrated geologic–engineering models have shown that little oil remains to be recovered at Appleton Field and a significant amount of oil remains to be recovered at Vocation Field through a strategic infill drilling program. The drive mechanisms for primary production in Appleton and Vocation Fields remain effective; therefore, the initiation of a pressure maintenance program or enhanced recovery project is not required at this time.

The integrated geologic-engineering model developed for a low-relief paleohigh (Appleton Field) was tested for three scenarios involving the variables of present-day structural elevation and the presence/absence of potential reef thrombolite lithofacies. In each case, the predictions based upon the model were correct. From this modeling, the characteristics of the ideal prospect in the basement ridge play include a low-relief paleohigh associated with dendroidal/chaotic thrombolite doloboundstone and dolostone that has sufficient present-day structural relief so that these carbonates rest above the oil-water contact. Such a prospect was identified from the modeling, and it is located northwest of well Permit # 3854B (Appleton Field) and south of well # Permit #11030B (Northwest Appleton Field).

Table of Contents

INTRODUCTION

The University of Alabama, in cooperation with Texas A&M University, McGill University, Longleaf Energy Group, Strago Petroleum Corporation, and Paramount Petroleum Company, has undertaken an integrated, interdisciplinary geoscientific and engineering research project. The project is designed to characterize and model reservoir architecture, pore systems and rock-fluid interactions at the pore to field scale in Upper Jurassic Smackover reef and carbonate shoal reservoirs associated with varying degrees of relief on pre-Mesozoic basement paleohighs in the northeastern Gulf of Mexico. The project effort includes the prediction of fluid flow in carbonate reservoirs through reservoir simulation modeling that utilizes geologic reservoir characterization and modeling and the prediction of carbonate reservoir architecture, heterogeneity and quality through seismic imaging.

The Upper Jurassic Smackover Formation (Figure 1) is one of the most productive hydrocarbon reservoirs in the northeastern Gulf of Mexico. Production from Smackover carbonates totals 1 billion barrels of oil and 4 trillion cubic feet of natural gas. The production is from three plays: 1) basement ridge play, 2) regional peripheral fault play, and 3) salt anticline play (Figure 2). Unfortunately, much of the oil in the Smackover fields in these plays remains unrecovered because of a poor understanding of the rock and fluid characteristics that affects our understanding of reservoir architecture, heterogeneity, quality, fluid flow and producibility. This scenario is compounded because of inadequate techniques for reservoir detection and the characterization of rock-fluid interactions, as well as imperfect models for fluid flow prediction. This poor understanding is particularly illustrated for the case with Smackover fields in the basement ridge play (Figure 3) where independent producers dominate the development and management of these fields. These producers do not have the financial resources and/or staff

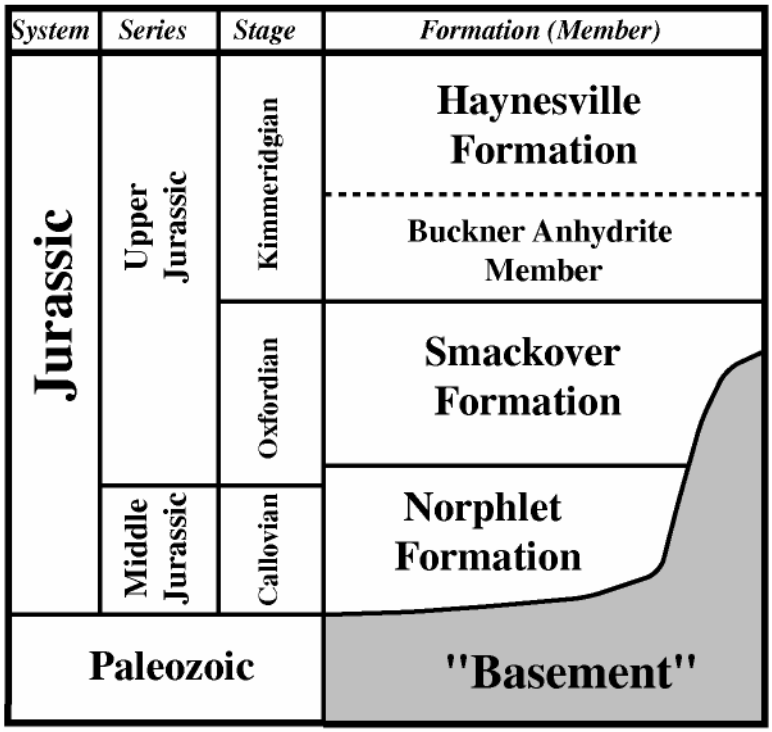

Figure 1. Jurassic stratigraphy in the study area.

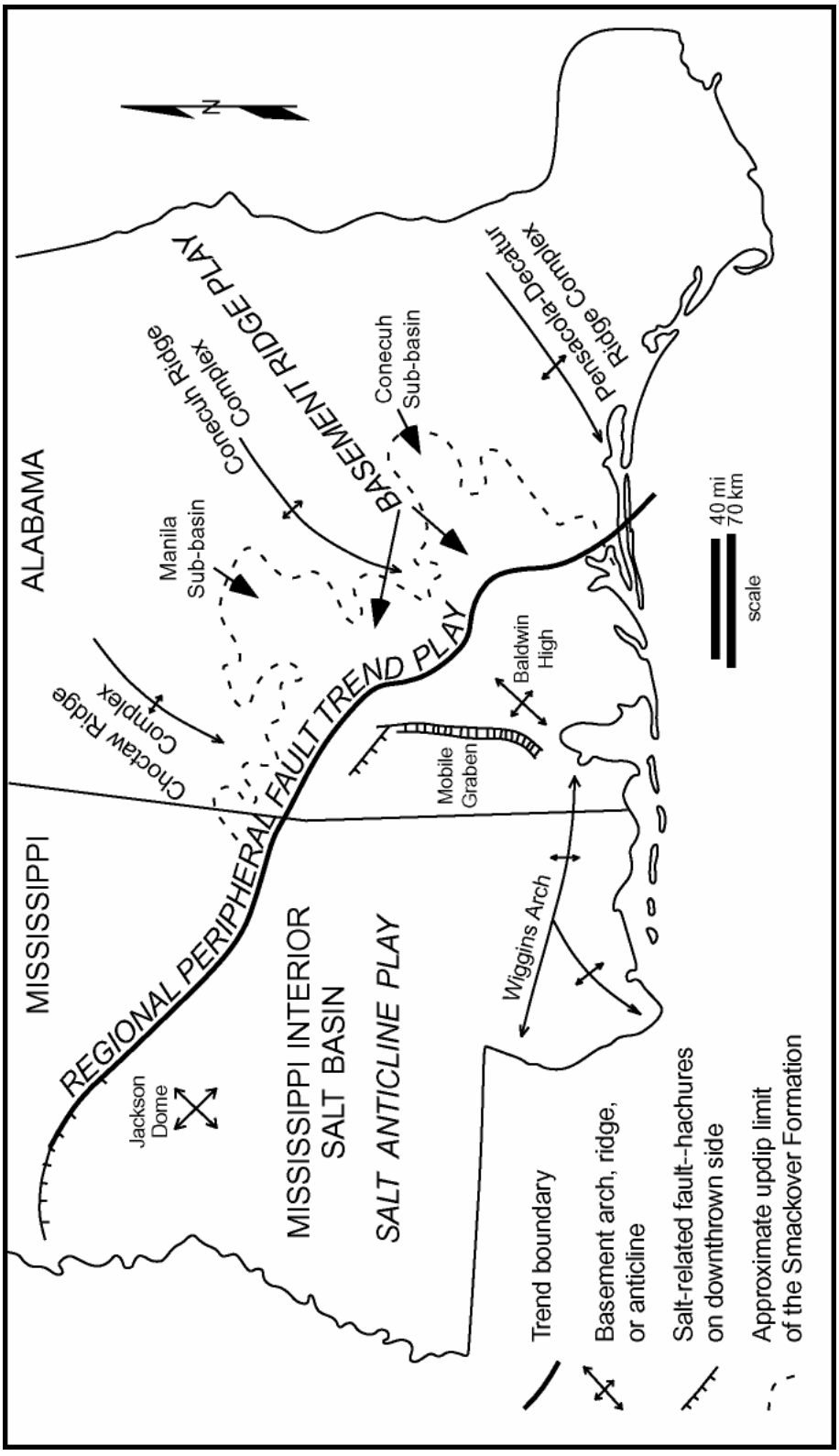

Figure 2. Major petroleum trends in study area.

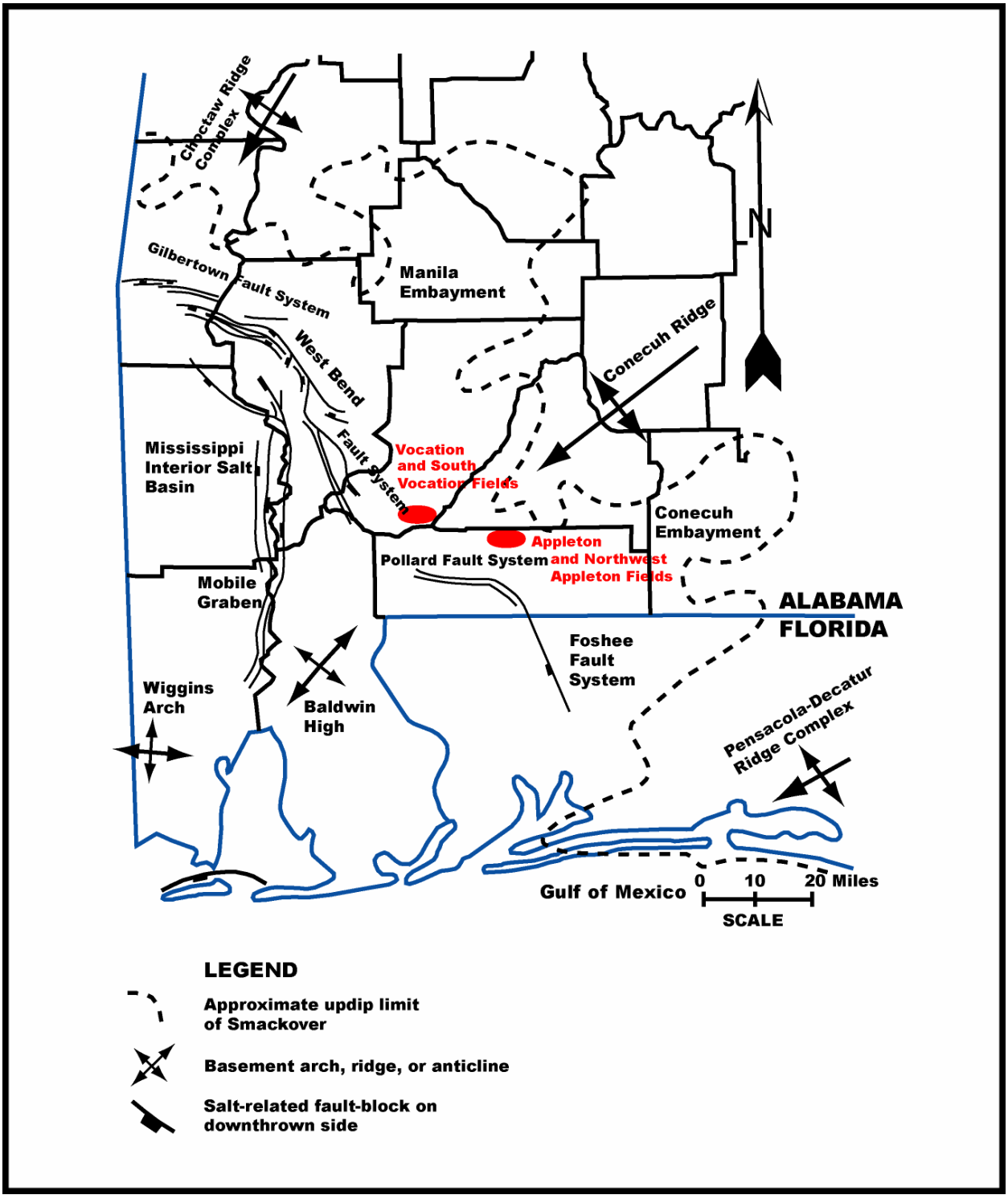

Figure 3. Location of Appleton and Northwest Appleton and Vocation and South Vocation Fields.

expertise to substantially improve the understanding of the geoscientific and engineering factors affecting the producibility of Smackover carbonate reservoirs, which makes research and application of new technologies for reef-shoal reservoirs all that more important and urgent. The research results from studying the fields identified for this project will be of direct benefit to these producers.

This interdisciplinary project is a 3-year effort to characterize, model and simulate fluid flow in carbonate reservoirs and consists of 3 phases and 11 tasks. Phase 1 (1 year) of the project involves geoscientific reservoir characterization, rock-fluid interactions, petrophysical and engineering property characterization, and data integration. Phase 2 (1.5 years) includes geologic modeling and reservoir simulation. Phase 3 (0.5 year) involves building the geologic-engineering model, testing the geologic-engineering model, and applying the geologic-engineering model.

The principal goal of this project is to assist independent producers in increasing oil producibility from reef and shoal reservoirs associated with pre-Mesozoic paleotopographic features through an interdisciplinary geoscientific and engineering characterization and modeling of carbonate reservoir architecture, heterogeneity, quality and fluid flow from the pore to field scale.

The objectives of the project are as follows:

1. Evaluate the geological, geophysical, petrophysical, and engineering properties of reef-shoal reservoirs emphasizing Appleton (Figure 4) and Vocation (Figure 5) Fields.
2. Construct a digital database of integrated geoscience and engineering data for reef-shoal carbonate reservoirs associated with basement paleohighs.

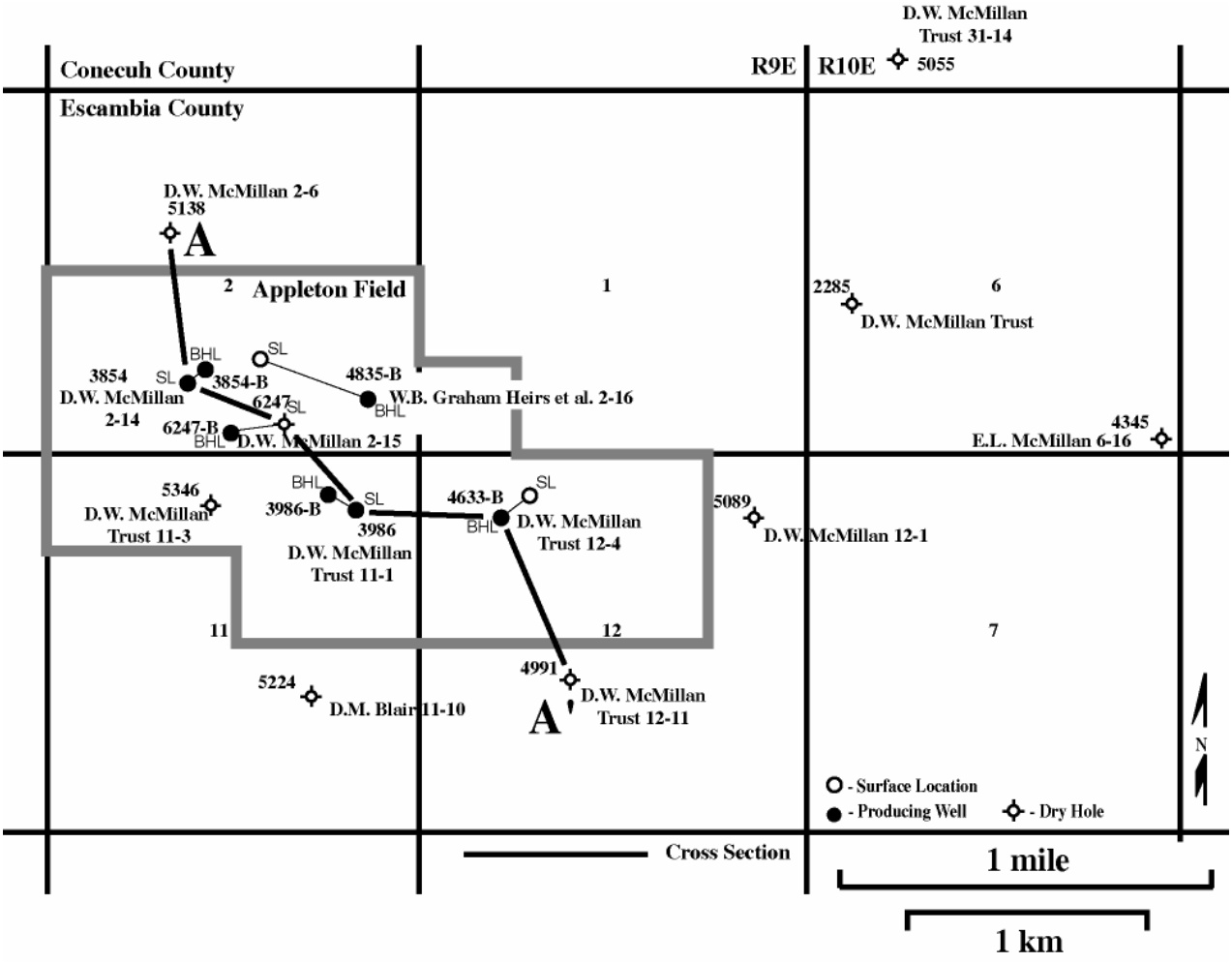

Figure 4. Appleton Field Unit area.

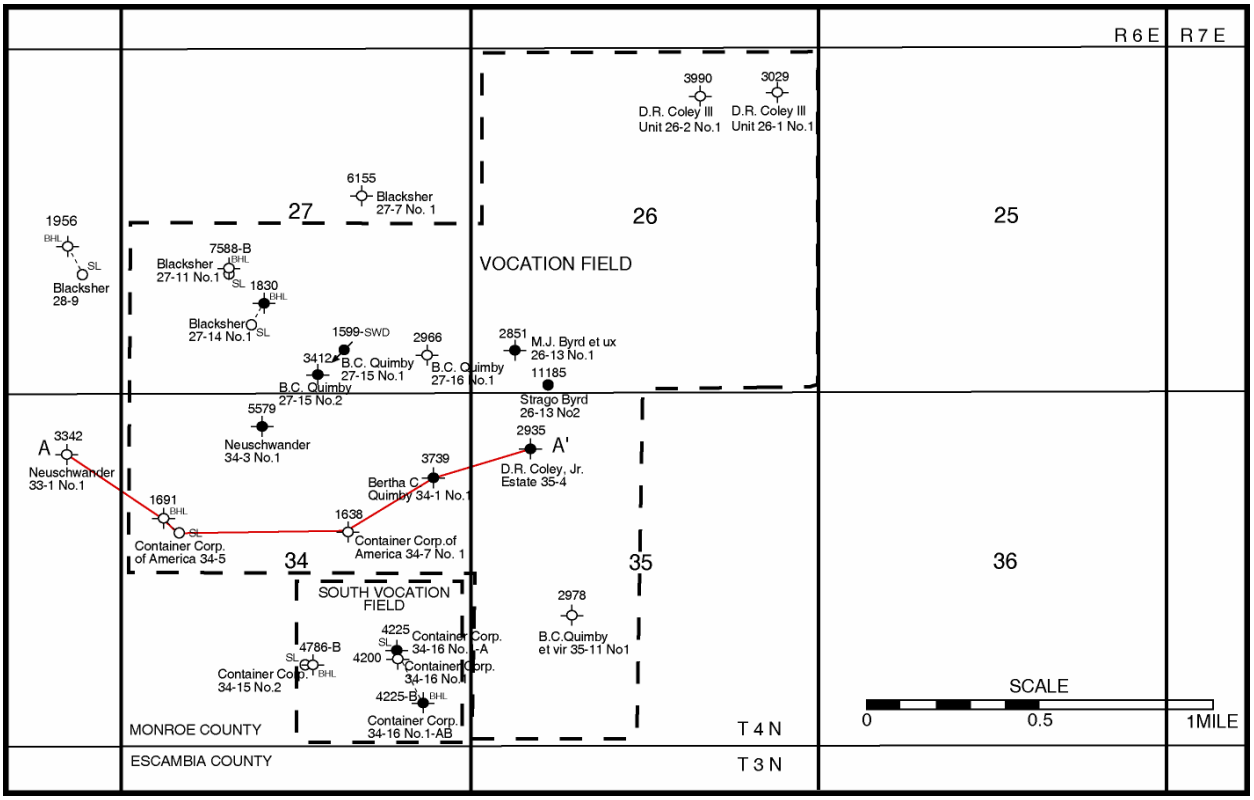

Figure 5. Vocation Field area.

3. Develop an integrated geologic models, based on geological, geophysical, petrophysical and engineering data and analysis for improving reservoir detection, reservoir characterization, reservoir imaging, flow simulation, and performance prediction for reef-shoal carbonate reservoirs using the case studies of Appleton and Vocation Fields.
4. Test and apply the integrated geologic models on prospective Smackover reef-shoal reservoirs associated with basement paleohighs.

This project has direct and significant economic benefits because the Smackover is a prolific hydrocarbon reservoir in the northeastern Gulf of Mexico. Smackover reefs represent an underdeveloped reservoir, and the basement ridge play in which these reefs are associated represents an underexplored play. Initial estimations indicate the original oil resource target available in this play approximates 90 million barrels. To date, 30 million barrels of oil have been produced from 54 fields. Any newly discovered fields are expected to have 1 to 3 million barrels of oil in recovery potential. The combined oil production from the Smackover fields (Appleton and Vocation Fields) studied in this project total 5 million barrels of oil. The results from this project should lead to increased oil producibility from existing and newly discovered fields similar to Appleton and Vocation Fields. Production of these domestic resources will serve to reduce U.S. dependence on foreign oil supplies.

Completion of the project will contribute significantly to the understanding of: the geologic factors controlling reef and shoal development on paleohighs, carbonate reservoir architecture and heterogeneity at the pore to field scale, generalized rock-fluid interactions and alterations in carbonate reservoirs, the geological and geophysical attributes important to geologic modeling of reef-shoal carbonate reservoirs, the critical factors affecting fluid flow in carbonate reservoirs, the elements important to the development of a carbonate integrated geologic model, and the

geological, geophysical, and/or petrophysical properties important to improved carbonate reservoir detection, characterization, imaging and flow prediction.

EXECUTIVE SUMMARY

The University of Alabama, in cooperation with Texas A&M University, McGill University, Longleaf Energy Group, Strago Petroleum Corporation, and Paramount Petroleum Company, has undertaken an integrated, interdisciplinary geoscientific and engineering research project. The project is designed to characterize and model reservoir architecture, pore systems and rock-fluid interactions at the pore to field scale in Upper Jurassic Smackover reef and carbonate shoal reservoirs associated with varying degrees of relief on pre-Mesozoic basement paleohighs in the northeastern Gulf of Mexico. The project effort includes the prediction of fluid flow in carbonate reservoirs through reservoir simulation modeling which utilizes geologic reservoir characterization and modeling and the prediction of carbonate reservoir architecture, heterogeneity and quality through seismic imaging.

The project has direct and significant economic benefits because the Smackover is a prolific hydrocarbon reservoir in the northeastern Gulf of Mexico. To date, 30 million barrels of oil have been produced from 54 fields that have been discovered and developed in the basement ridge play. Smackover reef and carbonate facies associated with paleohighs in this play represent underdeveloped reservoirs. The combined oil production from the Smackover fields (Appleton and Vocation Fields) studied in this project total 5 million barrels of oil. The results from this project should lead to increased oil producibility from existing and newly discovered fields similar to Appleton and Vocation Fields.

The primary goal of the project is to increase the profitability, producibility and efficiency of recovery of oil from existing and undiscovered Upper Jurassic fields characterized by reef and carbonate shoals associated with pre-Mesozoic basement paleohighs.

The objectives of the project are: (1) to evaluate the geological, geophysical, petrophysical and engineering properties of reef-shoal reservoirs using Appleton and Vocation Fields as case studies; (2) construct a digital database of integrated geoscience and engineering data for reef-shoal reservoirs associated with basement paleohighs; (3) develop integrated geologic models, based on geological, geophysical, petrophysical, and engineering data and analysis, for improving reservoir detection, characterization, imaging, flow simulation and performance prediction for reef-shoal reservoirs using the case studies of Appleton and Vocation Fields; and (4) test and apply the integrated geologic models to prospective Smackover reef-shoal reservoirs associated with basement paleohighs.

The objectives have been achieved through the accomplishments resulting from the following research tasks: geoscientific reservoir property characterization, geophysical seismic attribute characterization, petrophysical property characterization, engineering property characterization, rock-fluid interactions (diagenesis), geologic modeling, reservoir simulation, testing and applying the integrated geologic–engineering models, and technology transfer.

Geoscientific reservoir property characterization has shown that the main Smackover lithofacies are subtidal, reef flank, reef crest, shoal flank, shoal crest, lagoon, tidal flat and sabkha. The reef lithofacies consist of thrombolite layered, chaotic and dendroidal subfacies. The shoal complex consists of the lagoon/subtidal and shoal flank and crest lithofacies. These reef and shoal reservoir lithofacies are developed on the flanks of high-relief crystalline

basement paleohighs (Vocation Field example) and on the crest and flanks of low-relief crystalline basement paleohighs (Appleton Field example).

Seismic attribute characterization has shown that seismic attributes can be used to predict subsurface rock properties, such as the presence/absence of porosity and porosity thickness in the Smackover reservoir lithofacies, associated with basement paleohighs. Porous intervals were generally greater and thicker on the flanks of the paleohighs, rather than the crests of these features, due to greater accommodation space and improved growth conditions for reef organisms. This volume-based seismic attribute study was also used to determine lithofacies distribution and thickness and to define the vertical and lateral heterogeneity in Smackover reservoirs.

Petrophysical property characterization has shown that the shoal and reef thrombolite lithofacies are the main reservoir lithofacies. The reservoir quality of the thrombolite lithofacies is greater than the shoal lithofacies because the thrombolite reservoir consists of a pore system comprised of a higher percentage of large-sized pores and larger pore throats. The shoal pore system is dominated by moldic and dolomite intercrystalline pores. The dendroidal and chaotic thrombolite reservoirs have higher producibility than the layered thrombolite reservoirs because they have overall higher permeabilities and greater interconnectivity due to their vertical and horizontal branching growth pattern. Thrombolite flow units are characterized by dolomite intercrystalline and vuggy pores.

Engineering property characterization has shown that reservoirs at Appleton and Vocation Fields have a heterogeneous nature. Porosity and permeability data show that the reef reservoirs are of higher quality than the shoal reservoirs. The primary production mechanism in Vocation Field is a combination drive consisting of fluid/rock/gas expansion and water from an underlying

and/or adjoining aquifer. The primary production mechanism in Appleton Field is a strong bottom up water drive. New well pressure test data acquired for Appleton Field show that the reservoir pressures at Appleton Field currently range from 4423 to 5125 psia.

Rock-fluid interactions (diagenesis) studies show that although the primary control on reservoir architecture and geographic distribution of Smackover reservoirs is the fabric and texture of the depositional lithofacies, diagenesis (chiefly dolomitization) is a significant factor that preserves and enhances reservoir quality. Porosity in the thrombolite doloboundstone lithofacies is a mixture of primary shelter and fenestral porosity overprinted by secondary dolomite intercrystalline and vuggy porosity. Porosity in the shoal dolograinstone lithofacies is primary interparticle porosity overprinted by secondary moldic and dolomite intercrystalline. Although seepage reflux and mixing zone diagenetic processes are mechanisms for the formation of Smackover dolostone, the evaporative pumping mechanism is favored to explain the intense and extensive dolomitization of the Appleton and Vocation reservoir flow units.

Geologic modeling of the Appleton and Vocation paleohighs and associated lithofacies has shown that these features are complex structures. The structure at Appleton Field is a northwest-southeast trending, low-relief composite paleotopographic high with two water levels. The well production differences in the field are related to the heterogenous nature of the reservoirs. The greater production from the eastern part of the composite paleohigh is attributed to the higher relief, which results in the placement of more thrombolite dolostone above the oil-water contact. The structure at Vocation Field is a high-relief composite paleotopographic high with multiple water levels. This composite feature consists of one main north-south oriented elongated feature with three crests that remained subaerially exposed throughout the time of Smackover deposition. The Vocation structure is bounded to the east and north by high-angle normal faults.

Reef growth was limited to the eastern and northern flanks (leeward side) of the structure due to Smackover paleoenvironmental conditions.

Reservoir simulation of the reservoirs at Appleton and Vocation Fields used the 3-D geologic models for these reservoirs as a foundation for the simulation modeling. Reservoir simulation at Appleton Field shows that 50% of the recoverable oil in this field has been produced; thus, little oil remains to be recovered. Of the oil remaining, the areas around well Permits #3854B, #6247 and #4735B (western part of the structure) have the most potential to recover additional oil. Reservoir simulation at Vocation Field shows that a significant amount of oil remains to be recovered in this field through infill drilling. The area north of well Permit #4786B and south of well Permits #1638 and #1691 and the area southeast of well Permits #1599 and #3412 and northwest of well Permit #3739 have high potential for recovering additional oil from this field.

The integrated geologic-engineering model developed for a low-relief paleohigh (Appleton Field) was tested using three scenarios involving the variables of present-day structural elevation and the presence or absence of potential reef thrombolite lithofacies. In each case, the predictions based upon the model were correct. The integrated model was also used to evaluate existing reservoir management strategies at Appleton and Vocation Fields. It was concluded that the drive mechanisms for primary production in these fields remain effective; and therefore, no recommendations for the initiation of a pressure maintenance program or an enhanced recovery project were justified at this time. It was determined that these fields would benefit from additional infill drilling, particularly Vocation Field, at the strategic drill sites identified from the reservoir simulation modeling. From the integrated geologic model, a drill site northwest of well Permit #3854B (Appleton Field) and south of well Permit #11030B (Northwest Appleton Field)

was identified as a location with high potential to encounter thrombolite doloboundstone and dolostone on a low-relief paleohigh.

To date, technology transfer activities have included conducting two technology workshops in Jackson, Mississippi, making 31 technical presentations at regional and national meetings, and publishing 40 technical publications on the research results from this project.

EXPERIMENTAL RESULTS

Geoscientific Reservoir Characterization.--This task was designed to characterize reservoir architecture, pore systems and heterogeneity based on geological and geophysical properties. This work has been done using well logs, cores, and other data for Vocation Field and for Appleton Field. The first phase of the task involved core descriptions, including lithologies, sedimentary structures, lithofacies, depositional environments, systems tracts, and depositional sequences. Graphic logs were constructed from the core studies depicting the information described above. Core samples were selected for petrographic, XRD, and microprobe analyses. The graphic logs were compared to available core analysis and well log data. The core features and core analyses were calibrated to the well log patterns. The next phase was the link between core and well log analysis and reservoir modeling. It involved the preparation of stratigraphic and structural cross sections to illustrate structural growth, lithofacies and reservoir geometry, and depositional systems tract distribution. Maps were prepared to illustrate lithofacies distribution, stratigraphic and reservoir interval thickness (isolith and isopach maps), and stratal structural configurations. These cross sections and maps, in association with the core descriptions, were utilized to make sequence stratigraphic, environment of deposition, and structural interpretations. Standard industry software, such as StratWorks and Z-Map, were used in the preparation of the cross sections and subsurface maps. The next phase included

identification and quantification of carbonate mineralogy and textures (grain, matrix and cement types), pore topology and geometry, and percent of porosity and was performed to support and enhance the visual core descriptions. These petrographic, XRD and microprobe analyses were used to confirm and quantify the observations made in the core descriptions. This analysis provides the opportunity to study reservoir architecture and heterogeneity at the microscopic scale. The last phase involved the study of pore systems in the reservoir, including pore types and throats. This phase examined pore shape and geometry and the nature and distribution of pore throats to determine the features of the pore systems that are affecting reservoir producibility. The geoscientific characterization of the Smackover at Appleton and Vocation Fields has been done by Mancini, Benson, Llinas, Parcell and Panetta at the University of Alabama. This work is part of the dissertation research of Llinas.

The architecture and heterogeneities of reservoirs that are a product of a shallow marine carbonate setting are very complex and a challenge technically to predict. Carbonate systems are greatly influenced by biological and chemical processes in addition to physical processes of deposition and compaction. Carbonate sedimentation rates are primarily a result of the productivity of marine organisms in subtidal environments. In particular, reef-forming organisms are a crucial component to the carbonate system because of their ability to modify the surrounding environments. Reef growth is dependent upon many environmental factors, but one crucial factor is sea-floor relief (paleotopography). In addition, the development of a reef structure contributes to depositional topography. Further, the susceptibility of carbonates to alteration by early to late diagenetic processes dramatically impacts reservoir heterogeneity. Reservoir characterization and the quantification of heterogeneity, therefore, becomes a major task because of the physiochemical and biological origins of carbonates and because of the

masking of the depositional rock fabric and reservoir architecture due to dissolution, dolomitization, and cementation. Further, the detection, imaging, and prediction of carbonate reservoir heterogeneity and producibility is difficult because of an incomplete understanding of the lithologic characteristics and fluid-rock dynamics that affect log response and geophysical attributes.

Appleton Field. All available whole cores (11) from Appleton Field have been described and thin sections (379) from these cores have been studied. Graphic logs were constructed describing each of the cores (Figures 6 through 16). Depositional facies were determined from the core descriptions. From the study of thin sections, the petrographic characteristics of these lithofacies have been described, and the pore systems inherent to these facies have been identified (Table 1). The core data and well log signatures have been integrated and calibrated on these graphic logs.

For Appleton Field (Figure 4), the well log and core data have been entered into a digital database and structural maps on top of the basement (Figure 17), reef (Figure 18), and Smackover/Buckner (Figure 19) have been constructed. An isopach map of the Smackover interval has been prepared (Figure 20), and thickness maps of the sabkha facies (Figure 21), tidal flat facies (Figure 22), shoal complex (Figure 23), tidal flat/shoal complex (Figure 24) and reef complex (Figure 25) facies have been constructed. A cross section (Figure 26) illustrating the thickness and facies changes across Appleton Field has been prepared.

Based on the description of cores (11) and thin sections (379), 14 lithofacies have been identified in the Smackover/Buckner at Appleton Field. Analysis of the vertical and lateral distributions of these lithofacies indicates that these lithofacies were deposited in one or more of eight depositional environments: 1) subtidal, 2) reef flank, 3) reef crest, 4) shoal flank, 5) shoal

crest, 6) lagoon, 7) tidal flat, and 8) sabkha in a transition from a catch-up carbonate system to a keep-up carbonate system. These paleoenvironments have been assigned to four Smackover/Buckner genetic depositional systems for three-dimensional stratigraphic modeling. Each of these systems has been interpreted as being time-equivalent from that work, two principal reservoir facies, reef and shoal were identified at Appleton Field.

Based on the description of cores and thin sections, three subfacies have been recognized in the reef facies. These subfacies include thrombolitic layered, chaotic and dendroidal. Each represents a different and distinct microbial growth form which has inherent properties that affect reservoir architecture, pore systems, and heterogeneity. The layered growth form is characterized by a reservoir architecture that is characterized by lateral continuity and high vertical heterogeneity. The chaotic form has a reservoir architecture that is characterized by high vertical and lateral continuity. The dendroidal form has a reservoir architecture that is characterized by high vertical and moderate lateral continuity and moderate heterogeneity. The pore systems in each of these reservoir fabrics consist of shelter and enlarged pore types. The enlargement of these primary pores is due to dissolution and dolomitization resulting in a vuggy appearing pore system. Three subfacies have been recognized in the shoal facies. These subfacies are the lagoon/subtidal, shoal flank, and shoal crest. The lagoon/subtidal subfacies has a mud-supported architecture and therefore is not considered a reservoir. The shoal flank has a grain-supported architecture but has considerable carbonate mud associated with it, and therefore, has low to moderate reservoir capacity. The shoal crest has a grain-supported architecture with minimal carbonate mud, and therefore, has the highest reservoir capacity of the shoal subfacies. The pore systems of the shoal flank and shoal crest reservoir facies consist of intergranular and enlarged pore types. The enlargement of the primary pores is due to dissolution

and dolomitization. Heterogeneity in the shoal reservoir is high due to the rapid lateral and vertical changes in this depositional environment. Graphic logs were constructed for each of the cores. The core data and well log signatures are integrated and calibrated on these graphic logs.

Appleton Field was discovered in 1983 with the drilling of the D.W. McMillan 2-14 well (Permit #3854). The discovery well was drilled off the crest of a composite paleotopographic structure, based on 2-D seismic and well data. The well penetrated Paleozoic basement rock at a depth of 12,786 feet. The petroleum trap at Appleton was interpreted to be a simple anticline associated with a northwest-southeast trending basement paleohigh. After further drilling in the field, the Appleton structure was interpreted as an anticline consisting of two local paleohighs. The D.W. McMillan 2-15 well (Permit #6247) was drilled in 1991. The drilling of this well resulted in the structural interpretation being revised to consist of three local paleohighs. In 1995, 3-D seismic reflection data were obtained for the Appleton Field area. The interpretation of these data indicated three local highs with the western paleohigh being separated into a western and a central feature.

Based on the structural maps that we have prepared for the Appleton Field, we have concluded that the Appleton structure is a low-relief, northwest-southeast trending ridge comprised of local paleohighs. This interpretation is based on the construction of structure maps on top of the basement, on top of the reef, and on top of the Smackover/Buckner from well log data and 3-D seismic data.

The Smackover reservoir at Appleton Field has been influenced by antecedent paleotopography. The Smackover thickness ranges from 177 feet in the McMillan 2-14 well (Permit #3854) to 228 feet in the McMillan Trust 11-1 well (Permit #3986) in the field. As observed from the cross sections based on well log data and on seismic data, the sabkha facies

thins over the composite paleohigh, while the reservoir lithofacies are thicker on the paleohigh. Thickness maps of the sabkha facies, tidal flat facies, shoal complex, tidal flat/shoal complex, and reef complex facies illustrate the changes in these lithofacies in the Appleton Field.

Vocation Field. All available whole cores (11) from Vocation Field have been described and thin sections (237) from the cores have been studied. Graphic logs were constructed describing each of the cores (Figures 27 through 37). Depositional facies were determined from the core descriptions. From this work, an additional 73 thin sections are being prepared to provide accurate representation of the lithofacies identified. From the study of thin sections, the petrographic characteristics of these lithofacies have been described, and the pore systems

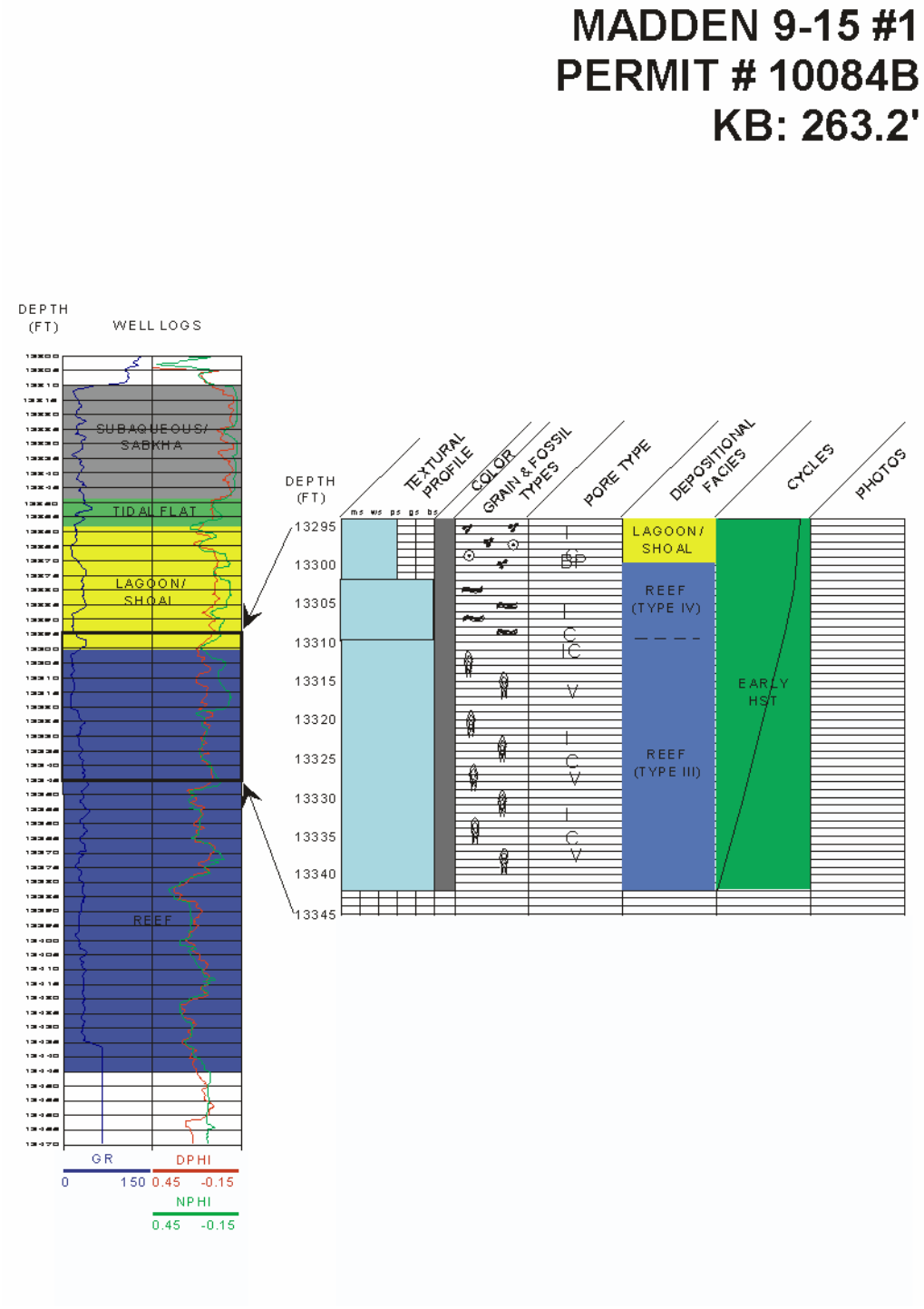

Figure 6. Graphic log for well Permit # 10084B
by W.C. Parcell

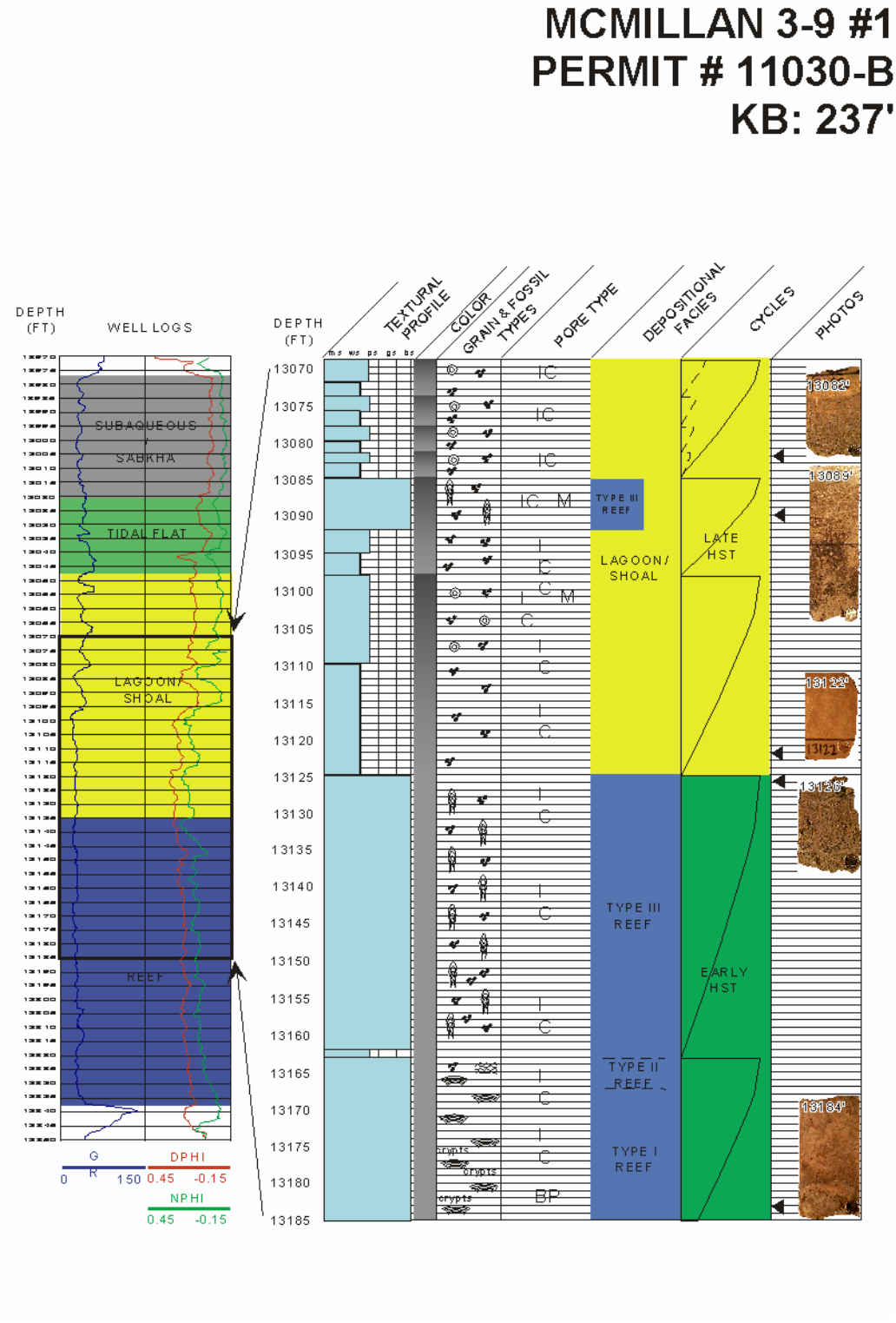

Figure 7. Graphic log for well Permit # 11030B
by W.C Parcell

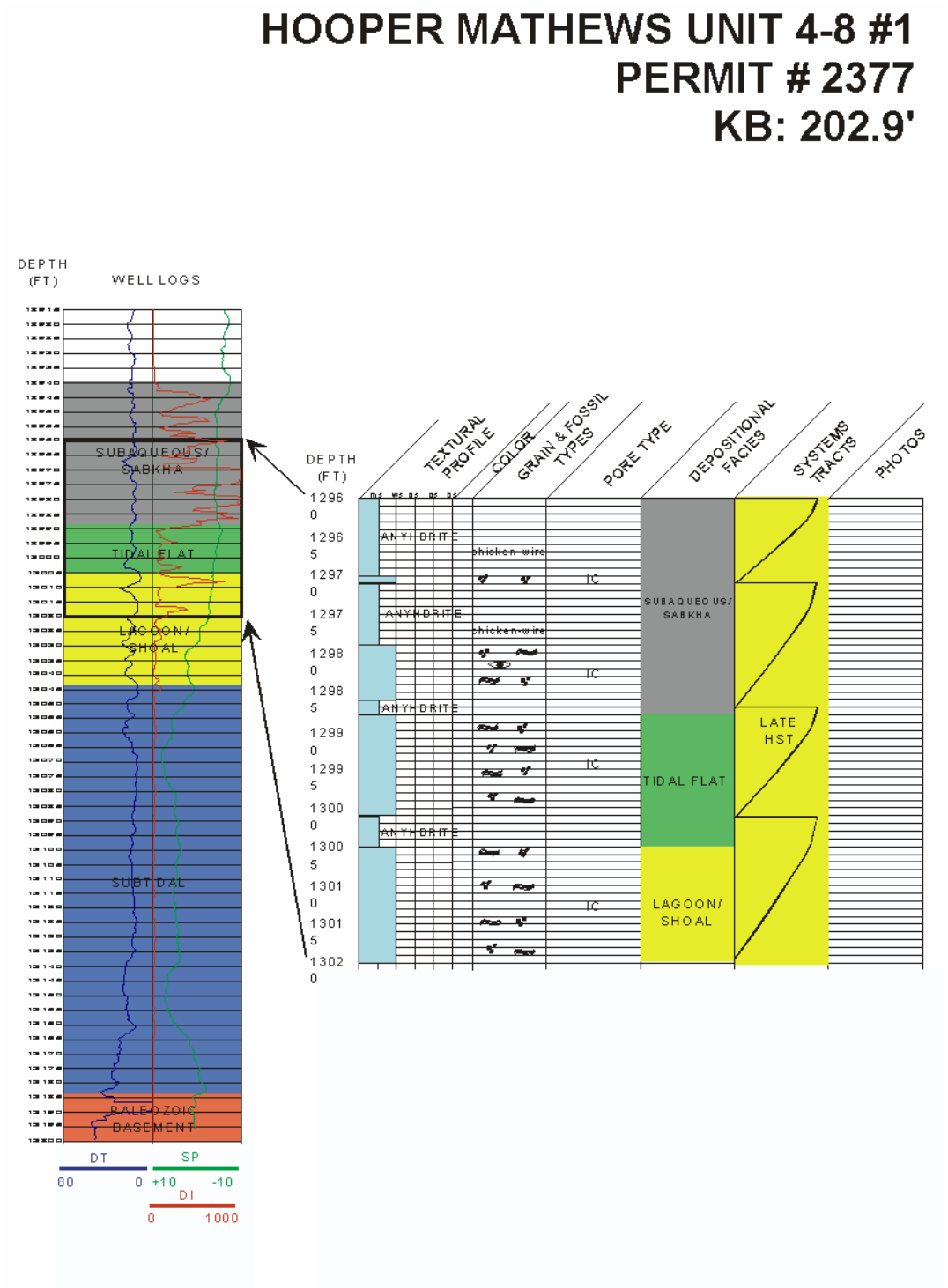

Figure 8. Graphic log for well Permit # 2377
by W.C. Parcell

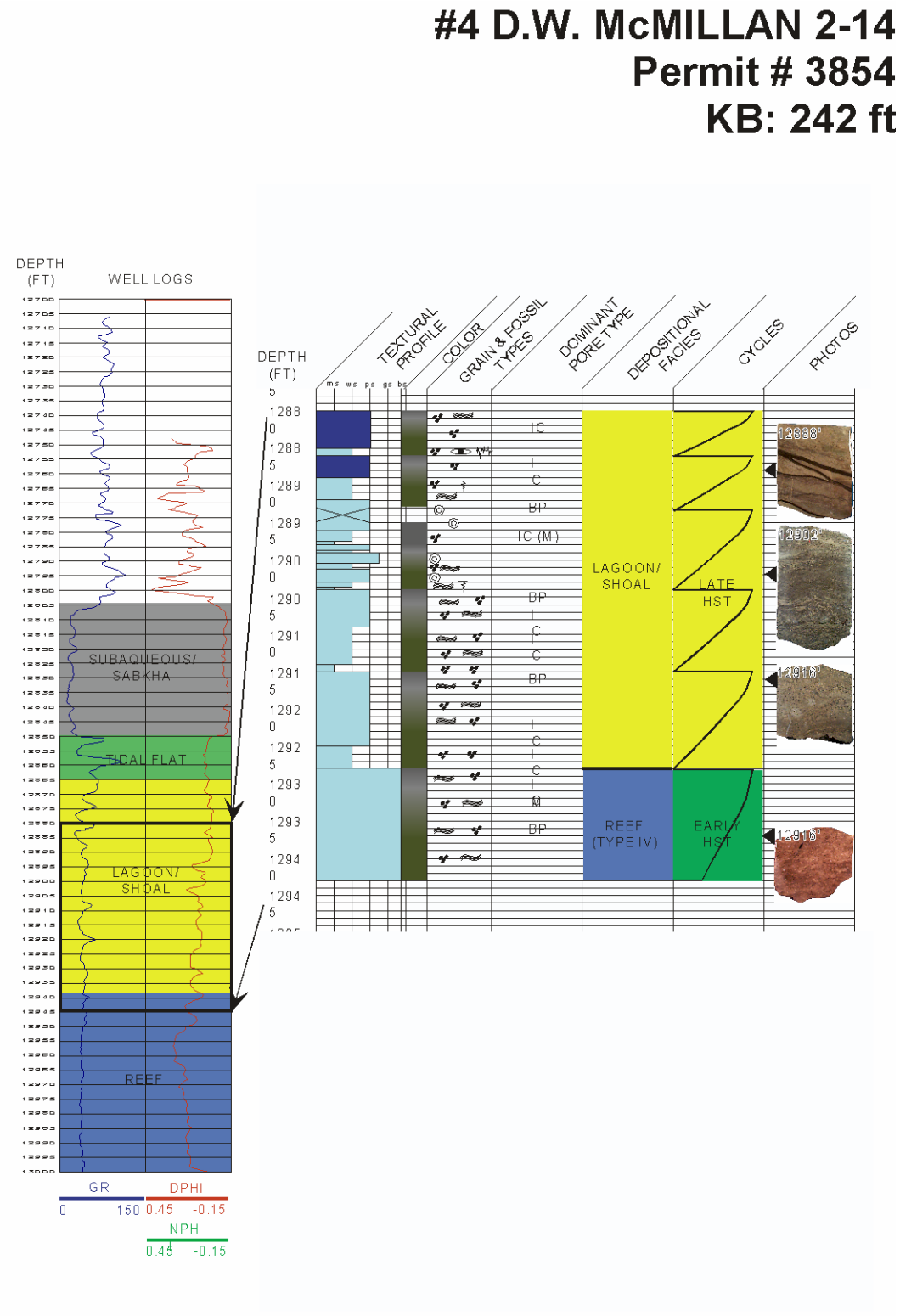

Figure 9. Graphic log for well Permit # 3854
by W.C. Parcell

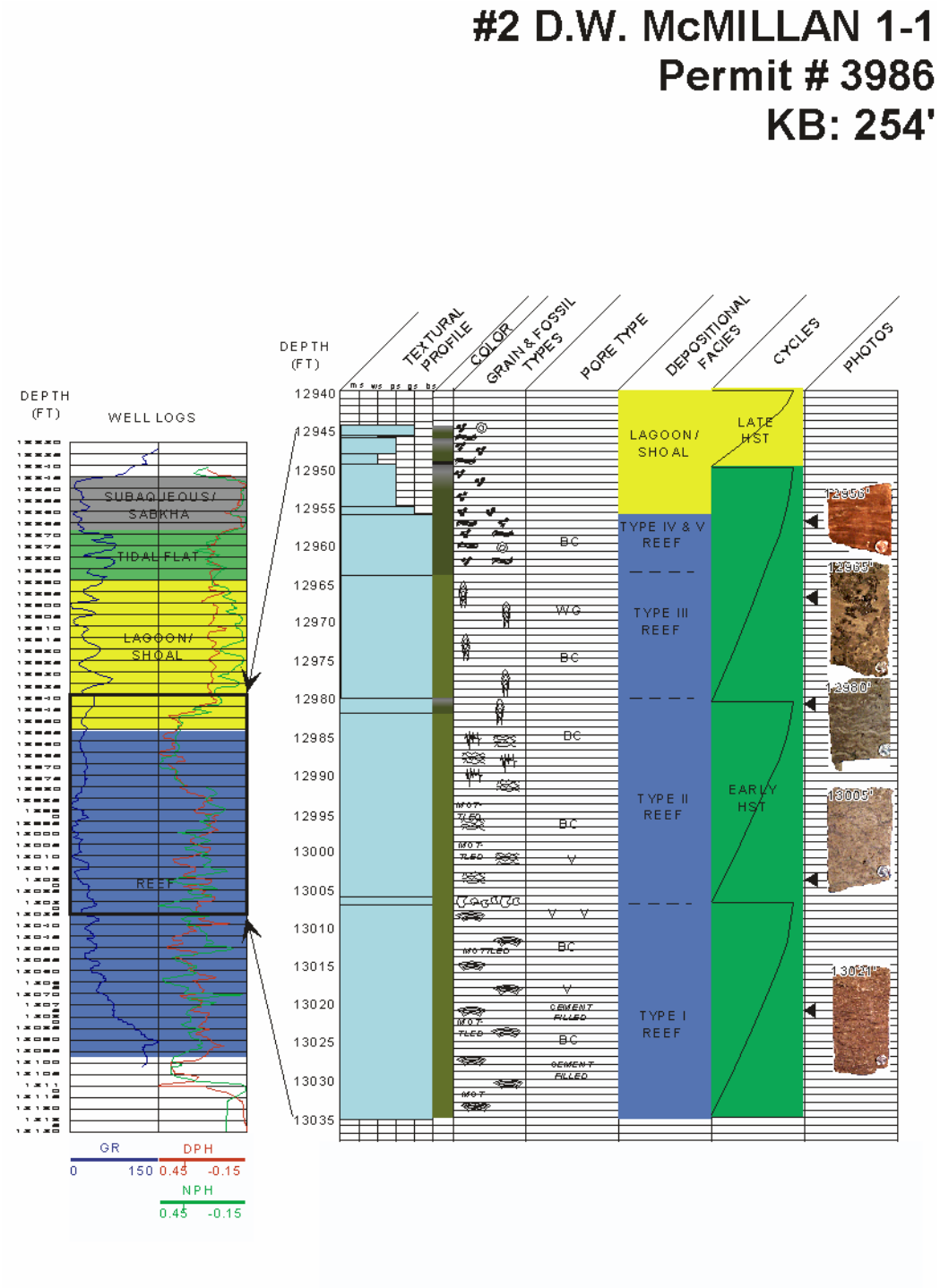

Figure 10. Graphic log for well Permit # 3986
by W.C. Parcell

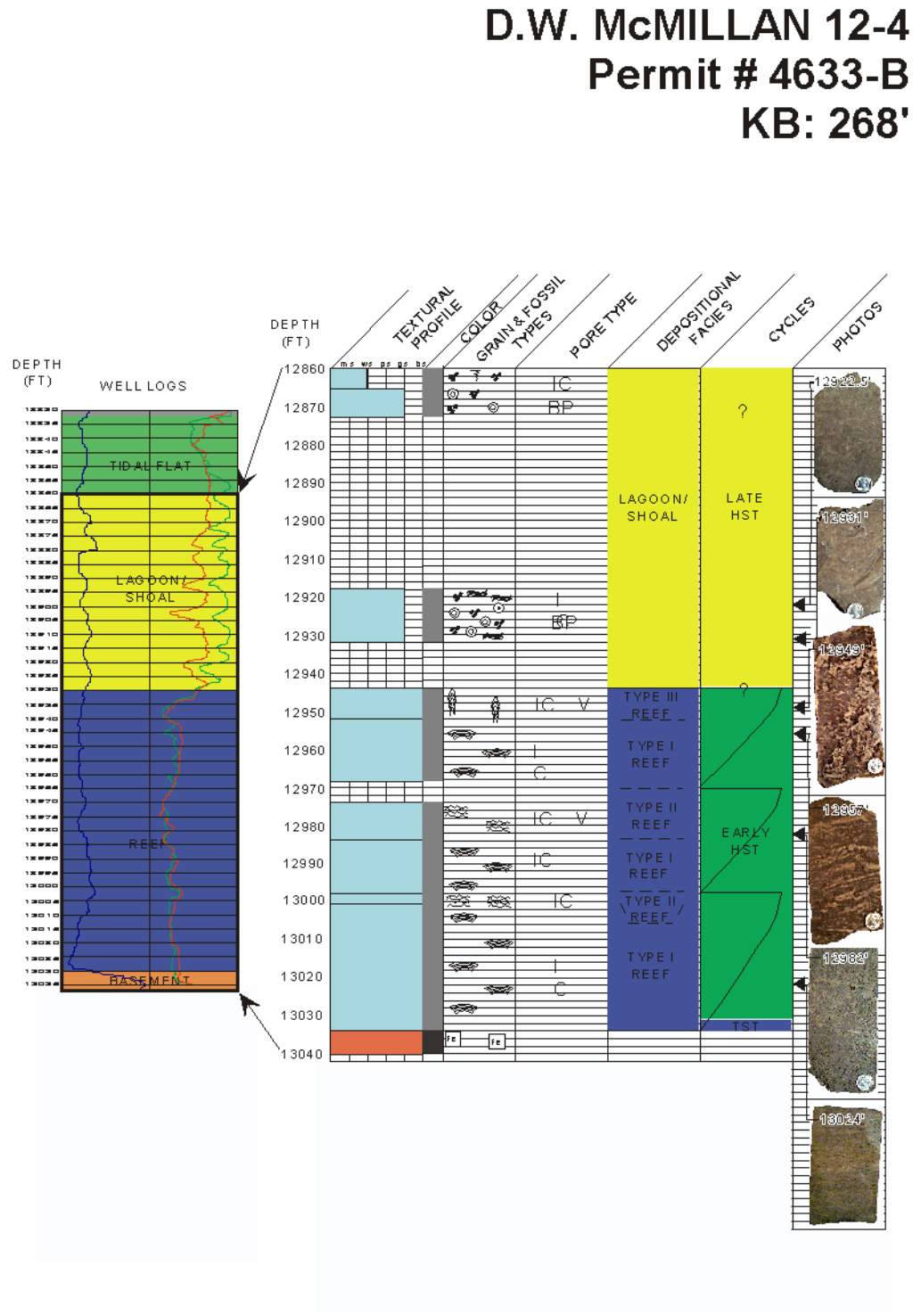

Figure 11. Graphic log for well Permit # 4633B
by W.C. Parcell

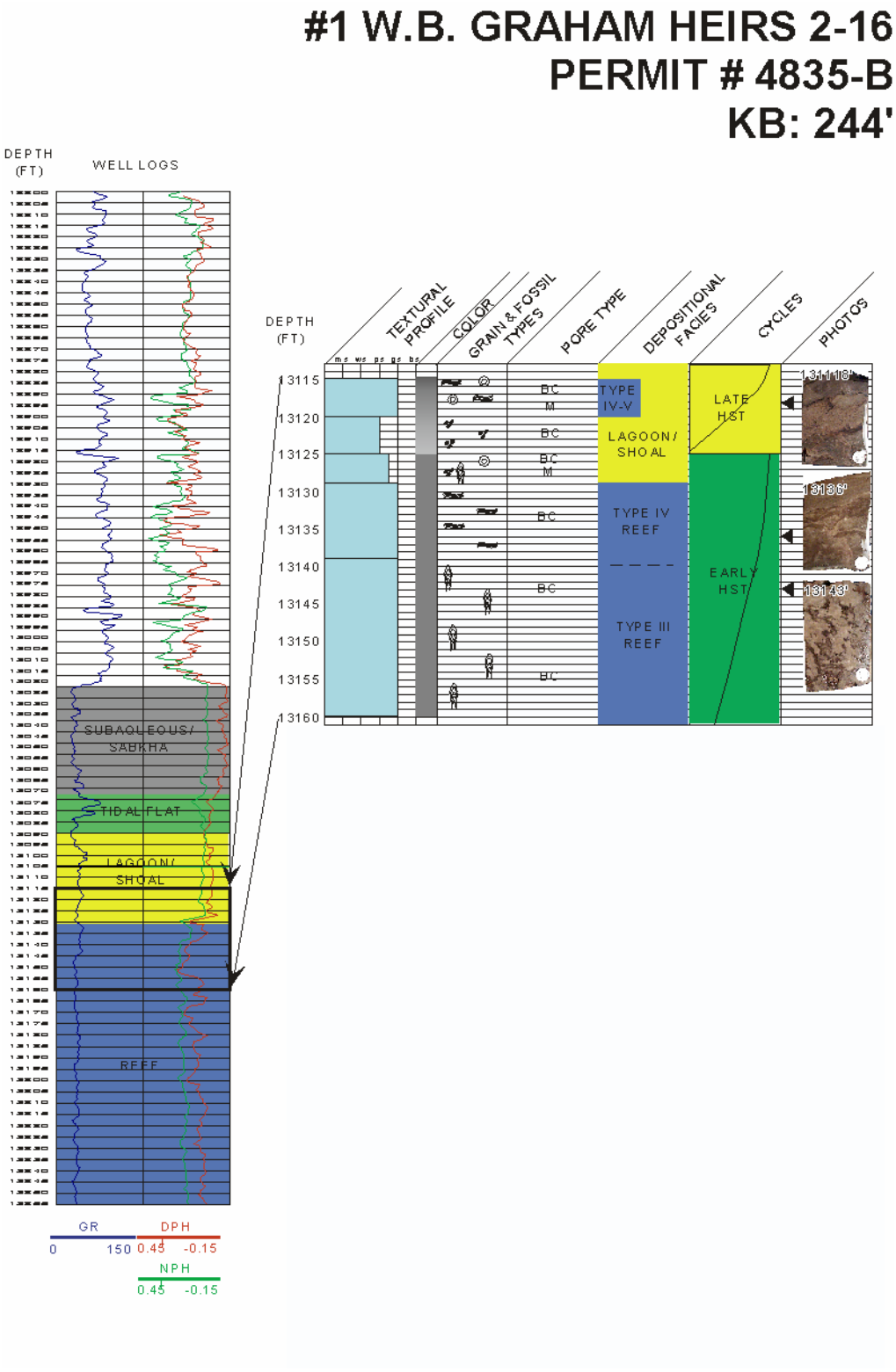

Figure 12. Graphic log for well Permit # 4835B
by W.C. Parcell

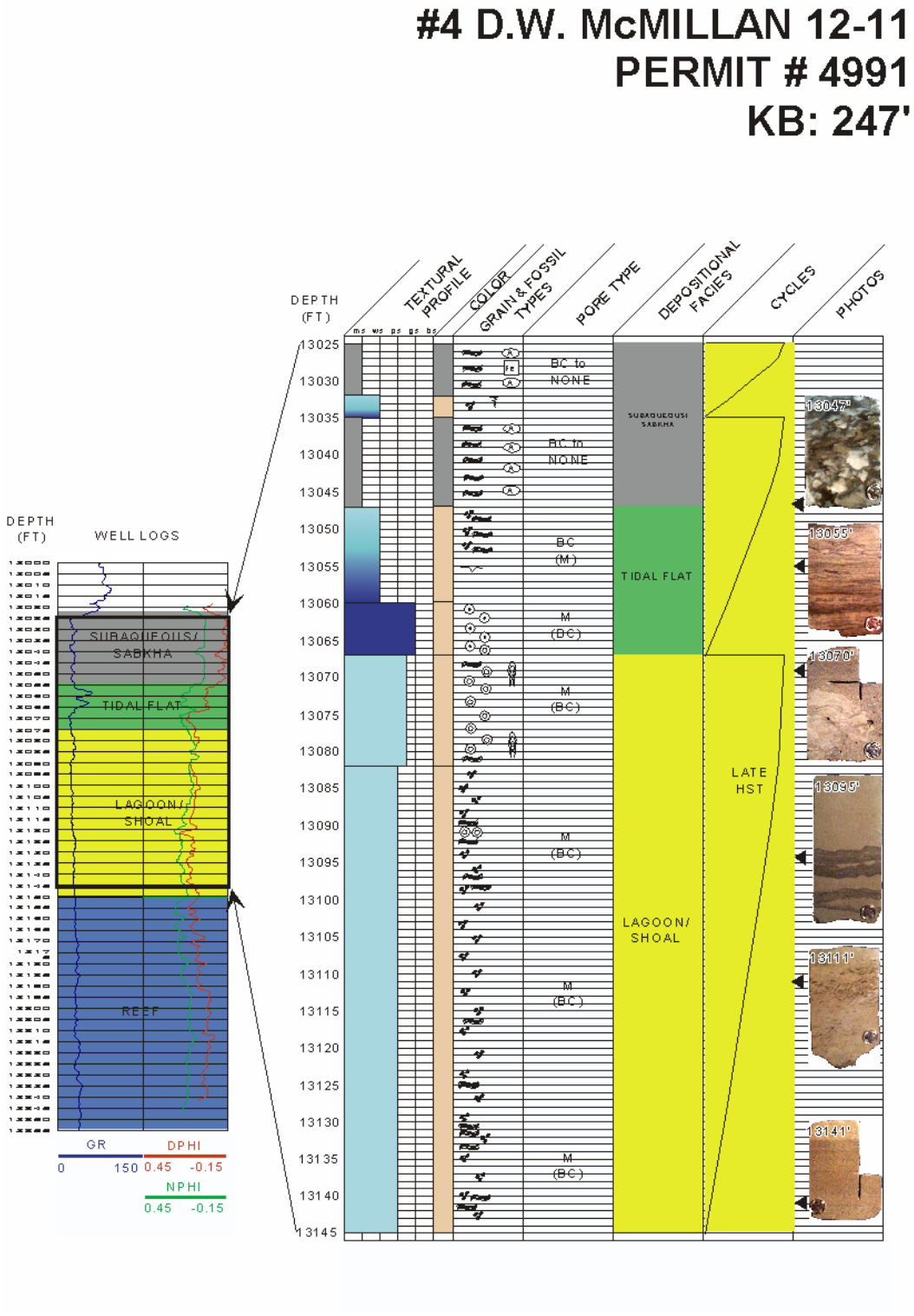

Figure 13. Graphic log for well Permit # 4991
by W.C. Parcell

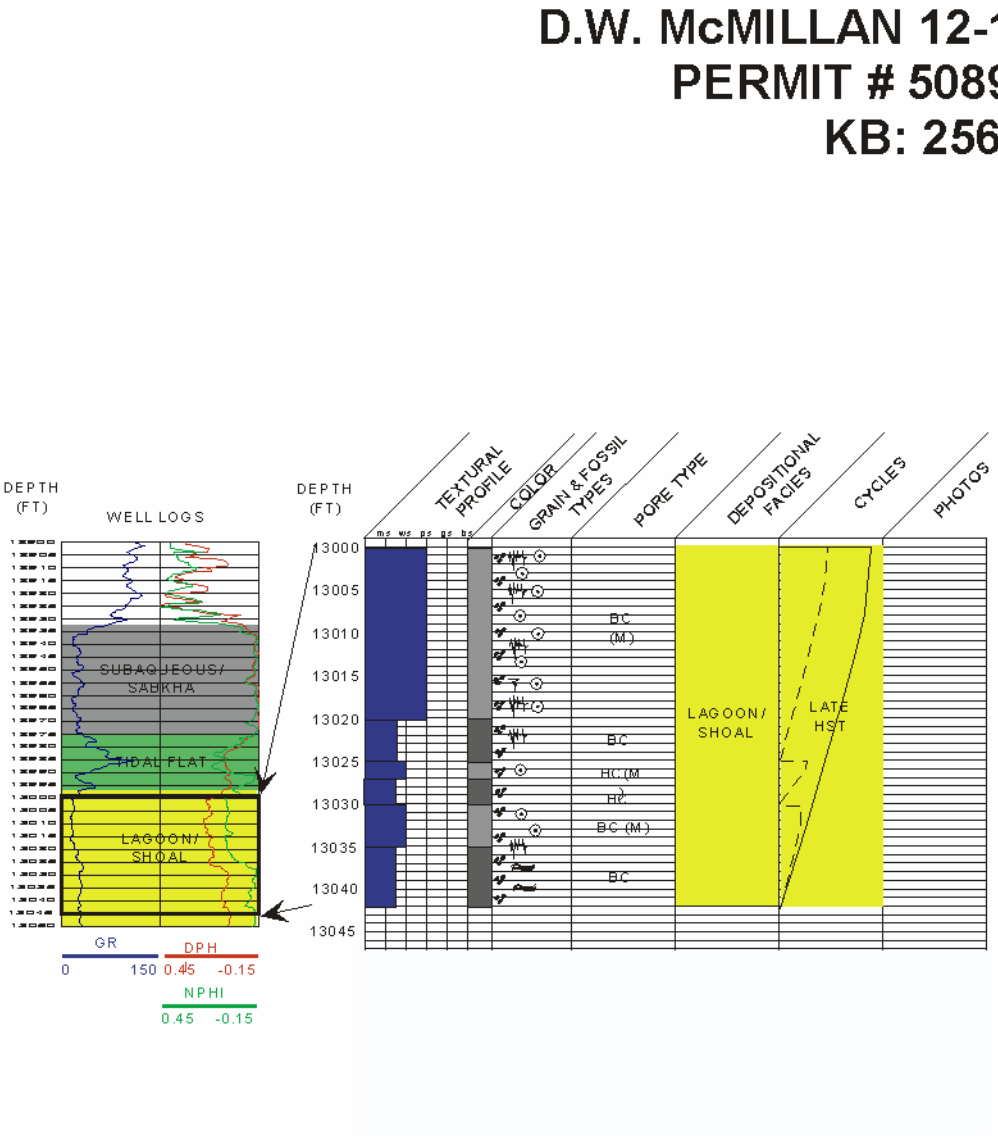

Figure 14. Graphic log for well Permit # 5089
by W.C. Parcell

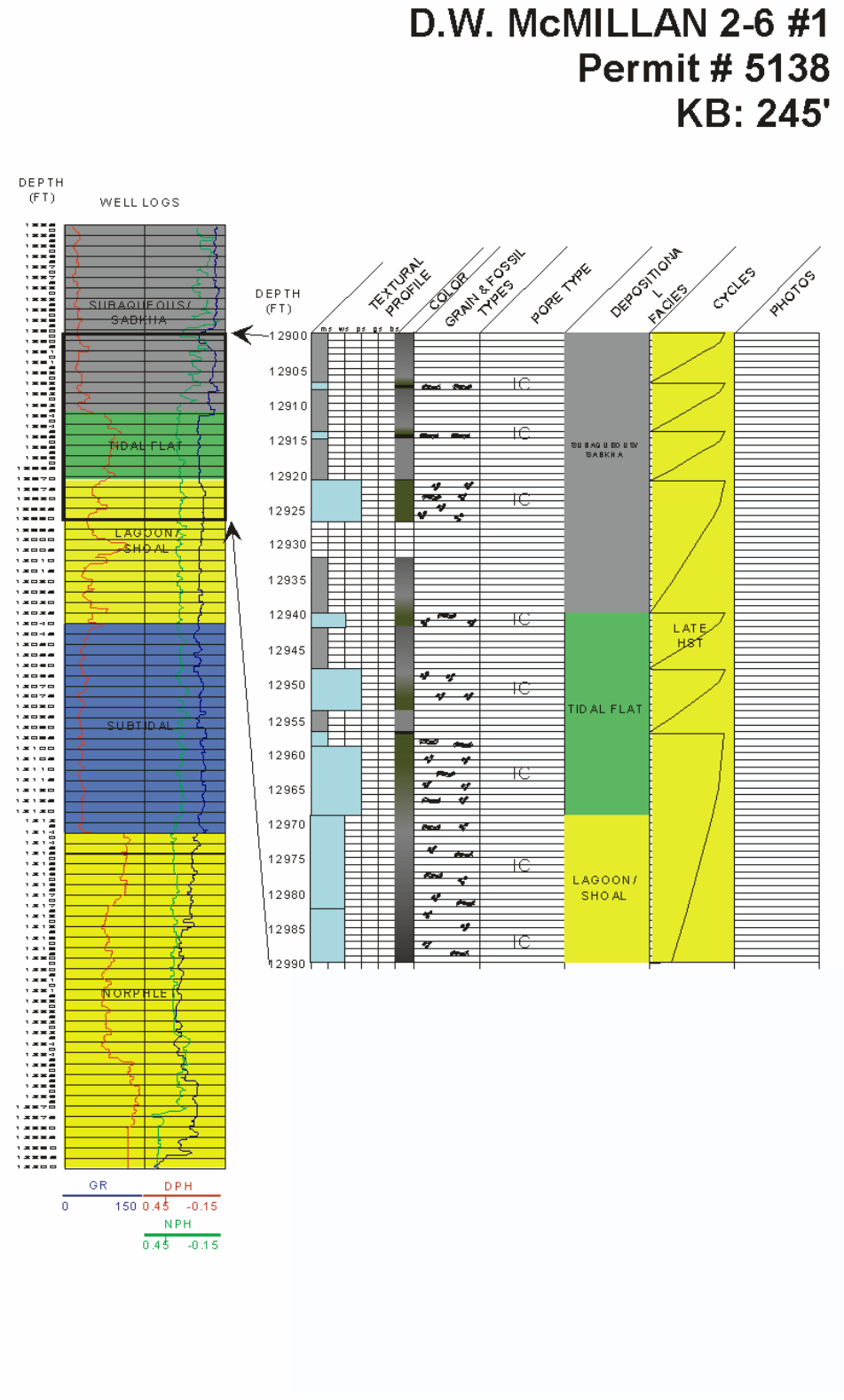

Figure 15. Graphic log for well Permit # 5138
by W.C. Parcell

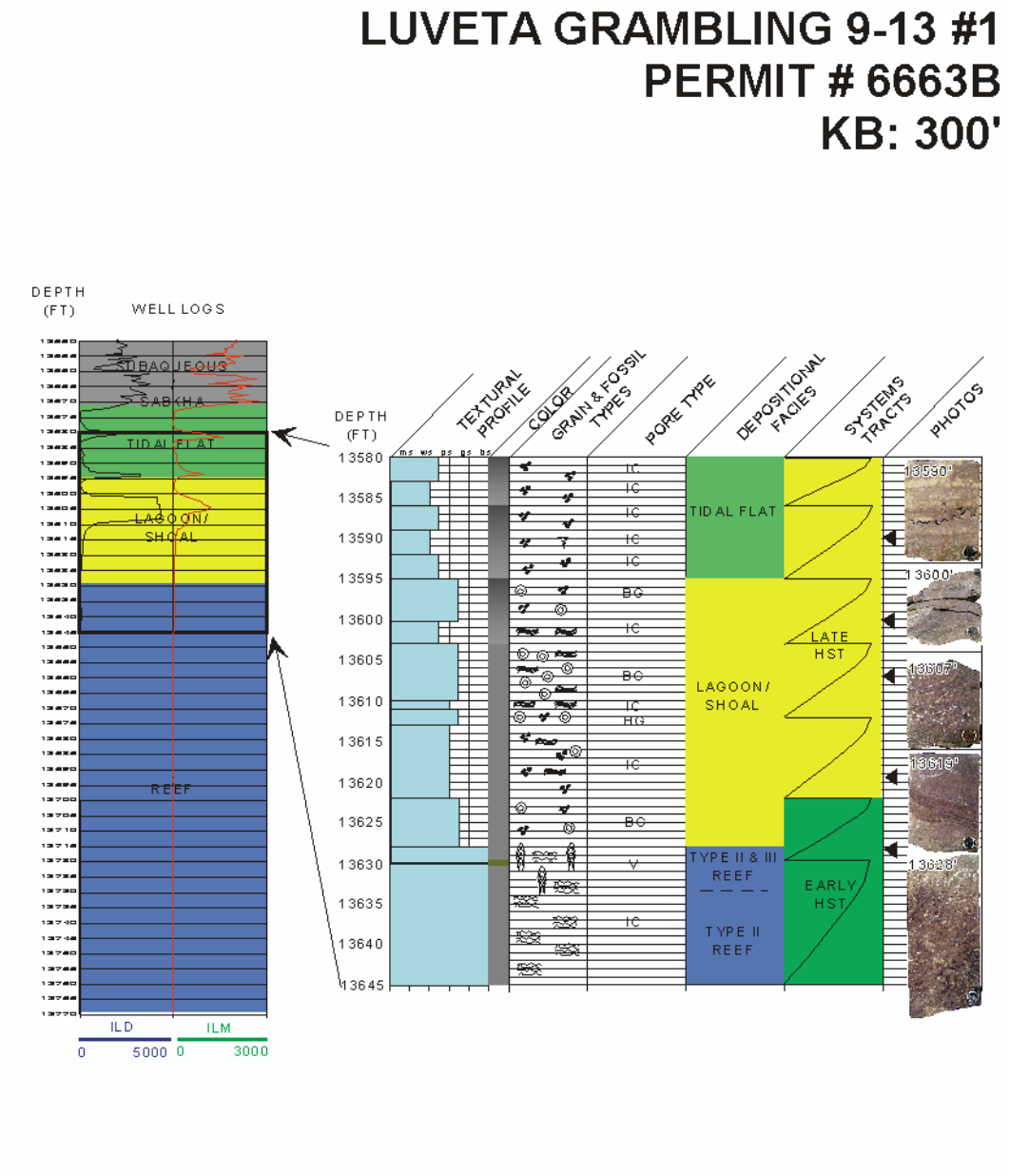

Figure 16. Graphic log for well Permit # 6663B
by W.C. Parcell

Table 1. Characteristics of Smackover Lithofacies in the Appleton Field Area.

Lithofacies	Lithology	Allochems	Pore Types	Porosity	Permeability
Carbonate mudstone	Dolostone and anhydritic dolostone	None	Intercrystalline	Low (1.2 to 2.5%)	Low (0.01 md)
Peloidal wackestone	Dolostone to calcareous dolostone	Peloids, ooids, intraclasts	Intercrystalline, moldic	Low to moderate (2.6 to 12.4%)	Low (0.01 to 0.11 md)
Peloidal packstone	Dolomitic limestone	Peloids, ooids, oncoids, intraclasts	Interparticulate, moldic, intercrystalline	Low to moderate (1.1 to 12.4%)	Low to moderate (0.01 to 0.51 md)
Peloidal/oncoidal packstone	Dolostone to calcareous dolostone	Peloids, oncoids, intraclasts	Interparticulate	Low (1.2 to 6.1%)	Low (0.01 md)
Peloidal/oolitic packstone	Dolostone	Peloids, ooids, skeletal grains, intraclasts	Moldic, intercrystalline, interparticulate	Low (1.3 to 4.5%)	Low (0.01 md)
Peloidal grainstone	Calcareous dolostone	Peloids, oncoids, algal grains, intraclasts	Interparticulate, fenestral, moldic, interparticulate, vuggy	Low to high (1.0 to 19.9%)	Low to high (0.01 to 722 md)
Oncoidal grainstone	Calcareous dolostone to dolostone	Oncoids, peloids, intraclasts	Interparticulate, intraparticulate, fenestral	Low to moderate (1.4 to 11.9%)	Low to high (0.01 to 8.27 md)
Oolitic grainstone	Dolostone to limestone	Ooids, peloids, oncoids, intraclasts	Interparticulate, moldic, intercrystalline	Moderate to high (8.3 to 20.7%)	Moderate to high (3.09 to 406 md)
Oncoidal/peloidal/ oolitic grainstone	Dolostone to calcareous dolostone	Oncoids, peloids, ooids, algal grains	Interparticulate, moldic, vuggy	Low to high (1.9 to 19%)	Low to high (0.01 to 219 md)
Algal grainstone	Dolomitic limestone to calcareous dolostone	Algal grains, oncoids, peloids, ooids	Interparticulate, moldic, vuggy, fenestral, intercrystalline	Low to high (1.7 to 23.1%)	Low to high (0.01 to 63 md)
Microbial boundstone (bafflestone)	Dolostone	Algae, intraclasts, oncoids, peloids	Shelter, vuggy, interparticulate, intercrystalline	High (11.0 to 29.0%)	High (8.13 to 4106 md)
Microbial bindstone	Dolostone	Algae, peloids, ooids	Shelter, vuggy, fenestral, moldic, interparticulate	High (11.9 to 20.7%)	High (11 to 1545 md)
Algal laminite	Dolostone to dolomitic limestone	Algae, peloids, oncoids, intraclasts	Interparticulate, intercrystalline	Low (1.1 to 7.0%)	Low (0.01 md)
Anhydrite	Anhydrite	None	None	Low (1.0%)	Low (0.01 md)

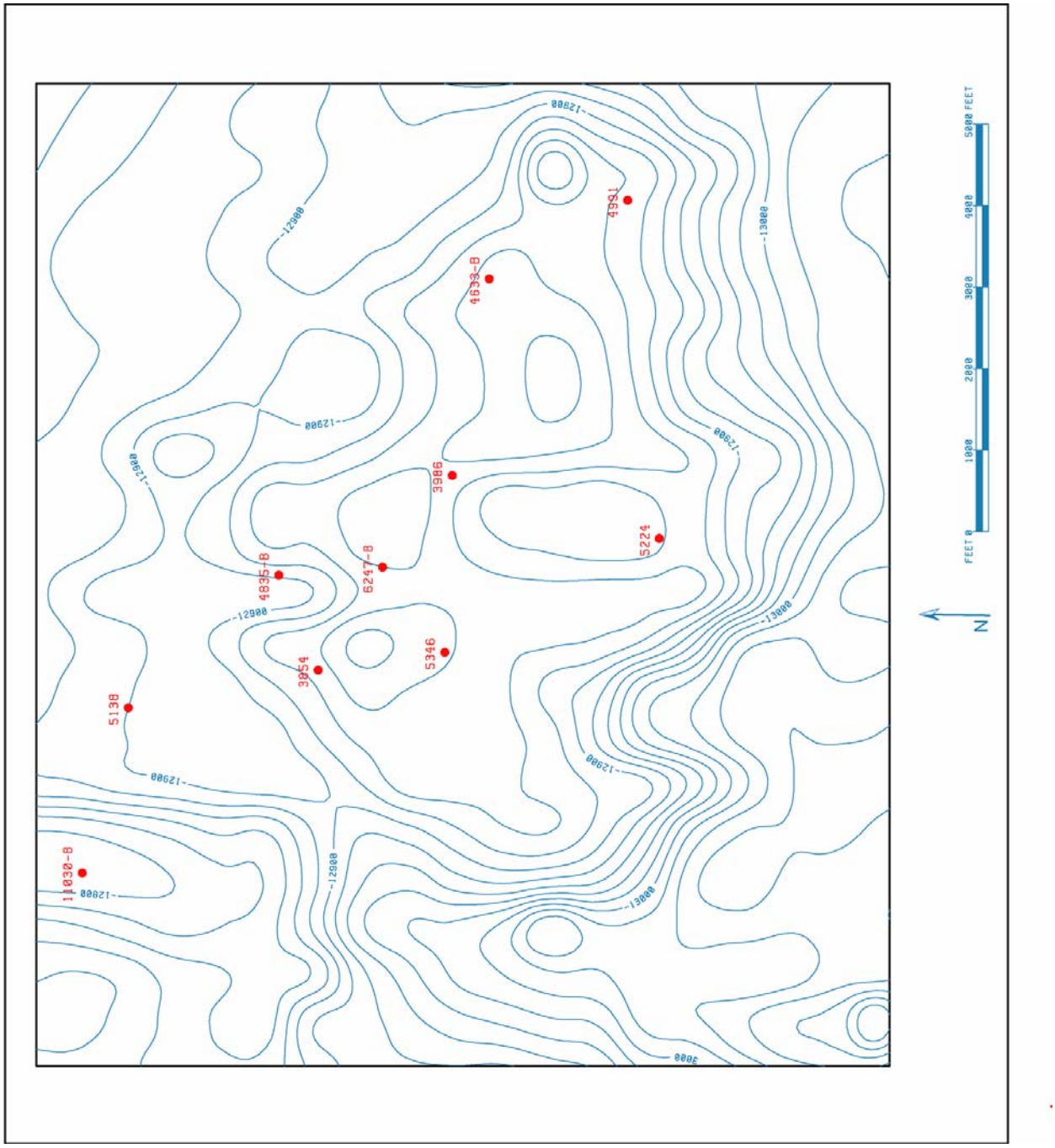

Figure 17. Structure on top of basement (from seismic data).

By B. J. Panetta

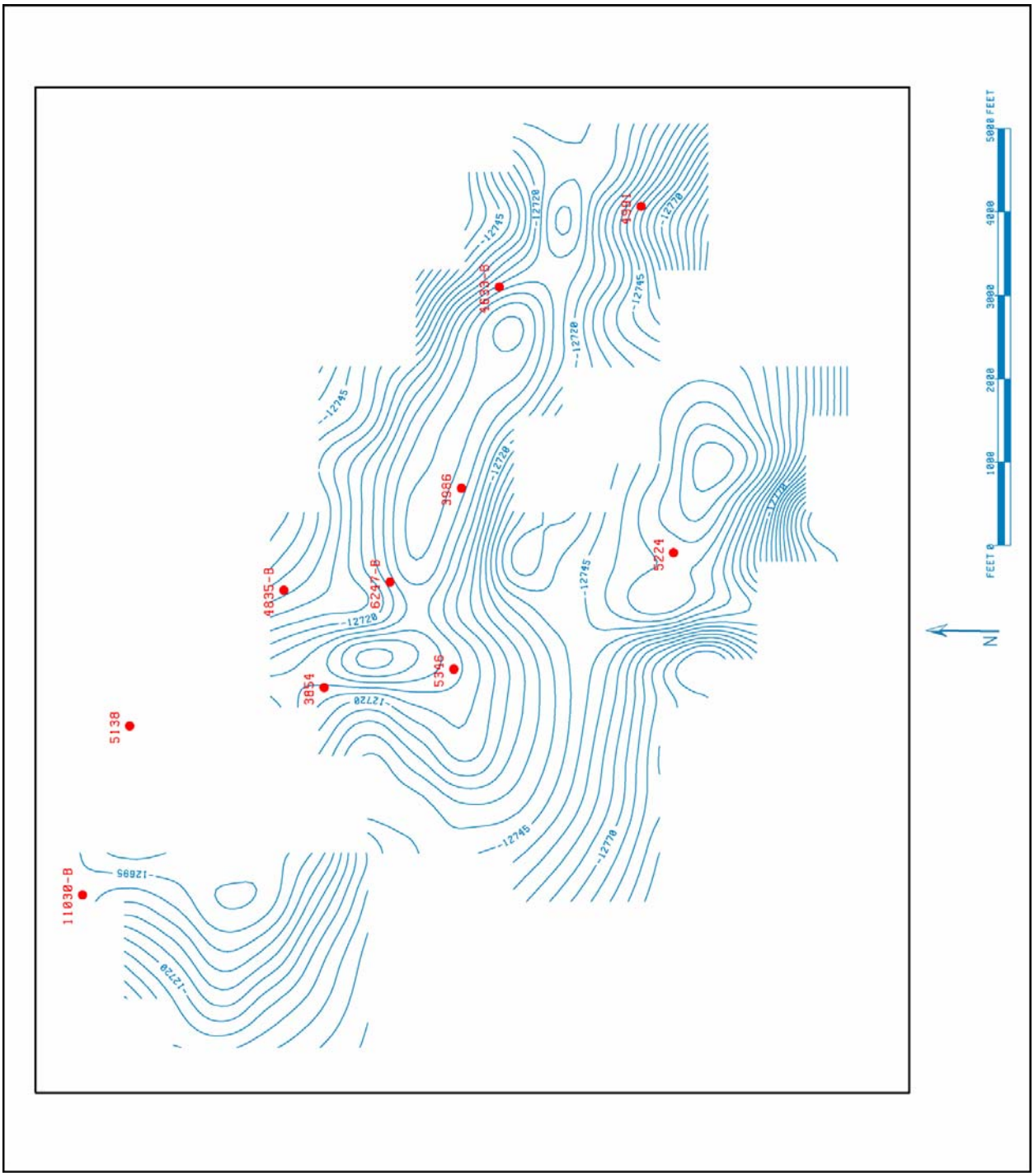

Figure 18. Structure on top of reef (from seismic data).

By B. J. Panetta

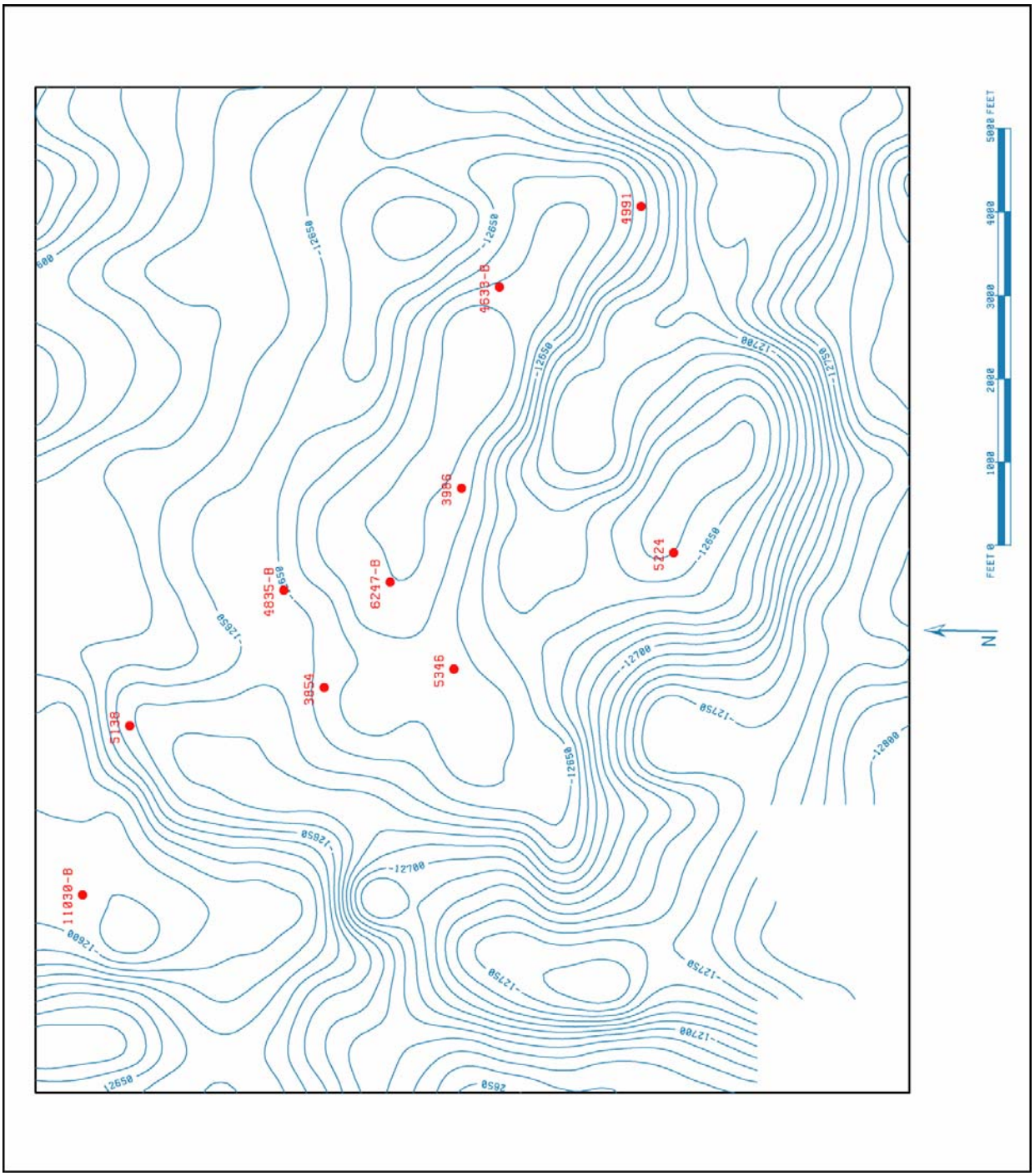

Figure 19. Structure on top of Smackover/Buckner (from seismic data).

By B. J. Panetta

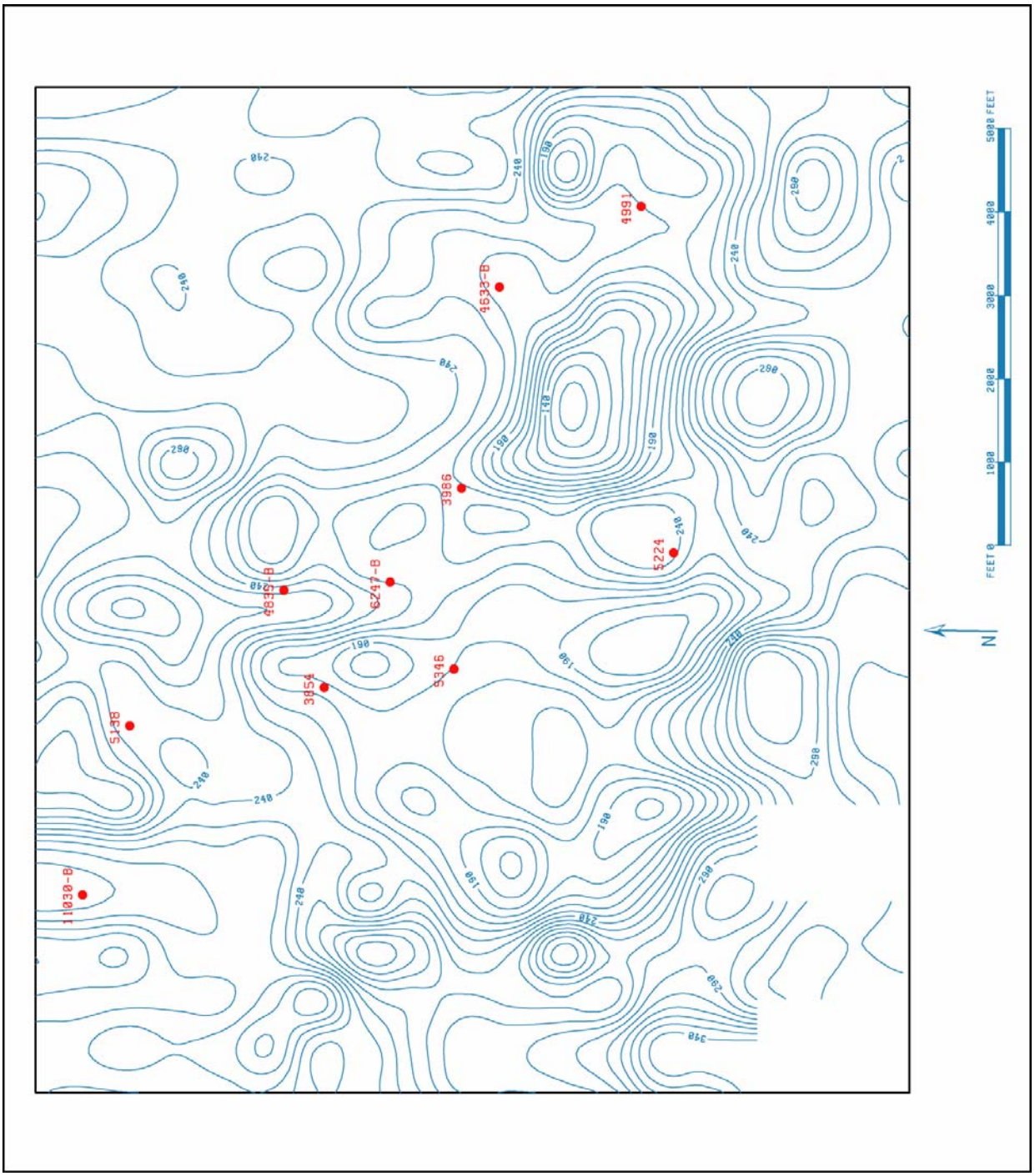

Figure 20. Isopach map of Smacover interval (from seismic data).

By B. J. Panetta

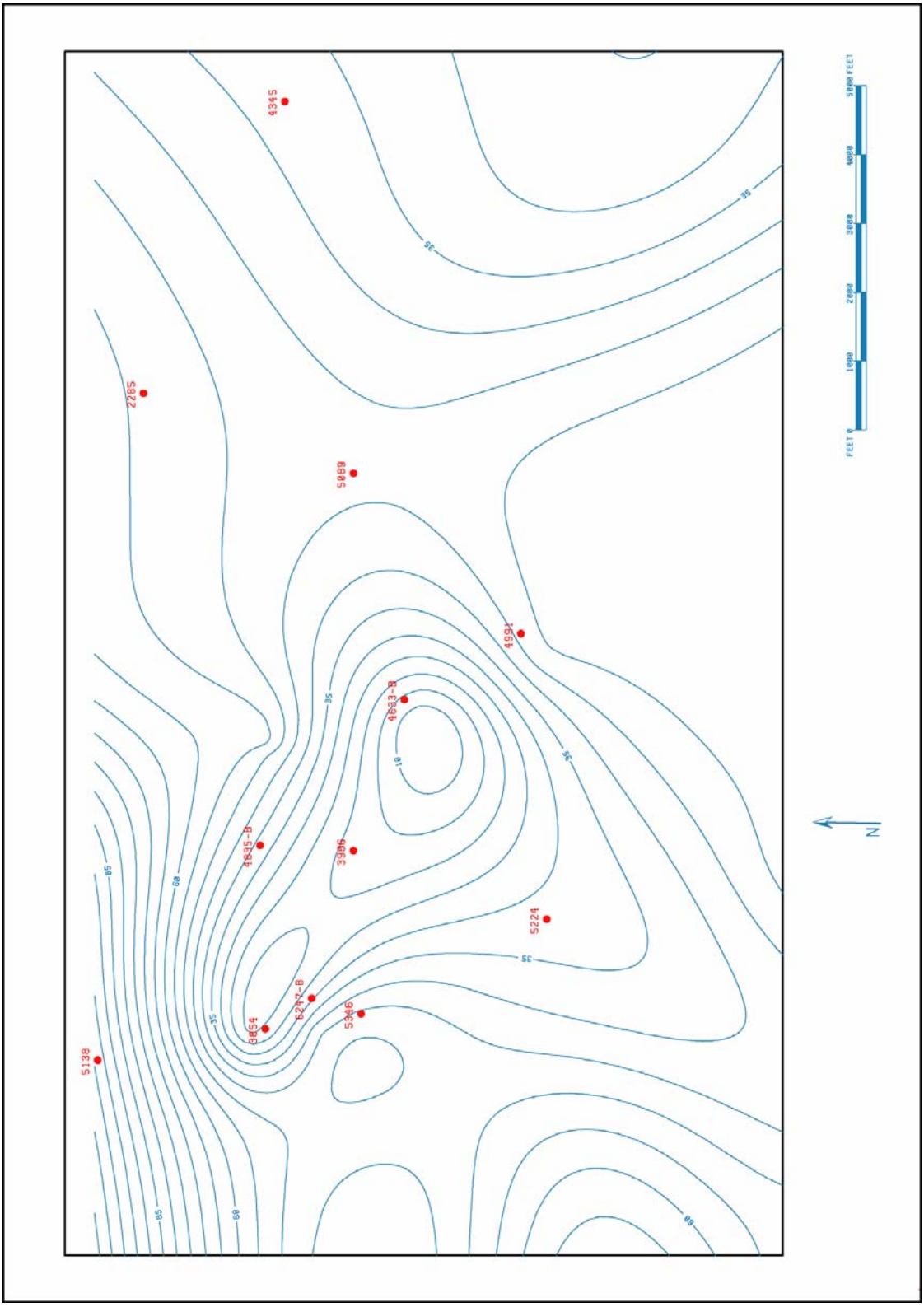

Figure 21. Thickness map of sabkha facies (from log data).

By B. J. Panetta

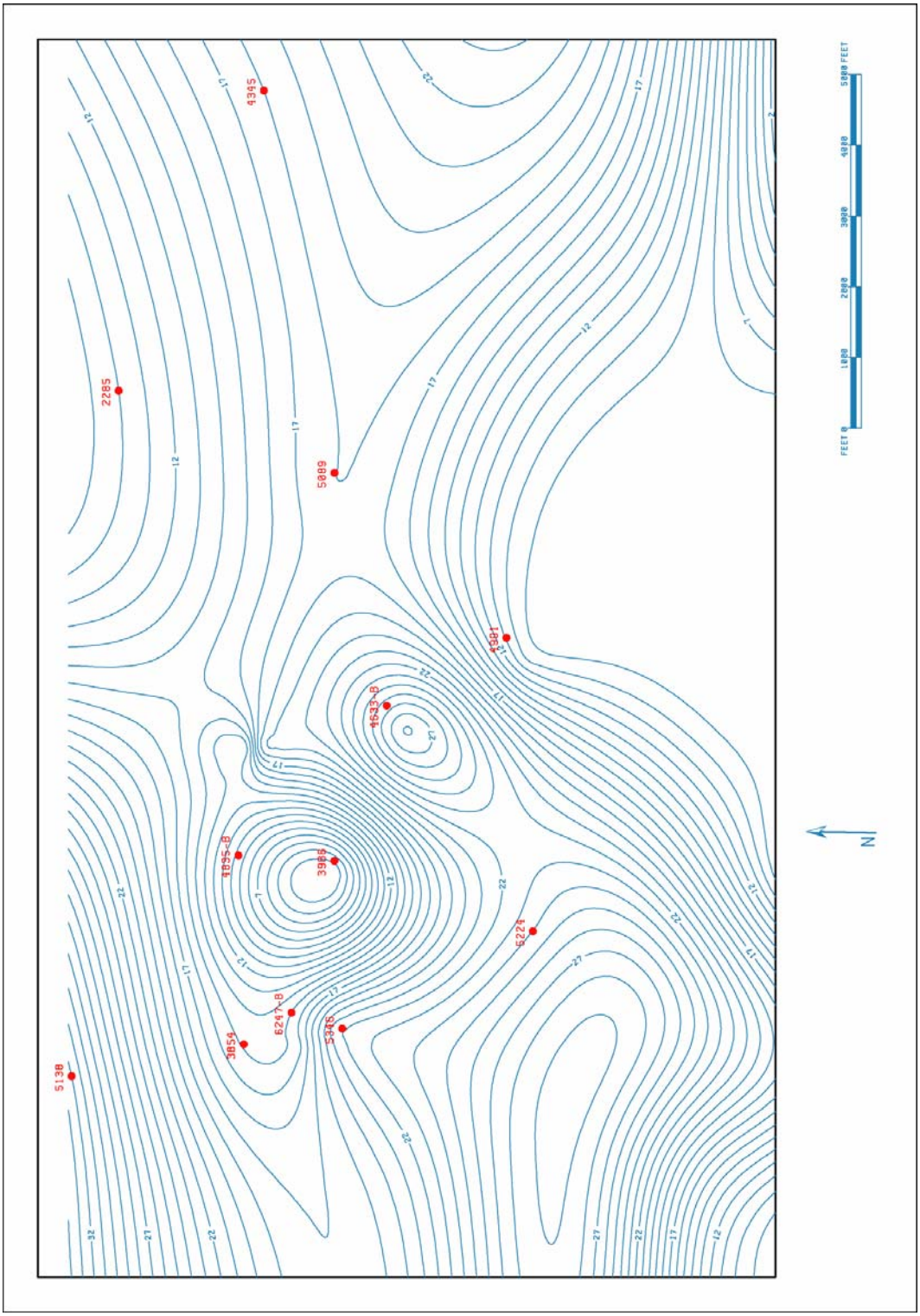

Figure 22. Thickness map of tidal flat facies (from log data).

By B. J. Panetta

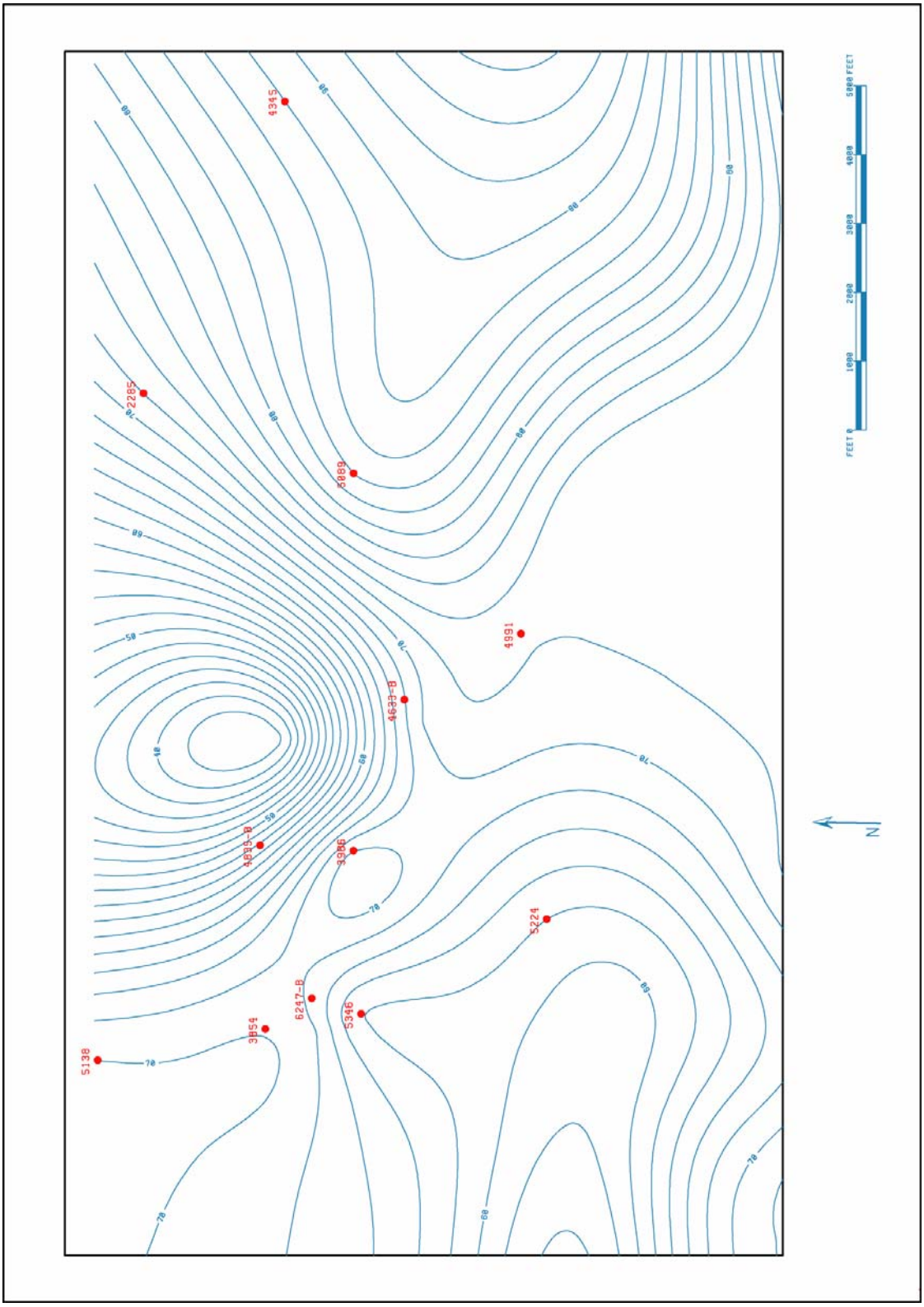

Figure 23. Thickness map of shoal facies (from log data).

By B. J. Panetta

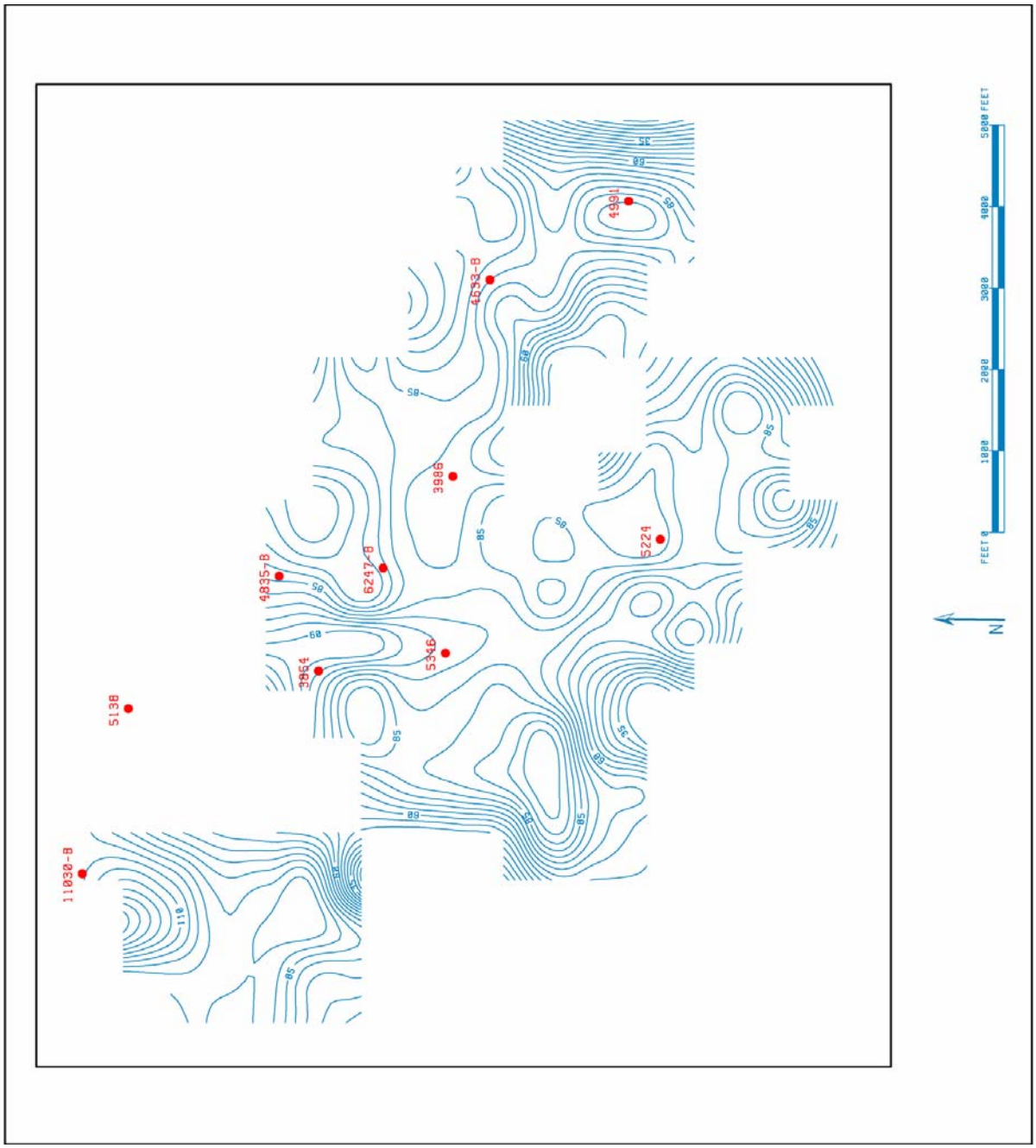

Figure 24. Thickness map of tidal flat and shoal facies (from seismic data).

By B. J. Panetta

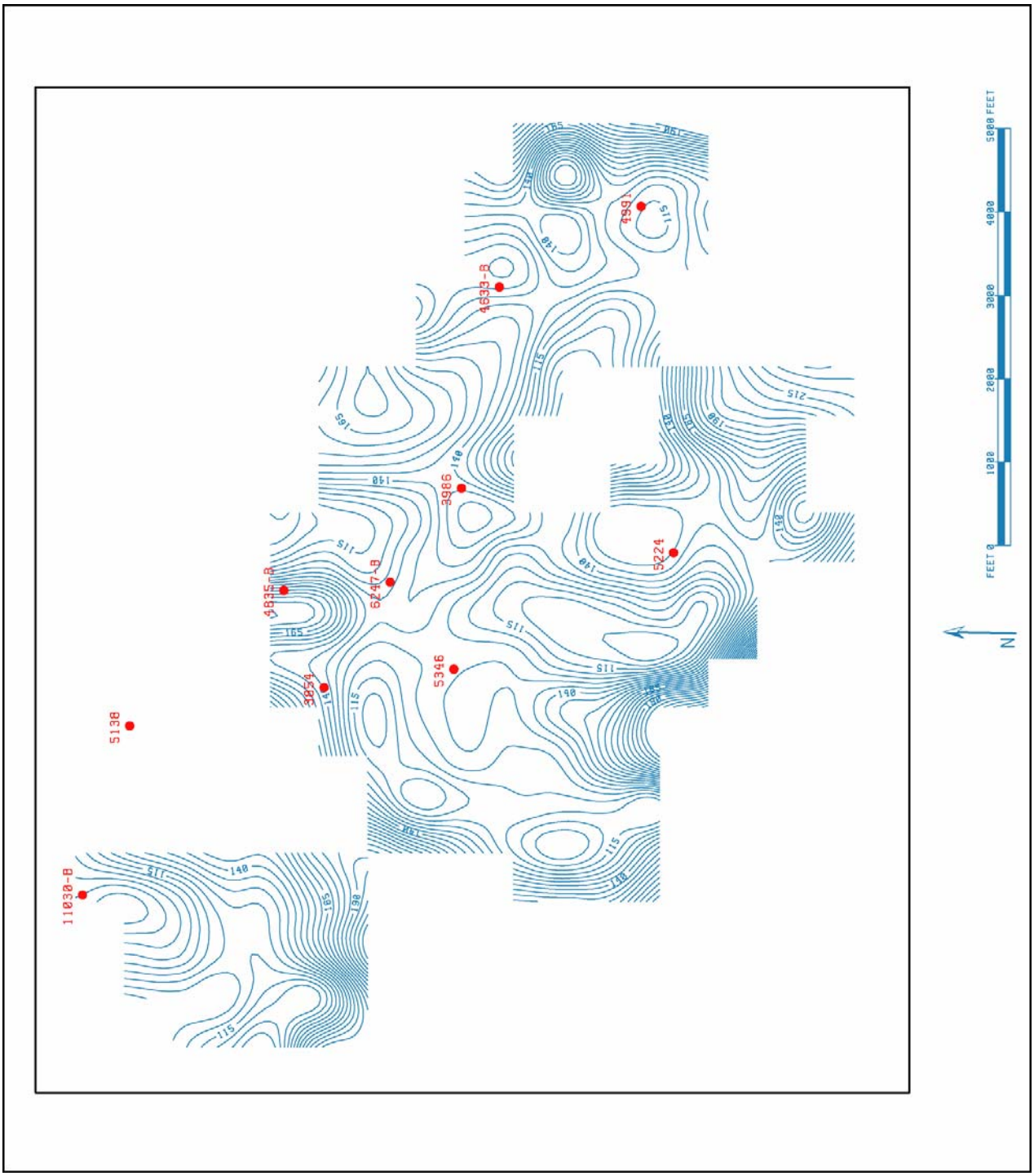

Figure 25. Thickness map of reef facies (from seismic data).

By B. J. Panetta

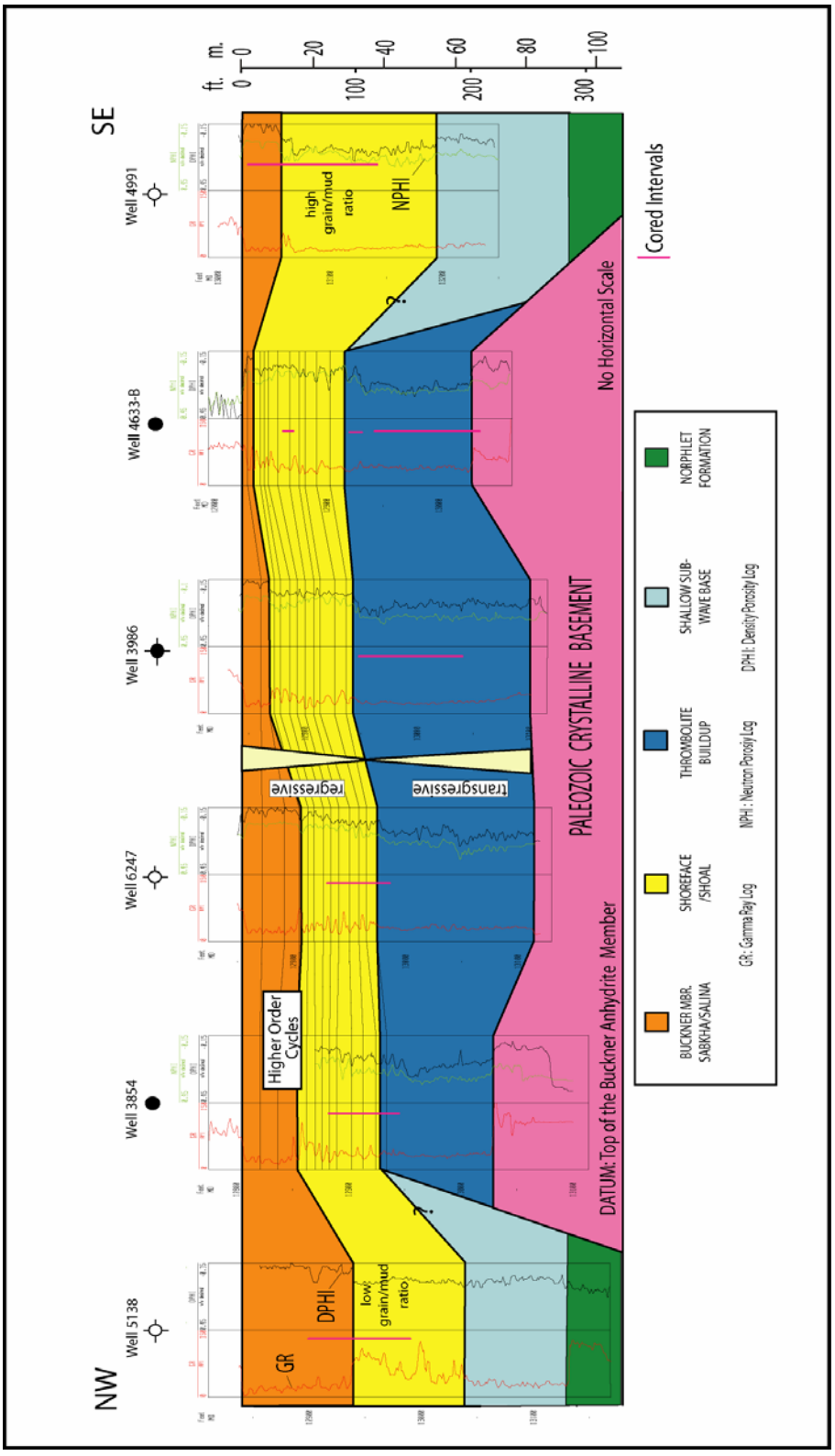

Figure 26. Northwest-southeast stratigraphic well log cross section illustrating the lateral and vertical variation of depositional facies identified in the Smackover/Buckner interval in the Appleton Field area.

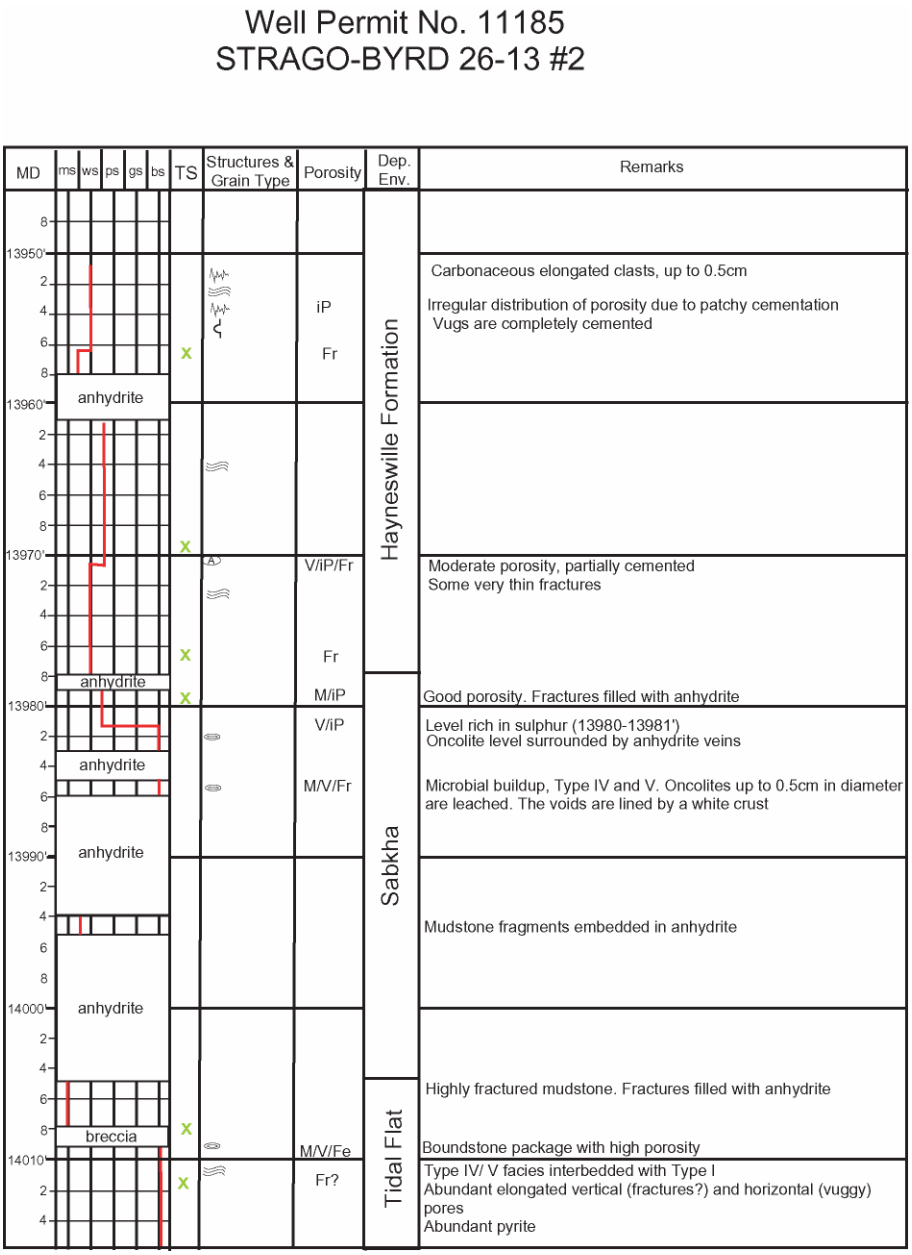

Figure 27. Core description for well permit # 11185.

By Juan Carlos Llinas.

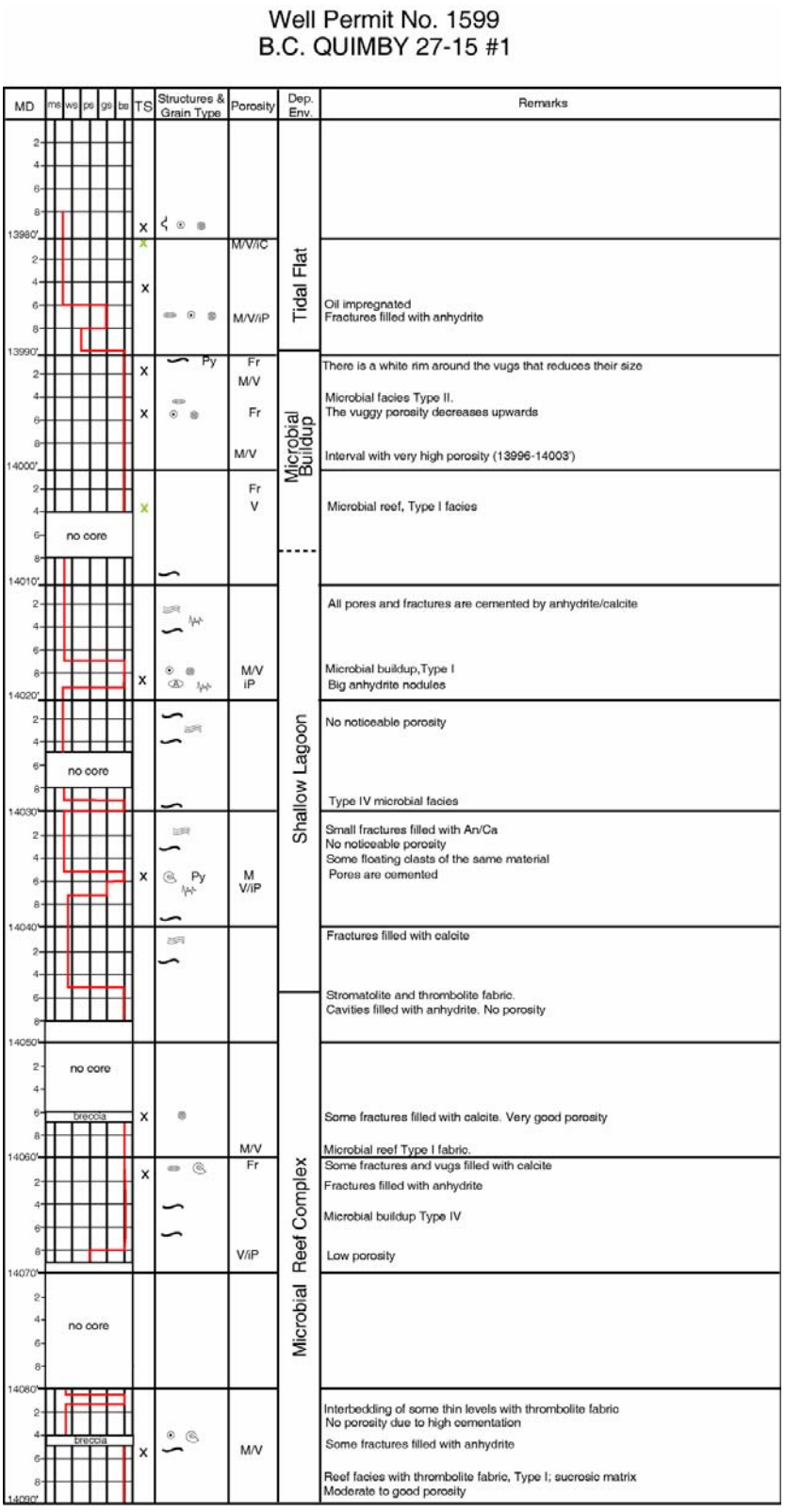

Figure 28. Core Description for well permit # 1599. By Juan Carlos Llinas.

Well Permit No. 1599 (cont.)
B.C. QUIMBY 27-15 #1

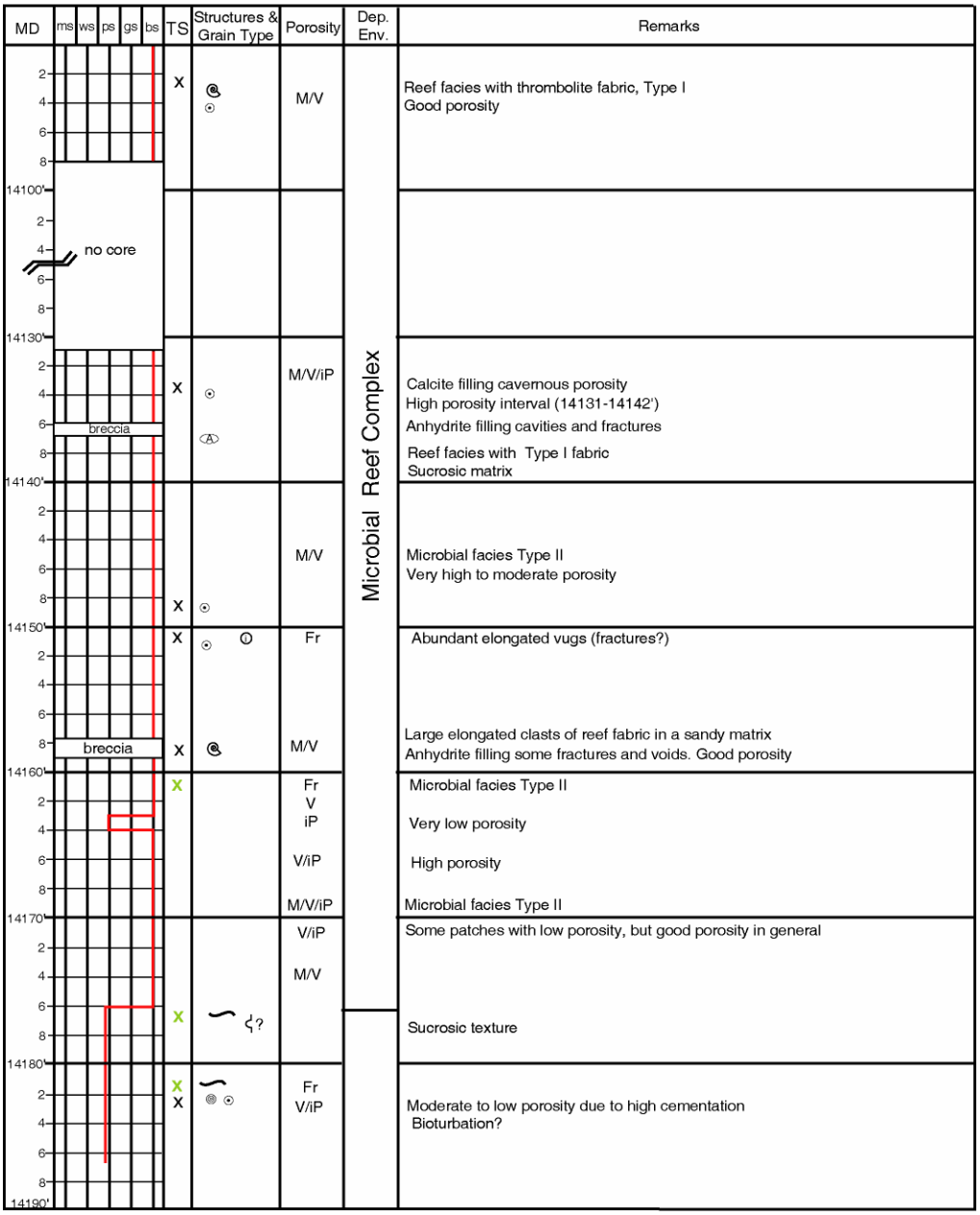

Figure 28 (continued). Core description for well permit # 1599.

By Juan Carlos Llinas.

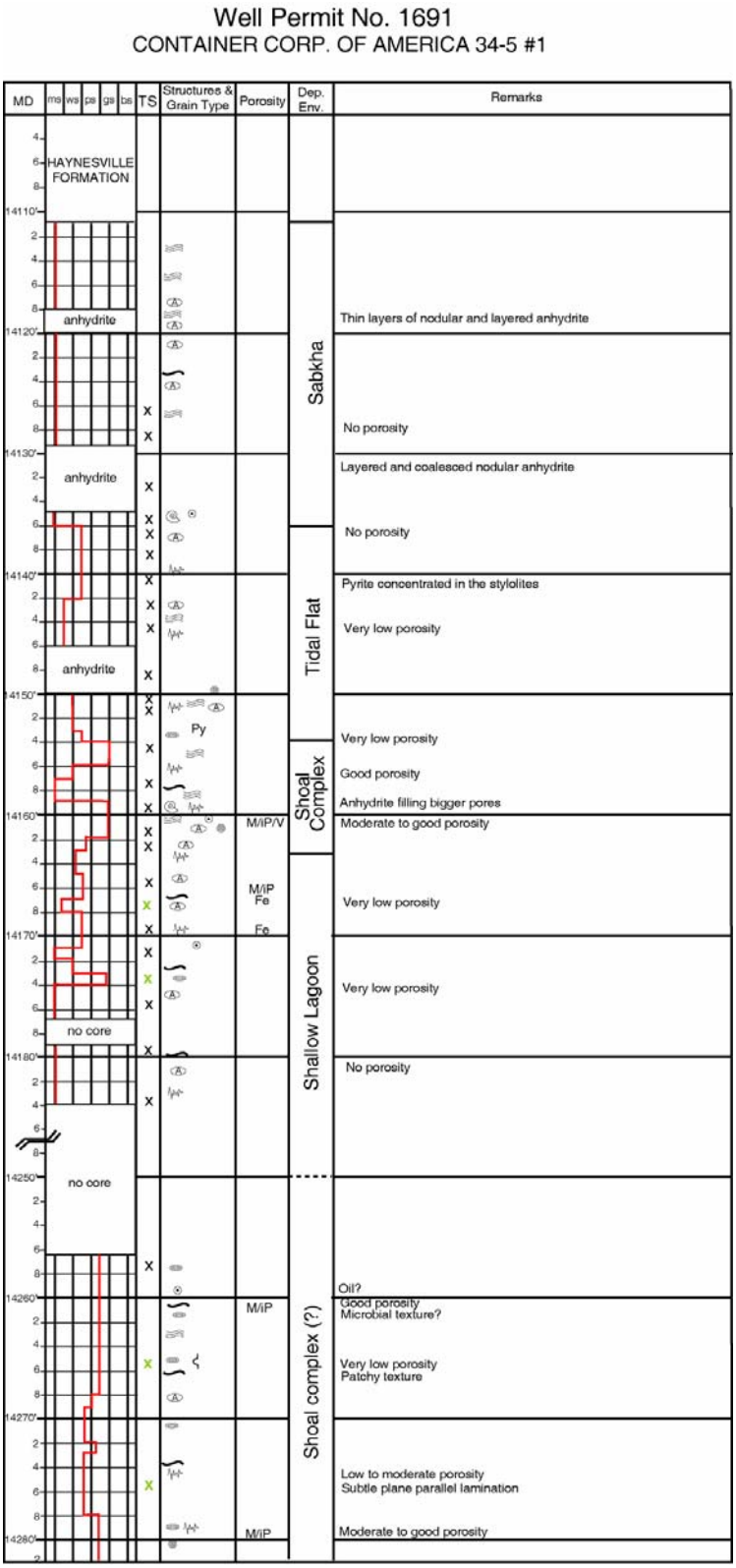

Figure 29. Core description for well permit # 1691. By Juan Carlos Llinas.

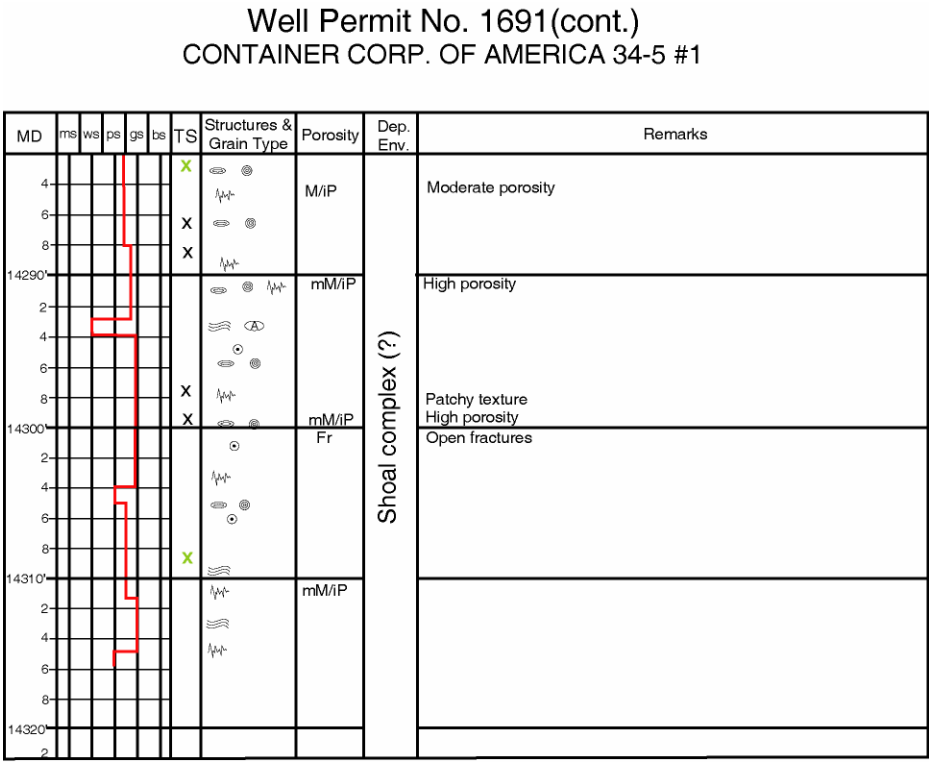

Figure 29 (continued). Core description for well permit # 1691.

By Juan Carlos Llinas.

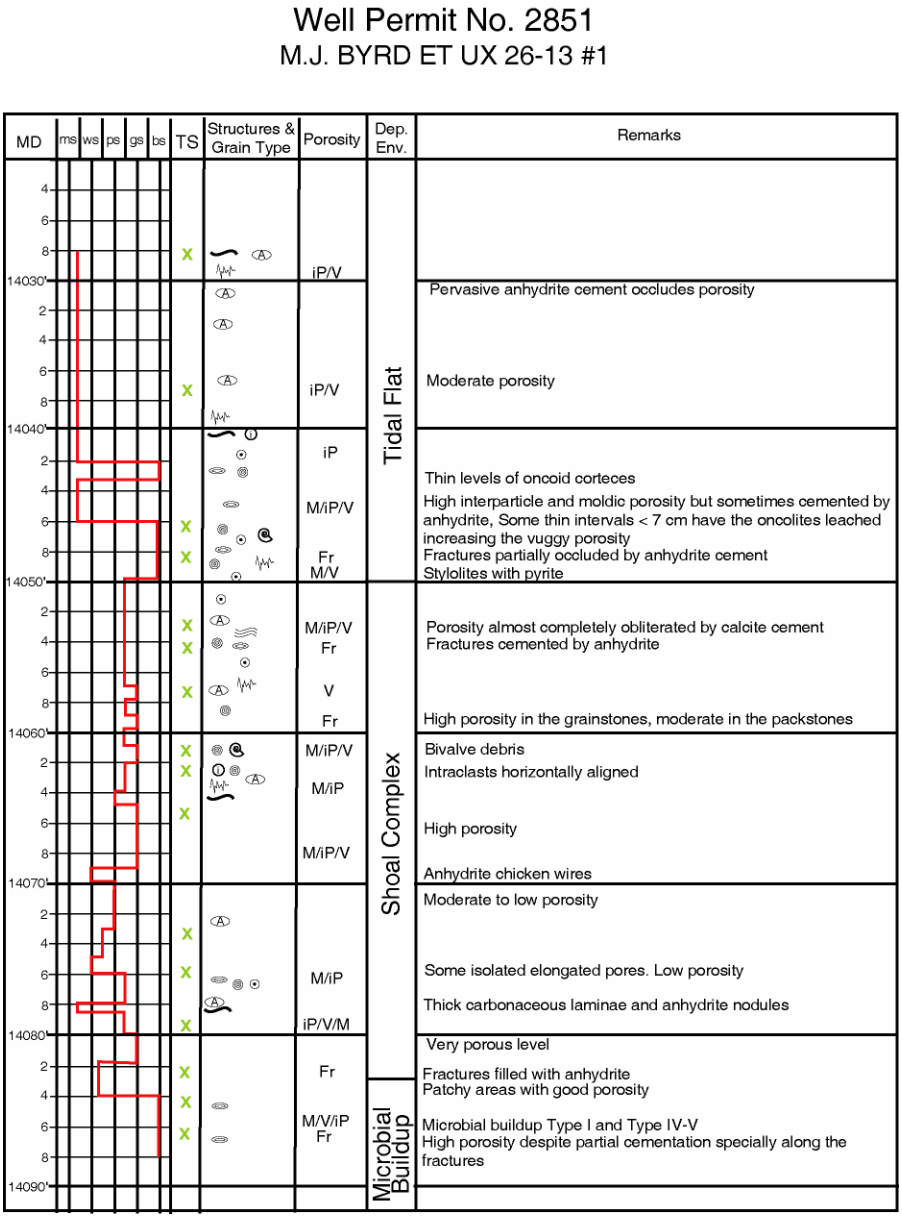

Figure 30. Core description for well permit # 2851.

By Juan Carlos Llinas.

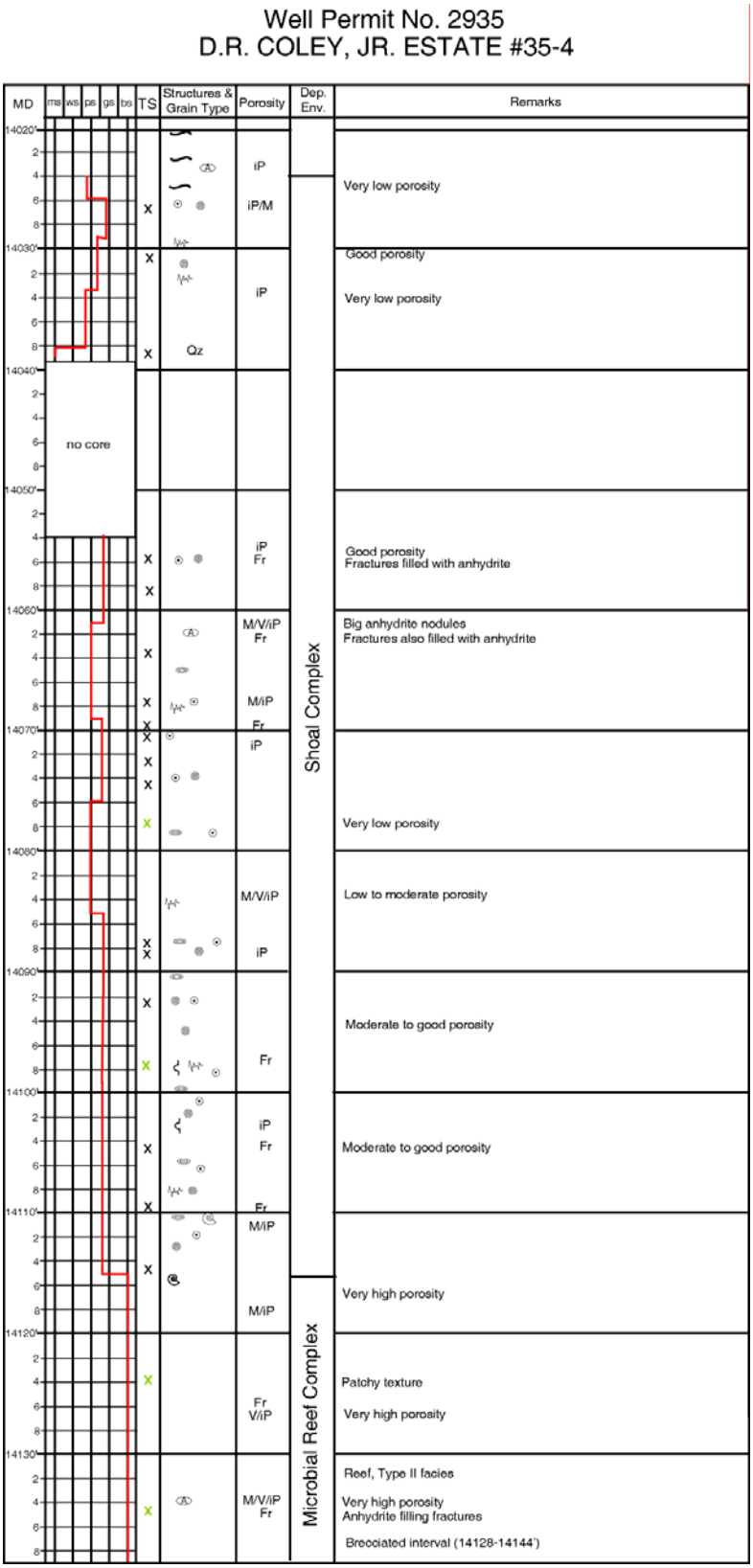

Figure 31. Core description for well permit # 2935. By Juan Carlos Llinas.

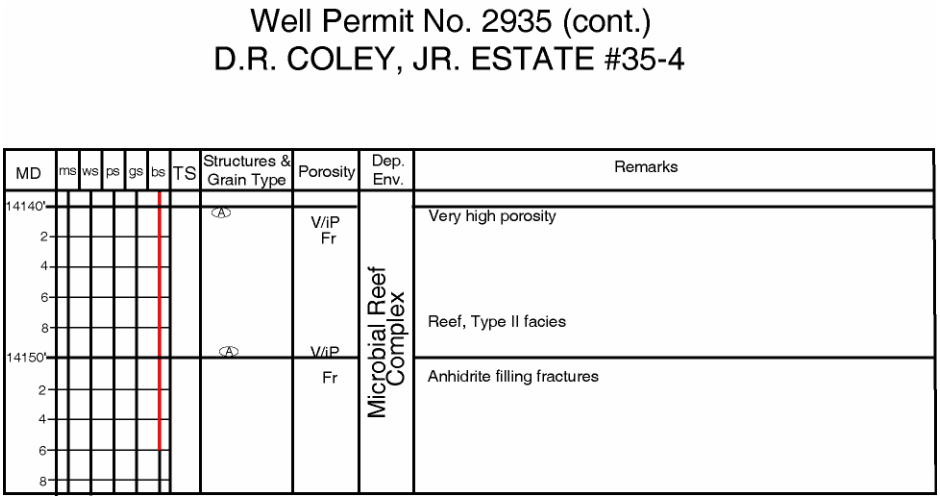

Figure 31 (continued). Core description for well permit # 2935.

By Juan Carlos Llinas.

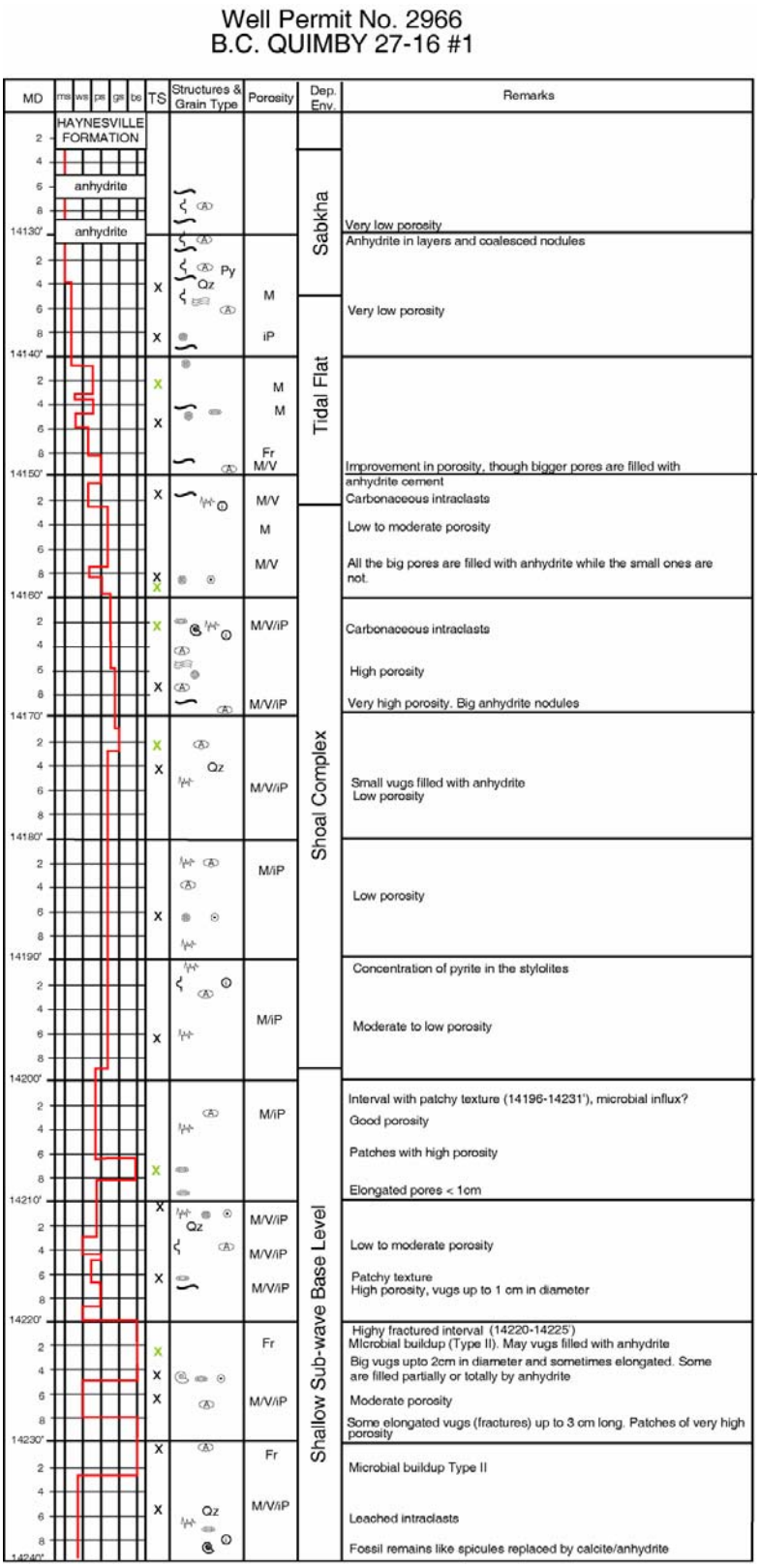

Figure 32. Core description for well permit # 2966. By Juan Carlos Llinas.

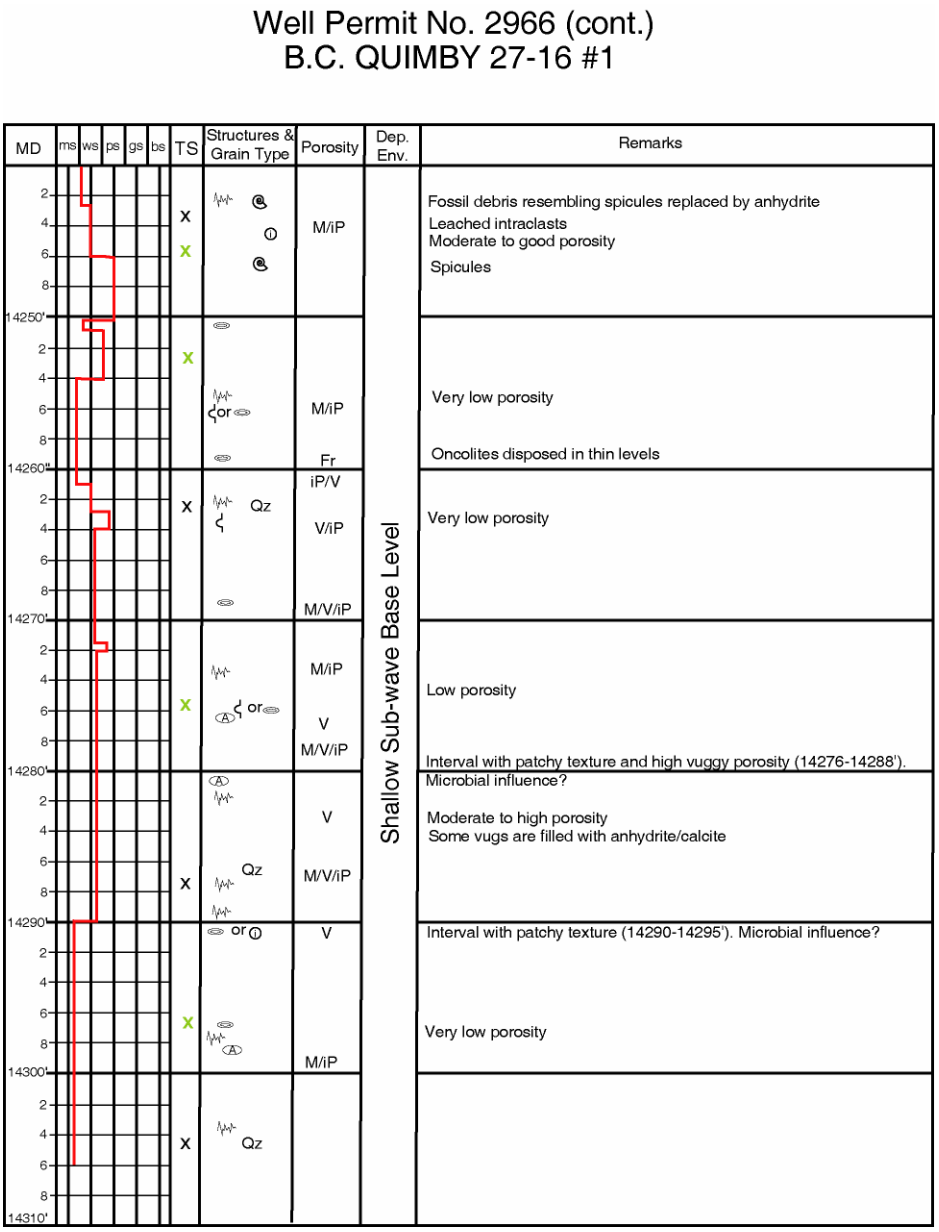

Figure 32 (continued). Core description for well permit # 2966.

By Juan Carlos Llinas.

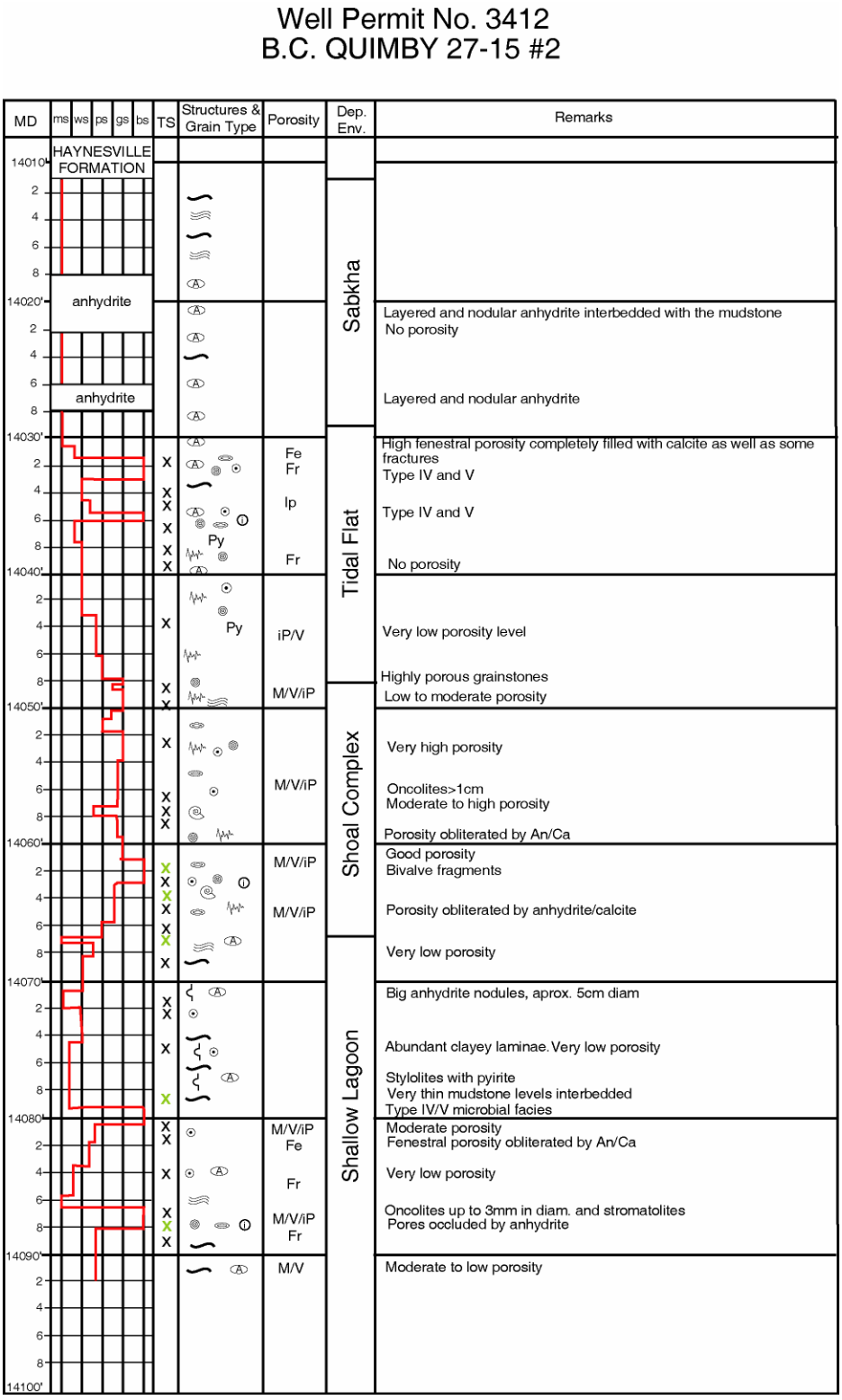

Figure 33. Core description for well permit # 3412. By Juan Carlos Llinas.

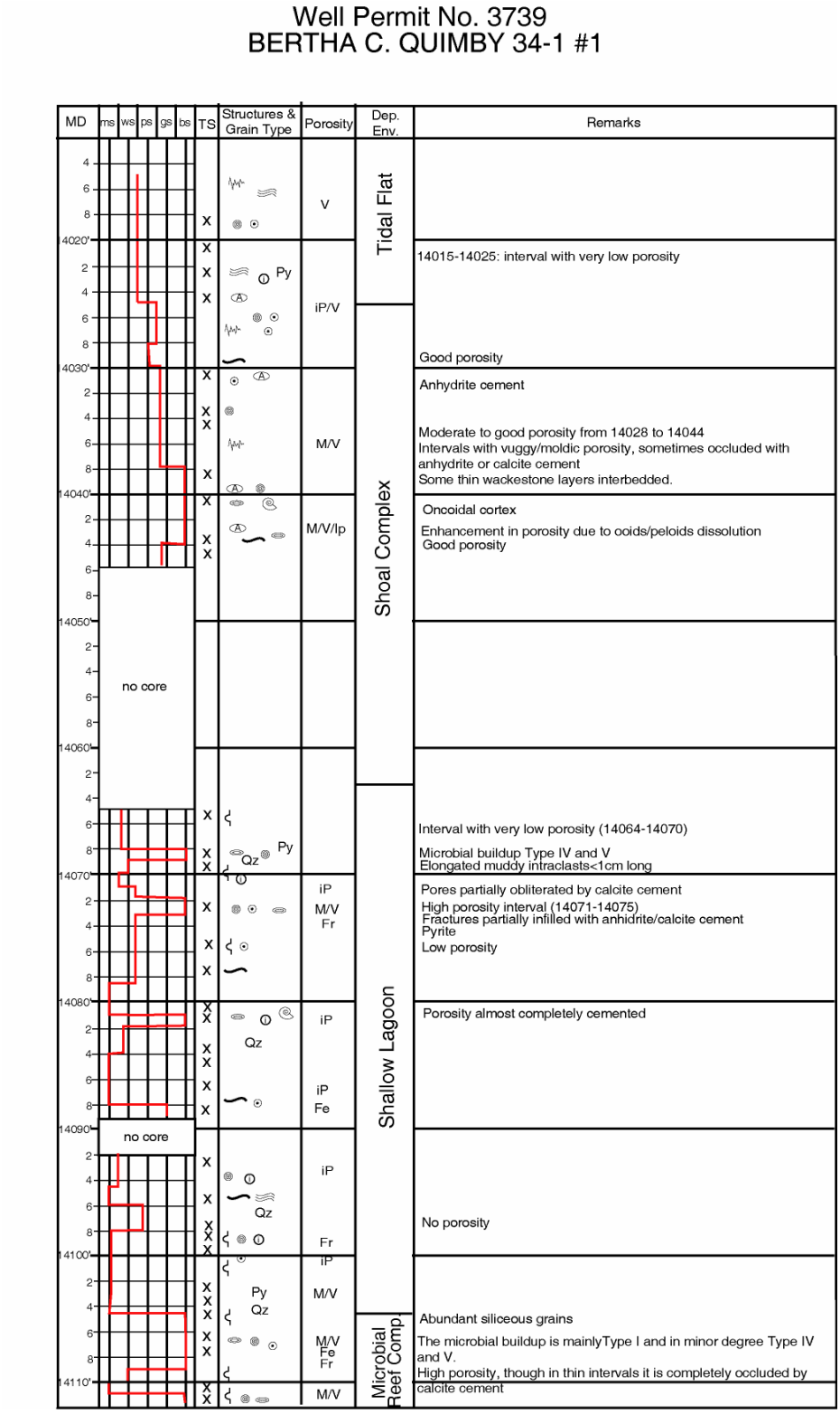

Figure 34. Core description for well permit # 3739. By Juan Carlos Llinas.

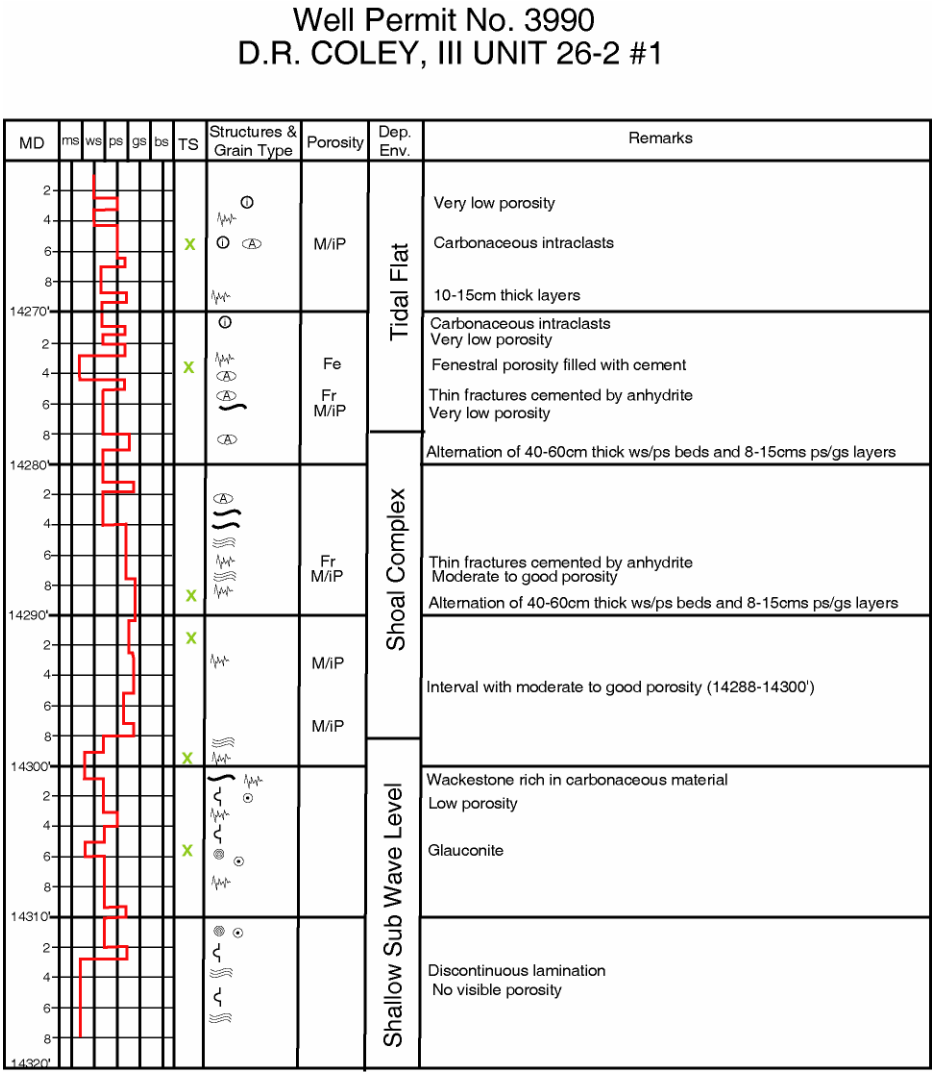

Figure 35. Core description for well permit # 3990.

By Juan Carlos Llinas.

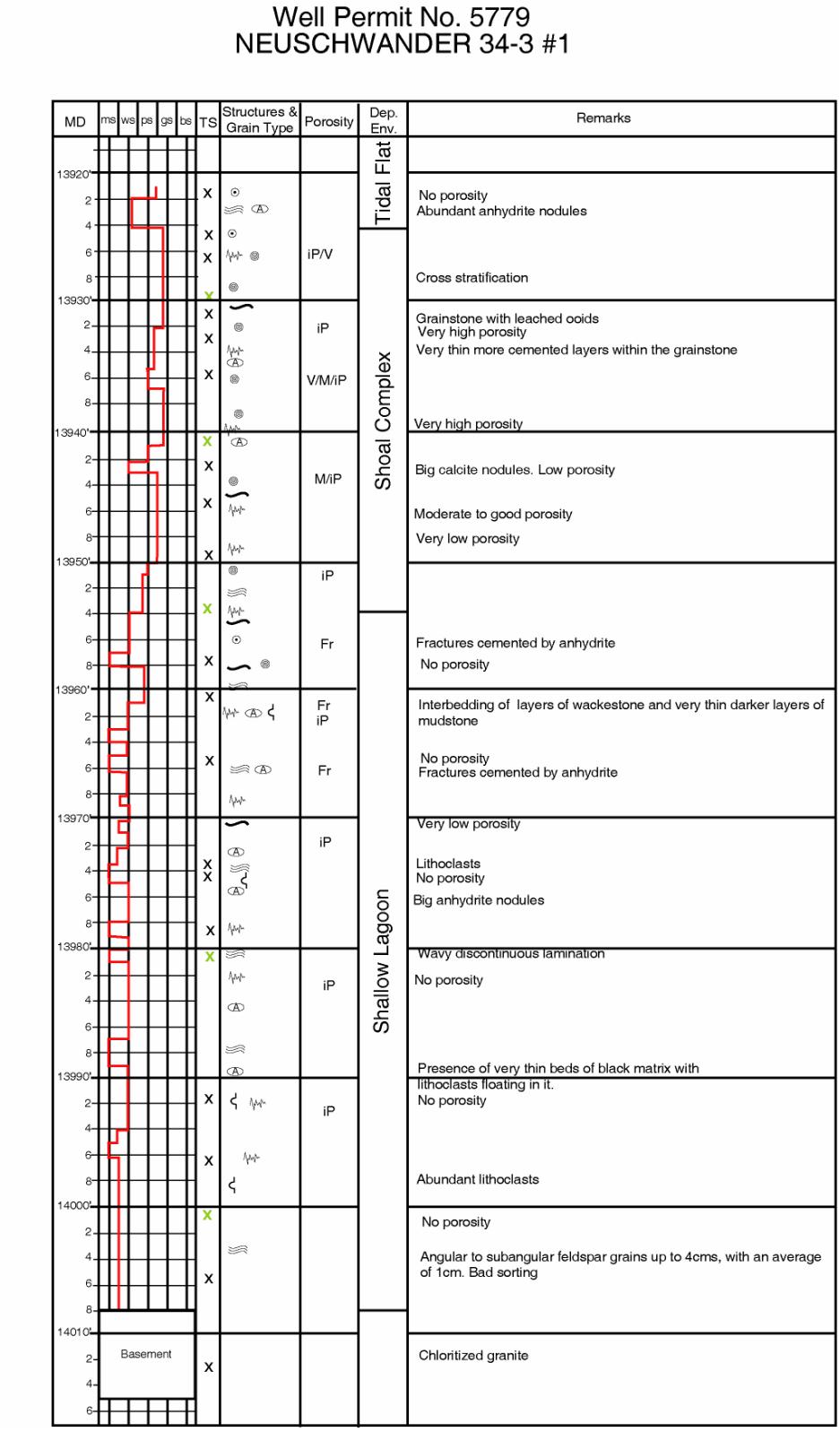

Figure 36. Core description for well permit # 5779. By Juan Carlos Llinas.

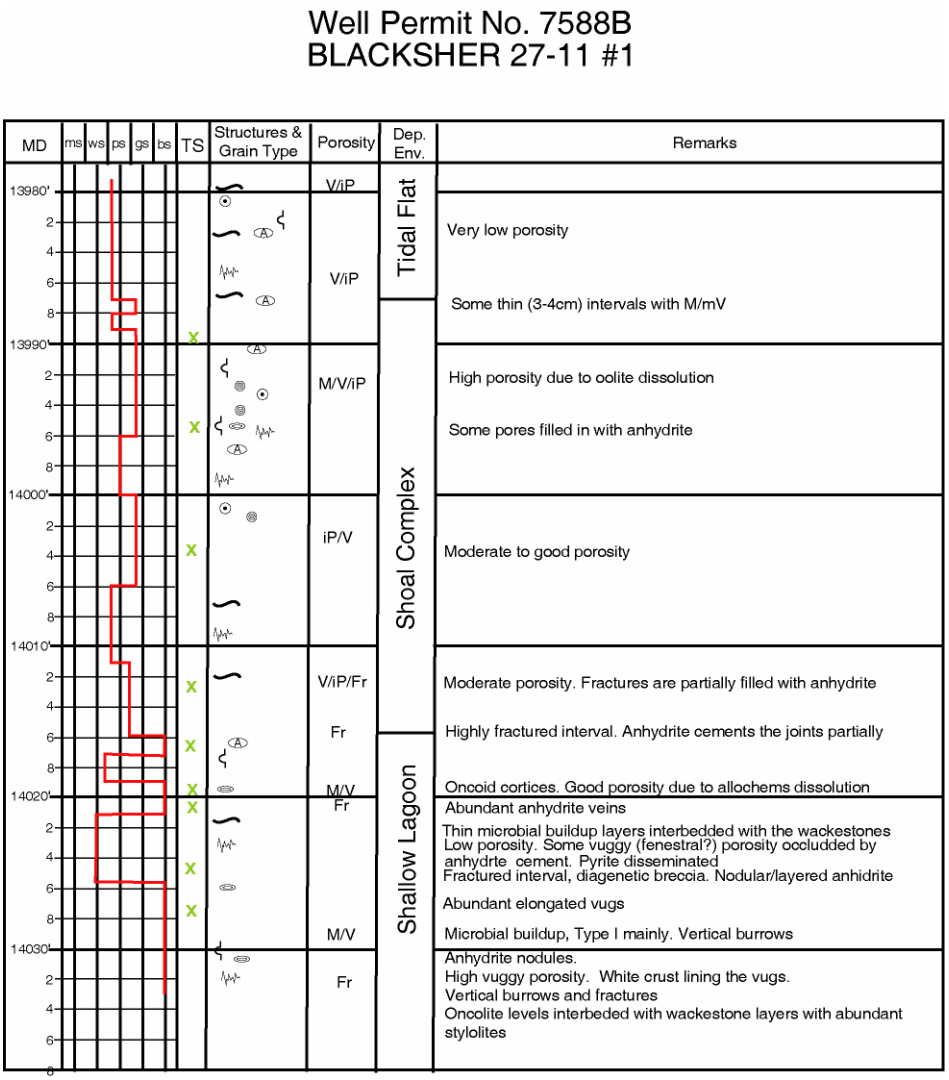

Figure 37. Core description for well permit # 7588B.

By Juan Carlos Llinas.

inherent to these facies have been identified (Table 2). The core data and well log signatures have been integrated and calibrated on the graphic logs.

For Vocation Field (Figure 5), the well log and core data have been entered into a digital database and structural maps on top of the reef (Figure 38), and Smackover/Buckner (Figure 39) have been constructed. An isopach of the Smackover interval has been prepared (Figure 40) and a thickness map of the reef complex facies (Figure 41) illustrating the thickness and facies changes across Vocation Field has been prepared. A cross section (Figure 42) illustrating the thickness and facies changes across the field has been constructed.

Smackover deposition in the Vocation Field area is the product of the interplay of carbonate deposition, paleotopography, and subsidence mainly of tectonic origin during a third order eustatic sea level rise. Based on core descriptions, five shallow-marine environments in the Smackover Formation were identified: microbial reef complex, shallow subtidal, shallow lagoon, shoal complex, and tidal flat/sabkha. The last environment includes the Buckner Anhydrite Member that in Vocation field is relatively thin with an average thickness of 20 to 30 feet. These subenvironments define an overall aggradational and finally progradational shallowing upward cycle developed in a restricted evaporate-carbonate setting.

The microbial reef complex facies is present in the lower part of the Smackover Formation. It is very heterogeneous and consists of bafflestone (thrombolitic chaotic), bindstone (thrombolitic layered) and oncoidal crusts, interbedded with dolomudstone/dolowackestone layers. Stylolitic laminae are common. Allochems are bioclasts mainly of algae and bivalve fragments, oncoids, peloidal clots, intraclasts, and ooids. The amount and types of pores are highly variable, including primary shelter, interparticle and intraparticle porosity and secondary

Table 2. Characterization of Smackover Lithofacies in the Vocation Field Area.

Lithofacies	Lithology	Allochems	Pore Types	Porosity (percent)	Permeability (md)
ooid-dominated, grain-supported (grainstone/packstone)	dolostone, limestone	ooids, oncoids, peloids	moldic, interparticulate, intercrystalline	high (1.5-28.3)	high (0-2,230)
ooid-dominated, matrix-supported (wackestone)	dolostone	ooids, oncoids, peloids	moldic	moderate (1.2-14.0)	moderate (0-8)
oncoid-dominated grain-supported (grainstone/packestone)	dolostone	oncoids, peloids, ooids, intraclasts	interparticulate, moldic, vuggy	high (1.6-20.1)	high (0-1,635)
oncoid-dominated matrix-supported (wackestone)	dolostone	oncoids, peloids	vuggy, moldic	low (2.5-8.3)	low (0-0.39)
peloid-dominated grain-supported (grainstone/packestone)	dolostone, limestone	peloids, oncoids, ooids	interparticulate, intercrystalline, vuggy	high (0.8-25.6)	high (0-587)
peloid-dominated matrix-supported (wackestone)	dolostone, anhydritic dolostone	peloids, oncoids	intercrystalline	moderate (1.0-18.2)	moderate (0-39)
mudstone	dolostone, limestone	none	fracture	low (1.2 to 8.8)	low (<0.01)
algal stromatolite (boundstone)	dolostone	algae, peloids, oncoids	fracture, vuggy, fenestral	low (1.1-8.8)	moderate (0-16)
algal boundstone	dolostone	algae, peloids, oncoids	vuggy, fracture, breccia, moldic	high (3.0-33.6)	high (0-2,998)

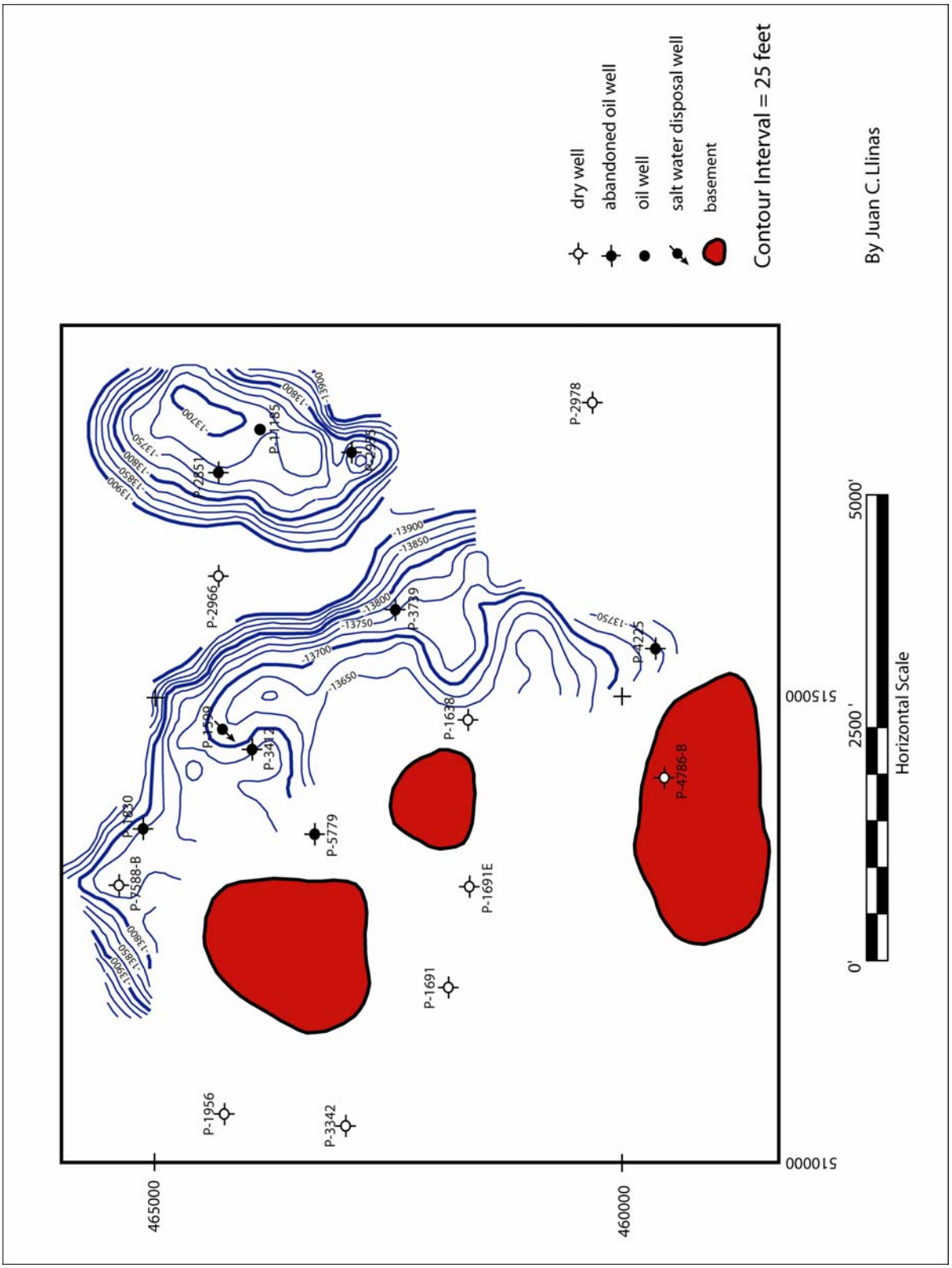

Figure 38. Contour map of the top of the microbial reef complex.

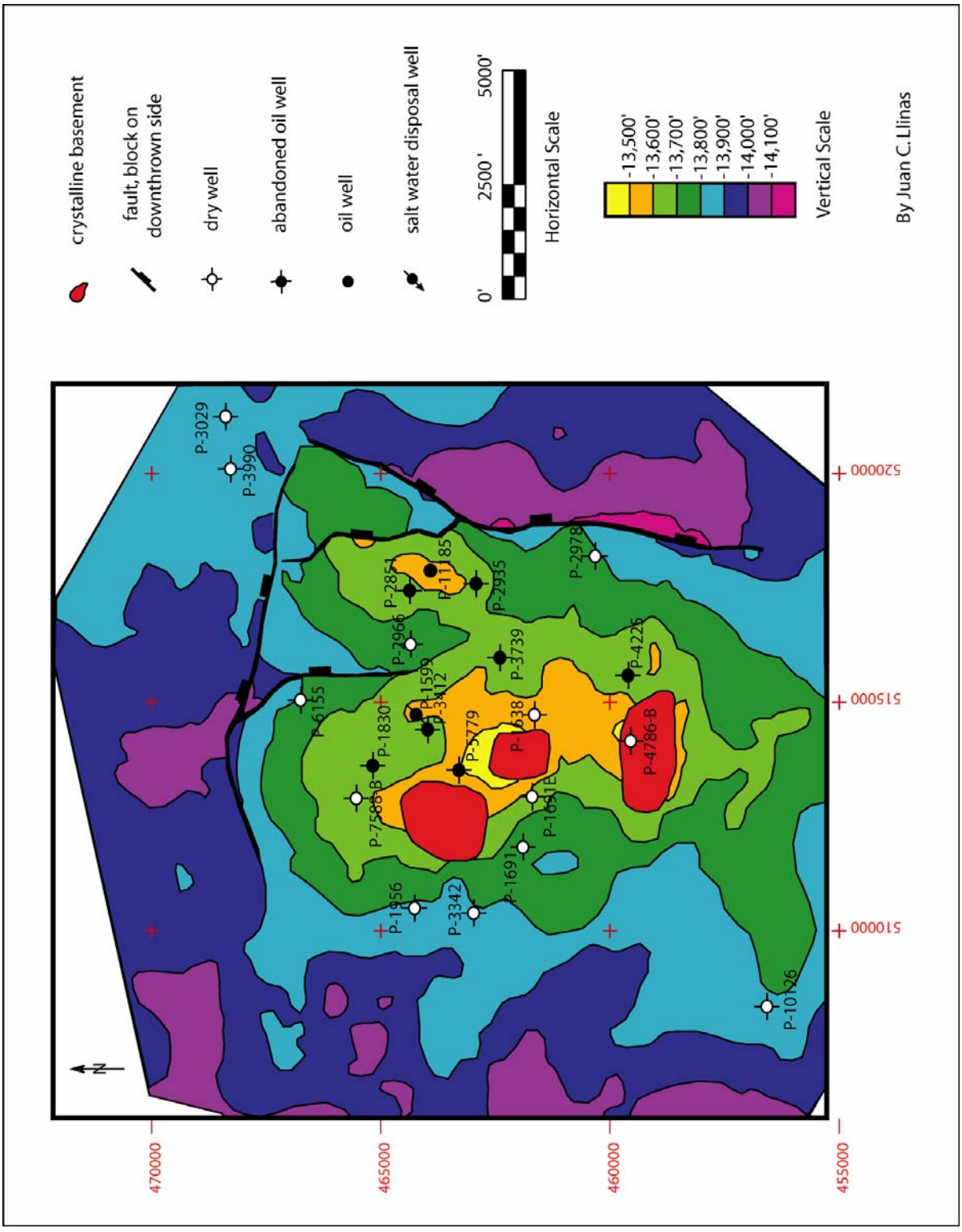

Figure 39. Structure contour map of the top of the Smackover Formation.

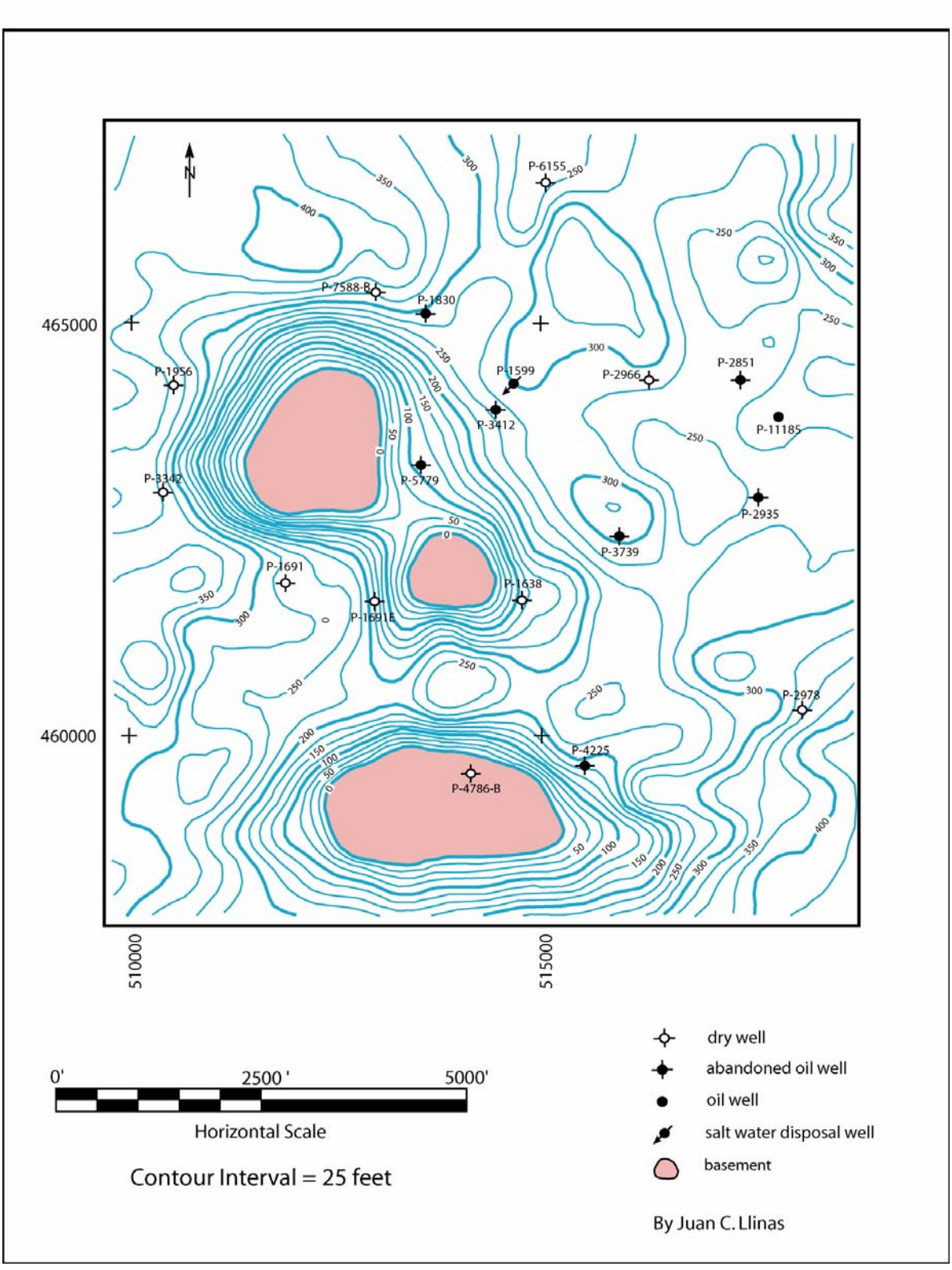

Figure 40. Isopach map of the Smackover Formation.

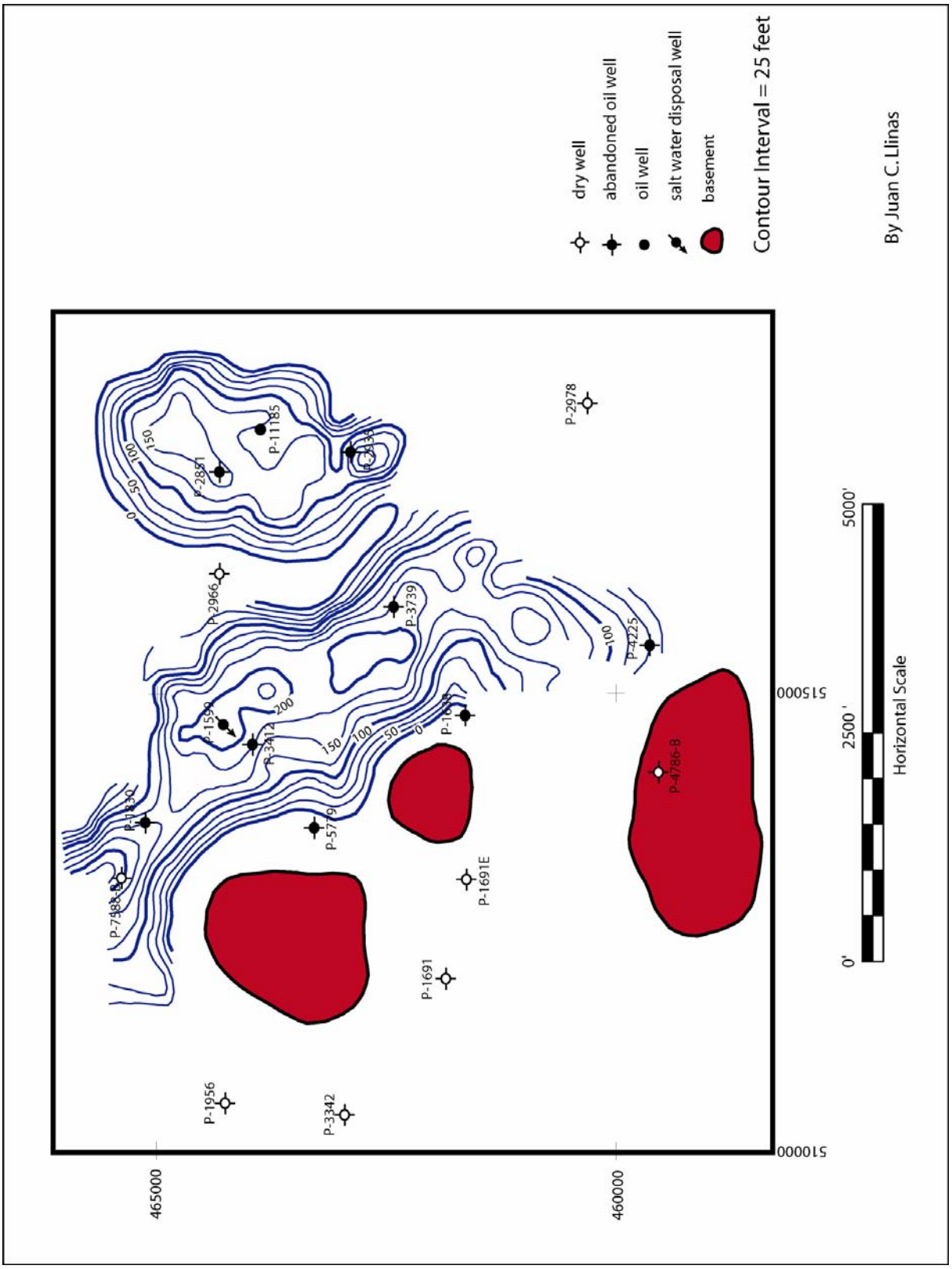

Figure 41. Isopach map of the microbial reef complex.

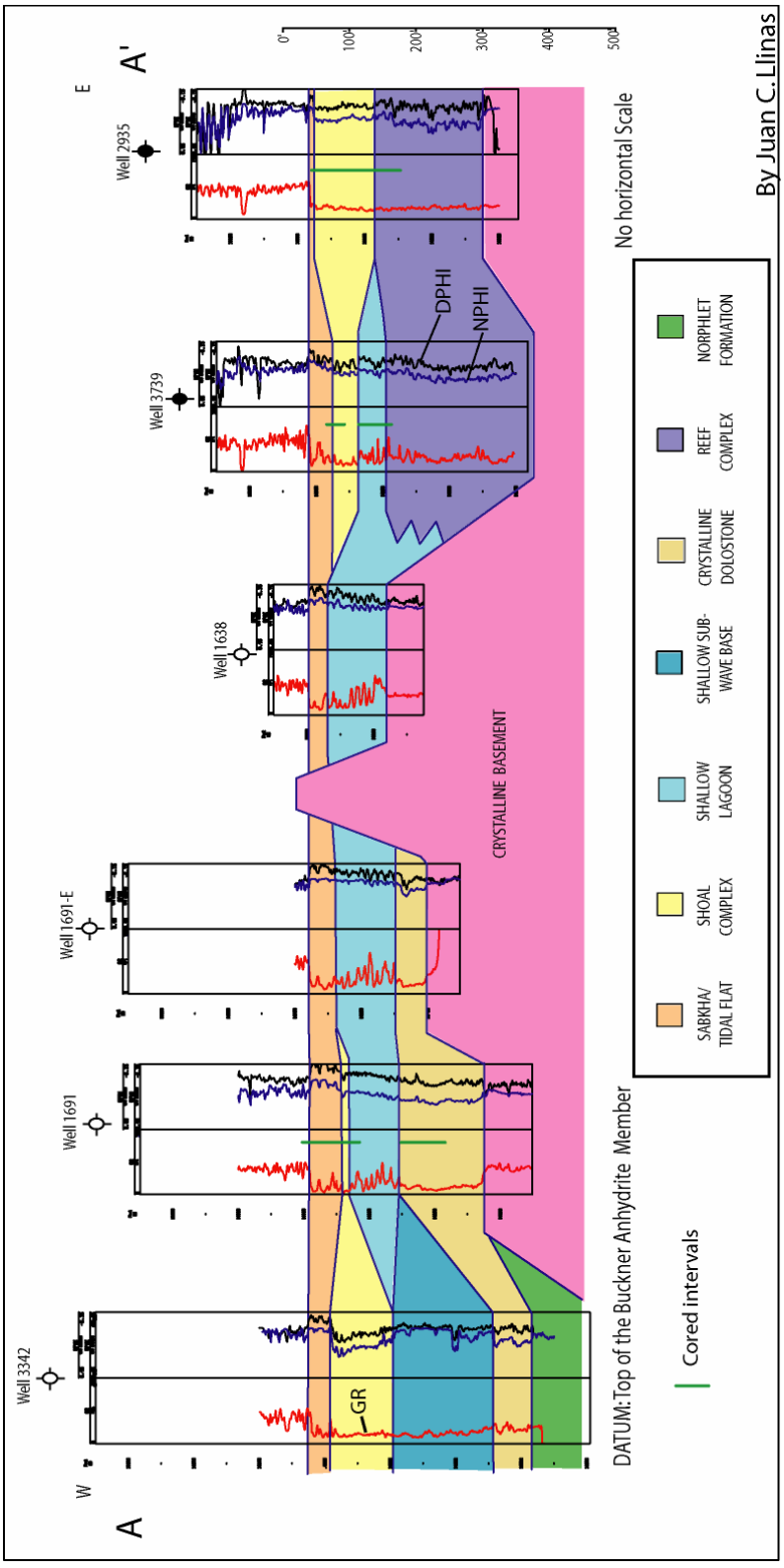

Figure 42. Cross section across Vocation Field.

solution enlarged/vuggy, moldic, and fracture pores. In some cases, anhydrite partially occludes vuggy pores and fractures. Significant development of microbial buildups are located on the northeastern side (leeward side) of the basement structure, while in the western side of the structure (windward side) grainy sediments were deposited, but their original texture is difficult to identify due to intense dolomitization.

The shallow subtidal facies is also present in the lower part of the Smackover succession but in off-structure locations. It is composed of dark brown skeletal dolowackestone with subtle plane parallel to wavy lamination. Some intervals display patchy textures indicative of microbial influence. Allochems are mainly peloids, and sporadic ooids and skeletal debris, such as echinoderm spines and bivalve fragments. Stylolites and horsetail lamination enriched in authigenic pyrite are very common. Scarce and small anhydrite nodules are also present.

The shallow lagoon facies represents deposits accumulated behind a reef and/or shoal barrier. It is composed of light brown dolowackestone to dolopackstone interbedded with darker dolomudstone and argillaceous beds. Microbial buildups of up to 10-feet thick and fine-grained grainstone are sporadically present. Allochems are scarce and consist mainly of isolated peloids, ooids, oncoids, and intraclasts. Localized wavy lamination showing effects of bioturbation is common in this facies.

Deposited in the upper parts of the Smackover Formation, the shoal complex facies comprises most of the producing intervals in the field. It consists of carbonate sand bars consisting of ooid/oncoidal dolograinstone/dolopackstone in thick, sometimes cross-stratified layers, interbedded with thinner dolopackstone/dolowackestone beds. Allochems are mainly ooids and oncoids though intraclasts and peloids are also common in the shoal flanks. Anhydrite in the form of nodules or as cement is an important constituent of this facies. Porosity is

moderate to high and consists of primary interparticle and secondary moldic, intraparticle, and vuggy pores, and microfractures. Some intervals display low porosity (<5%) values due to cementation and compaction processes.

The shoal complex is the uppermost depositional facies of the Smackover Formation and consists of laminated dolomudstone to dolowackestone interbedded with thick anhydrite layers and microbial laminites (stromatolites). Stylolites and anhydrite nodules of varied sizes are very common. Allochems are peloids with less common ooids and bioclasts. Porosity is commonly low (< 6 %) due to the presence of dense anhydrite layers and the fine-grained texture of the carbonate sediments, although in some cases the extensive dolomitization of this facies has generated beds with high intercrystalline porosity. It consists of primary fenestral and secondary moldic and microfracture porosity. Sporadic beds with solution enlarged pores are also present.

Vocation Field was discovered in 1971 with the drilling of the B.C. Quimby 27-15 (Permit #1599) well. The discovery well was drilled near the crest of a paleotopographic structure based on 2-D seismic and well log data. The well penetrated Paleozoic basement rock at a depth of 14,209 feet.

The Vocation field structure has been interpreted as a high relief composite paleotopographic feature of the updip basement ridge play. It lies on the western flank of the Conecuh Ridge in the southeastern margin of the Manila Sub-basin. Its position is updip of the subcrop limit of the Louann Salt and 10 miles northeast of the regional peripheral fault trend. The trap in Vocation field is combined (structural-stratigraphic), as the result of the onlap of reservoir facies against the basement paleohigh. The structure at Vocation field is a composite feature formed by Paleozoic granitic basement highs with irregular relief and steep slopes on the flanks. It consists of a main north-south trending basement feature with three local highs that

remained subaerially exposed until the end of Smackover deposition. To the northeast, a smaller feature with lower elevations has been successfully tested by three wells. This smaller structure and the low area that separates it from the main feature were preferentially colonized by microbial reefs, probably due to the presence of gentler depositional slopes formed by crystalline igneous rocks. These surfaces provided the stable hardground necessary for the establishment and growth of the microbial reef. The Vocation structure is characterized by embayed margins and by high angle normal faulting that affected the Smackover Formation on the eastern and northern flanks. Seismic data interpretation shows greater thicknesses of the Smackover section on the downthrown blocks of the faults that cut the structure on the eastern flank indicating that these faults were active during Smackover deposition.

The depositional sequence of the Smackover Formation varies dramatically in thickness in the field from 0 ft (Well Permit 4786-B) in structurally elevated areas where the Smackover pinches out against crystalline basement rocks, to 440 ft off-structure (Well Permit 3029). On-structure, the Smackover section is the result of a shallowing-upward event in which four shallow marine subenvironments were identified as follows: microbial reef complex, consisting of baffle stone (chaotic thrombolites), bindstone (layered thrombolites) and oncoidal crusts, interbedded with skeletal and peloidal dolopackstone to dolowackestone layers; shallow lagoon, consisting of dolomudstone and dolowackestone to dolopackstone layers, with some bioturbated levels and thin isolated microbial buildups that formed in a low energy environment behind the reef and shoal complex; shoal complex, consisting of irregular and discontinuous sand bars made up of ooid, oncoid and peloid dolograinstone and dolopackstone in thick, sometimes cross-stratified layers of variable thickness interbedded with thinner dolopackstone to dolowackestone levels and thin horizons rich in anhydrite nodules especially in the upper layers; and sabkha-tidal

flat, consisting of laminated peloidal dolomudstone to peloidal dolowackestone interbedded with thick anhydrite layers and algal laminites (stromatolites). The Buckner Anhydrite Member, which is relatively thin in the area (0 to 40 ft), is included in this interval. In general, this facies is thicker close to the paleohigh crestal areas and progressively thinner toward the margins.

As in Appleton Field, the best potential reservoirs are associated with the microbial reef facies mainly in the levels with reticulate thrombolite texture, and with the grainstone-packstone shoal complex. The reservoir quality of these rocks is the result of the depositional fabric combined with the effects of diagenetic processes, such as dolomitization and dissolution that acted to increase the initial porosity and improved the connectivity of the pore network. Significant thicknesses of microbial boundstone have been found only in the northeastern side of the basement paleohigh but unfortunately below the oil/water contact. Instead, on the western flank, fine-crystalline, highly dolomitized limestone was deposited.

Geophysical Seismic Attribute Characterization.--3-D seismic-based analyses of the Smackover Formation at Appleton and Vocation Fields has been done by Tebo and Hart at McGill University. The work on Appleton Field described below is from Tebo's thesis (2003) at McGill University and a paper submitted in May 2003 for publication in the Journal of Sedimentary Research by Tebo and Hart. Results of the study of the Vocation Field are also included. The objective has been to integrate well logs and attributes derived from seismic data to generate porosity volumes that predict the 3-dimensional distribution of that property for the Smackover Formation in and around Appleton and Vocation Fields.

Seismic attribute studies represent a relatively new approach that has been developed and applied in the oil industry. This approach seeks to find empirical correlations between seismic attributes and log-derived physical properties (e.g., porosity, lithology, bed thickness) through methods such as multivariate linear regression (MLR) and artificial or probabilistic neural networks (ANN/PNN; Schultz *et al.* 1994 a & b; Russell *et al.* 1997; Hampson *et al.* 2001). Seismic attributes are derivatives or mathematical transforms of a basic seismic measurement and include amplitude, frequency, phase and other measures (Taner *et al.* 1979; Brown 1996; Chen and Sidney 1997). Some of these correlations have an obvious rock physics basis (e.g., tuning effects or changes in acoustic impedance; Robertson and Nogami 1984; Brown 1996), whereas the physical basis for other relationships is more poorly understood. Accordingly, some authors have advocated statistical approaches to correlate seismic attributes with physical properties measured by logs (Schultz *et al.* 1994a; Hampson *et al.* 2001). Criticisms of purely statistical approaches were offered by Hart (1999, 2002), and Mukerji *et al.* (2001) amongst others.

There are two main types of seismic attribute studies. Horizon or interval-based methods use attributes that are extracted or averaged along or between interpreted seismic horizons. These

attributes are then correlated to log-derived properties (e.g., average porosity, net thickness) to produce a map (e.g., Schultz *et al.* 1994a). Volume-based studies look for correlations between attributes and log properties on a sample-by-sample basis over a window that is defined by two seismic horizons (Hampson *et al.* 2001). This type of study produces a physical property volume, and thus better defines changes in physical properties and their corresponding geometries in 3-D space. The latter method is particularly useful for property prediction in thick and complex stratigraphic sequences where lateral and vertical facies changes are frequent.

Appleton Field. The primary database for Appleton Field consisted of 11 wells with logs and a 3-D seismic volume. Six of these wells with sonic logs are used for the attribute study. These logs were used to generate synthetic seismograms that were then employed to tie log and seismic data. Seismic data consisted of an approximately 5 x 3.5 km grid of post-stack time-migrated 3-D volume (Figure 43), with a 4 ms sample rate, a bin spacing of 165 x 165 ft (~50 x 50 m), and a 4 second two-way travel time (TWT) trace length. Supplementary data in the form of production data and core analyses were also used to help guide the interpretations.

A stratigraphic framework for the study was established through log analysis and construction of log cross-sections (Fig. 44). The geology was then tied to the seismic data by generating synthetic seismograms and 2-D seismic models (cf Tebo 2003; Figure 45). The well-tying procedure was critical in the analysis because it ensured that both data types were imaging and comparing the same stratigraphic interval. These stratigraphic picks were then mapped in the 3-D seismic volume, and the seismic horizons so defined were used for geologic interpretation and to constrain the attribute analysis.

A volume-based seismic attribute study as described by Russell *et al.* (1997) and Hampson *et al.* (2001) was used due to the thickness (80-230ft/24-70m) and expected stratigraphic complexity of this interval. Porosity was predicted, as measured by the density porosity log,

because of its direct relation to depositional facies at the Appleton Field (Benson 1988; Benson *et al.* 1996) and because it is an important variable controlling hydrocarbon production. The window of analysis was defined by the top and base of the Smackover Formation. The choice of which attribute(s) to generate and use was determined by the capabilities of the

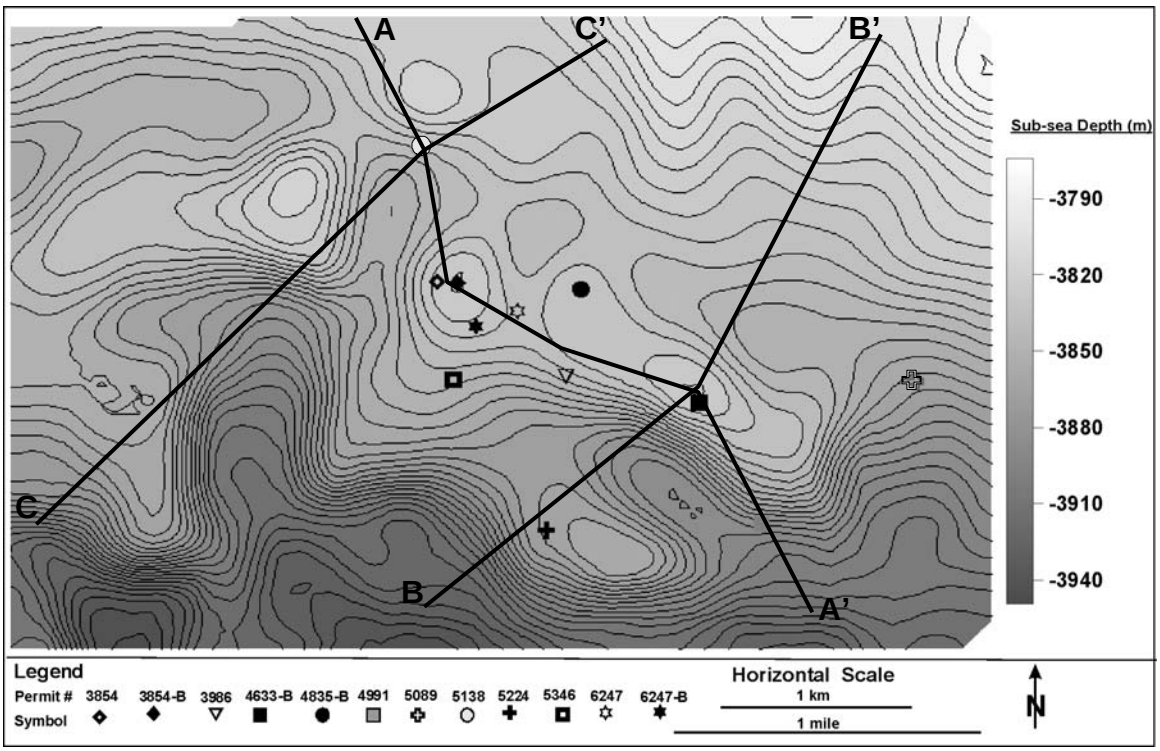

Figure 43: Seismic grid showing the aerial coverage of current survey area and well locations.

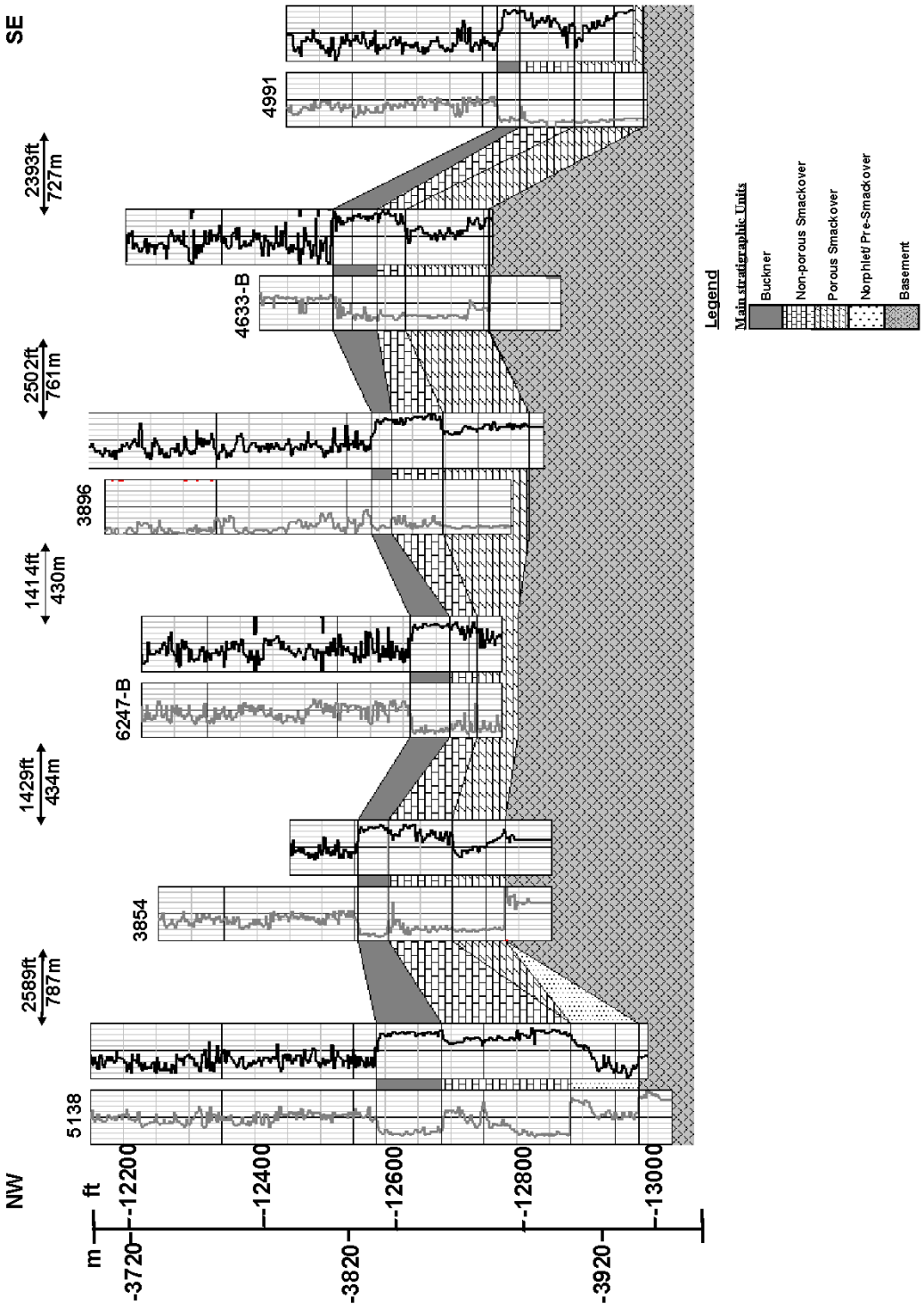

Figure 44: NW-SE well-to-well cross-section showing major stratigraphic units and their relationships. Cross-section was obtained along strike of paleohighs (A-A' transect of Figure 43). Note that the eastern paleohigh at well 4633-B is structurally higher than that in the west beneath well 3854. Grey curve = gamma ray, black curve = sonic.

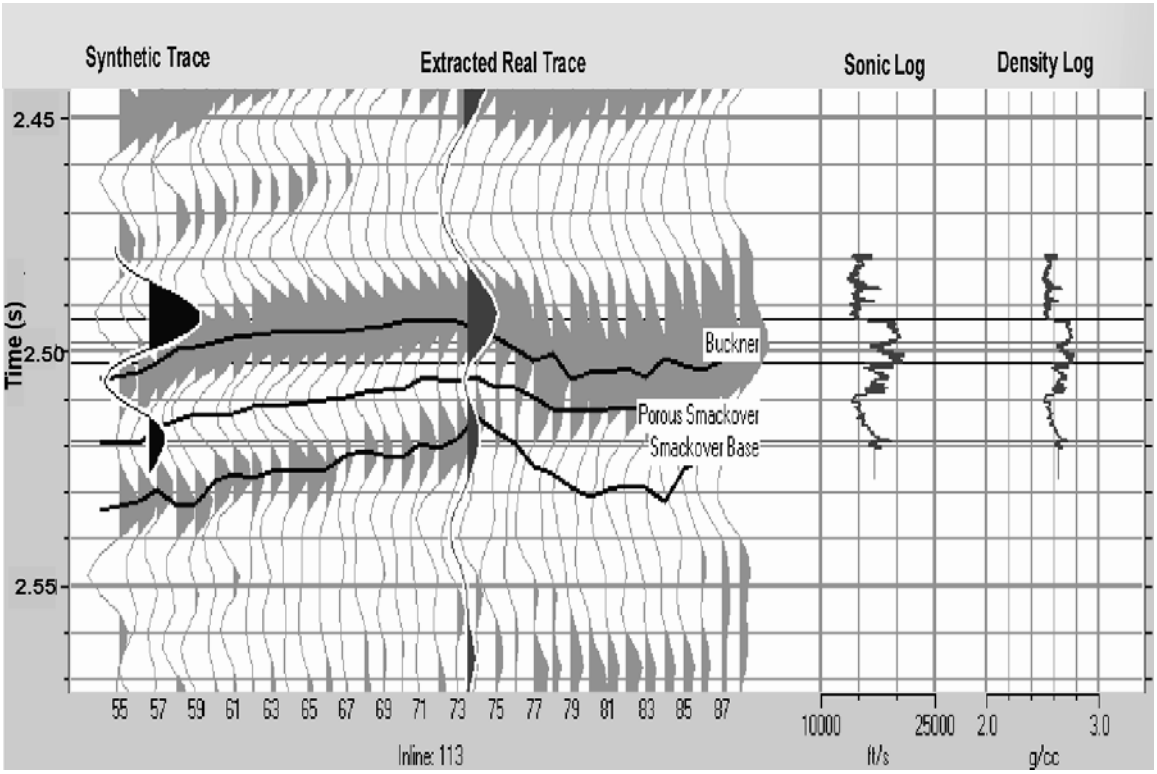

Figure 45: Example of synthetic seismogram (well 4633-B) used for tying well data to seismic. Black curve = log synthetic, grey = seismic trace extracted along wellbore at well location.

software, which offered 18 attributes that were extracted over the analysis window. Although not considered a "true" attribute by some authors (Schultz *et al.* 1994a), we also included inversion results (acoustic impedance derived from seismic data) as an attribute.

Porosity was predicted in 3-dimensions. This was done by obtaining a statistical relationship between the best set of predicting attributes and porosity using a probabilistic neural network (PNN). The relationship has the form:

$$P_{PNN}(z) = \frac{[P_1 e^{(-d^2_1/\sigma^2)} + P_2 e^{(-d^2_2/\sigma^2)} + P_3 e^{(-d^2_3/\sigma^2)}]}{[e^{(-d^2_1/\sigma^2)} + e^{(-d^2_2/\sigma^2)} + e^{(-d^2_3/\sigma^2)}]} \quad (1)$$

where: P_{PNN} = predicted porosity at each sample using probabilistic neural network, $P_{1\text{-}3}$ = actual porosity value, d^2_1 = distance between input point and the training data $[(X_1 - X_0)^2 + (Y_i - Y_0)^2]$ as measured in the multidimensional space spanned by the attributes, and σ is a scalar.

Application of this relationship led to the generation of a porosity volume from the seismic data volume. In essence, the method replaces each seismic trace within the analysis window by a porosity curve. This result is different to that obtained from a horizon-based attribute analysis, whereby an average porosity value might be produced at each trace location to generate a map (e.g., Hart and Balch 2000).

Porosity volume was derived and evaluated using quantitative and qualitative methods described by Hampson *et al.* (2001) and Hart (1999, 2002). In particular, and as described fully below, the statistical significance of the results, their geologic plausibility, and the physical basis for relationships between attributes and porosity was examined.

Based on velocity and density contrasts, Hart and Balch (2000) defined the following six units at Appleton Field: a) metamorphic and igneous rocks of "Basement", b) siliciclastics of the

Norphlet Formation, c) lower, porous dolomites of the Smackover that are restricted to the flanks and crests of basement structures (broadly corresponding to the Middle Smackover), d) generally non-porous Smackover dolomites that overlie the porous zone on-structure but form the entire thickness of the Smackover off-structure (Upper Smackover on-structure, Middle and Upper Smackover off-structure), e) Buckner Anhydrite, and f) siliciclastics of the Haynesville Formation (Figure 46).

Seismically, the top of the Buckner and top of the Smackover are imaged as a single high amplitude peak (Figure 47). This is because of both the relative thinness of the Buckner Anhydrite and low acoustic impedance contrast between these two units. The top of the porous Smackover is imaged as a trough that is only locally developed. The base of the Smackover Formation changes character from a peak, where relatively low acoustic impedance porous dolomites overlies basement, to a trough, where relatively high acoustic impedance tight dolomites overlie siliciclastics of the Norphlet Formation, within the study area.

Mapping indicates that five main structural culminations occur in and around the Appleton Field, with four of these (Figures 43 and 48) being present during Smackover deposition. Their NW-SE orientation is parallel to structural paleostrike and perpendicular to the direction of transgression. The Porous Smackover is thickest on the southward flanks and thinner on the crests of paleohighs (Figure 44). This pattern is attributed to greater accommodation space and increasing water depth resulting from rising sea levels during Smackover deposition. The

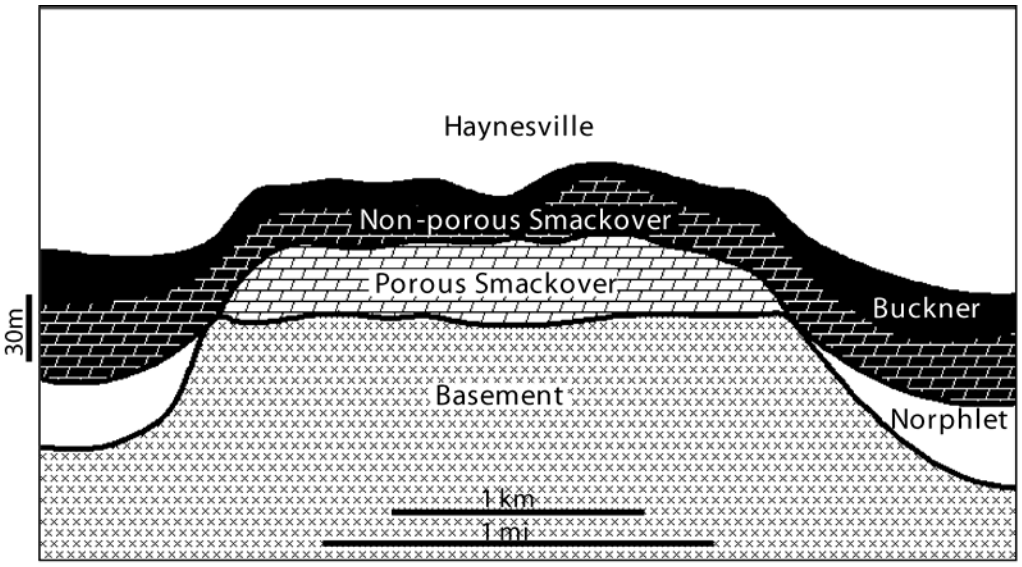

Figure 46: Geologic model depicting the relationship of the main stratigraphic units at Appleton Field (from Hart and Balch, 2000).

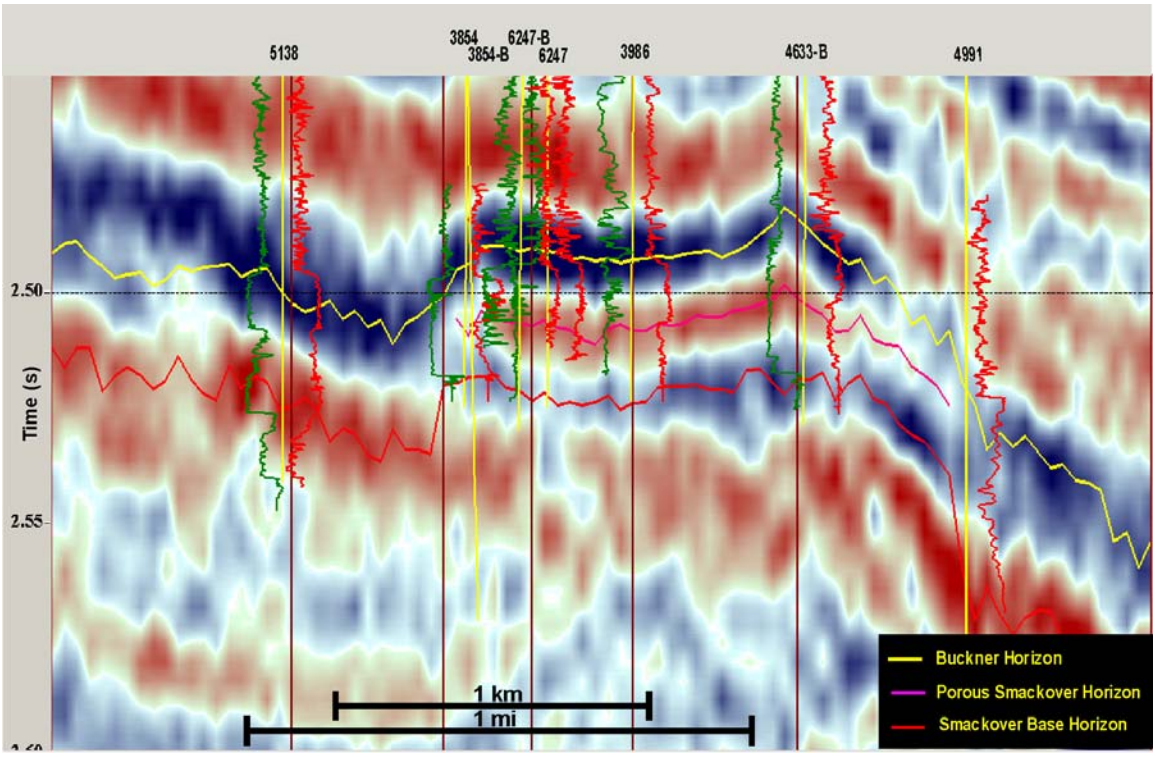
5138
3854
3854-B
6247-B
6247
3986
4633-B
4991
2.50
Time (s)
2.55
1 km
1 mi
Buckner Horizon
Porous Smackover Horizon
Smackover Base Horizon

(a)

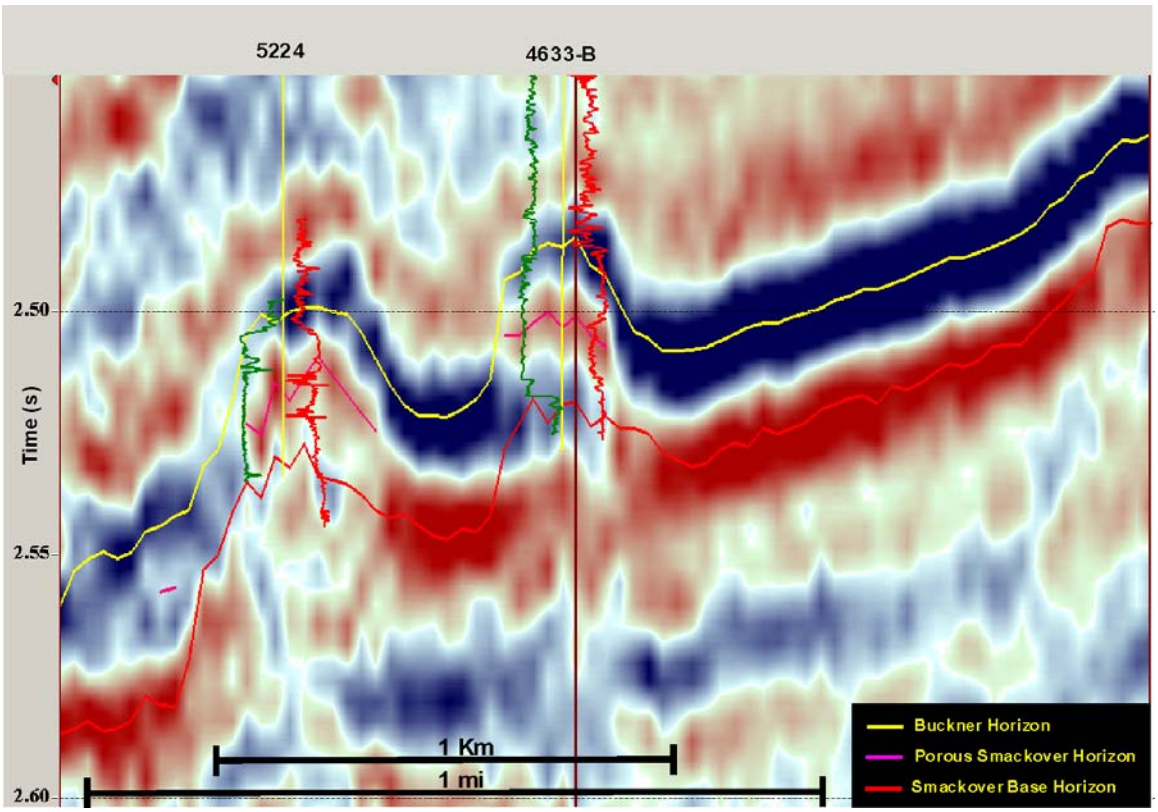
5224
4633-B
2.50
Time (s)
2.55
2.60
1 Km
1 mi
Buckner Horizon
Porous Smackover Horizon
Smackover Base Horizon

(b)

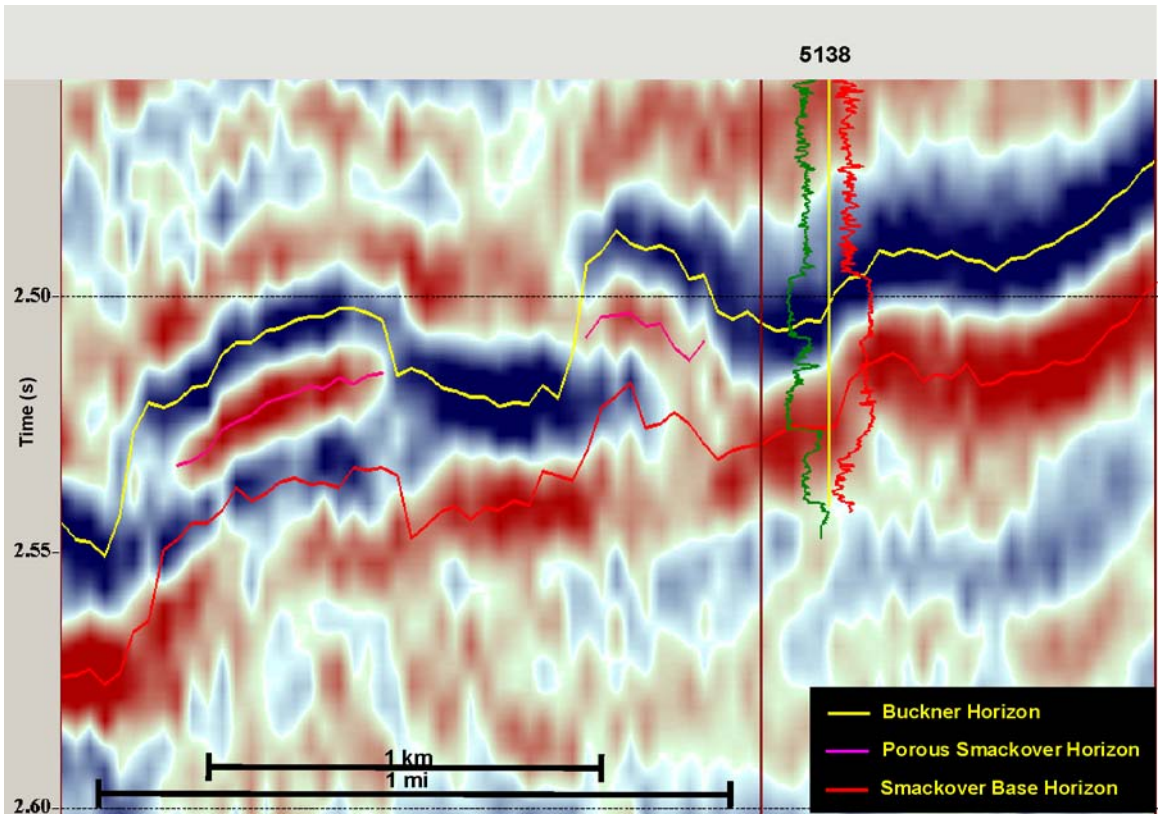

(c)

Figure 47: Transects showing seismic data across Appleton Field; note location of the porous Smackover on paleostructure. (a) NW-SE transect parallel to strike (A-A' in Fig. 3), and shows horizon picks ans seismic character of the mapped formations (red = trough, blue = peak); (b) & (c) dip sections (B-B', C-C' in Fig. 43) across Appleton Field.

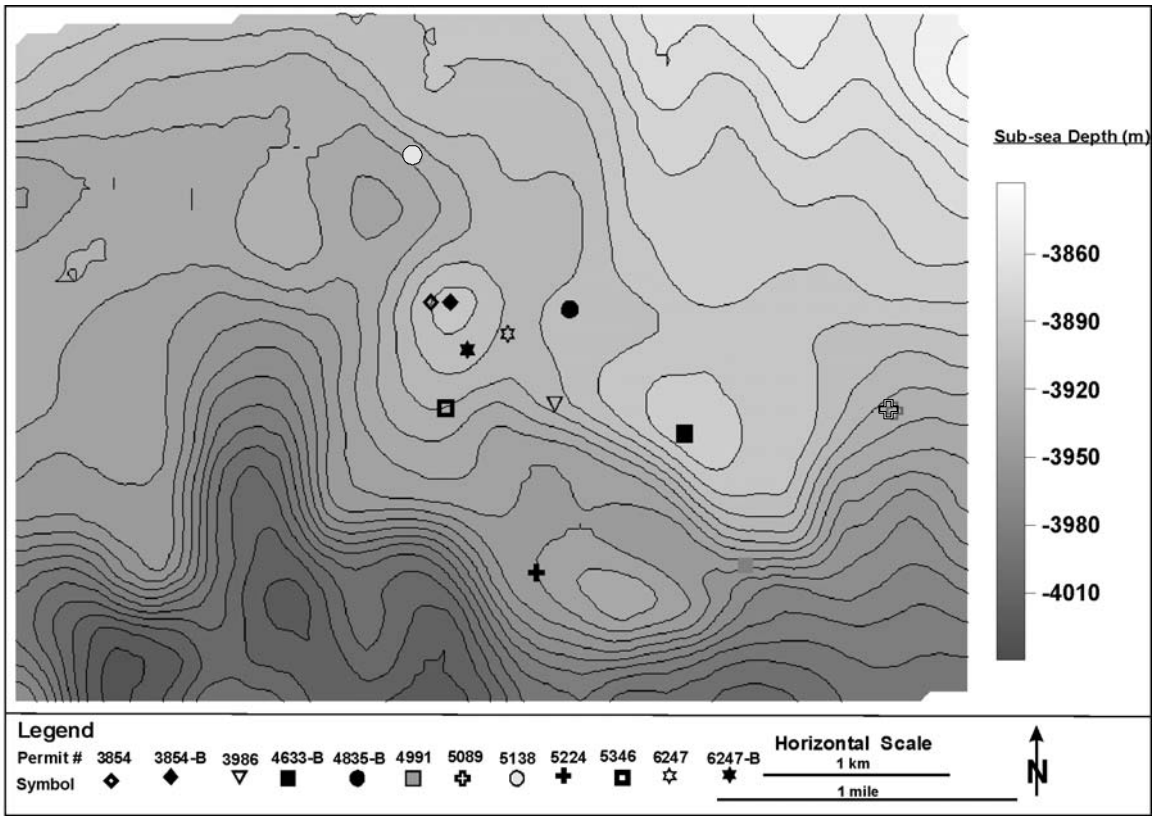

Figure 48: Structure map (depth sub-sea) of the base of the Smackover Formation. This shows main pre-existing structural culminations that controlled facies deposition, three at the Appleton Field in the east, and one to the NW. The structural high to the SW had no closure prior to Smackover deposition.

combination of paleostructure, steep seaward slope and eustatic sea level rise provided optimal conditions (e.g., temperature, salinity, substrate, etc.) for reef growth.

Step-wise linear regression and validation testing (Hampson *et al.* 2001) indicated that four of the nineteen attributes represent the optimum combination of attributes required to predict porosity (Figure 49). These four attributes are:

1. Derivative. Overall, this was the best single-predicting attribute, with a correlation coefficient of 73%. Chen and Sidney (1997) defined derivative as the difference between the seismic trace amplitude of one sample and the preceding sample. Calculated as such, derivative shows the onset and variation of energy for the Porous Smackover unit (Figure 50a).

Forward modeling (described by Tebo, 2003) demonstrated that areas with highest porosity, and consequently greater acoustic impedance contrast with overlying and underlying rocks, had the most positive derivative. At Appleton Field, porosity is strongly related to depositional facies (Benson 1988) and therefore variations in derivative are indicative of facies changes.

2. Derivative Reflection Strength (DRS). This is the rate of change of reflection strength over time (Figure 50b). Reflection strength is amplitude independent of phase, and it shows the location of maximum energy within an event, which may be different from that of the maximum amplitude (Taner *et al.* 1979; Figure 50c). Reflection strength as an attribute loses vertical resolution, which is captured more effectively by its derivative. The derivative of reflection strength is therefore most useful in characterizing vertical interfaces and discontinuities resulting from stratigraphic (facies), lithologic, or fluid changes.

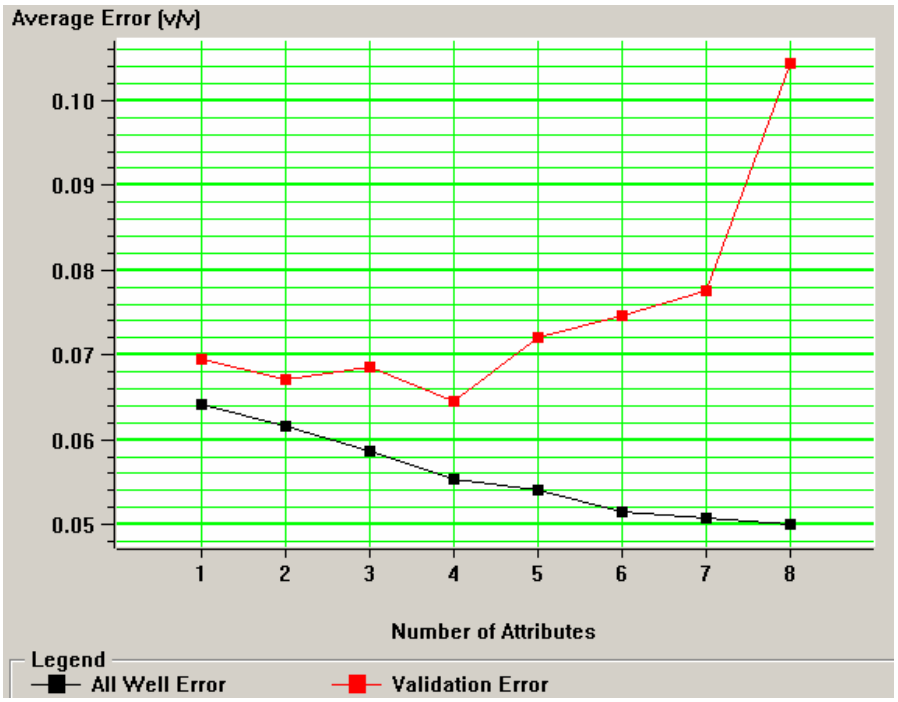

Figure 49: Validation plot, showing the optimum number of attributes to use in predicting porosity from density porosity logs using stepwise multilinear regression. This optimum number of attributes is reached when the validation error (red curve) associated with adding a new attribute to the predicting relationship fails to decrease convincingly. The black curve shows the training error. The training error generally decreases with an increase in number of attributes. See Hampton *et al.* (2001) for a full description and justification of this method.

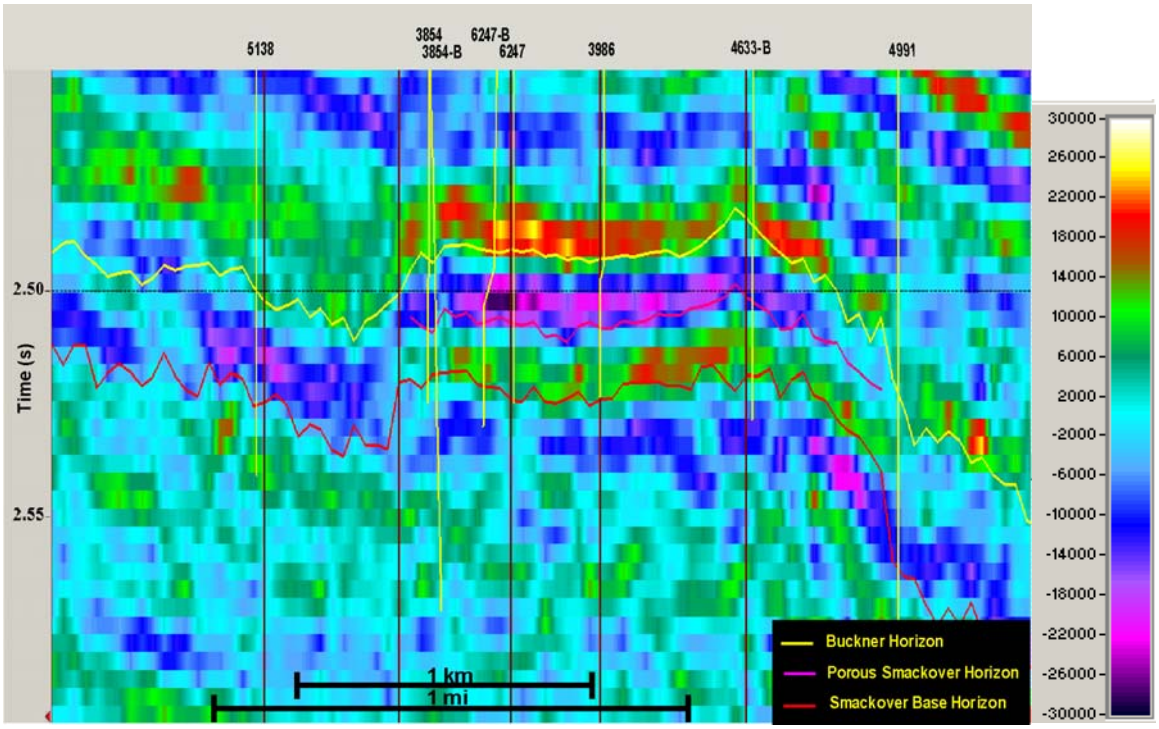
5138
3854
3854-B
6247-B
6247
3986
4633-B
4991
2.50
2.55
Time (s)
30000
26000
22000
18000
14000
10000
6000
2000
-2000
-6000
-10000
-14000
-18000
-22000
-26000
-30000
Buckner Horizon
Porous Smackover Horizon
Smackover Base Horizon
1 km
1 mi

(a)

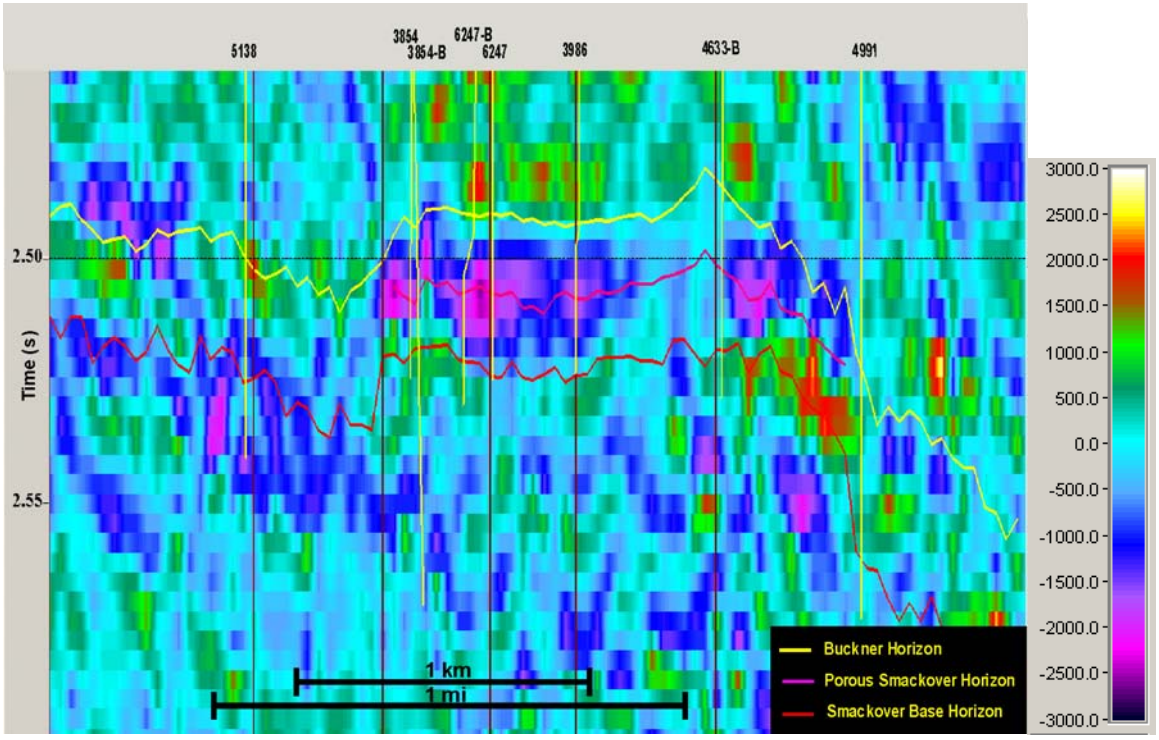
5138
3854
3854-B
6247-B
6247
3986
4633-B
4991
2.50
2.55
Time (s)
3000.0
2500.0
2000.0
1500.0
1000.0
500.0
0.0
-500.0
-1000.0
-1500.0
-2000.0
-2500.0
-3000.0
Buckner Horizon
Porous Smackover Horizon
Smackover Base Horizon
1 km
1 mi

(b)

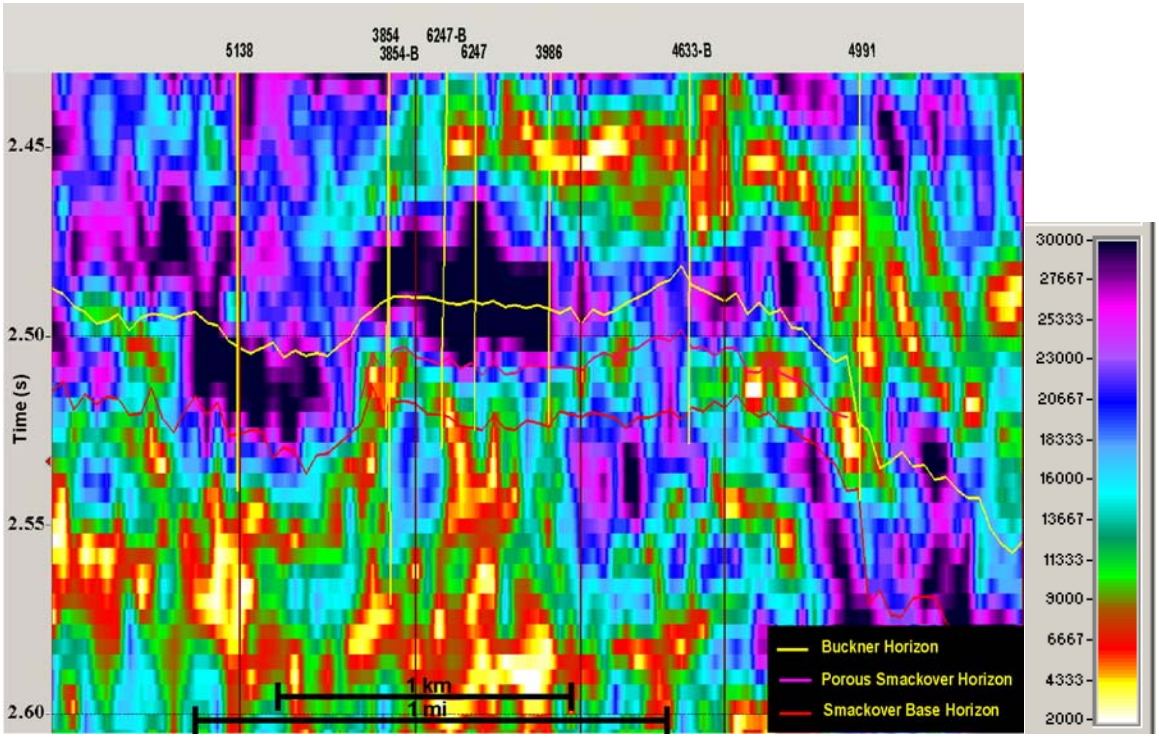

(c)

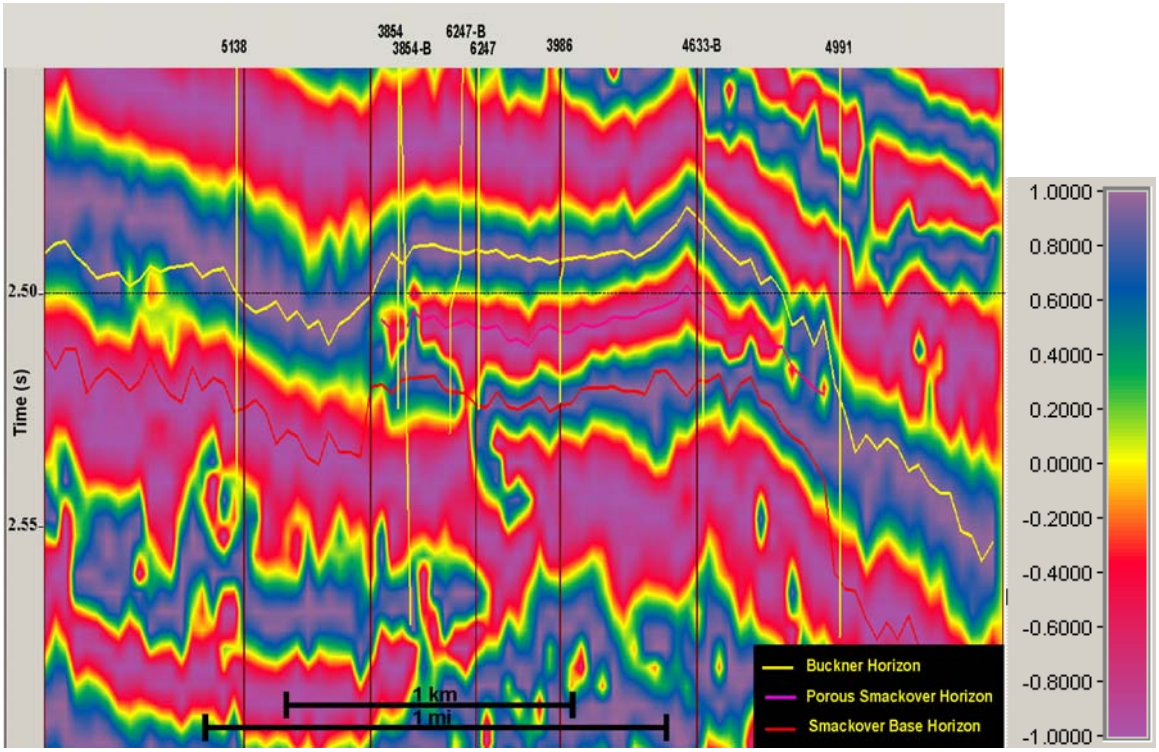

(d)

Figure 50: NW-SE transects through attribute volumes corresponding to Figure 47a. These show the physical relationship between the predicting attributes and porosity within the porous interval. (a) Derivative (b) Derivative of reflection strength (c) Reflection strength (this attribute is shown to illustrate the importance of its derivative (b) in imaging vertical changes) (d) Cosine instantaneous phase. See Figure 43 for location of transects.

Tebo (2003) showed that major changes observed in DRS resulted primarily from thickness variation of the porous unit, while acoustic impedance contrast had little effect. Figures 50b and 10c show transects through DRS and reflection strength (RS) volumes respectively. High porosity areas were seen to have higher values in DRS and lower values in RS volumes (both denoted in hot colors to enhance similarities). Lateral variations in DRS observed within the porous interval show discontinuity in porosity distribution.

3. Cosine Instantaneous Phase. This attribute is derived from instantaneous phase. Because cosine instantaneous phase avoids the 180^{o} phase discontinuity that occurs with instantaneous phase, it generates a better and smoother display of phase variations. Instantaneous phase is phase independent of amplitude, and emphasizes the continuity of reflection events (Taner *et al.* 1979). Within the Smackover interval, changes in cosine instantaneous phase correlated in magnitude and sign to the corresponding amplitude changes of the various stratigraphic units (Figure 50d). No criteria could be identified from this attribute volume nor from model results that might directly relate to changes in porosity within the porous interval. However, on the whole, this attribute defined precisely the lateral extent and stratigraphic configuration of the porous unit.
4. 1/Smoothed Inversion Results. We used a model-based inversion over a 700 ms window that included the interval of interest. Full details are provided in Tebo (2003). In a general way, seismic inversion attempts to derive an acoustic impedance volume from the seismic data by removing the embedded seismic wavelet. Acoustic impedance in the Smackover is inversely proportional to porosity (i.e., high porosity equals relatively low velocity and density; Figure 51). Because well data are used directly in the inversion process to generate the acoustic impedance volume, the results need to be smoothed

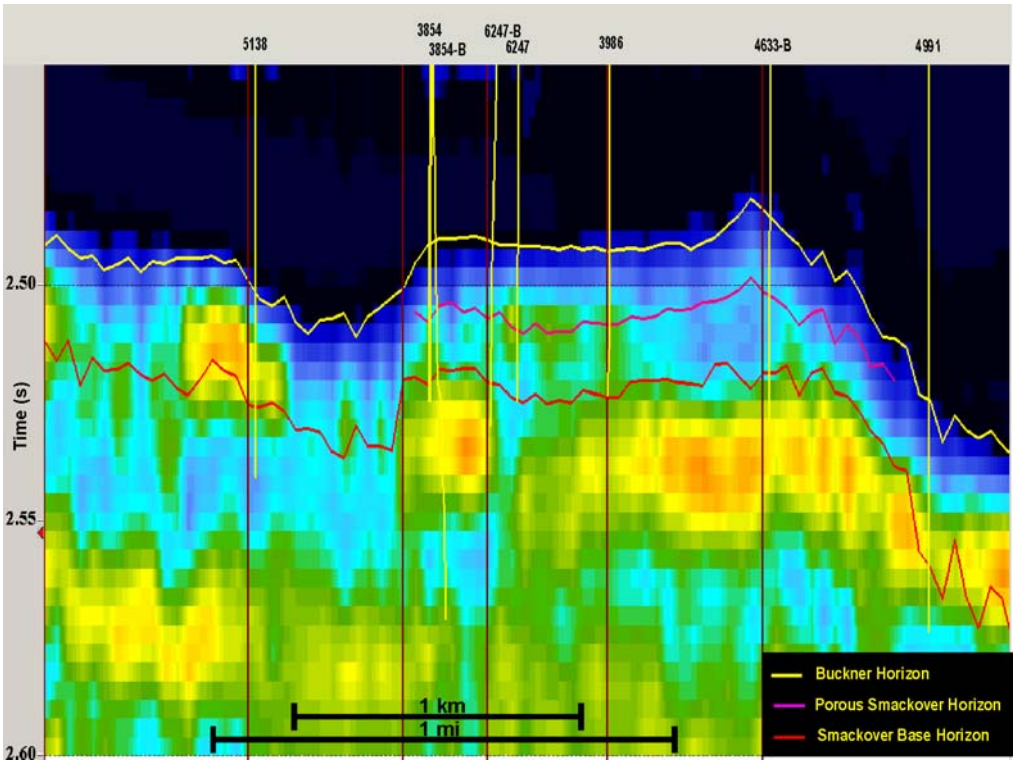
5138
3854
3854-B
6247-B
6247
3986
4633-B
4991
2.50
Time (s)
2.55
2.60
1 km
1 mi
Buckner Horizon
Porous Smackover Horizon
Smackover Base Horizon

(a)

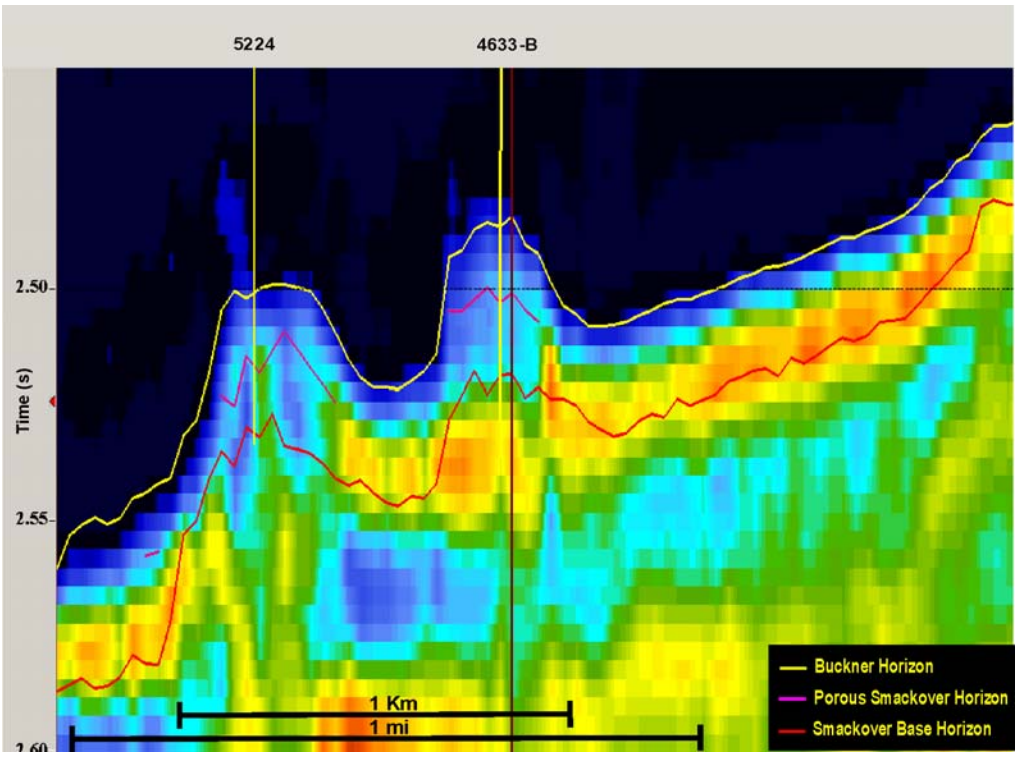
5224
4633-B
2.50
Time (s)
2.55
1 Km
1 mi
Buckner Horizon
Porous Smackover Horizon
Smackover Base Horizon

(b)

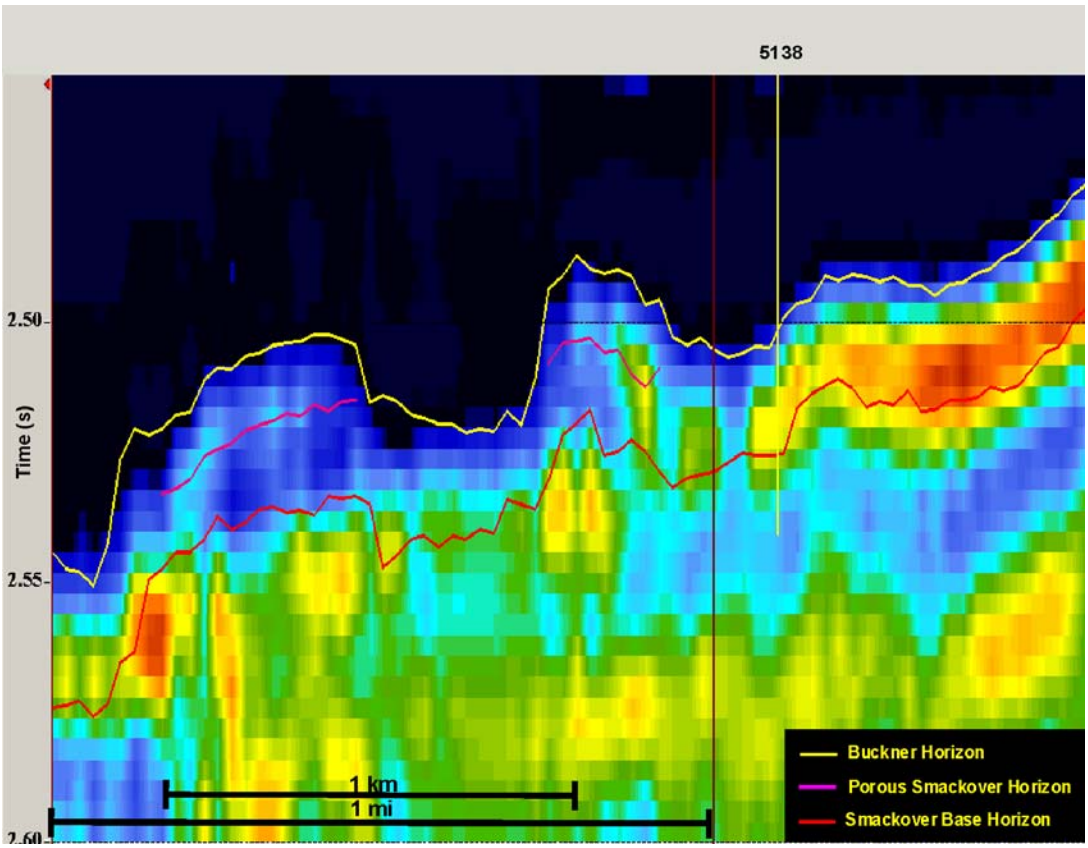

(c)

Figure 51: Transects, corresponding to those shown in Figure 47, showing the acoustic impedence structure of the Smackover Formation. Impedences are generally lower in the porous Smackover and the Norphlet Formation. (a) Strike section, (b) & (c) Dip sections. Units = ft/s*g/cc. See Figure 43 for location of transects.

before inversion results may be used as an attribute. Otherwise, statistical correlations between the inversion results and well data might be suspect.

The PNN-trained relationship with four attributes provided a correlation of 93%, with RMS error of 1.7%. Figure 52 shows that the PNN is able to capture subtle trends in the porosity log. The predictive equation for PNN derived from the analysis was applied to the seismic data to create a porosity volume.

Examination of the porosity volume shows that, like the thickness of the porous interval, porosity is generally higher on the forereef flanks than the crests of paleohighs, although there are other restricted areas (e.g., the highest point of the crests) of high porosity (Fig. 53). Slices through the Smackover interval of the PNN volume highlight this trend (Fig. 54). We generated a porosity thickness (Øh) map for the Smackover Formation to better examine the relationship between porosity development and paleostructure. A 12% porosity cut-off was used as the porosity indicator (12% porosity is the lower limit for production in the Appleton Field), and then calculated the cumulative thickness (in time) of porosity for the Smackover Formation. We then multiplied this value by the average velocity (ft/s) for the Smackover to get thickness (ft). This thickness map (Fig. 55) clearly shows better development of porosity on the forereef flanks than on the crests of structures. This result is geologically realistic given the facies types and their growth forms described from core studies (Table 3).

Tebo (2003) also used multivariate linear regression (MLR) to generate a porosity volume. That result had a lower correlation coefficient (81%) than the PNN and was less geologically reasonable. Leiphart and Hart (2001) noted similar results in their study. This is because the PNN better captures non-linear relationships between attributes and physical properties than the MLR.

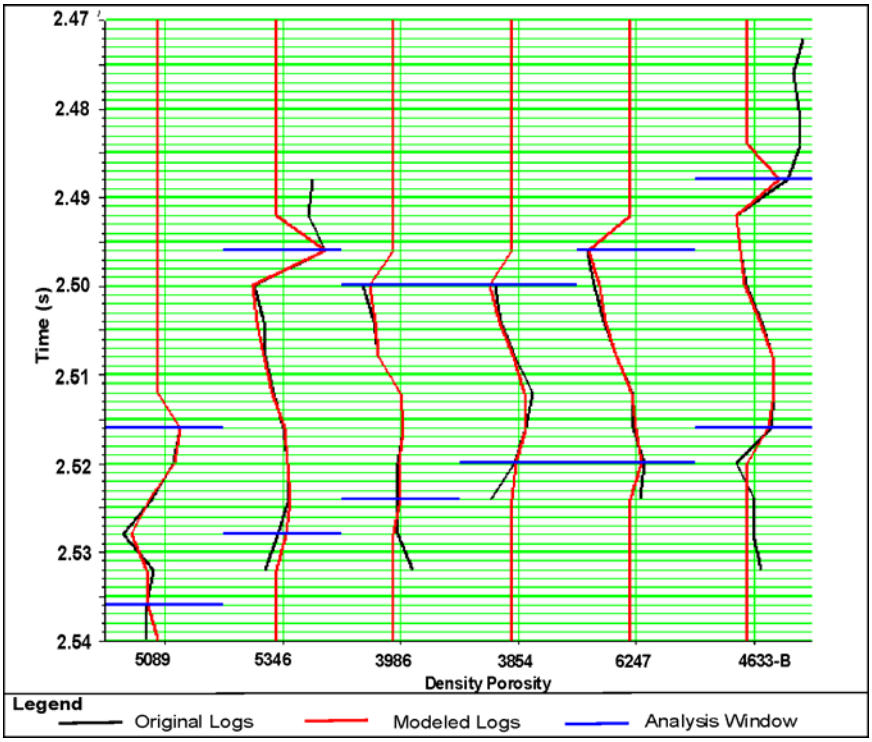
2.47
2.48
2.49
2.50
2.51
2.52
2.53
2.54
Time (s)
5089
5346
3986
3854
6247
4633-B
Density Porosity
Legend
Original Logs
Modeled Logs
Analysis Window

(a)

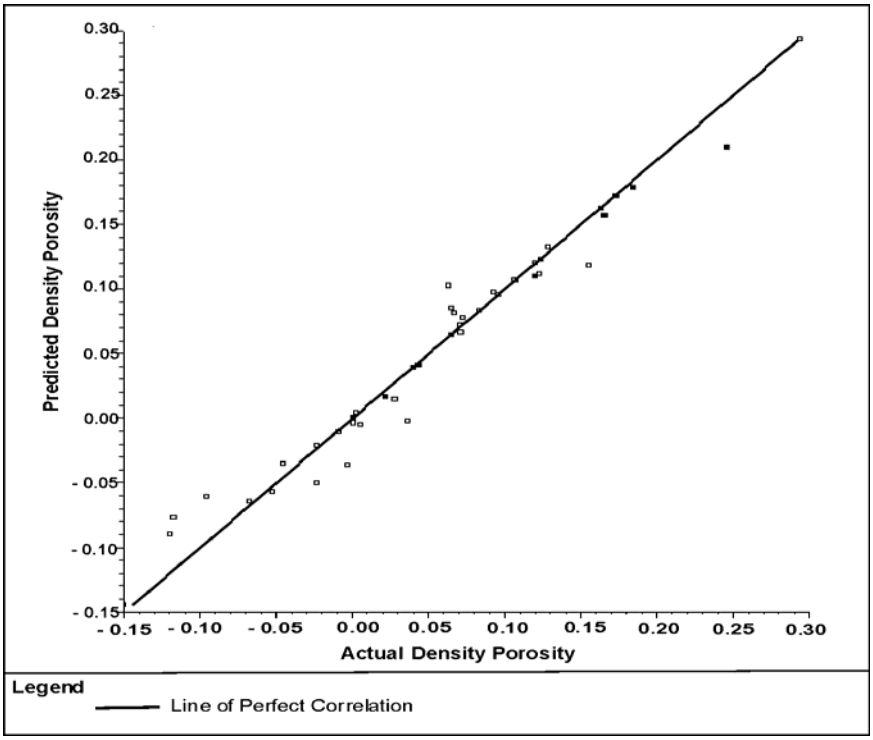
0.30
0.25
0.20
0.15
0.10
0.05
0.00
- 0.05
- 0.10
- 0.15
Predicted Density Porosity
- 0.15
- 0.10
- 0.05
0.00
0.05
0.10
0.15
0.20
0.25
0.30
Actual Density Porosity
Legend
Line of Perfect Correlation

(b)

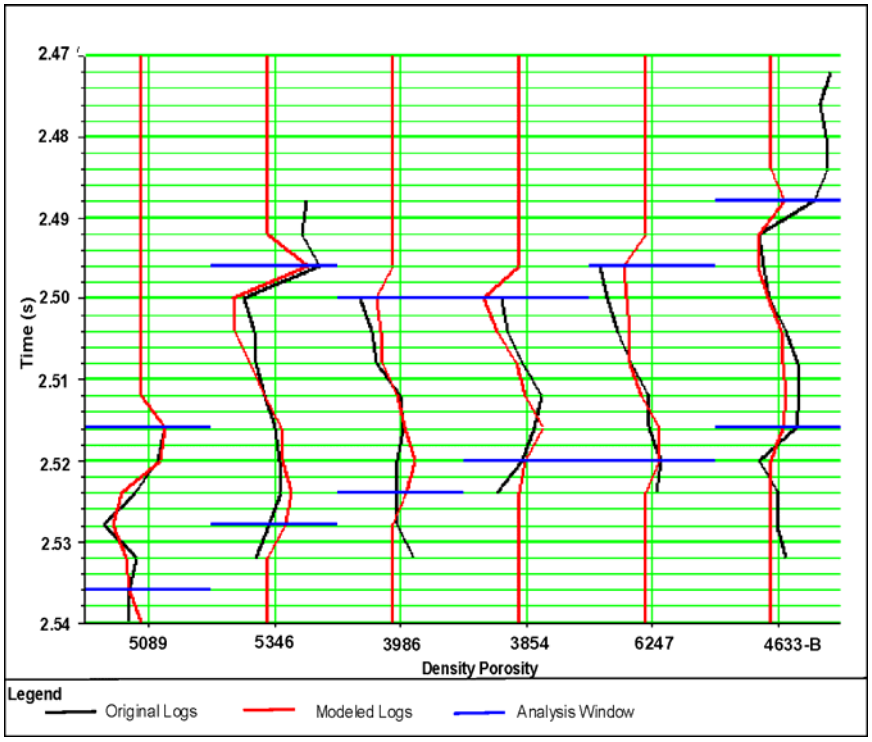

(c)

Figure 52: Visual correlation of actual and modeled/predicted porosity using PNN. (a) On application of multiattribute equation. Note how good the PNN-derived relationship is in modeling subtle changes in porosity within the Smackover Formation. (b) On crossplotting actual vs. predicted porosity values. (c) This figure shows how accurately the porosity at each well can be modeled using the PNN-derived empirical relationship, when that well is excluded from the analysis. Porosity increases to the right of the curve.

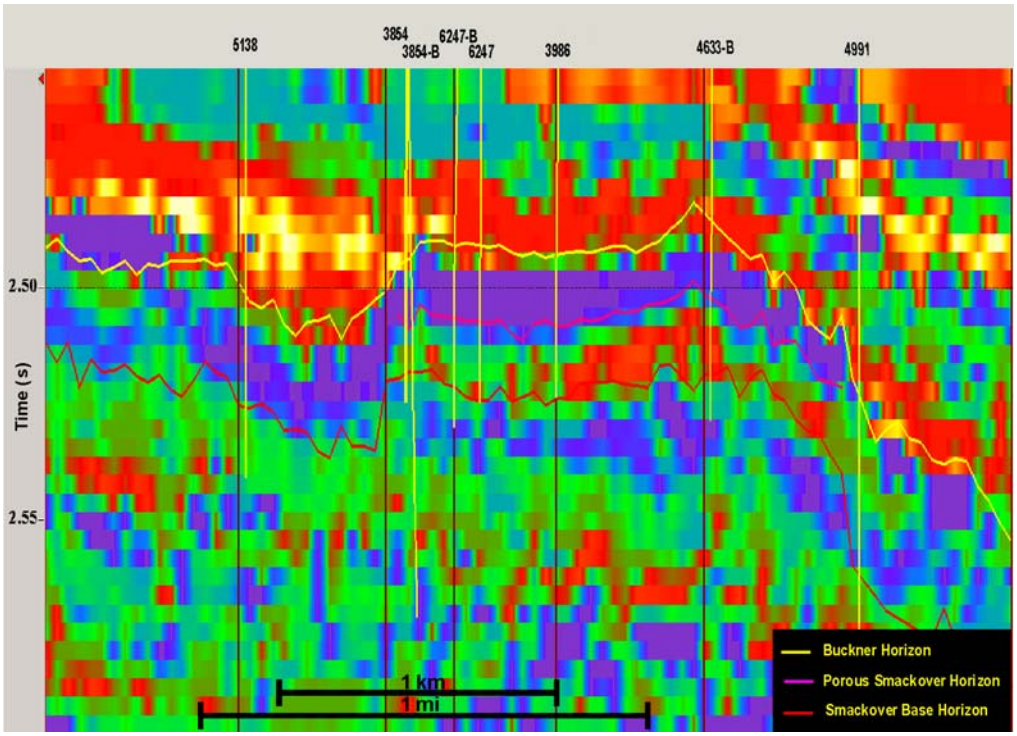
5138
3854
3854-B
6247-B
6247
3986
4633-B
4991
2.50
2.55
Time (s)
1 km
1 mi
Buckner Horizon
Porous Smackover Horizon
Smackover Base Horizon

(a)

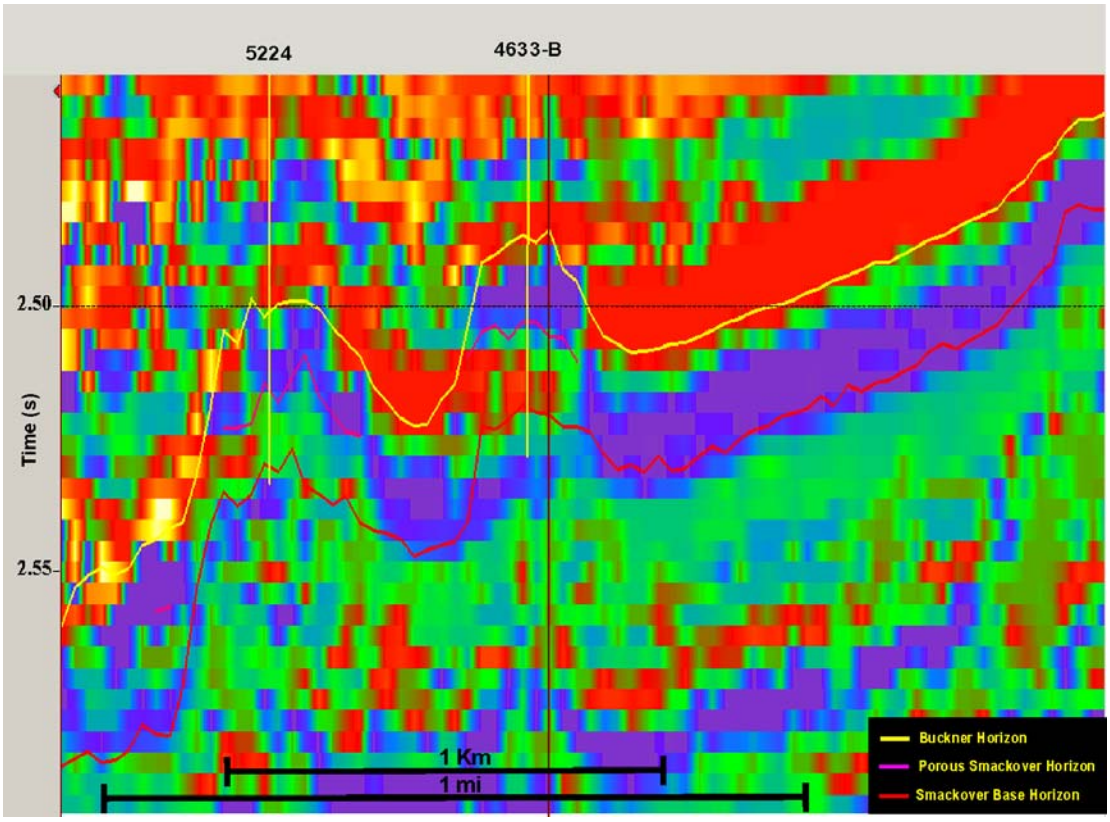
5224
4633-B
2.50
2.55
Time (s)
1 Km
1 mi
Buckner Horizon
Porous Smackover Horizon
Smackover Base Horizon

(b)

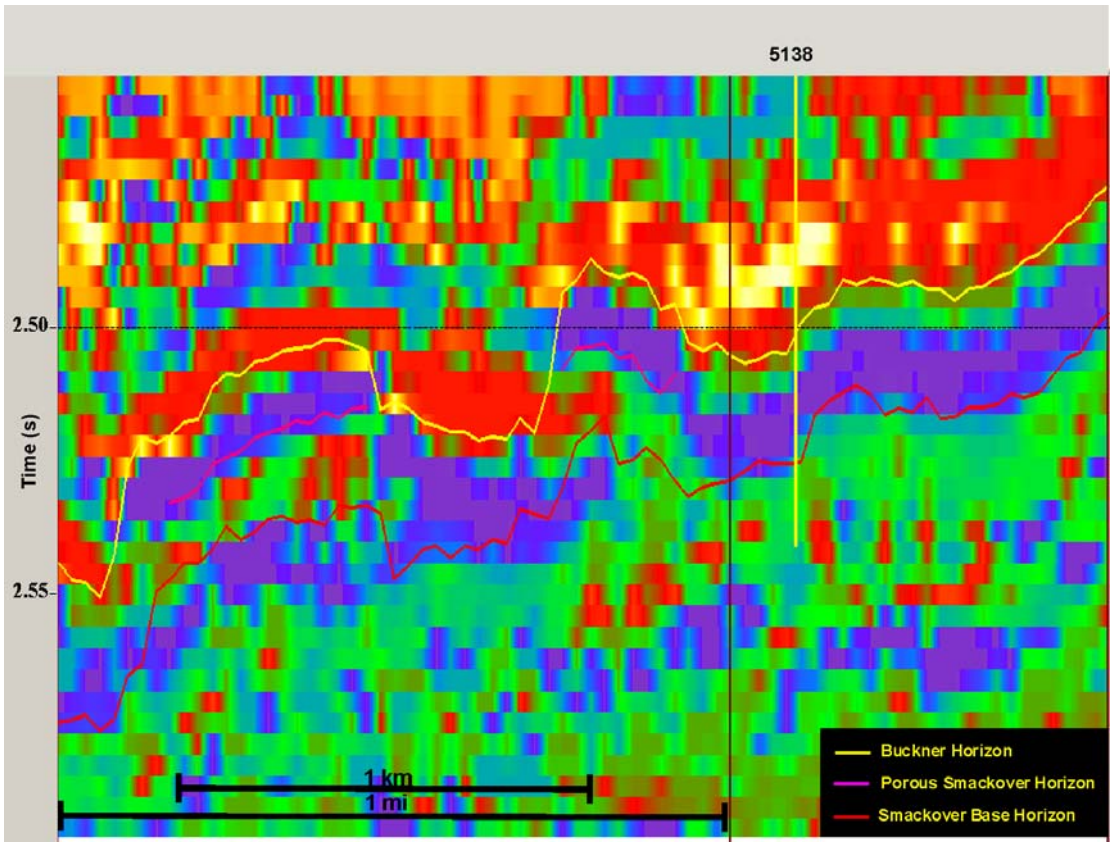

(c)

Figure 53: Strike (a) and dip sections (b & c) through the PNN porosity volume. All sections show that higher porosities (hot colors) are best developed on the seaward flanks of structure. See Figure 43 for location of transects.

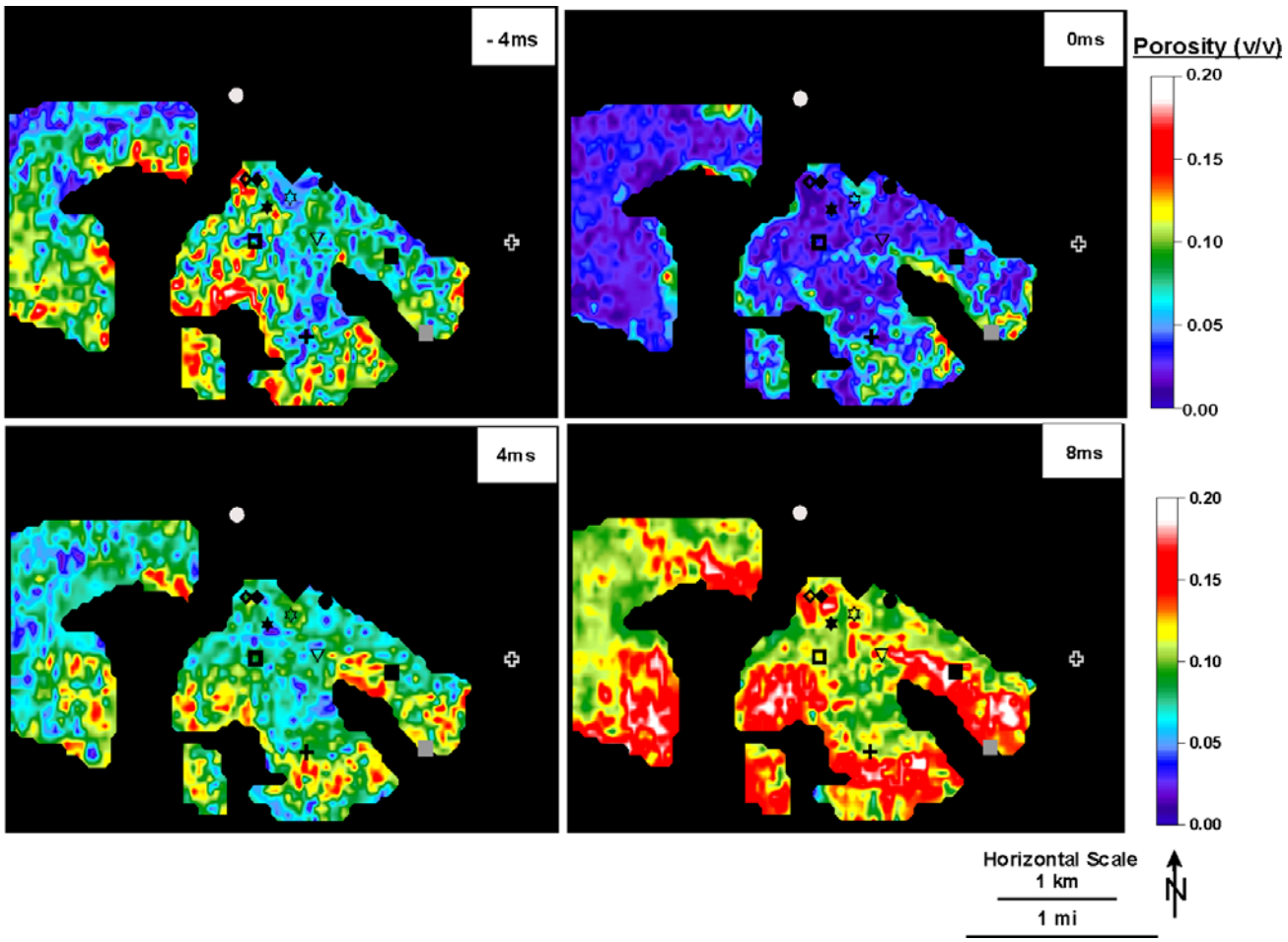

Figure 54: Slices through the porosity volume (porosity values are in decimals (v/v) i.e., volume of voids/total volume of rock, and not percentages), starting 4 ms above the porous Smackover pick. Porosity at -4ms above this pick was attributed to shoal grainstone facies, which constitute the other major reservoir facies in the Appleton Field. Note the overall association of higher porosities (hot colors) with the southern (paleoseaward) flanks of structure, which we attribute primarily to changes in facies type and growth form. Well symbols are indicated in Figure 43 and 48.

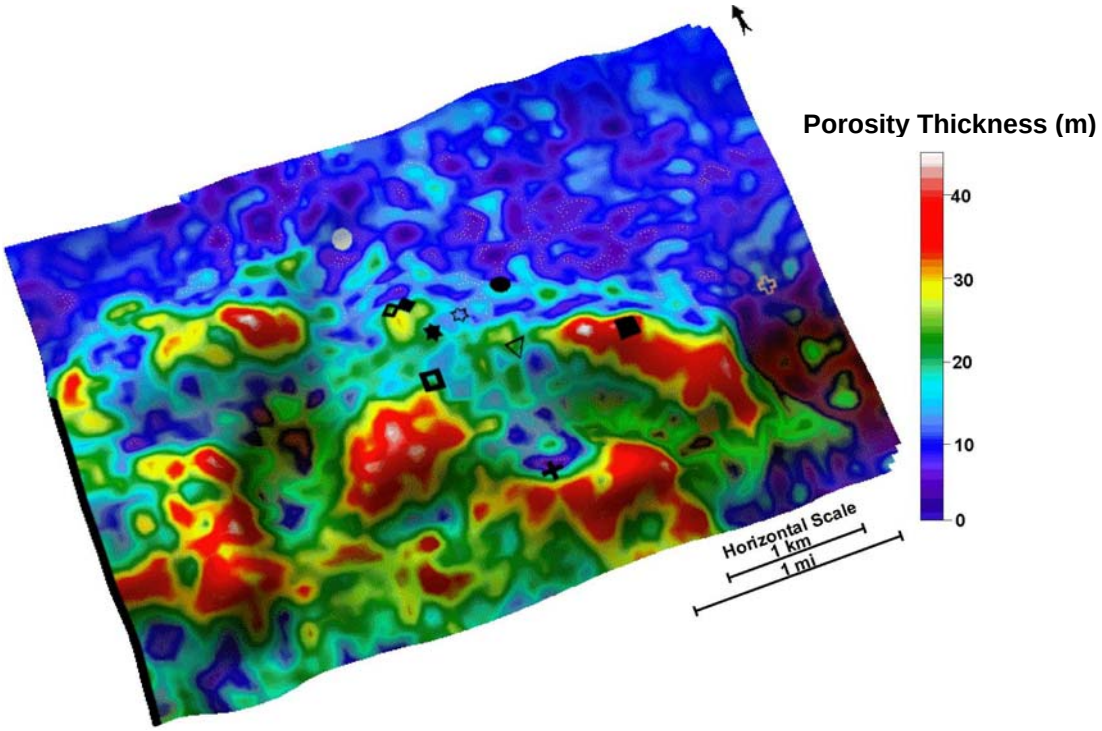

Figure 55: Porosity thickness map of the Smackover Formation overlain on the Buckner/Smackover structure map for better display. Note the overall porosity thickness (hot colors) on the southern flanks of structure. Observed differences in the distribution of porosity are mainly a result of the non-linear relationship between the predicting attributes and the seismic data. Well symbols are indicated in Figures 43 and 48.

Table 3: Reef type, depositional fabric/growth forms, and their reservoir characteristics observed at the Appleton Field, SW Alabama. (Modified from Parcell, 2000).

Reef	Depositional	Reservoir characteristics at
Type I	Layered thrombolites (higher energy)	Good reservoir, lateral permeability
Type II	Reticulate/Chaotic thrombolites (moderate energy)	Good reservoir, lateral-vertical permeability
Type III	Dendroid thrombolites (lower energy)	Best reservoir, vertical permeability
Type IV	Isolated stromatolitic crusts (moderate energy)	Poor reservoir, low permeability
Type V	Oncoidal packstone/ Grainstone (higher energy)	Poor reservoir, low permeability (better if primary fabric is not occluded)

The results from this study are consistent with carbonate sedimentologic and sequence stratigraphic principles. Preferential development of reservoir facies on paleohighs at Appleton Field and similar areas has been attributed to the favorable substrate provided by these features, relative fluctuations of sea level, and carbonate productivity (Kopaska-Merkel *et al.* 1994; Benson *et al.* 1996). Fluctuations in relative sea level interacted with paleobathymetry and other environmental factors to control the growth form, fabric and, ultimately, diagenetic alteration of the carbonate deposits. At Appleton, these changes have been described from core and logs studies by Benson *et al.* (1996), Parcell (2000), and Mancini and Parcell (2001). The buildups at Appleton Field are mainly thrombolitic (Parcell 2000; Mancini and Parcell 2001). The preferential development of porosity in the forereef environment in this field was attributed to the low background sedimentation and low to moderate energy levels, which enhanced the proliferation of deeper water dendroid thrombolites (Leinfelder 1993, 1996; Parcell 2000; Mancini and Parcell 2001). The high accommodation potential of the forereef environment permitted these buildups to attain thicknesses in excess of 30 m. Just as conventional 3-D seismic data permit more accurate mapping of structural and stratigraphic features than may be undertaken using log and/or core information alone (Brown 1996, Hart 2000), it is believed that the 3-D seismic attribute-based porosity prediction more accurately portrays the 3-D distribution of dendroid thrombolites and other porous facies than the results of previous studies. This interpretation is based on previous studies of diagenesis at Appleton Field, which suggested that dolomitization was responsible for porosity preservation and enhancement, rather than widespread development or obliteration (Saller and Moore 1986; Prather 1992; Kopaska-Merkel *et al.* 1994; Haywick *et al.* 2000).

Several previous studies have examined porosity development at Appleton Field, and related porosity to depositional history. Differences between these studies and the results lie in the choice of analytical methods used and the nature (e.g., quantitative or qualitative) of the results.

Hart and Balch (2000) used a horizon-based attribute study to predict porosity thickness at Appleton Field. Their results suggested that the porous Smackover unit was best developed on the crests rather than the flanks of the paleohighs (Figure 56a). They suggested that porosity development on the southern flanks of structure might be related to forereef talus deposits. Although some evidence points to the limited existence of talus deposits (e.g., oncoids, which are characteristic to talus deposits have been observed in cores from the Appleton Field and other Upper Jurassic reef-dominated fields; Jansa *et al.* 1989, Pratt *et al.* 1992, Pratt 1995, Parcell 2000), the results suggest that talus-derived porosity is not a major contributor to porosity development in this field. Transects through the porosity volume (e.g., Figures 53a-c) depict porous units on the forereef flanks of structures that are disproportionately thick, compared to the thickness of porous reef crest units, for reef front talus deposits. Instead the results are more compatible with models that relate preferential porosity development to thrombolite facies at Appleton Field.

The results presented herein have a stronger statistical basis than those presented by Hart and Balch (2000) and, perhaps equally important, are 3-D rather than 2-D in nature. The 3-D

(a)

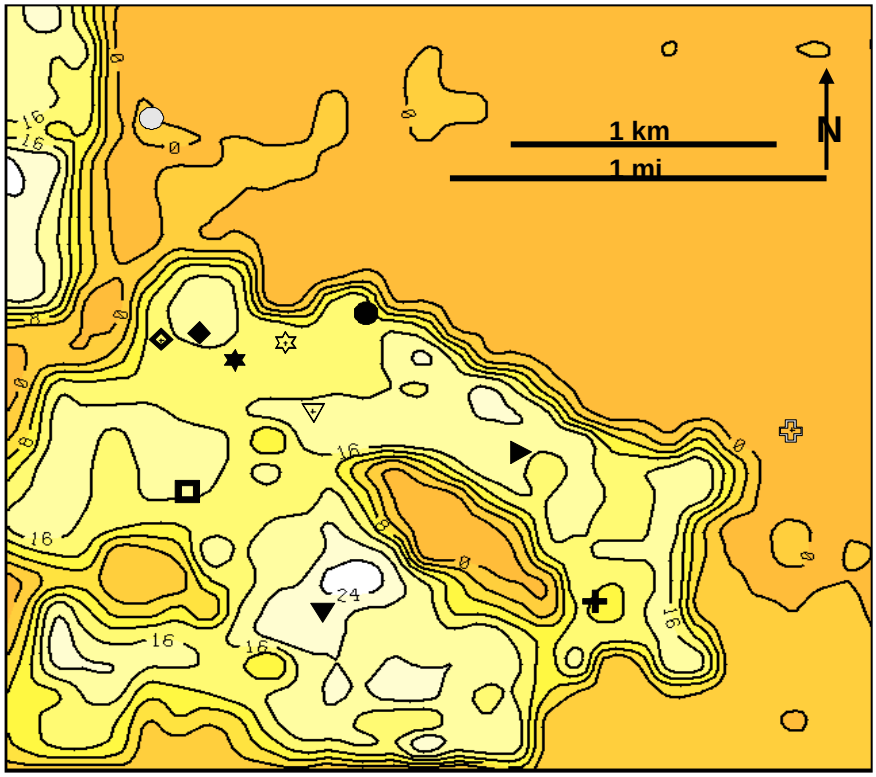

(b)

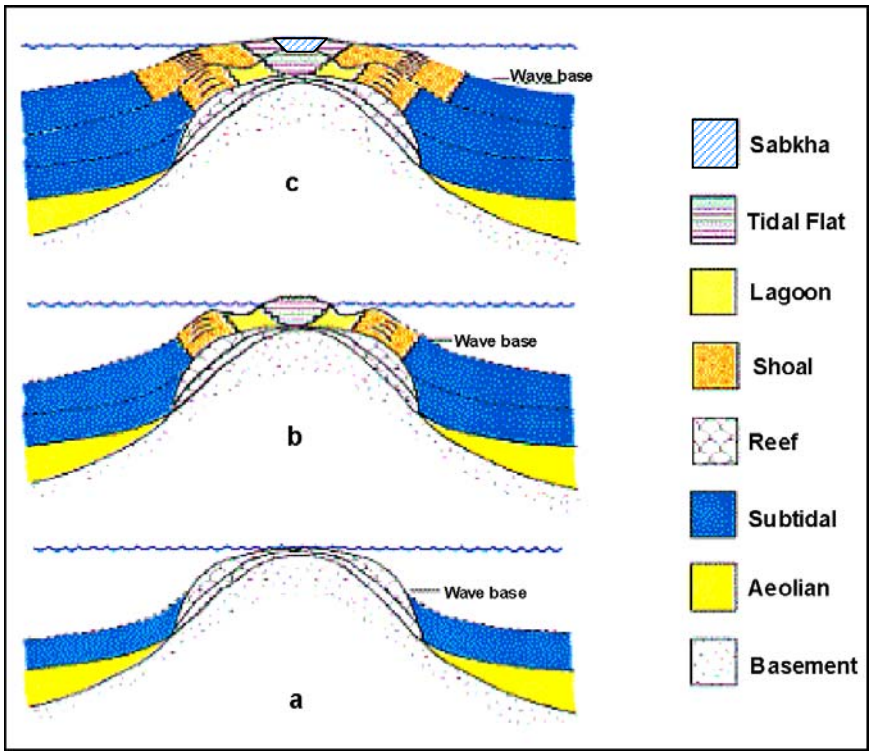

Figure 56: Existing models for the Appleton field. (a) Model of Hart and Balch (2000) depicting porosity distribution in the porous unit of the Smackover Formation, Appleton Field. Map created using a horizon-based seismic attribute study. (b) Model by Mancini *et al,* 1999. This illustrates facies distribution as a function of water depth on the basement paleohigh.

porosity volume may be viewed in ways (e.g., Figures 53 and 54) that facilitate geological analysis of the results, thereby improving the quality and robustness of the interpretation.

Mancini *et al.* (1999, 2000) suggested that the distribution of facies was dependent on the height of the paleohighs (Figure 56b) and associated paleowater depth at Appleton Field. Their model is mainly conceptual and not unique to their study area. As such, it does not provide a detailed guide to facies heterogeneity in the Smackover at Appleton Field. The result has the advantage of quantitatively portraying 3-D porosity changes, hence large-scale reservoir heterogeneities, in the area (Figures 53-55). As such, the result is of greater utility to those who might be interested in understanding fluid flow in this reservoir.

Attribute studies such as the one presented herein have several advantages over other methods (e.g., facies models, sequence stratigraphy, geostatistics, etc.) for defining the distribution of stratigraphic features and rock properties in three dimensions. The lateral continuity of a 3-D seismic volume generally allows formation tops and other features of contrast (e.g., reef margins, channels) to be more accurately mapped than may be done using wireline logs, core or 2-D seismic (Brown 1996, Hart 2000). Seismic attribute studies, and especially volume-based studies such as ours, integrate the high degree of lateral resolution from a 3-D seismic survey with the relatively better (compared to seismic data) vertical resolution of wireline logs. The result is a quantitative output that: a) is of greater utility for applied studies than facies maps, cross-section or conceptual models, b) has well-defined statistical properties (correlation with input, average error, etc.), and c) typically shows greater geologic “reality” than purely geostatistically based methods.

Several authors have presented workflows and precautions to be taken when working with seismic attribute studies (e.g. Schultz *et al.*1994a, Kalkomey 1997, Hampson *et al.* 2001, Hart

1999, 2002) and a full discussion of these aspects cannot be presented here. Instead, we emphasize the following selected points:

a) Data quality and quality control at all aspects of the interpretation process (e.g., horizon picking) are essential. In the case, we could only use six of the eleven wells for which we had logs. This is because the rest could not be adequately tied to the seismic data because of poor log quality and/or seismic data quality problems at the well location.

b) The use of a volume-based as opposed to a horizon-based method increases sample size, and hence the statistical basis of the analysis. As was observed during the multiattribute analysis, the sample size was substantially increased from six (one sample per well) to forty-three (an average of six samples per well). Hence, this method is most appropriate in areas of limited well control (Russell *et al.* 1997; Hampson *et al.* 2001).

c) Although the degree of statistical correlation between input and output variables, and between attributes and physical properties, is important, high correlation coefficients alone are not sufficient for accepting the results of an attribute study. The results must also be examined to determine whether they are geologically logical and whether they are supported by other data types (e.g. engineering data). The physical basis for the relationships between attributes and physical properties also needs to be established. Seismic modeling (Tebo, 2003) helped us to understand the meaning of the attributes employed in this study.

d) Seismic attribute studies do not eliminate the need for conventional geologic analyses. Instead, they are best thought of as a means of building upon those studies. For example, although we can use seismic attributes to image porosity at Appleton Field; it is only through the integration of the results with previous geological analyses that we

can understand the relative importance depositional facies and diagenesis in the creation of that porosity.

Vocation Field. This work was undertaken to predict the distribution of porosity at Vocation Field by integrating attributes derived from a 3-D seismic volume with log-derived physical properties. The purpose was twofold: 1) to generate a data-based porosity volume using Hampson-Russell's Emerge software that could be used in reservoir modeling, and b) to use the results to gain insights into the geologic controls on porosity development at Vocation Field.

Twenty-two wells with a varied suite of logs, along with their coordinates and deviation surveys were available for analysis (Figure 57, Table 4). Fourteen of these wells had both the sonic log (needed to generate synthetic seismograms) and the porosity (density and neutron) logs. Logs were edited for spikes or other problems. The 3-D seismic data used in this study covered a 5.2 x 4.9 km (3.2 x 3.0 mi) grid, of which a 4.3 km^2 (2.7 mi^2) grid was used for analysis. The seismic data had a bin spacing of 110 x 110 ft (~33 x 33 m) and a trace length of 3 s two-way travel time (TWT). Also available for comparison and interpretation were core descriptions and production information for some of the wells. No checkshot surveys were available.

Given the lack of checkshot information, wells needed to be tied to seismic data using the log and seismic picks provided to us. The following procedure to generate synthetic seismograms was used:

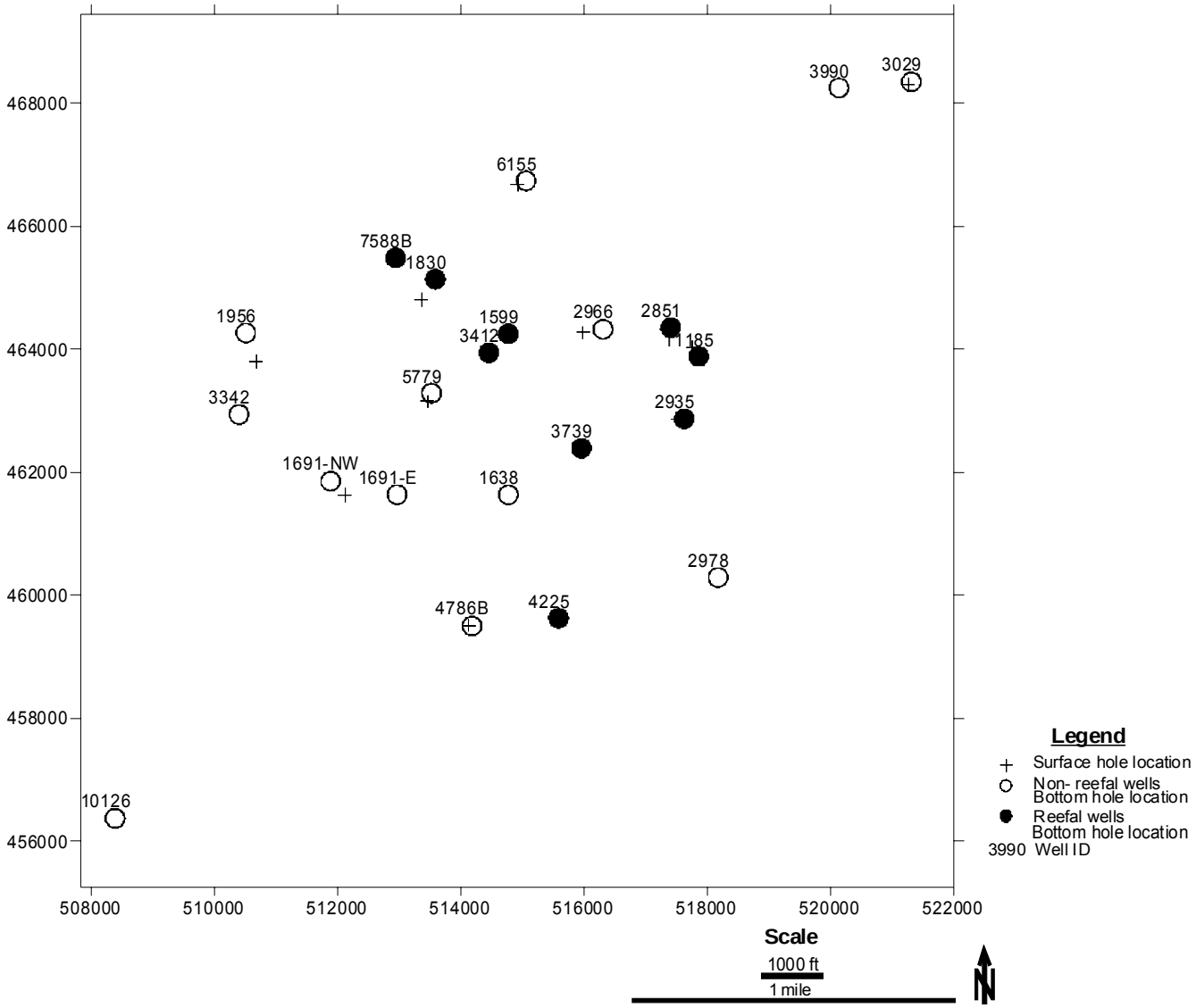

Figure 57: Well locations at Vocation Field. Wells classified based on presence or absence of reef facies.

Table 4: Cross section of logs available for the Vocation Field.

Permit #	GR	NPHI	DPHI	DT	ILM	ILD	SP	SFL	CALI	RHOB	LLS
10126	X	X	X	X	X	X	X	X	0	0	0
11185	X	X	X	X	X	X	X	X	0	0	0
1599	X	X	X	X	X	X	X	X	0	0	0
1638	X	X	X	X	X	X	X	X	0	0	0
1691-NW	X	X	X	0	X	X	X	X	0	0	0
1691-E	X	X	X	0	X	X	X	X	0	0	0
1830	X	X	X	0	X	X	X	X	0	0	0
1956	X	X	X	0	X	X	X	0	0	0	X
2851	X	X	X	X	X	X	X	0	0	0	X
2935	X	X	X	X	X	X	X	X	0	0	0
2966	X	X	X	X	X	X	X	X	0	0	0
2978	X	X	X	X	X	X	X	X	0	0	0
3029	X	X	X	X	X	X	X	X	0	0	0
3342	X	X	X	0	X	X	X	X	0	0	0
3412	X	X	X	X	X	X	X	X	0	0	0
3739	X	X	X	0	X	X	X	X	0	0	0
3990	X	X	X	X	X	X	X	X	0	0	0
4225	X	X	X	0	X	X	X	X	0	0	0
4786B	X	X	X	X	X	X	X	X	0	0	0
5779	X	X	X	X	X	X	X	X	0	0	0
6155	X	X	X	X	X	X	X	X	0	0	0
7588B	X	X	X	0	X	X	X	X	0	0	0
X = curve, 0 = No curve											

•Statistical wavelet extraction: A wavelet that matched the frequency content of the seismic data was needed. To generate this wavelet, the following parameters were used:

•Time window: A window length of 600ms (2300 – 2900ms), twice the length of the wavelet was used.

•Seismic data: A subset of the seismic data, 130 inlines by 130 crosslines, was used to minimize the influence of bad data particularly noticeable at survey edges but large enough to improve statistics of the extracted wavelet.

A wavelet with a dominant frequency of ~35Hz (Figure 58) was generated.

•The statistical wavelet was convolved with the well-derived reflectivity series to create synthetic seismograms for wells with sonic logs. The synthetics were then compared to the seismic data at well locations. A series of constant phase rotations was applied to this wavelet and each time the resulting synthetic trace was correlated to the seismic. The synthetic with the best overall correlation, determined by the correlation coefficient, was chosen. The phase at which this occurs was assumed to be identical to the incident wavelet (Figure 59).

Of the total 22 wells, 14 had all logs needed for this study. Of that number, it was possible to generate synthetics that adequately tied (correlation coefficient > 0.75) with the seismic data for 6 wells. Problems existed with the other wells:

•Horizon picks: Lateral variations in seismic phase presented problems in maintaining consistent seismic picks.

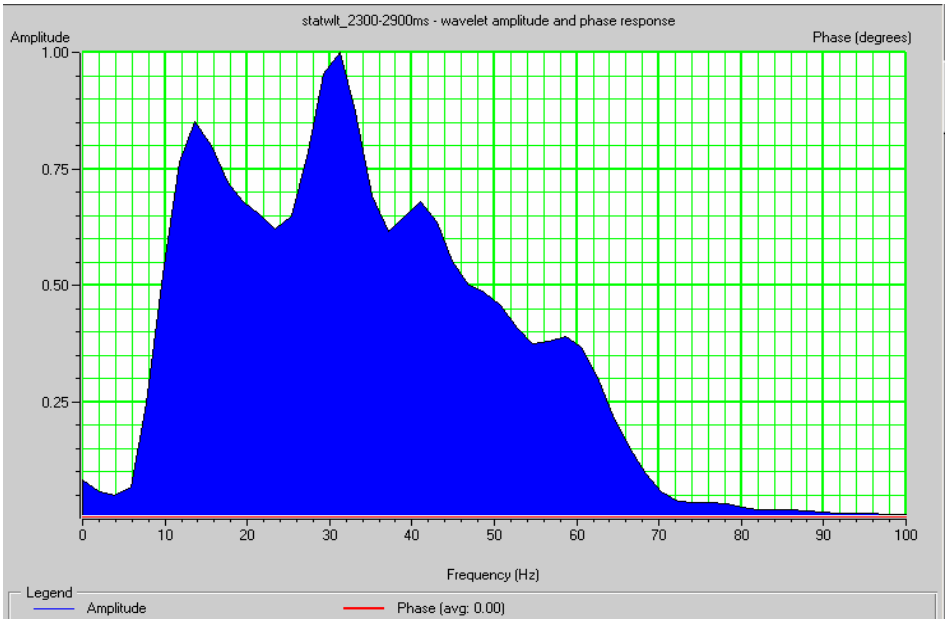

(a)

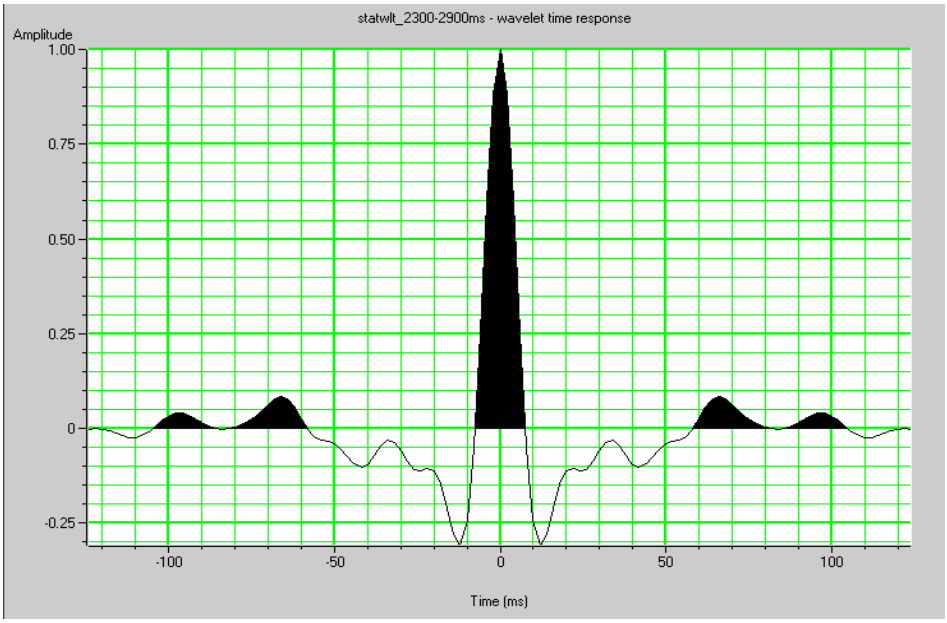

(b)

Figure 58: Estimated (statistical) seismic wavelet: (a) amplitude spectrum showing the range of frequencies embedded in the wavelet, dominant frequency range is between 25-35 Hz, (b) wavelet shape in time domain.

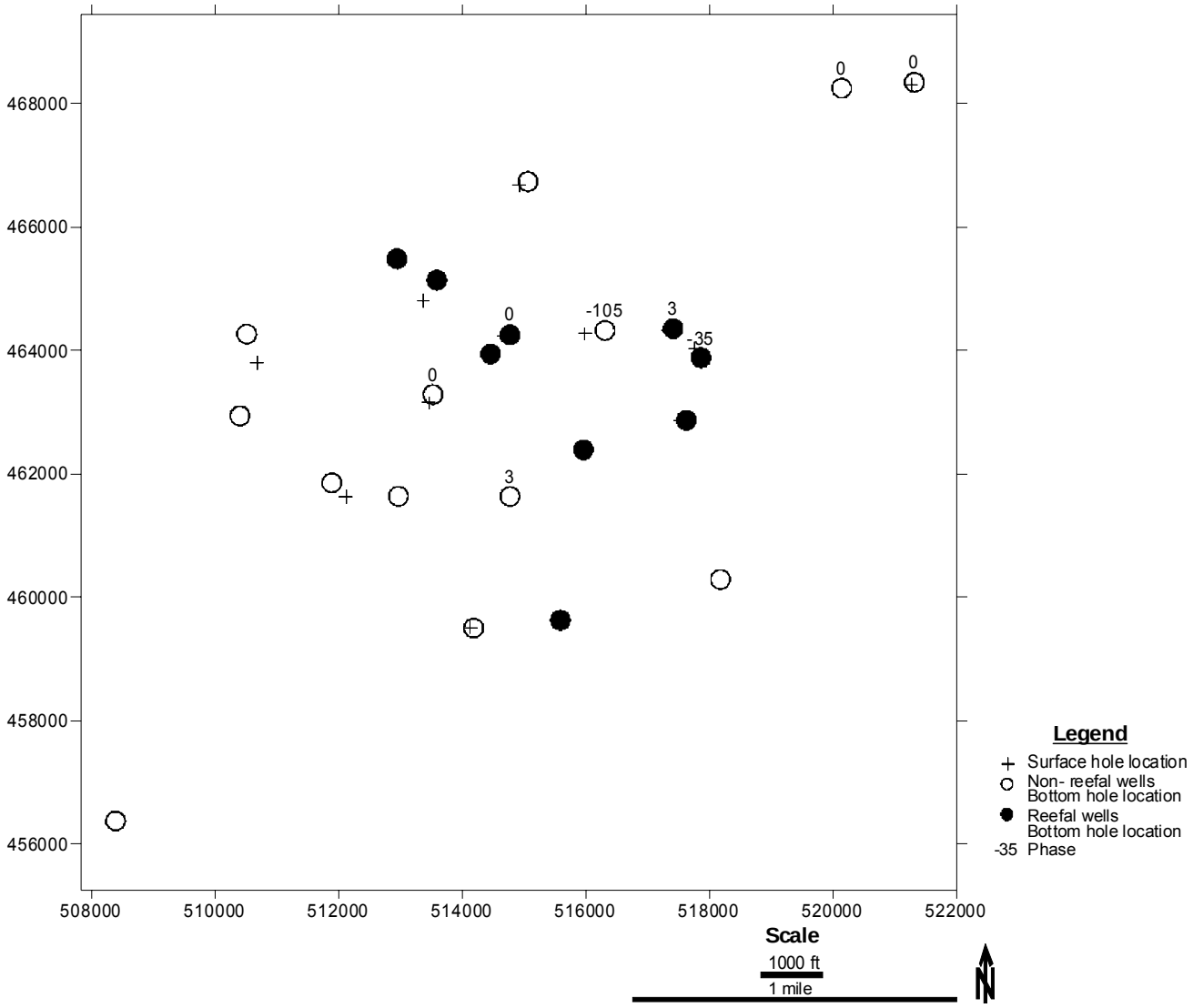

Figure 59: Seismic grid showing phase rotation necessary to obtain a statistically significant synthetic tie. Note phase variation in the east, which could be attributed to structural changes in that area. Wells with excessive phase rotations were not included in subsequent attribute analyses.

(e.g., Well 2966). Wells that required extreme phase changes in the source wavelet for the synthetic seismograms compared to the others (e.g., Wells 2966, 11185) were not used for the Emerge attribute analysis.

- Log length: Most of the digital logs within and around the Vocation Field have a limited vertical extent. Most extend only a few feet above and below the Smackover Formation, while some started below, or were not logged to the end of this formation. For this reason, adequate synthetic seismograms could not be generated due to the lack of velocity information above and below the formation (Fig. 60, Table 5). Ideally, longer digital logs would be available for analysis.
- Seismic data quality: The overall quality of the available seismic data was somewhat poor in areas. Noisy data would prevent us from obtaining adequate well ties between logs and seismic data.

The six calibrated wells with the predicted property logs were trained with 23 attribute volumes, including the original seismic trace, that were derived by the Hampson-Russell software. Apparent porosity (the average of neutron and density porosity) was selected for prediction because it provided a better approximation of porosity (compared to core measurements) at Vocation Field than neutron, density or sonic porosity alone (See Table 6).

A volume-based method (Hampson *et al.*, 2001; see fuller description of the methodology in Section 2.5) was adopted due to the thickness (0-440ft/0-134m) and stratigraphic complexity (rapid facies changes) of this interval. For this study, multivariate linear regression and three types of neural networks were evaluated. The three neural networks we trained are:

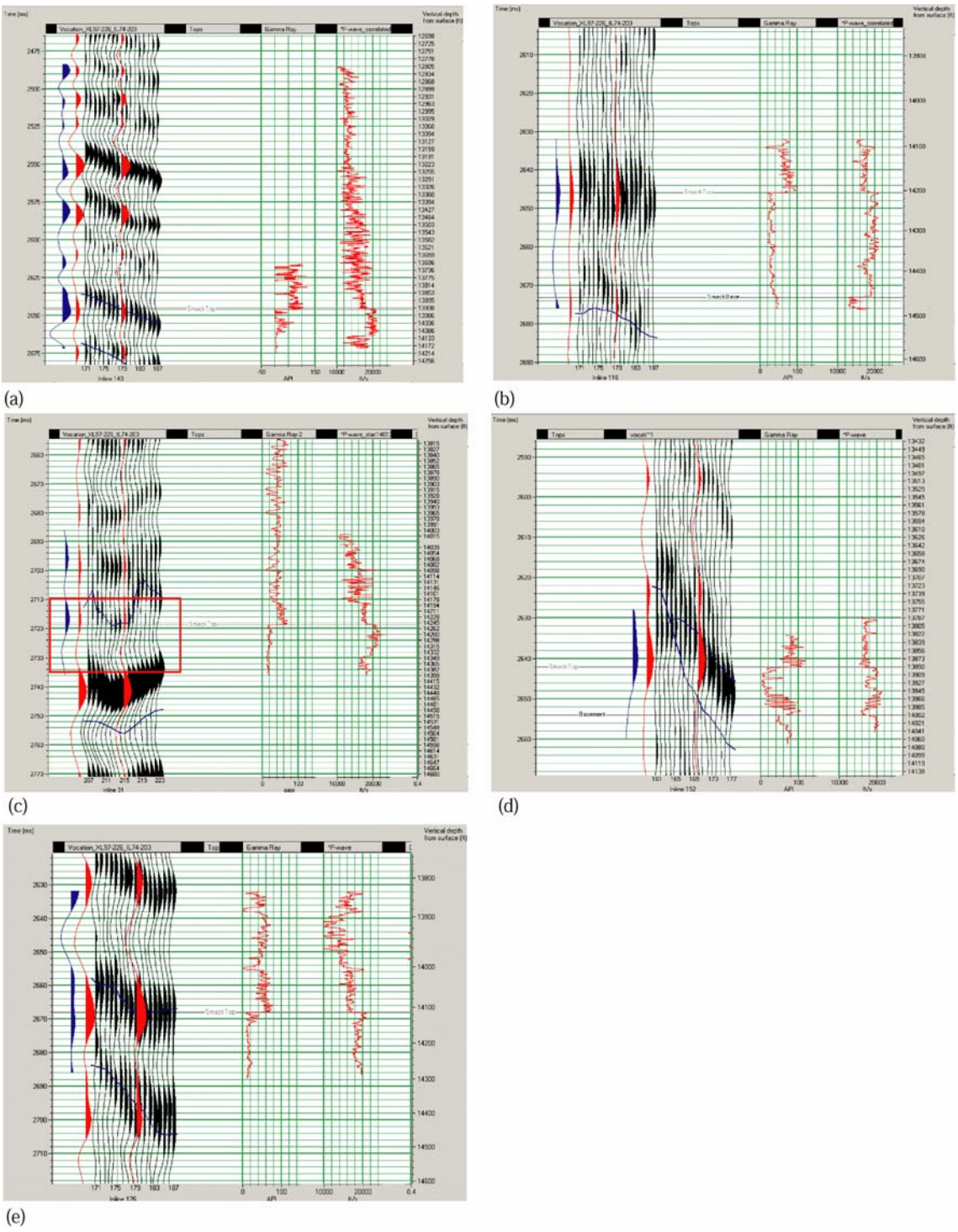

Figure 60: Synthetic seismograms of selected wells showing good ties: a) 1638, b) 2851, c) 3990, d) 5779, e) 2966. The synthetic for 2966 was generated using a -105° phase-rotated wavelet, judged to be an excessive amount. Blue wiggle = synthetic, red wiggle = seismic trace extracted along the wellbore.

Table 5: Summary statistics of available data and synthetic calibration for the Vocation Field.

Permit #	DT Logs	Reefal Facies	Cored	Well Status	Hole Type	Synthetic	Correlation Coefficient	Wavelet Phase
10126	yes	no	no	na	straight	no	-	-
11185	yes	yes	yes	producing	deviated	yes	0.5674	-35
1599	yes	yes	yes	temp plugged- oil	deviated	yes	0.6695	0
1638	yes	no	no	na	straight	yes	0.7939	3
2851	yes	yes	yes	abandoned - oil	deviated	yes	0.8408	3
2935	yes	yes	yes	abandoned - oil	deviated	no	could not tie	-
2966	yes	no	yes	na	deviated	yes	0.8857	-105
2978	yes	no	no	na	straight	no	could not tie	-
3029	yes	no	no	na	deviated	yes	0.748	0
3412	yes	yes	yes	abandoned - oil	straight	no	-	-
3990	yes	no	yes	na	straight	yes	0.8782	0
4786B	yes	no	no	na	deviated	no	-	-
5779	yes	no	yes	abandoned - oil	deviated	yes	0.9618	0
6155	yes	no	no	na	deviated	no	-	-
1691-NW	no	no	yes	na	deviated	no	-	-
1691-E	no	no	no	na	deviated	no	-	-
1830	no	yes	no	abandoned - oil	deviated	no	-	-
1956	no	no	no	na	deviated	no	-	-
3342	no	no	no	na	straight	no	-	-
3739	no	yes	yes	abandoned - oil	straight	no	-	-
4225	no	yes	no	abandoned - oil	deviated	no	-	-
7588B	no	yes	yes	na	deviated	no	-	-

Table 6: Comparison of porosity measured by different porosity logs. PHID = Density porosity, PHIN = Neutron porosity, PHIA = Apparent porosity ([PHID + PHIN]/2).

Permit #	PHIDmax	PHINmax	PHIAmax	PHIDavg	PHINavg	PHIAavg	Coremax	Coreavg	Misc
10126	0.222	0.162	0.112	0.047	0.077	0.023			
11185	0.182	0.226	0.184	0.039	0.133	0.086	0.130	0.061	
1599	0.387	0.324	0.169	0.084	0.115	0.055	0.350	0.109	No base
1638	0.038	0.100	0.061	-0.044	0.041	-0.002			
1691-E	0.088	0.151	0.118	-0.054	0.033	-0.011			
1691-NW	0.055	0.223	0.139	-0.026	0.141	0.058			
1830	0.101	0.232	0.159	-0.002	0.105	0.052	0.250	0.105	
1956	0.157	0.293	0.221	-0.006	0.068	??			
2851	0.185	0.204	0.187	0.008	0.113	0.060	0.250	0.106	
2935	0.137	0.259	0.198	0.012	0.146	0.079	0.200	0.091	
2966	0.14	0.217	0.163	-0.015	0.157	0.071			No base
2978	0.283	0.274	0.277	0.010	0.139	0.075			
3029	0.166	0.281	0.207	0.006	0.110	0.058			
3342	0.126	0.259	0.192	0.006	0.088	0.047			
3412	0.281	0.187	0.190	-0.009	0.068	0.039	0.175	0.052	No base
3739	0.160	0.233	0.179	0.061	0.155	0.108	0.150	0.062	No base
3990	0.121	0.191	0.144	0.030	0.144	0.087			No base
4225	0.112	0.236	0.174	-0.015	0.081	0.033	0.150	0.038	
4786B	x	x	x	X	X	X	x	X	No Smackover
5779	0.108	0.160	0.134	-0.019	0.067	0.024	0.225	0.059	
6155	0.174	0.263	0.199	0.036	0.141	0.088			
7588B	0.335	0.283	0.263	0.02	0.148	0.082			No base

- Probabilistic Neural Network (PNN) – Probabilistic Neural Networks are described in the section on Appleton Field (Section 2.5).
- Trend cascaded Probabilistic Neural Network (PNN) – This method is used to improve MLR prediction, and works best in data, such as Vocation Field, which have no significant trends within the analysis window. In this option, the network first performs linear regression using the attributes identified from the MLR analysis. This MLR-predicted log is smoothed, and a PNN is then used to predict the high frequency component (residual) of the logs that is not found in the smoothed MLR log. The final trend-cascaded log is the sum of the PNN residual and smoothed MLR logs. This is a new option for the Emerge software that was not available during the Appleton Field project.
- Multi-layer Feed Forward Network (MLFN) – The properties of this network are described in Masters (1994). The validity of this network is dependent on the number of nodes to use in the hidden layer and the number of iterations. The number of nodes, analogous to the degree of polynomial, is determined by the following method:

  Number of nodes = 2/3 x (Number of attributes x Operator length).

  The number of iterations basically controls computation time.

The top and base of the Smackover Formation were used to define the interval of interest (Figure 61). The Buckner Anhydrite Member of the Haynesville Formation was used as the seismic proxy for the top of the Smackover Formation. Seismically this top was found to vary laterally in phase (see Figures 59 & 60). This could be attributed to lateral changes in phase of the wavelet embedded in the seismic data, lateral changes in lithology or some other factor.

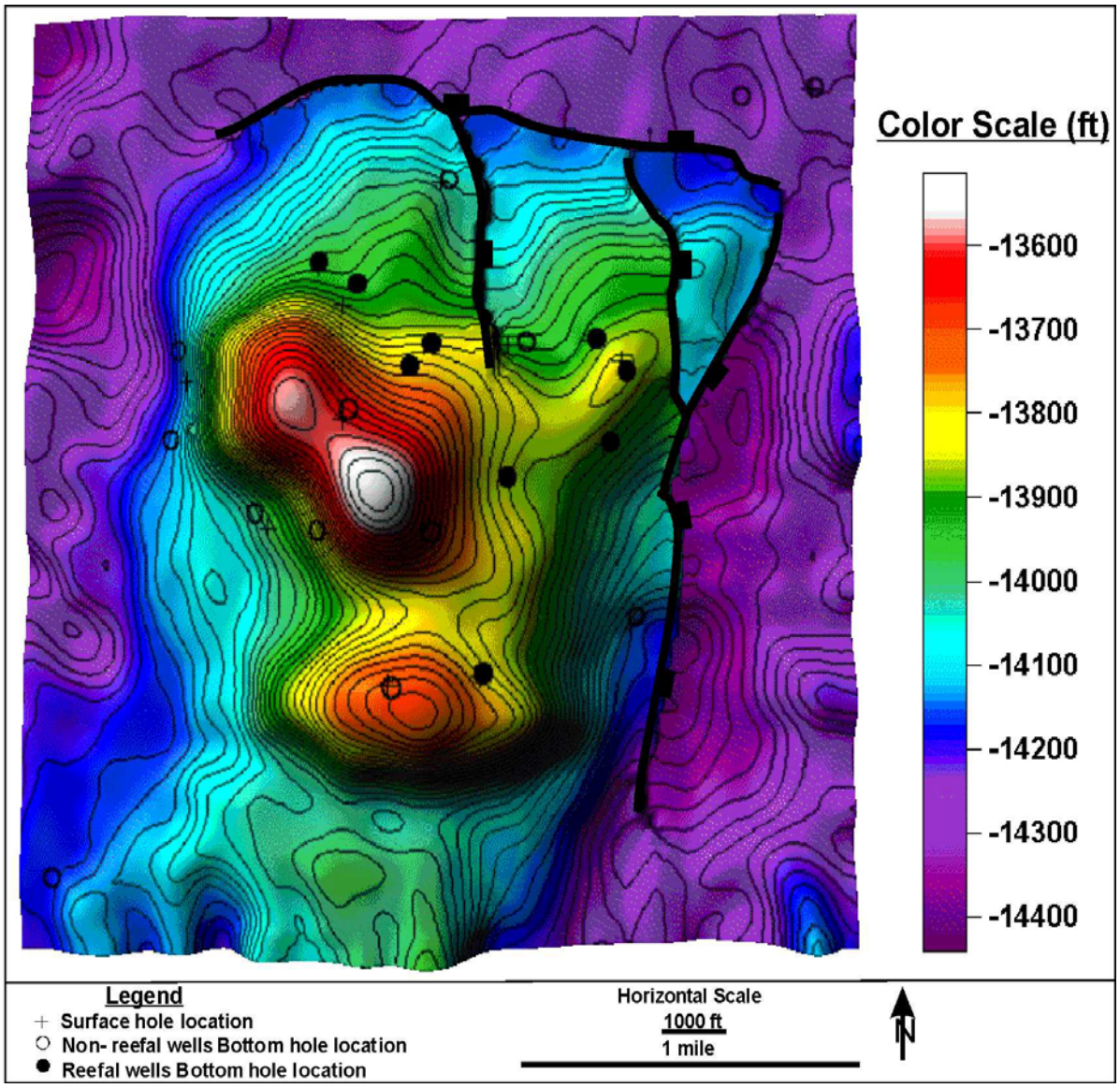

Figure 61: Depth-structure map (sub-sea) from seismically interpreted Smackover base horizon. Thick black lines represent faults and their dip directions.

As was the case at Appleton Field, the phase of the base of the Smackover Formation in the Vocation dataset was dependent on the physical properties of the units underlying the Smackover Formation. This pick constituted a medium to high amplitude peak where the Smackover is underlain by the Basement, and a medium to high amplitude trough, when the formation is underlain by siliciclastics of the Norphlet Formation.

The best predicting attribute was the integrated trace, with a correlation coefficient of 46% (Figure 62). MLR results showed that 3 attributes were optimal in predicting apparent porosity (Figure 63), these attributes were: integrated trace, time, and filter 25/30-30/35 (Tables 7 and 8).

- Integrated trace: This attribute is the integral of the seismic trace, which essentially is a band-limited (recursive) inversion, with low acoustic impedance being represented by negative numbers, and high acoustic impedance being represented by positive numbers. A crossplot of this attribute and apparent porosity of the trained wells reveals that higher porosity areas are associated with negative values of integrated trace, hence the relationship of high porosity and low acoustic impedance (Figure 62b).
- Time: This mainly is a ramp function that adds a trend to the computed reservoir property, in this case apparent porosity. A crossplot of this attribute and porosity shows a positive correlation, which could be attributed to a relationship between structure and porosity development (Figure 64).
- Filter 25/30 – 30/35Hz: This attribute is related to the spectral decomposition of the seismic wavelet. As observed for the amplitude spectrum of the wavelet computed over the interval of interest (Figure 58), the majority of the spectrum falls within this given frequency range. This attribute is related to rock properties, specifically to mapping bed thickness, geologic

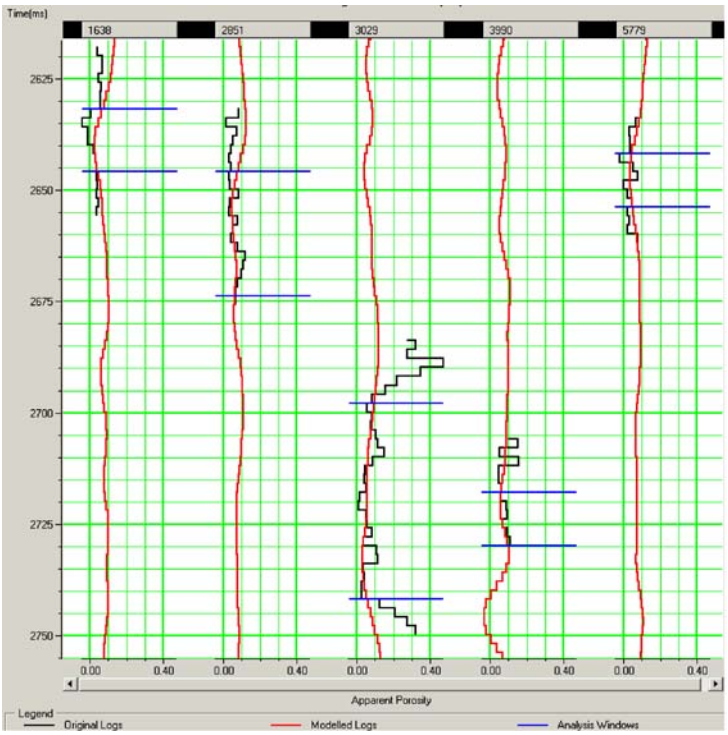

(a)

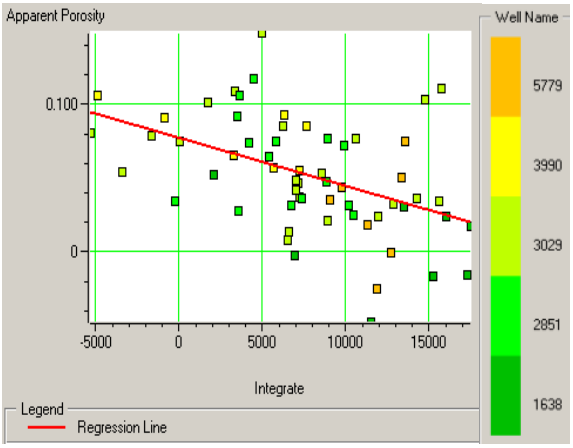

(b)

Figure 62: a) Comparison of modeled porosity logs (red curve) derived from the application of the best single-predicting attribute (integrated trace), and actual porosity logs (black curve). The blue lines across logs define the window for which this analysis is valid; b) Crossplot of actual porosity values from logs against integrated trace illustrates the negative relationship between this attribute and porosity. Higher porosities are associated with negative integrated trace values.

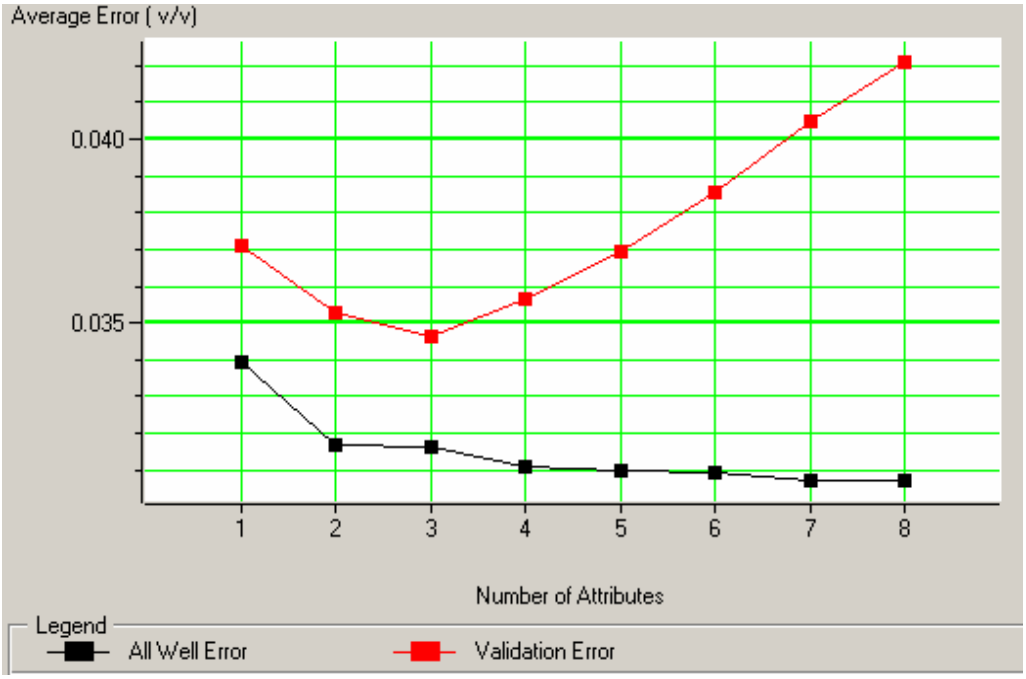

Figure 63: Validation plot, showing variation in all-well error and validation error in predicting porosity from apparent porosity logs using stepwise linear regression. The increase in validation error after the third attribute indicates that the optimum number of attributes to use is three. See Hampson *et al.* (2001) for a full description and justification of the method.

Table 7: Multiattribute list showing the best predicting 8 attributes, prediction error decreases with the addition of each attribute. Each added attribute consists the preceding set of attributes.

No. of attributes	Target	Final Attribute	Training Error	Validation Error
1	Apparent Porosity	Integrate	0.033962	0.037084
2	Apparent Porosity	Time	0.031673	0.035277
3	Apparent Porosity	Filter 25/30 – 35/40	0.031607	0.034657
4	Apparent Porosity	Instantaneous Phase	0.031104	0.035650
5	Apparent Porosity	Dominant Frequency	0.030976	0.036948
6	Apparent Porosity	Amplitude Weighted Phase	0.030954	0.038529
7	Apparent Porosity	Filter 55/60 – 65/70	0.030735	0.040484
8	Apparent Porosity	Second Derivative	0.030697	0.042113

Table 8: Attributes and their weights/sigmas contributed towards creating the empirical relationship (multiattribute transform) for porosity prediction using different analytical methods.

Attribute Name	Attribute Transform	MLR Weight	PNN_No Trend Sigmas	PNN_Trend Sigmas
Integrate	None	-2.79471e-006	0.267086659401869	0.0905277336448514
Time	None	0.000335289	0.525753681217157	1.37145498622836
Filter 25/30 – 35/40	None	-4.396e-010	0.554705532426393	0.269098355541889
Constant	-	-0.827684	0.704166667846342	0.462500001303852
Target Transform	None	0	-	-
Trend Length	-	1	-	-

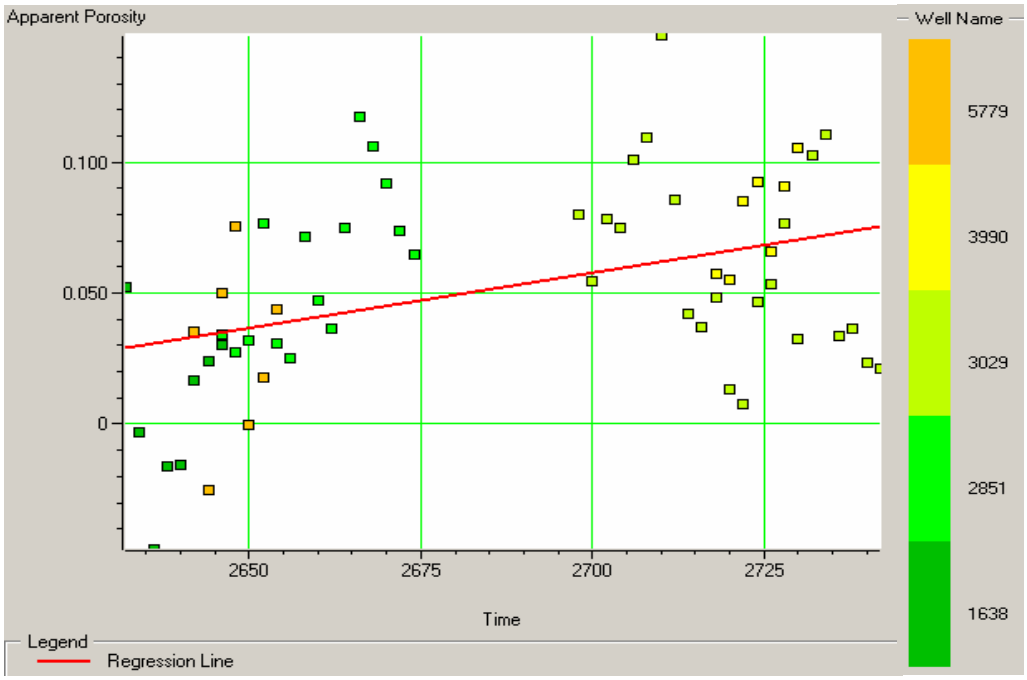

Figure 64: Crossplot of time vs. porosity indicates the presence and nature of relationship between these two variables. The trend indicates that higher porosity is generally found lower in the section.

discontinuities and/or absorption effects (Peyton *et al.*, 1998; Partyka *et al.*, 1999; Taner, 2001).

Applying the three-attribute transform obtained from the MLR increased the prediction coefficient to 56% (Figures 65a & b). A 45% correlation shows how well this transform could be used to predict trained logs excluded from the analysis in the validation analysis (Figure 65c).

Although the neural networks trained with MLR-derived attributes generally increased the statistical accuracy of the porosity prediction, the improvement was not uniform. The performance of each network was evaluated based on the correlation of predicted and actual porosity, their average error incurred upon application of the transform, the ability to predict porosity at each well excluded from the training dataset (cross correlation/validation), and visual correlation of predicted and actual porosity logs (Table 9; Figures 66, 67 and 68). The "regular" (no trend-cascaded) PNN showed the least improvement, followed by the MLFN. The best (statistically and geologically) porosity prediction and resolution was produced by the trend cascaded PNN. This method also best modeled the higher frequency changes within the Smackover Formation in the trained wells (Figure 67a).

Furthermore, comparison of PhiH (porosity thickness) maps calculated from all four porosity volumes (using a cut off of 8%) shows that the PNN trend-cascaded map best represents thickness distribution (Figure 69). Below are some probable reasons for differences in predicted and actual porosity thickness:

- Resolution: From crossplots, histograms of predicted and actual porosity, and maximum porosity maps created for the Smackover Formation we observed that all methods do not predict the absolute range of porosity captured by logs (Figures 65b, 66b, 67b, 68b, 70, & 71). This can be related, at least in part, to the resolution of the logs. Most high porosity

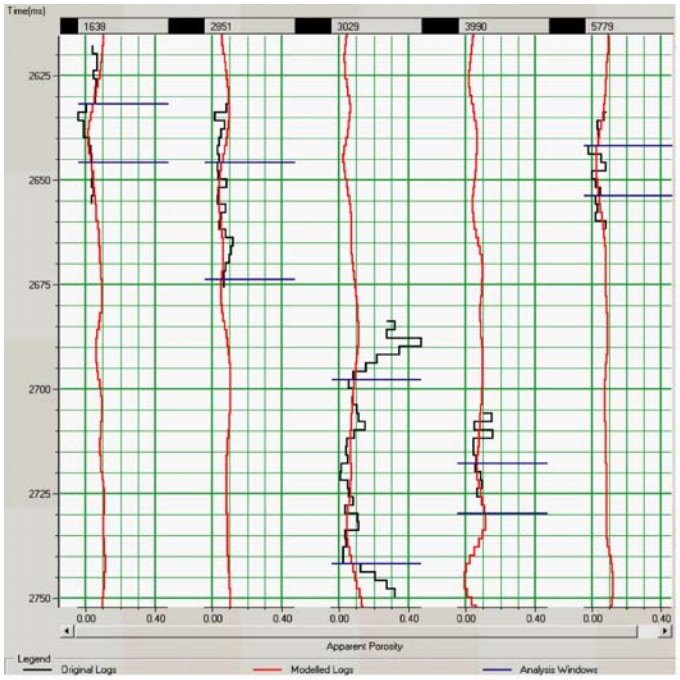

(a)

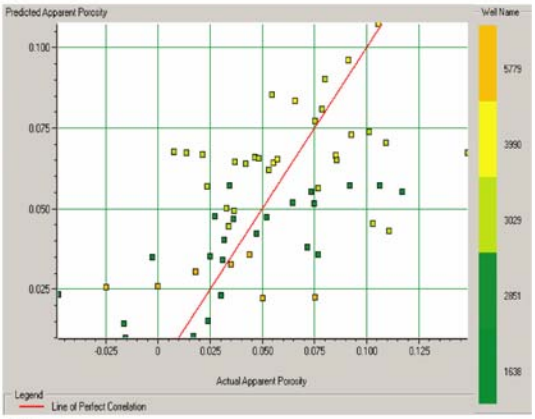

(b)

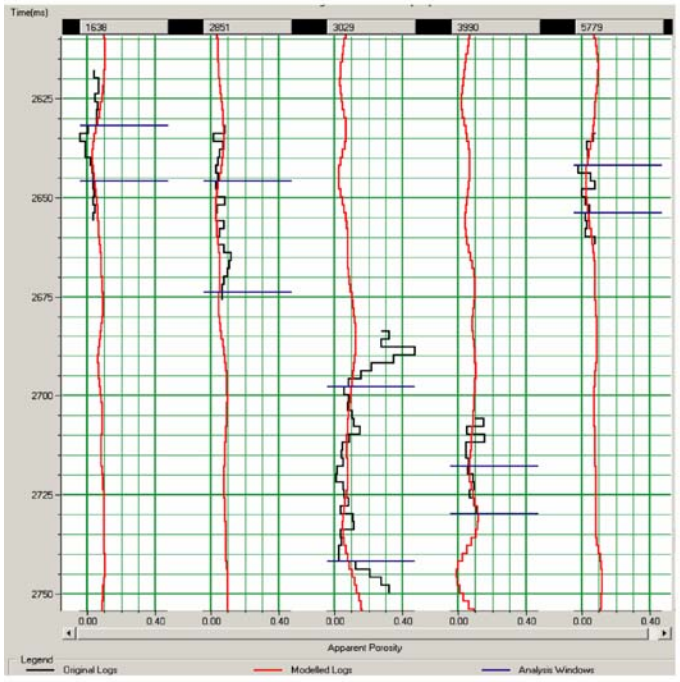

(c)

Figure 65: Visual correlation of actual and modeled porosity using MLR, a) on application of multiattribute equation, and b) on cross-plotting actual vs. predicted porosity values. Note the difference in range of actual and predicted porosity. c) Shows how accurately the porosity at each well can be modeled using the derived empirical relationship, when that well is excluded from the analysis. Porosity increases to the right of the curve.

Table 9: Table of correlation coefficients and average errors to evaluate performance of multiattribute transforms from the different analytical methods used in analysis. Best method determined by high correlation coefficients and correspondingly low average errors.

Analytical Method	Corr. Coeff. on Application	Average Error	Corr. Coeff. on validation	Average Error
Linear regression	0.46028	0.0339616	-	-
Multilinear regression	0.56333	0.0316073	0.44699	0.034657
No Trend PNN	0.72437	0.0270095	0.44425	0.034484
MLFN	0.73498	0.0259411	0.45239	0.037869
Trend PNN	0.87894	0.0189337	0.54557	0.033390

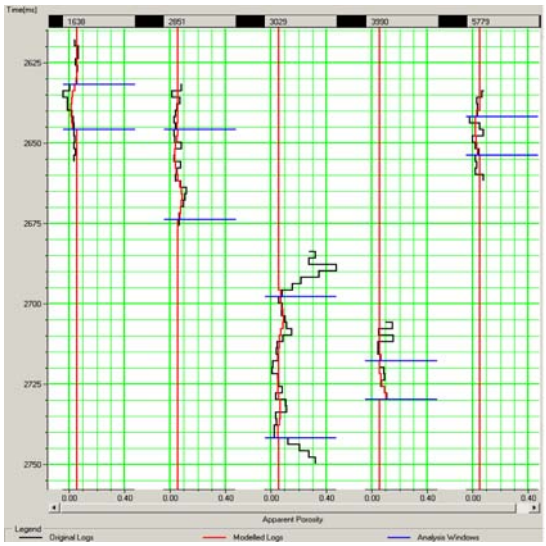

(a)

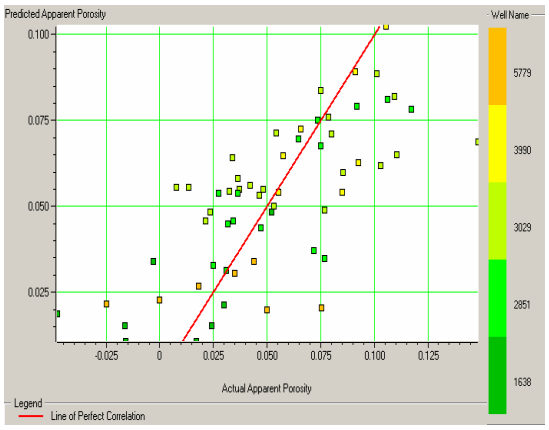

(b)

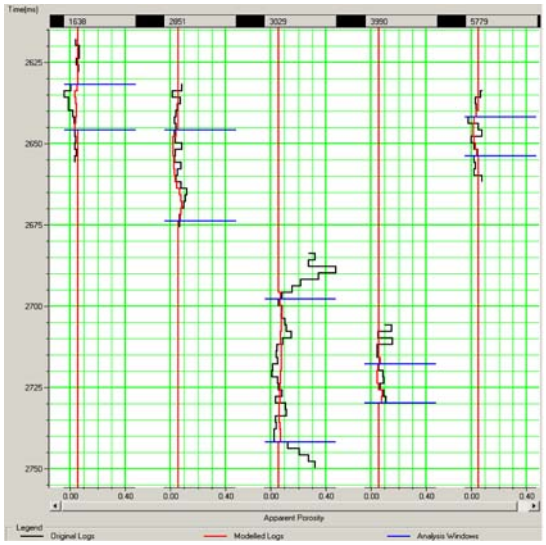

(c)

Figure 66: Visual correlation of actual and modeled porosity using a no trend-cascading PNN, a) on application of PNN results using all wells, and b) on cross-plotting actual vs. predicted porosity values. Also note the differences in range of actual and predicted porosity. c) Shows how accurately the porosity at each well can be modeled using the derived empirical relationship, when that well is excluded from the analysis. Porosity increases to the right of the curve.

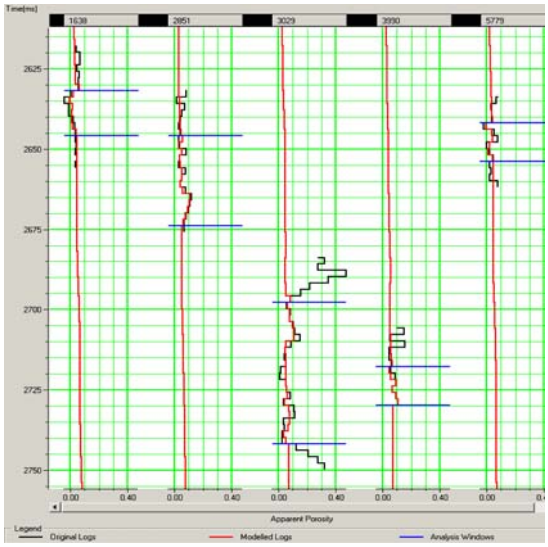

(a)

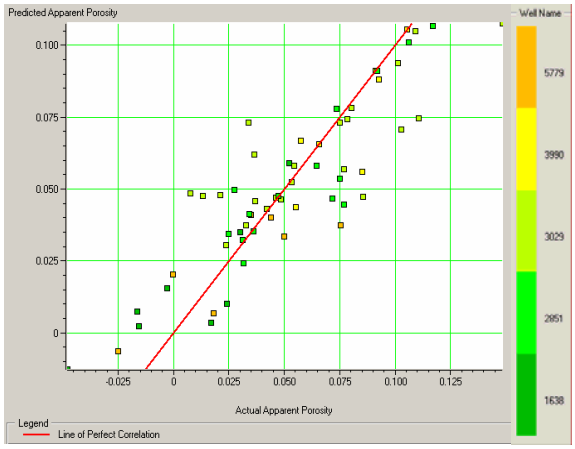

(b)

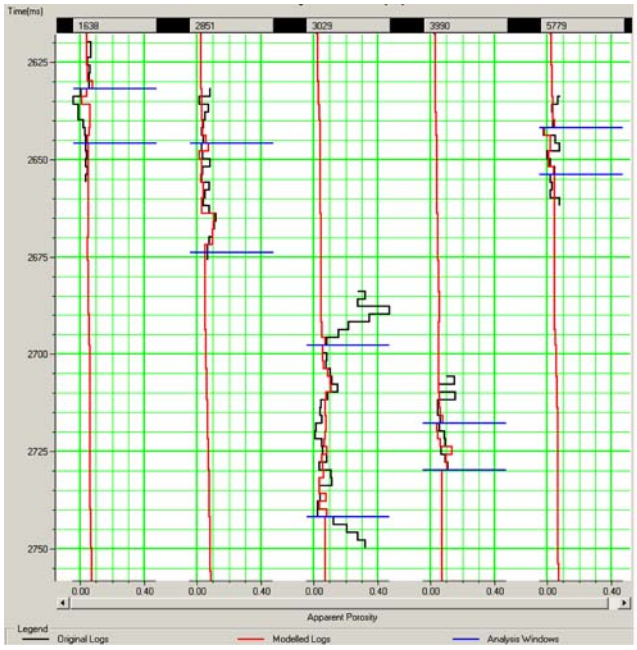

(c)

Figure 67: Visual correlation of actual and modeled porosity using the MLR trend-cascading PNN, a) on application of results using all wells, and b) on cross-plotting actual vs. predicted porosity values. Also note the difference in range of actual and predicted porosity. c) Shows the accuracy of porosity prediction at each well using the derived empirical relationship, when that well is excluded from the analysis. Porosity increases to the right of the curve. Note how ell this PNN-derived relationship captures subtle changes in porosity within the analysis window when compared to other methods.

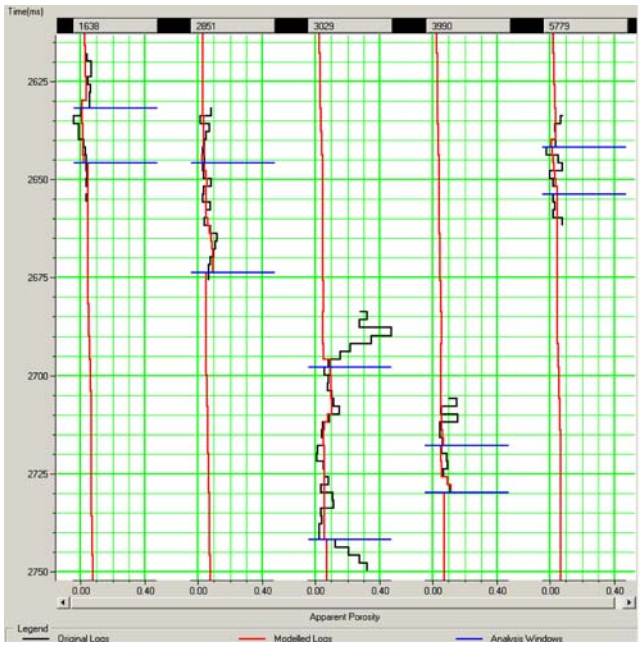

(a)

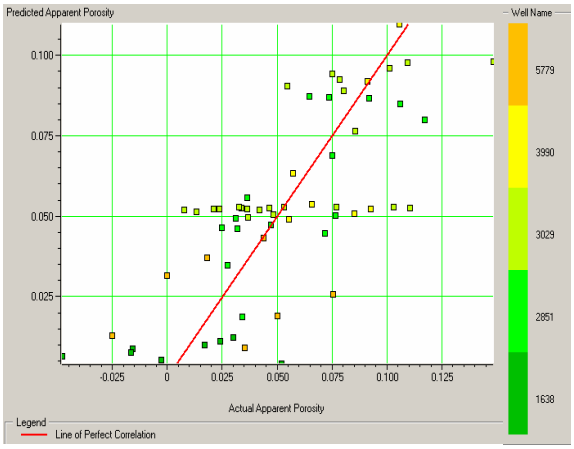

(b)

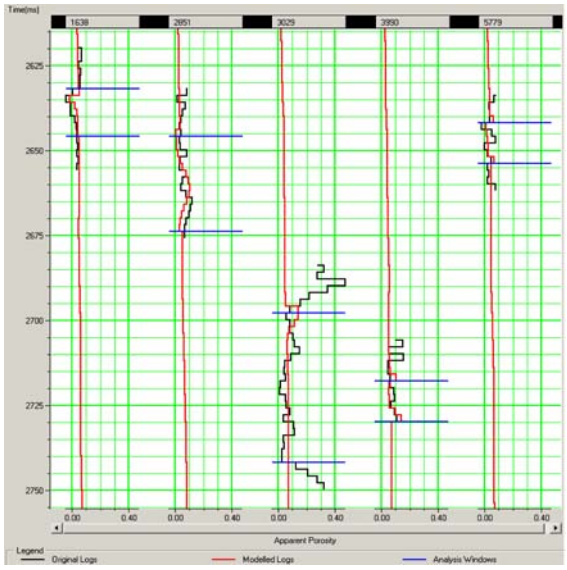

(c)

Figure 68: Visual correlation of actual and modeled porosity using MLFN. (a) on application of MLFN results using all wells, and b) on cross-plotting actual vs. predicted porosity values. Also note the difference in range of actual and predicted porosity. c) Shows how accurately the porosity at each well can be modeled using the derived empirical relationship, when that well is excluded from the analysis. Note how poorly the derived relationship models subtle changes in porosity within the analysis window, especially at well 3029. Porosity increases to the right of the curve.

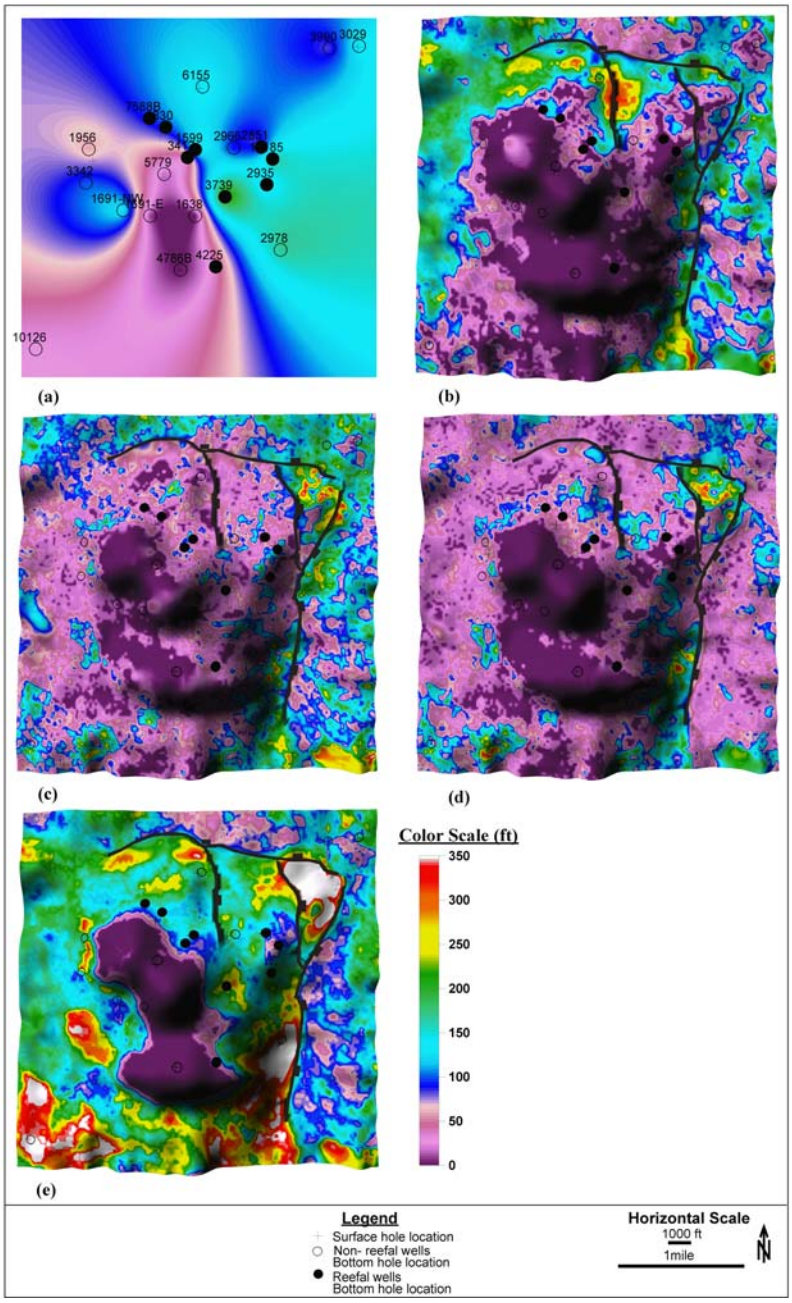

Figure 69: Porosity thickness map of the Smackover Formation overlain on the Buckner/Smackover depth-structure map for better display; a) based on contouring of wells only, b) MLR result, c) MLR trend-cascading PNN result, d) no trend cascaded PNN, and e) MLFN. Note the overall lack of porosity at the crests of structure, and thicker porosity to the flanks of structure and along faults. Also note the prediction of high/thick porosity zones associated with faults in eastern part of the study area. Observed differences in the distribution of porosity are mainly a result of the method used.

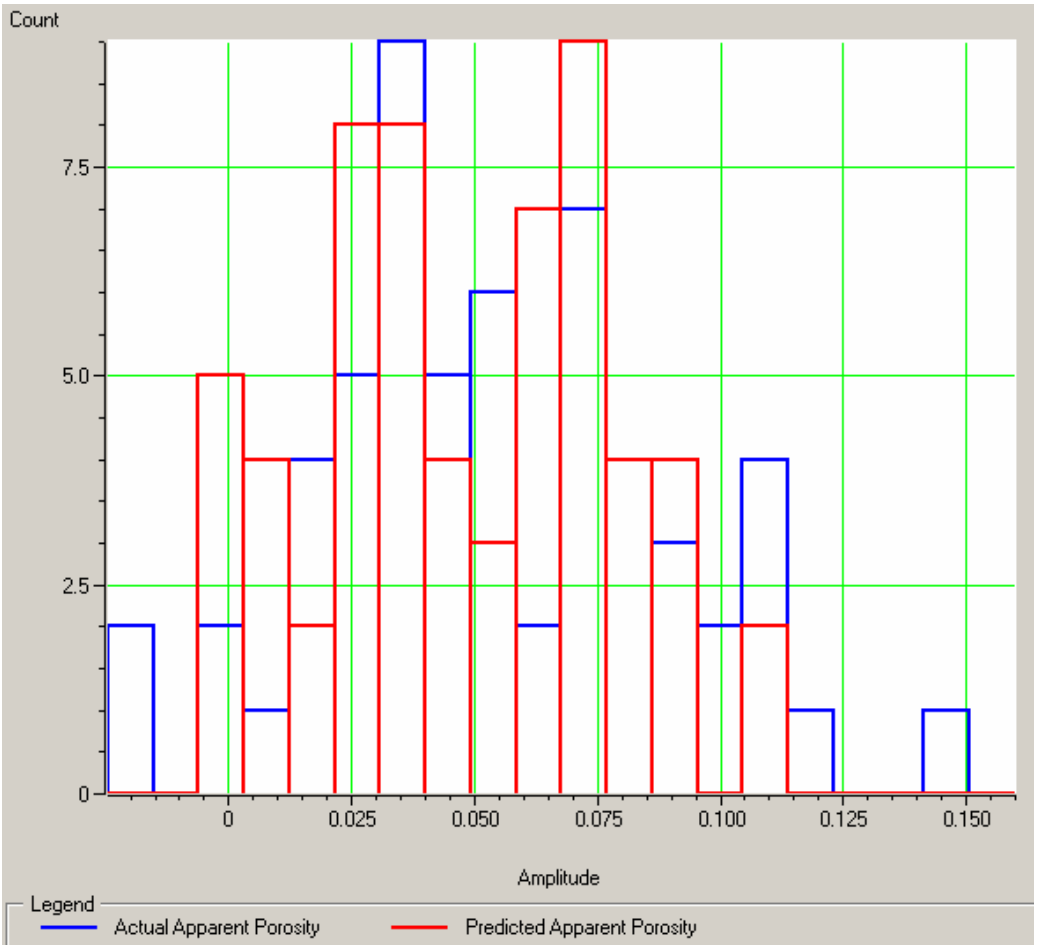

Figure 70: Histogram comparing the actual range of porosity values and those predicted using the MLR trend-cascaded PNN method (statistically and geologically preferred method).

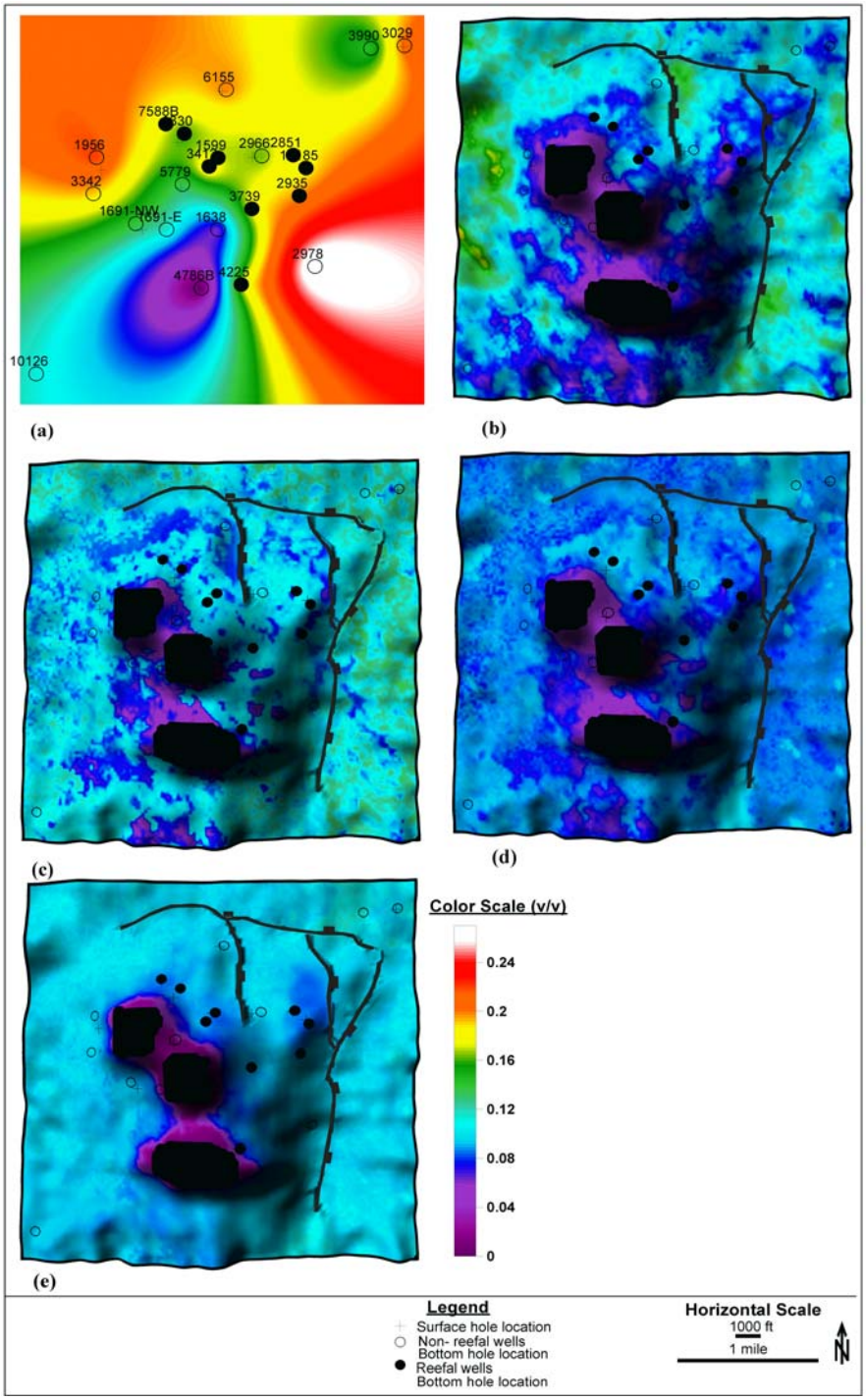

Figure 71: Maps showing the maximum porosity for the Smackover Formation. a) based only on contouring of well data, b) MLR result, c) MLR trend-cascaded PNN result, d) conventional PNN result, e) MLFN result. Note how low these are compared to actual porosity values at well locations.

intervals are very thin. As a result, these zones are “lost” when the logs are converted to time and resampled at 2ms (same as seismic data) by the Hampson-Russell software. The relatively high velocity of the rocks in this area (velocity of the Smackover Formation approximately 19,000 ft/s) acts to decrease the resolution (wavelength = velocity/frequency).

- Sampling bias: Only 6 of the 22 wells in the study area were used because only these six wells could be adequately tied to the seismic data. These six wells did not capture the full range of porosity in the study area. For example, the well with the highest apparent porosity, 2978 (>27%) and that with the thickest porosity, 3739, were not used in the analysis. Accordingly, sampling bias could have affected the nature of the empirical relationships (MLR or neural networks) that were established between porosity and seismic attributes.
- Method of calculation: Because PhiH is calculated for the Smackover Formation, discrepancies in seismic picks (compare Figures 72a & b) or log picks are bound to introduce some degree of error in the calculated thickness maps. The base of the Smackover was not picked in some wells although it may have been present. Some other wells TD in the Smackover and so a true value of PhiH cannot be calculated for them.

Powers (1990) suggested that the distribution of porosity in the Smackover at Vocation Field resembles a ‘halo’, with non-productive wells in the supratidal deposits immediately surrounding paleohighs; productive wells spanning the lagoonal to supratidal areas, and more non-productive wells in the deeper basin away from paleohighs. The trend-cascaded PNN thickness map most closely models this trend (Figure 69c).

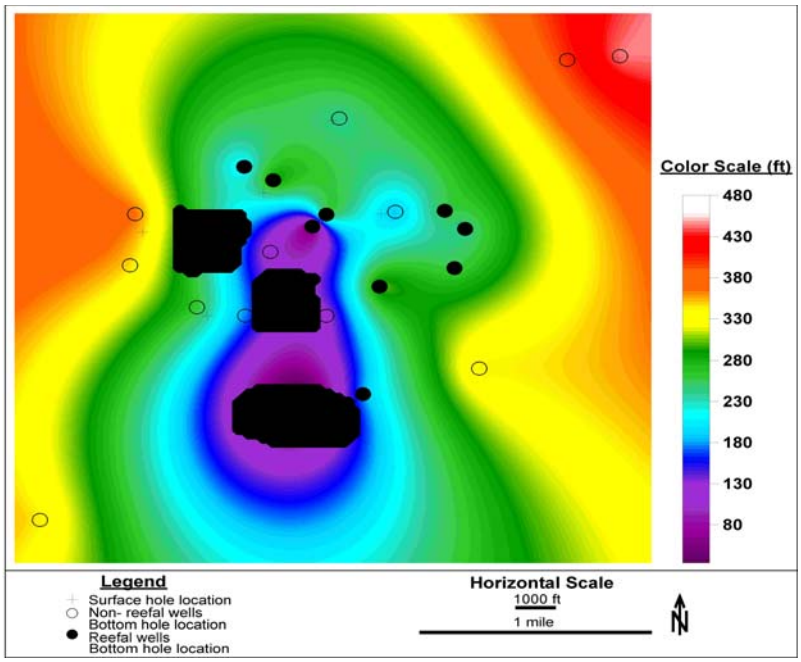

(a)

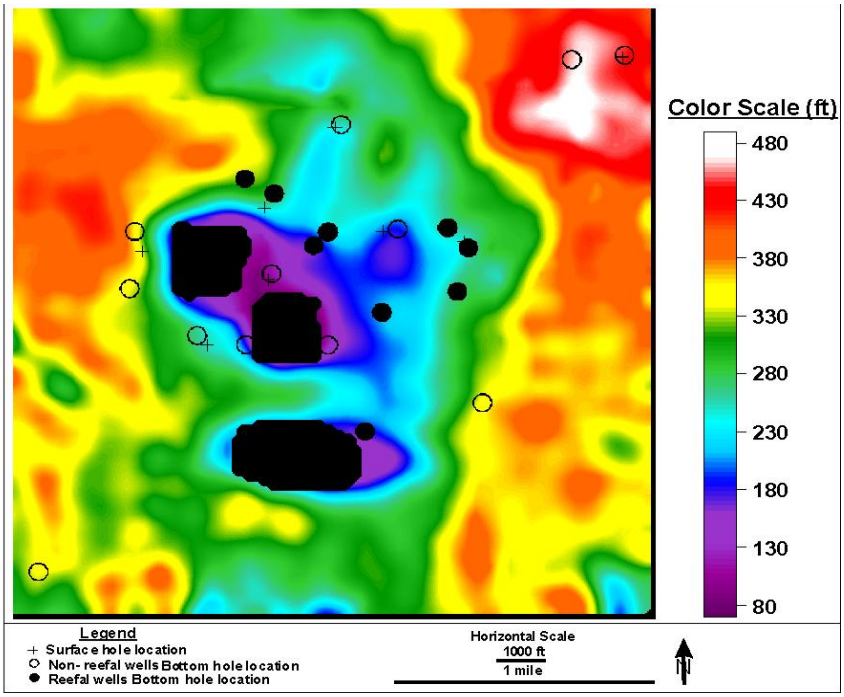

(b)

Figure 72: a) Well-based and b) 3-D seismic-based isopach maps for the Smackover. These thickness maps show that the Smackover Formation thickens away from paleohighs.

Slices at 2ms intervals into the Porous Smackover (microbial reef) show that reef growth in this field, and as in the Appleton Field, is governed primarily by water depth and the presence of paleostructure. These slices depict reef growth from near basinal depth, at lower sea levels, to progressively shallower water depths as sea level rose in the Oxfordian (10 ms to 0 ms). This trend is most observed at wells 3739 and 11185 that are structurally lowest and highest respectively (Figure 73). Furthermore, well 11185 is presently the only producing well at the Vocation Field (Mancini, 2002) due its location on the crest of low relief structure, high porosity thickness, and being surrounded by thick porous intervals. Reef growth and porosity development in the Smackover at Vocation Field is further highlighted by W-E transects through both the seismic and PNN trend-cascaded porosity volume, which also show the presence of shoal-derived porosity in the upper Smackover directly beneath the Buckner/Smackover horizon and microbial reefs flanking the paleohighs (e.g., Figure 74).

The relationships seen between zones of high porosity and faults in all thickness maps might indicate that faults served as conduits for dolomitizing fluids (Figures 69 and 71). Although none of the wells used in the Emerge analysis penetrate these areas, the 2978 well, which has the highest porosity of the wells available to us, is in or adjacent to one of these zones (Figures 69 and 71). More significantly, this well has no reefal facies (Table 5) and so porosity must not be associated with this primary depositional facies. Hydrothermal dolomitization, which produced porosity and permeability in tight basinal limestones of units like the Trenton-Black River interval of the Appalachian Basin, could be present in this area. Whatever its origin, we consider the presence of high porosity in the 2978 well as supporting the attribute-based porosity prediction.

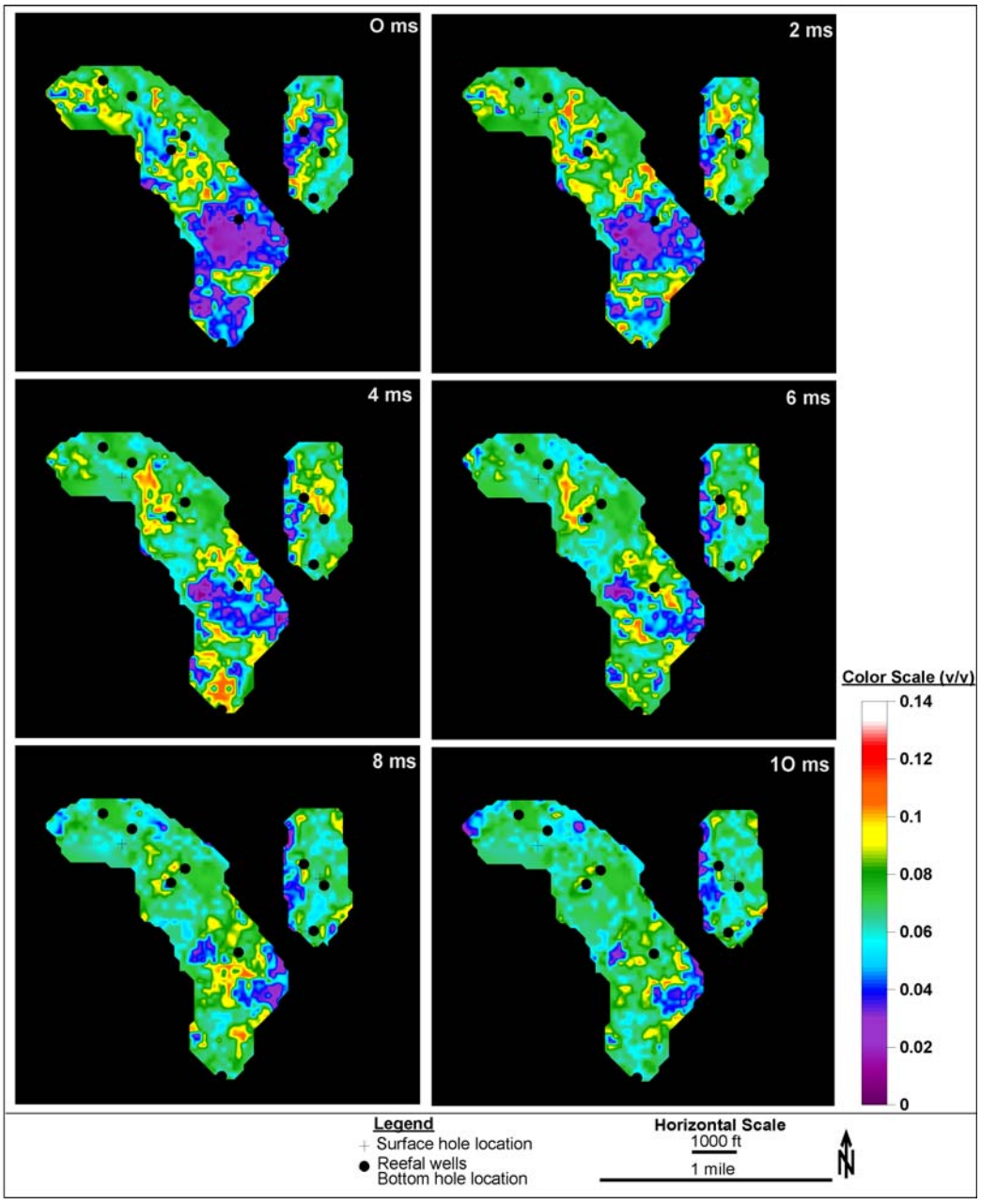

Figure 73: Slices through the porosity volume (porosity values are in decimals, v/v), starting at the porous Smackover pick. Porosity above this pick was attributed to shoal grainstone facies, which constitute the other major reservoir facies in the Vocation and Appleton Fields. The overall distribution of porosity in this interval is intricately related to structure (see Figure 61b), which we have attributed primarily to conditions related to reef growth. See Figure 57 for well permit numbers.

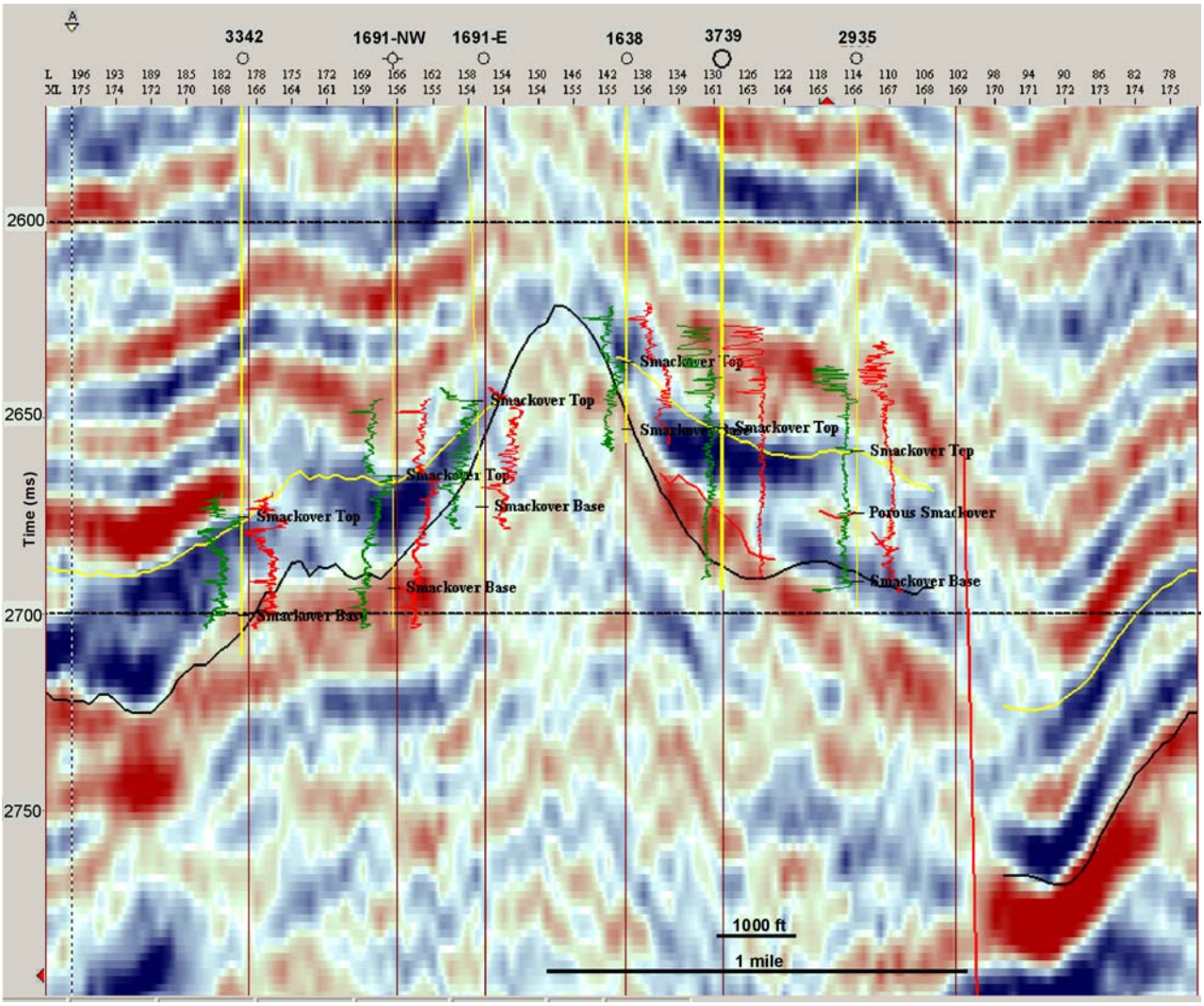
3342
1691-NW
1691-E
1638
3739
2935
2600
2650
2700
2750
Time (ms)
Smackover Top
Smackover Base
Porous Smackover
1000 ft
1 mile

(a)

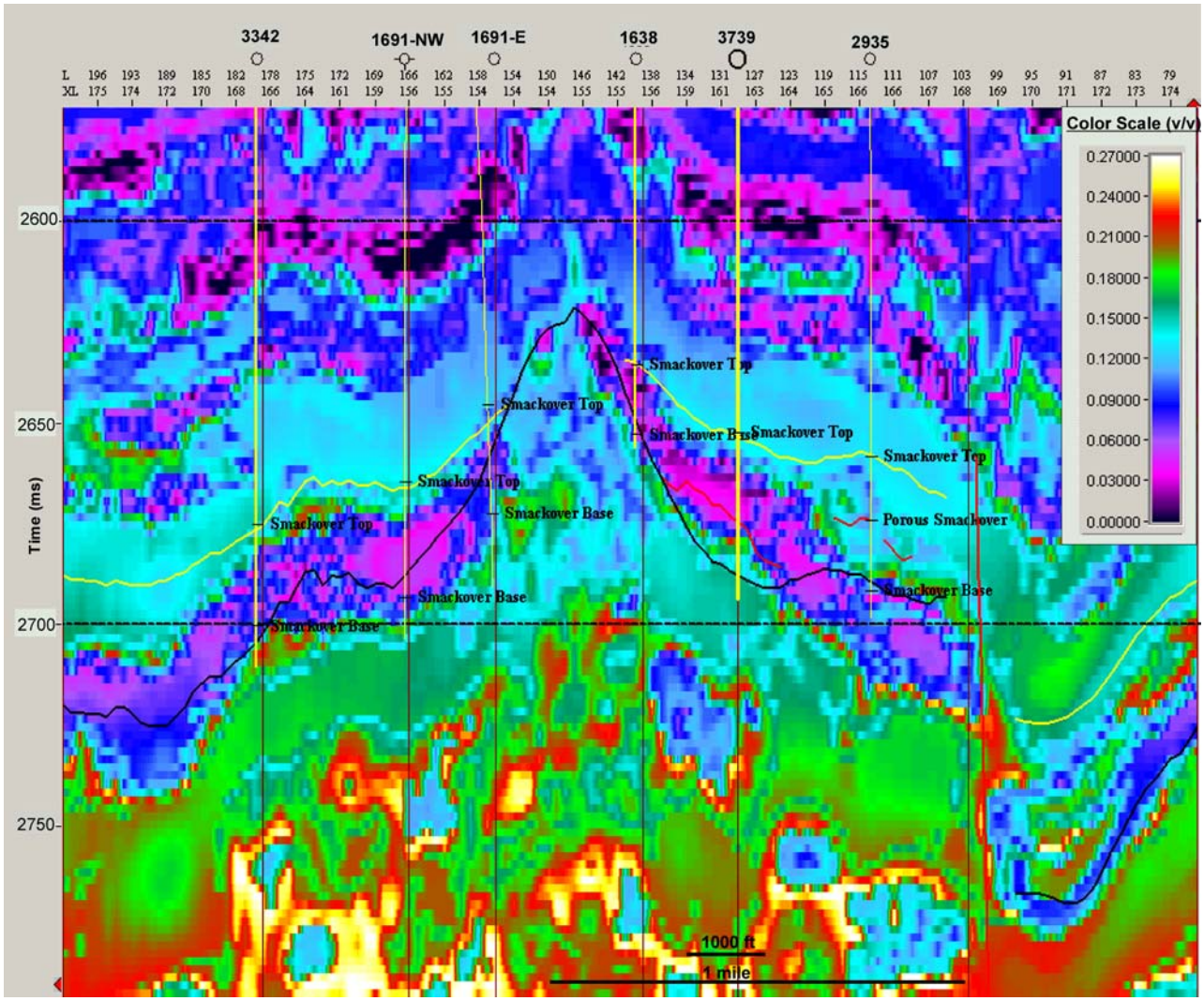

(b)

Figure 74: W-E transects across Vocation Field (A-A'). a) Original amplitude data shows horizon picks and seismic character of the mapped formations (red = trough, blue = peak). Note location of porous (reef) Smackover on flanks of paleostructure. b) Section through the MLR trend-cascaded PNN porosity volume shows a preference for higher porosities (hot colors) to be on the seaward flanks of structure, and also around faults. High porosity directly below the Buckner/Smackover pick is attributed to the shoal grainstone facies. Note porosity predictions are valid only within the Smackover Formation. Transect location shown in Figure 61a.

Petrophysical Property Characterization.--The mapping and ranking of flow units in the reservoirs at Appleton and Vocation Fields have been done by Morgan and Ahr at Texas A&M. The work described below is from Morgan's (2003) thesis at Texas A&M University.

Flow units in the Smackover Formation at Vocation and Appleton Fields were identified, mapped, and ranked. Pore categories by origin, pore and pore throat geometries, pore-scale diagenetic history, and core-scale depositional attributes were logged using conventional petrographic and lithological methods and advanced techniques. Resulting data were combined with core descriptions, mercury-injection capillary pressure data, and wireline log data to produce flow unit maps at the field scale.

Appleton and Vocation Fields produce from grainstone buildups and microbial reefs. Specific microbial fabrics were found to have significant influence on pore facies and flow unit quality rankings and ultimately on reservoir quality in these fields. Microbial reefs are composed of five fabric categories and growth forms that reflect variations in water geochemistry, energy level, sedimentation rate and substrate type. They include Type I layered thrombolite with characteristic mm/cm-scale crypts, Type II reticulate and "chaotic" thrombolite, Type III dendroidal thrombolite, Type IV isolated stromatolitic crusts, and Type V oncoidal packstone/grainstone dominated by oncoids that grew on soft to firm substrates in high-energy conditions. Types I, II and III buildups are the most productive reservoirs. Of these, Type III thrombolite buildups contain the highest quality reservoir rocks, which consist of extensively dolomitized dendroidal fabrics that have well-connected intercrystalline dolomite and vuggy porosity. Types IV and V microbialites make poor reservoir rocks because Type IV fabrics are not conducive for communication throughout this facies, and Type V oncoidal facies exhibit isolated moldic and vuggy porosity with low to moderate permeability.

The correlation of median pore aperture size (MPA) (Tables 10 and 11) to mercury permeability (K) (Figure 75) is moderately strong ($R^2 = 0.91$). This correlation suggests that pore aperture size has a direct link to permeability distribution. One observation from Figure 75 is that reef and solution enhanced pore types tend to have larger pore apertures and higher permeability values. A second observation is that multiple pore types tend to increase pore throat size and permeability, suggesting that there may be more than one mechanism which controls pore throat size and permeability. Combining these observations, one can see that the pore type has significant impact on permeability distribution.

Table 10. Common pore type associations in the MICP sample set, with the average porosity and MPA.

Common pore type associations	Average sample porosities (%)	Average MPA (μm)
interparticle (IP), intraparticle (IPA)	9.65	14.9
interparticle, intraparticle, moldic (M)	7.2	30
interparticle, cement reduced intercrystalline (CRIC)	4.3	1.19
reef (R), solution enhanced intercrystalline (SEIC)	20.0	12.6
reef, solution enhanced interparticle (SEIP), moldic, solution enhanced intercrystalline	12.0	8.09
reef, intercrystalline, cement reduced intercrystalline	4.1	8. 39
reef, solution enhanced interparticle, solution enhanced intercrystalline, moldic, vuggy (V)	15.4	20.63

Table 11. MICP data set: plugs chosen for MICP and measurements.

Well permit #	Core depth	Pore types	Facies type	Hg median pore aperture (mm)	Hg % porosity	Hg permeability (md)
1599	13,987.0	IP, IPA, M	oolitic gs	30	7.2	210
2935	14,078.0	IP, CRIC	peloidal gs	1.19	4.3	0.396
3986	12,970.0	R, SEIP, SEIC, M, V	Type III reef	21.9	14.4	280
3986	12,999.0	R, SEIP, SEIC, M, V	Type II reef	26.10	15.1	410
3986	13,024.0	R, IC, CRIC	Type I reef	8.93	4.1	17.6
4633-B	12,948.0	R, SEIP, M, SEIC	Type III reef	8.09	12.0	44.8
4633-B	12,969.0	R, SEIC	Type I reef	12.6	20.0	196
4633-B	12,984.0	R, SEIP, SEIC, M, V	Type II reef	13.9	16.7	225
5779	13,946.0	IP, IPA	oolitic gs	14.9	9.65	86.7

The correlation of mercury (Hg) permeability (K) to core analysis (CA) permeability (Fig. 76), shows a moderate correlation ($R^2 = 0.62$). The difference in correlation values likely is due

to the difference in data sampling since the core analysis is taken at one point every half foot and the mercury derived sample is from plugs at exact depths selected from thin section observations. Since there is a higher variability in the core analysis permeability values that were sampled, a range of permeability values within a two-foot interval of the mercury-injection capillary pressure (MICP) data depth is shown in the graph.

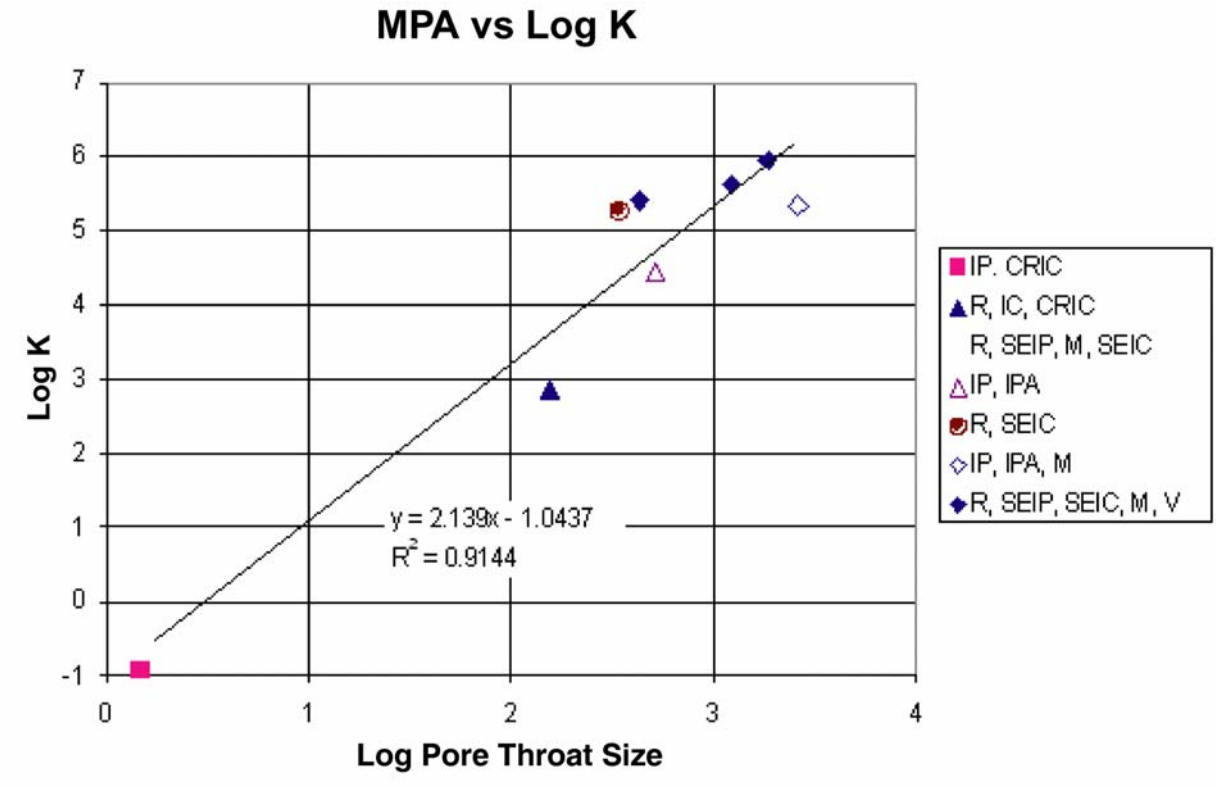

Figure 75. Comparison of median pore aperture size (MPA) and permeability (K).

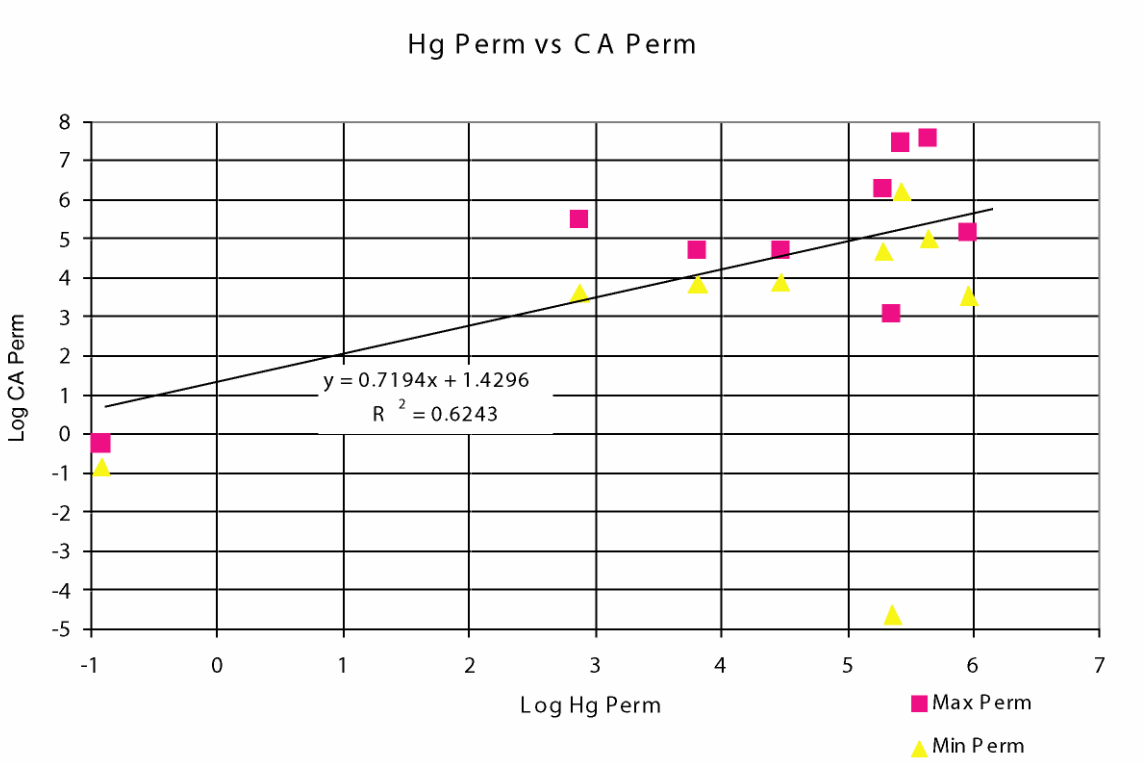

Figure 76. Comparison of mercury derived (Hg) permeability and core analysis (CA) derived permeability. It should be noted that there are two core analysis data points per mercury derived point to account for variability encountered in the interval sampled.

Core analysis porosity and mercury derived porosity was correlated (Fig. 77). This correlation had a moderate correspondence, not quite as strong as the permeability data. The correlation coefficient is due to the difference in sampling intervals.

Results of the MICP data and the corresponding pore types are shown in Table 10. Rocks that contained a combination of reef, solution enhanced interparticle, solution enhanced intercrystalline, moldic and vuggy porosities had the highest reservoir porosities, followed closely by those which also had a combination of some of these types but lacking the solution enhanced interparticle and vuggy porosity. The rocks with the lowest porosities and MPA values contained more than one pore type, but included cement reduced intercrystalline porosity. This observation suggests that porosity and pore throat size decrease as cement forms in the pore space.

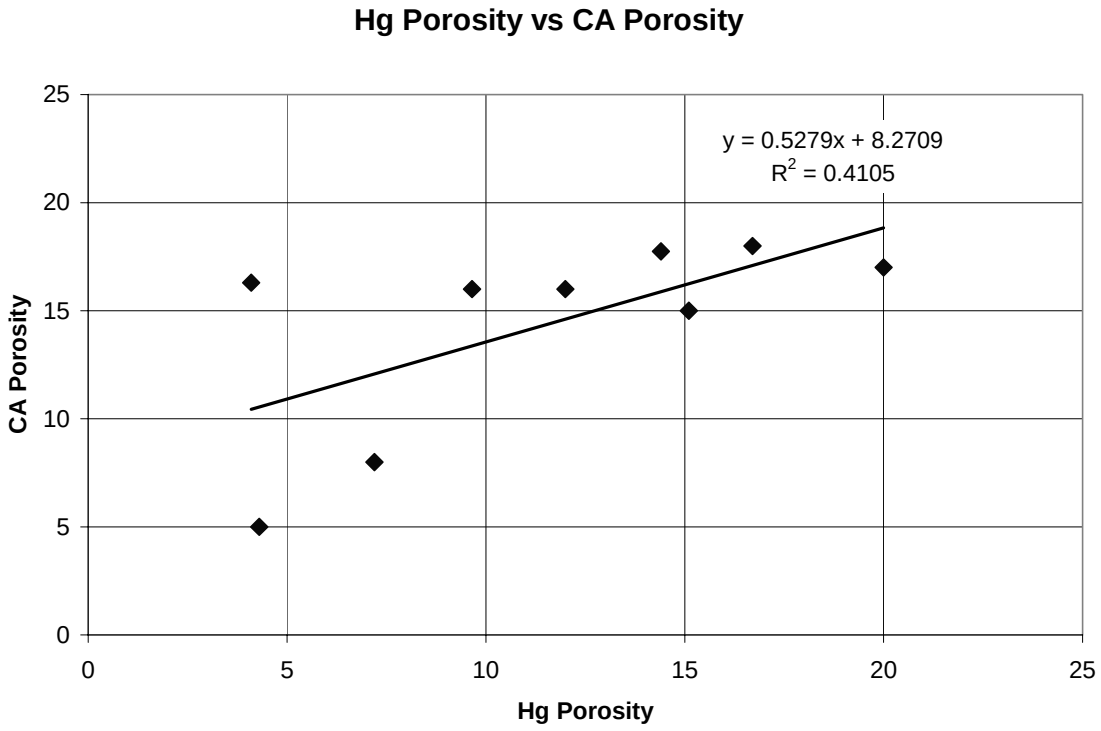

Figure 77. Comparison of mercury (Hg) derived porosity and core analysis (CA) derived porosity.

Using porosity as a predictor for MPA, permeability, or rock type would not be a robust method This is mainly due to the high degree of variability in porosity ranges that correspond to rock types and MPA. The main impact on the variability is the diagenetic overprint in the reservoir which contributes to the wide range of porosities that can be associated with a given MPA or rock type. In order to be able to use porosity as a predictor for MPA and rock type, more samples are required so that a range of porosities and their corresponding MPA and rock types can be established.

Porosity and permeability data from core analysis were compared to thin section descriptions to enable the correlation of petrophysical data with the petrologic information. Triaxial (x-y-z) plots were made to establish relationships between porosity-permeability (reservoir quality) and texture, pore types, and diagenetic attributes.

Diagenesis was observed to have had the greatest effect on reservoir quality. The main variable that effects permeability distributions was observed to be pore types in Figure 75. Pore types and porosity were controlled by lithology and grain types. The ranges of porosity and permeability that are associated with the various pore types are shown in Figures 78 and 79.

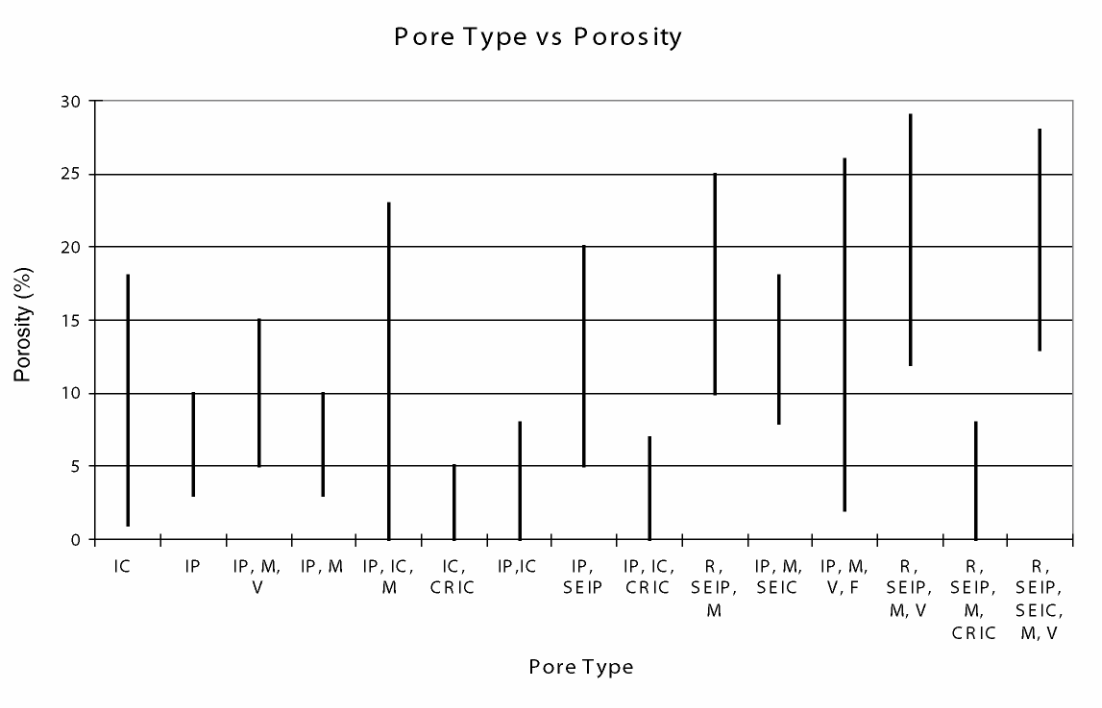

Figure 78. Graph of pore type versus porosity. It should be noted that no one pore type has a porosity range which is distinctive.

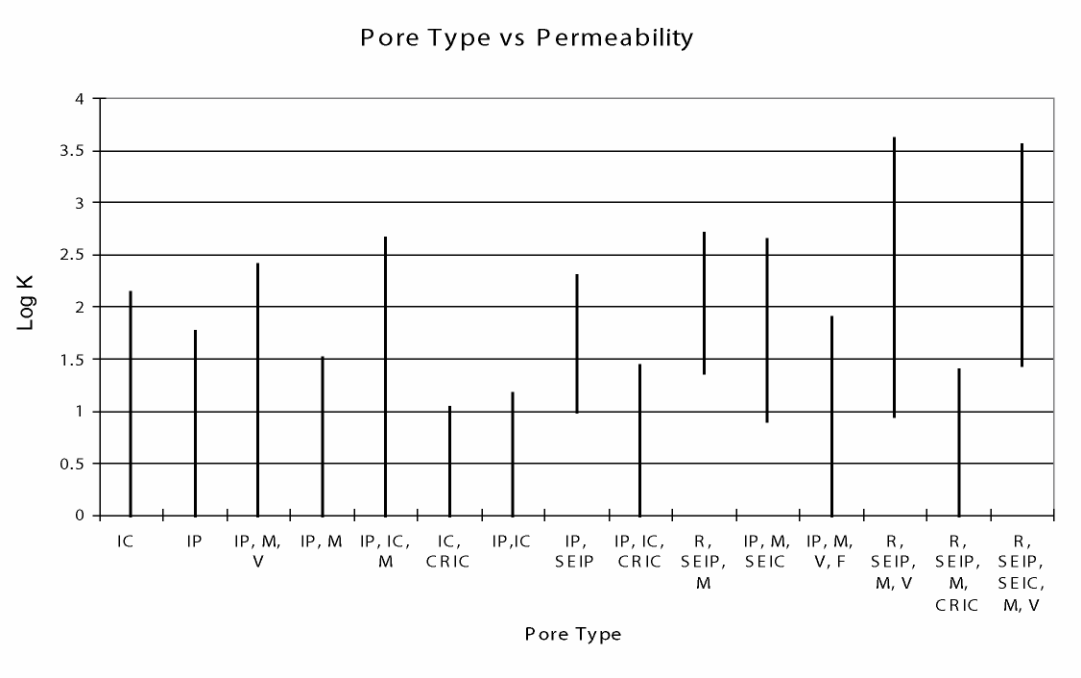

Figure 79. Graph of pore type versus permeability.

One of the advantages of having a set of data such as illustrated in Figures 78 and 79 is that trends can be identified where certain pore types are absent or present. For example, where the process of CRIC was active, porosity and permeability are greatly reduced even though other pore types in the same rock type may be a high-quality reservoir where the CRIC was not active. In some cases, the presence of moldic and vuggy porosity may increase the quality of the reservoir, but permeability may not be increased. A second benefit to graphing pore type versus porosity and permeability is that the graphs can be used as a "proxy" to predict porosity and permeability where no core analysis is available.

Reservoir quality rocks with intercrystalline dolomite porosity tend to be muddier rocks, such as mudstone and wackestone which are in the Vocation Field. The dominant grain type in these lithologies is peloids (if there are any visible grains). Typically there is little to no depositional porosity in these rocks. Thus, for these rocks to have reservoir quality, they must

undergo dissolution and diagenesis. Where these rocks were significantly dolomitized, porosities can be as high as 15 to 20%, with permeabilities of up to 180 md.

Porosity and permeability in grainier carbonates, such as packstone and grainstone, commonly have higher depositional porosity. Grainstone is dominantly oolitic, with some bioclast and oncoid grains. Packstone normally is composed of peloids and oncoids, with ooids as a minor component. These rocks have good depositional interparticle porosities with inter- and intraparticle porosity through dissolution. Moldic and vuggy porosity was also observed in the more diagenetically altered rocks, which exhibited higher porosity. Reservoir grade grainstone and packstone can have porosities that range from 10 to 23% with permeabilities that range from 1 to 620 md.

In nearly all microbial reef rocks, well-interconnected intercrystalline dolomite and vuggy porosity preferentially occurs in association with microbial growth patterns. In general, the porosity and permeability in surrounding mudstone-wackestone are of a high quality because the original lime mud was more densely packed than the microbialite. The thrombolite fabrics (Types I, II, III) produce well connected, intercrystalline porosity. Growth forms also factor into the ultimate reservoir quality. Type I (layered thrombolite) produce medium to coarse intercrystalline dolomite porosity. Core porosity values for Type I microbialite from wells at Appleton and Vocation Fields range from 6 to 23% and permeability values range from 1 to 2000 md. Although these values appear high, the degree of interconnectivity of pores depends on the microbial growth fabric associated with individual horizontal laminae. Individual laminae may have lateral permeability, but this microbial type is only of fair reservoir quality because of poor vertical connectivity. Type II (reticulate-“chaotic”) thrombolite boundstone also produces medium to coarse intercrystalline dolomite porosity, but pore interconnectivity is random, which is a reflection of the original “chaotic” growth pattern of the microbialite. Porosity values for

Type II thrombolites range from 3 to 23% and permeability values range from 0 to 1060 md. There are good reservoir quality zones in Type II buildups, but a predictable pattern is not readily distinguishable. Type III dendroidal thrombolites are characterized by medium to coarse intercrystalline dolomite porosity and vuggy porosity. Porosity values for Type III thrombolites range from 4 to 30% and permeability values range from 0 to 4000 md. The pore interconnectivity in these buildups is very good in both lateral and vertical dimensions because of the branching growth pattern of Type III microbialite. These buildups have the highest reservoir quality of all five types; but as stated earlier, Type III thrombolite buildups only develop on low relief basement structures (e.g., Appleton Field area).

Contoured “slice maps” of averaged porosity values from core analysis were constructed for each 10-foot stratigraphic interval in the Smackover Formation (Figures 80-91). Where core analysis was not present, porosity values were calculated from NPHI and DPHI logs. Permeability values corresponding to the porosity values were also averaged and mapped in the same fashion (Figure 92-103). These maps were then overlain in corresponding depth intervals, and were combined into ranked pairs.

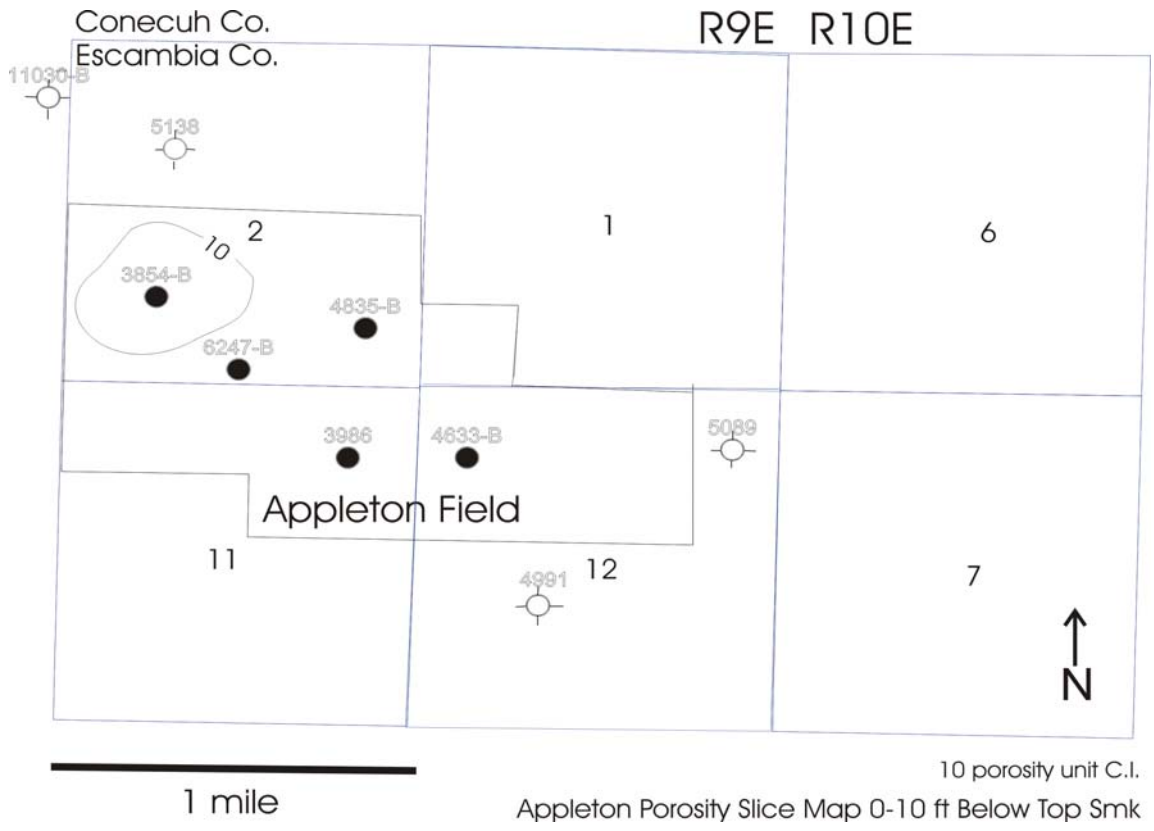

Figure 80. Appleton Porosity Slice Map 0 to 10 ft below Top of Smackover.

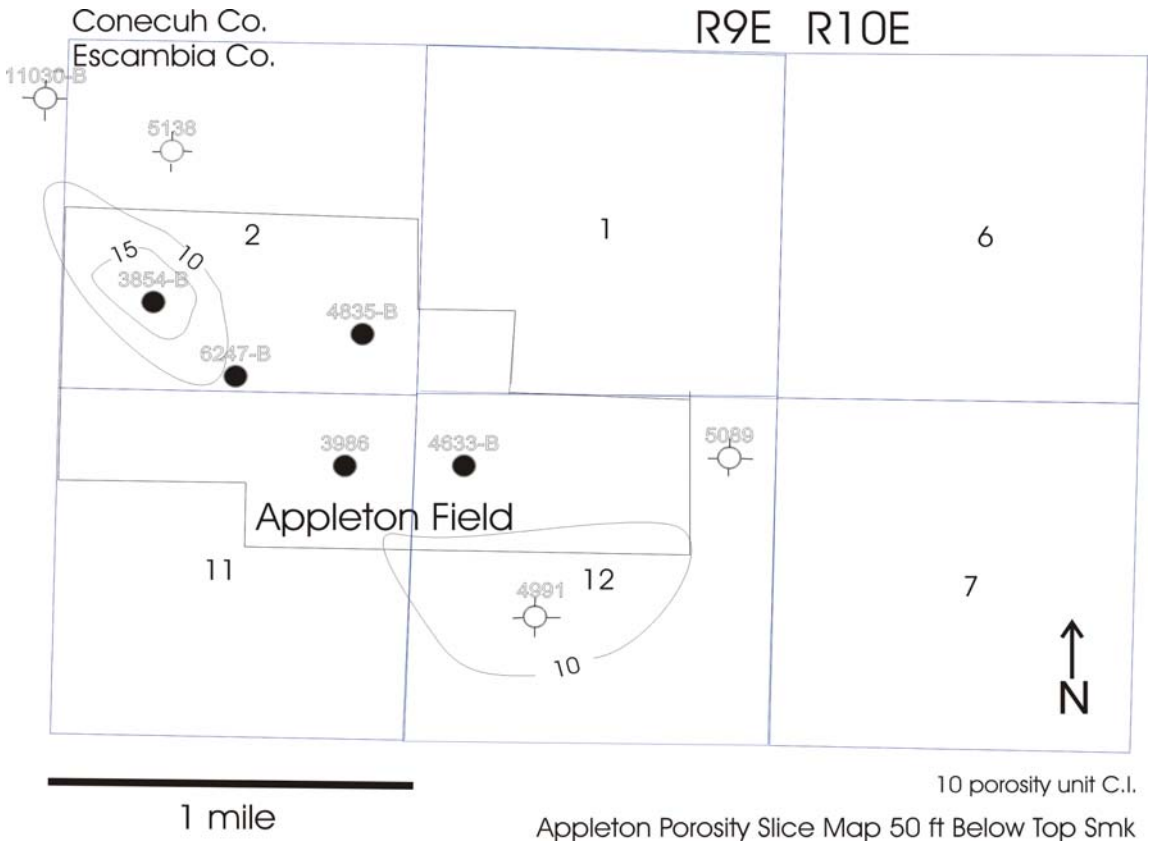

Figure 81. Appleton Porosity Slice Map 50 ft below Top of Smackover.

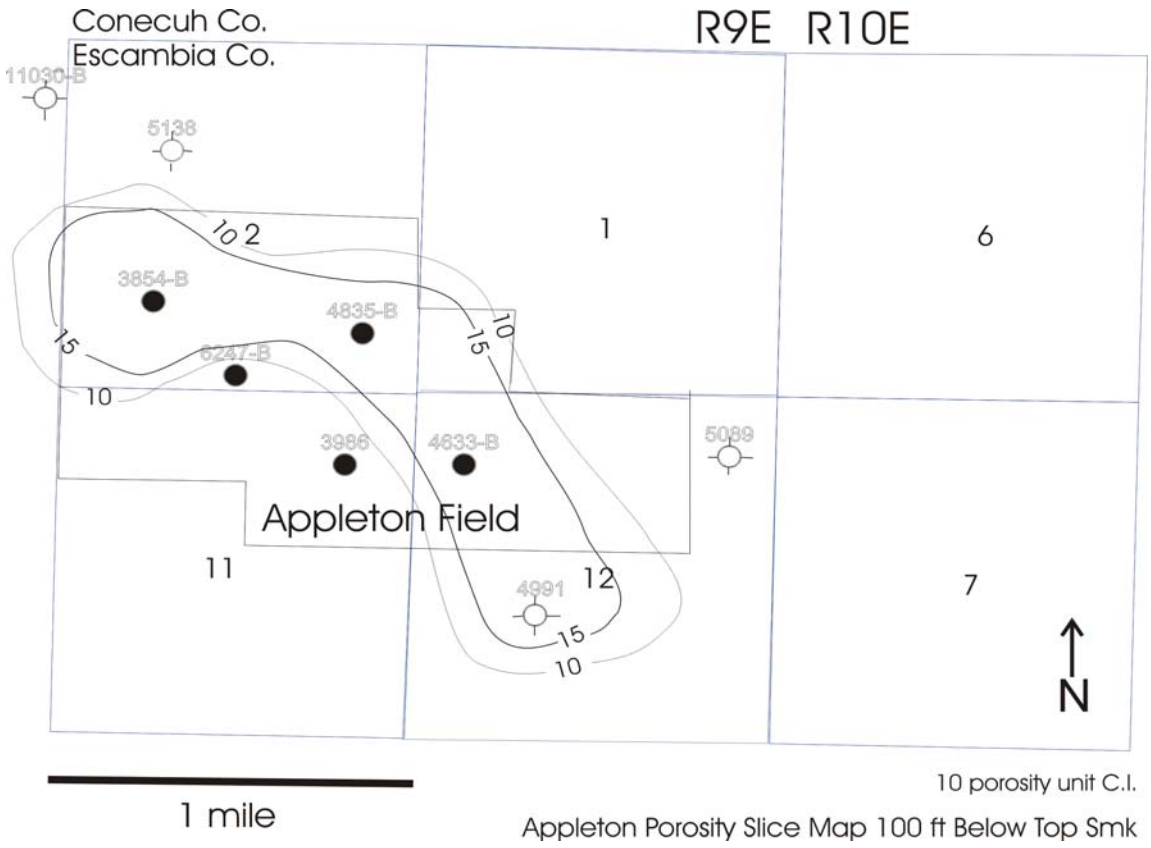

Figure 82. Appleton Porosity Slice Map 100 ft below Top of Smackover.

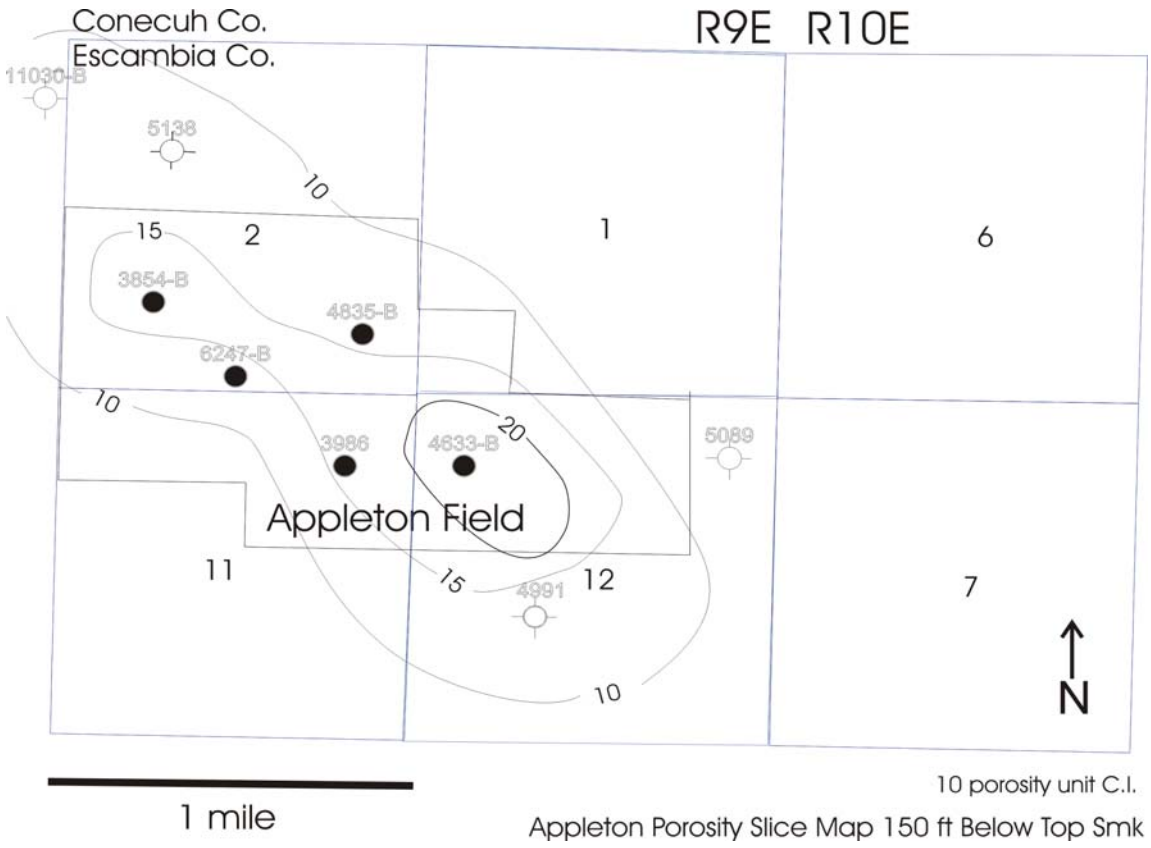

Figure 83. Appleton Porosity Slice Map 150 ft below Top of Smackover.

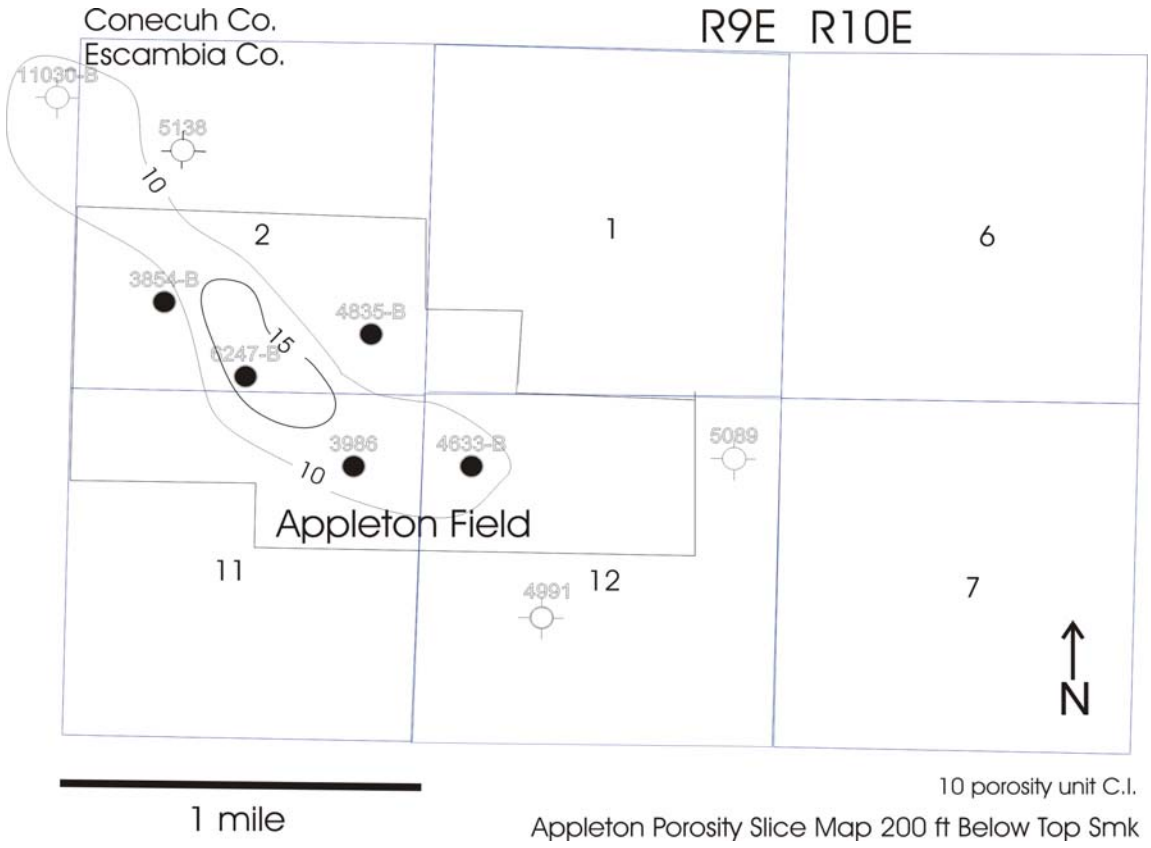

Figure 84. Appleton Porosity Slice Map 200 ft below Top of Smackover.

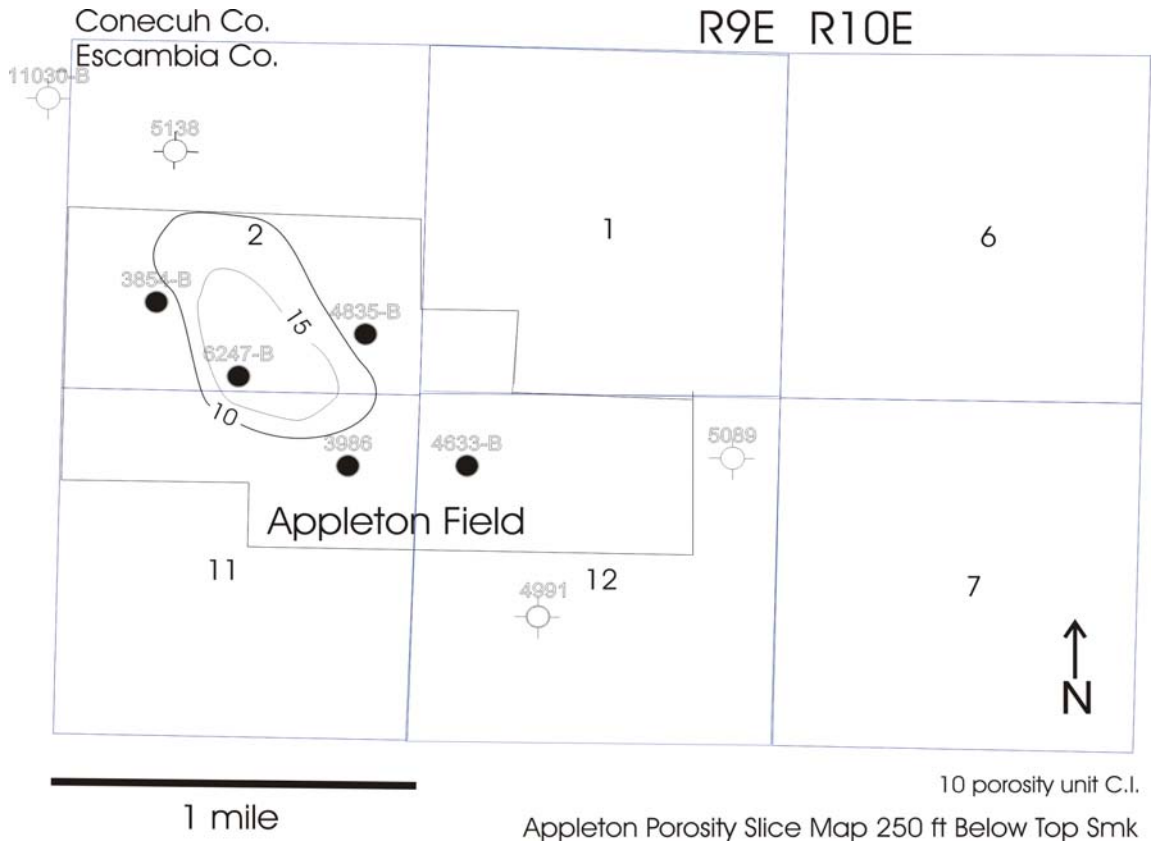

Figure 85. Appleton Porosity Slice Map 250 ft below Top of Smackover.

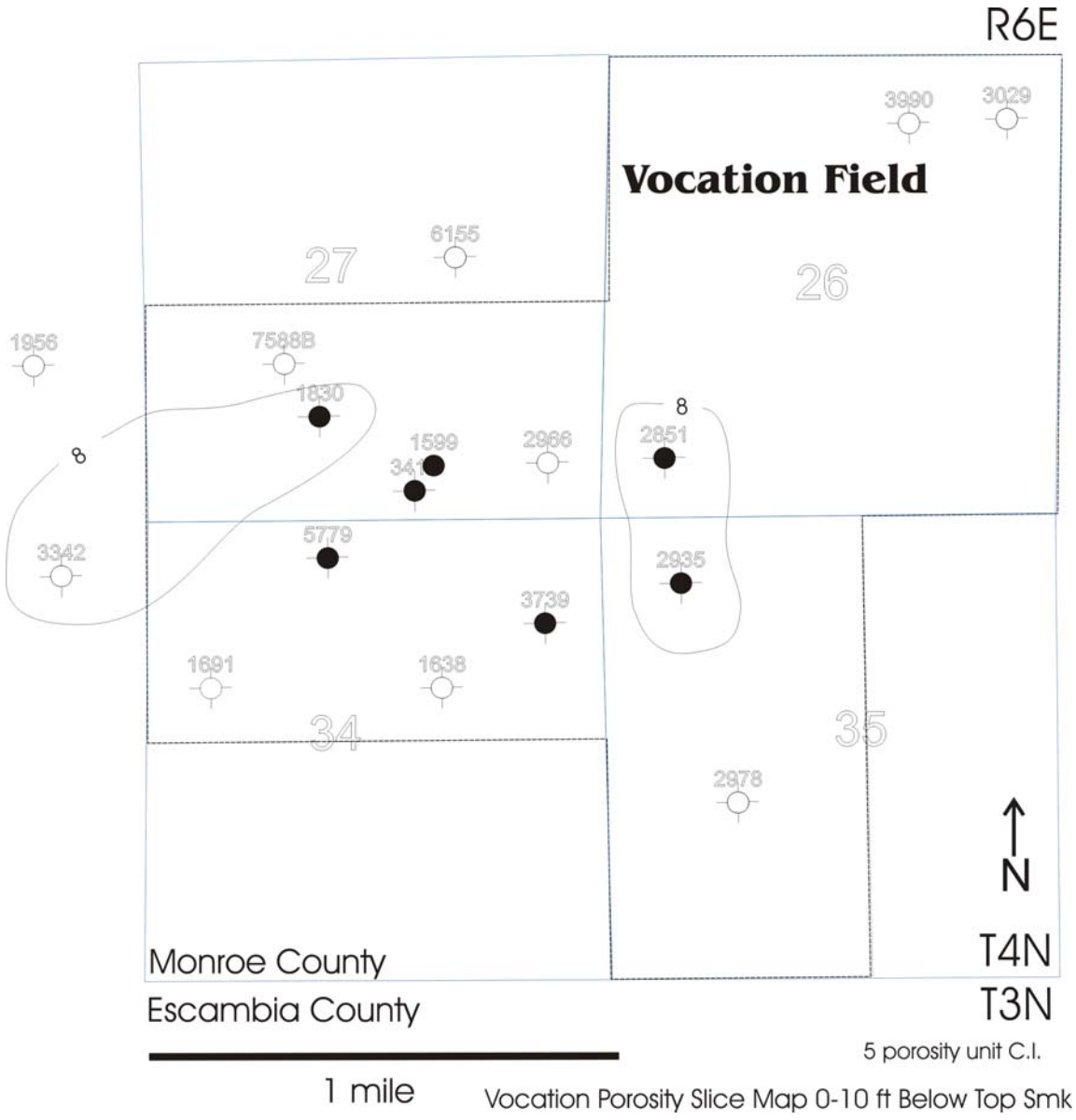

Figure 86. Vocation Porosity Slice Map 0-10 ft below Top of Smackover.

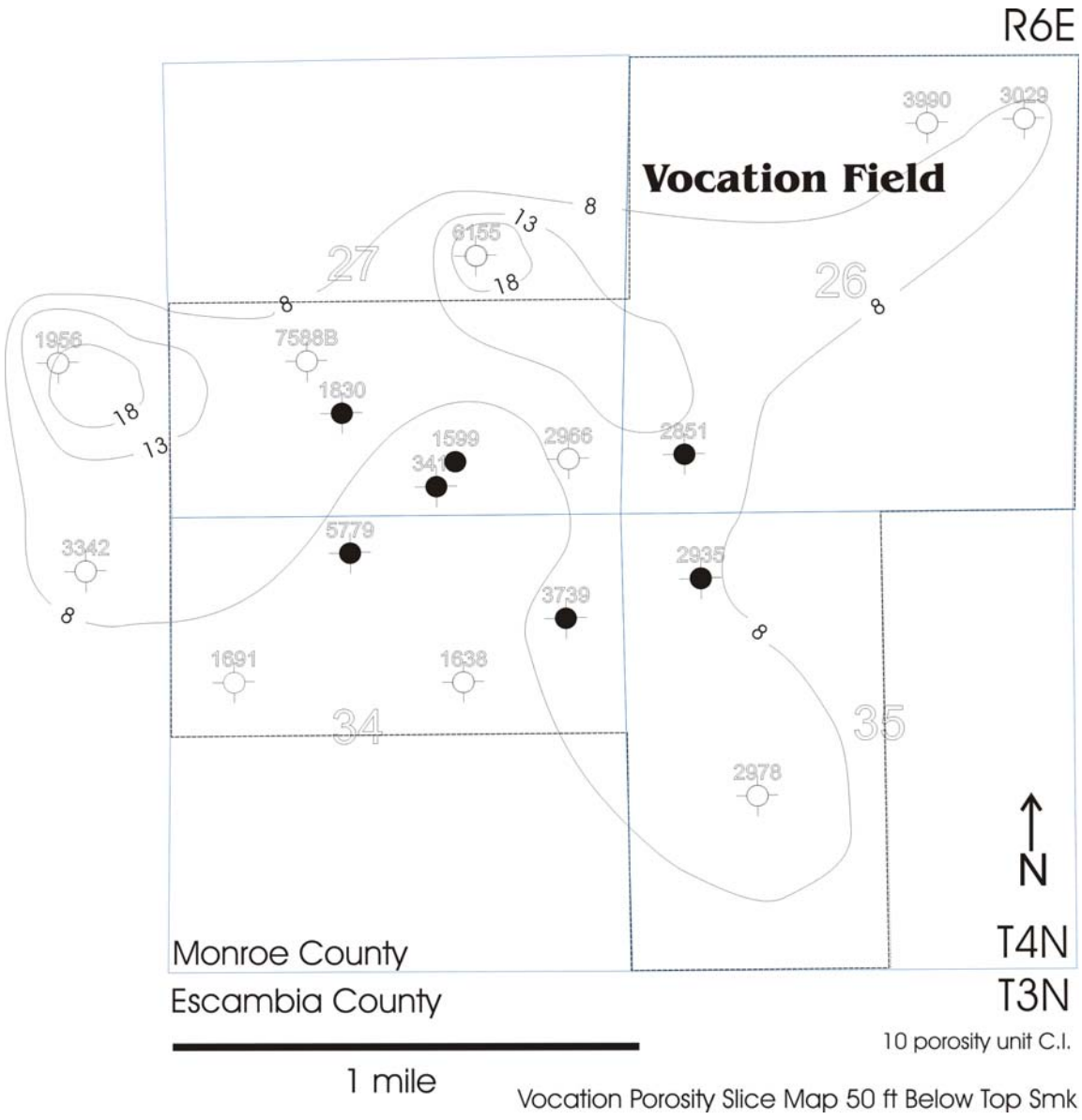

Figure 87. Vocation Porosity Slice Map 50 ft below Top of Smackover.

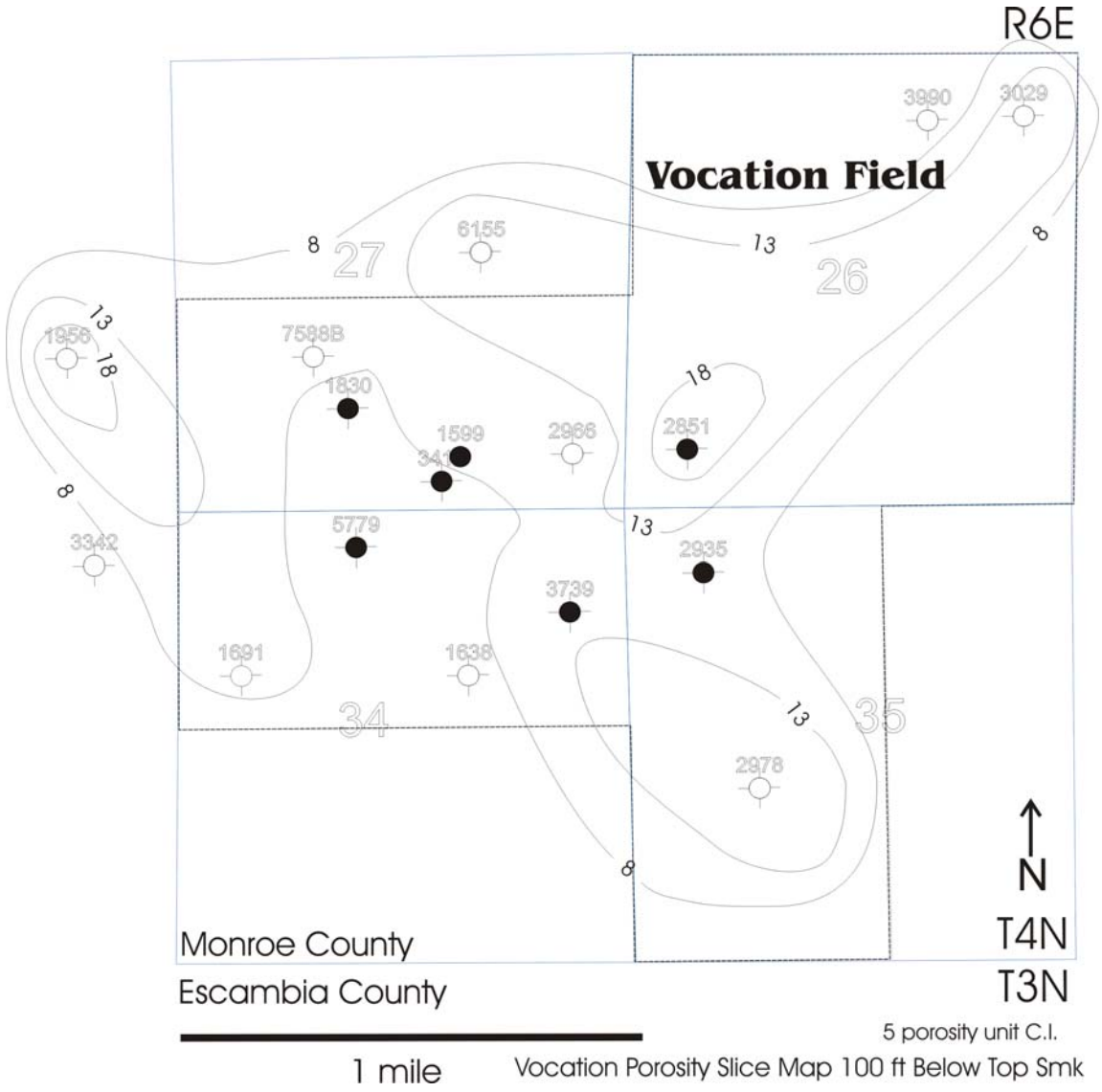

Figure 88. Vocation Porosity Slice Map 100 ft below Top of Smackover.

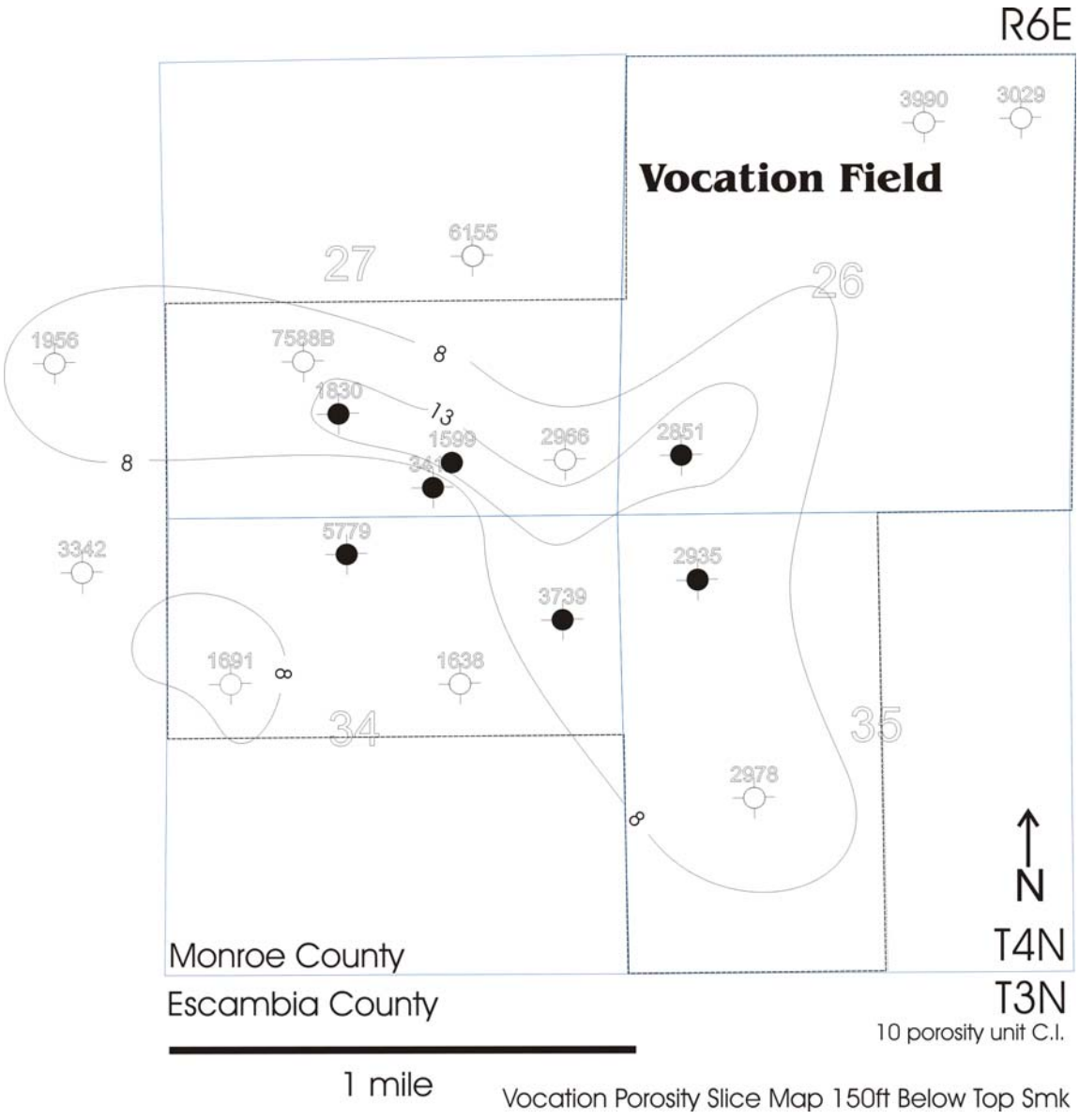

Figure 89. Vocation Porosity Slice Map 150 ft below Top of Smackover.

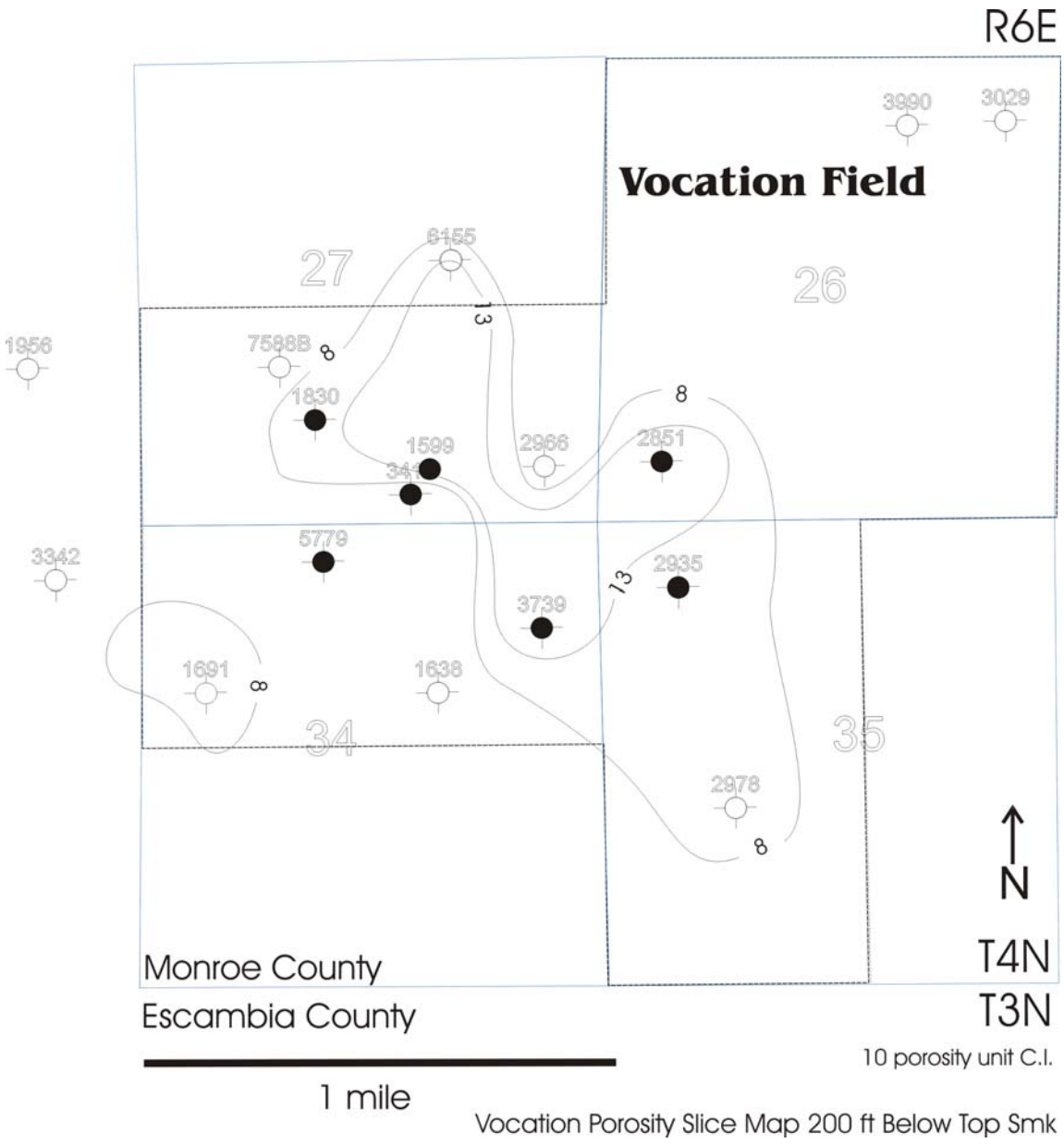

Figure 90. Vocation Porosity Slice Map 200 ft below Top of Smackover.

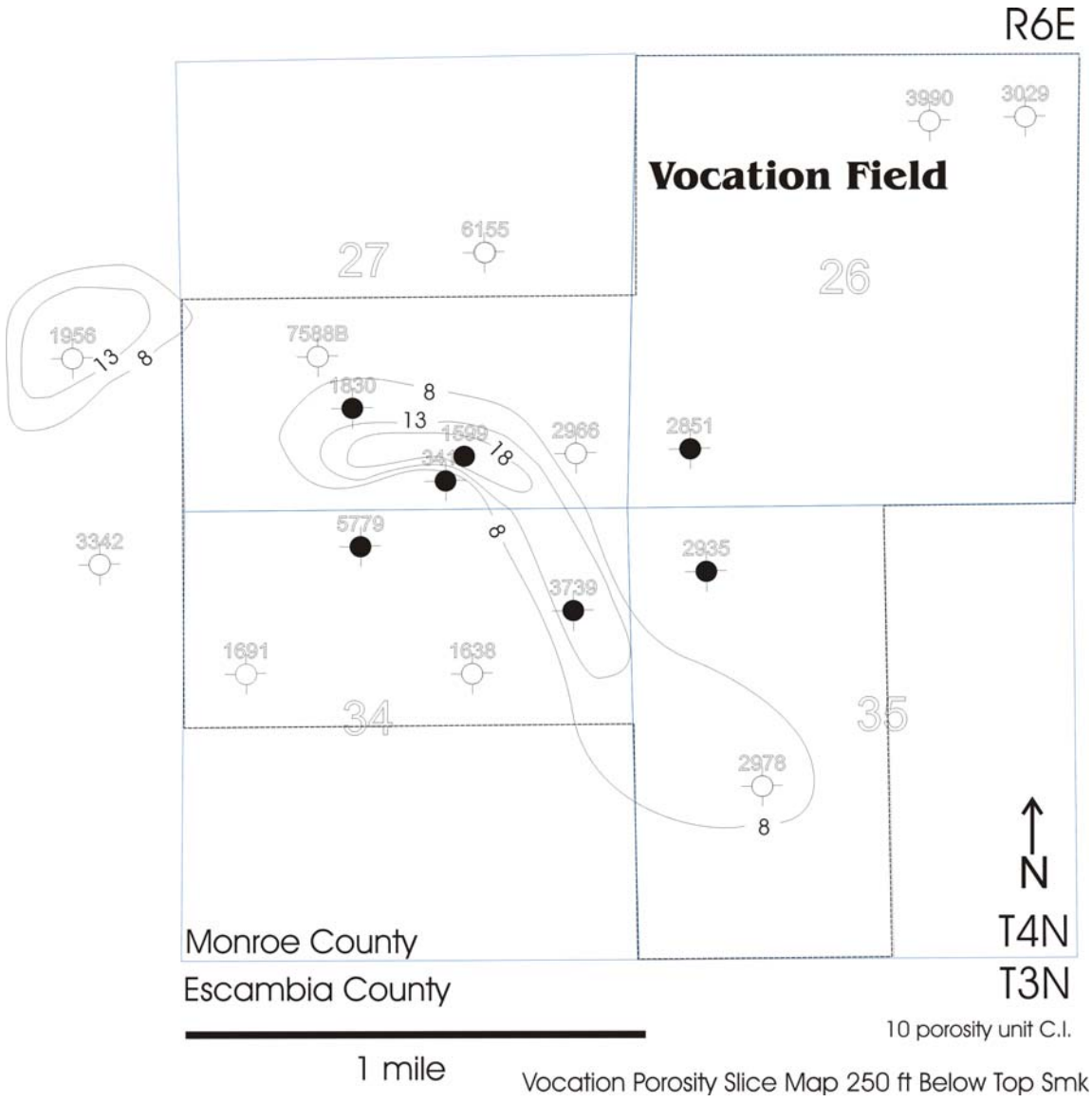

Figure 91. Vocation Porosity Slice Map 250 ft below Top of Smackover.

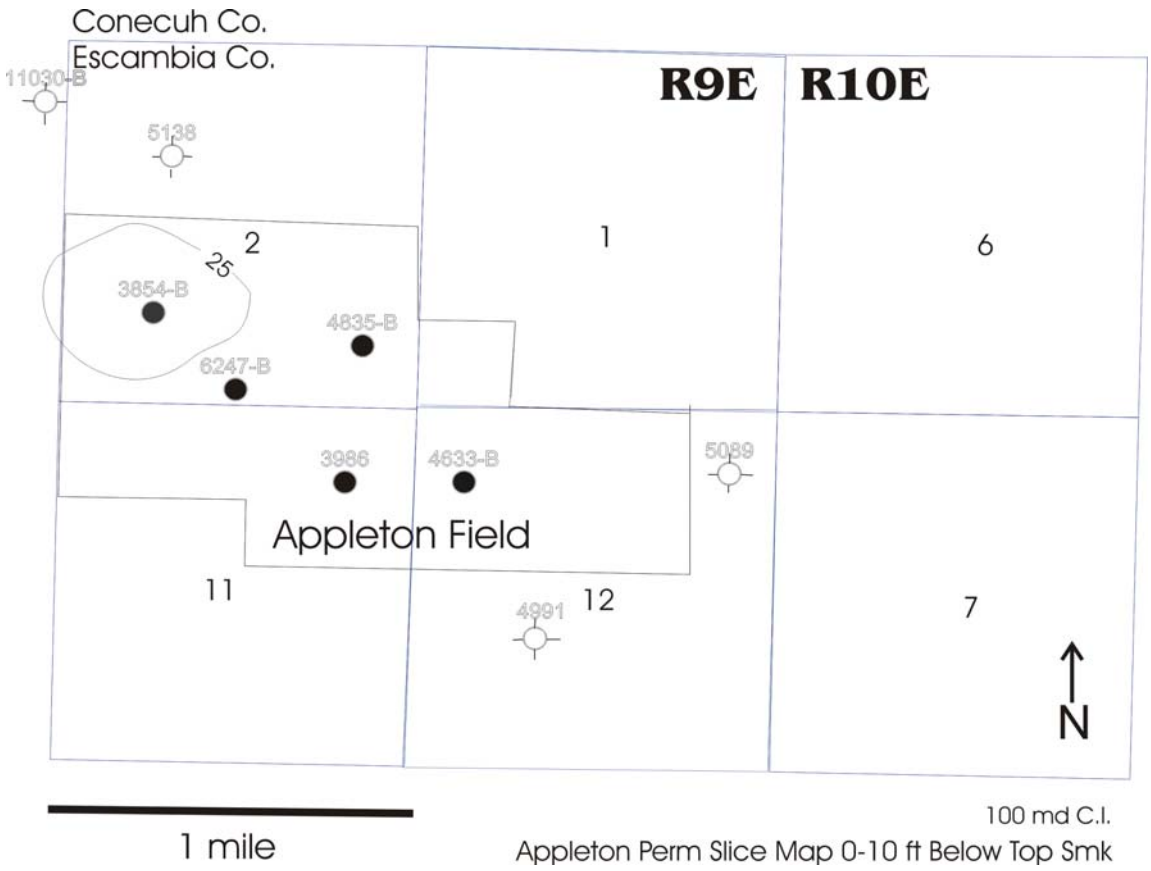

Figure 92. Appleton Permeability Slice Map 0-10 ft below Top of Smackover.

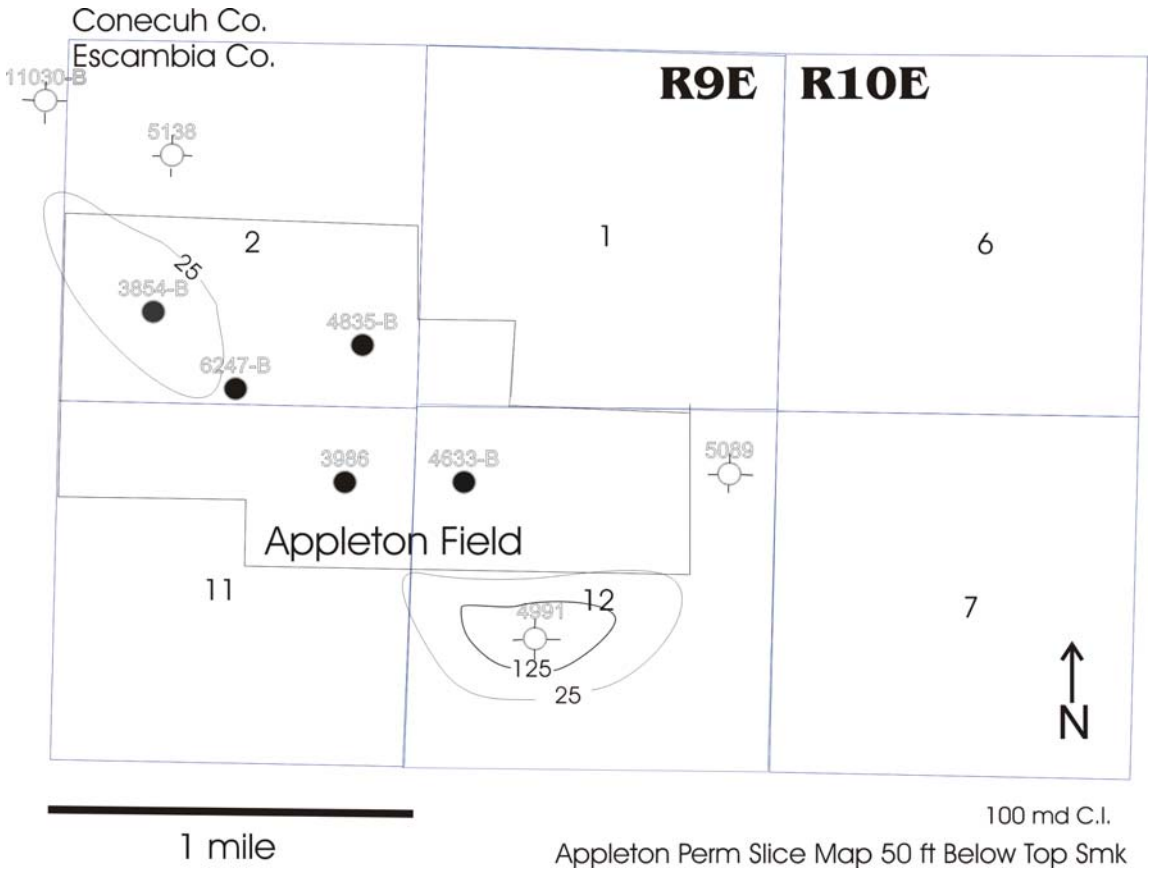

Figure 93. Appleton Permeability Slice Map 50 ft below Top of Smackover.

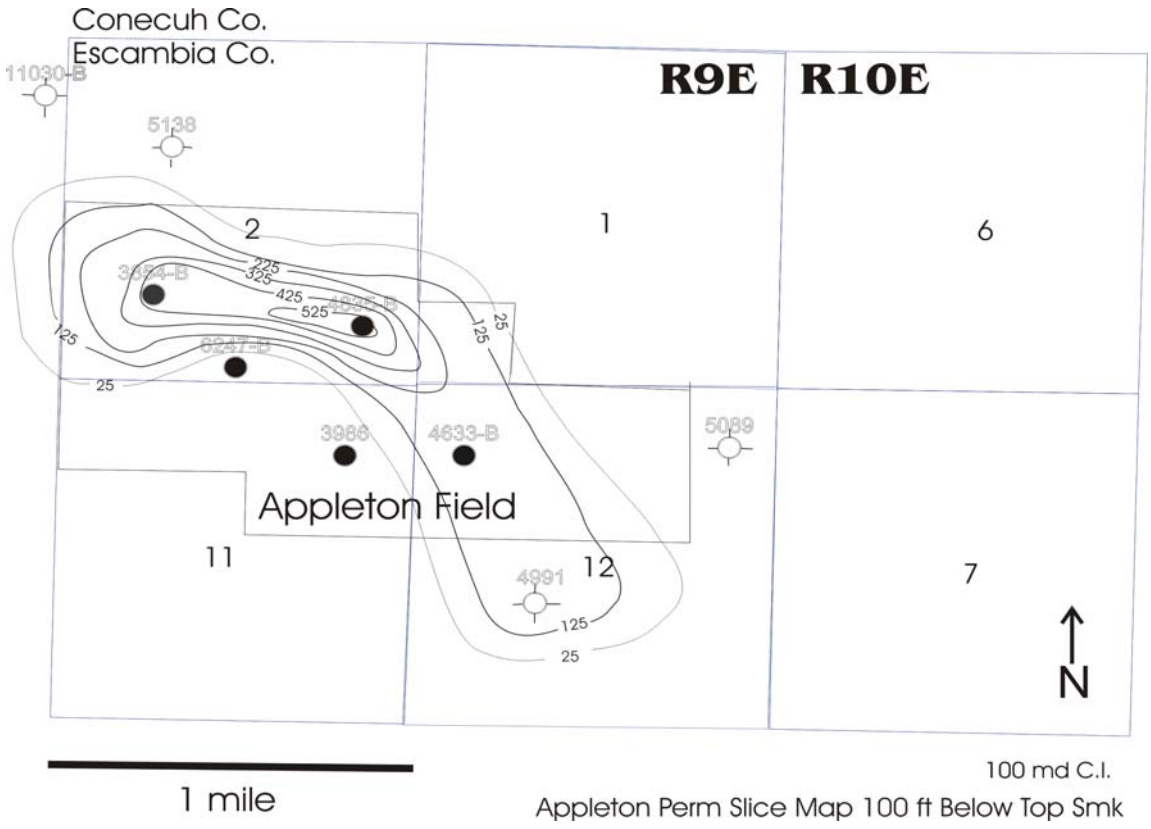

Figure 94. Appleton Permeability Slice Map 100 ft below Top of Smackover.

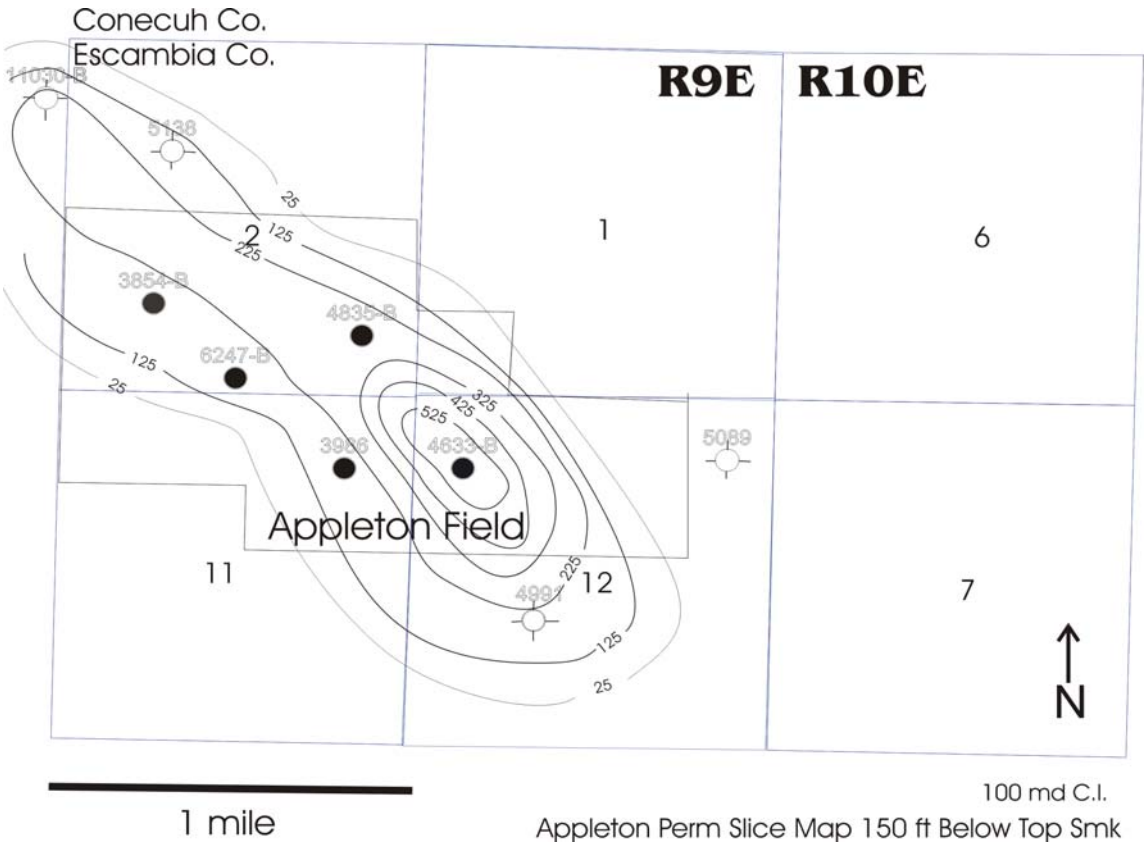

Figure 95. Appleton Permeability Slice Map 150 ft below Top of Smackover.

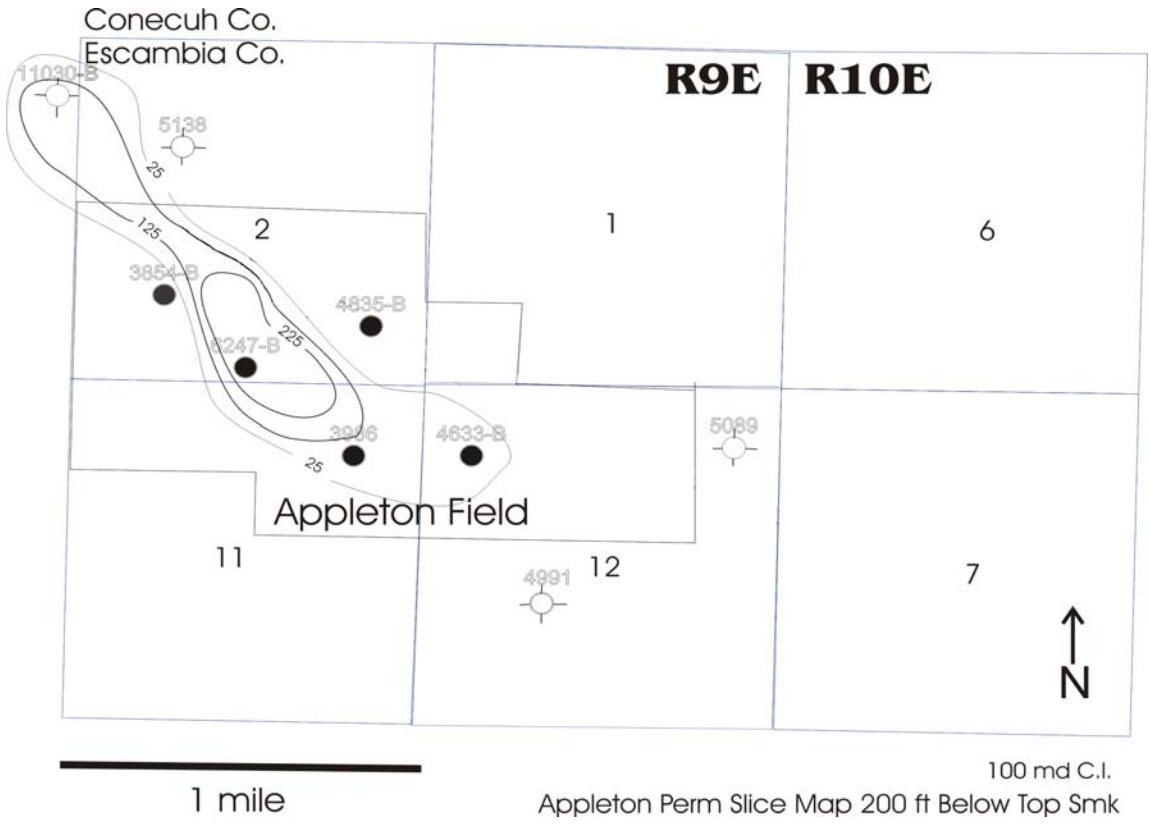

Figure 96. Appleton Permeability Slice Map 200 ft below Top of Smackover.

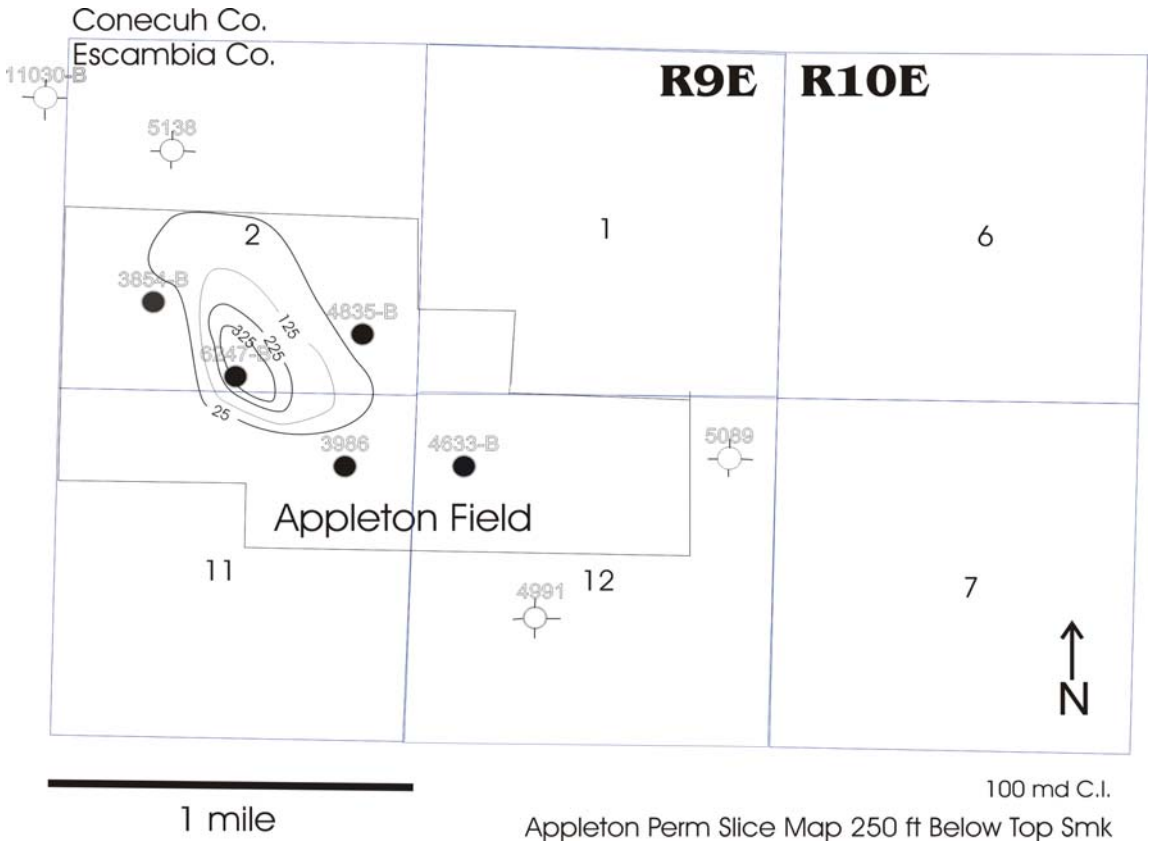

Figure 97. Appleton Permeability Slice Map 250 ft below Top of Smackover.

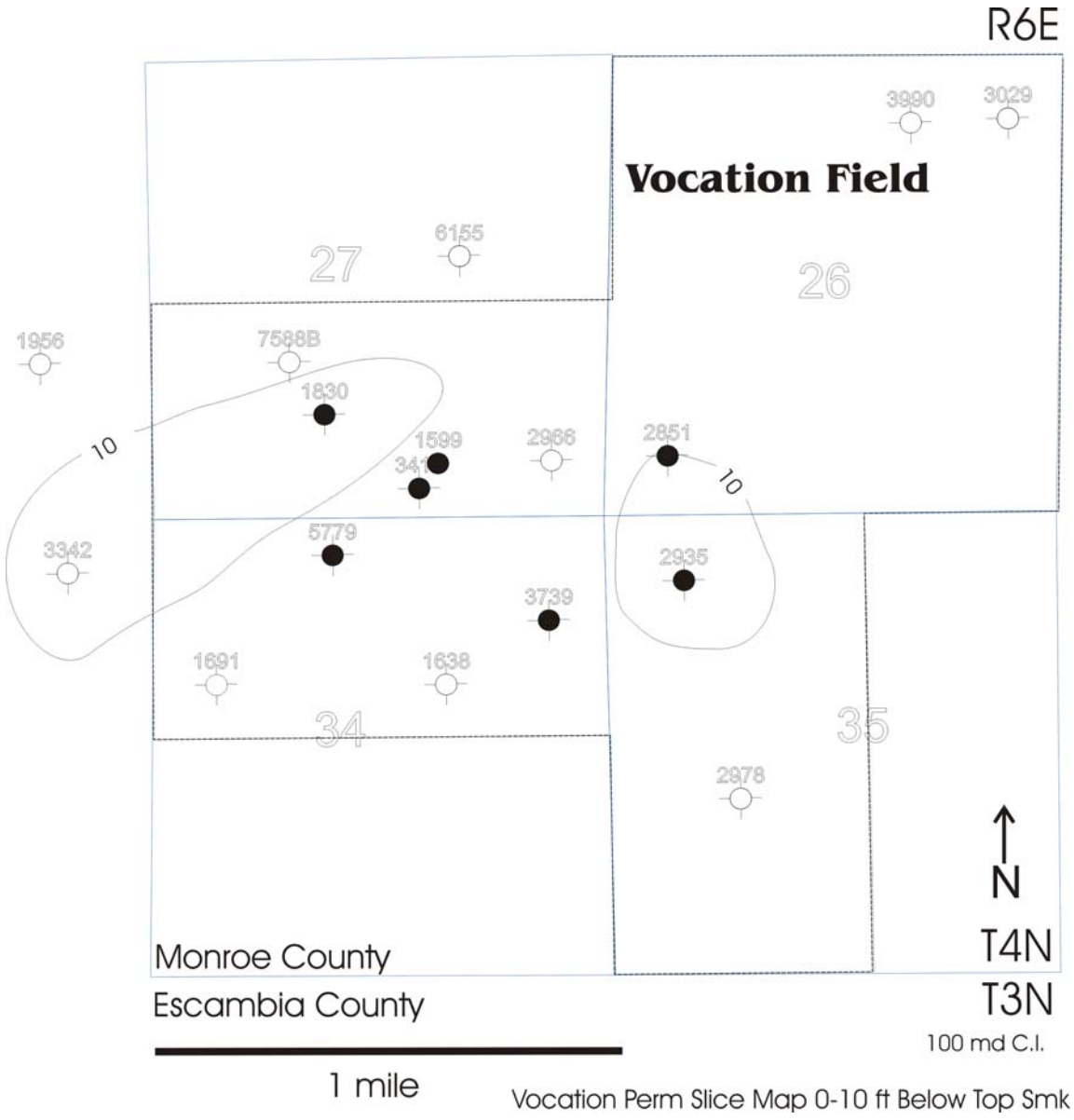

Figure 98. Vocation Permeability Slice Map 0-10 ft below Top of Smackover.

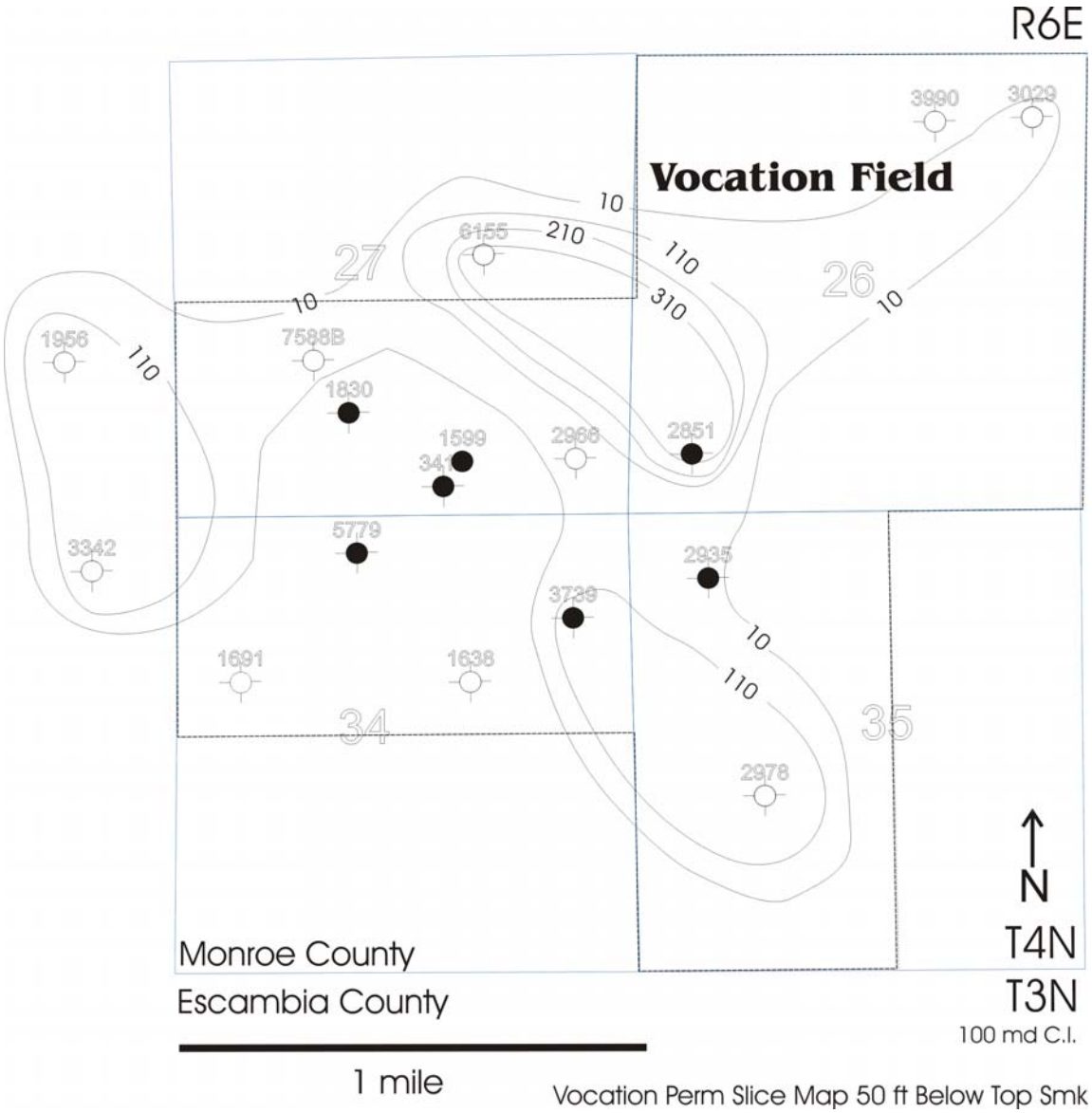

Figure 99. Vocation Permeability Slice Map 50 ft below Top of Smackover.

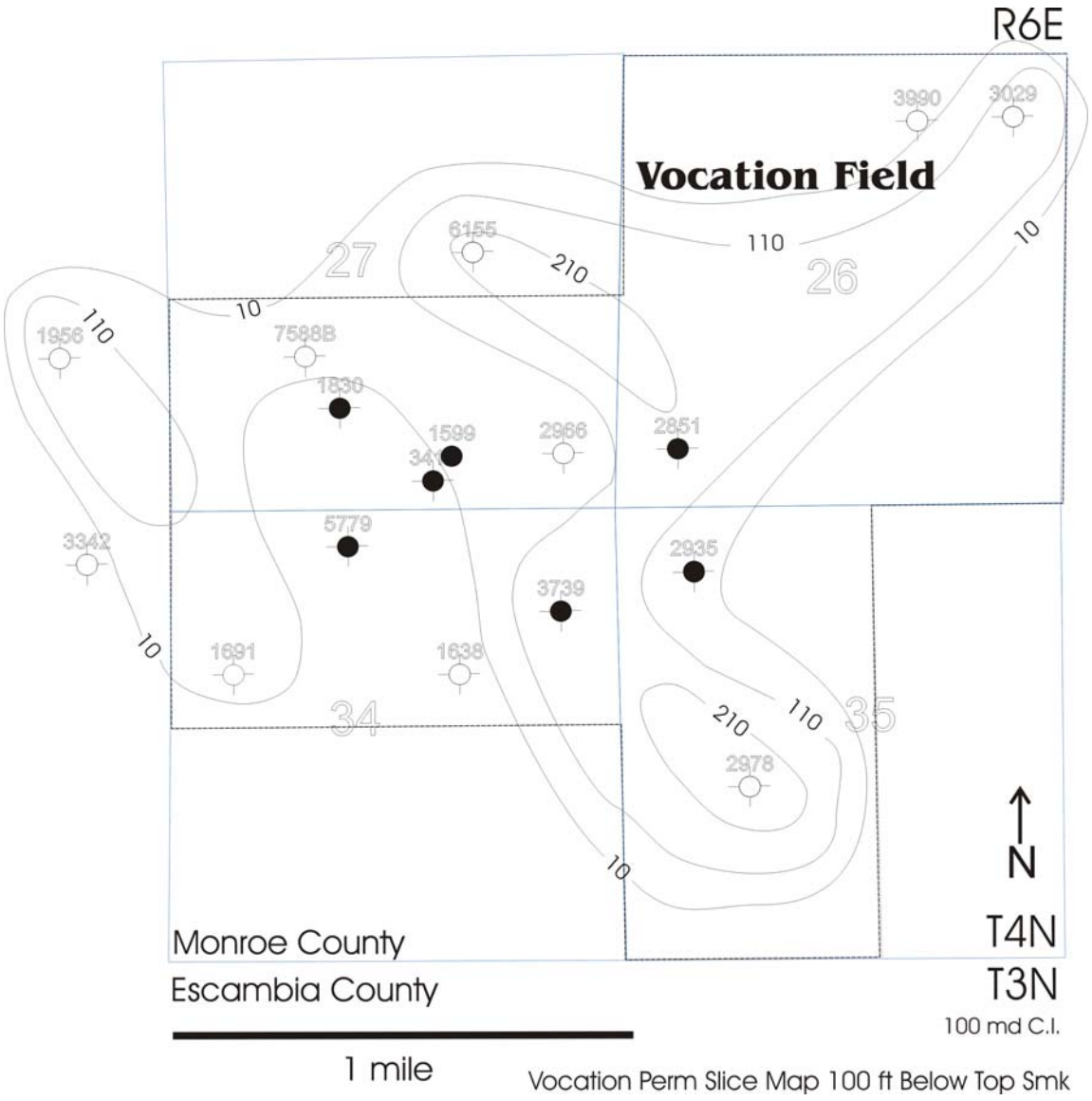

Figure 100. Vocation Permeability Slice Map 100 ft below Top of Smackover.

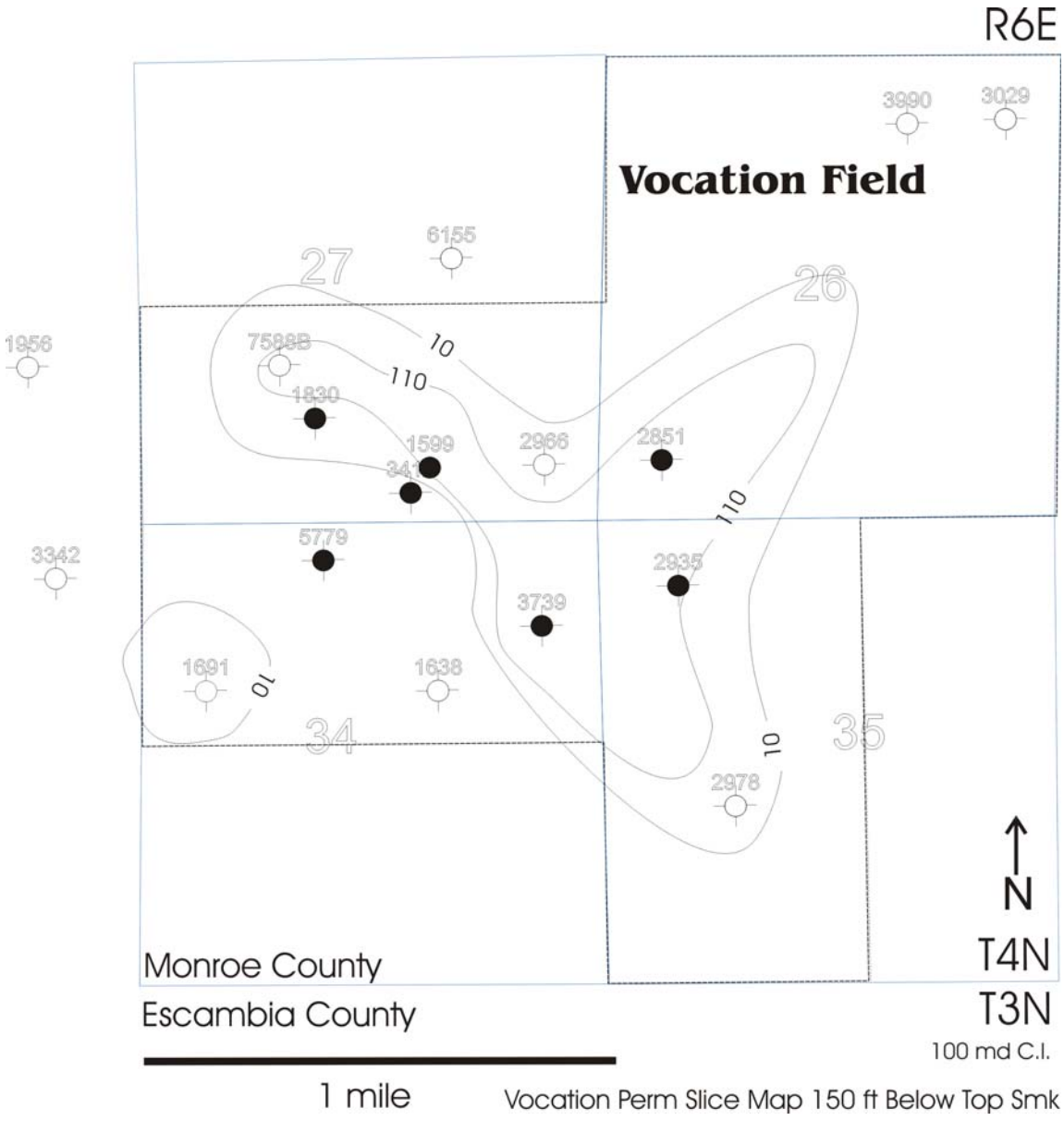

Figure 101. Vocation Permeability Slice Map 150 ft below Top of Smackover.

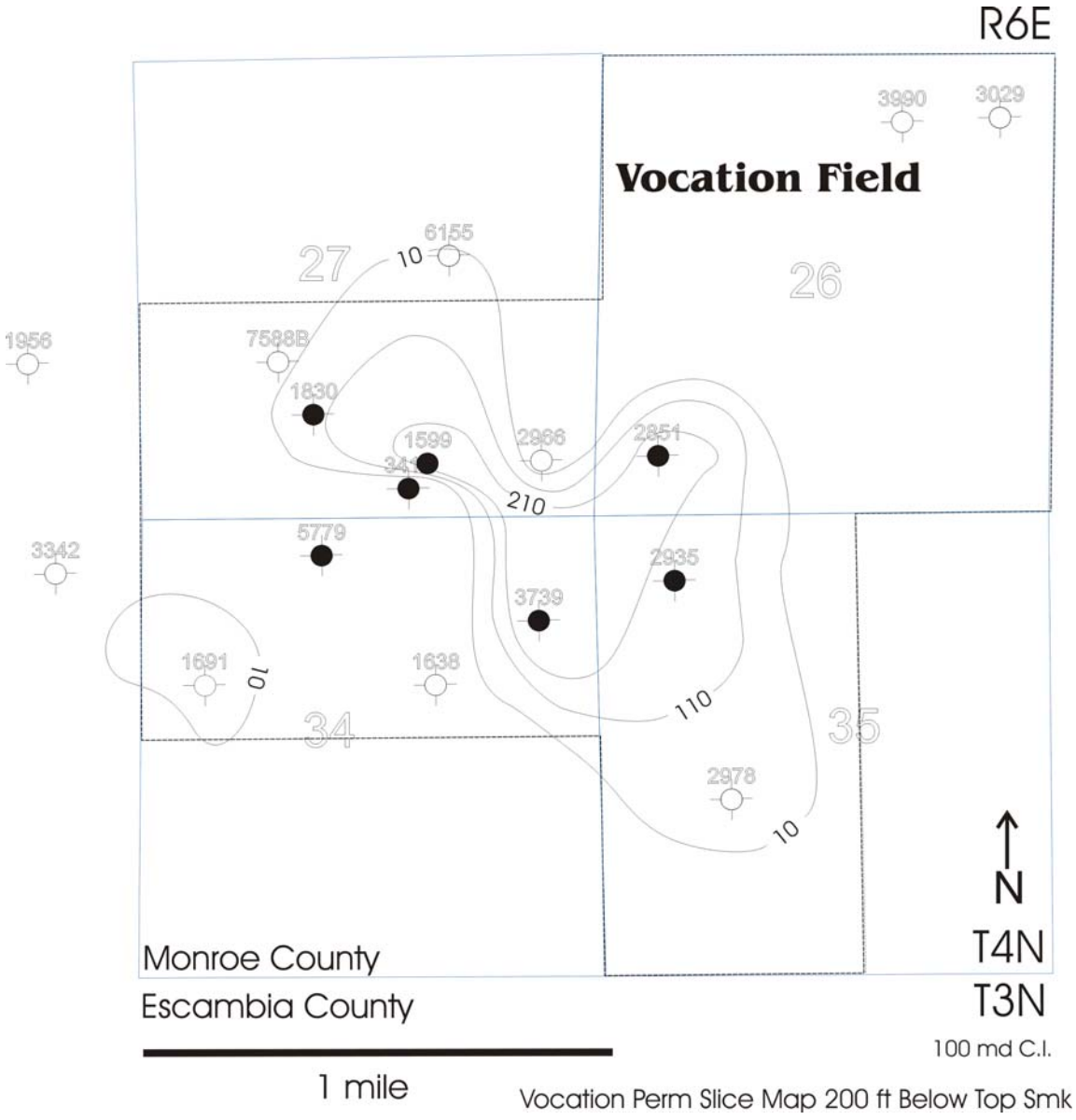

Figure 102. Vocation Permeability Slice Map 200 ft below Top of Smackover.

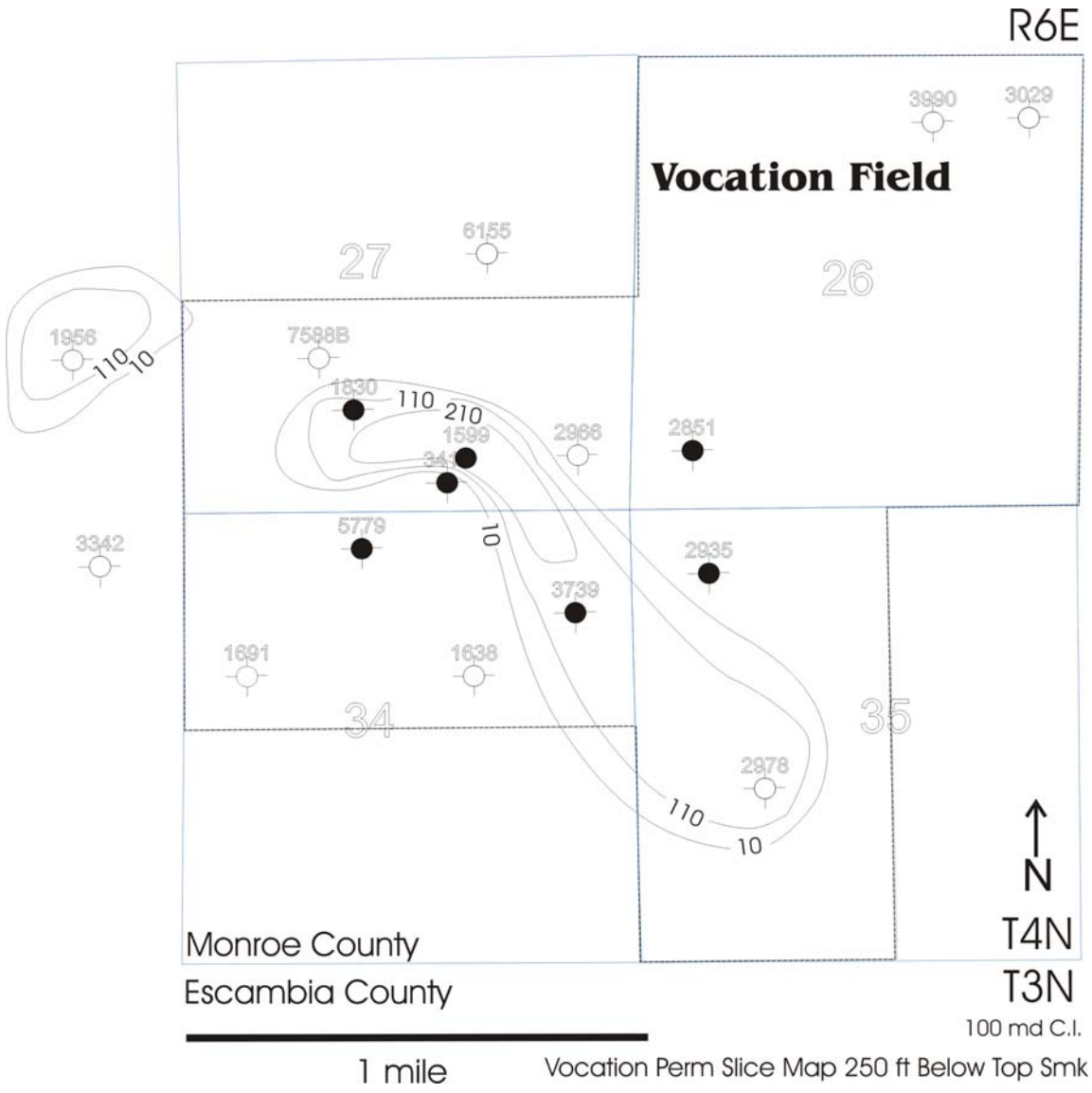

Figure 103. Vocation Permeability Slice Map 250 ft below Top of Smackover.

From the porosity and permeability pairings, nine classes (RQ) (Figure 104) were developed based on histograms of porosity and permeability trends in the fields. These ranges were also given a corresponding pattern for mapping. Rocks that were not reservoir quality, porosity values < 8% and permeability values < 10 md, were not mapped as a pattern since they are recognized as any area in which the pattern was not present. This decision allows for finer delineation of the flow units without adding more patterns. Superimposed on the patterns are MPA values from MICP which correspond to the various pairs. In two cases, more than one MPA value corresponded to a poroperm pair. This is because in most samples there are vugs of various sizes- with another range of varying sizes of connecting throats. These pairs were then contoured and mapped over 10-foot stratigraphic interval. (Figures 105-116). It should be noted here that only the maps drawn every 50 feet are illustrated due to the large number (180) of maps created for both fields. A histogram of porosity distribution and cumulative distribution frequency (Figure 117), and a histogram of permeability distribution and cumulative distribution frequency (Figure 118) are presented for Appleton and Vocation Fields.

The better reservoir quality classes such as RQ1, RQ2, and RQ3 are encountered where are combinations (R in reef facies and IP and SEIP-SEIC in non-reef facies) of pore types are predominant. Groups RQ4, RQ5, and RQ6 correspond to IP dominated pores accompanied by IPA, M, and IC. Reservoir groups RQ7 and RQ9 vary in the pore types associated with them, but it is noted that no SEIP or SEIC is associated with the pore types, and CRIC is unique to these groups.

The results of these comparisons are shown in Table 12 and Figure 119.

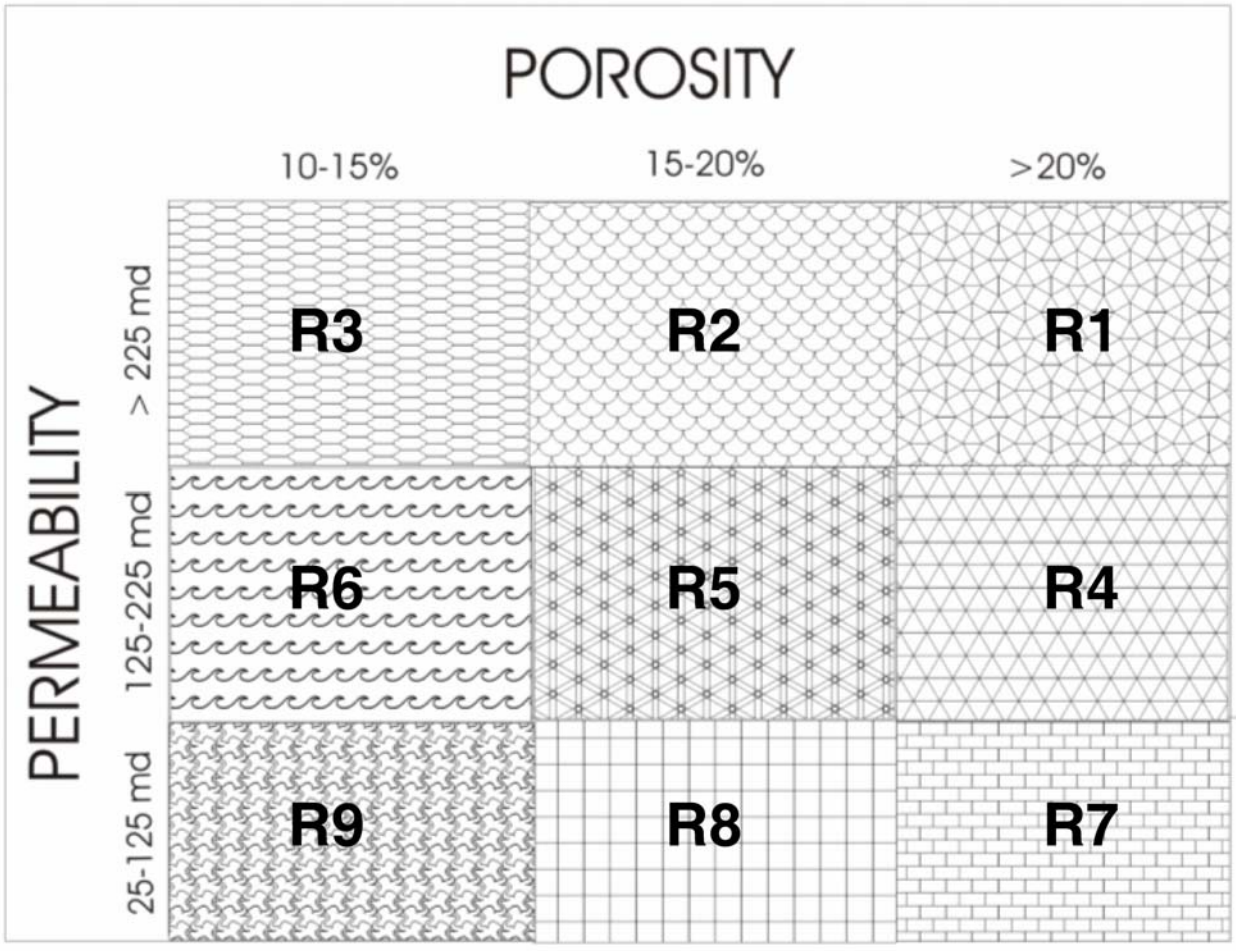

Figure 104. Vocation Reservoir Quality Map Key.

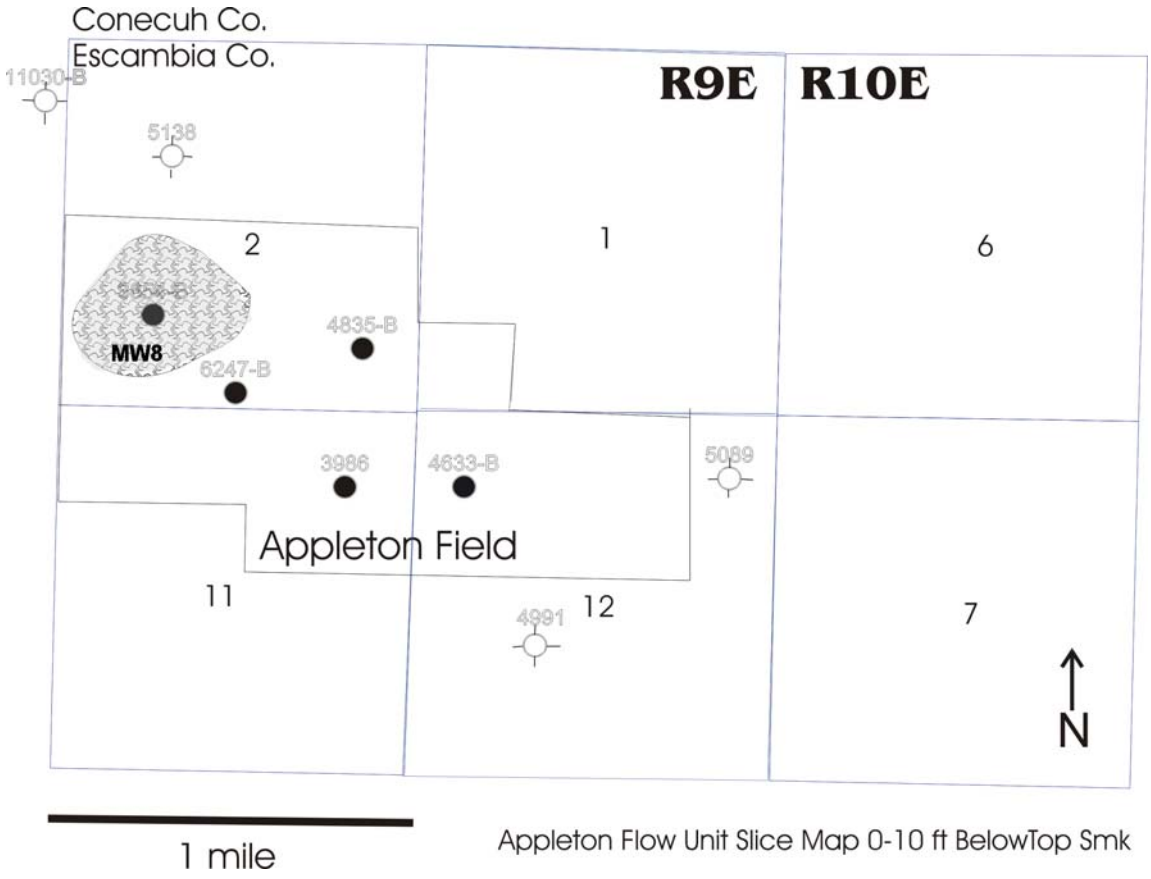

Figure 105. Appleton Flow Unit Slice Map 0-10 ft below Top of Smackover.

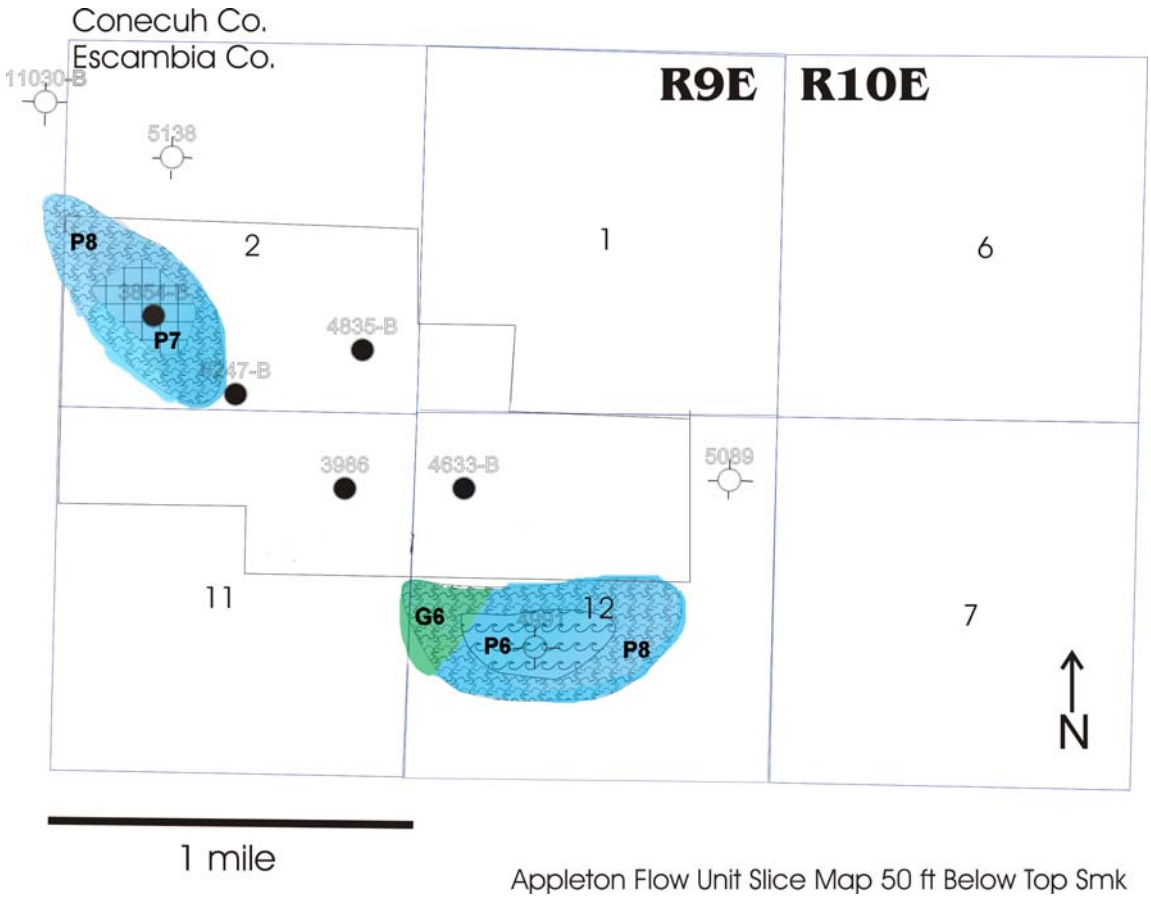

Figure 106. Appleton Flow Unit Slice Map 50 ft below Top of Smackover.

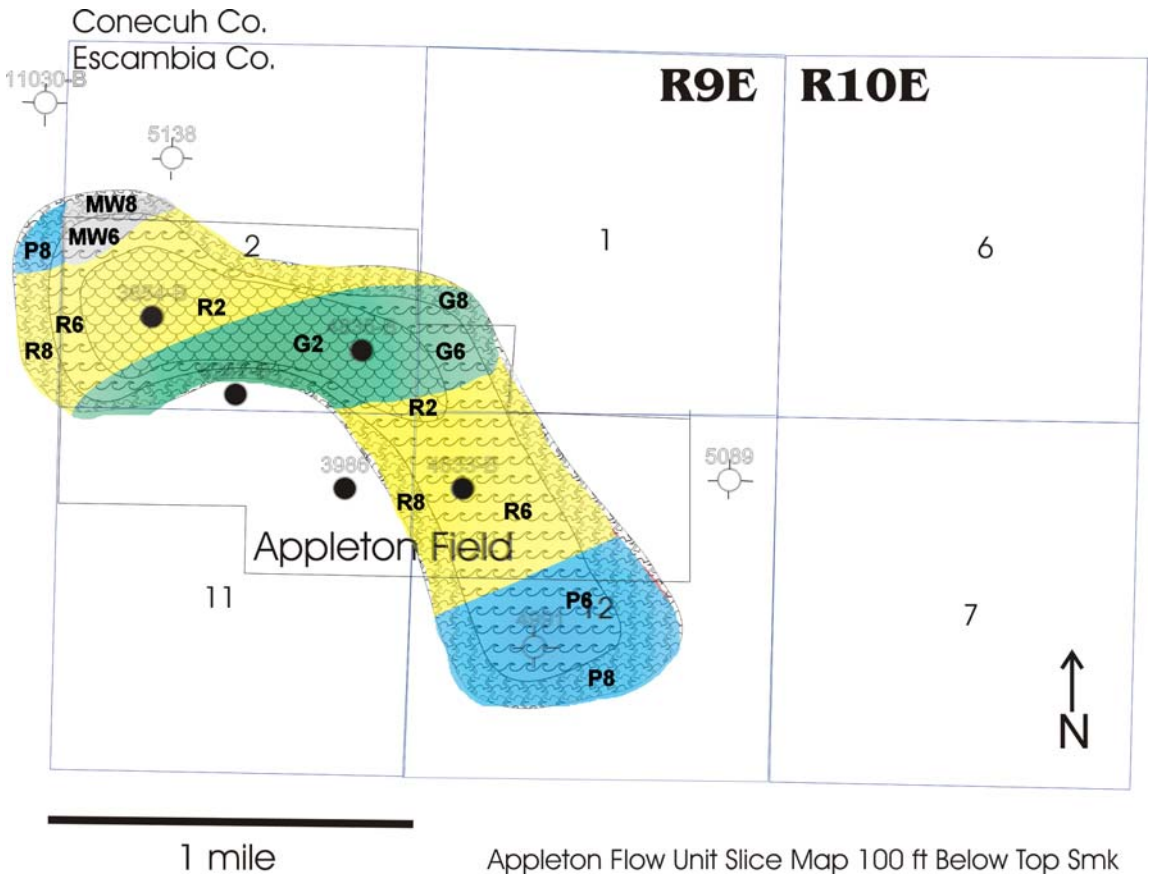

Figure 107. Appleton Flow Unit Slice Map 100 ft below Top of Smackover.

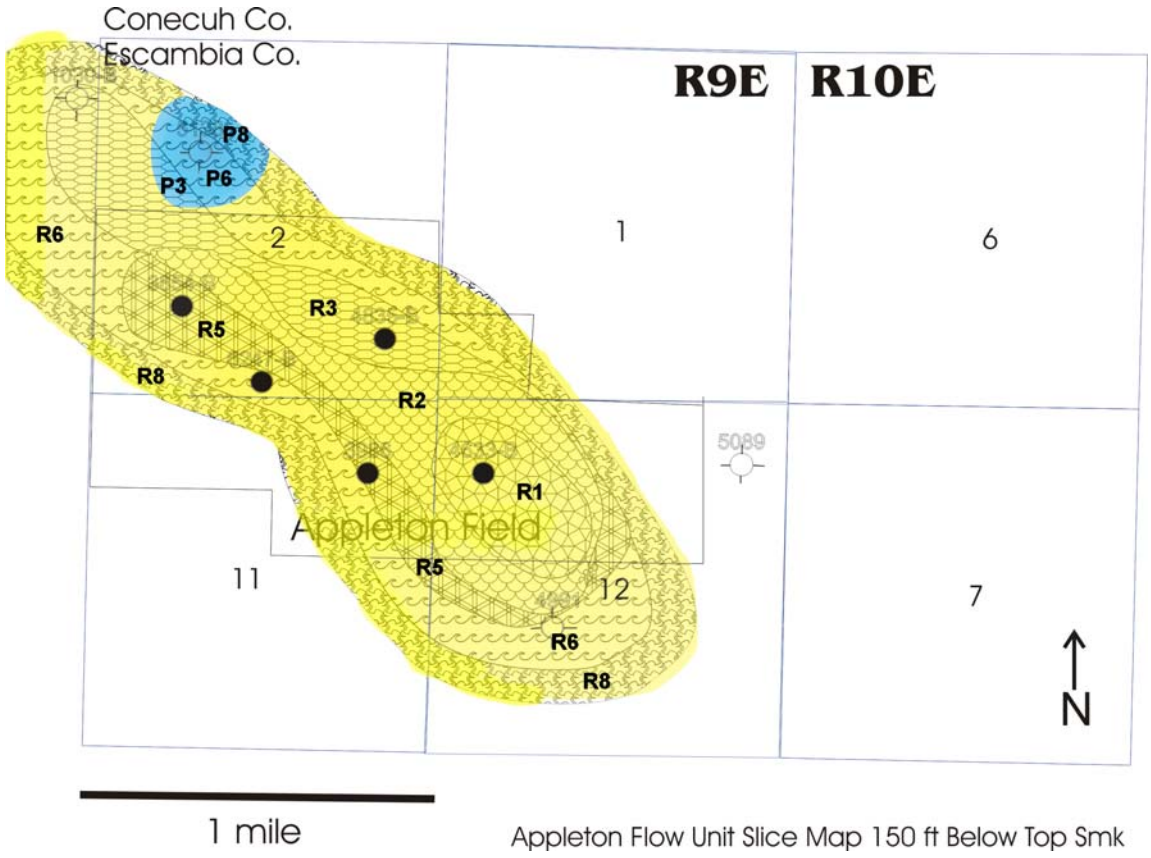

Figure 108. Appleton Flow Unit Slice Map 150 ft below Top of Smackover.

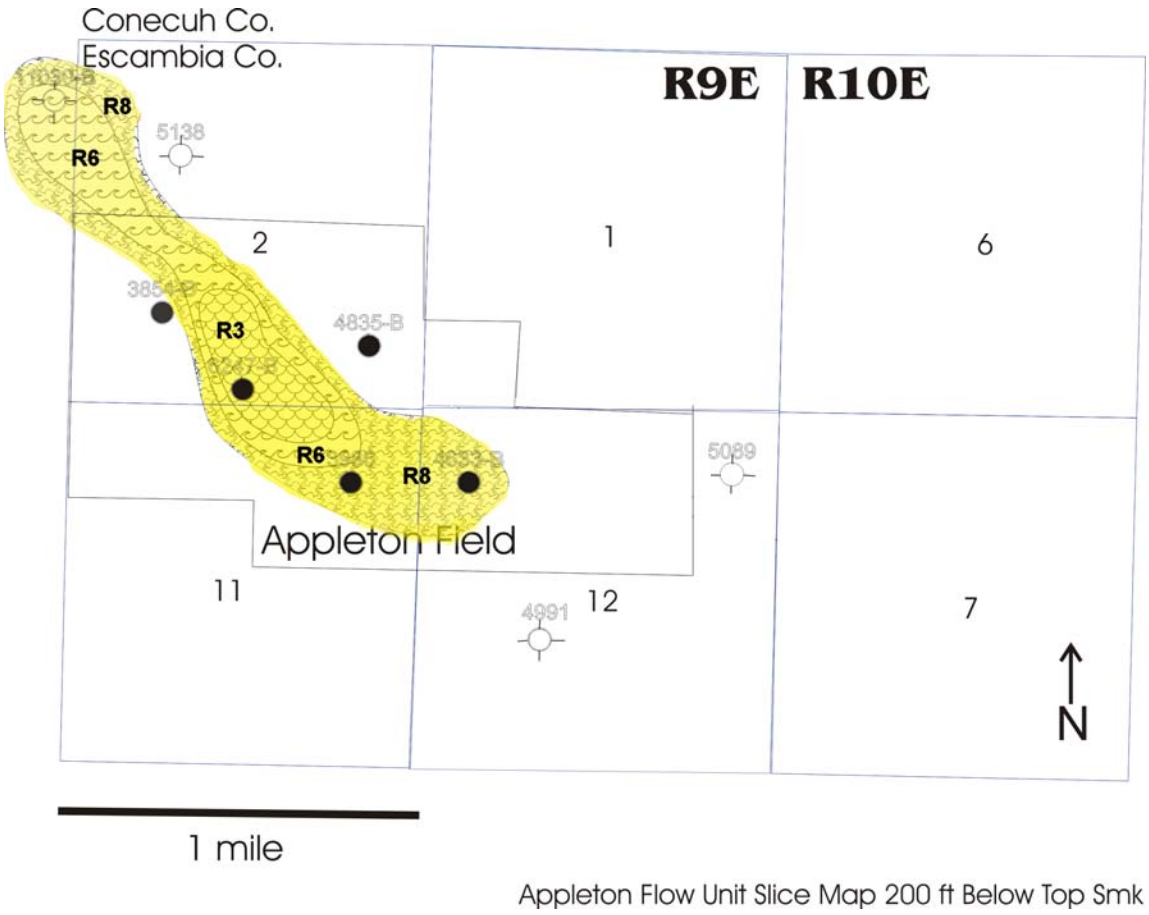

Figure 109. Appleton Flow Unit Slice Map 200 ft below Top of Smackover.

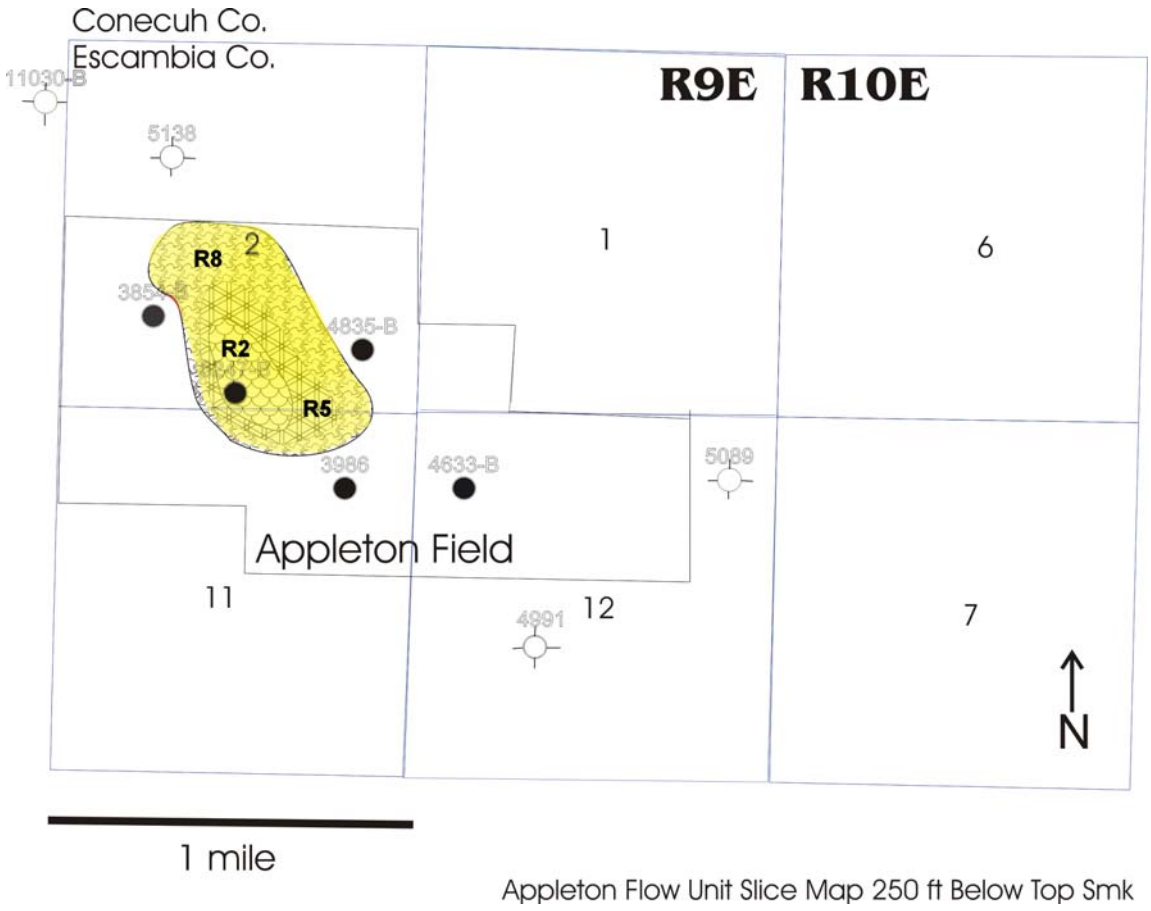

Figure 110. Appleton Flow Unit Slice Map 250 ft below Top of Smackover.

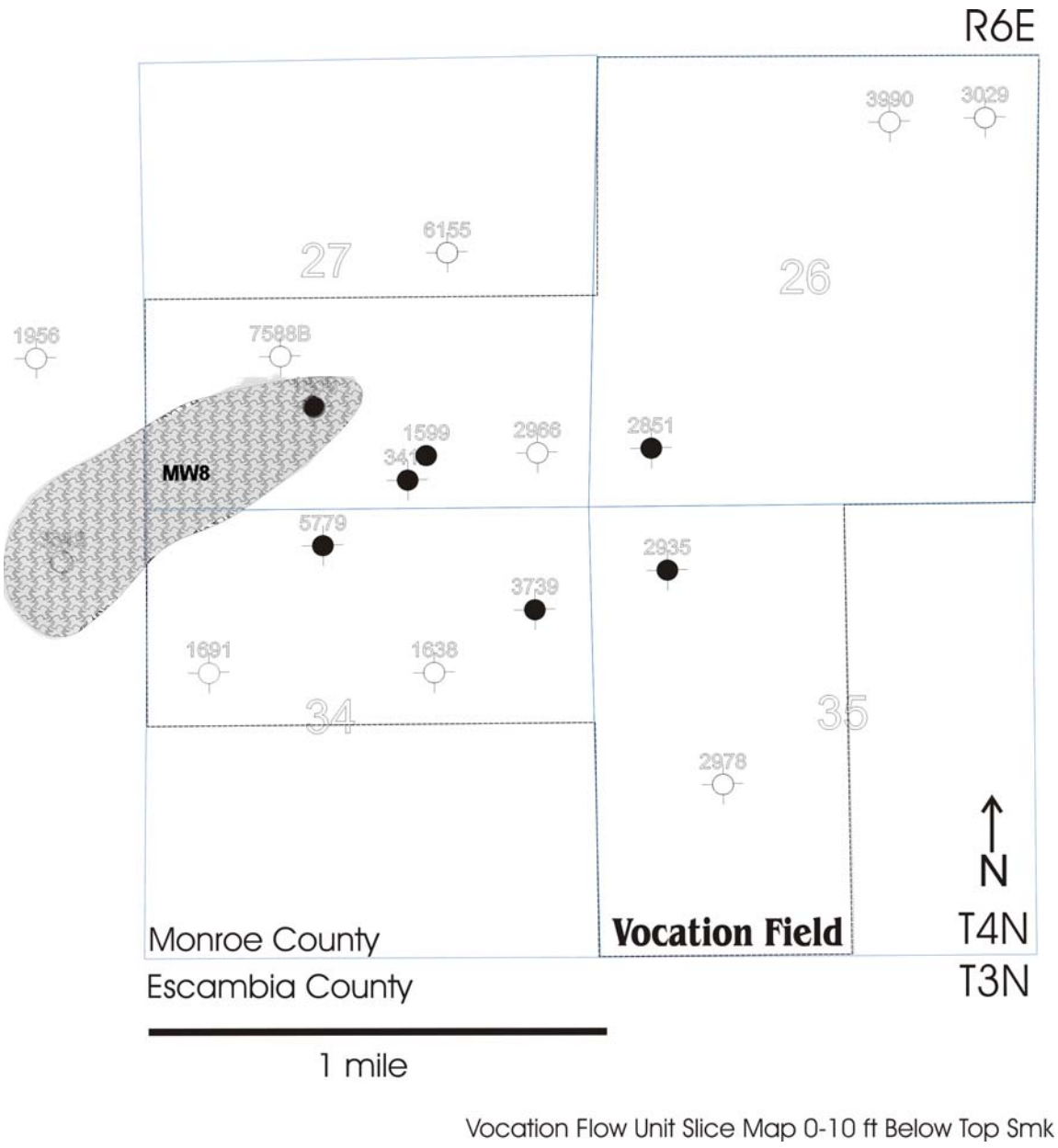

Figure 111. Vocation Flow Unit Slice Map 0-10 ft below Top of Smackover.

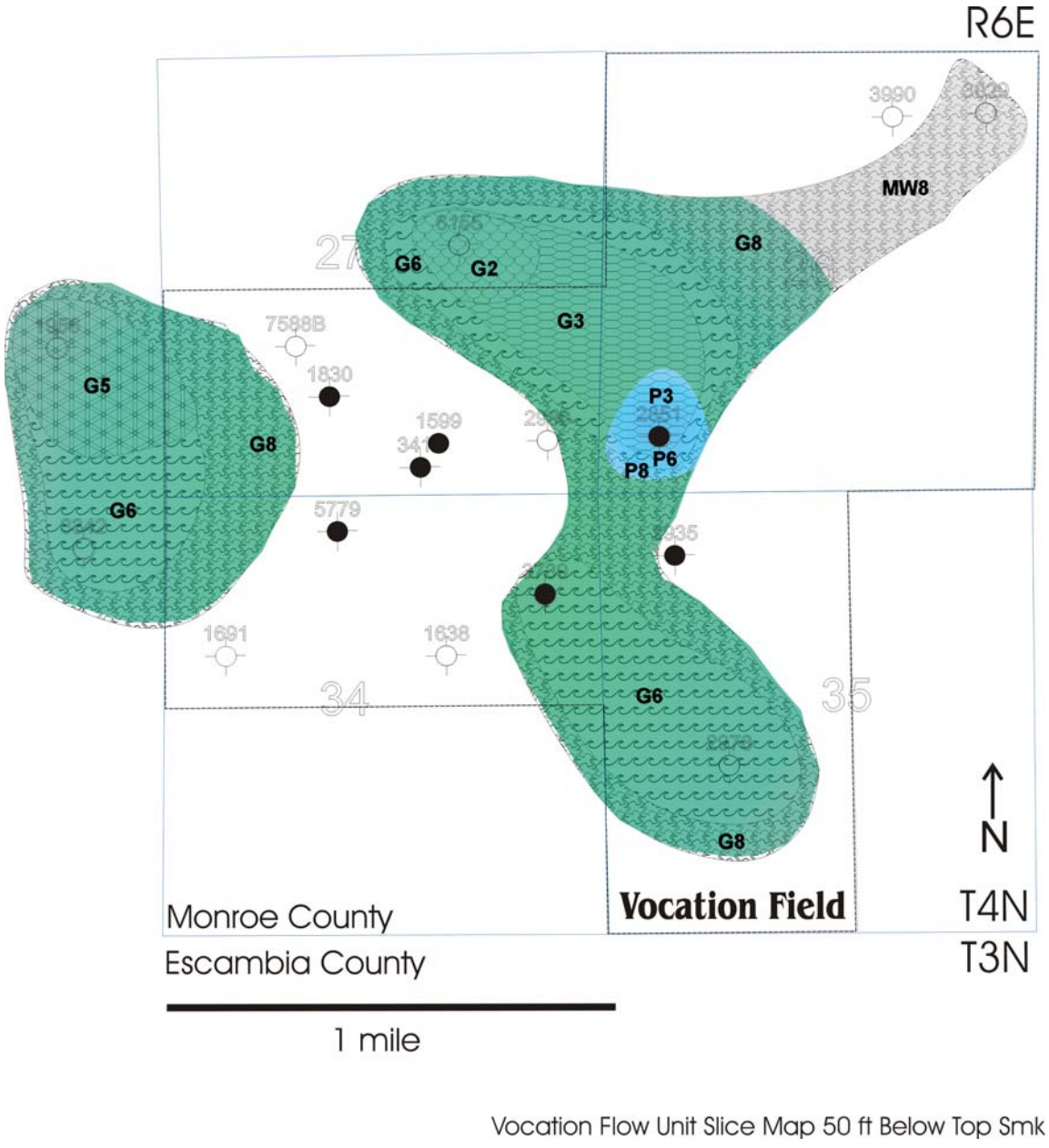

Figure 112. Vocation Flow Unit Slice Map 50 ft below Top of Smackover.

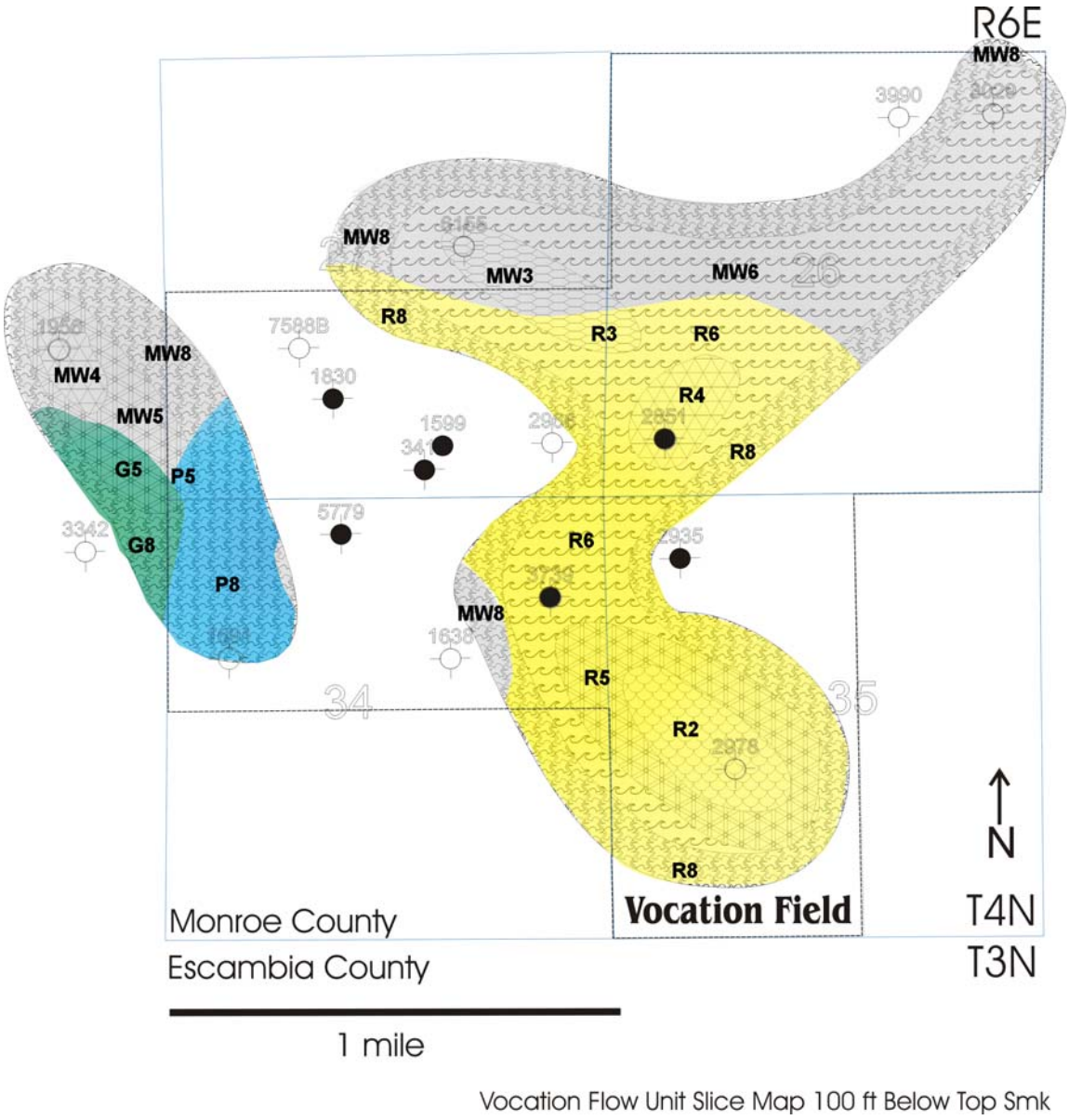

Figure 113. Vocation Flow Unit Slice Map 100 ft below Top of Smackover.

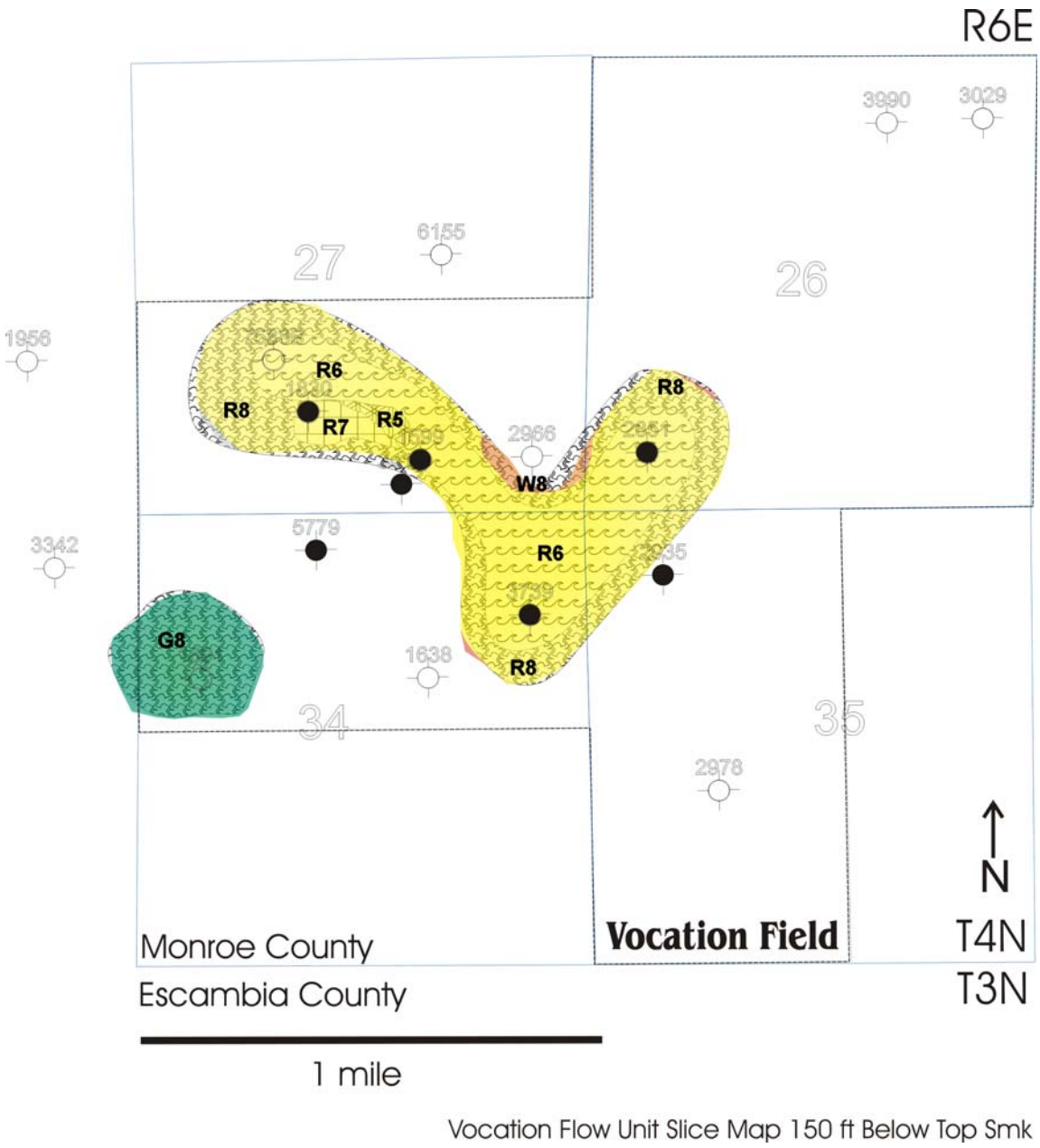

Figure 114. Vocation Flow Unit Slice Map 150 ft below Top of Smackover.

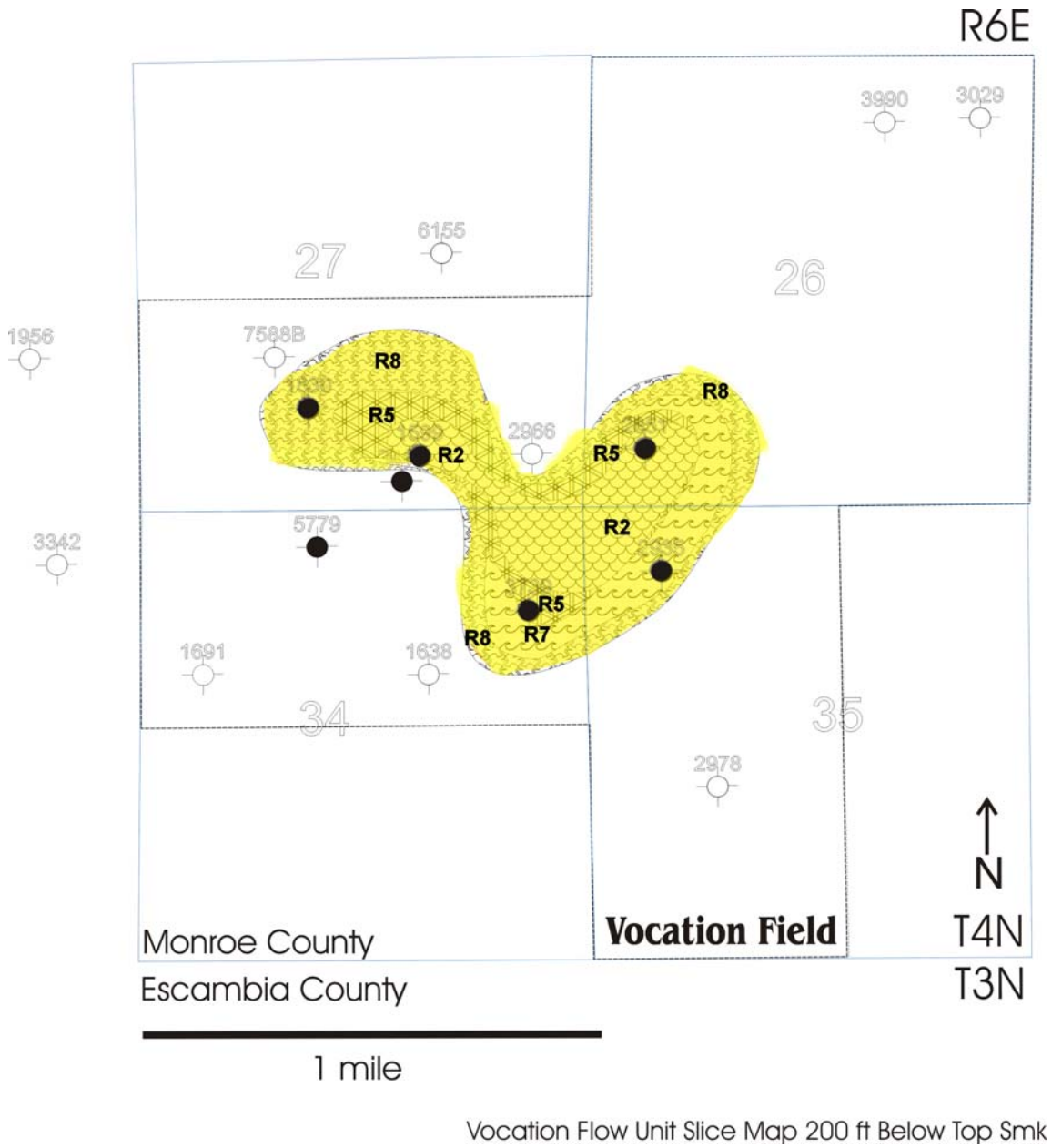

Figure 115. Vocation Flow Unit Slice Map 200 ft below Top of Smackover.

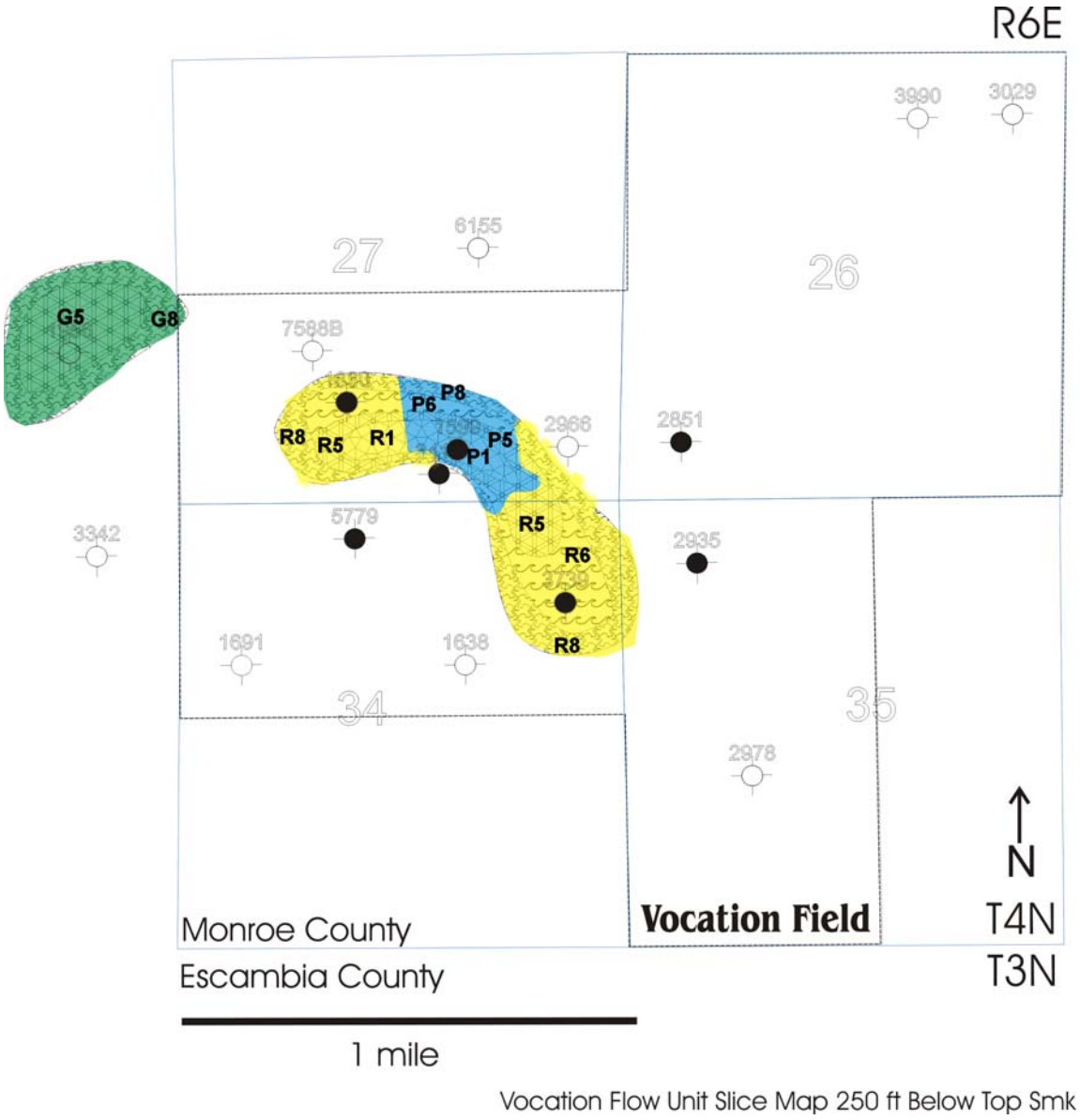

Figure 116. Vocation Flow Unit Slice Map 250 ft below Top of Smackover.

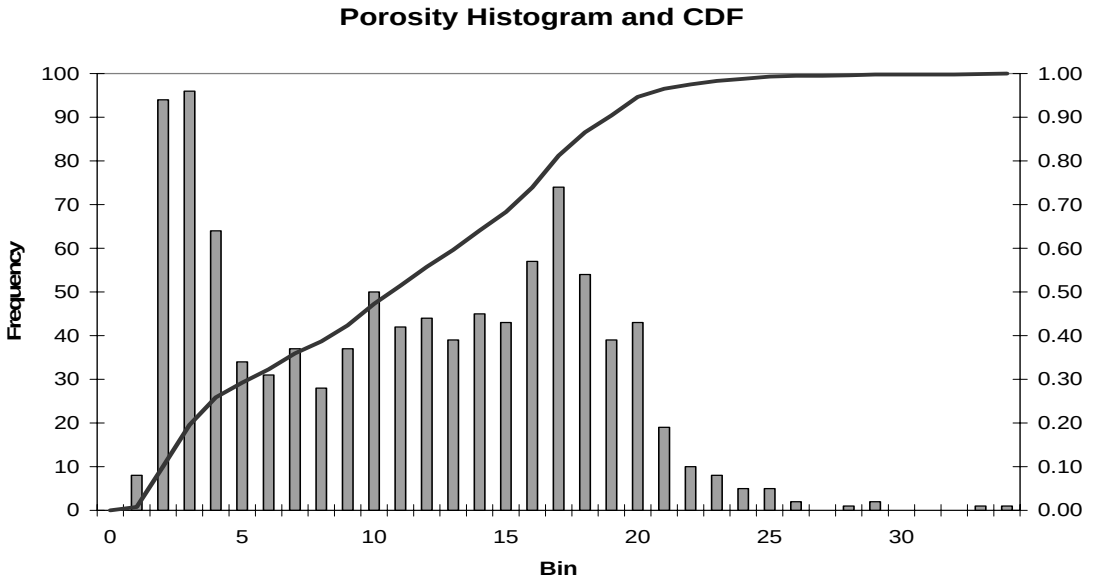

Figure 117. Histogram of porosity distribution and cumulative distribution frequency (CDF) in Appleton and Vocation fields.

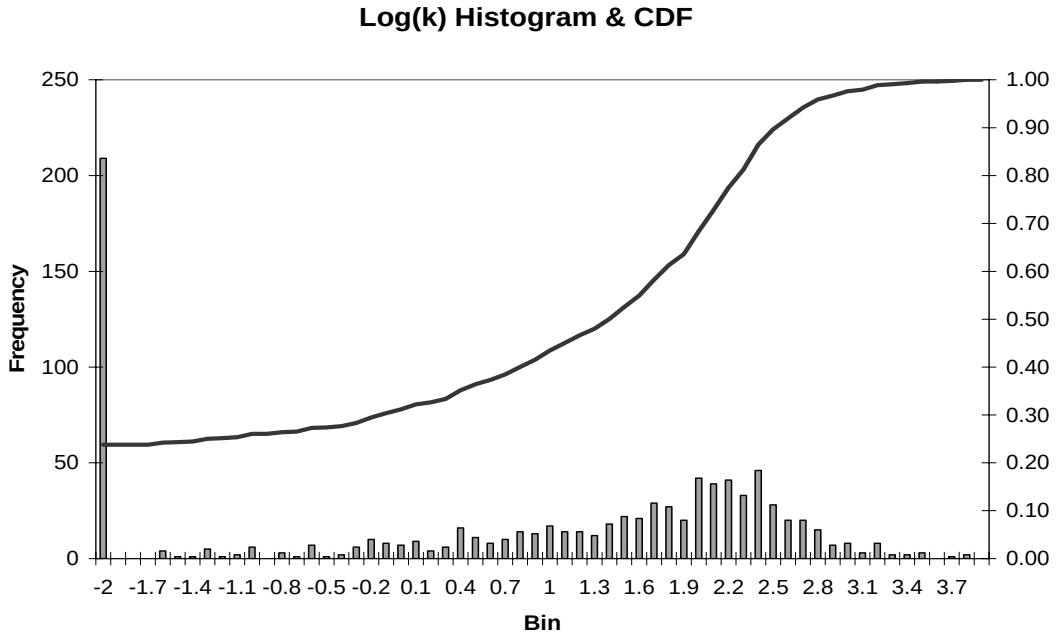

Figure 118. Histogram of permeability distribution and cumulative distribution frequency (CDF) in Appleton and Vocation fields.

Table 12. Typical petrologic characteristics of the various reservoir rankings.

Reservoir quality	Porosity range	Permeability range
RQ1	>19%	>400 md
RQ2	13-19%	>400 md
RQ3	>19%	80-400 md
RQ4	13-19%	80-400 md
RQ5	8-13%	80-400 md
RQ6	13-19%	10-80 md
RQ7	8-13%	10-80 md

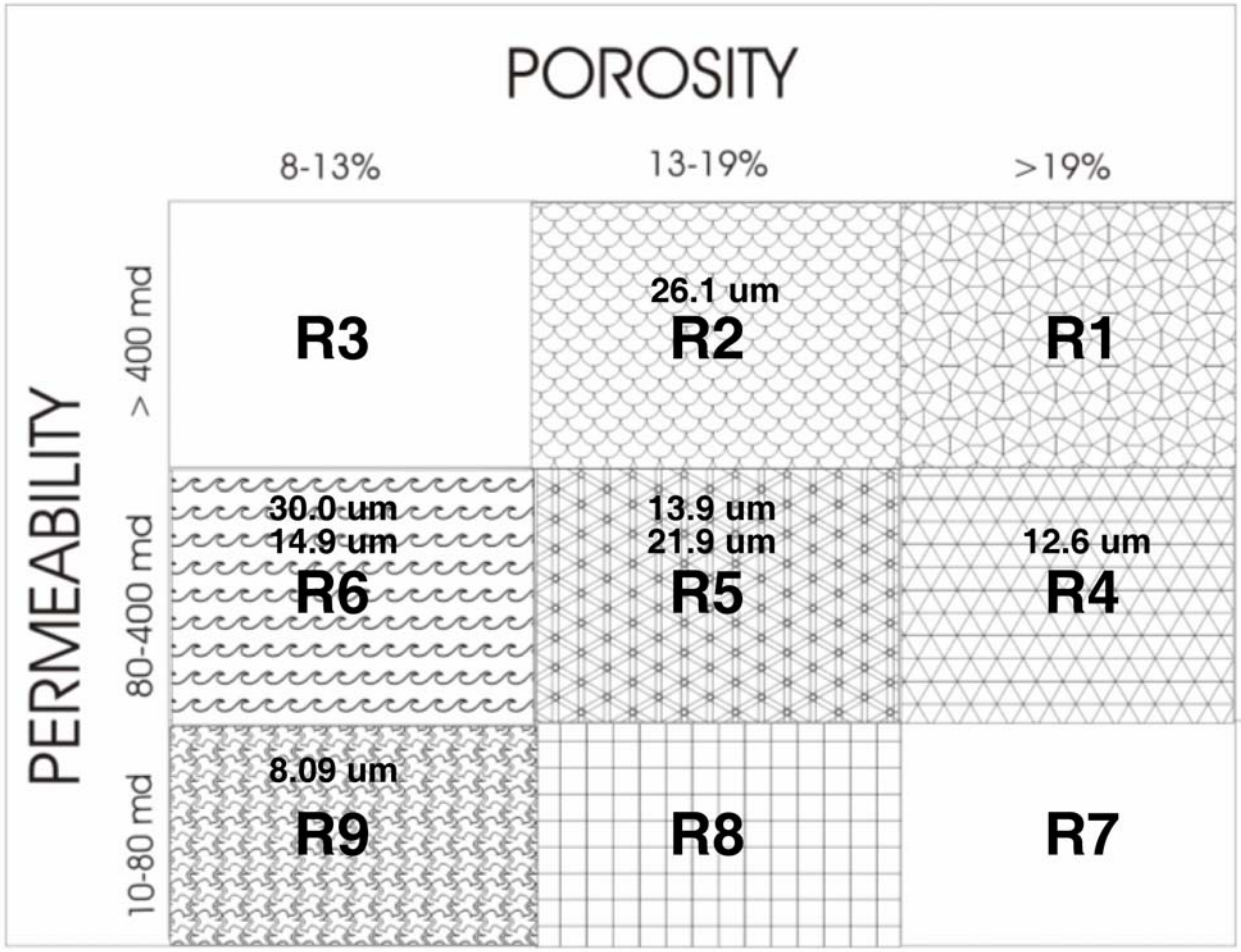

Figure 119. Reservoir quality pairs showing averaged porosity and permeability values along with corresponding MPA values over stratigraphic intervals for flow unit delineation.

Flow units are defined as the mappable portion of the total reservoir within which geological and petrophysical properties that affect the flow of fluids are consistent and are predictably different from the properties of other reservoir rock volumes. There are no set rules as to how to identify flow units, although they do have five common characteristics.

1. A flow unit is an internally consistent (not necessarily homogeneous) volume of reservoir rock which is composed of one or more reservoir quality lithologies.
2. A flow unit has a consistent range of porosity and permeability values.
3. A flow unit is correlative and mappable between wells.
4. Flow units are recognizable on wireline logs.
5. Flow units may be in communication with other flow units.

In this work, we define flow units, baffles, and barriers. Flow units are those segments of the reservoir that exhibit good, intermediate, or poor connectivity as determined by combined porosity/permeability pairs and by median pore throat sizes. Baffles are poor quality zones that extend and can be correlated across an area of two or more well locations. Barriers are those rocks with very low mercury recovery efficiency, low poroperm pairs, and usually have mud supported or cemented fabrics that can be correlated over one-fourth or more of the reservoir area. These rock types are usually but not always easily identifiable on wireline logs.

Flow units within Appleton and Vocation fields do not conform to facies boundaries or specific depths in the formation. Rather, they correlate with a combination of depositional and diagenetic attributes that are not readily identifiable as stratigraphic units; consequently, they are not always easily correlated between wells. Graphs of porosity-permeability versus rock types are illustrated in Figures 120-127. Seven flow units were identified and coded by reservoir quality (RQ1-7 and superimposed on top of lithofacies (MW—mudstone/wackestone, W—

wackestone, P—packstone, G—grainstone and R—reef boundstone). The lithofacies code corresponds with the first letters of the rock type. Reservoir quality is dependent upon different genetic pore types that have resulted from different styles and degrees of diagenesis that have overprinted depositional rock types and which are not consistently related to simple stratigraphic units within the field. This is evidenced by comparing structural maps in the field to porosity and permeability maps and noting which porosity and permeability trends more closely follow structure than lithofacies, indicating that diagenesis played a large role in porosity and permeability development.

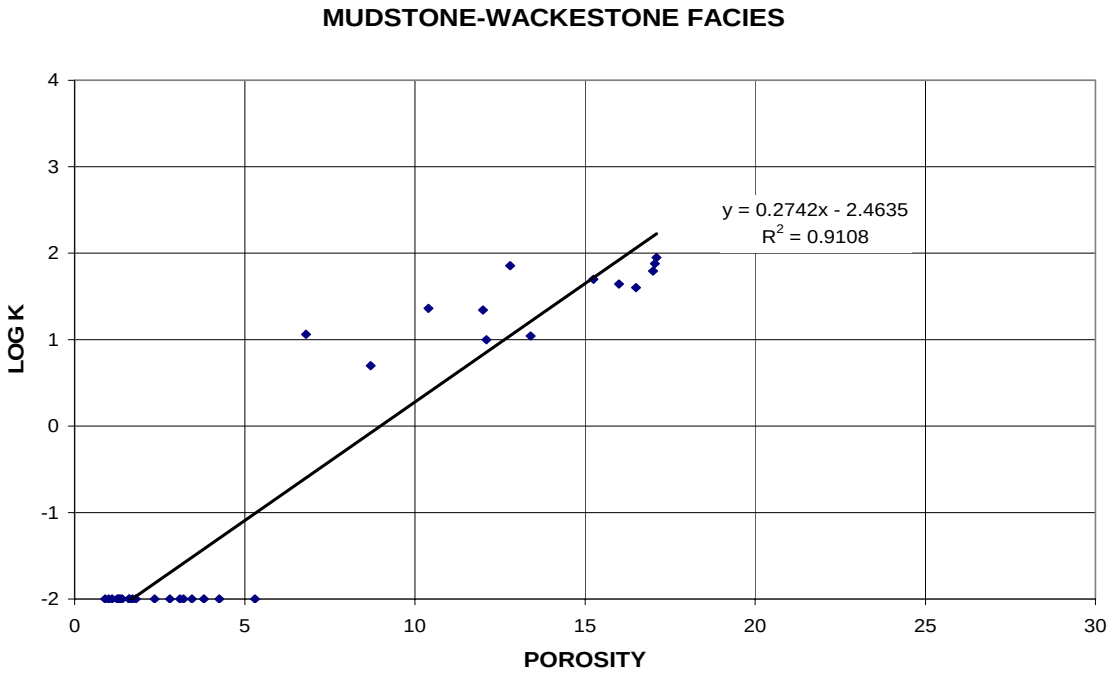

Figure 120. Porosity-permeability plot showing correlation to rock type in Appleton field.

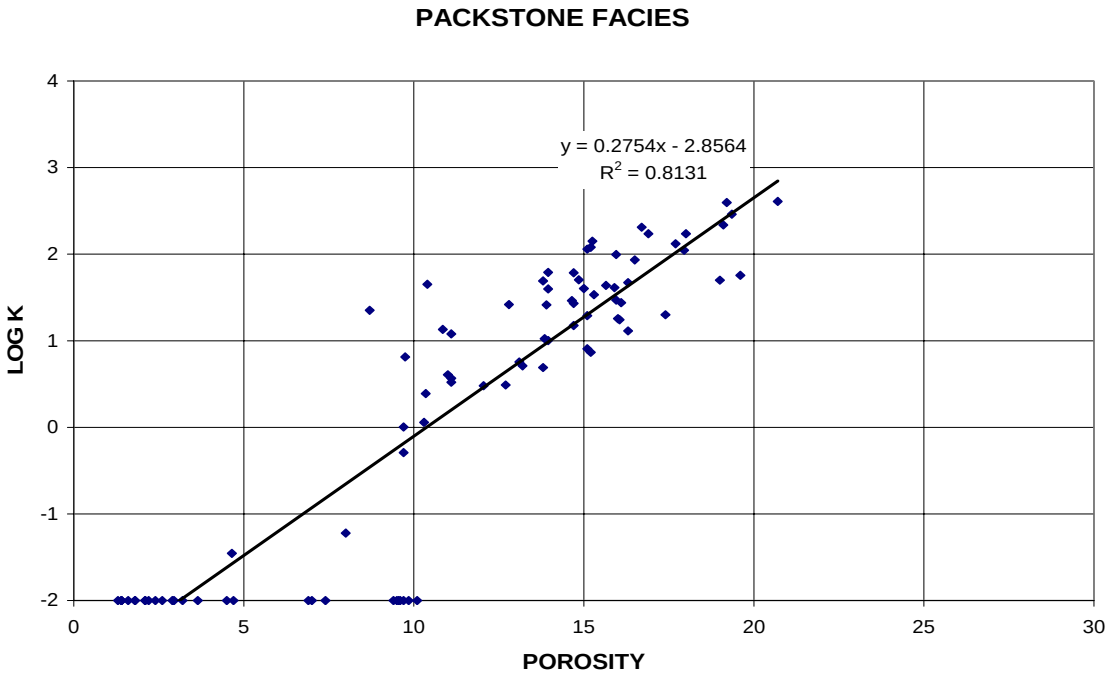

Figure 121. Porosity-permeability plot showing correlation to rock type in Appleton field.

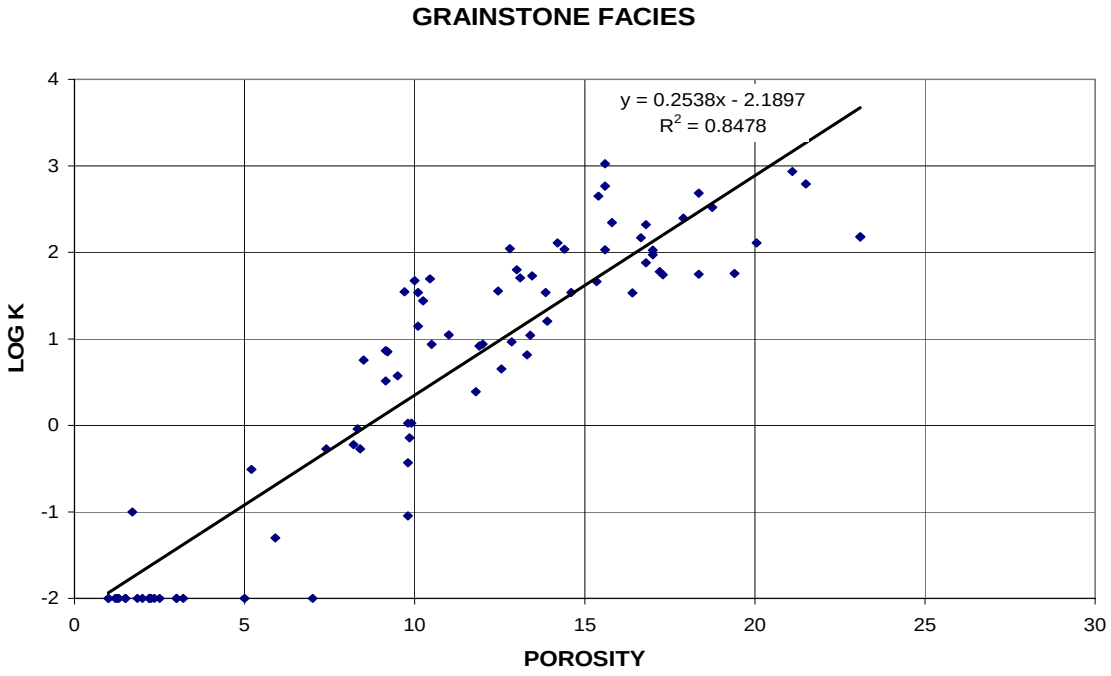

Figure 122. Porosity-permeability plot showing correlation to rock type in Appleton field.

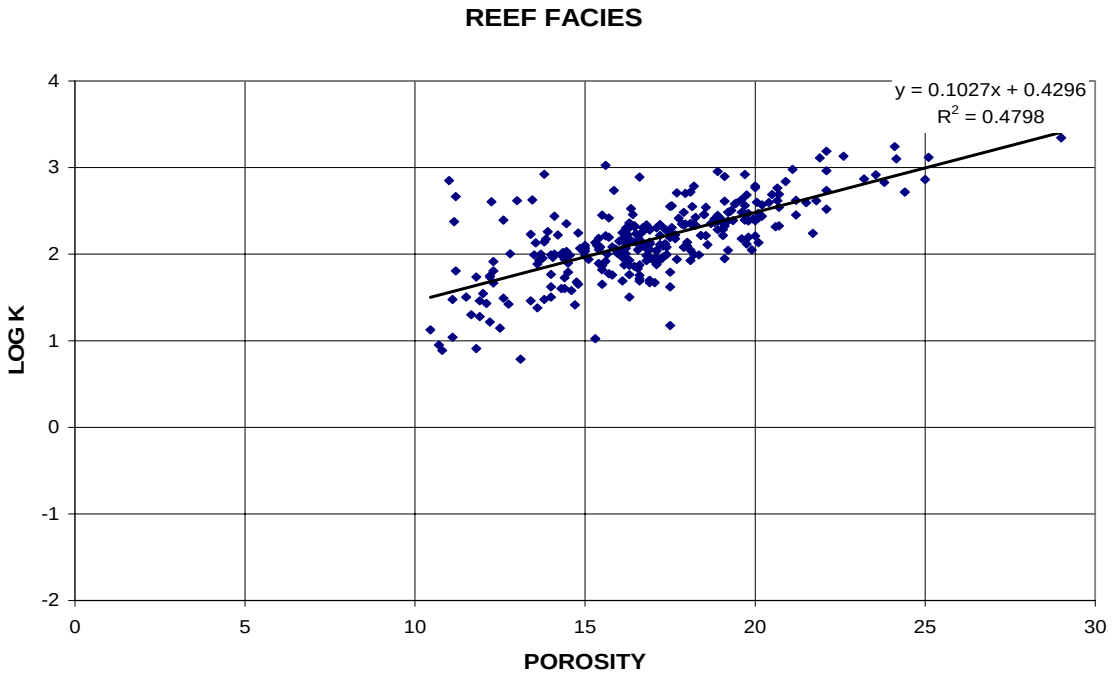

Figure 123. Porosity-permeability plot showing correlation to rock type in Appleton field.

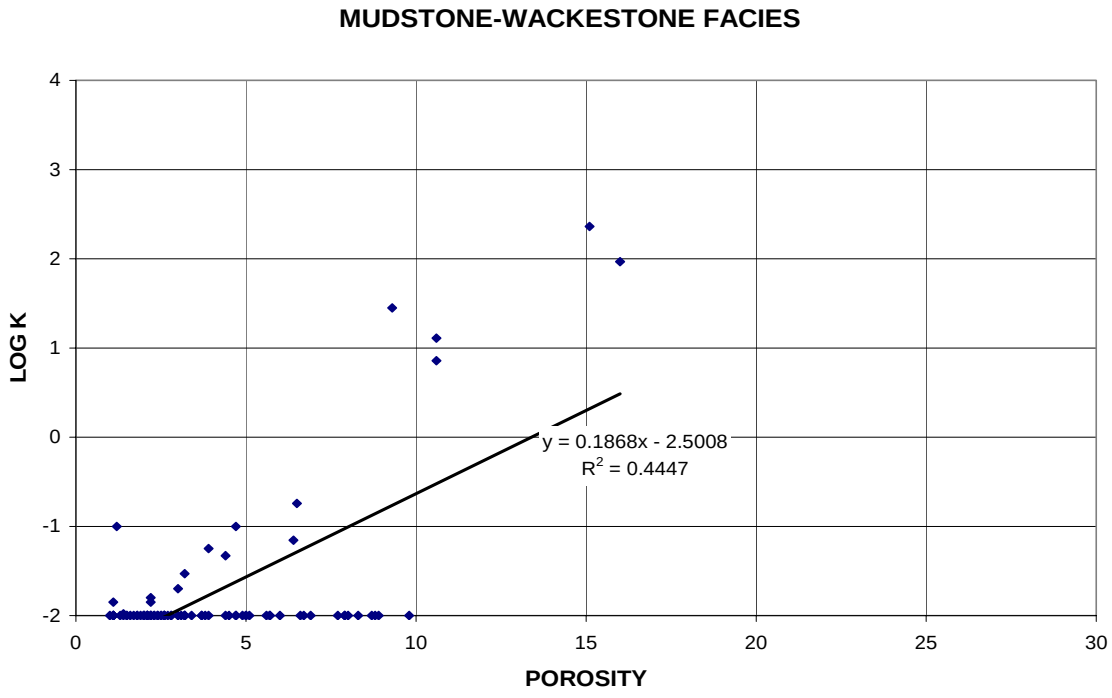

Figure 124. Porosity-permeability plot showing correlation to rock type in Vocation field.

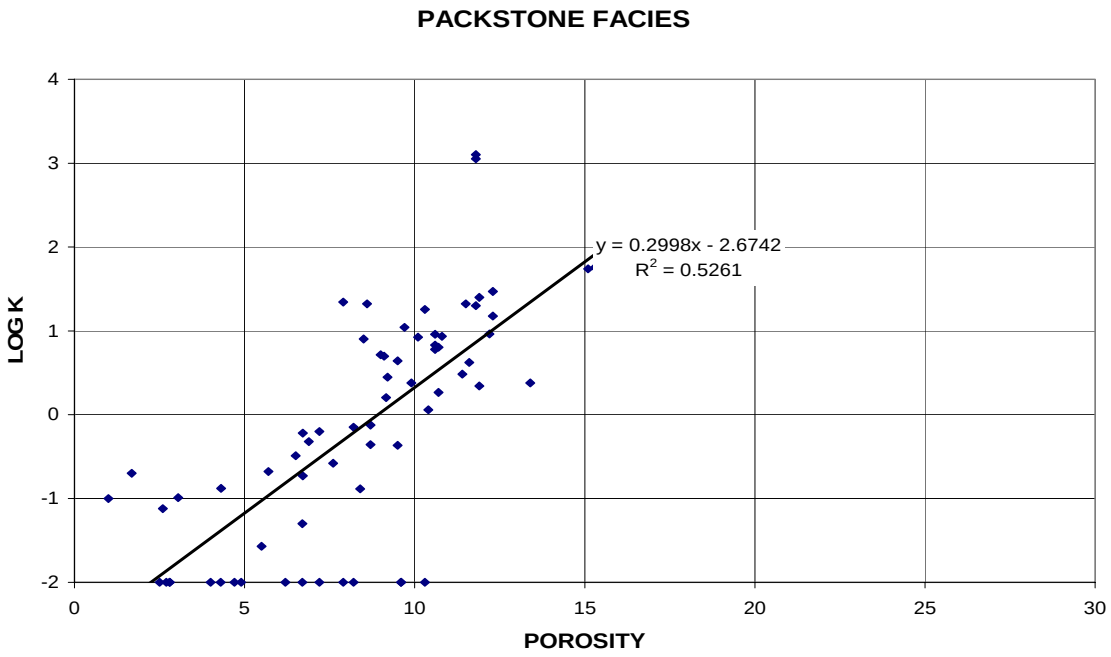

Figure 125. Porosity-permeability plot showing correlation to rock type in Vocation field.

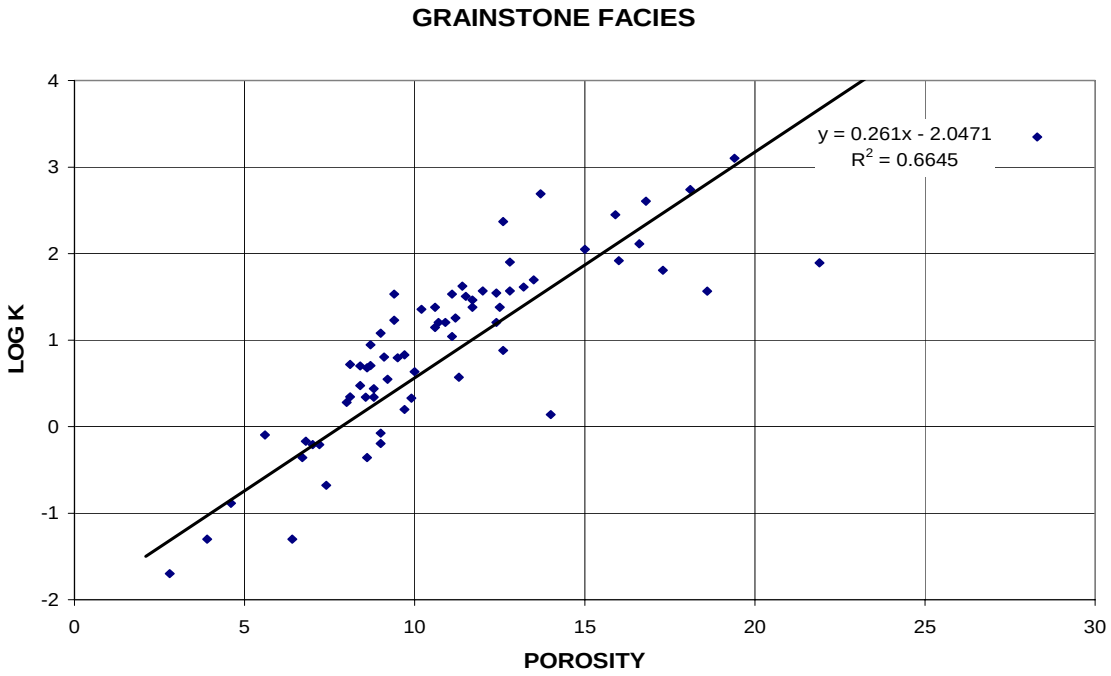

Figure 126. Porosity-permeability plot showing correlation to rock type in Vocation field.

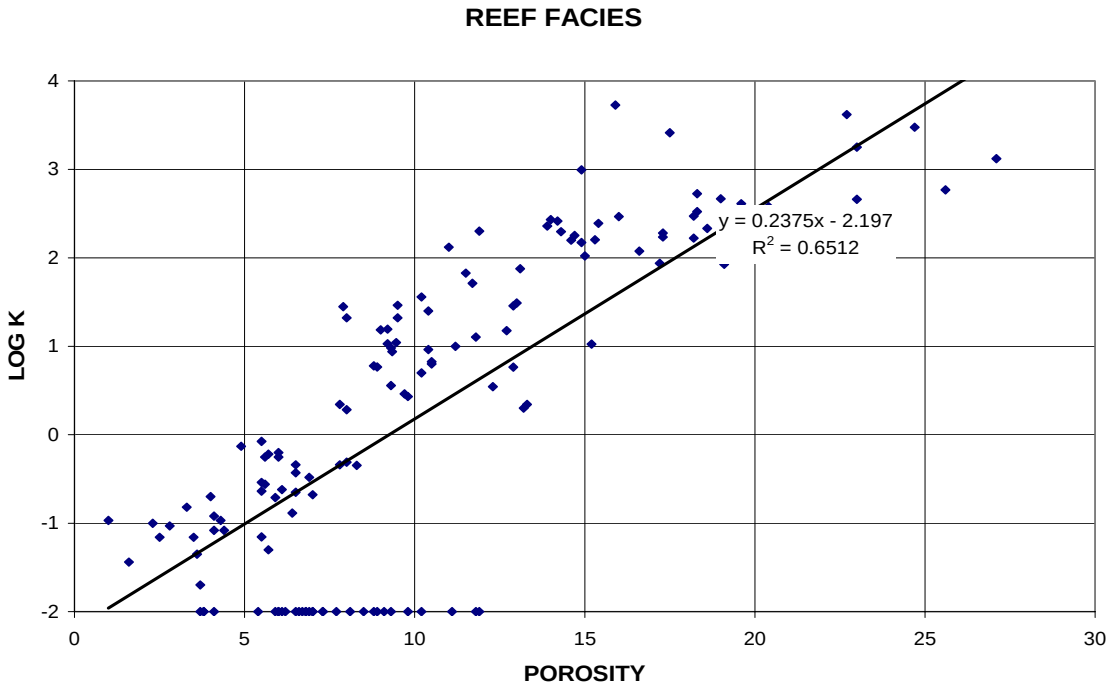

Figure 127. Porosity-permeability plot showing correlation to rock type in Vocation field.

The uppermost interval (0-80 feet below the top of the Smackover) at Appleton Field is dominated by muddier lithologies and RQ5-RQ7 quality flow units. These flow units are discontinuous both laterally and vertically. Reef boundstone facies dominate the lower part of the Smackover in this field and RQ1-RQ4, RQ5 and RQ7 are the more prevalent flow units in this reservoir interval. The highest poroperm values in the reservoir of Appleton Field are well developed beneath the structural culminations of the composite paleotopographic feature. The thickest zones (up to 80 ft) are developed near the crest of the paleostructures. Flow units in the field trend NW-SE throughout the entire Smackover interval which correspond to the same NW-SE paleotopographic trend in the field, implying a diagenetic impact to the porosity-permeability trend. In the lower portion of the reservoir at Appleton Field, flow units do closely tract lithofacies and in this case, log correlation based on lithofacies can be an excellent predictor of the distribution of reservoir quality rocks.

The uppermost interval (0-60 ft below the top of the Smackover) at Vocation Field is dominated by packstone and grainstone with reservoir quality values of RQ3-RQ7. A barrier between flow units is present in the center of the field separating reservoir flow units in the eastern and western parts of the field. This barrier in the flow units is due to different lithologies located in the center of the field that form a communication barrier between flow units. Deeper in the Smackover interval (greater than 100 ft below the top of the Smackover), reef boundstone and grainstone become the dominant lithofacies with reservoir quality ranging from RQ3-RQ7, with the reef boundstone having the highest reservoir quality. An increase in reservoir quality is observed at approximately 200 feet below the top of the Smackover. At this depth, the reservoir in the center of the field has the highest quality reservoir facies while the rocks in the eastern and western portions of the field do not include high quality reservoir rock. This high reservoir quality zone is due to the reef boundstone facies encountered in the reservoir in the center of the field which provides good lateral and vertical continuity. As in Appleton Field, there is a diagenetic overprint that is evident as flow units cut across lithofacies.

Engineering Property Characterization.--This task focused on the characterization of the reservoir rock and fluid properties of the reservoirs at Appleton and Vocation Fields. These properties can be obtained from petrophysical and engineering data. This task assesses the character of the reservoir fluids, as well as quantify the petrophysical properties of the reservoir rock. A major goal is to assess current reservoir pressure conditions and develop a simplified reservoir model. New pressure test data have been obtained to assess communication within the reservoir at Appleton Field, including among and within the various pay zones in the Smackover. This work will serve as a guide for the reservoir simulation modeling. Petrophysical and engineering data are fundamental to reservoir characterization. Petrophysical data are often considered static (non-time dependent) measurements, while engineering data are considered dynamic (time-dependent). Reservoir characterization is the coupling or integration of these two classes of data. The data are analyzed to identify fluid flow units (reservoir-scale flow sequences), barriers to flow, and reservoir compartments. Petrophysical data are essential for defining the quality of the reservoir, and engineering data (performance data) are crucial for assessing the producibility of the reservoir. Coupling these concepts, via reservoir simulation or via simplified analytical models, allows for the interpretation and prediction of reservoir performance under a variety of conditions. The first phase of the task involves the review, cataloging, and analysis of available core measurements and well log data. Core data have been correlated to the well log responses, and porosity-permeability relationships were established. The next phase focuses on the collection and cataloging of fluid property (PVT) data. In particular, basic (black oil) fluid property data are available, where these analyses include standard measurements of gas-oil-ratio (GOR), oil gravity, viscosity, and fluid composition. The objective of the fluid property characterization work is to develop relations for the analysis of

well performance data and for reservoir simulation. The final phase will be to develop a performance-based reservoir characterization of Appleton and Vocation Fields. This phase focuses exclusively on the analysis and interpretation of well performance data as a mechanism to predict recoverable fluids and reservoir properties. This analysis focuses on the production data, but other well performance data have been considered, in particular, pressure test data were analyzed and integrated into the reservoir description. The material balance decline type curve analysis is emphasized for the analysis of the data. Researchers at Texas A&M University have done this work. These researchers include Blasingame and students.

Appleton Field. Petrophysical and engineering property data have been gathered and tabulated for Appleton Field. These data include oil, gas and water production, fluid property (PVT) analyses (Table 13) and porosity and permeability information (Tables 14 and 15). Porosity and permeability characteristics of Smackover facies have been analyzed for each well using porosity histograms (Figures 128-132), permeability histograms (Figures 133-137) and porosity versus depth plots (Figures 138-142). Log porosity versus core porosity and porosity versus permeability plots for wells in the field have been prepared (Figures 143-147). Porosity versus permeability cross plots for Smackover facies have been prepared (Figures 148-152). Well performance studies through type curve (Table 16 and Figures 153-157) and decline curve analyses (Figures 158-162) have been completed for the wells in the field. The original oil in place and recoverable oil remaining for the field have been calculated (Table 17 and Figures 163-170).

Table 13. PVT Data for Appleton Field Reservoir

Permit#:	3854			
Well Name:	Appleton Unit 2-14 #1			
Field:	Appleton-Oil			
Pool:	Smackover			
County:	Escambia			
Date:	25-10-1983			
Pi (PSIA) :	6264	Boi	(RBBL/STB):	2.4676
Pb (PSIA) :	3416	Bob	(Rbbl/STB):	2.755
T:	245.3	Rsi	(SCF/STB):	2479.0
API:	48.3	Rsib	(SCF/STB):	900.0

Full Wellstream Recombination:

Component	MOL%
H2S	1.75
N2	1.38
CO2	5.7
C1	42.01
C2	10.06
C3	7.49
C4i	2.51
C4n	5.06
C5i	2.37
C5n	3.05
C6	3.06
C7	15.56
Total	100.00

Permit#:	3986			
Well Name:	Appleton Unit TR 5: McMillan Trust 11-1 #2			
Field:	Appleton-Oil			
Pool:	Smackover			
County:	Escambia			
Date:	19-03-1984			
Pi (PSIA) :	6270	Boi	(RBBL/STB):	2.2721
Pb (PSIA) :	3028	Bob	(Rbbl/STB):	2.5398
T:	252.0	Rsi	(SCF/STB):	2062.0
API:	46.4	Rsib	(SCF/STB):	812.0

Full Wellstream Recombination:

Component	MOL%
H2S	1.60
N2	4.03
CO2	1.19
C1	38.07
C2	9.86
C3	7.83
C4i	2.64
C4n	5.44
C5i	2.60
C5n	3.36
C6	2.81
C7	20.57
Total	100.00

Table 14 — Porosity and permeability characteristics in the Smackover.

Well	Minimum Porosity, (percent)	Maximum Porosity, (percent)	Average Porosity, (percent)	Minimum Permeability ,(md)	Maximum Permeability, (md)	Geometric Average Permeability ,(md)
3854B	3.2	24.4	13.6	0.54	618.1	21.8
3986	9.7	29.0	15.7	6.1	2200	108.3
4633B	9.2	24.1	17.0	0.37	1349	103.9
4835B	4.0	24.4	15.0	0.46	3345	191.4
6247B	1.0	6.7	2.7	0.055	0.1	0.07

Table 15 — Porosity and permeability characteristics in the Reef.

Well	Minimum Porosity, (percent)	Maximum Porosity, (percent)	Average Porosity, (percent)	Minimum Permeability ,(md)	Maximum Permeability, (md)	Geometric Average Permeability ,(md)
3854B	N/A	N/A	N/A	N/A	N/A	N/A
3986	10.7	22.1	14.5	8.9	1545	115.6
4633B	10.5	25.0	18.4	13.4	1748	274.0
4835B	16.0	20.8	17.9	225.8	563.8	345.9
6247B	1.0	14.3	5.6	0.025	18.8	1.79

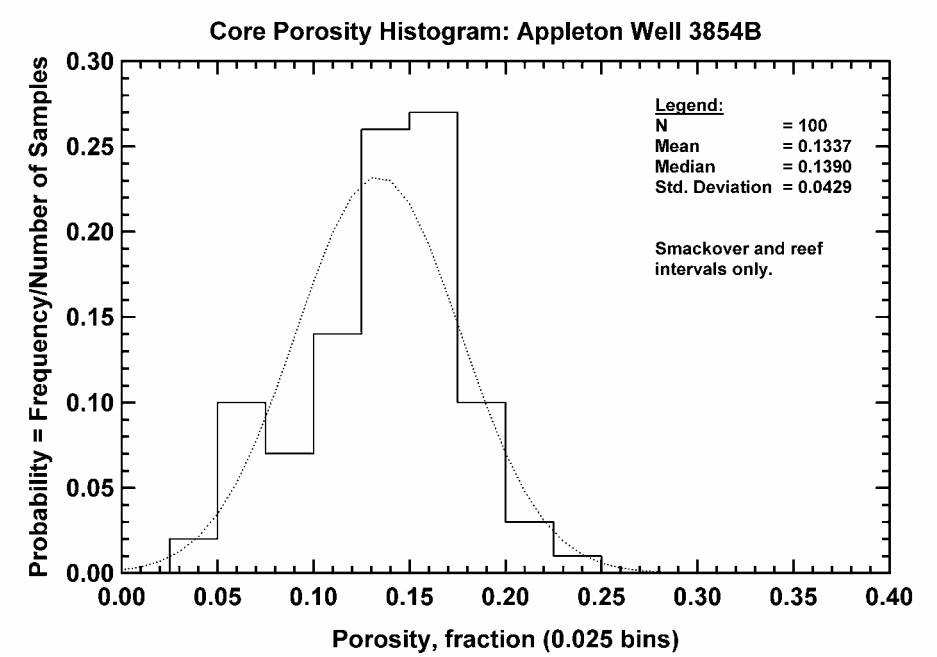

Fig. 128 — Core Porosity Histogram, Appleton Well 3854B

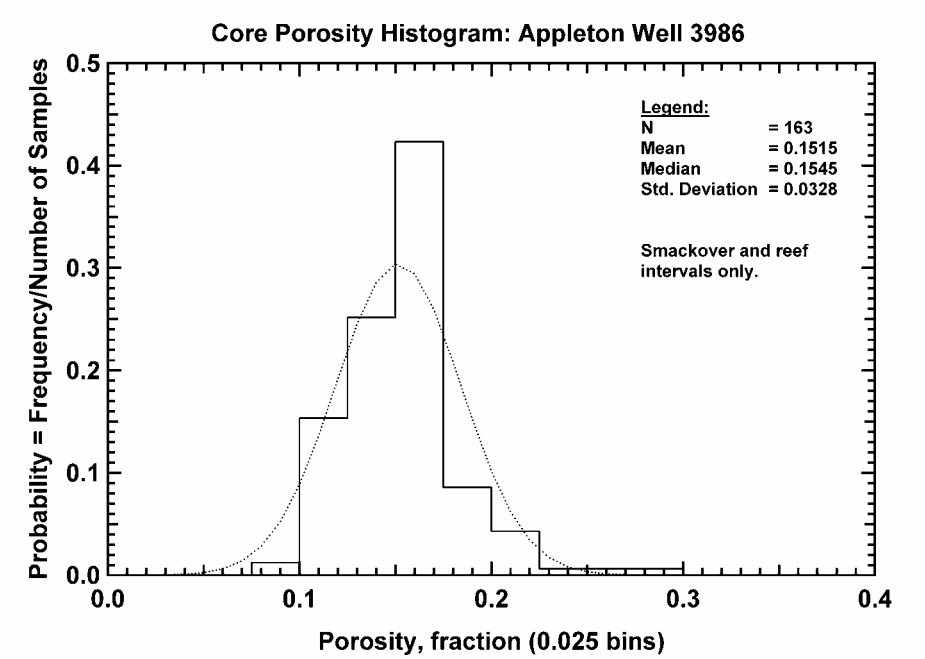

Fig. 129 — Core Porosity Histogram, Appleton Well 3986

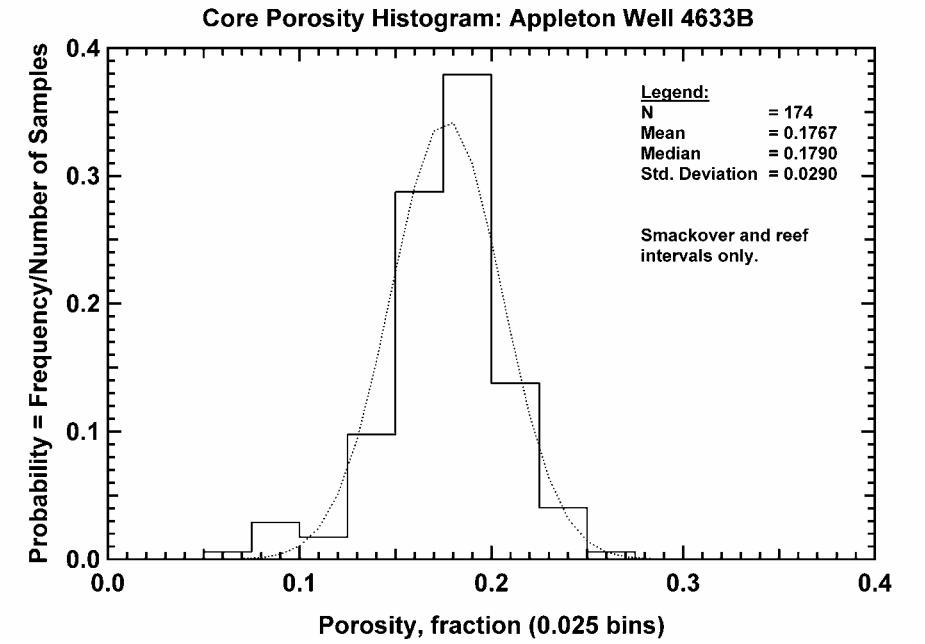

Fig. 130 — Core Porosity Histogram, Appleton Well 4633B

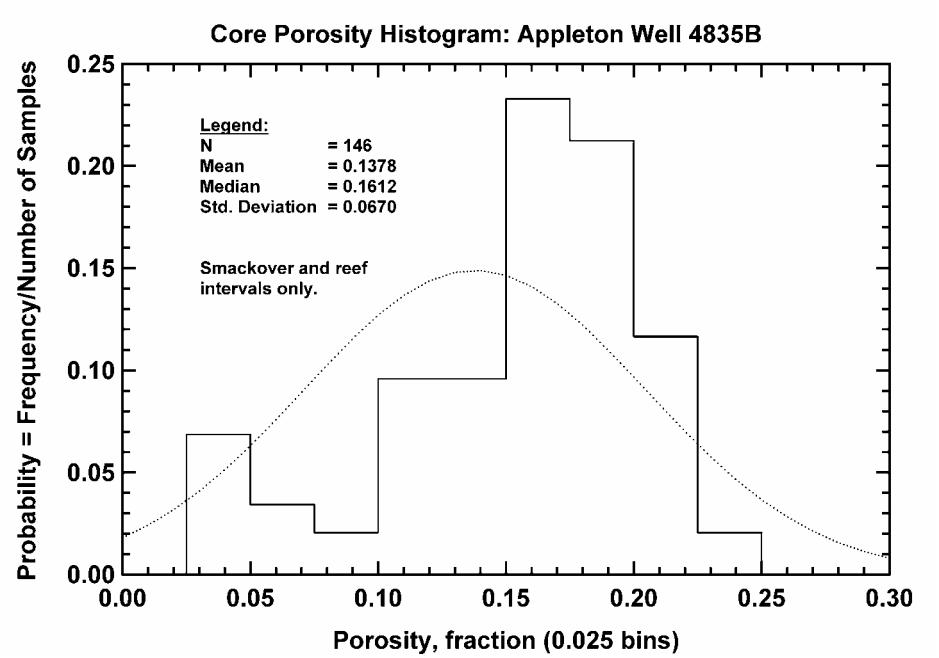

Fig. 131 — Core Porosity Histogram, Appleton Well 4835B

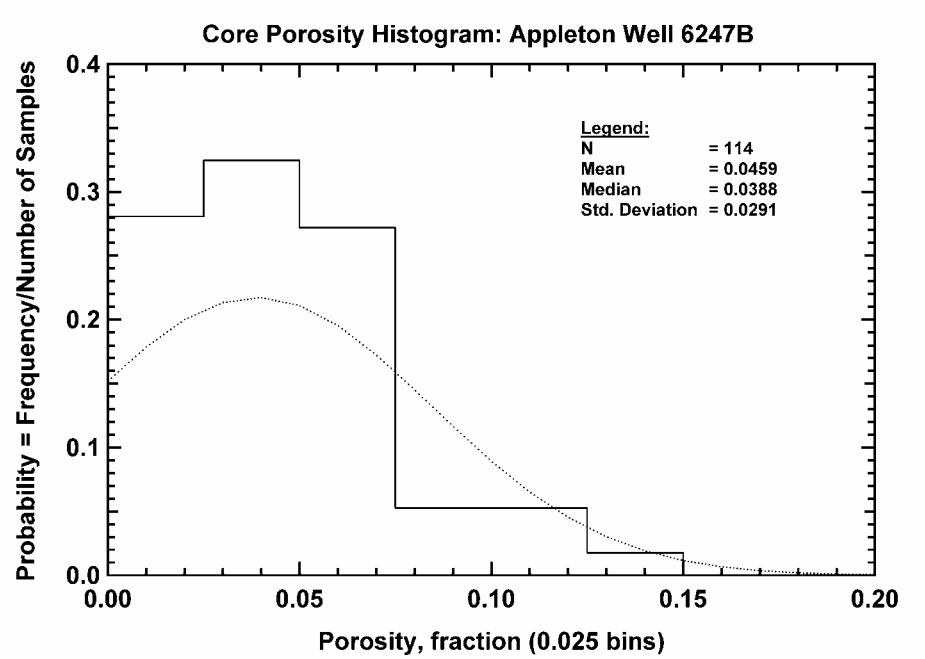

Fig. 132 — Core Porosity Histogram, Appleton Well 6247B

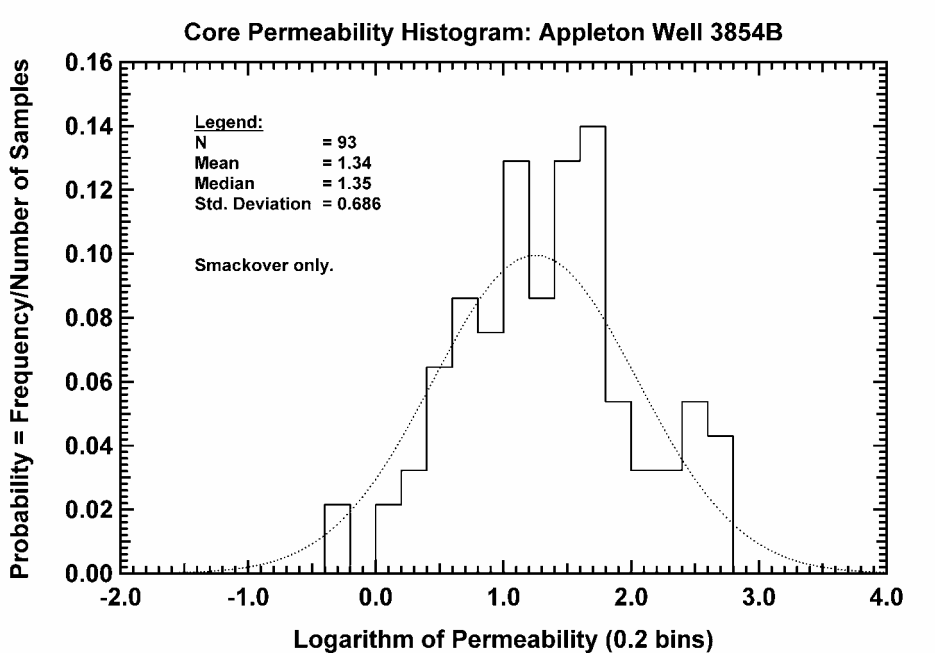

Fig. 133 — Core Permeability Histogram, Appleton Well 3854B

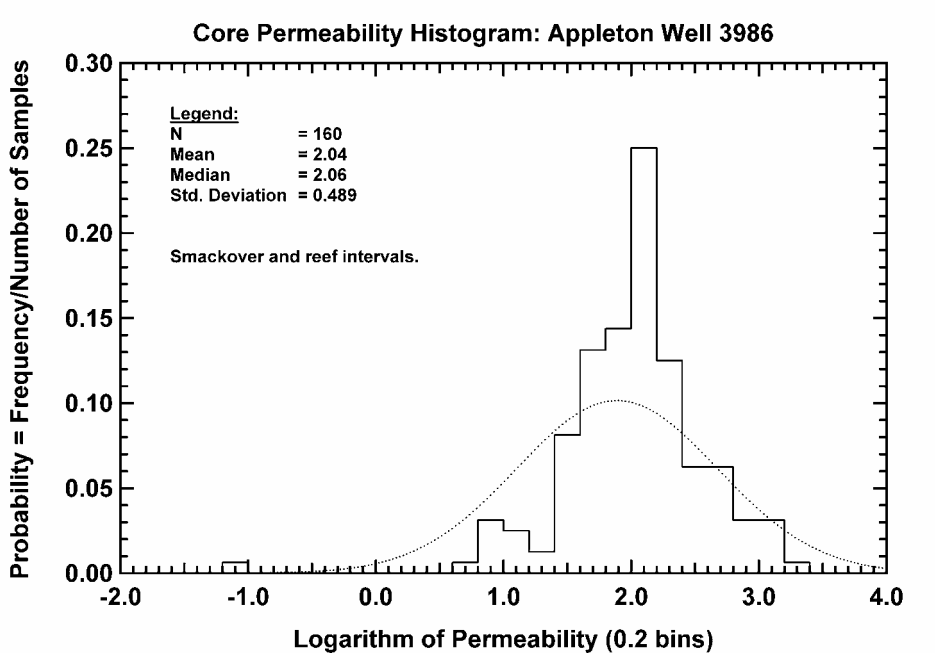

Fig. 134 — Core Permeability Histogram, Appleton Well 3986

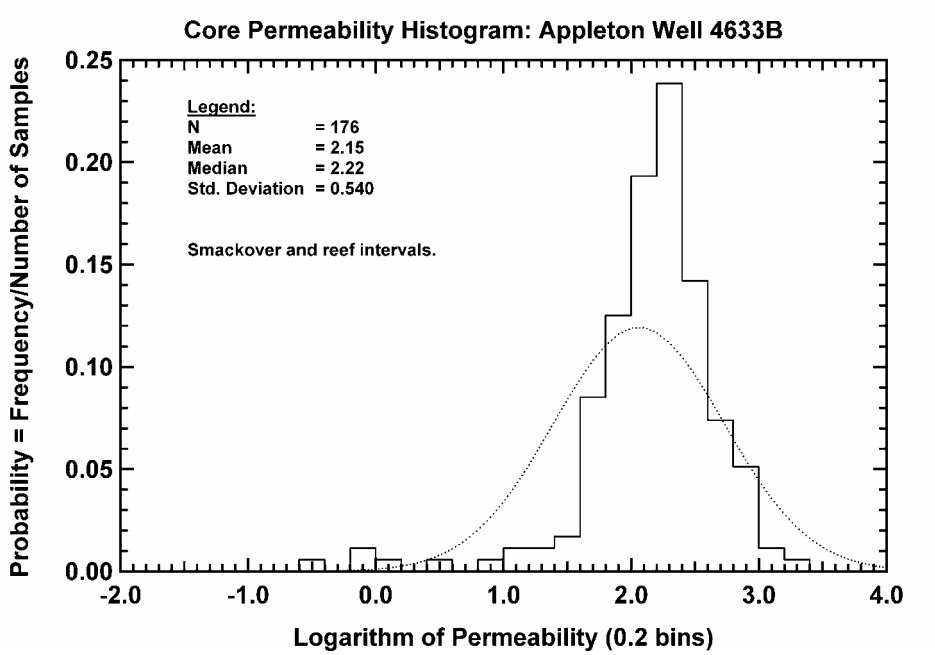

Fig. 135 — Core Permeability Histogram, Appleton Well 4633B

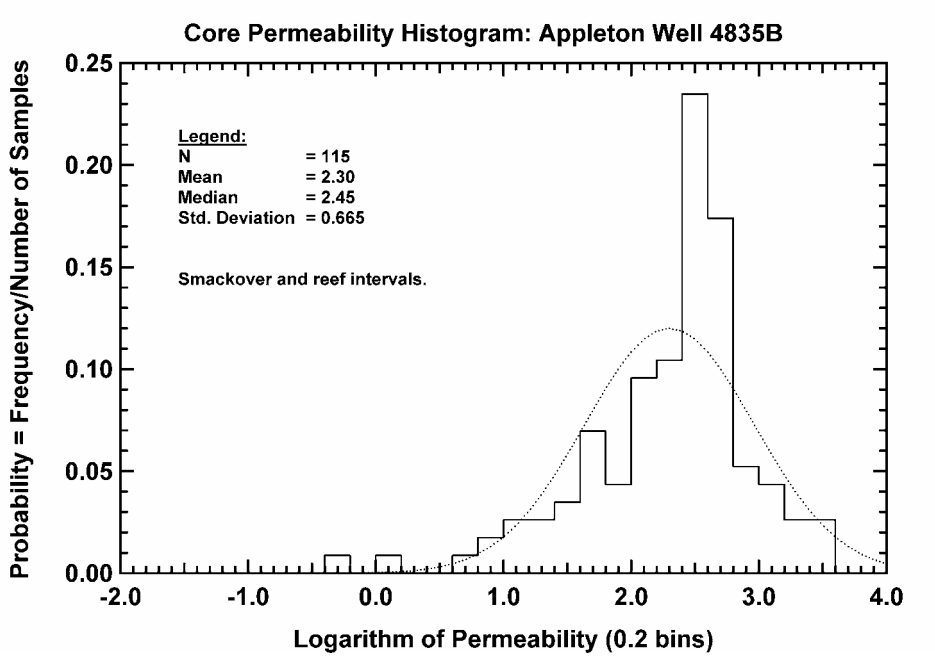

Fig. 136 — Core Permeability Histogram, Appleton Well 4835B

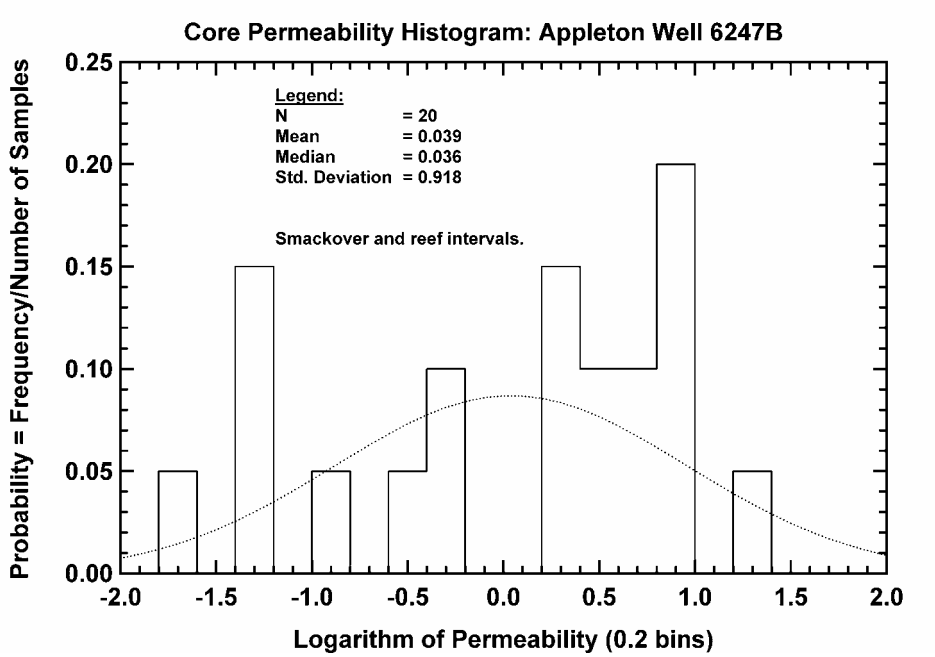

Fig. 137 — Core Permeability Histogram, Appleton Well 6247B

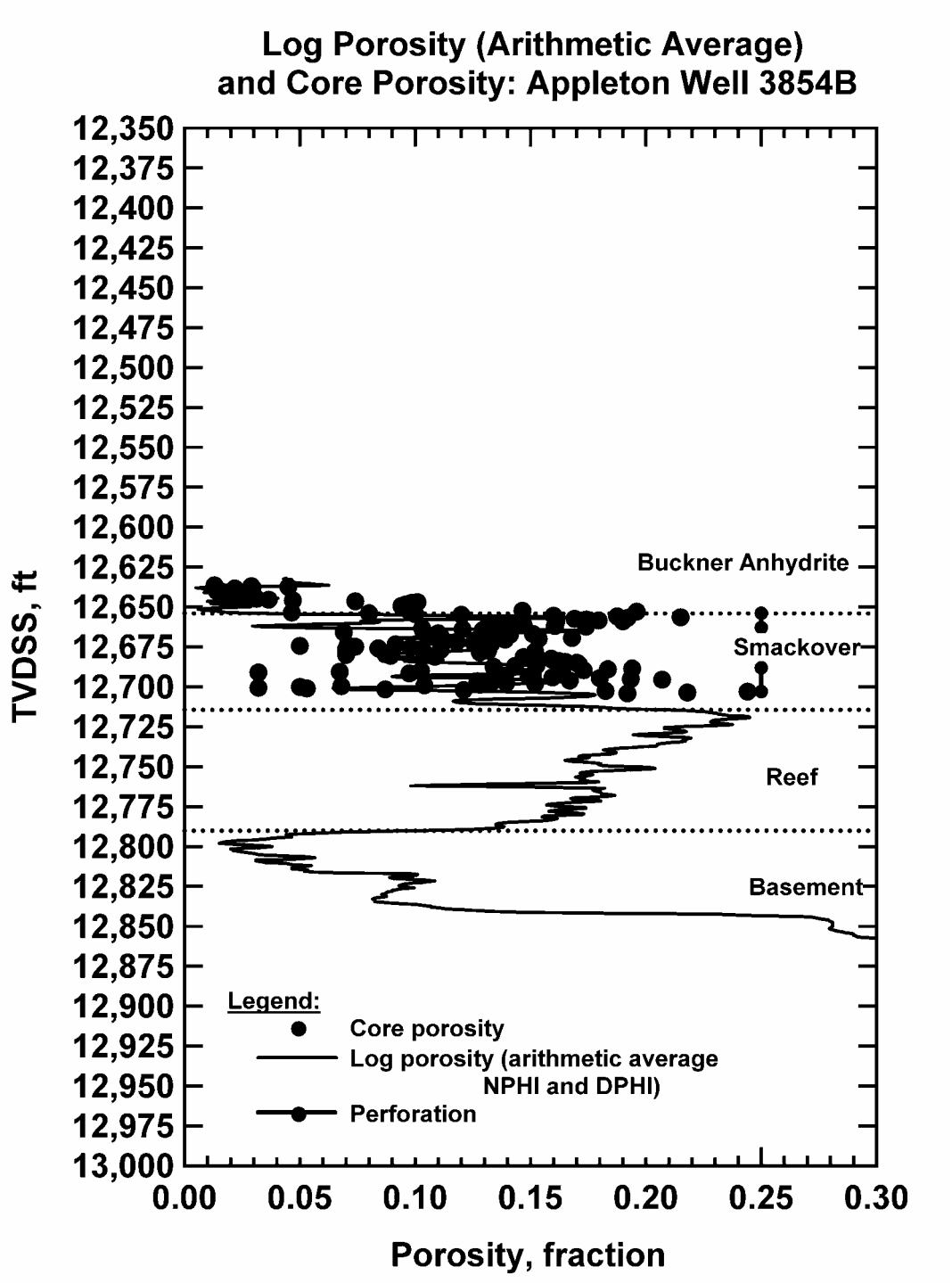

Fig. 138 — Porosity Variation with Depth, Appleton Well 3854B

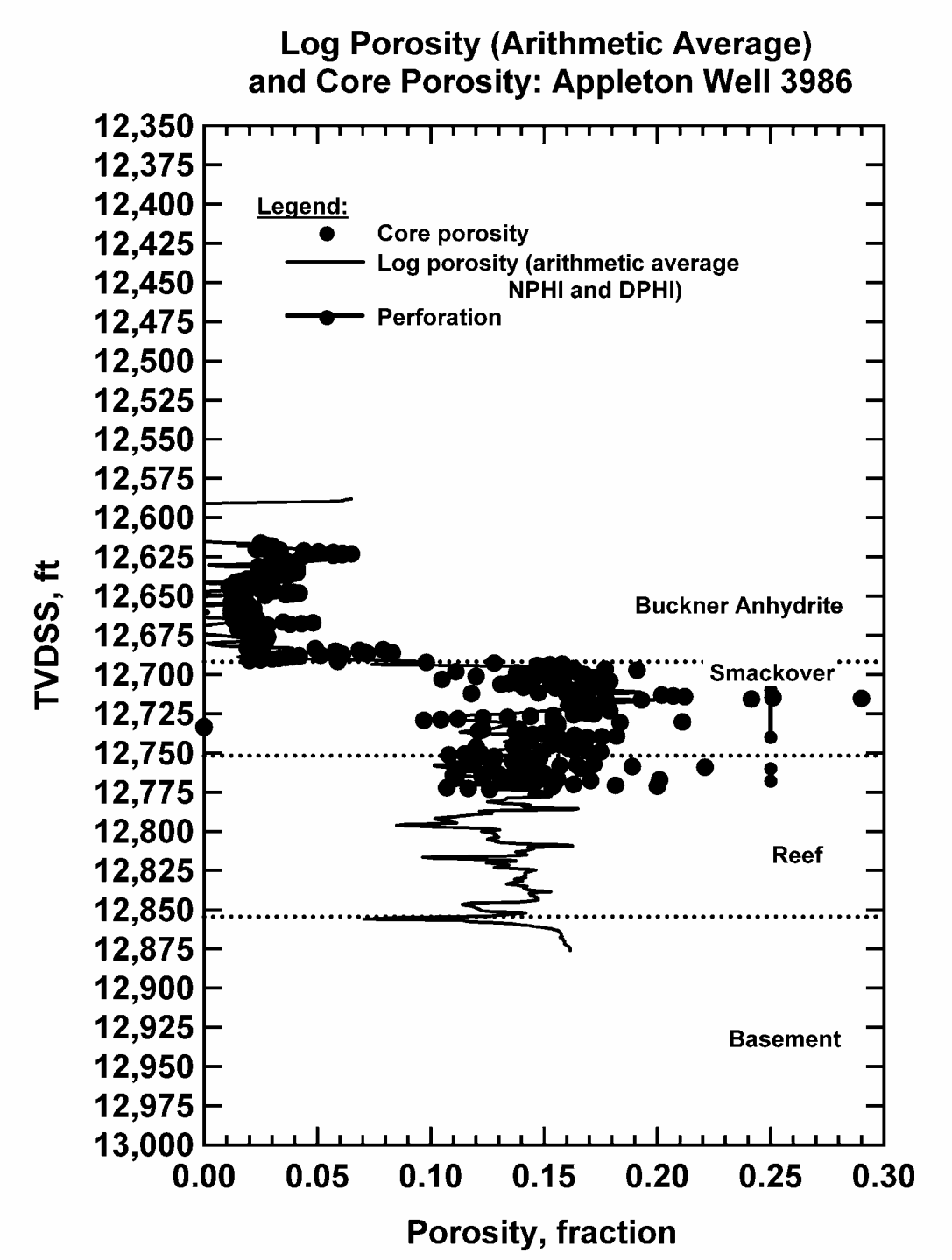

Fig. 139 — Porosity Variation with Depth, Appleton Well 3986

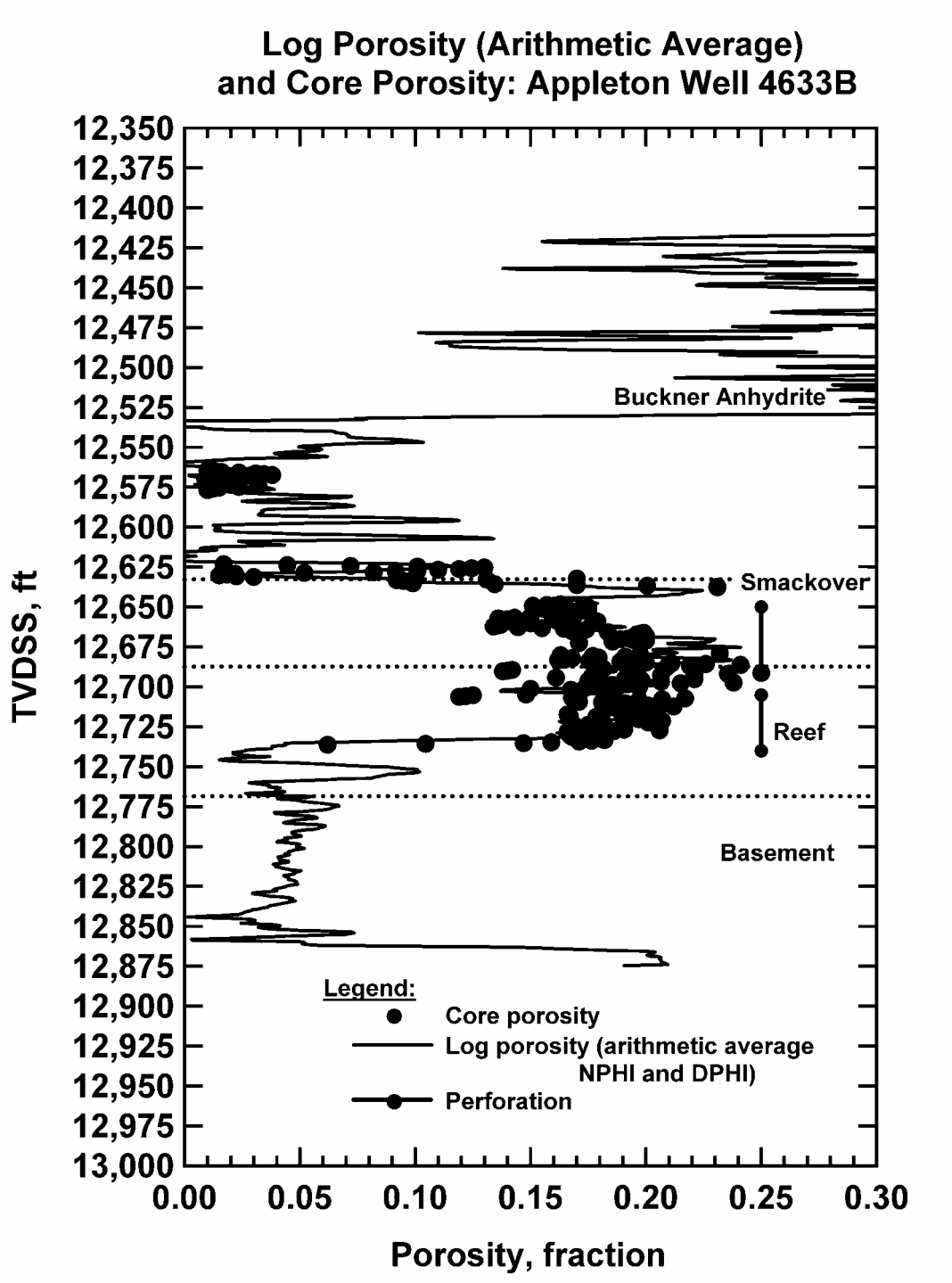

Fig. 140 — Porosity Variation with Depth, Appleton Well 4633B

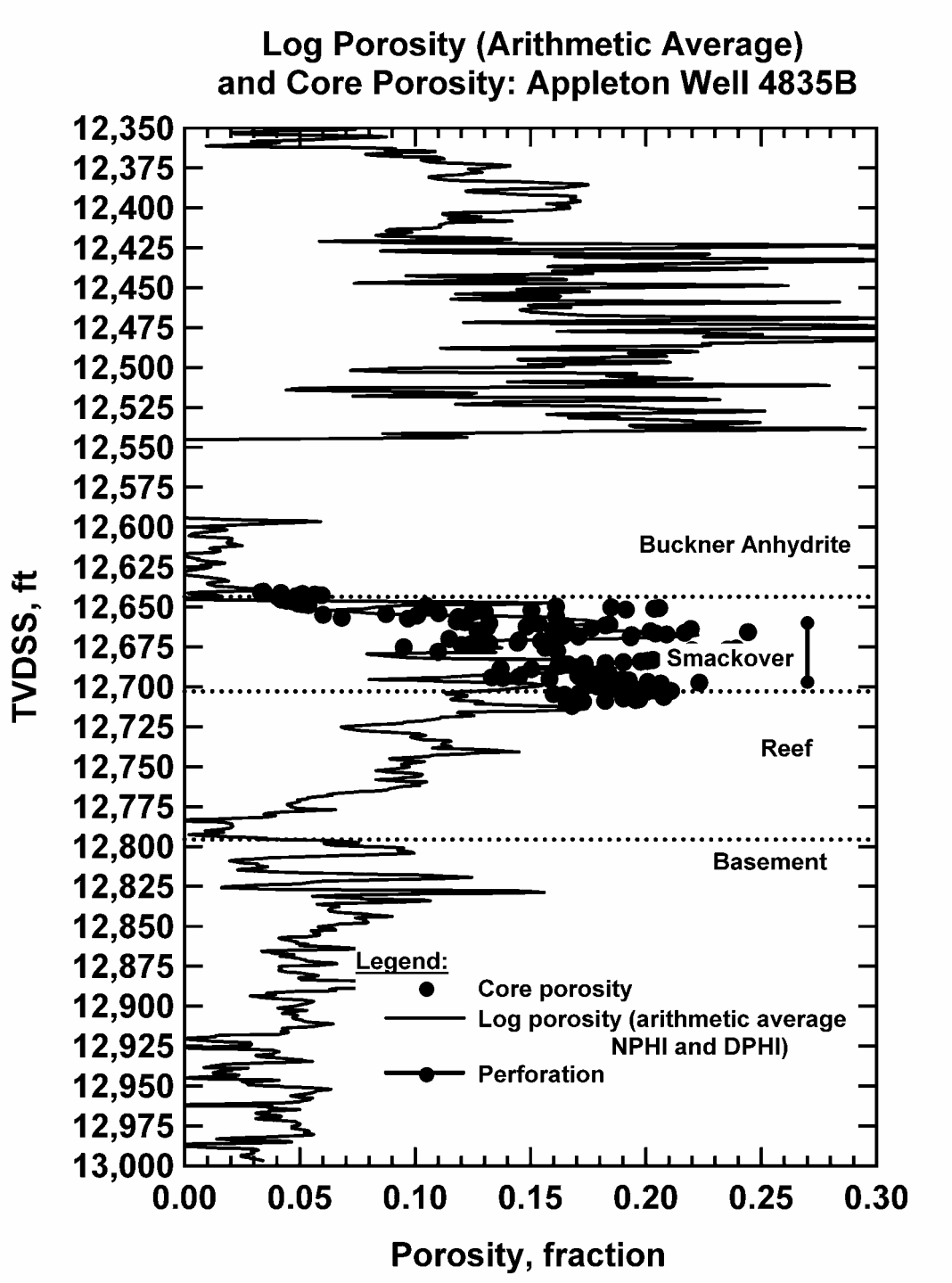

Fig. 141 — Porosity Variation with Depth, Appleton Well 4835B

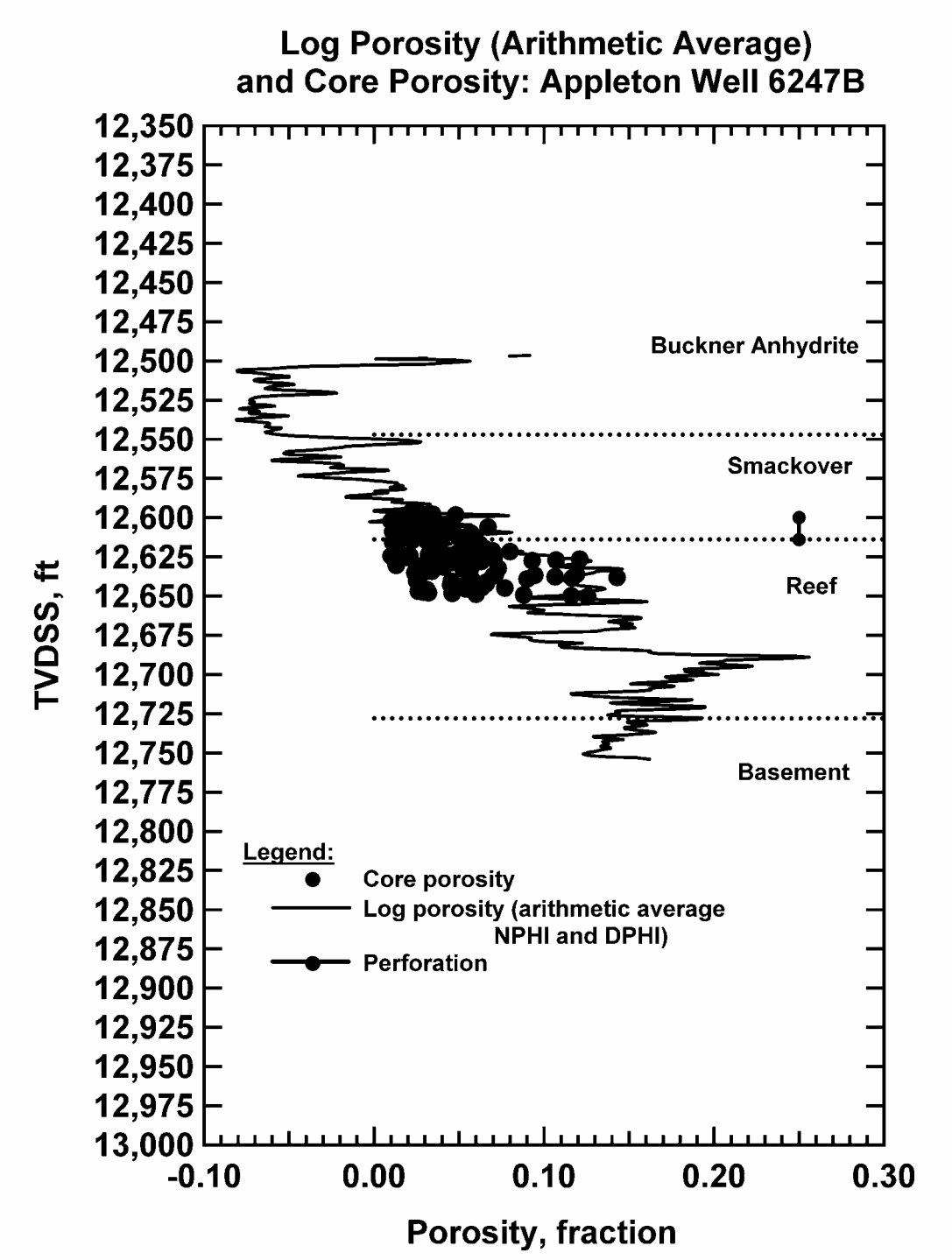

Fig. 142 — Porosity Variation with Depth, Appleton Well 6247B

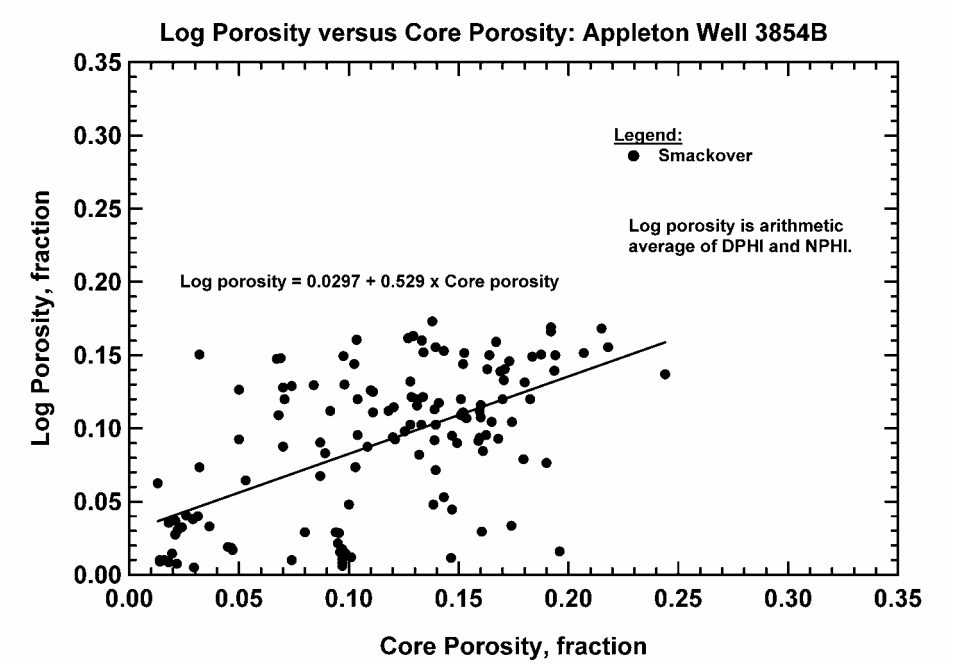

Fig. 143 — Log Porosity versus Core Porosity, Appleton Well 3854B

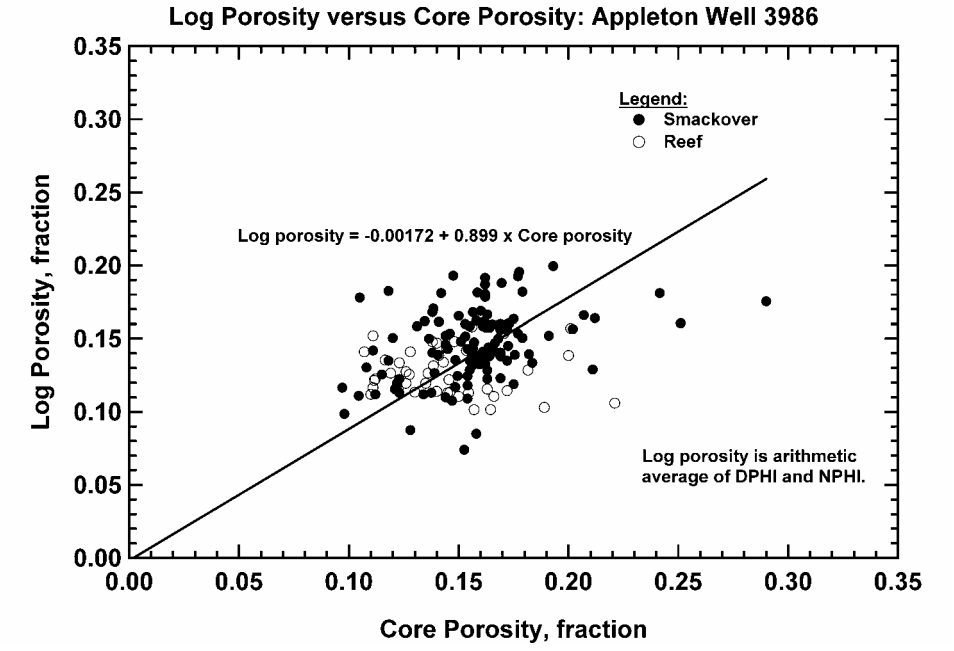

Fig. 144 — Log Porosity versus Core Porosity, Appleton Well 3986

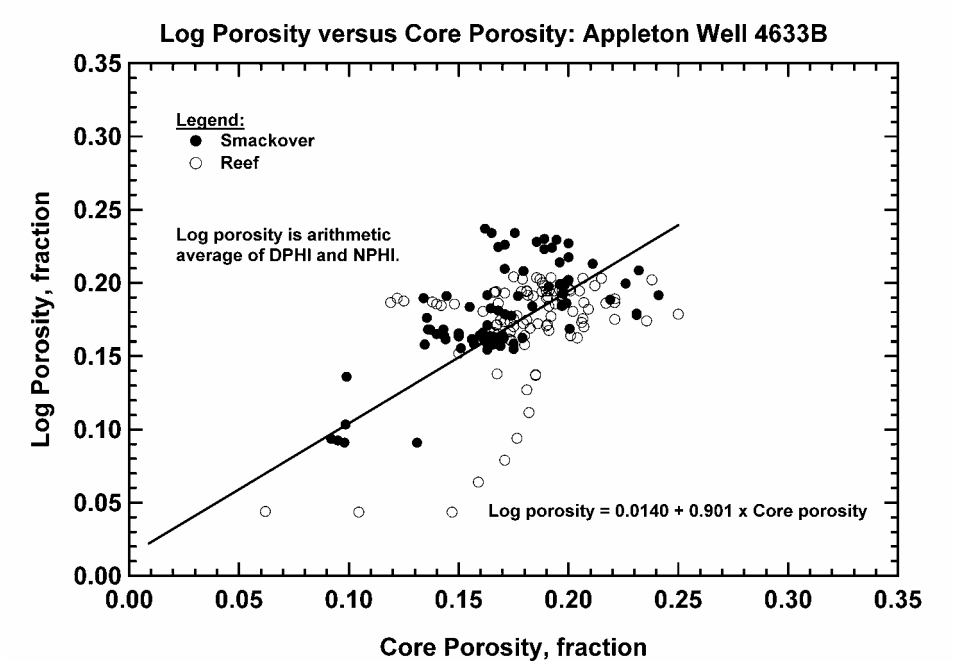

Fig. 145 — Log Porosity versus Core Porosity, Appleton Well 4633B

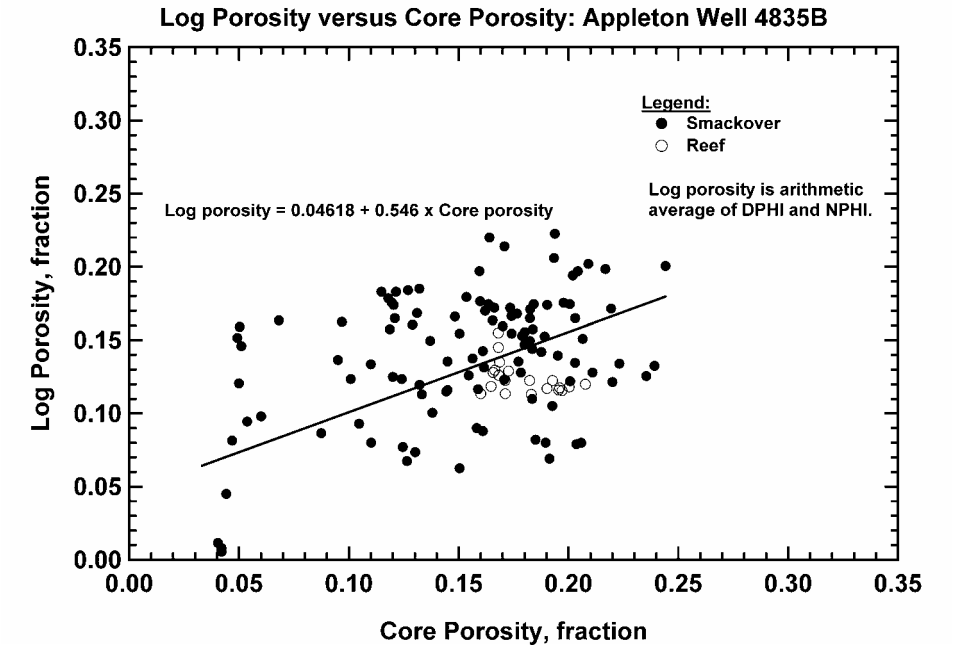

Fig. 146 — Log Porosity versus Core Porosity, Appleton Well 4835B

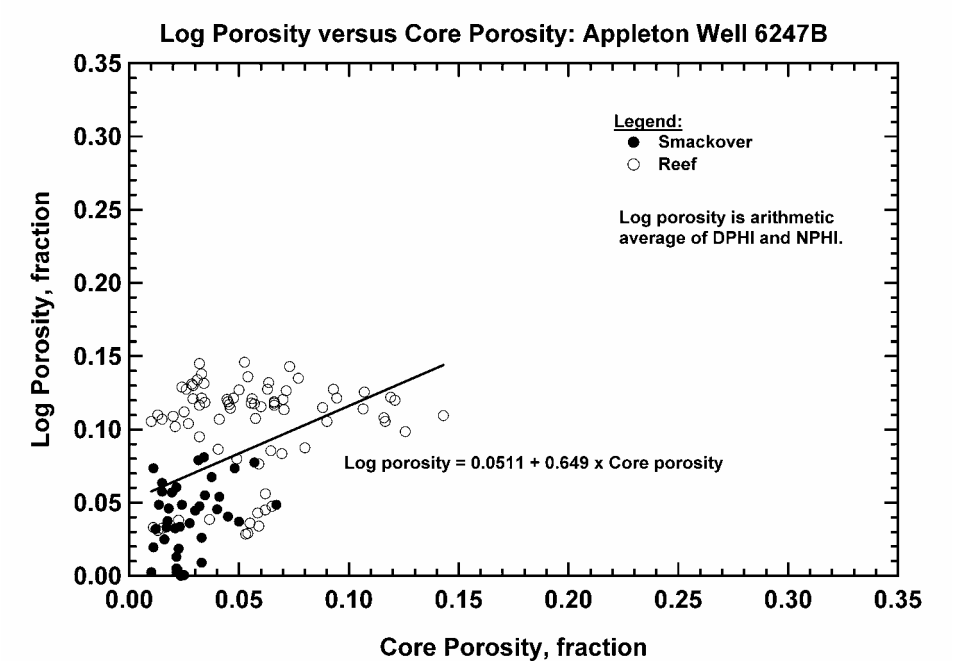

Fig. 147 — Log Porosity versus Core Porosity, Appleton Well 6247B

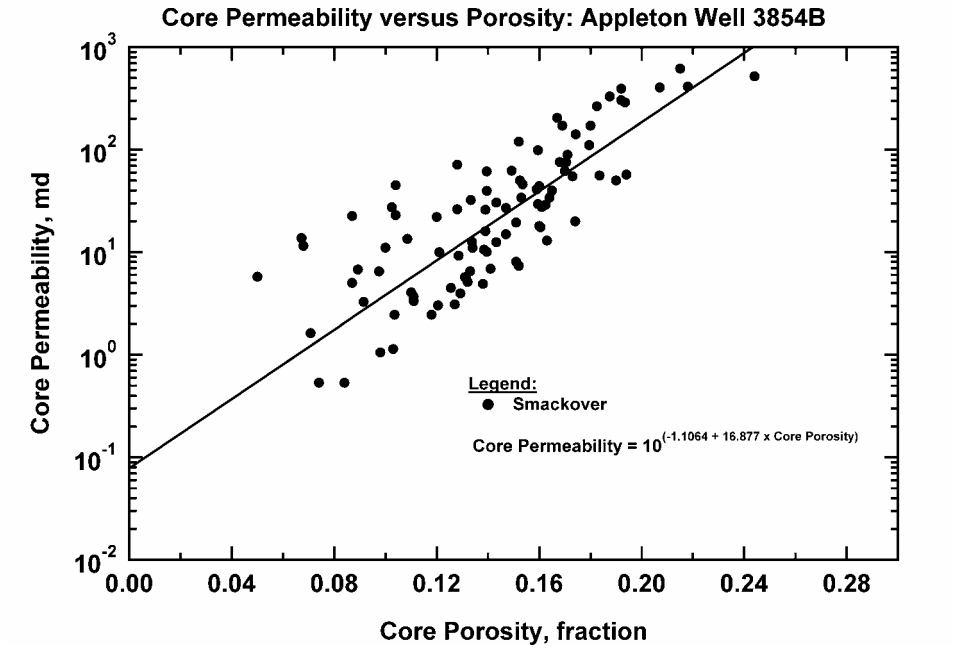

Fig. 148 — Core Permeability versus Core Porosity, Appleton Well 3854B.

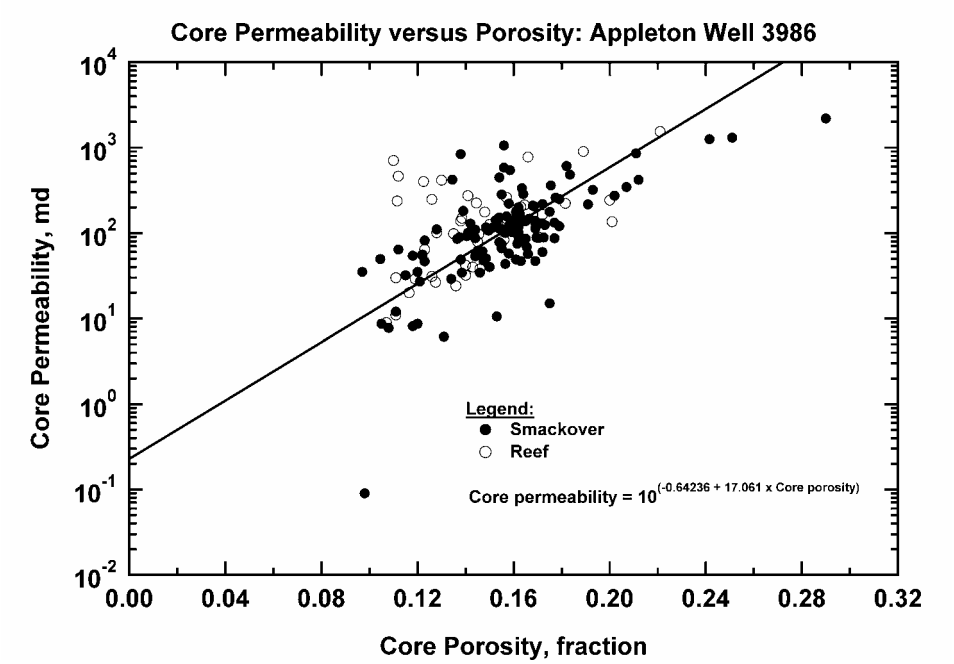

Fig. 149 — Core Permeability versus Core Porosity, Appleton Well 3986.

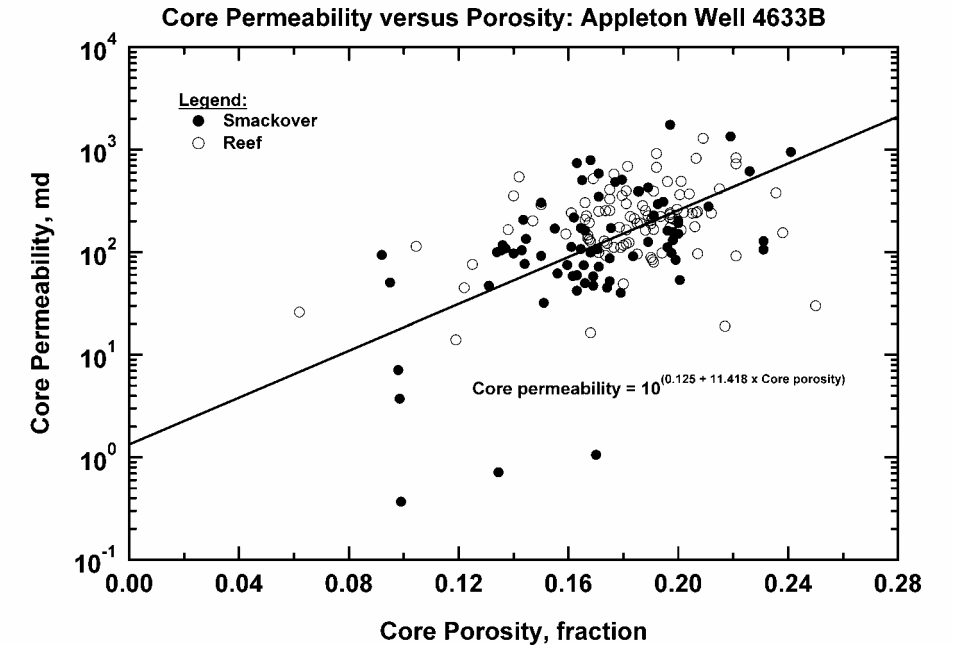

Fig. 150 — Core Permeability versus Core Porosity, Appleton Well 4633B.

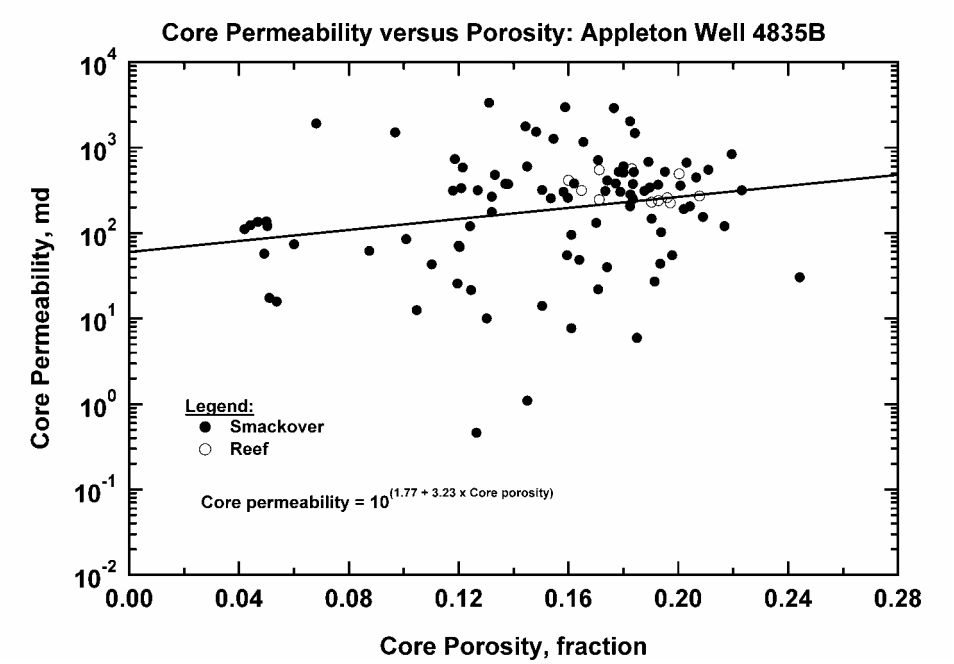

Fig. 151 — Core Permeability versus Core Porosity, Appleton Well 4835B.

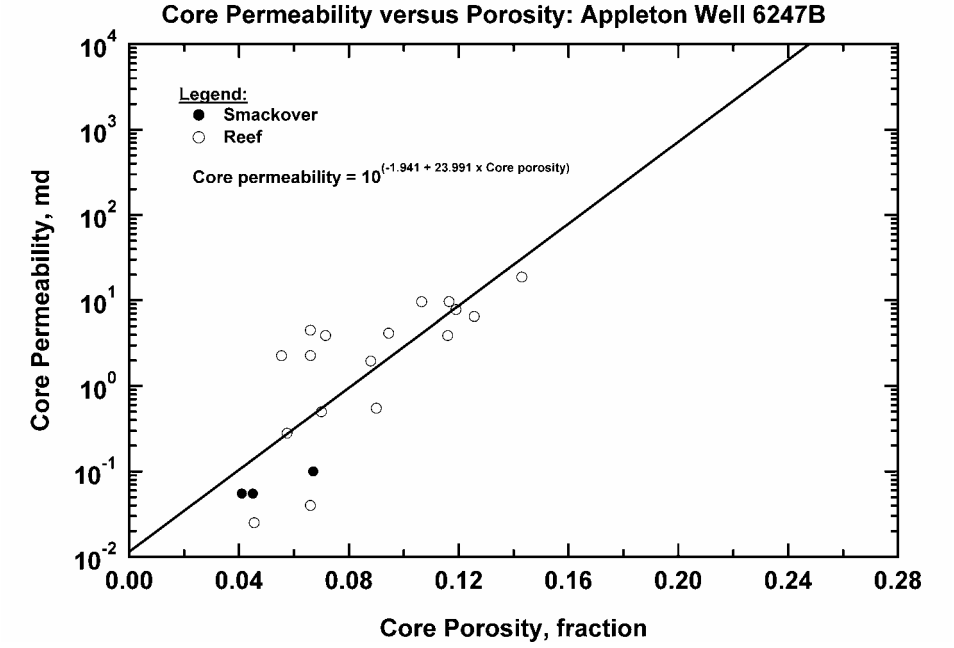

Fig. 152 — Core Permeability versus Core Porosity, Appleton Well 6247B.

Table 16 — Parameters Derived from Type Curve Analysis.

Well	Nc_t (STB/psi)	N (MSTB)	A (acres)	k_o (md)	s (dim-less)
3854B	471.6	25630	1600.5	1.14	-7.6
3986	50.1	2725	35.6	0.06	-5.7
4633B	510.1	27720	680.9	1.86	0.09
4835B	355.4	19320	617.6	3.00	0.12
6247B	62.8	3411	229.0	1.14	-4.7
Total		= 78806			

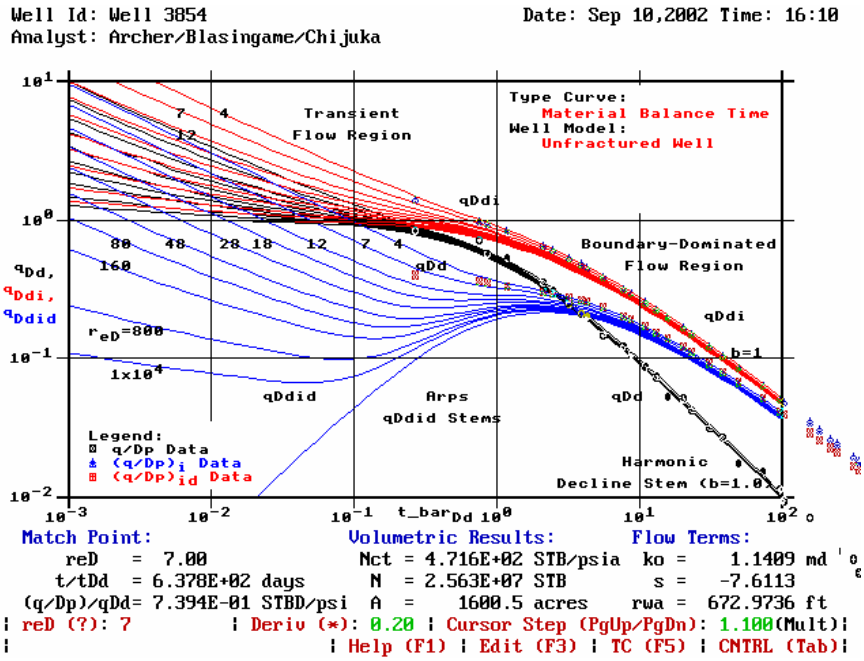

Fig. 153 — Type Curve Match, Appleton Well 3854.

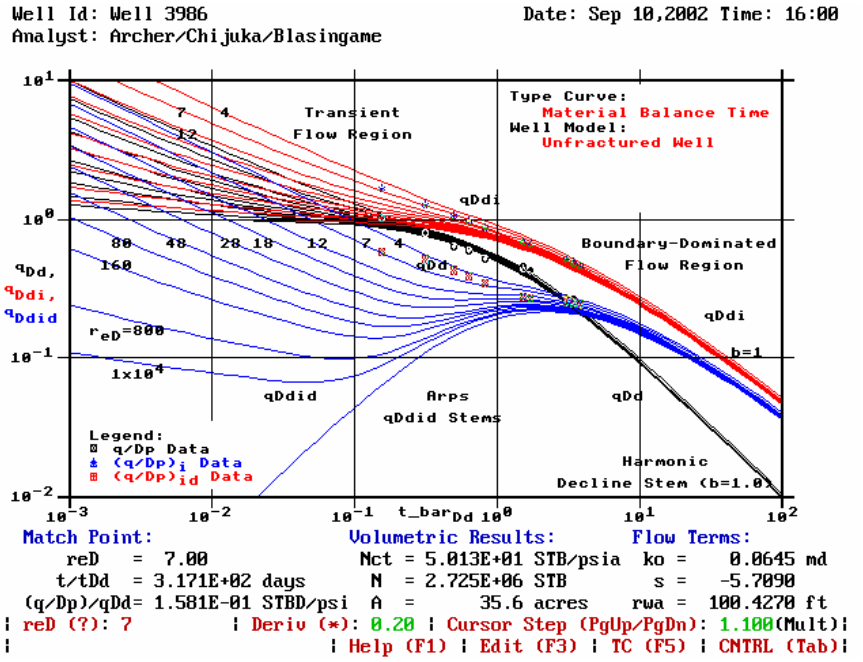

Fig. 154 — Type Curve Match, Appleton Well 3986.

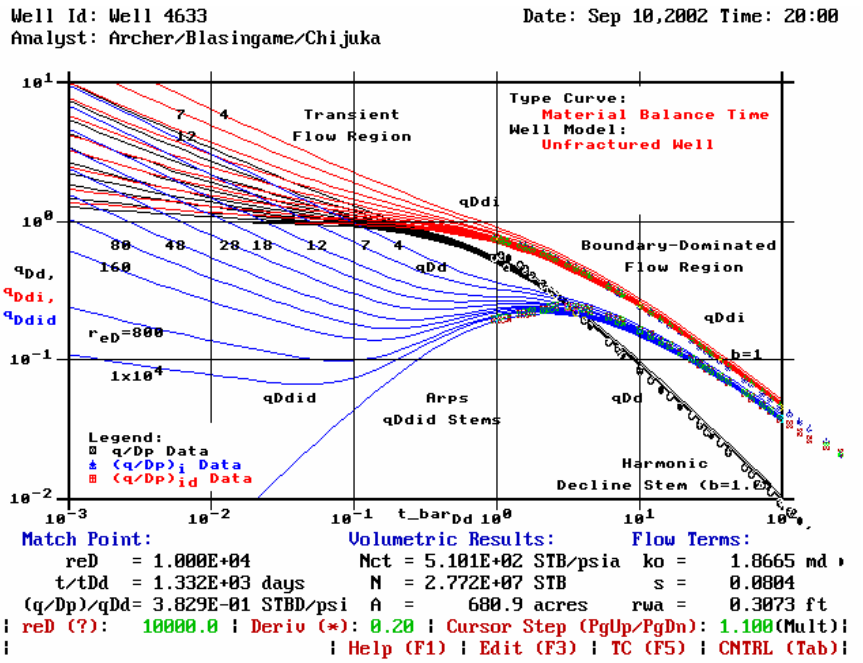

Fig. 155 — Type Curve Match, Appleton Well 4633B.

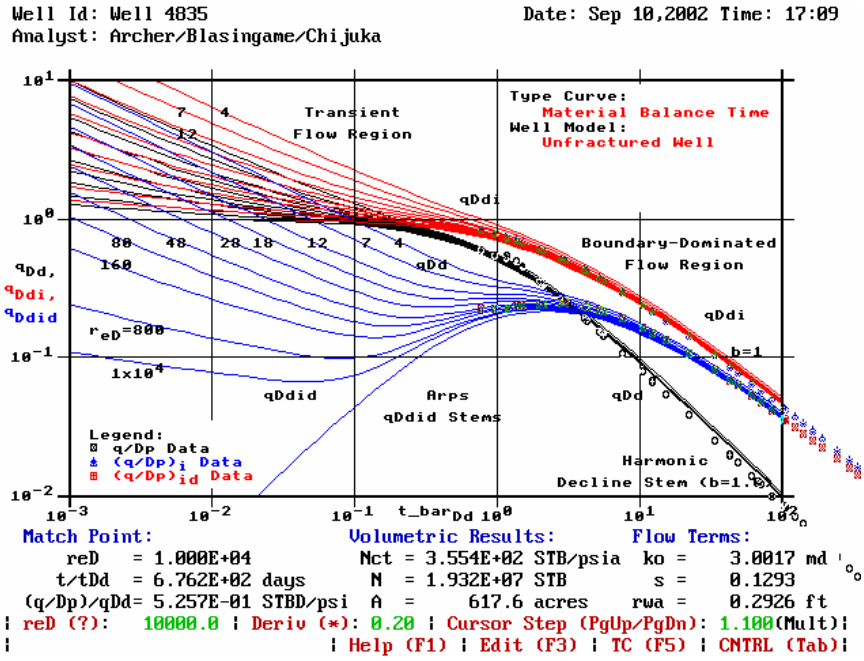

Fig. 156 — Type Curve Match, Appleton Well 4835B.

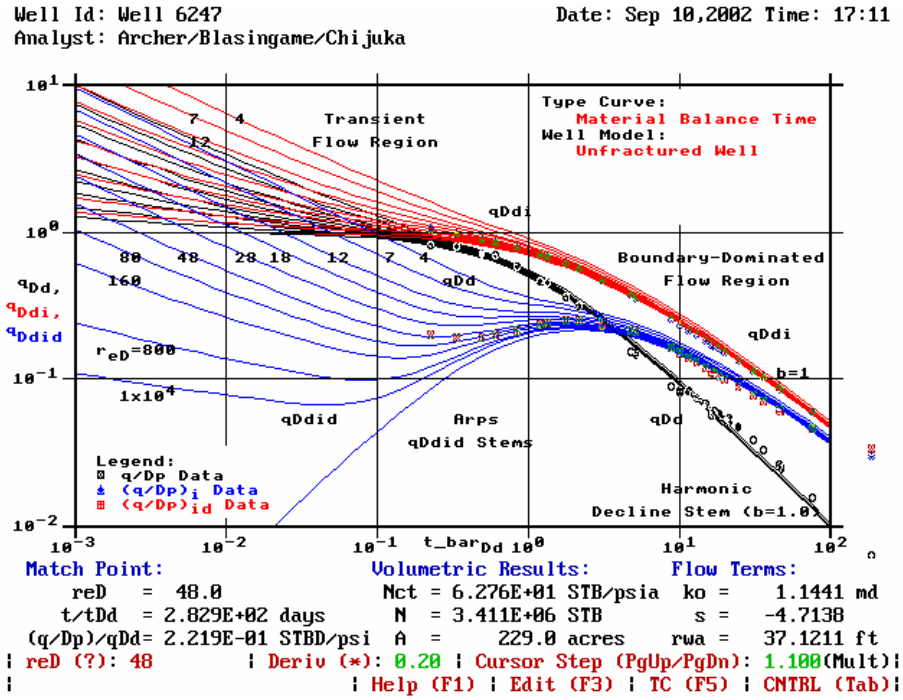

Fig. 157 — Type Curve Match, Appleton Well 6247B.

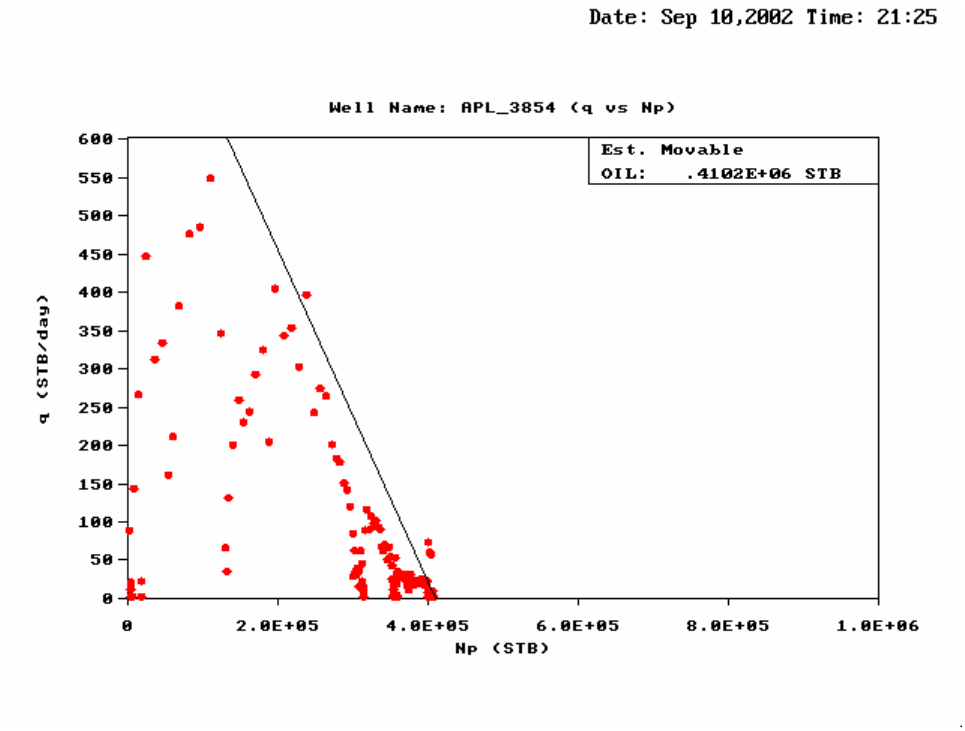

Fig. 158 — Estimate of Recoverable Oil, Appleton Well 3854B.

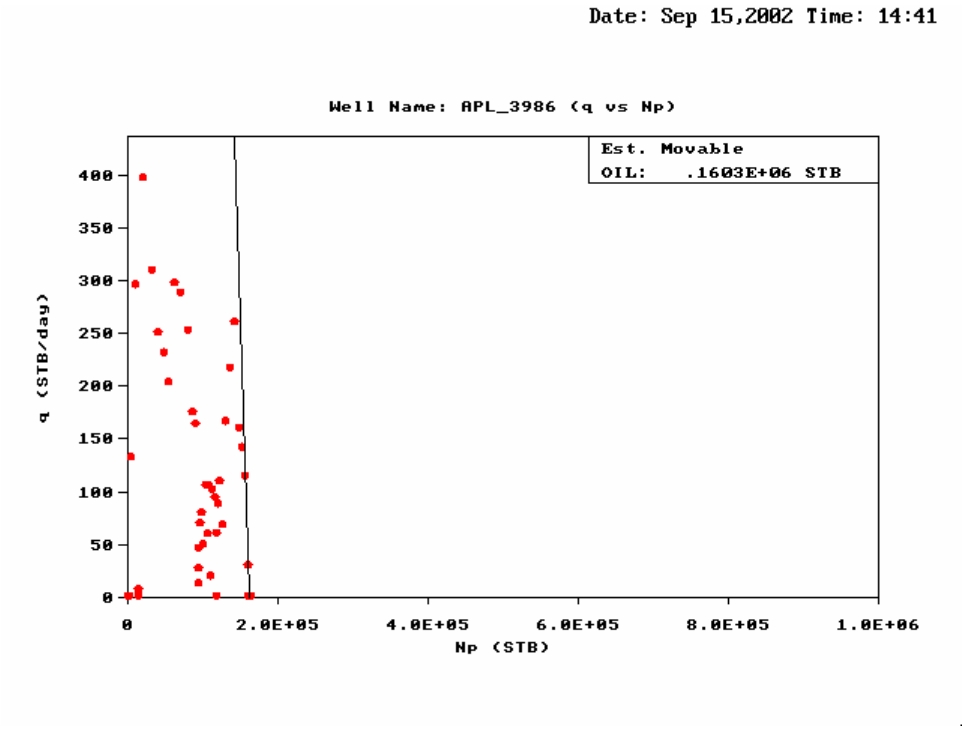

Fig. 159 — Estimate of Recoverable Oil, Appleton Well 3986.

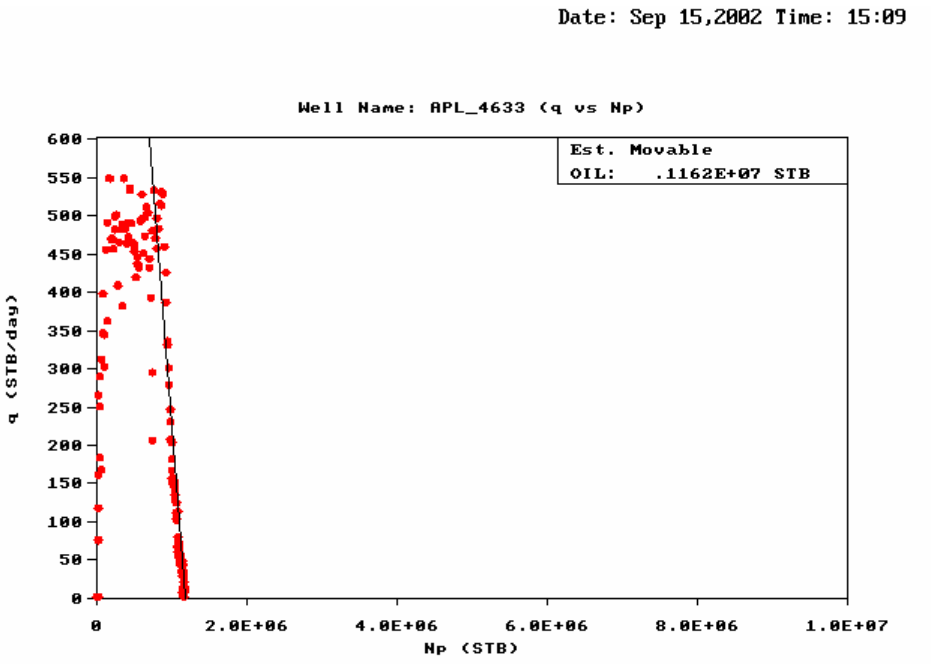

Fig. 160 — Estimate of Recoverable Oil, Appleton Well 4633B.

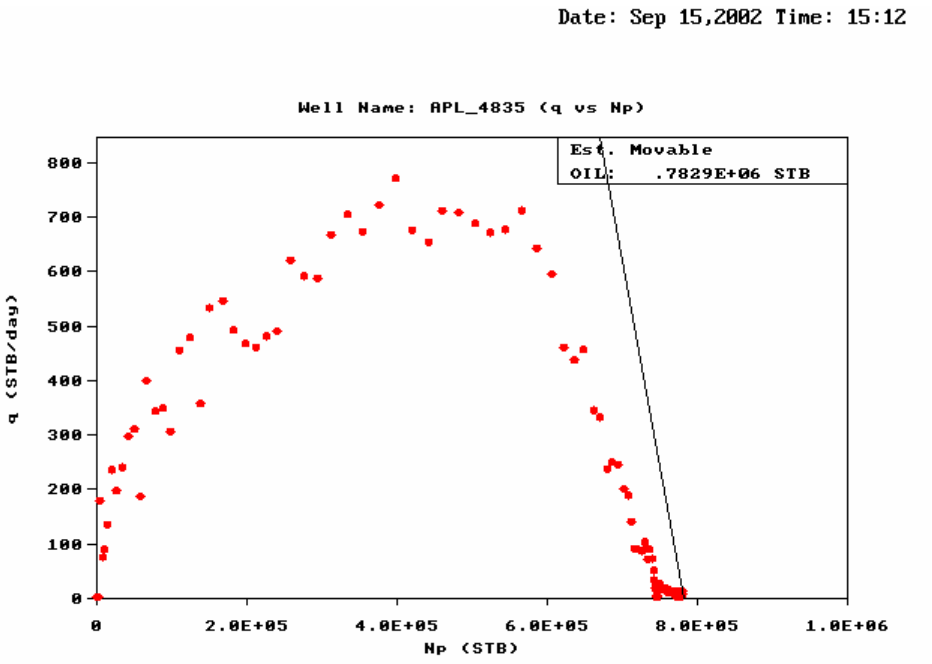

Fig. 161 — Estimate of Recoverable Oil, Appleton Well 4835B.

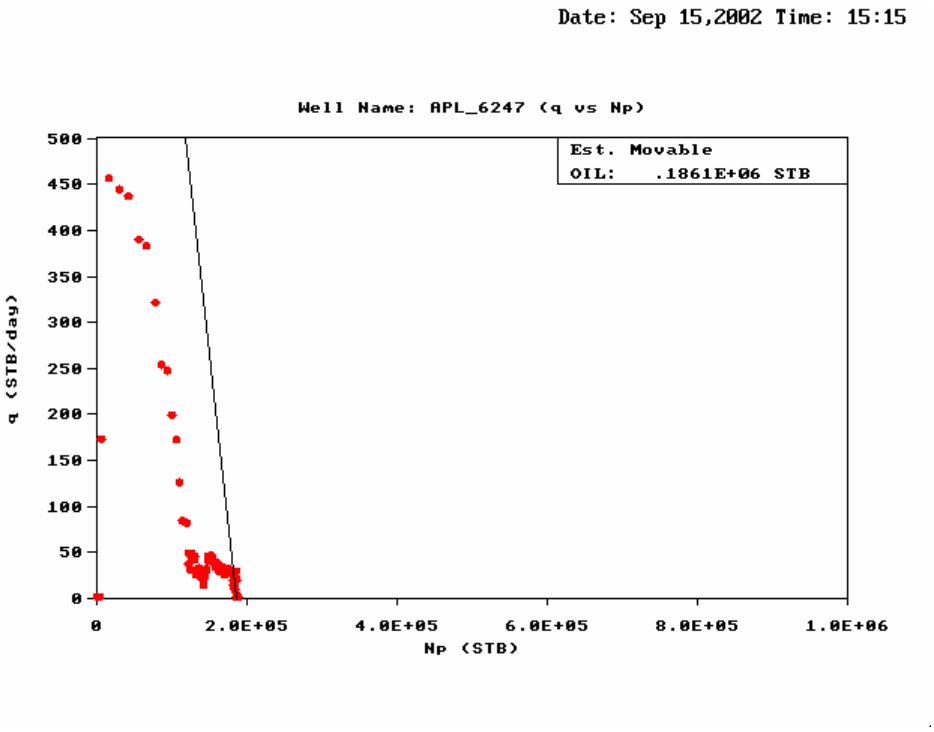

Fig. 162 — Estimate of Recoverable Oil, Appleton Well 6247B.

Table 17 – Oil Recovery and Recovery Factors.

Well	$N_{recoverable}$ (MSTB)	N_p (MSTB)	N (MSTB)	Recovery Factor N_p/N (dim-less)
3854B	410	410	25630	0.016
3986	160	160	2725	0.059
4633B	1160	1150	27720	0.041
4835B	783	780	19320	0.040
6247B	186	180	3411	0.053
Total	= 2699	= 2680	= 78806	= 0.034

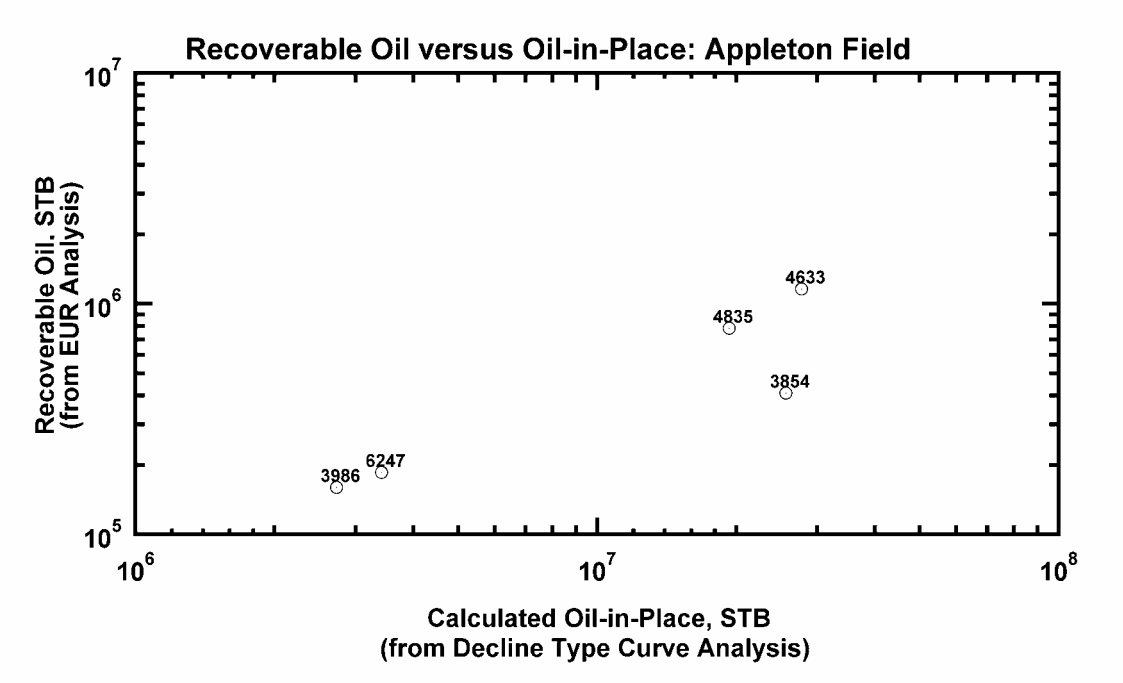

Fig. 163 — Recoverable Oil (*EUR* Analysis) versus Computed Original Oil-in-Place (Decline Type Curve Analysis), Appleton Oil Field.

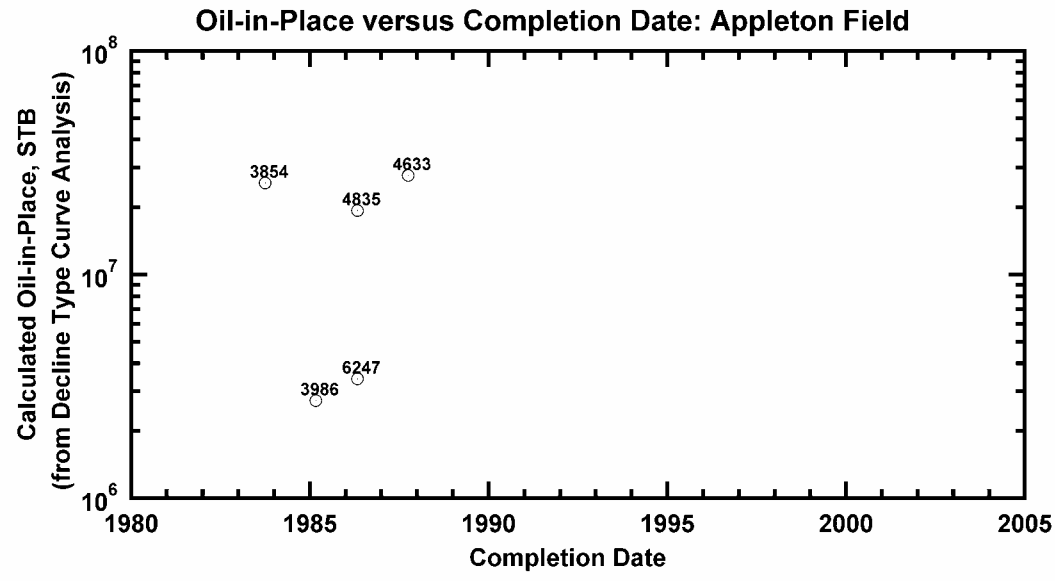

Fig. 164 — Computed Original Oil-in-Place versus Completion Date, Appleton Oil Field.

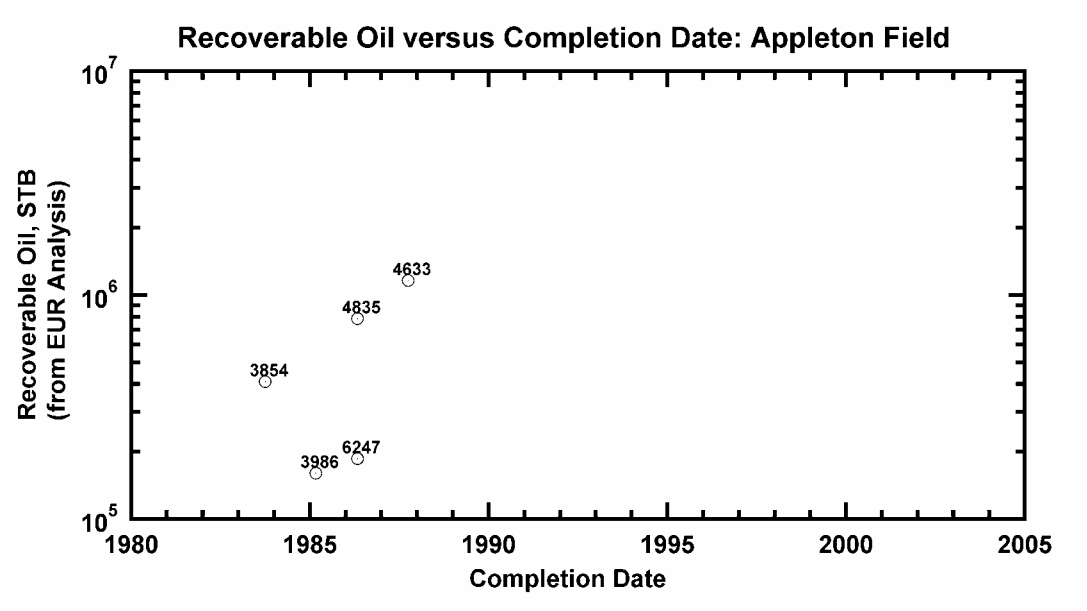

Fig. 165 — Recoverable Oil versus Completion Date, Appleton Oil Field.

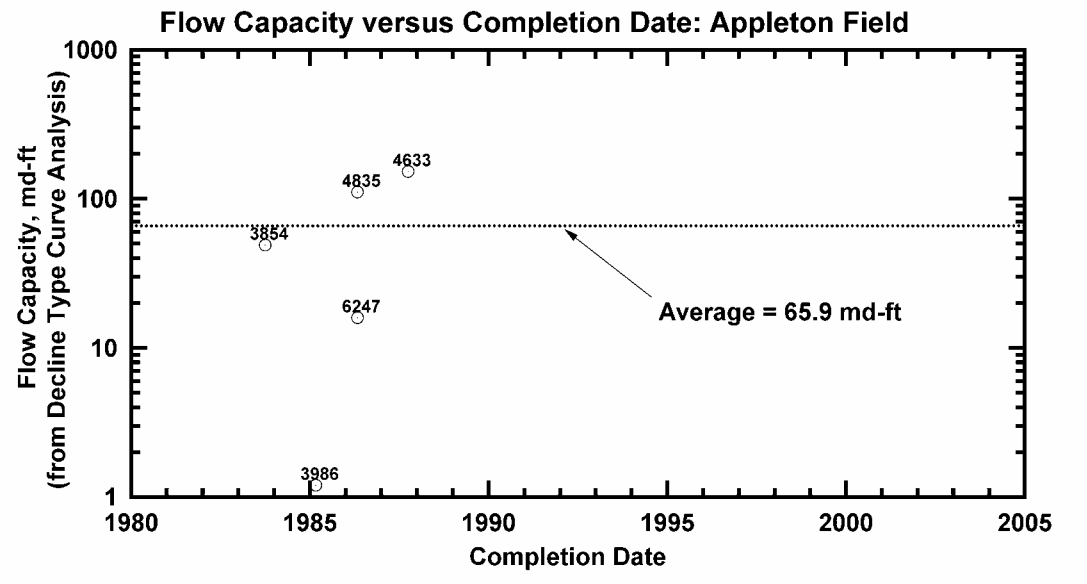

Fig. 166 — Flow Capacity versus Completion Date, Appleton Oil Field.

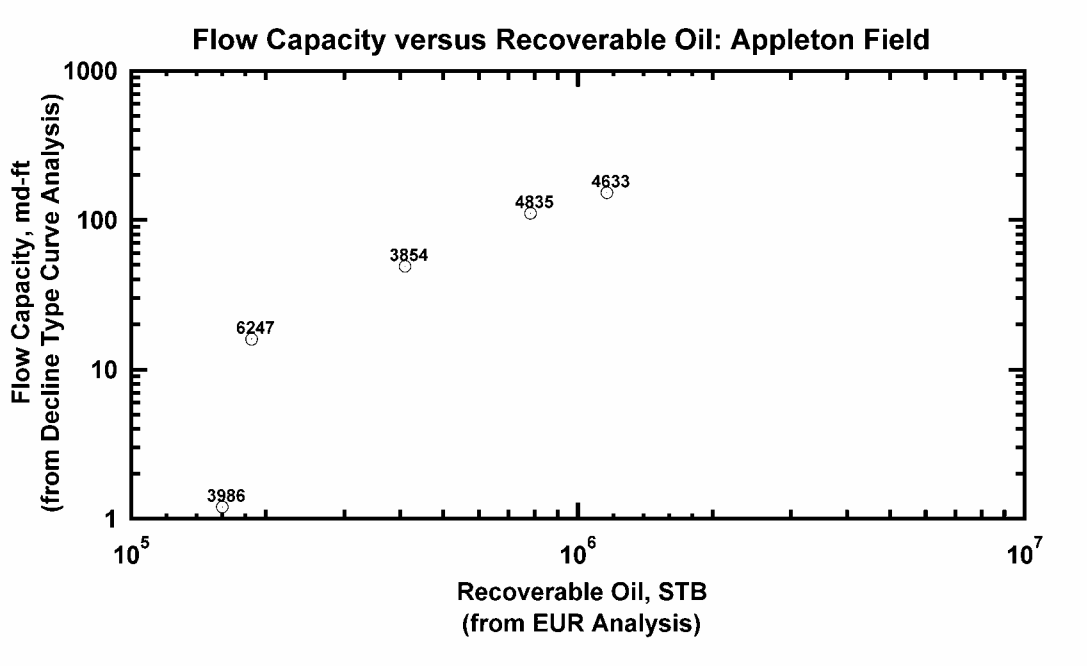

Fig. 167 — Flow Capacity versus Recoverable Oil, Appleton Oil Field.

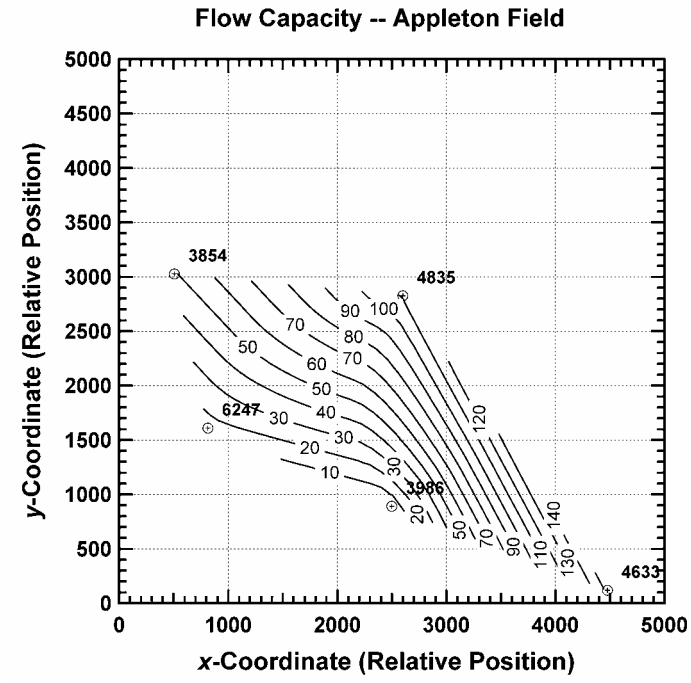

Fig. 168 — Contour Map of Flow Capacity, Appleton Oil Field.

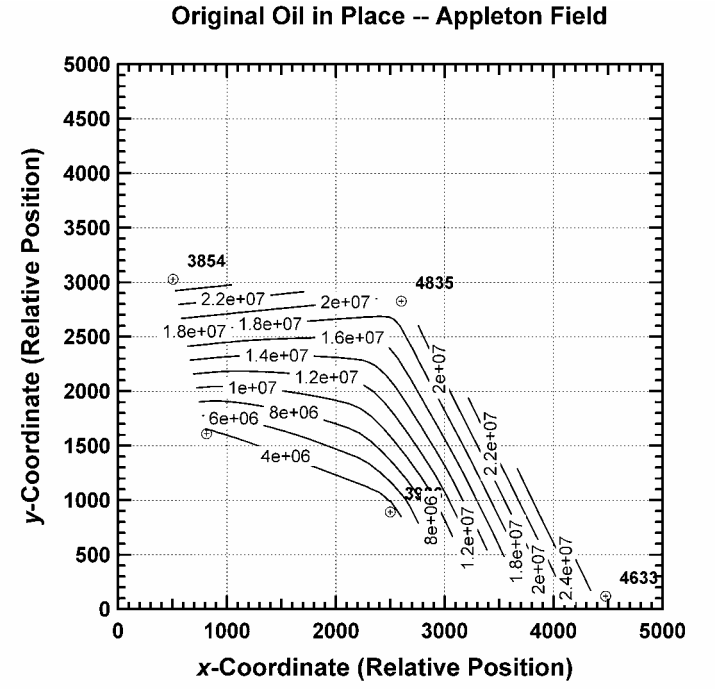

Fig. 169 — Contour Map of Original Oil-in-Place, Appleton Oil Field.

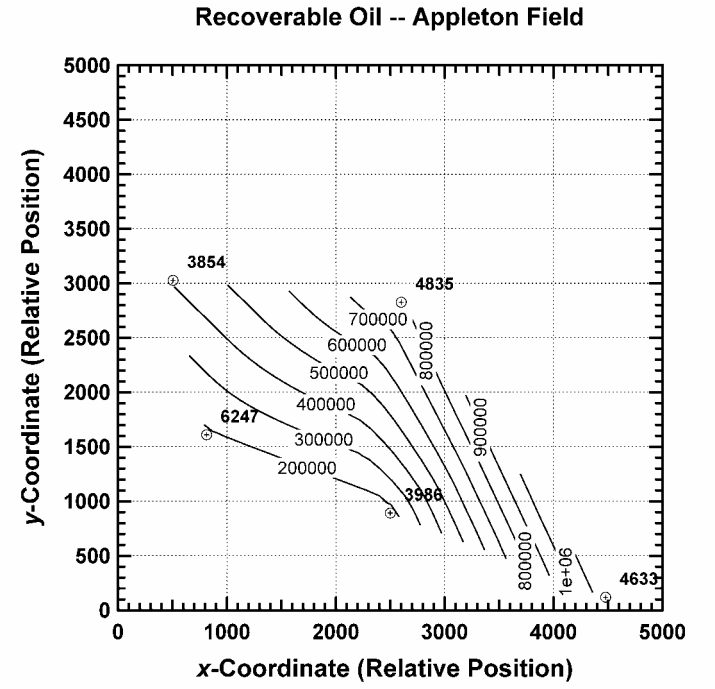

Fig. 170 — Contour Map of Recoverable Oil, Appleton Oil Field.

Analysis of the core and log data indicate that the reservoirs at Appleton Field have a heterogeneous nature. Porosity and permeability data show a significant difference in reservoir quality between the shoal and reef reservoirs, with the reef facies having better reservoir quality compared to the shoal facies. There is poor correlation between the core and log porosity measurements for these facies. The oil in place calculated for Appleton Field using well performance analysis is an optimistic total. Flow capacity of the wells in the field shows a trend of improving reservoir quality in a north and easterly direction, and recoverable oil from each well is strongly correlated with its flow capacity. Structural factors do not appear to have a strong influence on oil recovery at Appleton Field.

Well Test Analysis/Reservoir Description. In this work two well test sequences from wells in Appleton Field (Wells Graham 2-16 and McMillan 14-2-3) were analyzed using modern well test analysis methods. We note that the testing records appear to indicate very short drawdown periods (Graham 2-16 (4 hr) and McMillan 14-2-3 (10 hr)), followed by relative long shut-in periods on the order of 70-80 hr. Having noted this, we were able to perform analyses and have obtained results which we believe are reasonably correct. We note that the results for the "raw" and "smoothed" data sets are "forced" — *i.e.*, the analysis for each data set is forced to yield the same results.

The results for these well test analyses are provided in the table given below:

Table 18 —Well Test Analysis Results for Graham Well 2-16 and McMillan Well 14-2-3 (testing sequence of November 2003). Appleton Field (Alabama, USA)

Graham Well 2-16	***Raw Data***	***Smoothed Data***
Constant Rate Analysis	**Figs. 1.b-1.d**	**Figs. 1.e-1.g**
Wellbore Storage Coefficient, C_s	0.15 RB/psi	0.15 RB/psi
Permeability, *k*	7.5 md	7.5 md
Skin Factor, *s*	7	7
Variable Rate Analysis (Assumed)	**(Not Shown)**	**(Not Shown)**
Wellbore Storage Coefficient, C_s	0.005 RB/psi	0.005 RB/psi
Permeability, *k*	4.8 md	4.8 md
Skin Factor, *s*	2.9	2.9
McMillan Well 14-2-3	***Raw Data***	***Smoothed Data***
Constant Rate Analysis	**Figs. 2.b-2.d**	**Figs. 2.e-2.g**
Wellbore Storage Coefficient, C_s	0.02 RB/psi	0.02 RB/psi
Permeability, *k*	25.3 md	25.3 md
Skin Factor, *s*	98.7	98.7
Variable Rate Analysis (Assumed)	**(Not Shown)**	**(Not Shown)**
Wellbore Storage Coefficient, C_s	0.025 RB/psi	0.025 RB/psi
Permeability, *k*	24.9 md	24.9 md
Skin Factor, *s*	97.5	97.5

These well test analysis (Figures 171 and 172) results are consistent with results from other data types we have for this field (*e.g.*, petrophysical data and well performance data). It is noted that the "constant rate" analysis presumes that the wells were on production continuously prior to shut-in, while the "variable rate" analyses presumes that the wells were produced, shut-in for installation of equipment, and then produced again (as prescribed in the Schlumberger well test report), then shut-in for the final pressure buildup sequences. Assumptions are made with regard to production and shut-in times for the "variable rate" cases, and it is noted that while we

were able to achieve good data matches for the radial flow regime (for permeability and skin factor estimation), the remainder of the data were poorly matched.

As noted, the permeabilities estimated from these well tests are corroborated with other data — however, the skin factor estimate of 98.7 for McMillan Well 14-2-3 (constant rate analysis) implies well damage (or poor communication between the reservoir and the well). Such a result typically implies a failure in the well completion — plugged perforations, gas or water blockage, etc. It appears that the McMillan Well 14-2-3 is performing at a fraction of its capability.

Another interesting result of these well tests is derived from the fact that the wells are shut-in for such long periods of time. There is a flattening of the wellbore pressure profiles for each case, implying that the pressure in the region of the well has stabilized. While this is somewhat of an extrapolation in terms of both theory and practice, the "average" reservoir pressures in the vicinity of these wells are as follows:

Graham Well 2-16: $\bar{p} \approx 4423\,\text{psia}$
McMillan Well 14-2-3: $\bar{p} \approx 5125\,\text{psia}$

These are only estimates, but given the "slowness" of pressure recovery at very late times in the pressure buildup sequence, it is concluded that these estimates are reasonable. We note that neither well test indicates boundaries of any type — which is relevant therefore, the nature of these data may warrant only qualitative scrutiny with regard to "theory."

In summary:

Graham Well 2-16: Reservoir permeability and skin factor estimates appear to be reasonable for Appleton Field and the average pressure estimate is probably valid to with 50-100 psia.

McMillan Well 14-2-3: Reservoir permeability estimate appears to be reasonable for Appleton Field. The skin factor estimate is extremely high and suggests damage/production impairment in the near-well region. The pressure profile from which the average pressure estimate is derived is somewhat more consistent that the data for Graham Well 2-16, as such, this average reservoir pressure estimate is probably more representative (*i.e.*, to within 10-20 psia)

Graham Well 2-16:

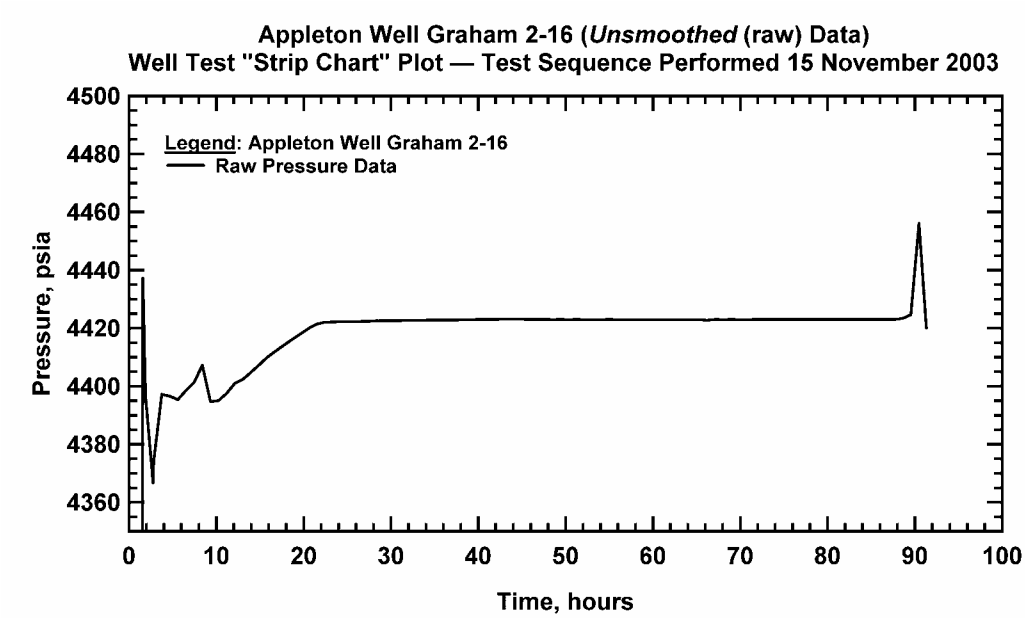

Figure 171a — "Strip Chart" Data Summary Plot (No Analysis) for Graham Well 2-16 (testing sequence of November 2003). Appleton Field (Alabama, USA)

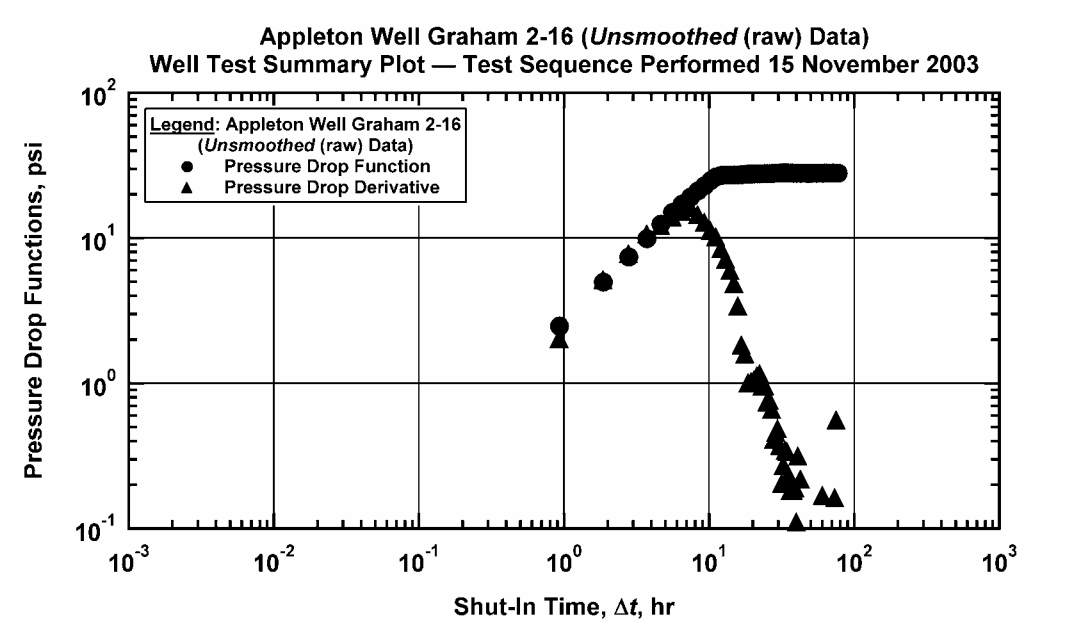

Figure 171b — Log-log Summary Plot (No Analysis) for Graham Well 2-16 (testing sequence of November 2003) — raw pressure buildup data case. Appleton Field (Alabama, USA)

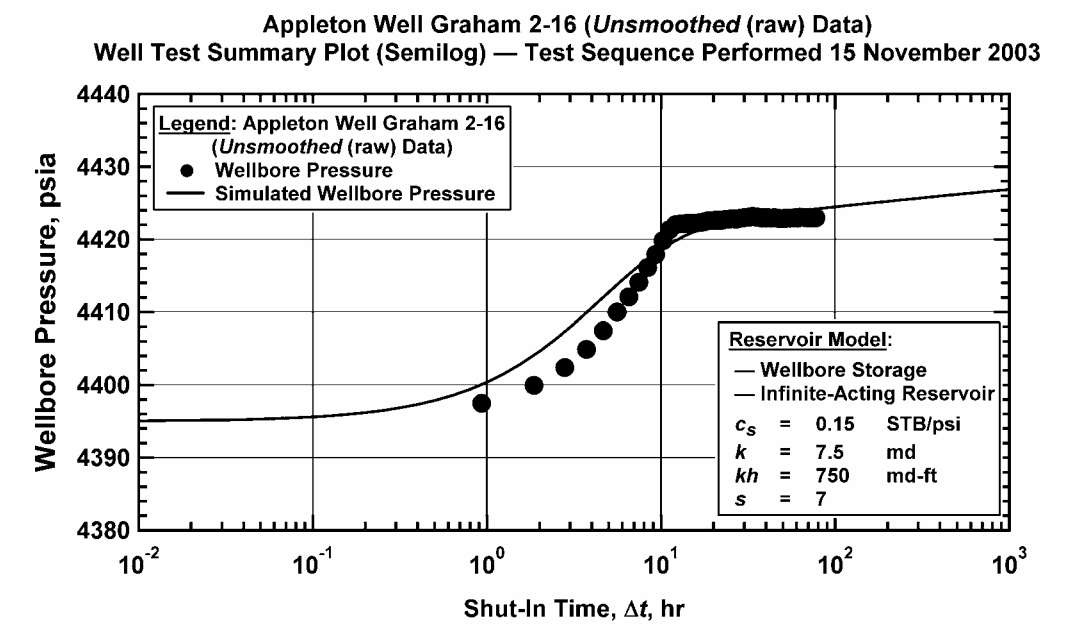

Figure 171c — Semilog Summary Plot (with Analysis) for Graham Well 2-16 (testing sequence of November 2003) — raw pressure buildup data case. Appleton Field (Alabama, USA)

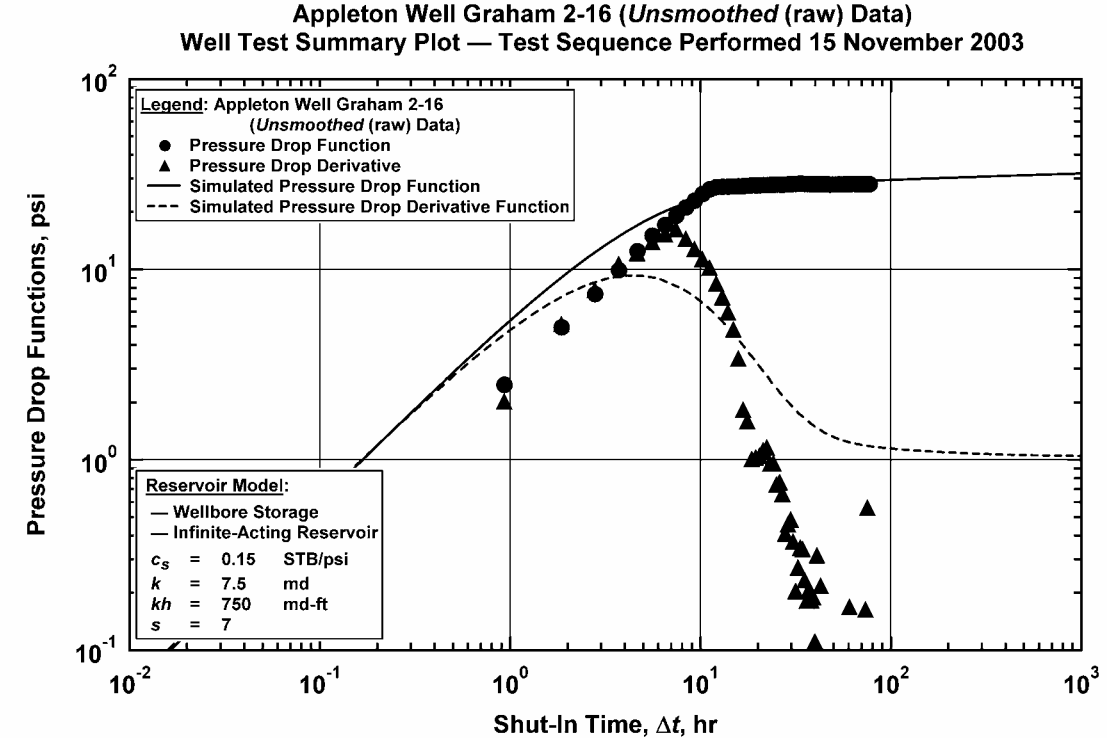

Figure 171d — Log-log Summary Plot (with Analysis) for Graham Well 2-16 (testing sequence of November 2003) — raw pressure buildup data case.

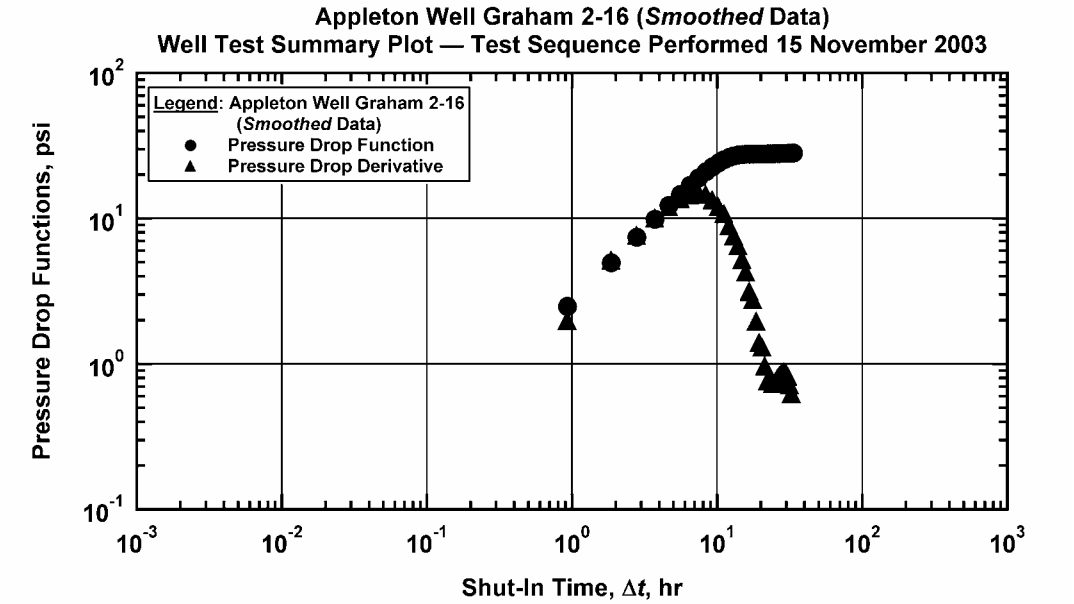

Figure 171e — Log-log Summary Plot (No Analysis) for Graham Well 2-16 (testing sequence of November 2003) — *smoothed* pressure buildup data case. Appleton Field (Alabama, USA)

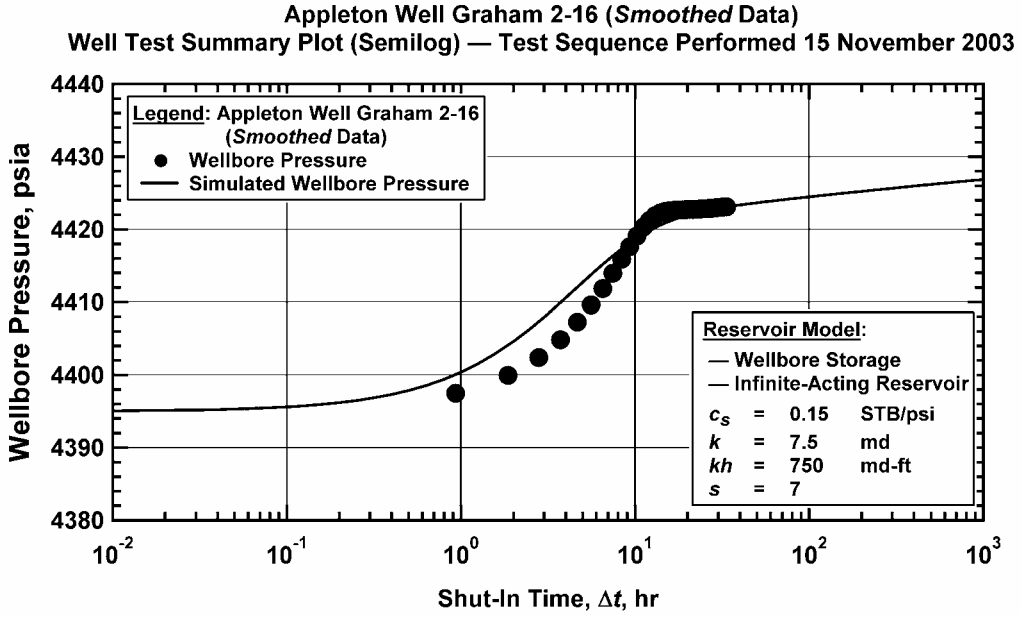

Figure 171f— Semilog Summary Plot (with Analysis) for Graham Well 2-16 (testing sequence of November 2003) — *smoothed* pressure buildup data case. Appleton Field (Alabama, USA)

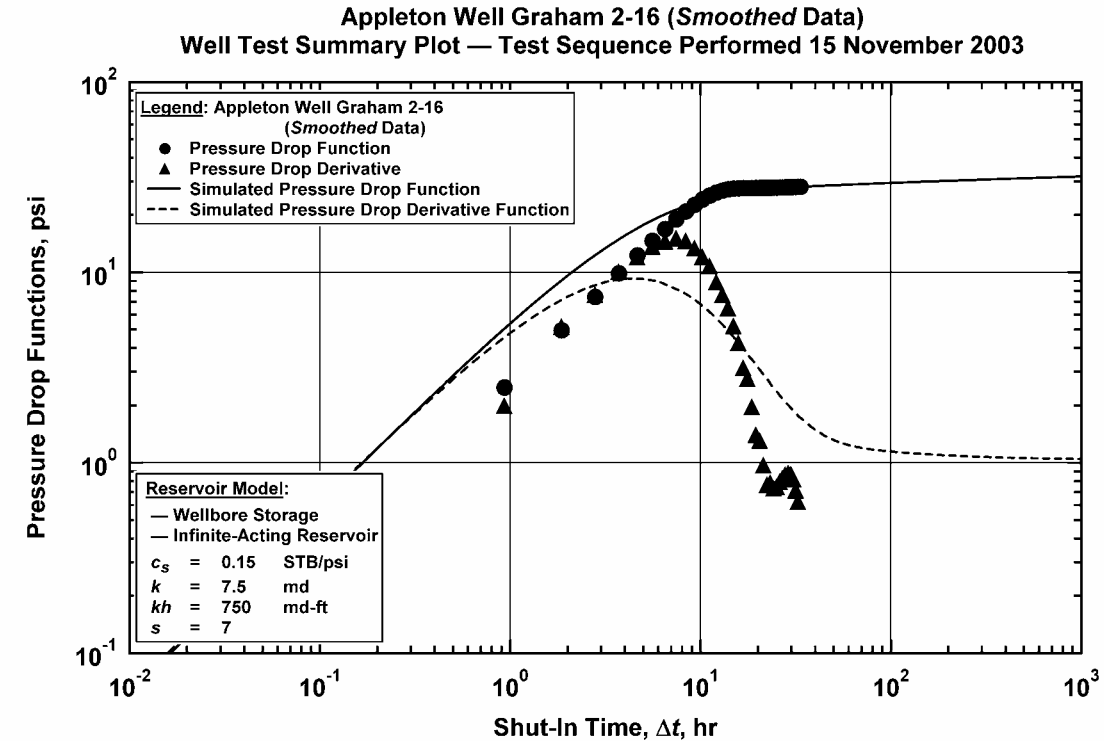

Figure 171g — Log-log Summary Plot (with Analysis) for Graham Well 2-16 (testing sequence of November 2003) — *smoothed* pressure buildup data case. Appleton Field (Alabama, USA)

McMillan Well 12-4-3:

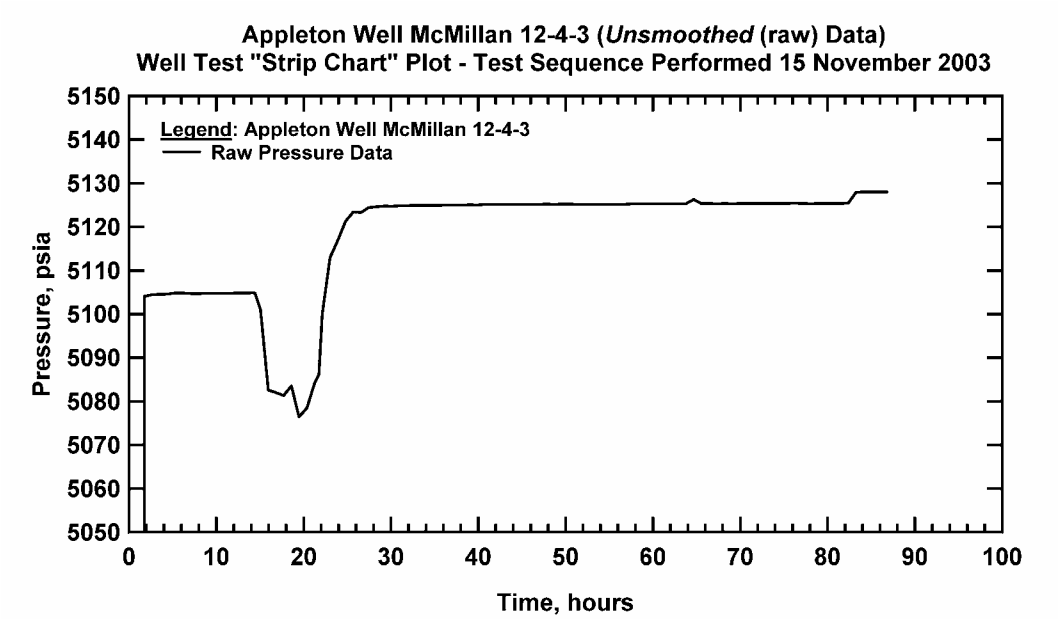

Figure 172a — "Strip Chart" Data Summary Plot (No Analysis) for Graham Well 2-16 (testing sequence of November 2003). Appleton Field (Alabama, USA)

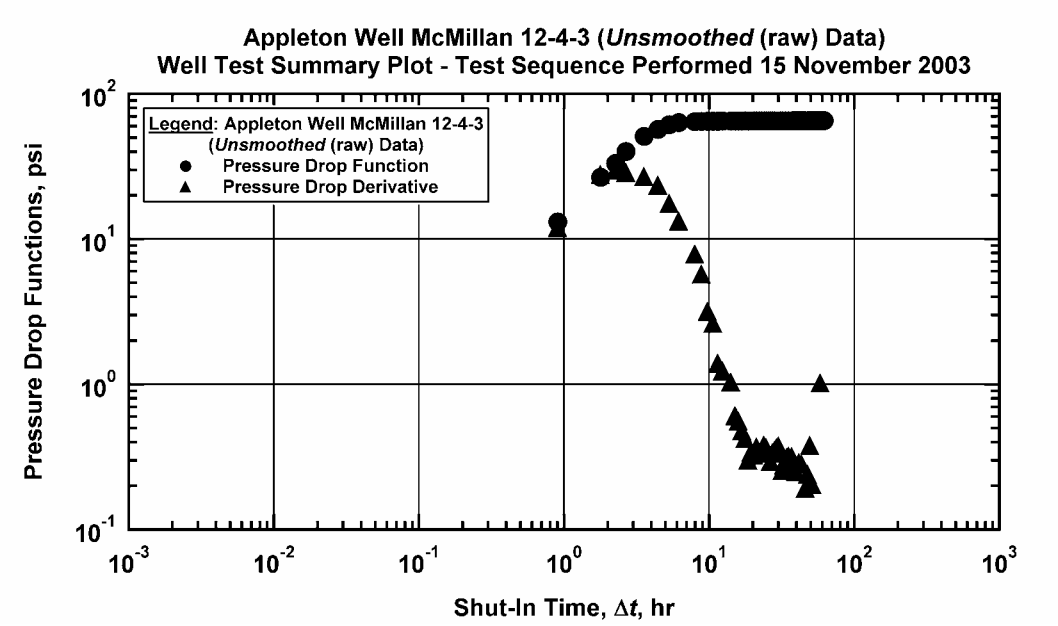

Figure 172b — Log-log Summary Plot (No Analysis) for Graham Well 2-16 (testing sequence of November 2003) — raw pressure buildup data case. Appleton Field (Alabama, USA)

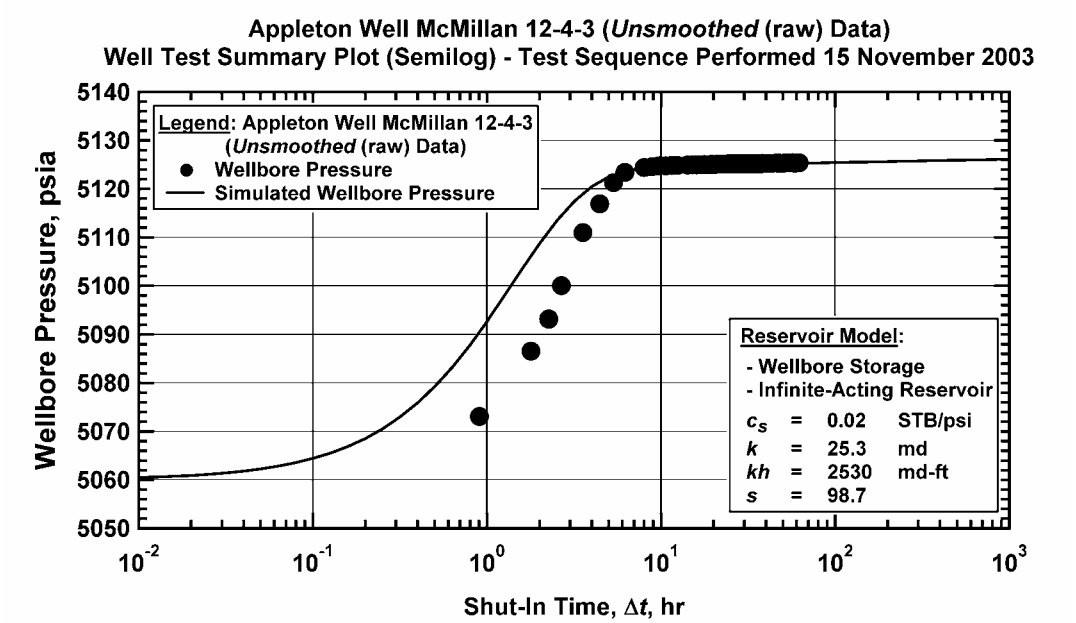

Figure 172c — Semilog Summary Plot (with Analysis) for Graham Well 2-16 (testing sequence of November 2003) — raw pressure buildup data case. Appleton Field (Alabama, USA)

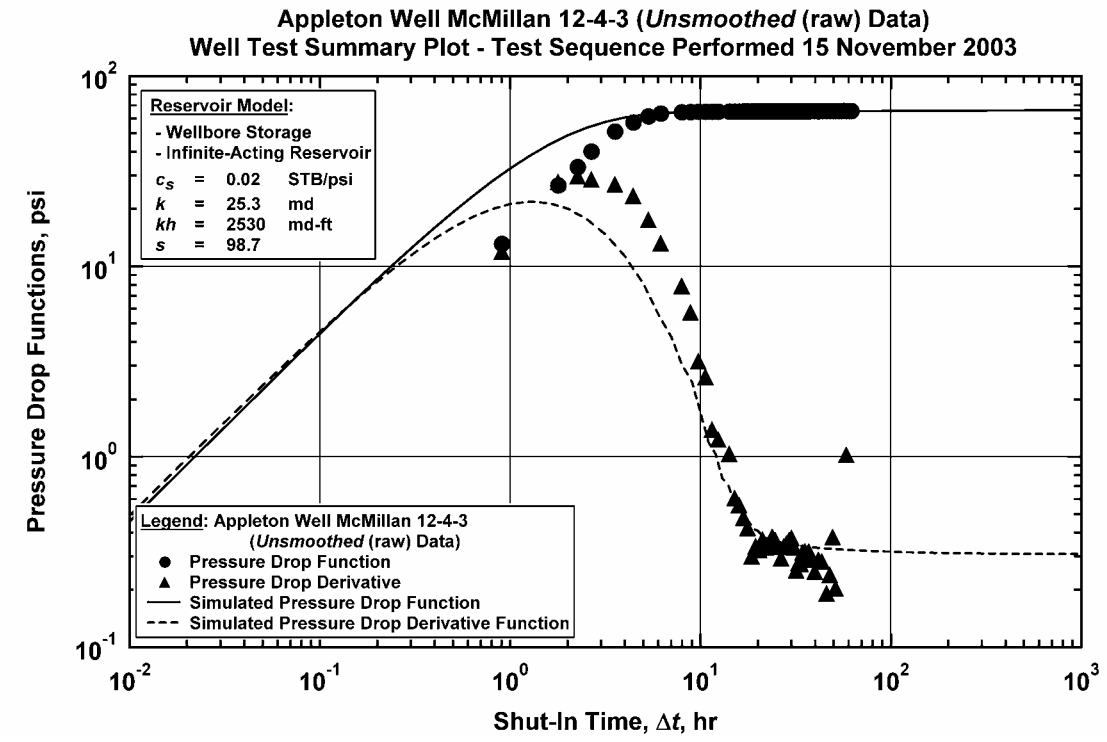

Figure 172d — Log-log Summary Plot (with Analysis) for Graham Well 2-16 (testing sequence of November 2003) — raw pressure buildup data case. Appleton Field (Alabama, USA)

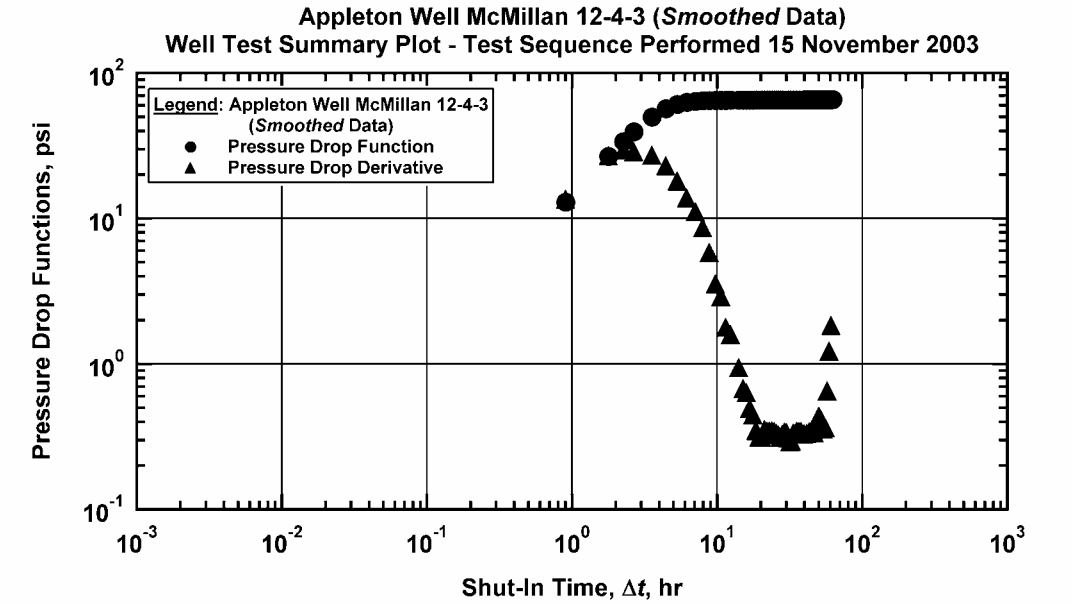

Figure 172e — Log-log Summary Plot (No Analysis) for Graham Well 2-16 (testing sequence of November 2003) — *smoothed* pressure buildup data case. Appleton Field (Alabama, USA)

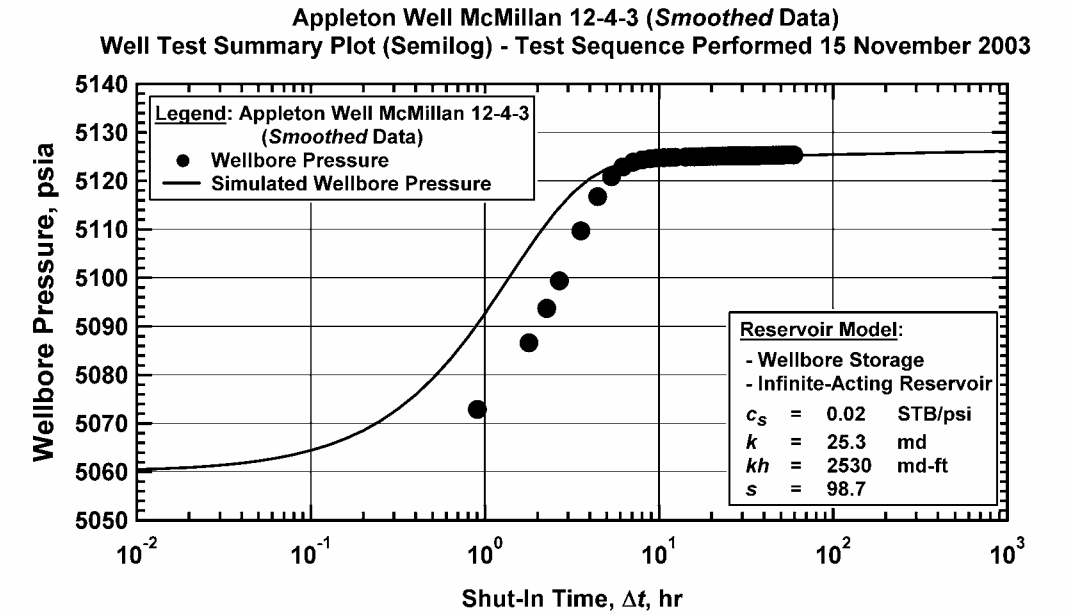

Figure 172f— Semilog Summary Plot (with Analysis) for Graham Well 2-16 (testing sequence of November 2003) — *smoothed* pressure buildup data case. Appleton Field (Alabama, USA)

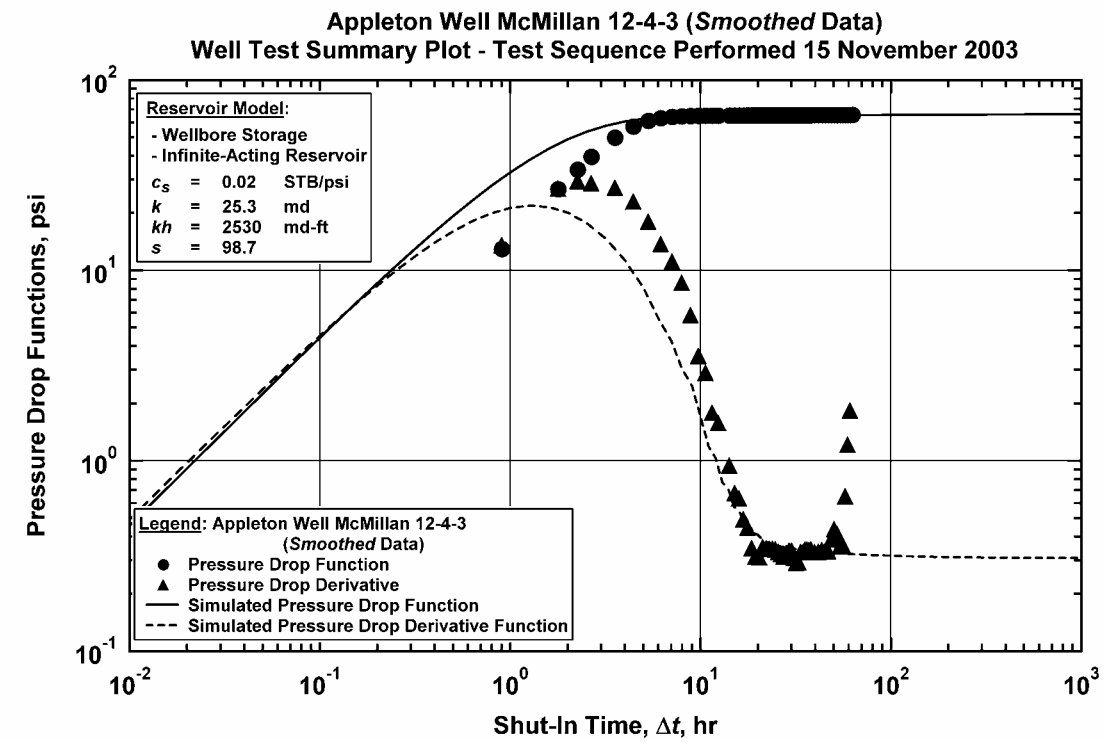

Figure 172g — Log-log Summary Plot (with Analysis) for Graham Well 2-16 (testing sequence of November 2003) — *smoothed* pressure buildup data case. Appleton Field (Alabama, USA)

Vocation Field. Petrophysical and engineering property data have been gathered and tabulated for Vocation Field. These data include oil, gas and water production, fluid property (PVT) analyses (Table 19) and porosity and permeability information (Tables 20-24). Porosity and permeability characteristics of Smackover facies have been analyzed for each well using porosity histograms (Figures 173-181), permeability histograms (Figures 182-190) and porosity versus depth plots (Figures 191-199). Log porosity versus core porosity for wells in the field have been prepared (Figures 200-208). Porosity versus permeability cross plots for wells (Figures 209-216) and for Smackover facies have been prepared (Figures 217-220). Well performance studies through type curve (Figures 221-230 and Table 25) and decline curve analyses (Figures 231-240) have been completed for the wells in the field. Figure 241 presents an alternative calculation of recoverable oil. The original oil in place and recoverable oil remaining for the field have been calculated (Table 26 and Figures 242-246). Contour maps of flow capacity have been constructed (Figures 247-249).

Analysis of the core and log data indicate that the reservoirs at Vocation Field have a heterogeneous nature. Porosity and permeability show a significant difference in reservoir quality between the shoal and reef reservoirs, with the reef reservoir having better reservoir quality compared to the shoal facies. There is reasonable correlation between the core and log porosity measurements for these facies. The correlation between core permeability and core porosity approximates a straight line representing a log linear model. This implies that the relationship between permeability and porosity at any point in the reservoir is more controlled by the location of the point structurally rather than in which lithofacies the point occurs. The primary production mechanisms in Vocation Field are believed to be depletion drive (fluid/rock/gas expansion) and

Table 19. PVT Data for Vocation Field Reservoir

Permit#:	1599-SWD-77-151-7			
Well Name:	B.C. Quimby 27-15 SWD #1			
Field:	Vocation-Oil			
Pool:	Smackover			
County:	Monroe			
Date:	11-05-1971			
Pi (PSIA) :	6837	Boi	(RBBL/STB):	2.1868
Pb (PSIA) :	3475	Bob	(Rbbl/STB):	2.529
T:	245.0	Rsi	(SCF/STB):	0.0
API:	55.3	Rsib	(SCF/STB):	0.0

Full Wellstream Recombination:

Component	MOL%
H2S	0.0
N2	7.11
CO2	0.63
C1	45.99
C2	6.73
C3	6.28
C4i	2.21
C4n	4.87
C5i	1.93
C5n	2.95
C6	4.51
C7	16.79
Total	100.00

Table 20 — Porosity and permeability characteristics in the Sabkha Interval.

Well	Minimum Porosity, (percent)	Maximum Porosity, (percent)	Average Porosity, (percent)	Minimum Permeability ,(md)	Maximum Permeability ,(md)	Geometric Average Permeability,(md)
1599	N/A	N/A	N/A	N/A	N/A	N/A
1830	N/A	N/A	N/A	N/A	N/A	N/A
2851	N/A	N/A	N/A	N/A	N/A	N/A
2935	N/A	N/A	N/A	N/A	N/A	N/A
3412	1.1	6.6	2.4	0.1	0.1	0.1
3739	N/A	N/A	N/A	N/A	N/A	N/A
4225	2.3	2.5	2.4	N/A	N/A	N/A
5779	N/A	N/A	N/A	N/A	N/A	N/A
11185	0.9	14.6	8.3	N/A	N/A	N/A

Table 21 — Porosity and permeability characteristics in the Tidal Flat Interval.

Well	Minimum Porosity, (percent)	Maximum Porosity, (percent)	Average Porosity, (percent)	Minimum Permeability ,(md)	Maximum Permeability ,(md)	Geometric Average Permeability ,(md)
1599	N/A	N/A	N/A	N/A	N/A	N/A
1830	14.6	23.6	21.3	5.9	162.0	56.6
2851	1.0	12.0	7.0	7.9	14.1	11.0
2935	N/A	N/A	N/A	N/A	N/A	N/A
3412	2.4	10.9	5.5	0.3	10.4	1.5
3739	3.7	8.6	5.1	9.0	9.0	9.0
4225	1.2	3.5	2.0	0.04	0.04	0.04
5779	2.1	3.7	2.9	N/A	N/A	N/A
11185	0.9	9.9	5.1	0.13	75.0	3.3

Table 22 — Porosity and permeability characteristics in the Shoal Complex Interval.

Well	Minimum Porosity, (percent)	Maximum Porosity, (percent)	Average Porosity, (percent)	Minimum Permeability, (md)	Maximum Permeability, (md)	Geometric Average Permeability, (md)
1599	N/A	N/A	N/A	N/A	N/A	N/A
1830	10.7	22.0	15.8	5.6	400.0	54.0
2851	2.1	20.1	9.9	0.02	1321.5	8.6
2935	1.6	15.3	9.7	0.05	57.0	4.5
3412	1.7	15.3	6.4	0.2	466.7	15.8
3739	1.6	13.7	7.9	0.04	18.0	1.8
4225	0.8	13.0	5.1	0.04	266.0	1.8
5779	2.7	21.9	13.3	0.04	1263.0	44.7
11185	N/A	N/A	N/A	N/A	N/A	N/A

Table 23 — Porosity and permeability characteristics in the Lagoon Interval.

Well	Minimum Porosity, (percent)	Maximum Porosity, (percent)	Average Porosity, (percent)	Minimum Permeability, (md)	Maximum Permeability, (md)	Geometric Average Permeability ,(md)
1599	8.0	19.0	12.5	2.8	1119.2	31.3
1830	2.5	15.3	7.6	0.3	57.0	4.1
2851	N/A	N/A	N/A	N/A	N/A	N/A
2935	N/A	N/A	N/A	N/A	N/A	N/A
3412	1.7	11.1	4.3	0.2	8.6	1.1
3739	1.8	14.0	5.7	0.02	50.0	1.4
4225	2.0	7.5	3.4	0.02	0.2	0.06
5779	1.9	8.1	2.7	0.02	2.2	0.1
11185	N/A	N/A	N/A	N/A	N/A	N/A

Table 24 — Porosity and permeability characteristics in the Reef Interval.

Well	Minimum Porosity, (percent)	Maximum Porosity, (percent)	Average Porosity, (percent)	Minimum Permeability ,(md)	Maximum Permeability, (md)	Geometric Average Permeability ,(md)
1599	2.5	33.6	9.3	0.8	5730.0	71.9
1830	5.2	18.6	12.1	0.3	196.0	12.0
2851	2.7	24.9	12.3	0.06	740.0	29.2
2935	3.2	18.3	8.2	0.02	332.0	5.8
3412	N/A	N/A	N/A	N/A	N/A	N/A
3739	1.7	7.8	5.5	2.7	68.0	10.3
4225	N/A	N/A	N/A	N/A	N/A	N/A
5779	N/A	N/A	N/A	N/A	N/A	N/A
11185	N/A	N/A	N/A	N/A	N/A	N/A

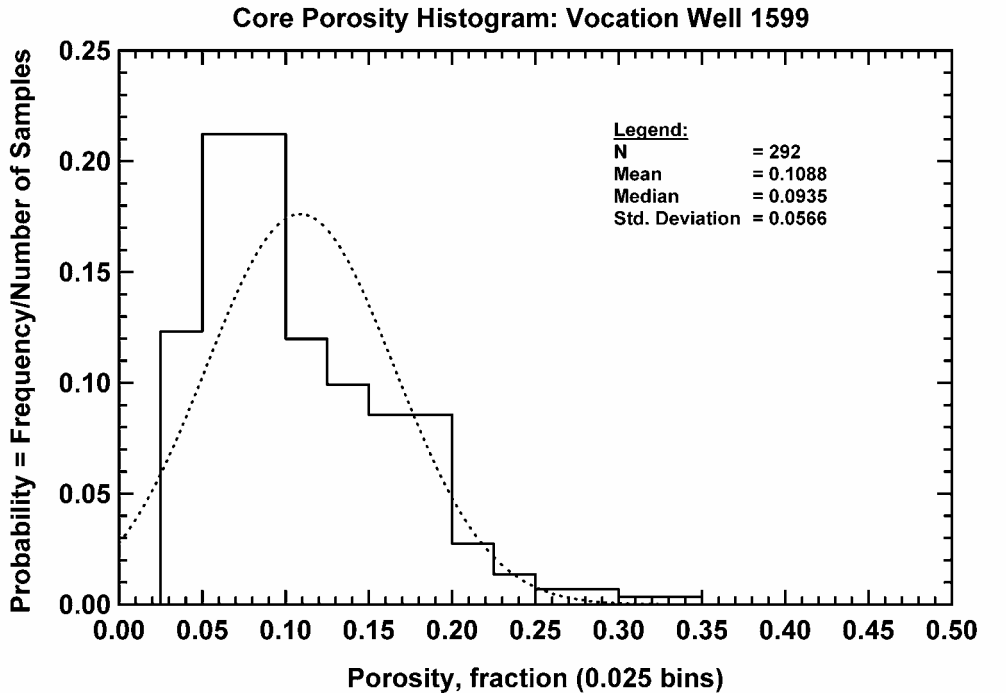

Figure 173 — Core Porosity Histogram, Vocation Well 1599.

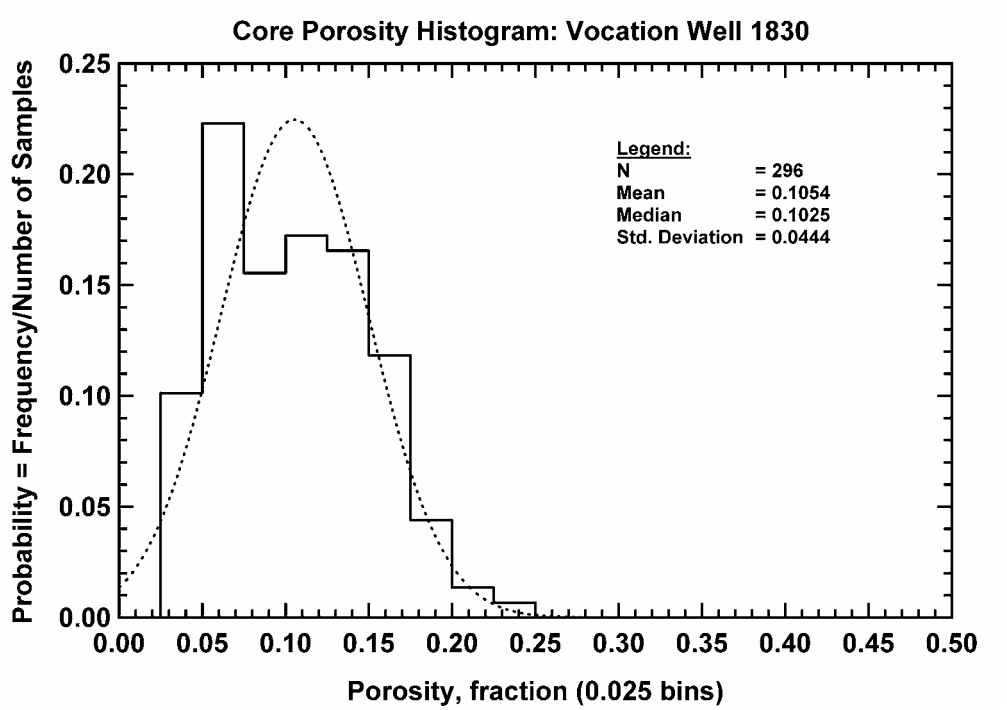

Figure 174 — Core Porosity Histogram, Vocation Well 1830.

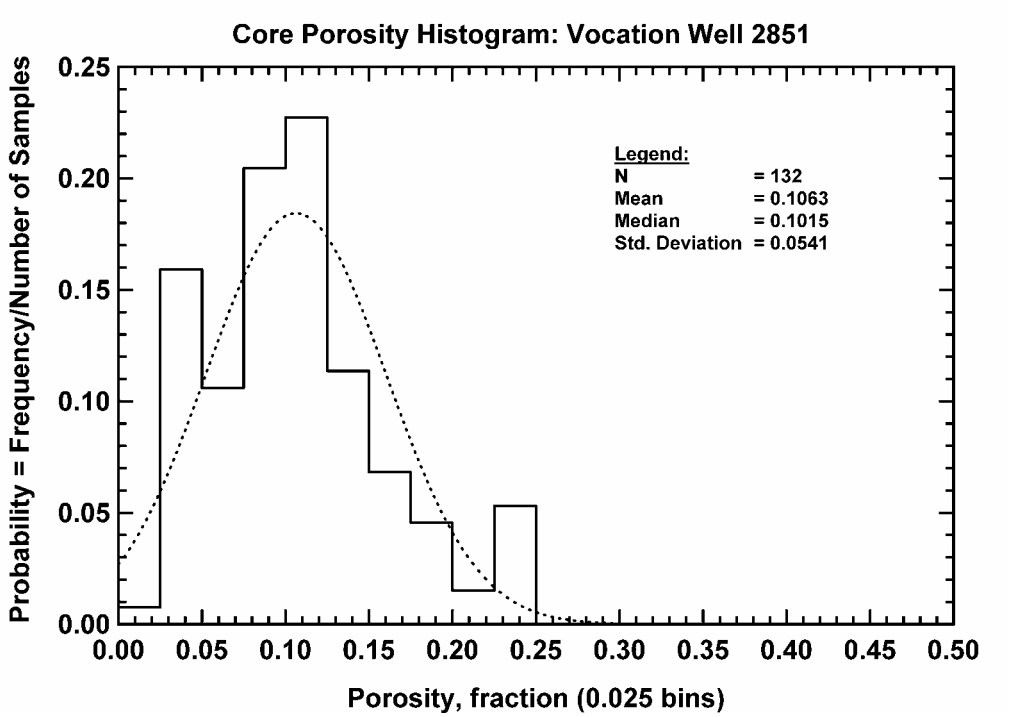

Figure 175 — Core Porosity Histogram, Vocation Well 2851.

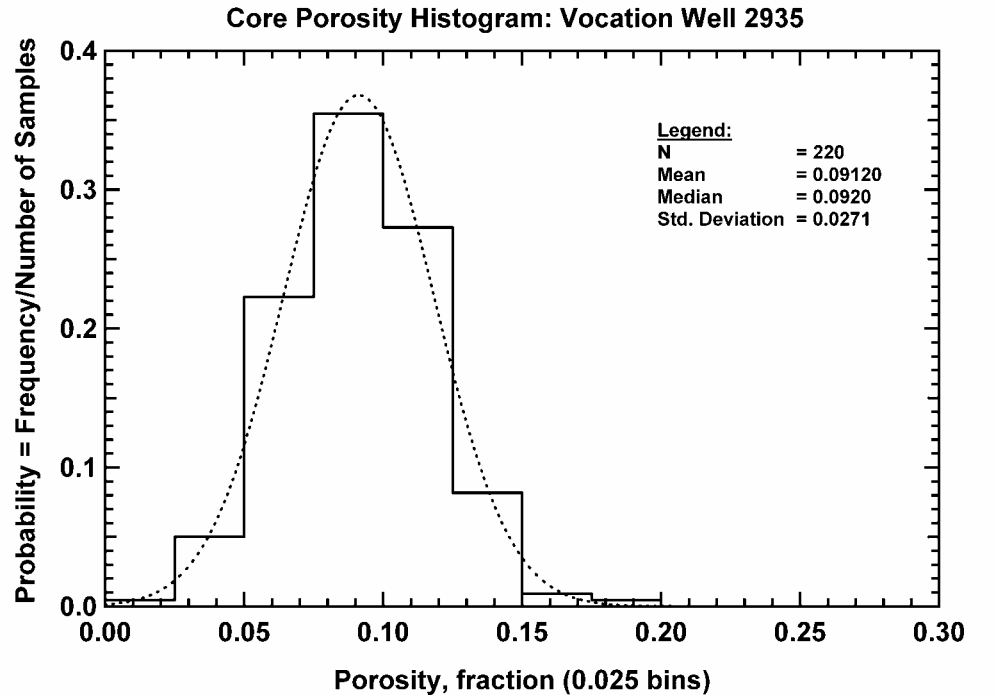

Figure 176 — Core Porosity Histogram, Vocation Well 2935.

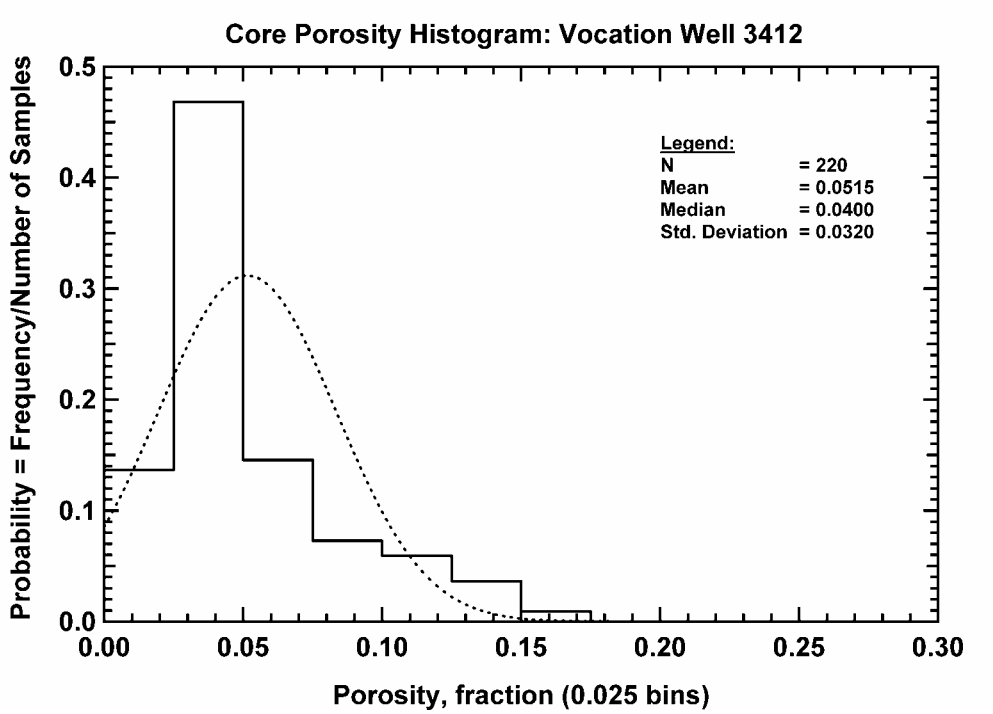

Figure 177 — Core Porosity Histogram, Vocation Well 3412.

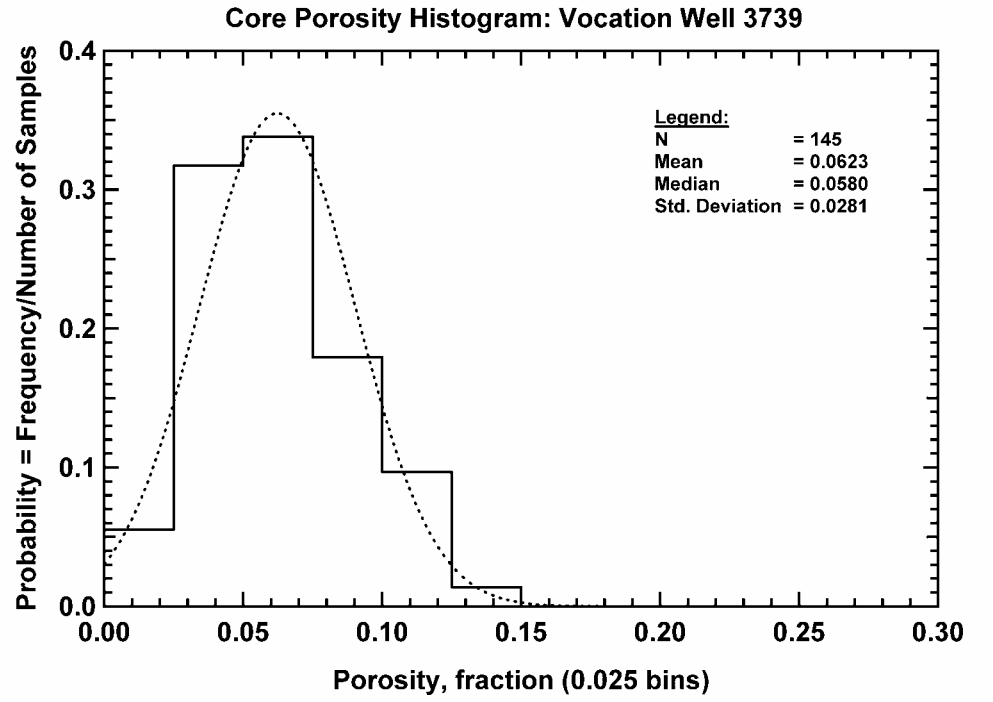

Figure 178 — Core Porosity Histogram, Vocation Well 3739.

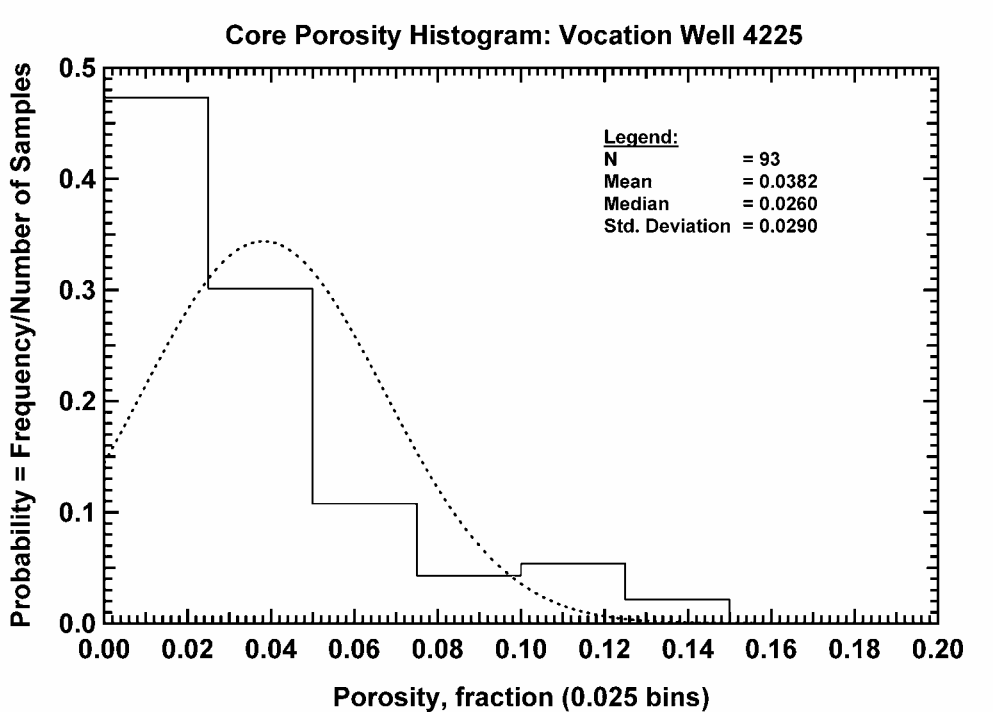

Figure 179 — Core Porosity Histogram, Vocation Well 4225.

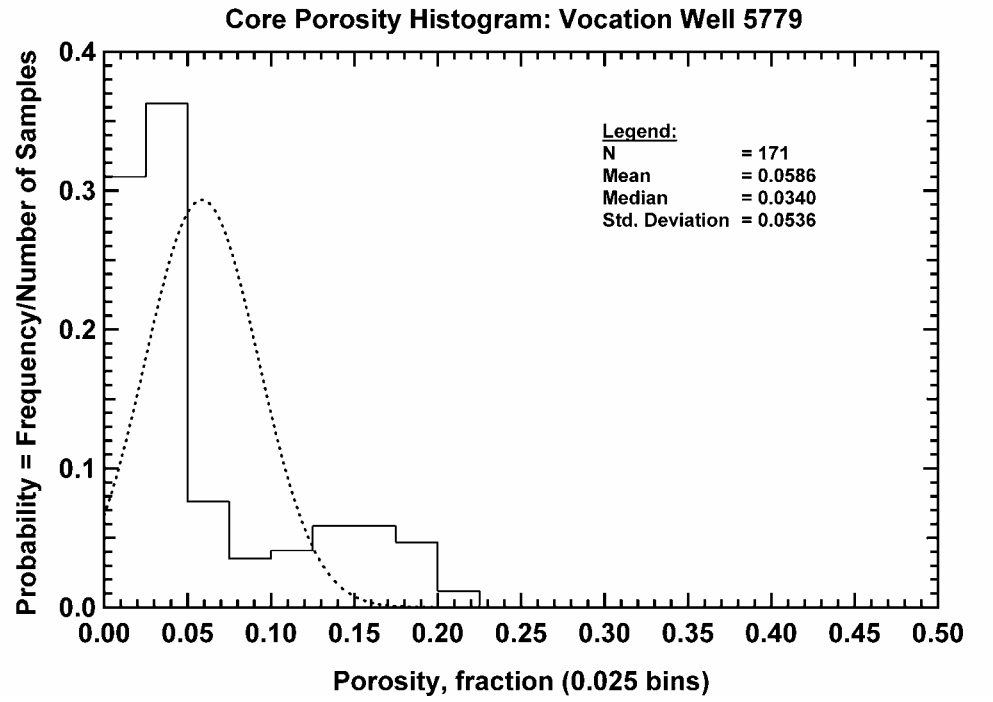

Figure 180 — Core Porosity Histogram, Vocation Well 5779.

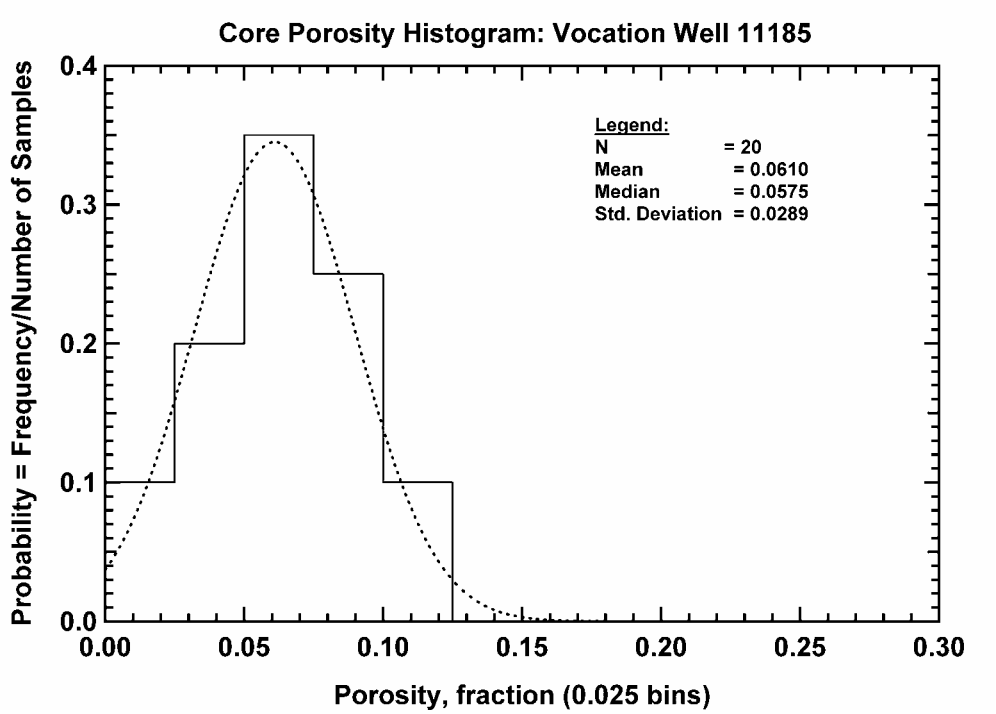

Figure 181 — Core Porosity Histogram, Vocation Well 11185.

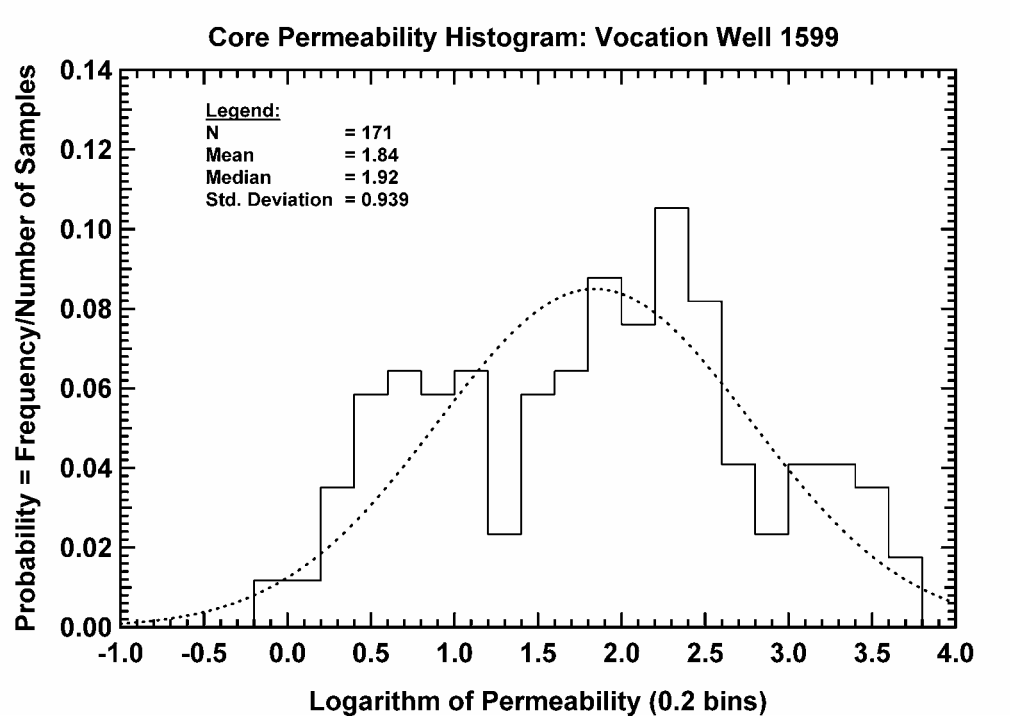

Figure 182 — Core Permeability Histogram, Vocation Well 1559.

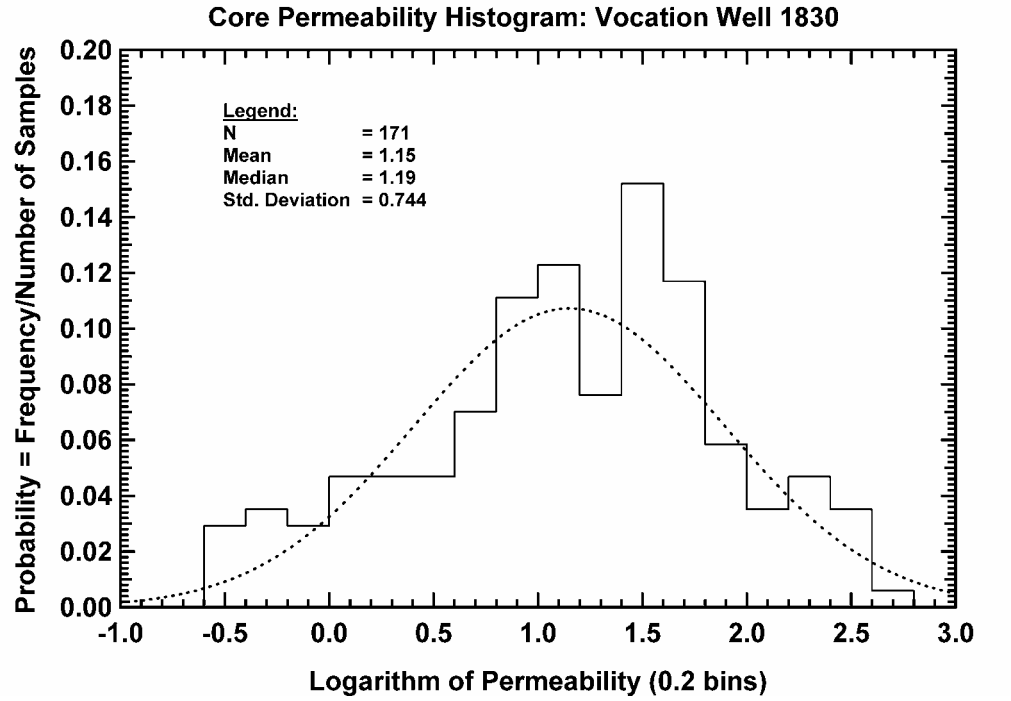

Figure 183 — Core Permeability Histogram, Vocation Well 1830.

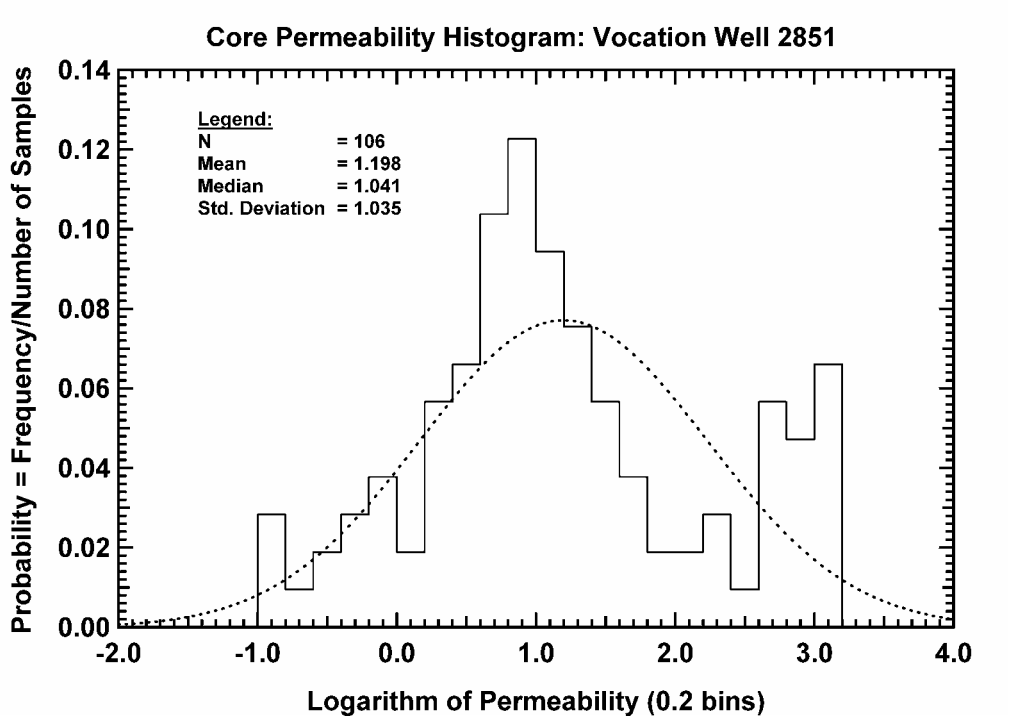

Figure 184 — Core Permeability Histogram, Vocation Well 2851.

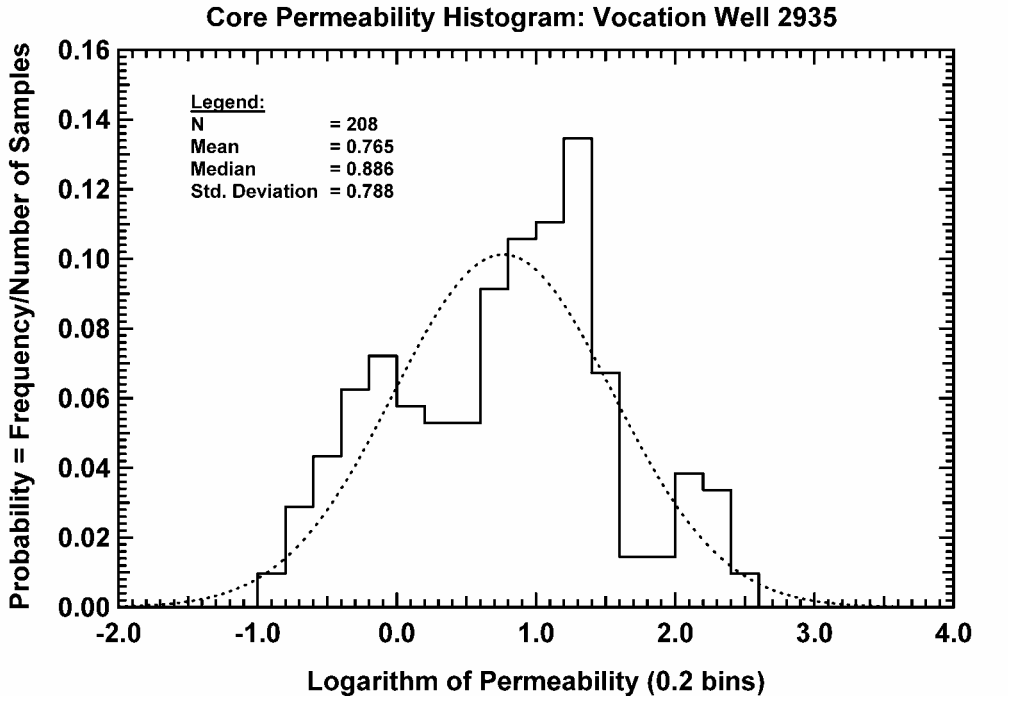

Figure 185 — Core Permeability Histogram, Vocation Well 2935.

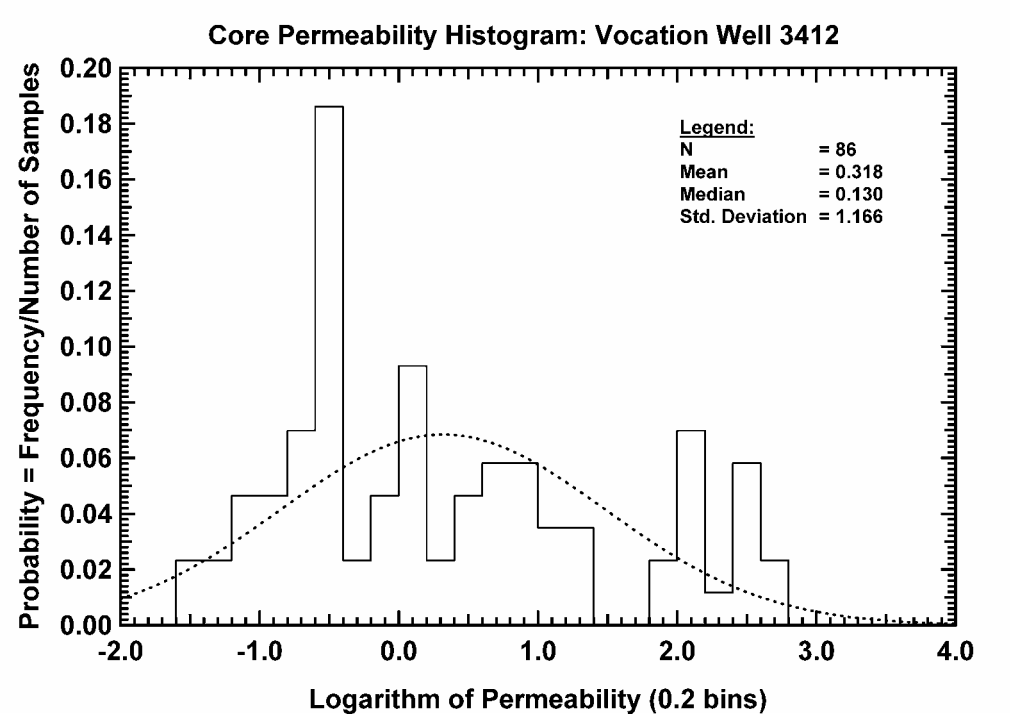

Figure 186 — Core Permeability Histogram, Vocation Well 3412.

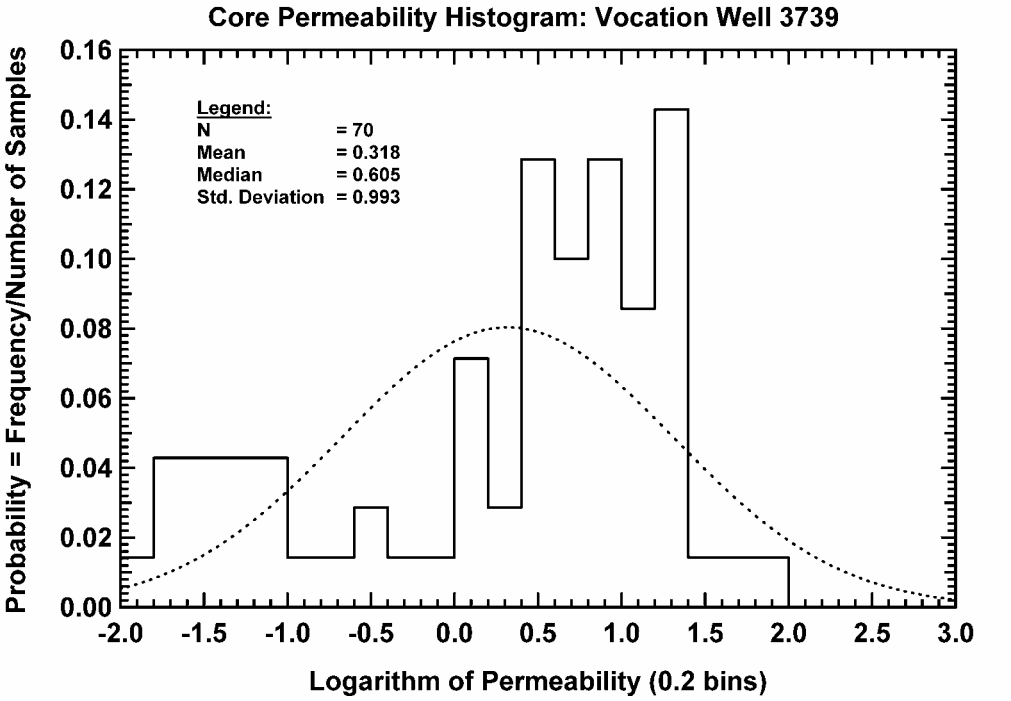

Figure 187 — Core Permeability Histogram, Vocation Well 3739.

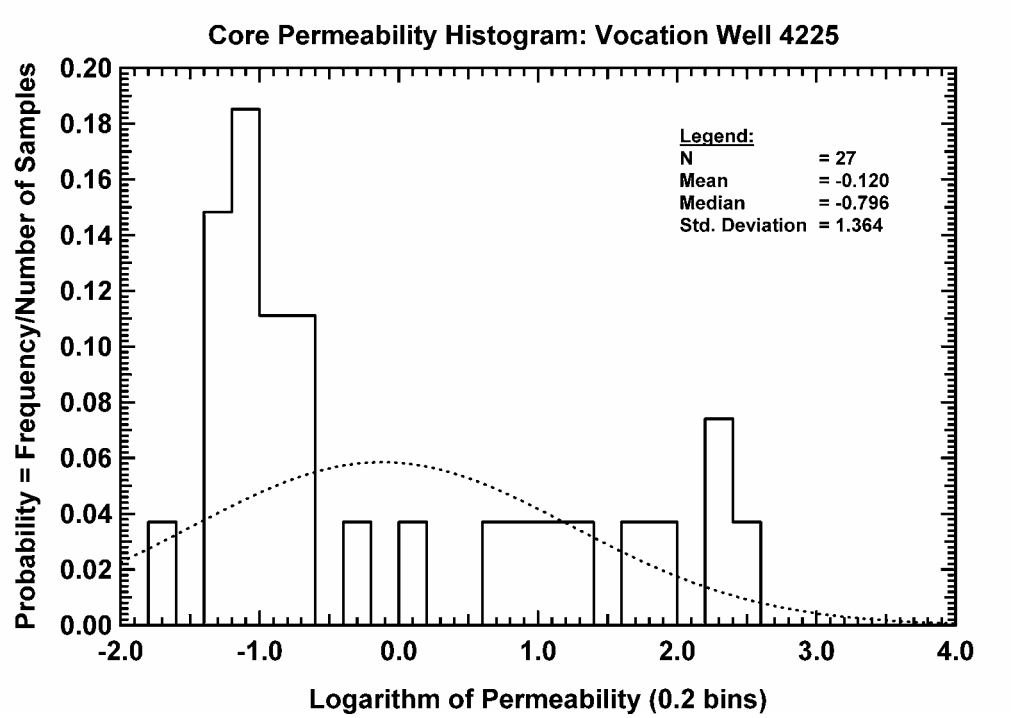

Figure 188 — Core Permeability Histogram, Vocation Well 4225.

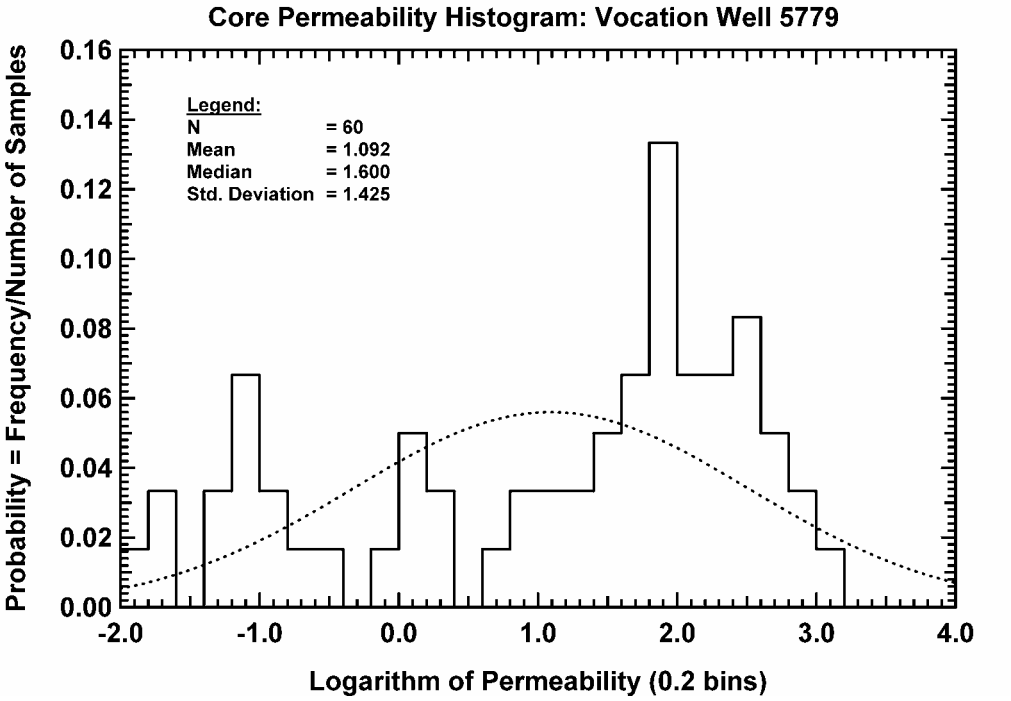

Figure 189 — Core Permeability Histogram, Vocation Well 5779.

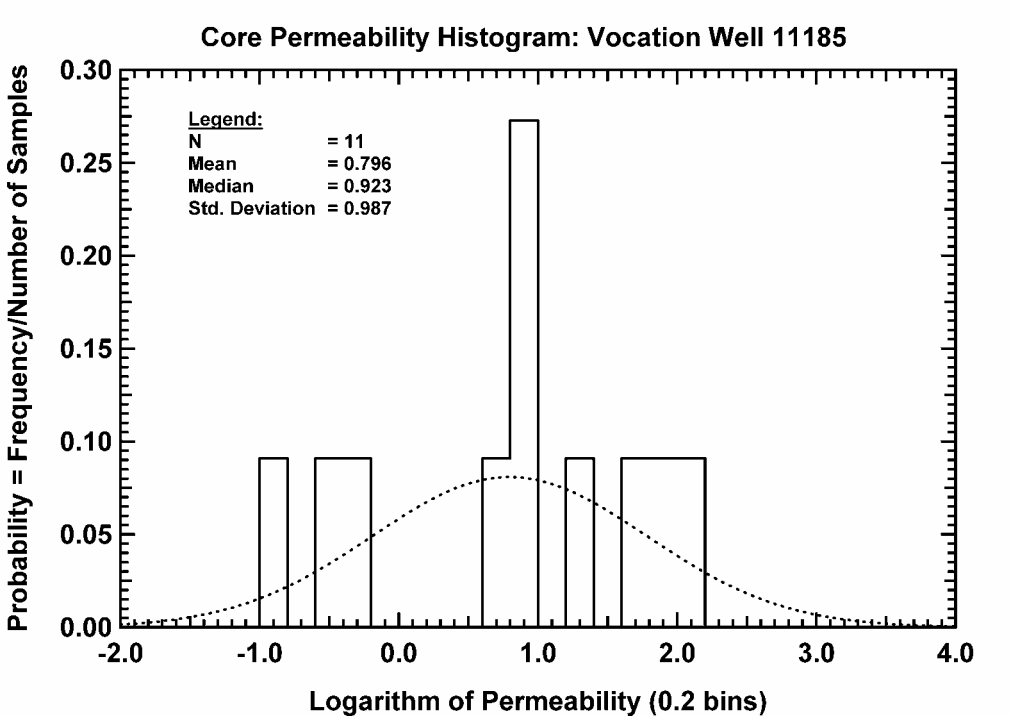

Figure 190 — Core Permeability Histogram, Vocation Well 11185.

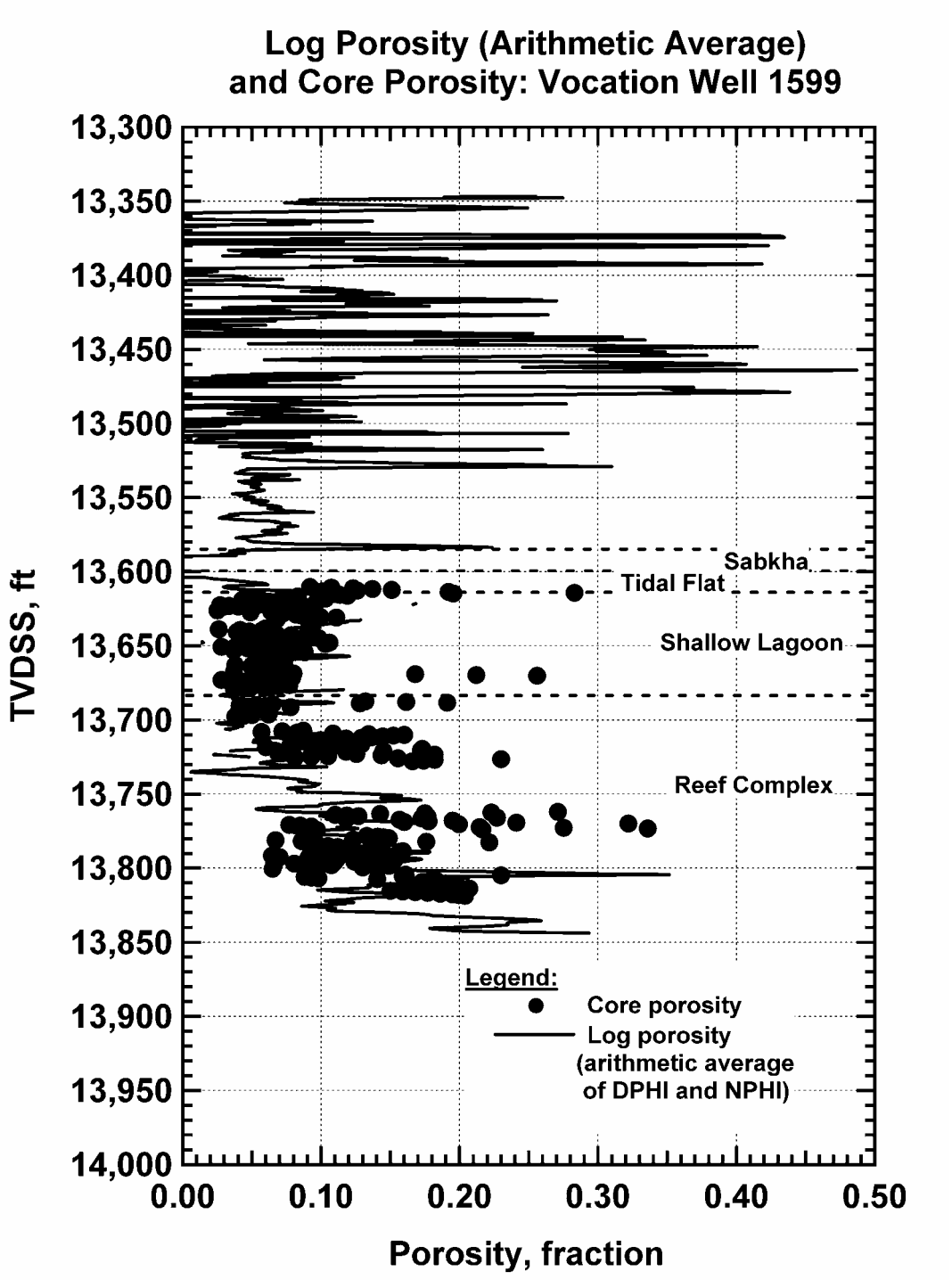

Figure 191 — Porosity Variation with Depth, Vocation Well 1599.

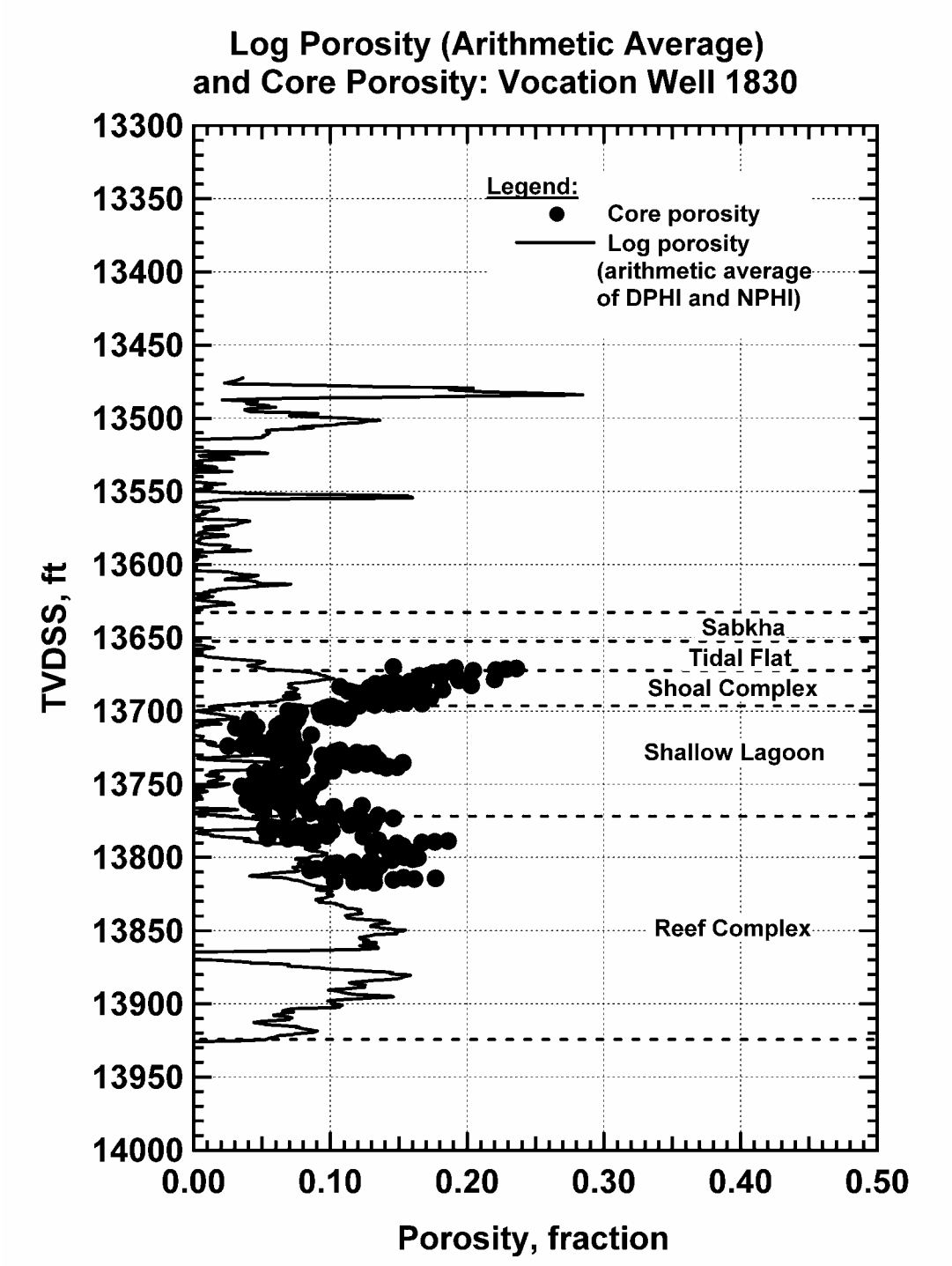

Figure 192 — Porosity Variation with Depth, Vocation Well 1830.

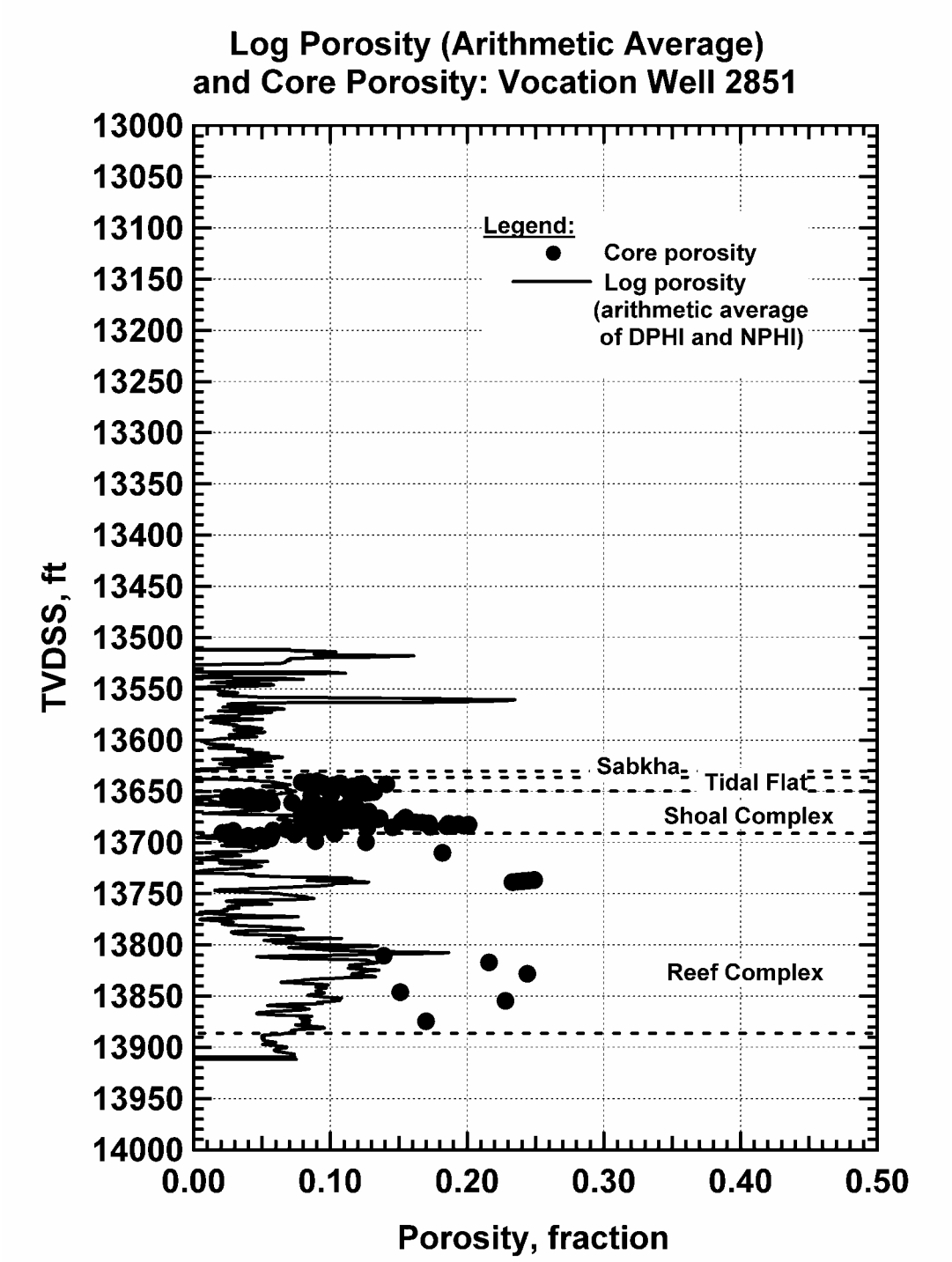

Figure 193 — Porosity Variation with Depth, Vocation Well 2851.

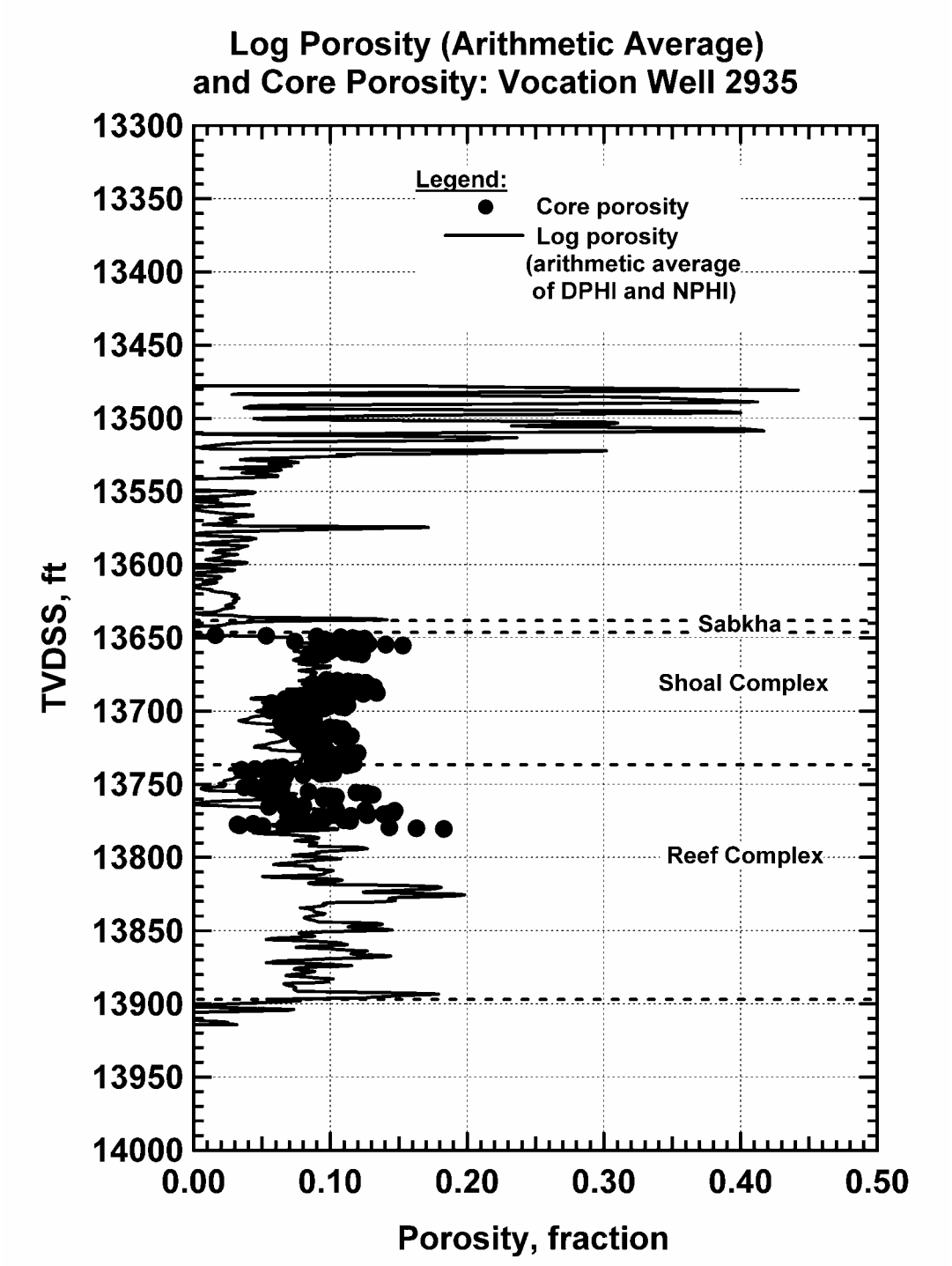

Figure 194 — Porosity Variation with Depth, Vocation Well 2935.

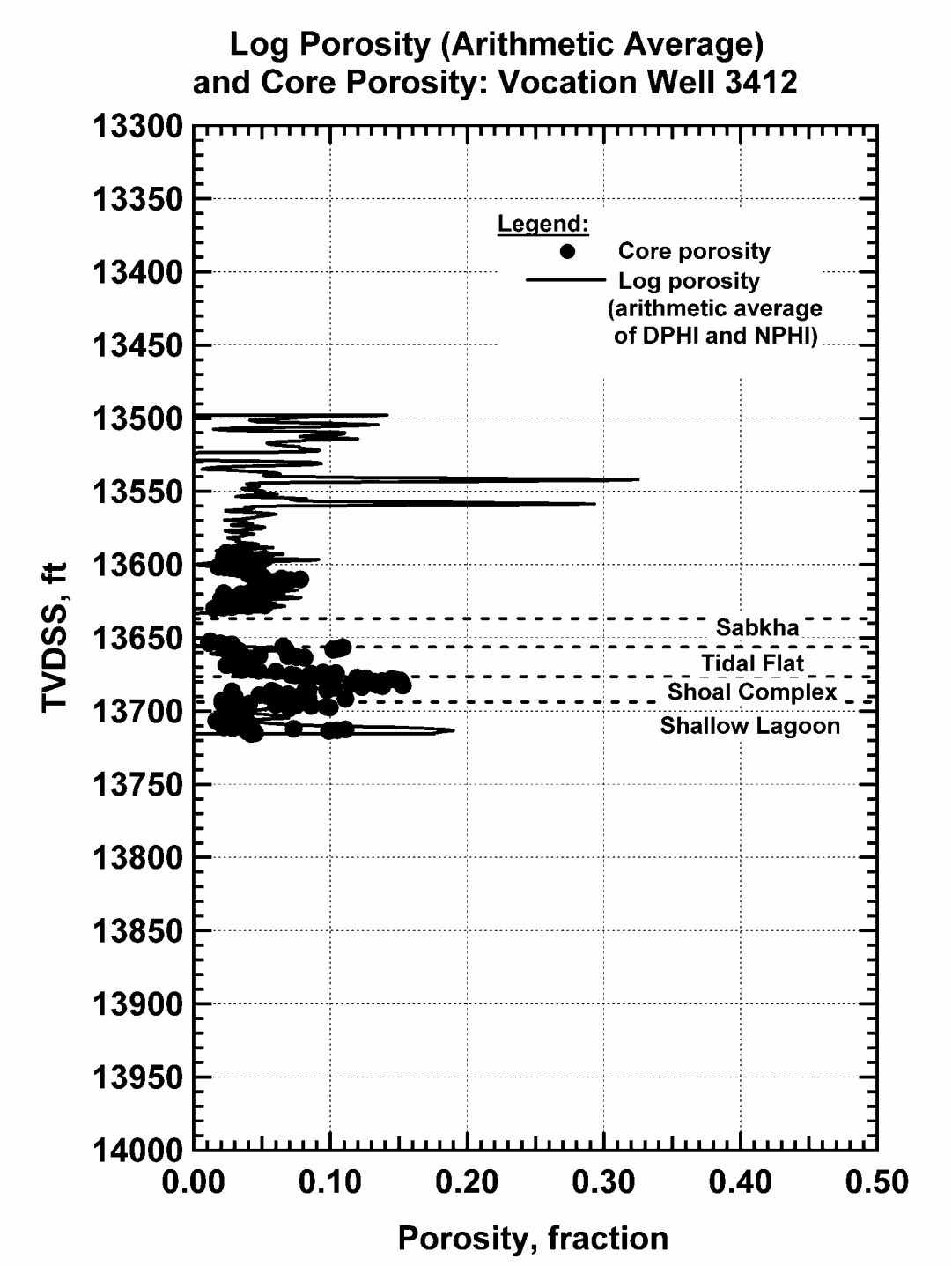

Figure 195 — Porosity Variation with Depth, Vocation Well 3412.

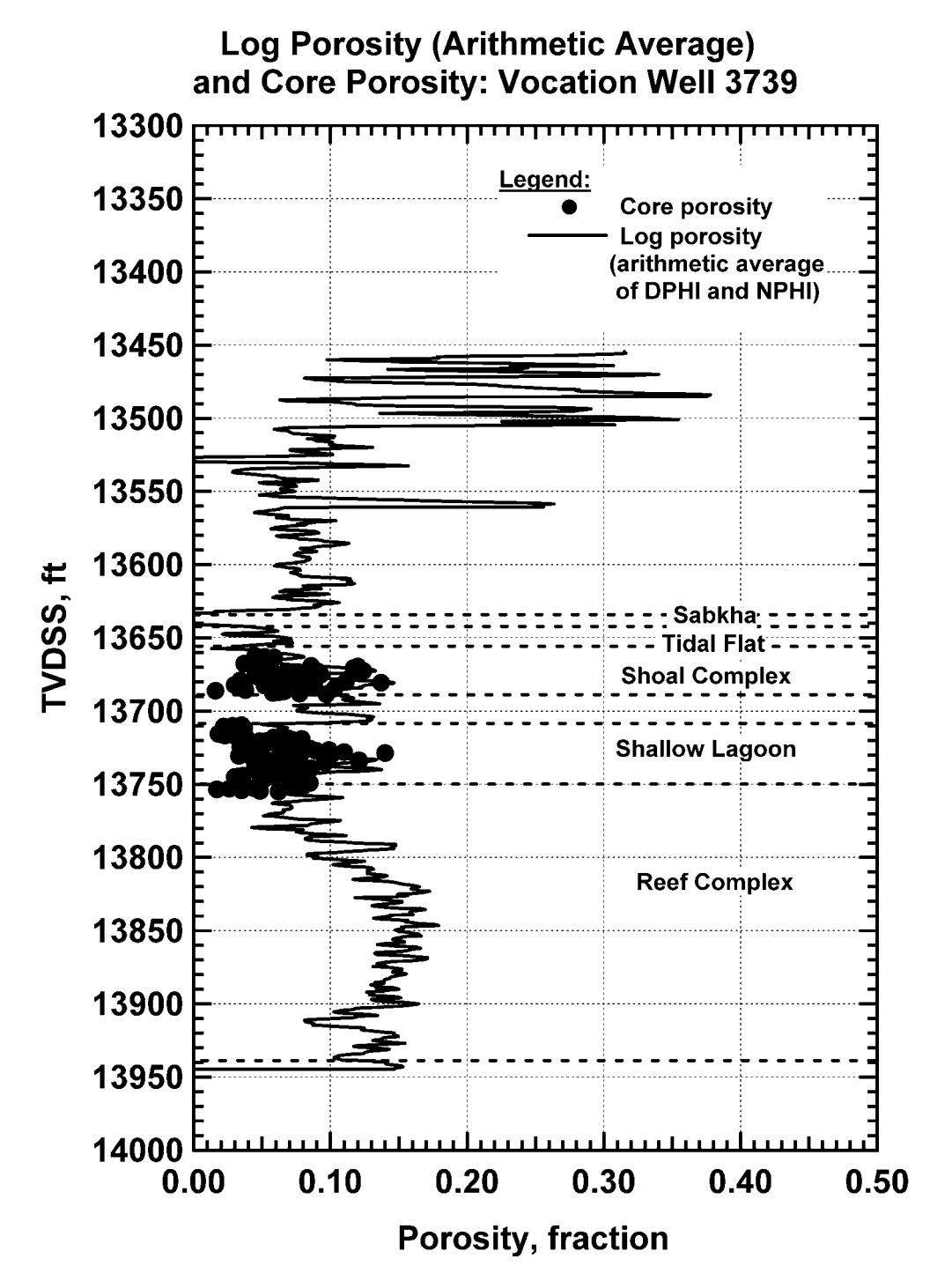

Figure 196 — Porosity Variation with Depth, Vocation Well 3739.

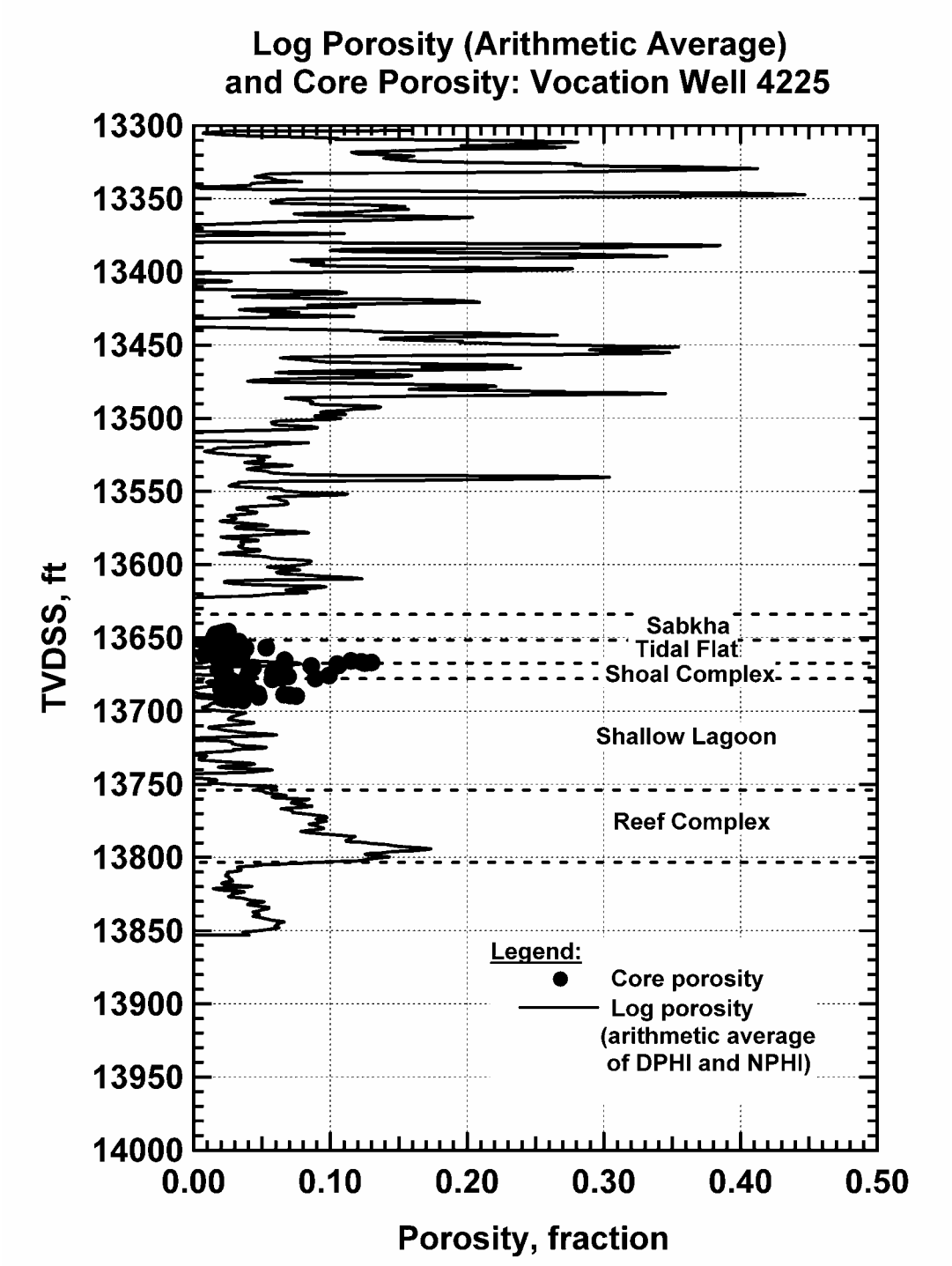

Figure 197 — Porosity Variation with Depth, Vocation Well 4225.

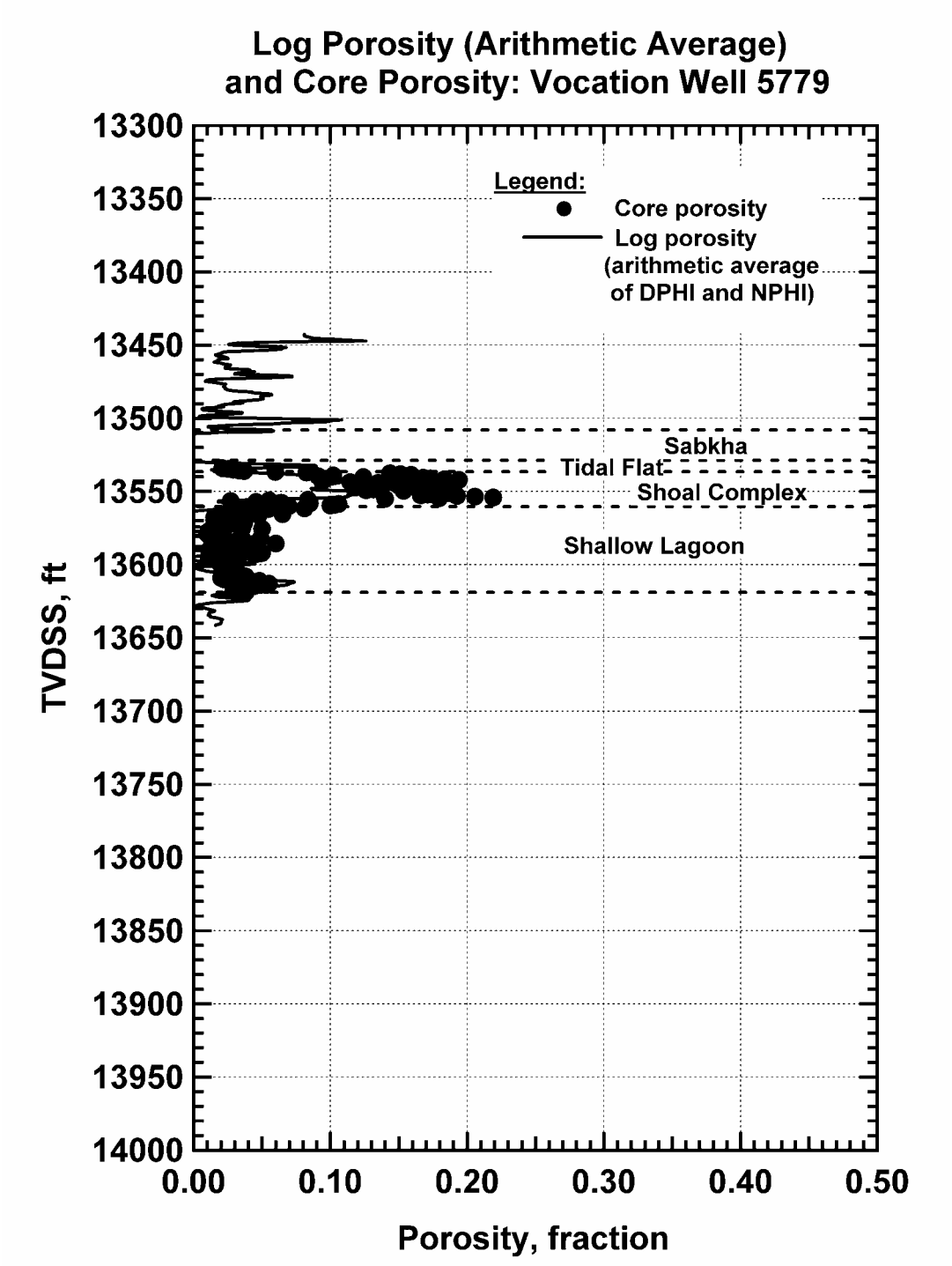

Figure 198 — Porosity Variation with Depth, Vocation Well 5779.

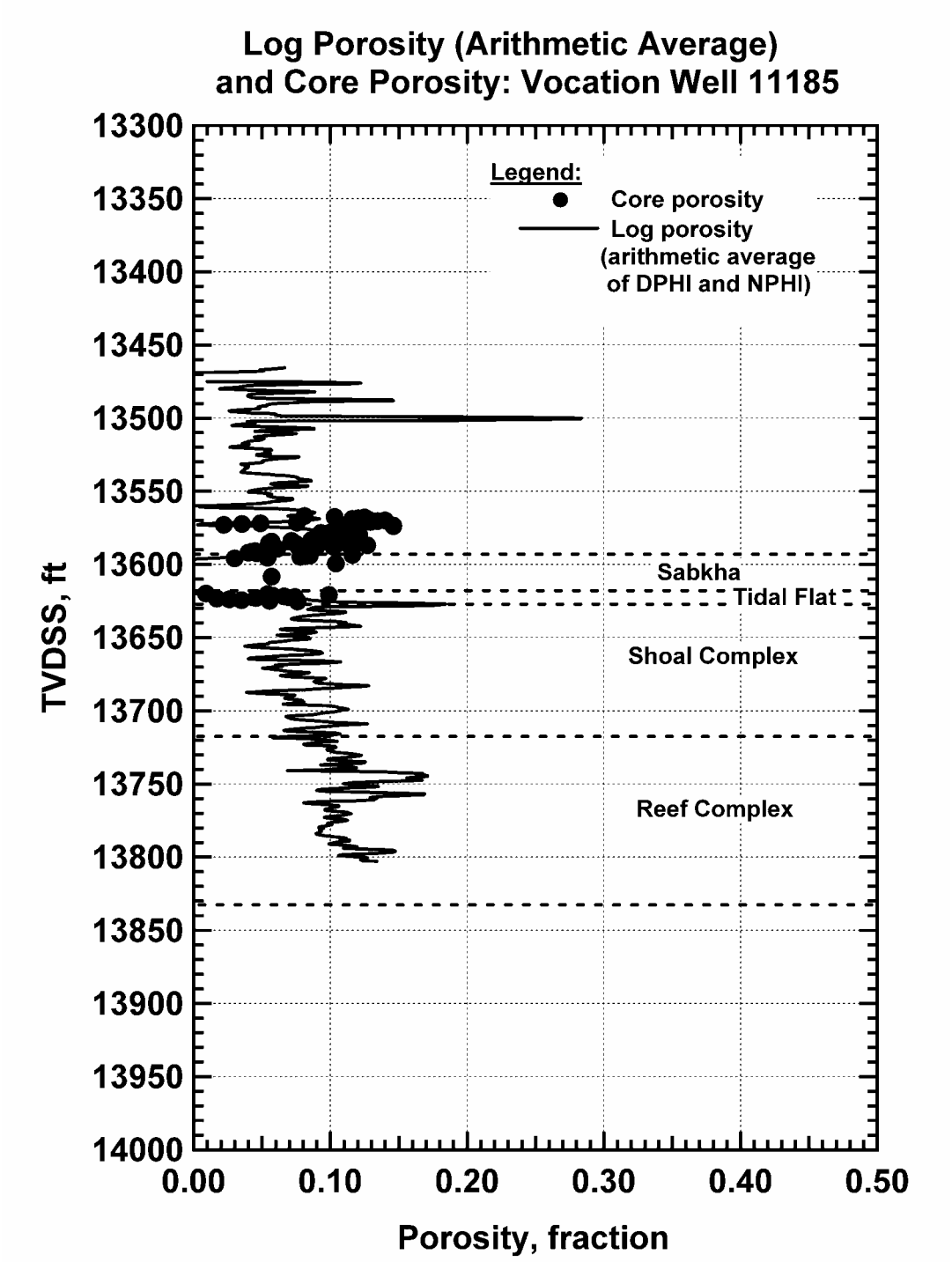

Figure 199 — Porosity Variation with Depth, Vocation Well 11185.

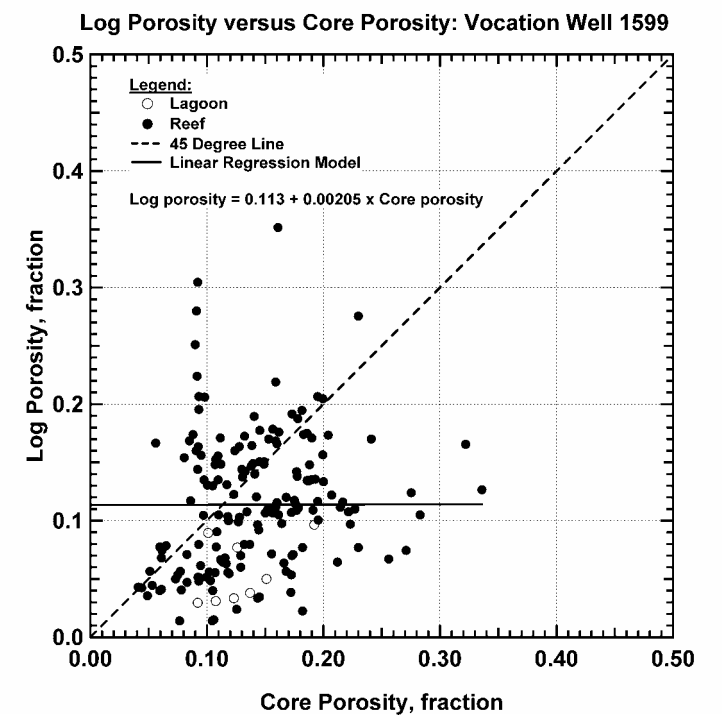

Figure 200 — Log Porosity versus Core Porosity, Vocation Well 1599.

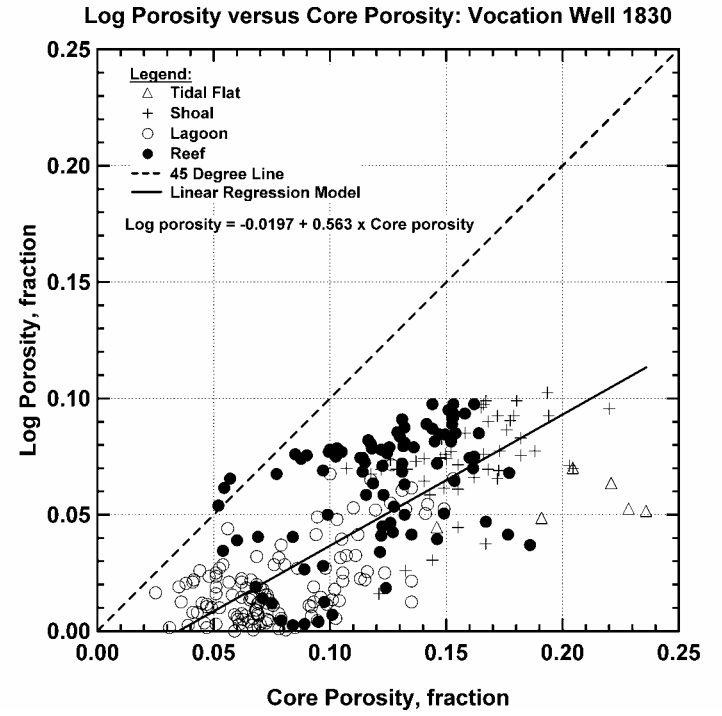

Figure 201 — Log Porosity versus Core Porosity, Vocation Well 1830.

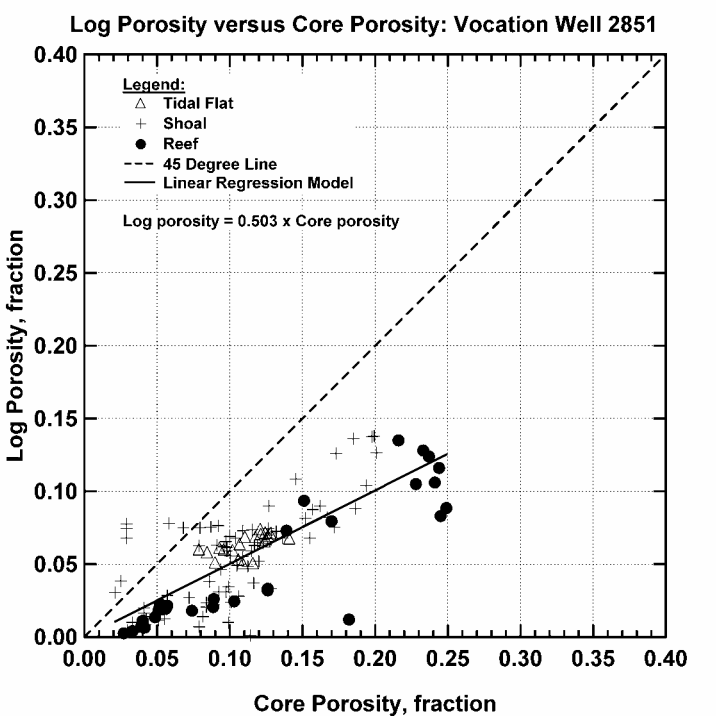

Figure 202 — Log Porosity versus Core Porosity, Vocation Well 2851.

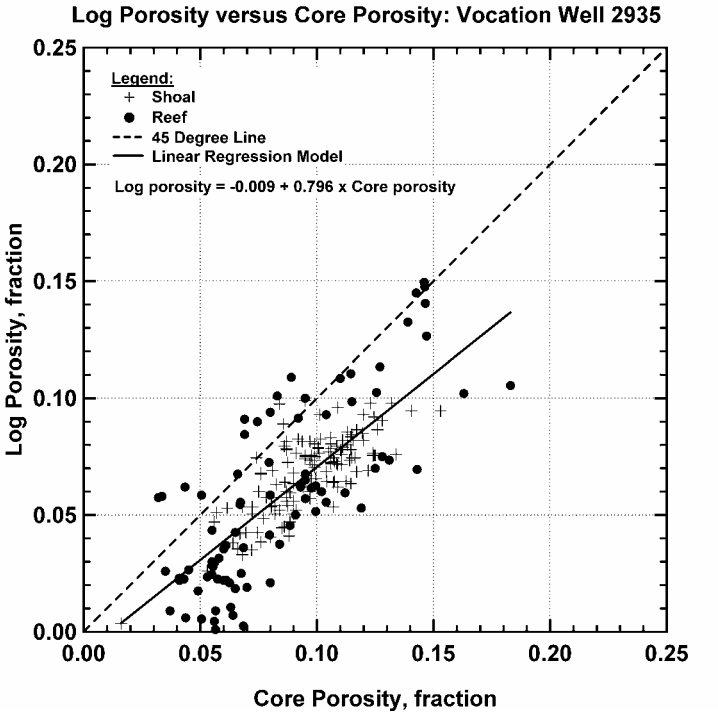

Figure 203 — Log Porosity versus Core Porosity, Vocation Well 2935.

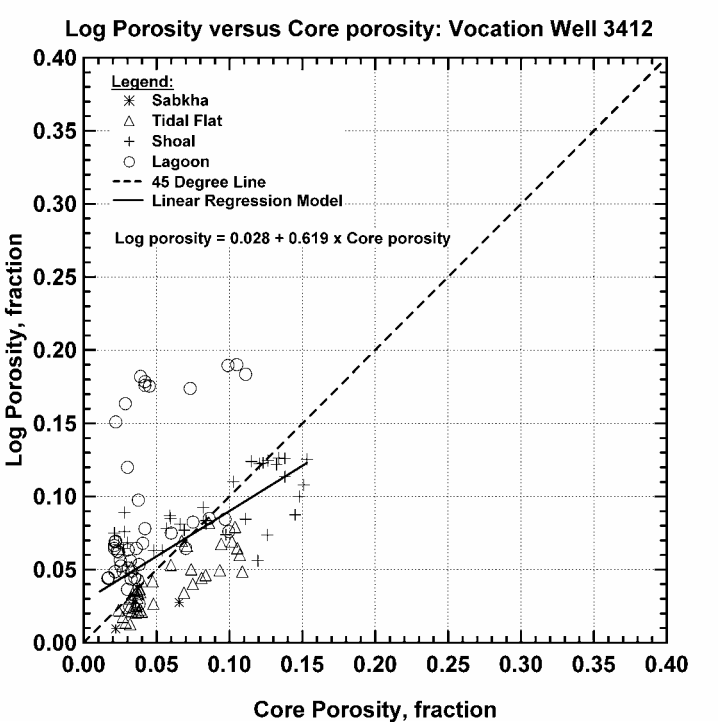

Figure 204 — Log Porosity versus Core Porosity, Vocation Well 3412.

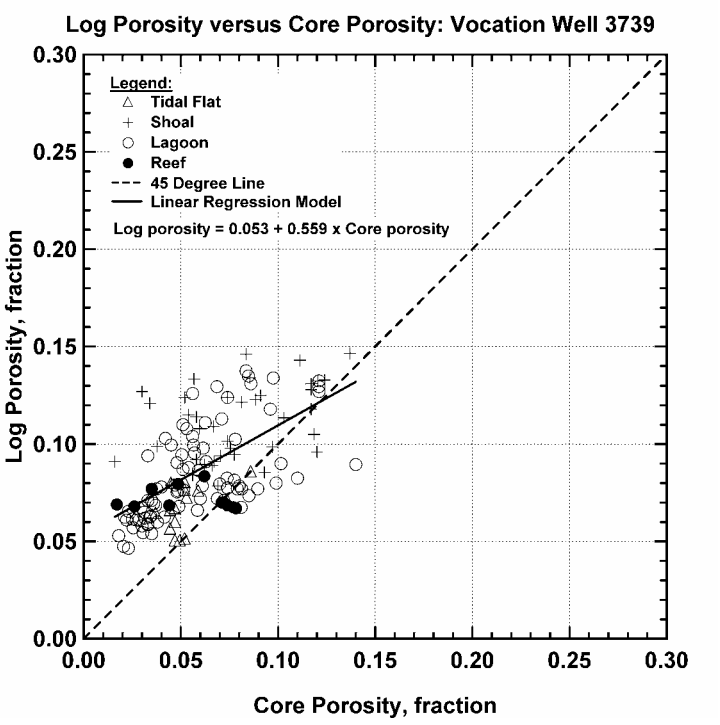

Figure 205 — Log Porosity versus Core Porosity, Vocation Well 3739.

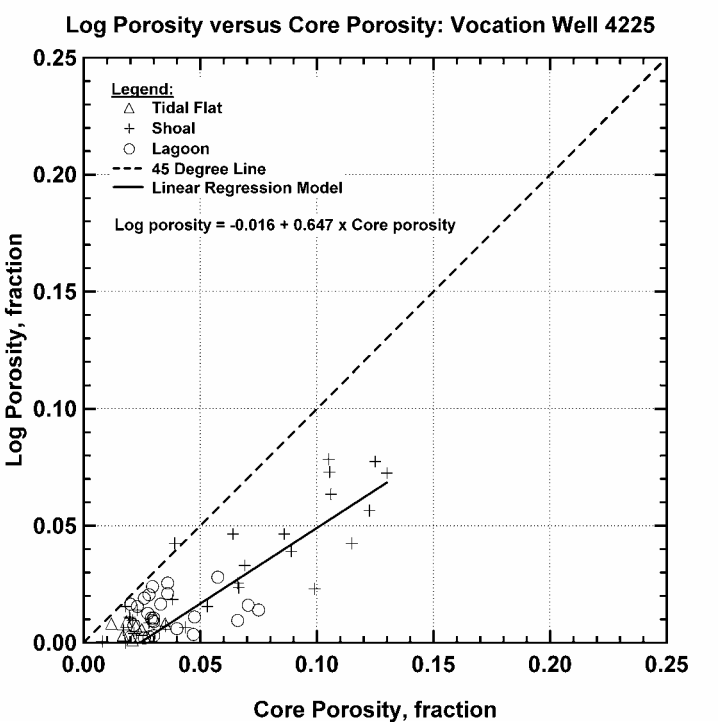

Figure 206 — Log Porosity versus Core Porosity, Vocation Well 4225.

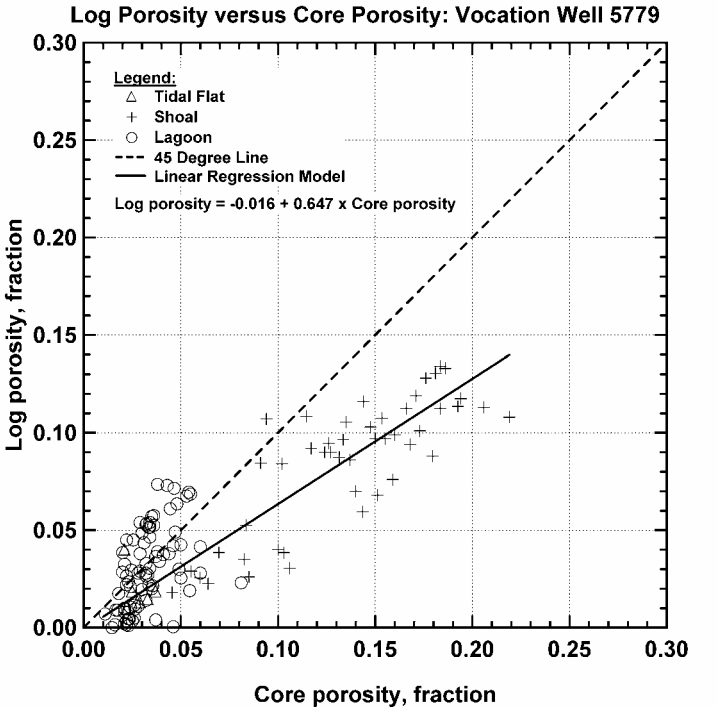

Figure 207 — Log Porosity versus Core Porosity, Vocation Well 5779.

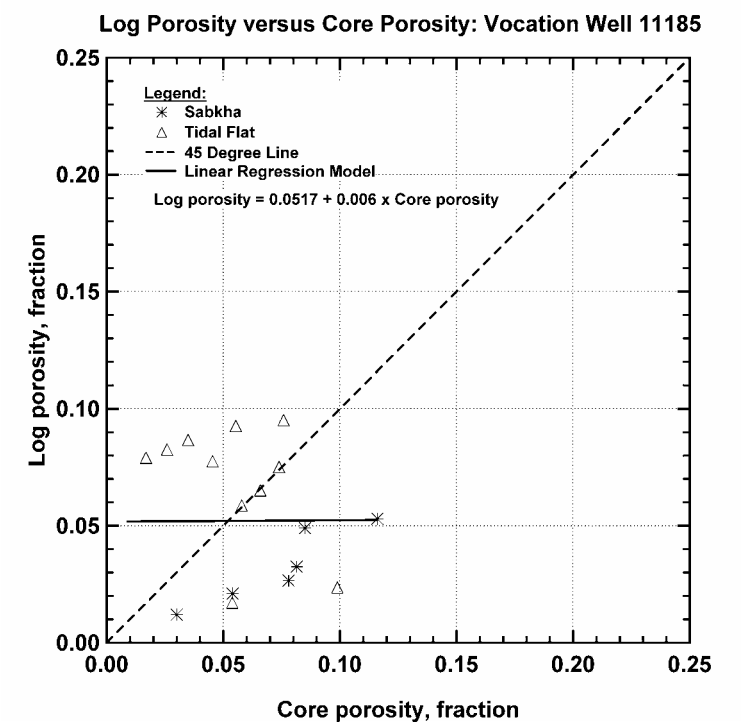

Figure 208 — Log Porosity versus Core Porosity, Vocation Well 11185.

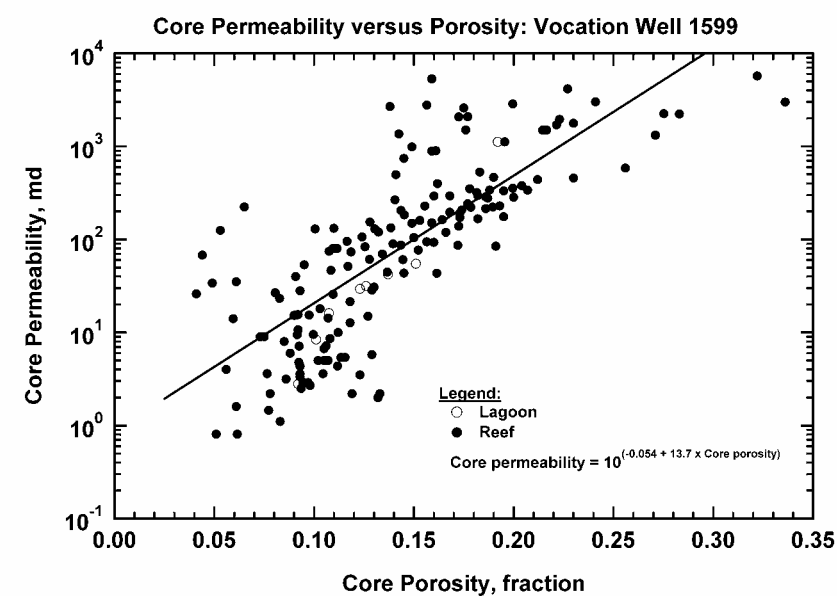

Figure 209 — Core Permeability versus Core Porosity, Vocation Well 1599.

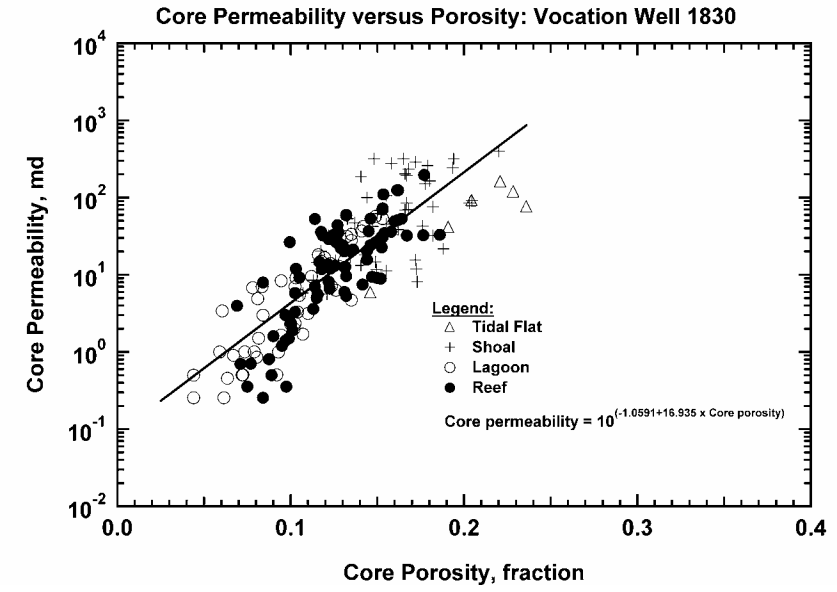

Figure 210 — Core Permeability versus Core Porosity, Vocation Well 1830.

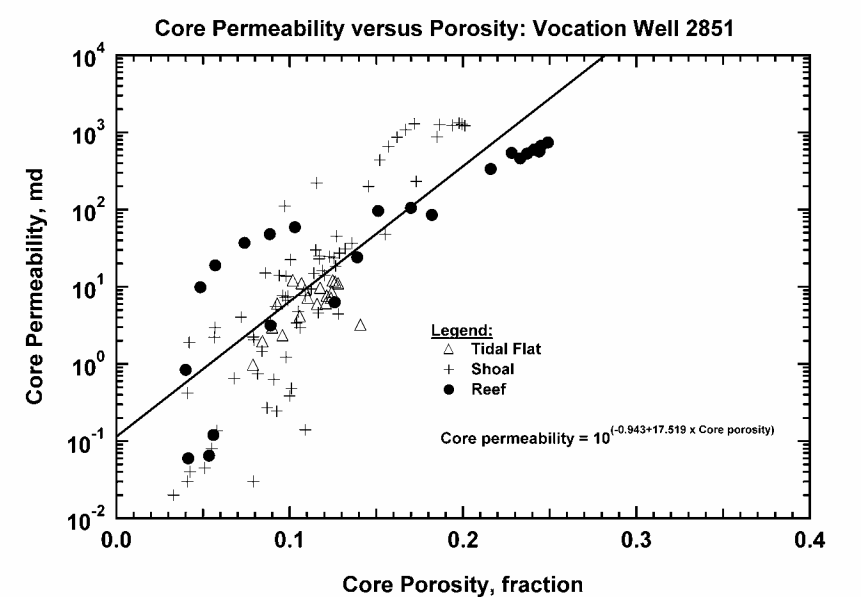

Figure 211 — Core Permeability versus Core Porosity, Vocation Well 2851.

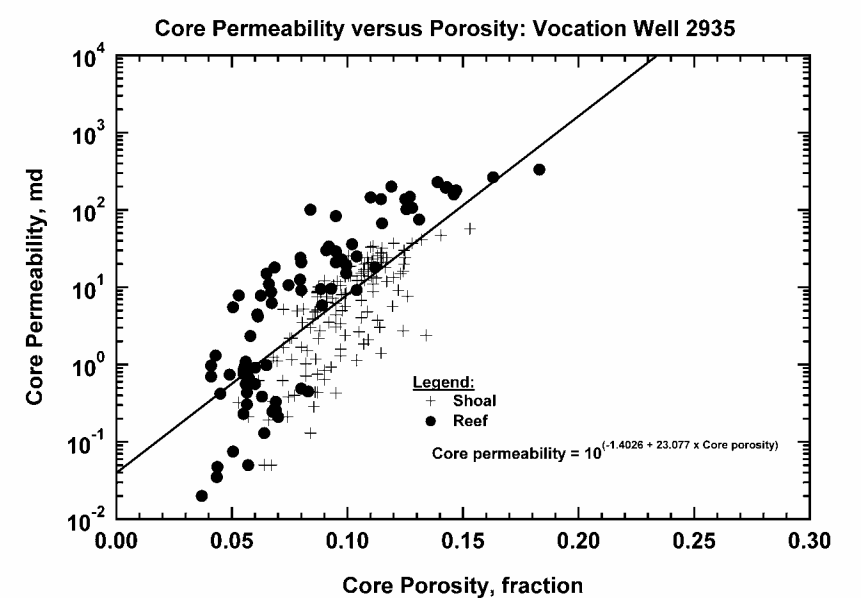

Figure 212 — Core Permeability versus Core Porosity, Vocation Well 2935.

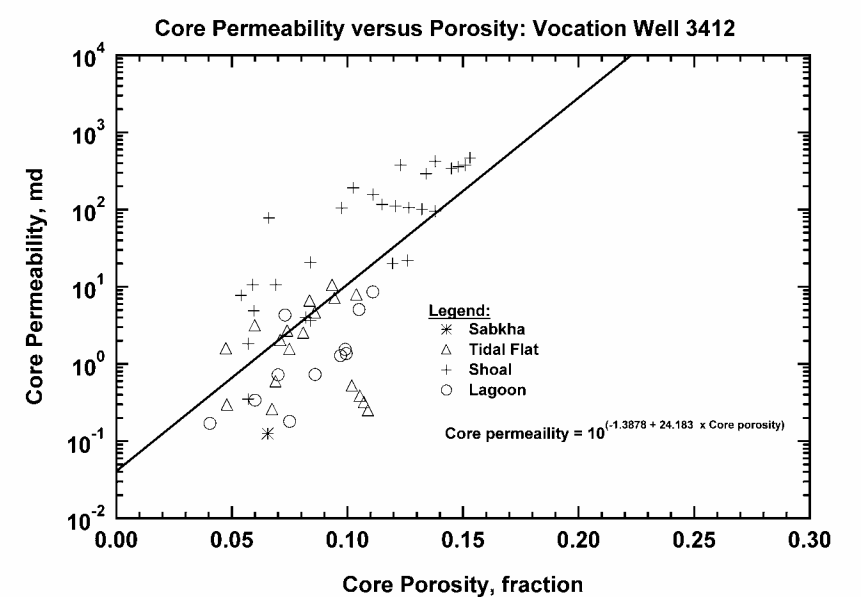

Figure 213 — Core Permeability versus Core Porosity, Vocation Well 3412.

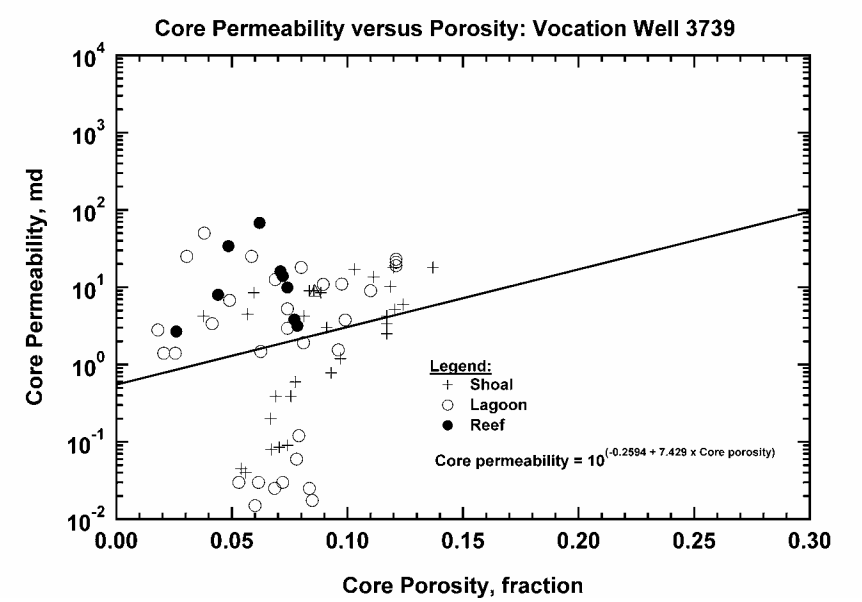

Figure 214 — Core Permeability versus Core Porosity, Vocation Well 3739

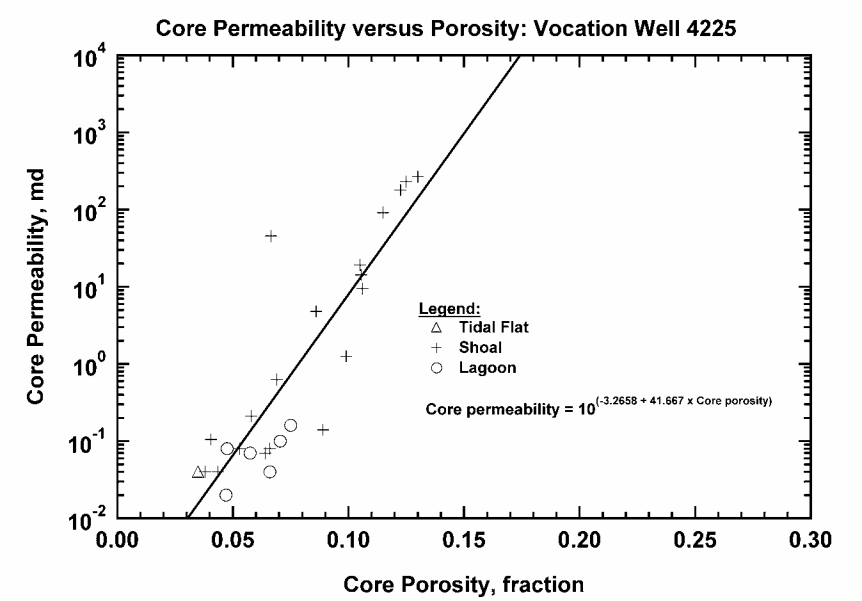

Figure 215 — Core Permeability versus Core Porosity, Vocation Well 4225.

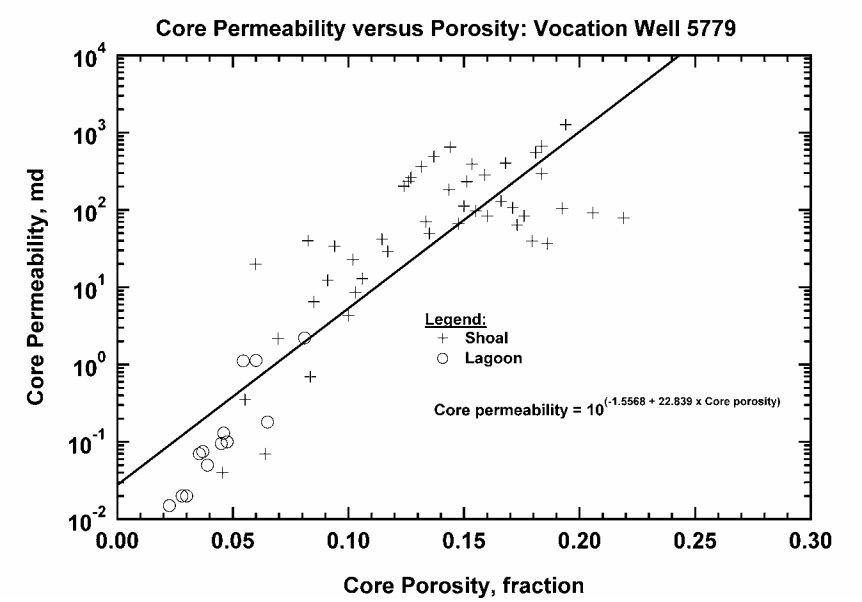

Figure 216 — Core Permeability versus Core Porosity, Vocation Well 5779.

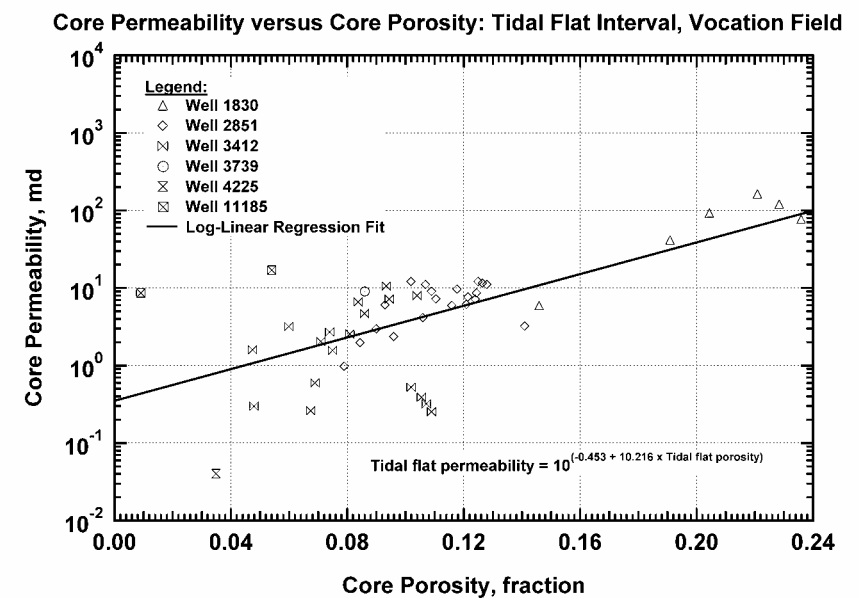

Figure 217 — Core Permeability versus Core Porosity, Tidal Flat.

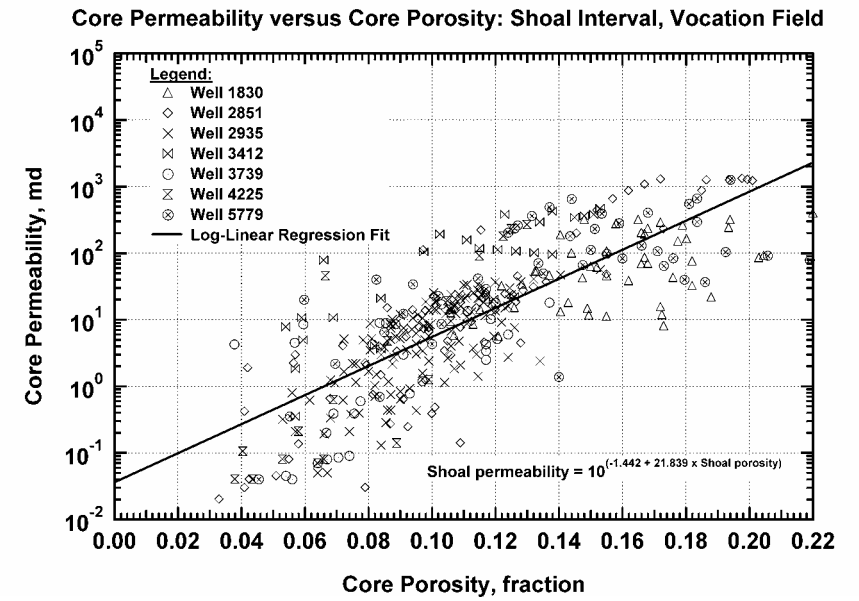

Figure 218 — Core Permeability versus Core Porosity, Shoal.

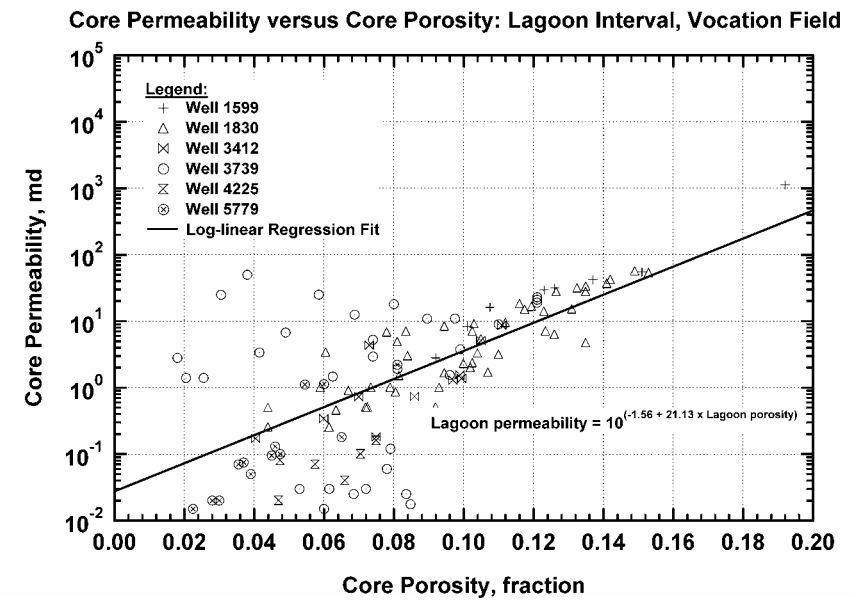

Figure 219 — Core Permeability versus Core Porosity, Lagoon.

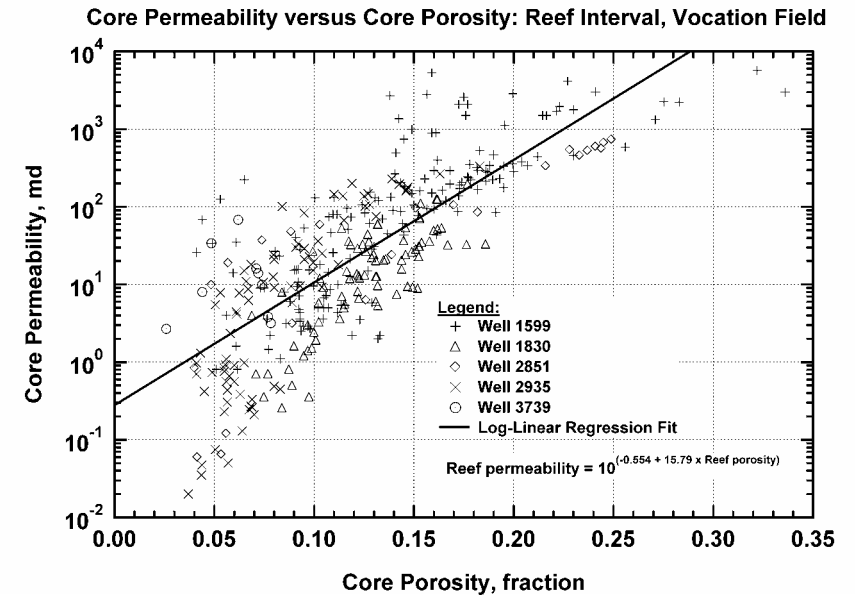

Figure 220 — Core Permeability versus Core Porosity, Reef.

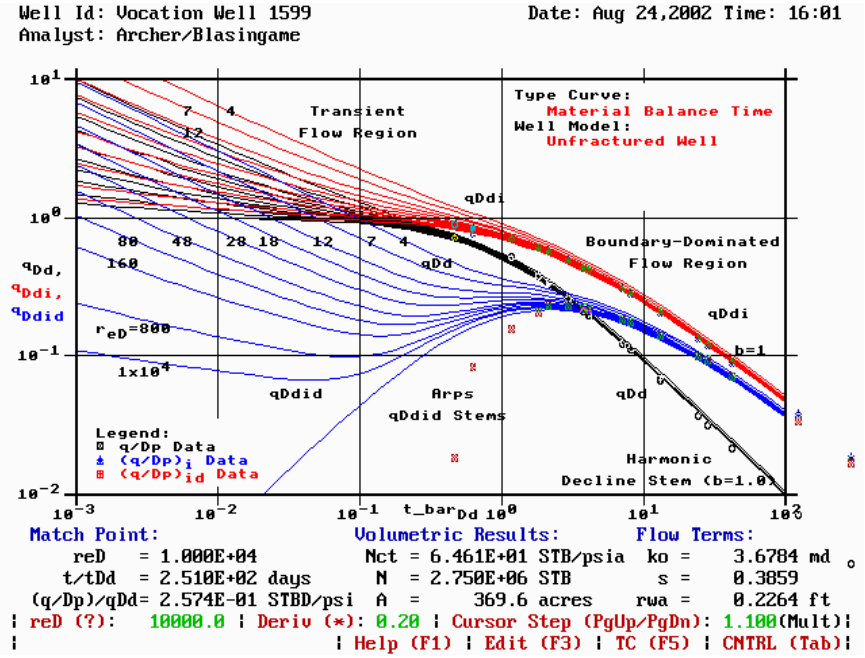

Figure 221 — Type Curve Match, Vocation Well 1599.

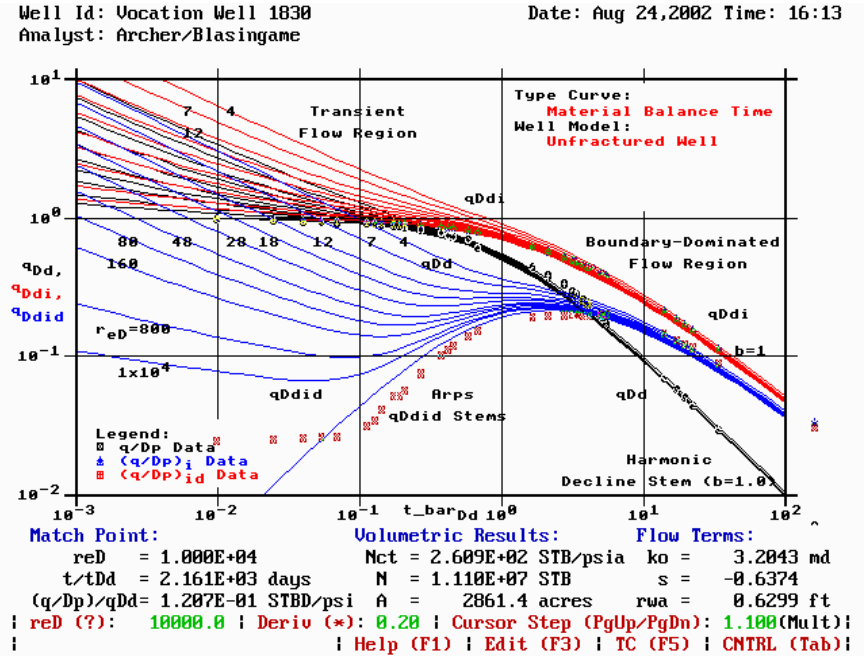

Figure 222 — Type Curve Match, Vocation Well 1830.

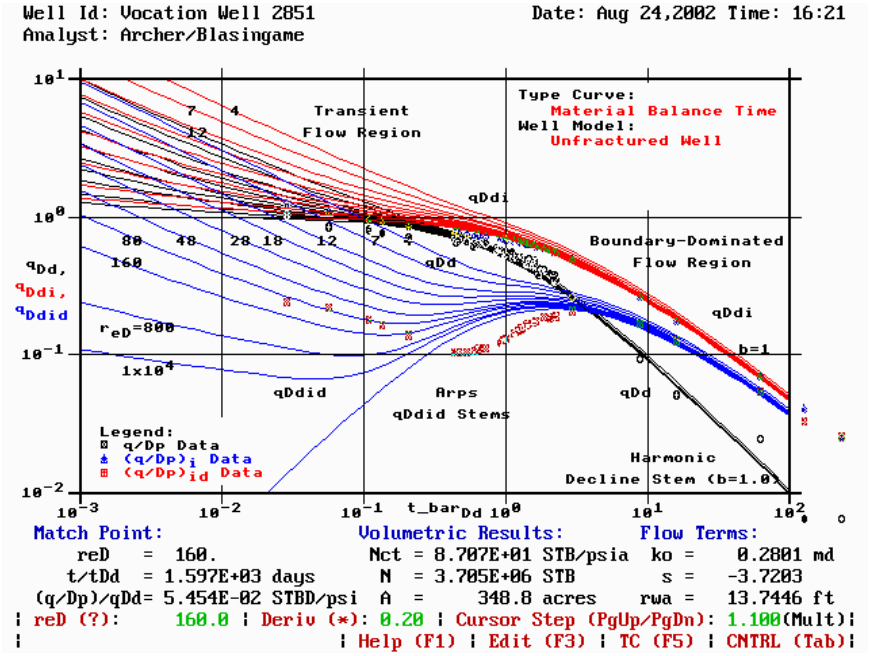

Figure 223 — Type Curve Match, Vocation Well 2851.

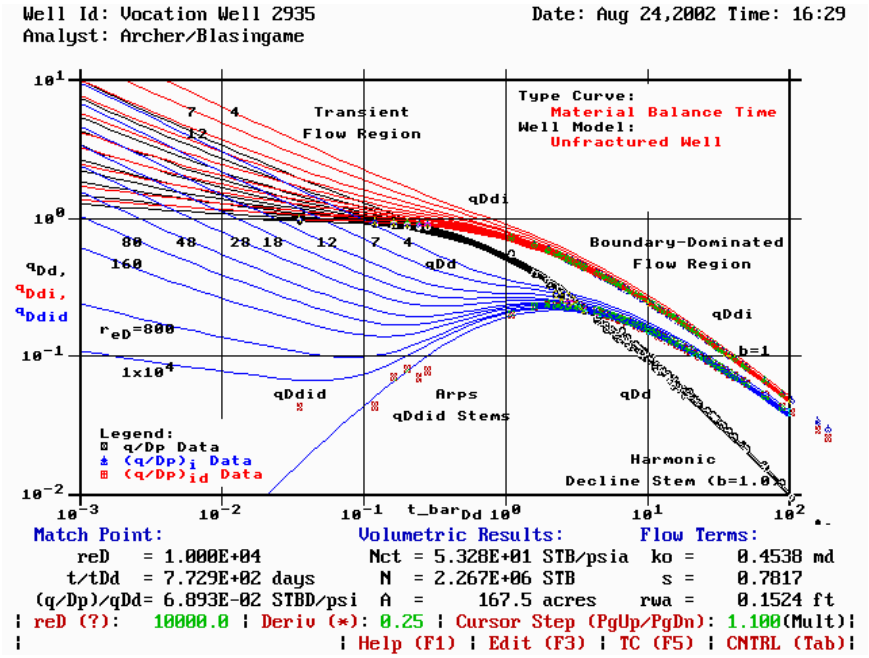

Figure 224 — Type Curve Match, Vocation Well 2935.

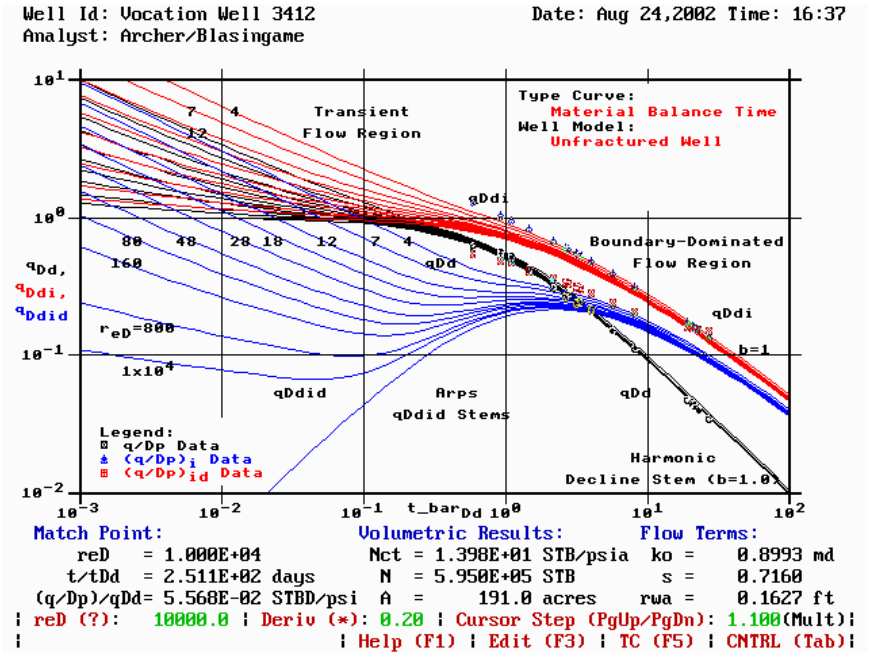

Figure 225 — Type Curve Match, Vocation Well 3412.

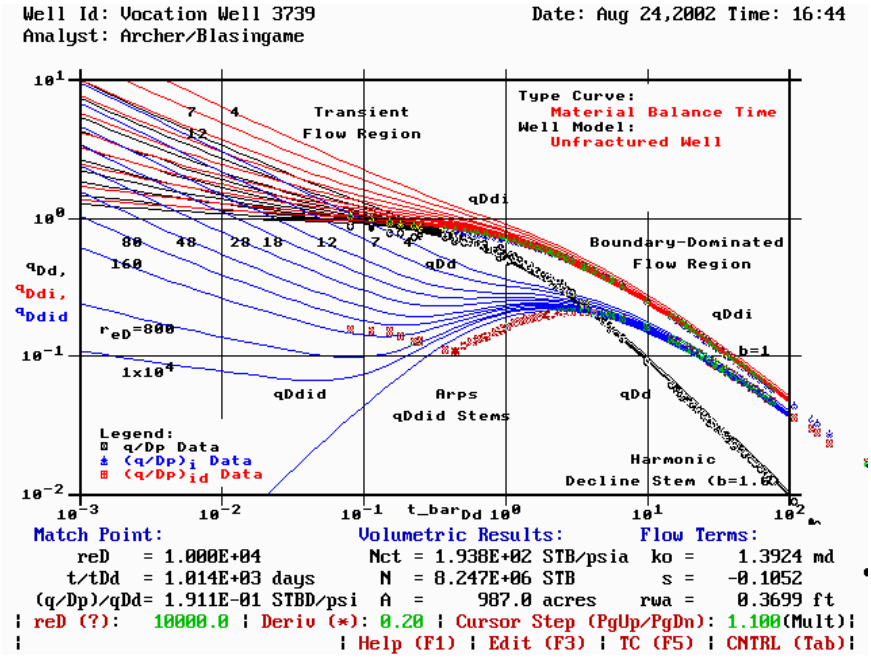

Figure 226 — Type Curve Match, Vocation Well 3739.

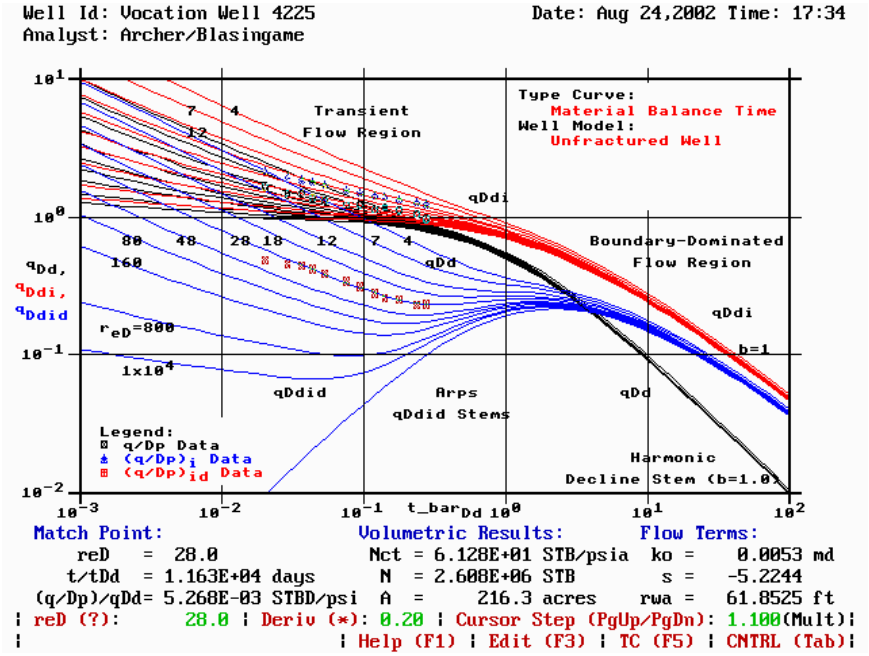

Figure 227 — Type Curve Match, Vocation Well 4225.

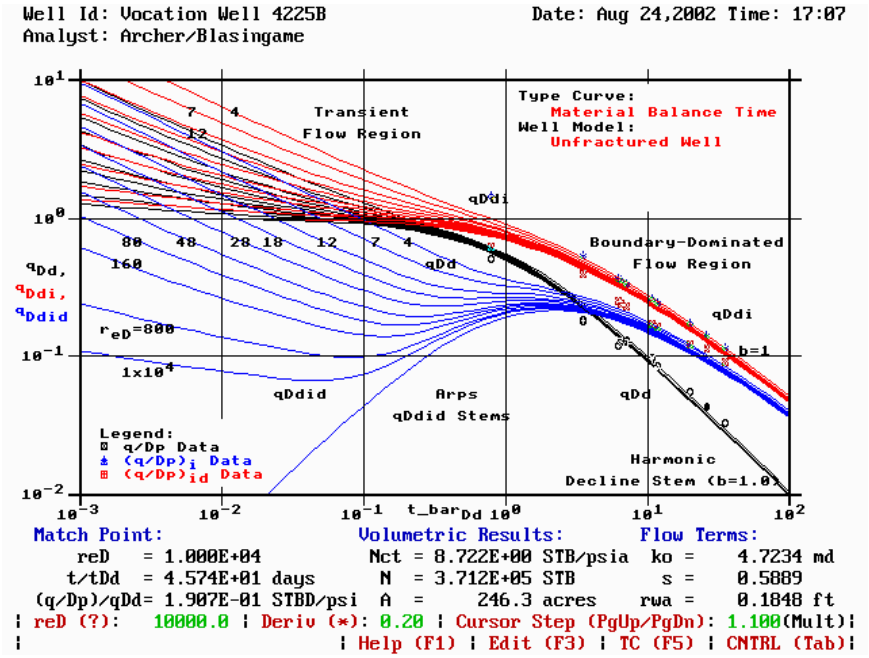

Figure 228 — Type Curve Match, Vocation Well 4225B.

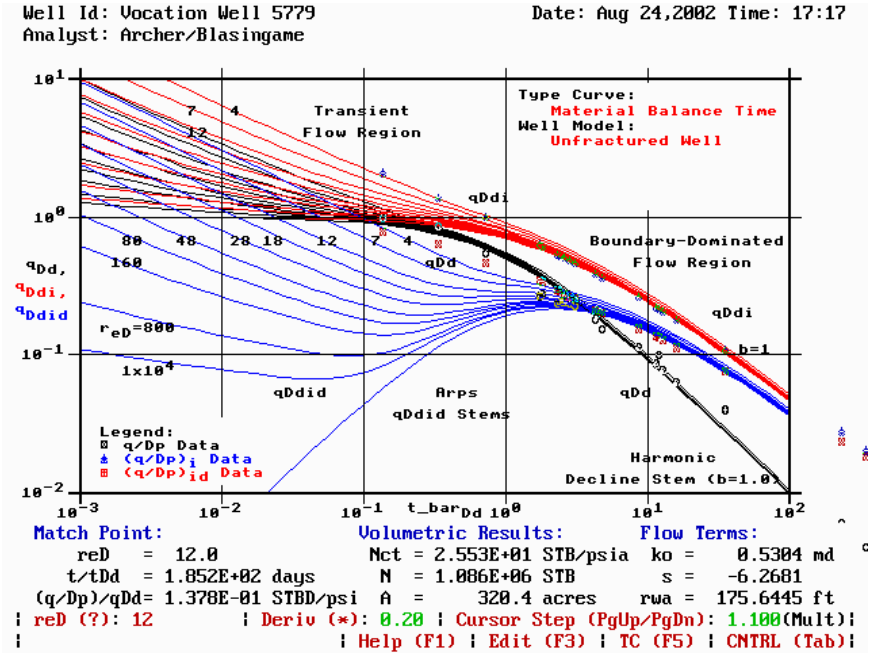

Figure 229 — Type Curve Match, Vocation Well 5779.

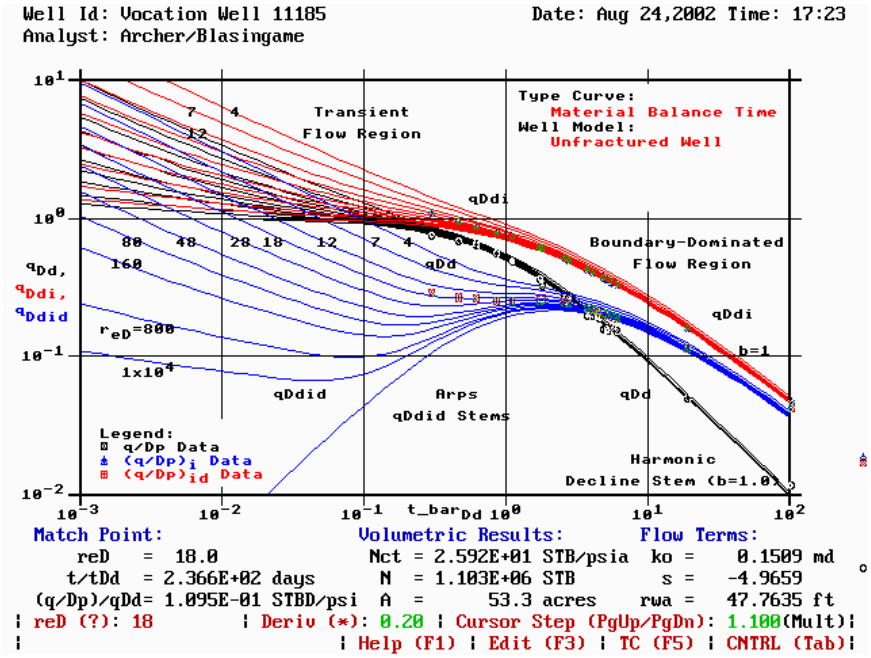

Figure 230 — Type Curve Match, Vocation Well 11185.

Table 25 — Parameters Derived from Type Curve Analysis.

Well	Nc_t (STB/psi)	N (MSTB)	A (acres)	k_o (md)	s (dim-less)
1599	64.6	2,750	369.6	3.68	0.38
1830	260.9	11,100	2861.4	3.20	0.63
2851	87.0	3,705	348.8	0.28	-3.72
2935	53.3	2,267	167.5	0.45	0.78
3412	13.9	595	191.0	0.90	0.72
3739	193.8	8,247	987.0	1.39	-0.10
4225	61.3	2,608	216.3	0.005	-5.2
4225B	8.7	371	246.3	4.72	0.58
5779	25.5	1,086	328.4	0.53	-6.26
11185	25.9	1,103	53.3	0.15	-4.96
Total		= 33,382			

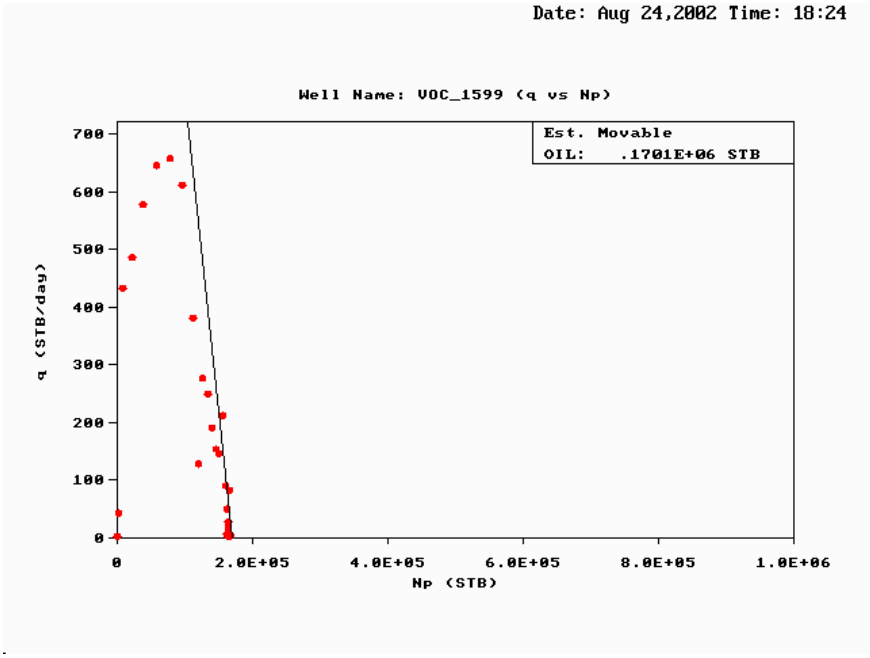

Figure 231 — Calculation of Recoverable Oil, Vocation Well 1599.

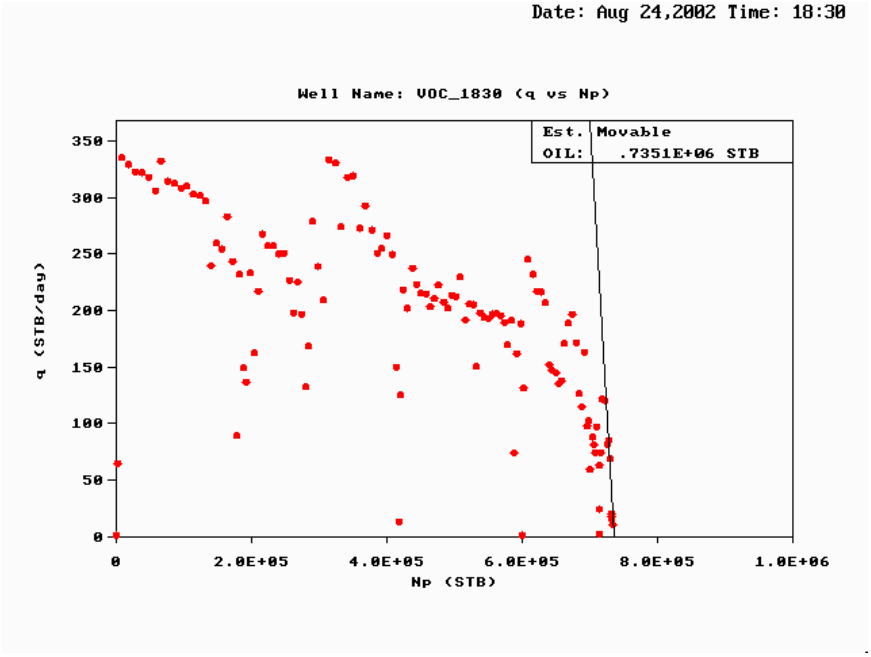

Figure 232 — Calculation of Recoverable Oil, Vocation Well 1830.

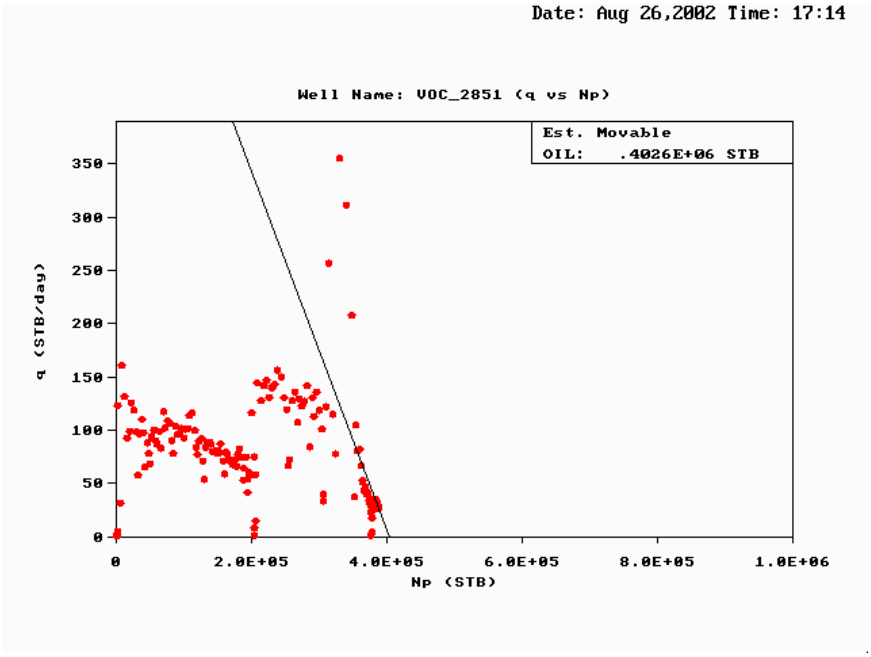

Figure 233 — Calculation of Recoverable Oil, Vocation Well 2851.

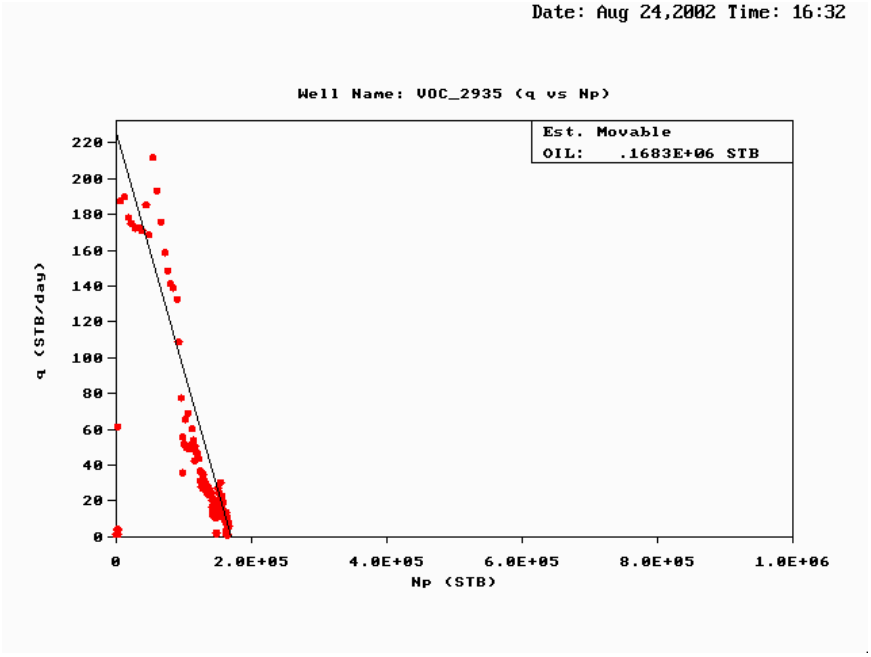

Figure 234 — Calculation of Recoverable Oil, Vocation Well 2935.

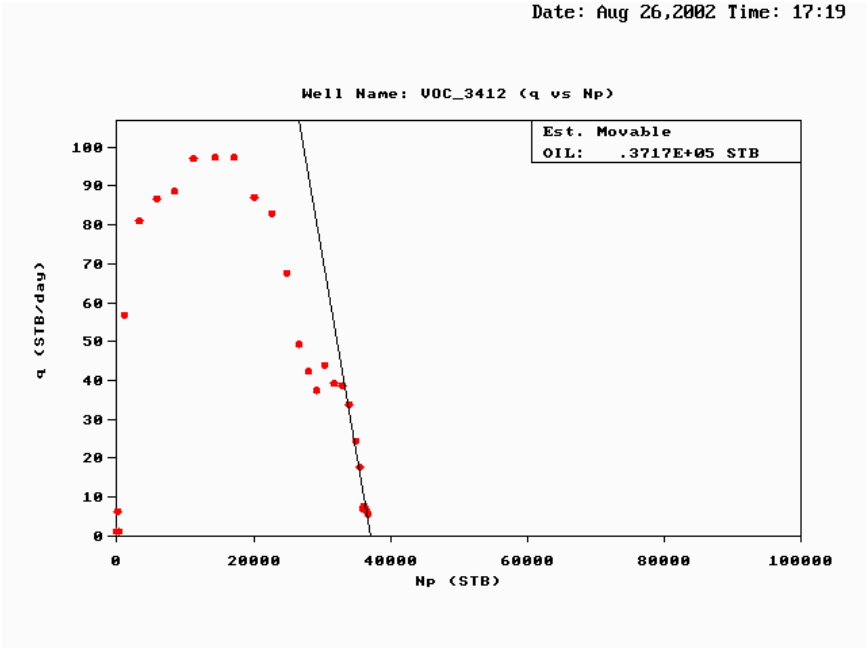

Figure 235 — Calculation of Recoverable Oil, Vocation Well 3412.

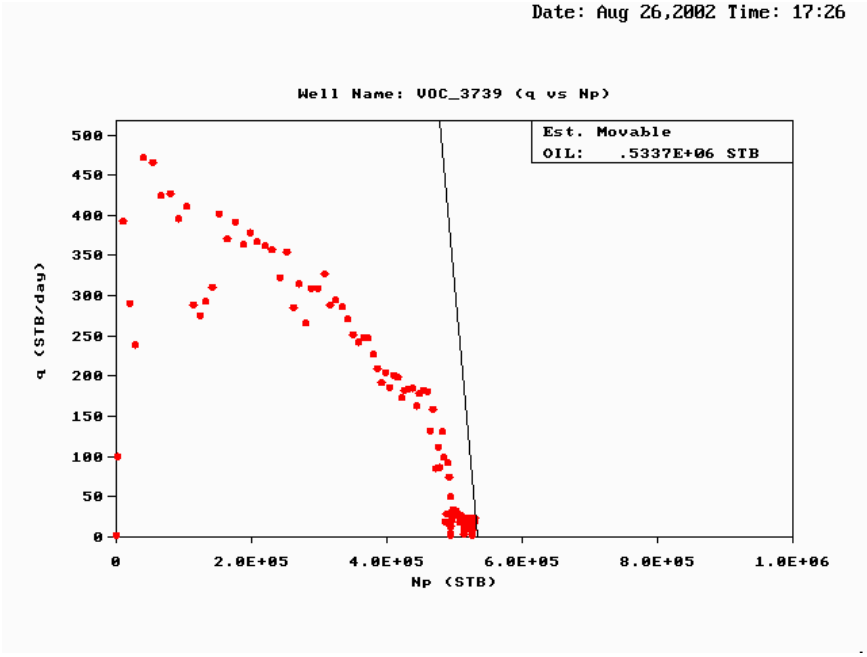

Figure 236 — Calculation of Recoverable Oil, Vocation Well 3739.

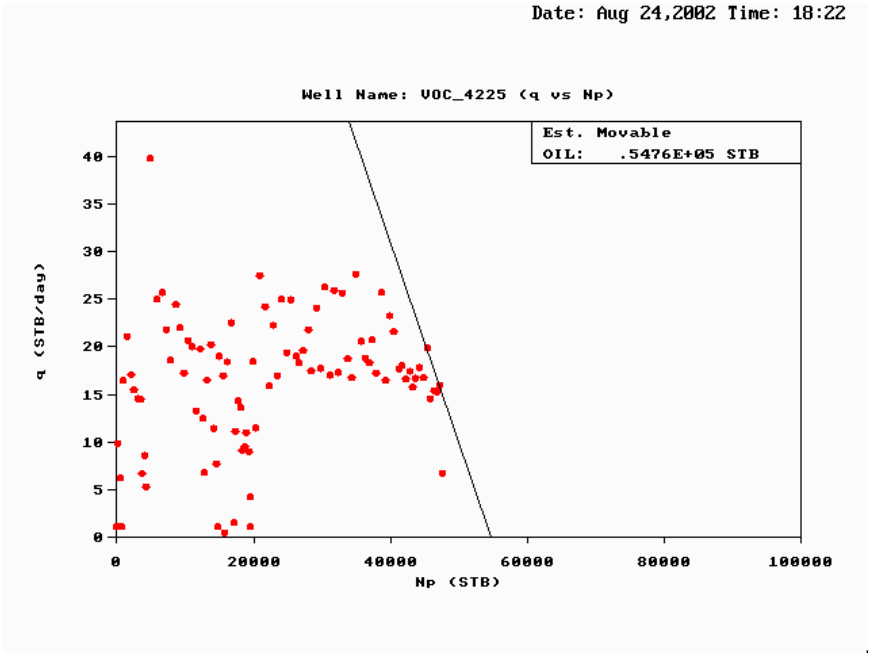

Figure 237 — Calculation of Recoverable Oil, Vocation Well 4225.

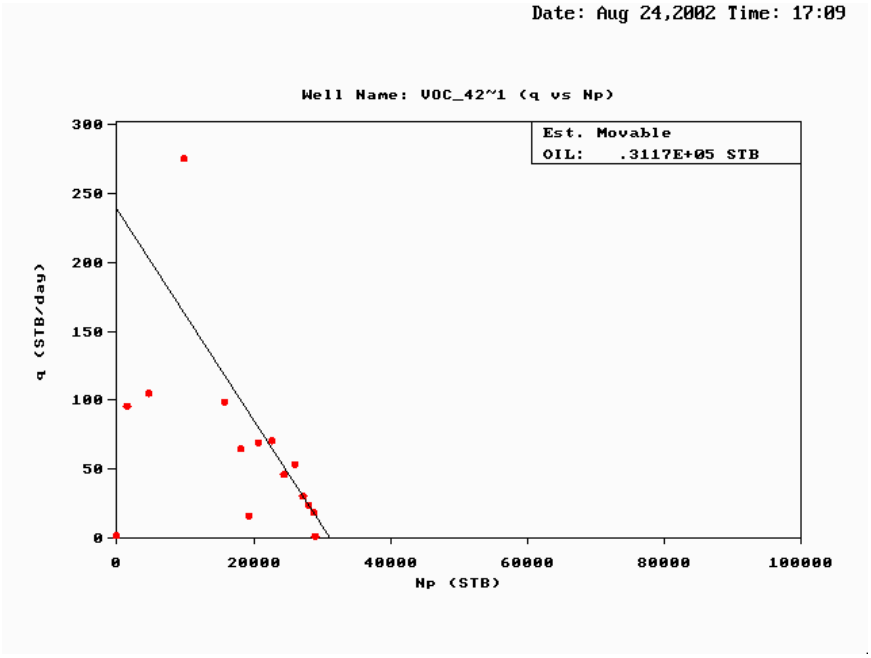

Figure 238 — Calculation of Recoverable Oil, Vocation Well 4225B.

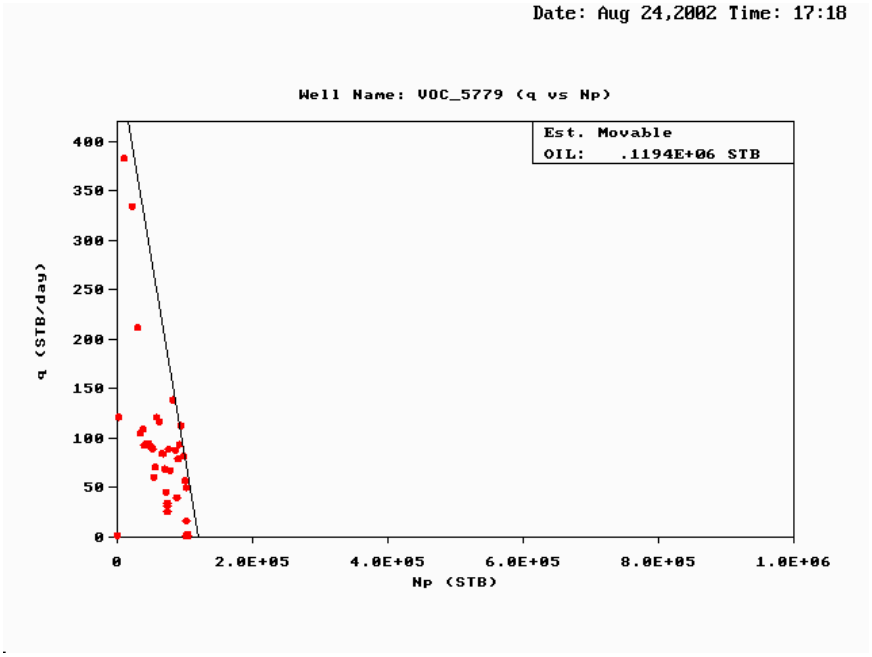

Figure 239 — Calculation of Recoverable Oil, Vocation Well 5779.

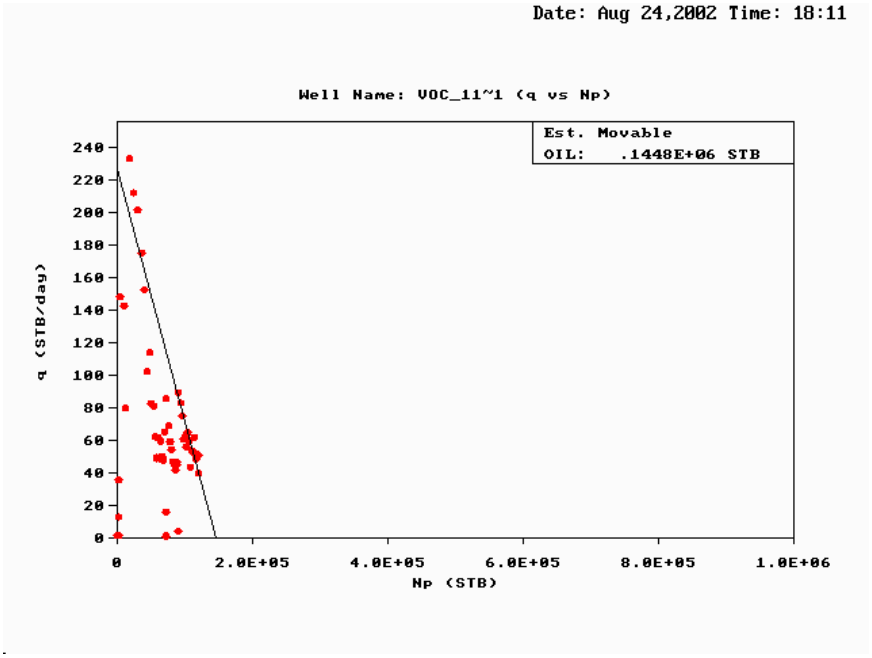

Figure 240 — Calculation of Recoverable Oil, Vocation Well 11185.

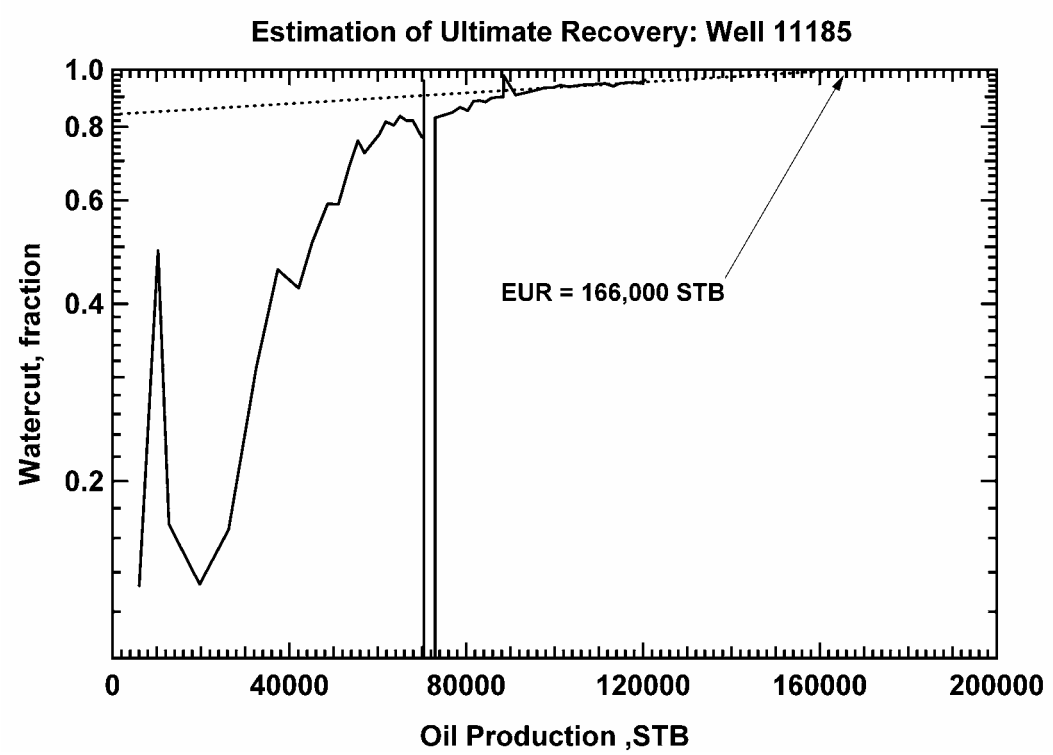

Figure 241 — Alternative Calculation of Recoverable Oil, Vocation Well 11185.

Table 26 – Oil Recovery and Recovery Factors.

Well	$N_{recoverable}$ (MSTB)	N_p (MSTB)	N (MSTB)	Recovery Factor N_p/N (dim-less)
1599	170	169	2,750	0.061
1830	735	733	11,100	0.066
2851	402	388	3,705	0.105
2935	168	165	2,267	0.072
3412	37	36	595	0.061
3739	534	529	8,247	0.064
4225	55	47	2,608	0.018
4225B	31	29	371	0.078
5779	119	102	1,086	0.094
11185	145	120	1,103	0.109
Total	= 2,331	= 2,318	= 33,832	= 0.069

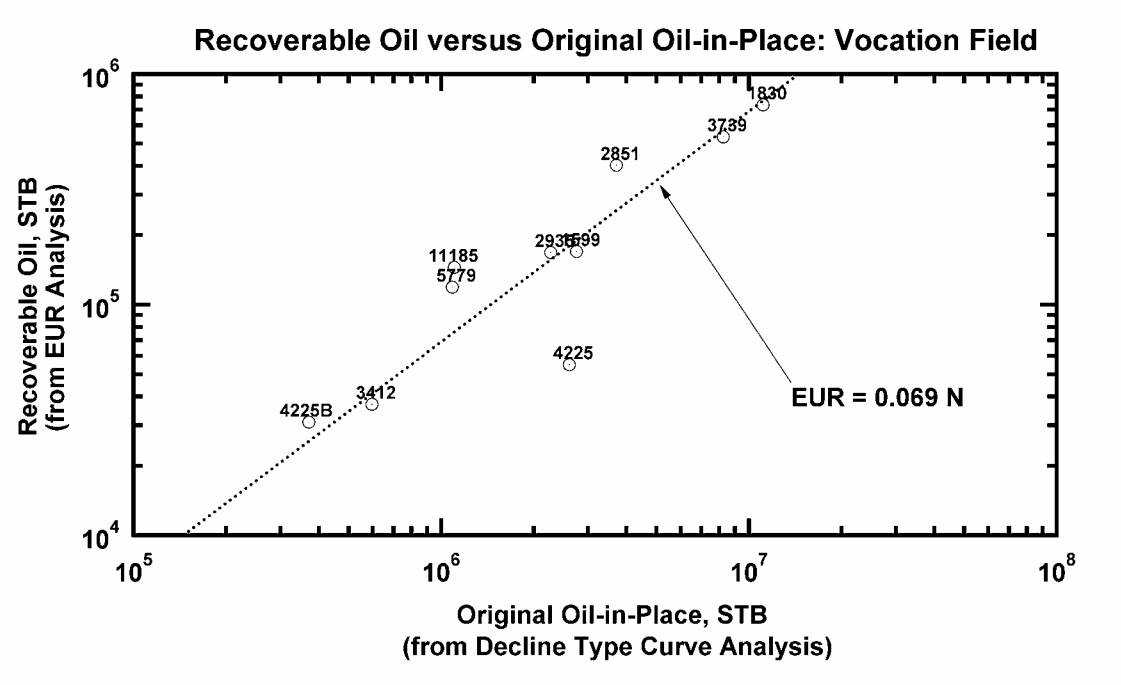

Figure 242 — Recoverable Oil (*EUR* Analysis) versus Computed Original Oil-in-Place (Decline Type Curve Analysis), Vocation Oil Field.

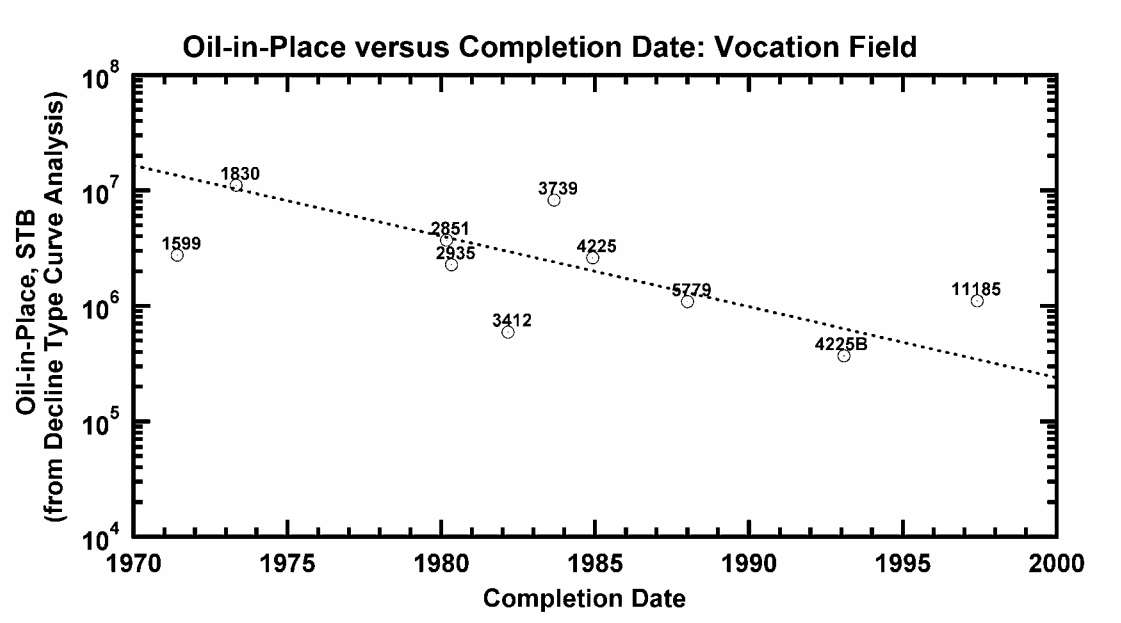

Figure 243 — Computed Original Oil-in-Place versus Completion Date, Vocation Oil Field.

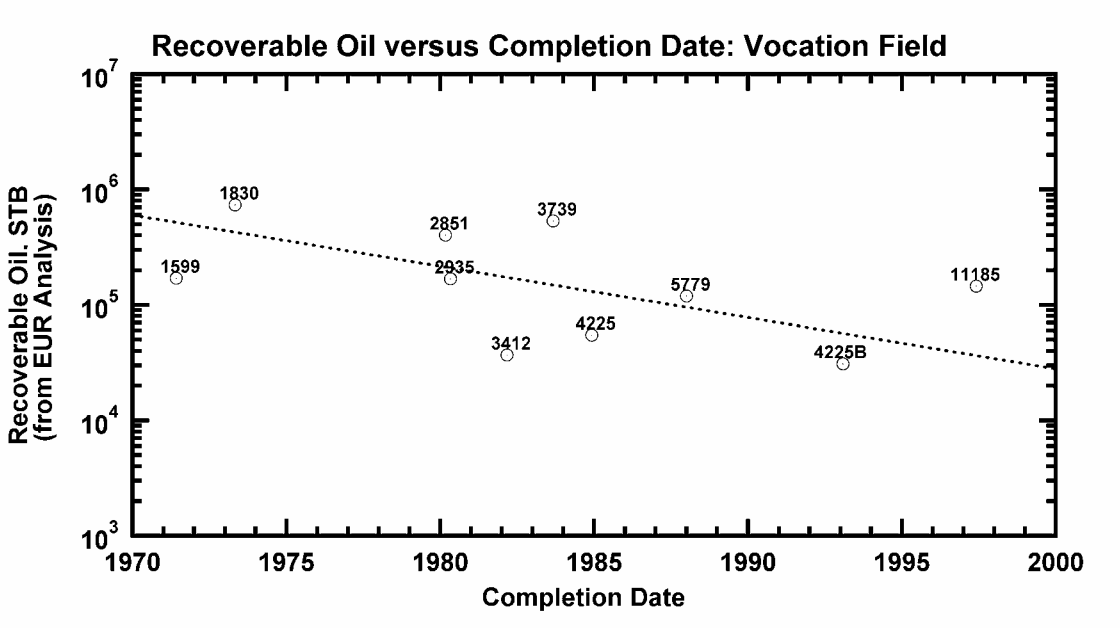

Figure 244 — Recoverable Oil versus Completion Date, Vocation Oil Field.

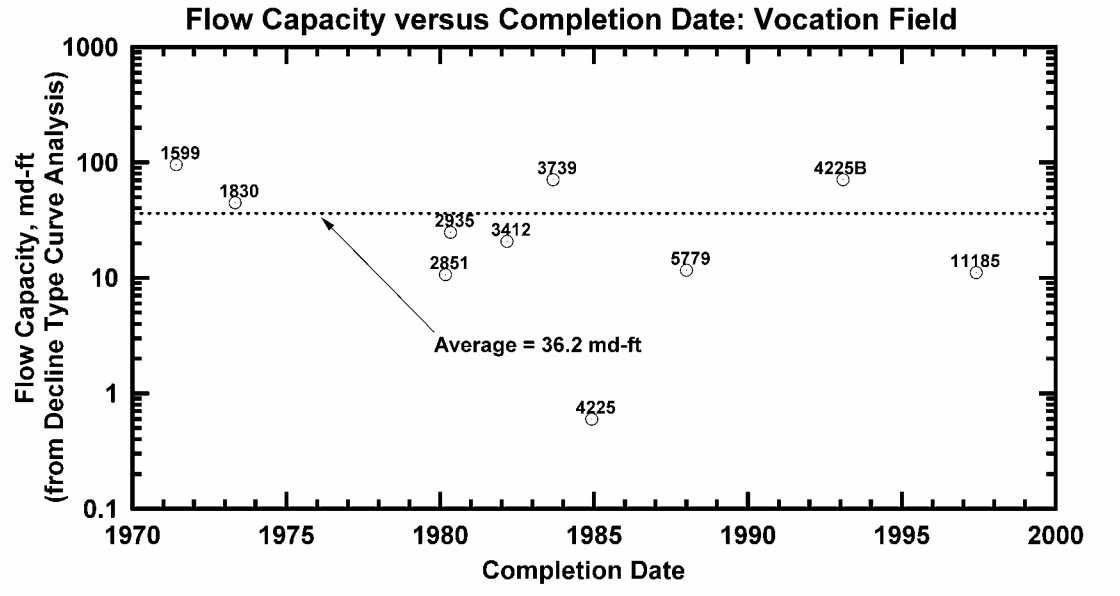

Figure 245 — Flow Capacity versus Completion Date, Vocation Oil Field.

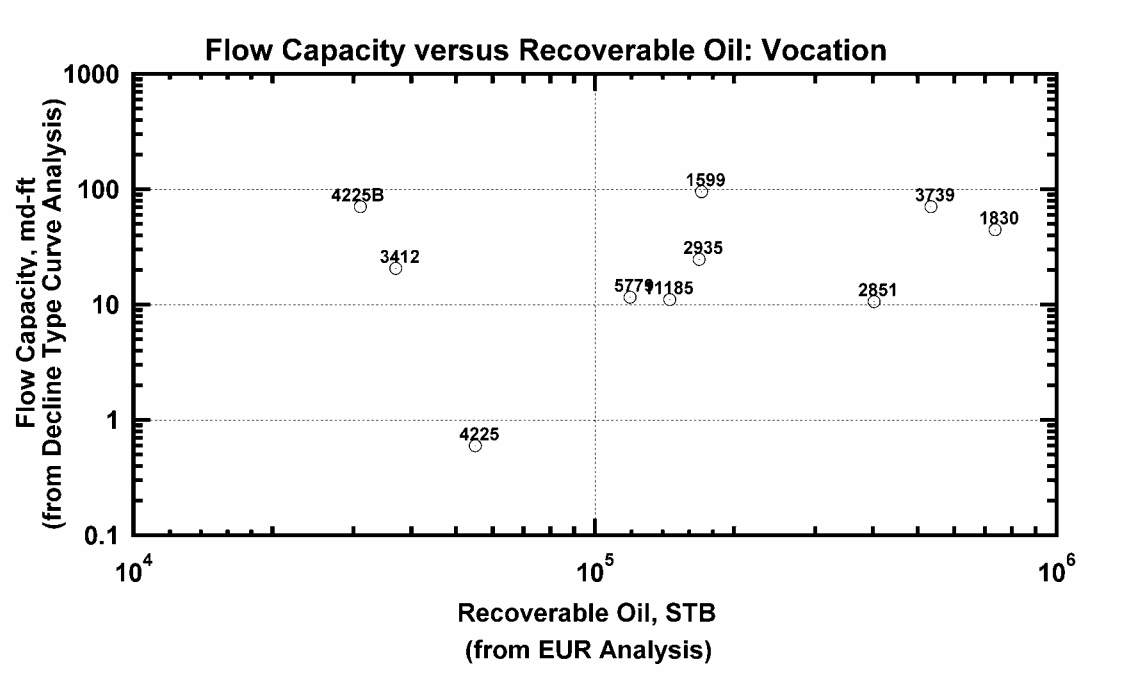

Figure 246 — Flow Capacity versus Recoverable Oil, Vocation Oil Field.

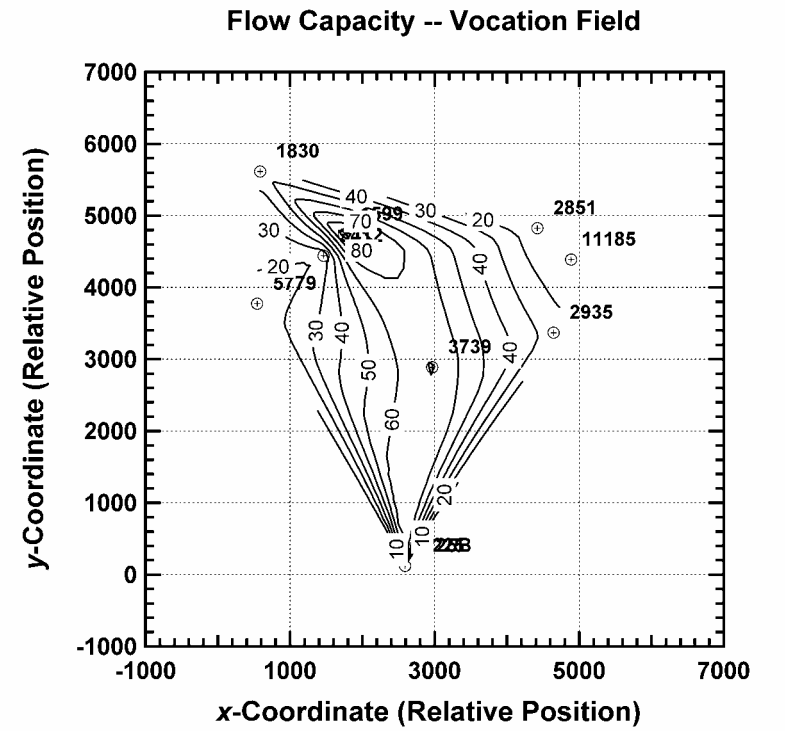

Figure 247 — Contour Map of Flow Capacity, Vocation Oil Field.

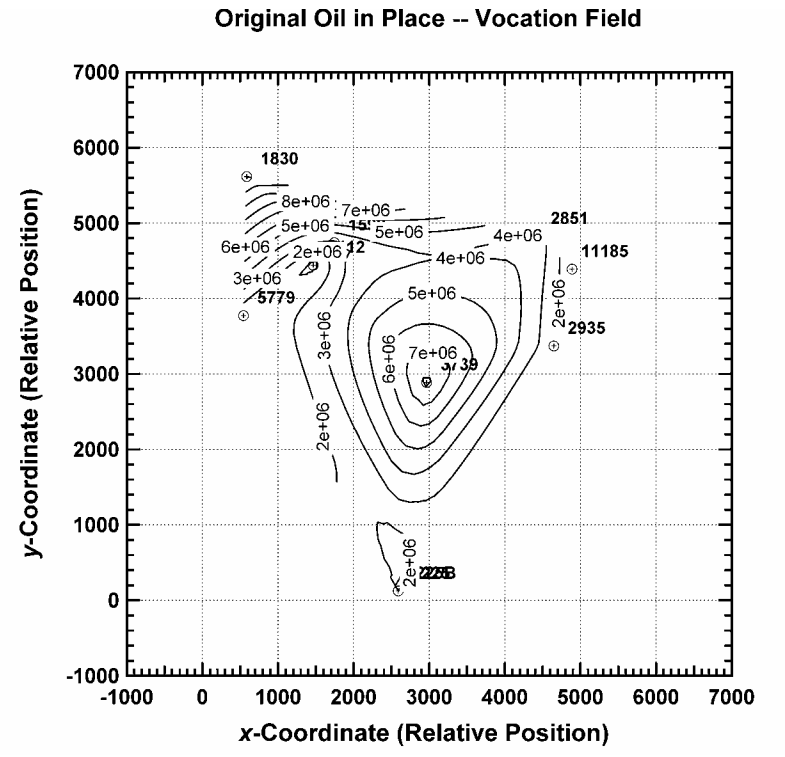

Figure 248 — Contour Map of Original Oil-in-Place, Vocation Oil Field.

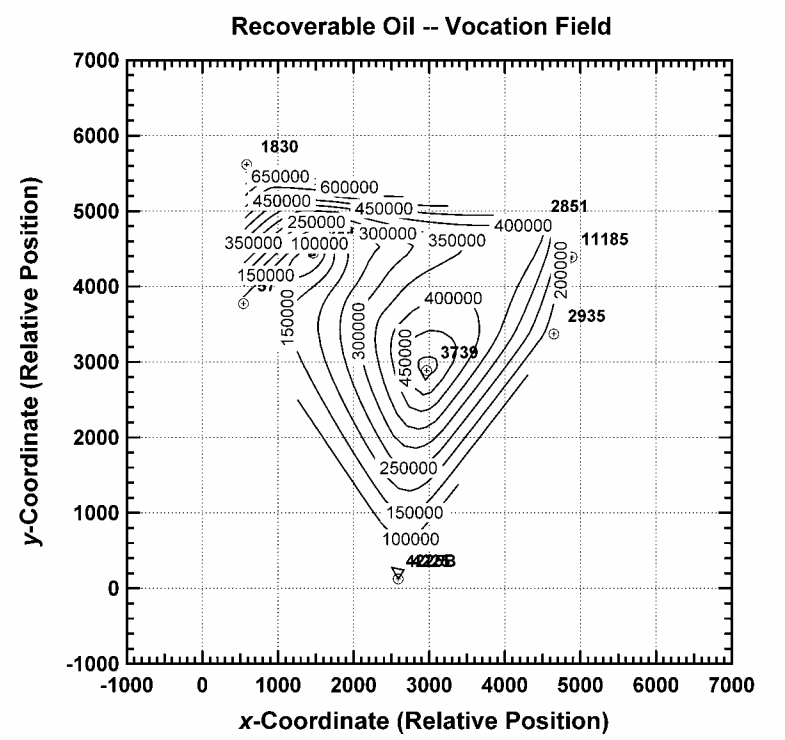

Figure 249 — Contour Map of Recoverable Oil, Vocation Oil Field.

water drive from an adjoining aquifer. The oil in place calculated for the field using well performance analysis is 33.8 million STB. It appears that oil recovery is not controlled by the flow capacity of a well, but rather is attributable to the proximity of a particular well's perforations to the oil-water contact.

Data Integration.--This task integrates the geological, geophysical, petrophysical and engineering data into comprehensive digital databases for reservoir characterization, modeling and simulation. Separate databases have been constructed for Appleton and Vocation Fields. This task serves as a critical effort to the project because the construction of a digital database is an essential tool for the integration of large volumes of data. This task also serves as a means to begin the process of synthesizing concepts. The task involves entering geologic data and merging these data with geophysical imaging information. Individual well logs serve as the standard from which the data are entered and compared. The researchers resolved any apparent inconsistencies among data sets through an iterative approach.

All geological, geophysical, petrophysical and engineering data generated from this study have been entered and integrated into digital databases for Appleton and Vocation Fields.

Rock-Fluid Interactions.--This task is a continuation of the study of reservoir architecture and heterogeneity at the microscopic scale. While macroscopic and mesoscopic heterogeneities are largely a result of structural and depositional processes, microscopic heterogeneities are often a product of diagenetic modification of the pore system. Macroscopic and mesoscopic heterogeneities influence producibility by compartmentalizing the reservoir and providing barriers to large-scale fluid flow. Microscopic heterogeneities, on the other hand, influence producibility by controlling the overall rate of fluid flow through the reservoir. This task involved an expansion of previous general studies of diagenesis within the Smackover to identify

those diagenetic processes that have influenced reef and shoal carbonates in paleohigh reservoirs using Appleton and Vocation Fields as examples. This work documents the impact of cementation, compaction, dolomitization, and dissolution on reef and shoal reservoirs. A detailed paragenetic sequence has been constructed for reservoir lithologies in each field to document the diagenetic history of these lithologies and to determine the timing of each individual diagenetic event. This task focuses on the evolution of the pore systems through time and on the identification of those diagenetic processes that played a significant role in the development of the existing pore systems. The goal of the task is to provide a basis for characterization of porosity and permeability with the reef and shoal reservoirs. Researchers Benson and Llinas at the University of Alabama conducted the diagenesis studies.

Appleton Field. Reservoir-grade porosity in the Smackover at Appleton Field occurs in microbial boundstone in the reef interval and in ooid, oncoidal, and peloidal grainstone and packstone in the upper Smackover. Porosity in the boundstone is a mixture of primary shelter porosity overprinted by secondary intercrystalline and vuggy porosity produced by dolomitization and dissolution that is pervasive throughout the field. Porosity in the grainstone and packstone is a mixture of primary interparticle and secondary grain moldic porosity overprinted by secondary dolomite intercrystalline porosity.

There is a distinct difference in reservoir quality between the grainstone/packstone and boundstone reservoir intervals. Although the difference in reservoir quality between these lithofacies is principally the result of depositional fabric, diagenesis acts to enhance or impair the reservoir quality of these lithofacies. Porosity in the grainstone/packstone reservoir interval in the McMillan 2-14 well (Permit #3854) ranges from 9.7 to 21.5% and averages 14.8%. Permeability ranges from 1.1 to 618 md, having a mean of 63.5 md. Porosity in the reef

boundstone reservoir interval in the McMillan Trust 12-14 well (Permit #4633-B) ranges from 11.9 to 25.0% and averages 18.1%. Permeability ranges from 14 to 1748 md, having a mean of 252 md.

The higher producibility for the reef lithofacies is attributed to the higher permeability of this lithofacies and to the nature of the pore system (pore-throat size distribution) rather than the amount of porosity. Pore-throat size distribution is one of the important factors determining permeability, because the smallest pore throats in cross-sectional areas are the bottlenecks that determine the rate at which fluids pass through a rock.

Although both the reef and shoal lithofacies accumulated in diverse environments to produce mesoscopic-scale heterogeneity, dolomitization and dissolution acted to reduce the microscopic-scale heterogeneity in these carbonate rocks (Figure 250). The grainstone/packstone accumulated in shoal environments and were later subjected to dolomitization and vadose dissolution. The resulting moldic pore system, which includes primary interparticulate and secondary grain moldic and dolomite intercrystalline porosities, is characterized by multisize pores that are poorly connected by narrow pore throats. Pore size is dependent on the size of the carbonate grain that was leached.

The boundstone accumulated in a reef environment and were later subjected to pervasive dolomitization and nonfabric-selective, burial dissolution. The intercrystalline pore system, which includes primary shelter and secondary dolomite intercrystalline and vuggy pores, is characterized by moderate-size pores having uniform pore throats. The size of the pores is dependent upon the original shelter pores, the dolomite crystal size, and the effects of late-stage

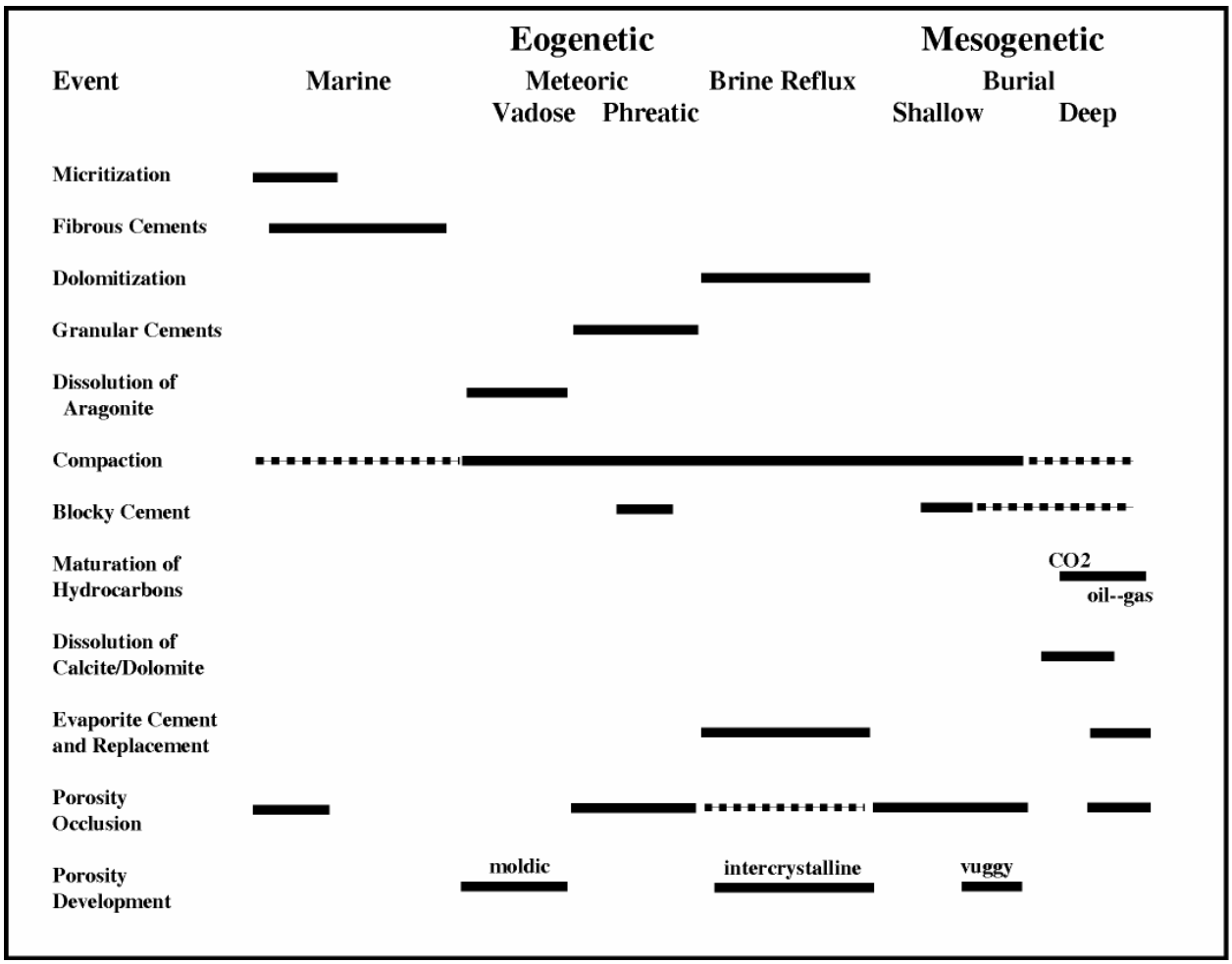

Figure 250 – Diagenetic sequence of the Smackover Formation at Appleton Field.

dissolution. The reef reservoir and its shelter and intercrystalline pore system, therefore, has higher producibility potential compared to the shoal reservoir and its moldic pore system.

As confirmed from well-log analysis and well production history, hydrocarbon production in Appleton field has occurred primarily from the boundstone of the Smackover reef interval, with secondary contributions from the shoal grainstone and packstone of the upper Smackover. Total reservoir thickness in the producing wells ranges from 20 ft (6 m) in the McMillan Trust 11-1 well (Permit #3986) to 82 ft (25 m) in the McMillan Trust 12-4 well (Permit #4633-B). With the exception of the McMillan 2-14 well (permit #3854), where production has been primarily from grainstone and packstone of the upper Smackover, the majority of the productive reservoir occurs in boundstone.

The higher production from the reef interval is attributed to the better reservoir quality of the boundstone and to the better continuity and connectivity of these carbonates. Whereas, the grainstone/packstone interval is discontinuous, both vertically and laterally, the boundstone interval appears to possess excellent vertical and lateral continuity.

In addition, although the microbial reef reservoir interval is more productive than the shoal reservoir interval at Appleton Field, the dendroidal thrombolites have higher reservoir quality than the layered thrombolites. Dendroidal thrombolites have a reservoir architecture characterized by high lateral and vertical pore interconnectivity and permeability, while layered thrombolites have good lateral but poorer vertical pore interconnectivity and permeability. Both thrombolite architectures are characterized by pore systems comprised of shelter and enlarged pores.

Vocation Field. The sequence of diagenetic events in the Smackover at Vocation Field occurred in the eogenetic and mesogenetic stages (Figure 251). The eogenetic stage is the time

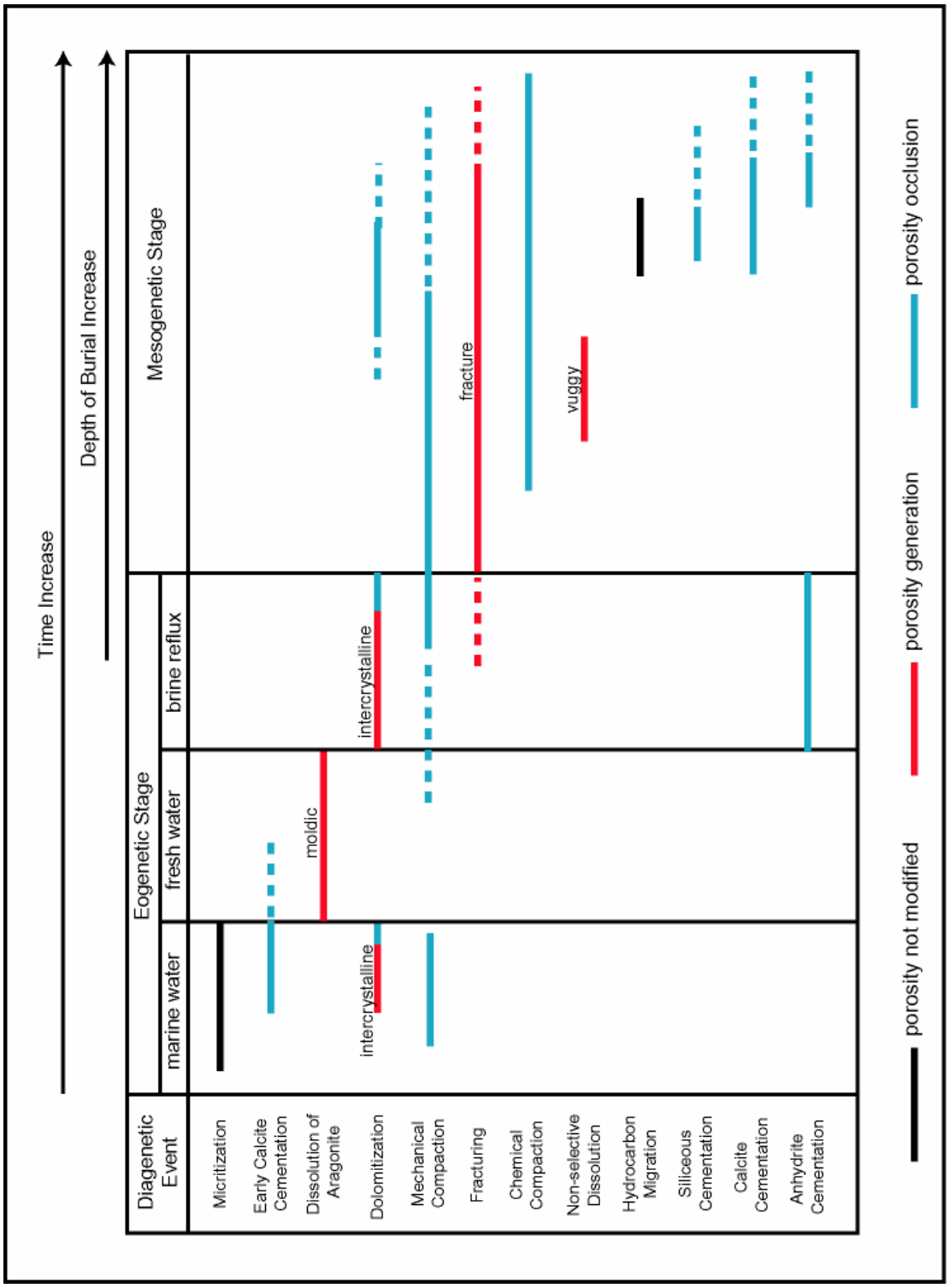

Figure 251. Diagenetic sequence of the Smackover Formation at Vocation Field.

interval between final deposition and the burial, below the influence of surface-derived fluids of marine, brine, or meteoric origin. The processes that occur within this stage are very active during relatively short periods of time. Generally, the sediments and rocks of the eogenetic zone are mineralogically unstable, or are in the process of stabilization, and therefore, porosity modification by dissolution, cementation, and dolomitization is quickly accomplished. The mesogenetic stage refers to the time interval in which sediments or rocks are buried below the influence of surficial diagenetic processes until final exhumation in association with unconformities. Progressively increased pressure and temperature and related rock-connate fluid interaction are the driving mechanisms for burial diagenesis. In general, diagenetic processes that occur in the mesogenetic zone operate at very slow rates but over long spans of geologic time.

Micritization is one of the earliest eogenetic events since it largely occurs near the sediment / water interface. It is produced by repeated boring activity of microorganisms such as algae and fungi over the allochem surfaces and the subsequent infill of the borings with micrite generating rims around the grains. This is a very common process in Smackover deposits especially in the shoal facies at Vocation Field. Another early diagenetic event is the selective dissolution of aragonite allochems generating moldic pores. It is produced by the action of meteoric waters undersaturated with respect to calcium carbonate and affected mainly tidal and shoal deposits because of their deposition very close to the sea water surface and probably reflecting a relative sea-level fall. Isopachous rims of marine calcite cement (later dolomitized) coating allochemical constituents have been found mainly in shoal facies and microbial reef facies in Vocation Field. The vast majority of marine cementation occurs very near the sediment water interface where sea water actively moves into the sediments. Precipitation of this early cement preserved primary porosity from subsequent compaction. Mechanical compaction starts to affect carbonate

sediments under early burial conditions destroying mainly primary intergranular pores. This process results in rotation and horizontal alignment of allochems and minor ductile grain deformation expressed by embayed contacts among the grains. Compaction was more intense where no early calcite cementation occurred. Dolomitization is one of the most significant digenetic events that affects the Smackover Formation in the study area because it created new intercrystalline pores that improved the connectivity of the pore network. Dolomitization is ubiquitously present in the entire Smackover interval in Vocation Field. It is expressed by neomorphism of calcareous allochems, matrix and cements into dolomite. This process also includes precipitation of dolomite cement. Gypsum and/or anhydrite precipitation also accompanied this process filling intergranular, vuggy and moldic pores, and as replacive nodules principally in the upper part of the Smackover Formation. Normally the size of the crystals is relative to the size of the grain being replaced. In some cases, penetrative dolomitization was able to obscure the primary texture preventing a reliable identification of the original rock. Rocks that experienced intense dolomitization display a sucrosic texture sometimes with high intercrystalline porosity.

Once carbonate sediment has been mechanically compacted, continued burial increases the chemical potential that eventually leads to the dissolution of the grains in a mesogenetic process known as pressure-solution. The result is the presence of abundant high amplitude stylolites, and anastomosing wispy seams and laminae of insoluble residue, mainly in the finer grained facies of the Smackover Formation. These features are impermeable barriers to fluid flow. Chemical compaction in the Smackover Formation is believed to be a significant source for later porosity occluding, subsurface cements. Fractures and microfractures are normally present in the Smackover Formation, especially in the microbial reef facies. Although time of formation is

difficult to define, this event occurred after dolomitization and lithification since normally the fractures cut dolomitized particles. The partial infill with dolomitic, calcitic and late stage anhydritic cements may imply that they began to form shortly after burial. The causes of fracturing can be a combination of compaction and local tectonic activity. In the Smackover Formation, the dissolution predates oil migration, and therefore, it is possible that its origin may be related to the presence of aggressive pore fluids enriched in CO_2 and organic acids associated with early phases of oil maturation. This process is the result of the decarboxilation (loss of -COOOH group) of organic material during the oil maturation process. Various types of cementing materials, including dolomitic, siliceous, calcitic, and anhydritic cements obliterated all types of porosity after burial. Ferroan dolomite cement is characterized by large crystals commonly with euhedral shapes and cloudy centers. This cement probably was precipitated immediately after the non-selective dissolution event since it normally fills vugs and cavities formed during this diagenetic episode. It often also fills moldic and intercrystalline pores. In some cases, the presence of saddle or baroque dolomite crystals with their characteristic undulose extinction indicates that dolomitization occurred under deep burial conditions. Saddle dolomite is commonly associated with hydrocarbons, and thus, implies late diagenetic formation by sulfate reduction processes. Siliceous cement is present in very small amounts in the form of isolated euhedral crystals. The source material for this cement is derived from pressure-solution processes affecting very fine authigenic quartz grains normally present in small amounts in Smackover deposits. Calcite cement is present normally as large sparitic crystals that embed crystals and allochems and fill the available pore space among them. Supersaturation in calcium carbonate of the formation fluids as the result of pressure-solution and late stage dissolution associated with hydrocarbon maturation may be responsible for the precipitation of the calcite

cement. The time of formation may be close to the time of oil migration. This cementation process remains active during the precipitation of late stage anhydrite cement as evidenced by the common presence of the intergrowth of these two types of cements. Anhydrite is another important late stage cement. It is considered one of the last events as inferred from the characteristic coarse, slightly corroded crystals sometimes with a poikilotopic character and because the anhydrite normally fills spaces that were partially occluded by other cements. The source of material for this cement may be provided by former dissolution events of carbonate rocks rich in sulfates due to pressure-solution and organic acid activity. Authors have suggested that this anhydrite is probably precipitated from ion-charged solutions migrating updip from the underlying Louann Salt.

Correlation between the depositional facies analysis of well cores and the petrophysical properties of these rocks leads to the conclusion that despite diagenesis, the depositional fabric defines the best reservoirs. In Vocation Field, the shoal complex and the microbial reef facies display the best porosity and permeability properties. Within the tidal flats and especially in the shallow lagoon environments, the deposition of isolated microbialite buildups and thin packstone-grainstone levels also have reservoir potential. Nonetheless, diagenesis can, in some cases, significantly affect and modify the distribution of reservoir grade rocks. Well Permit 2851 is an example of how penetrative dolomitization was able to generate reservoir grade intervals in tidal flat deposits that actually produced oil in this well. The opposite case is Well Permit 2966 where precipitation of dolomite and anhydrite cements obliterated porosity in the ooid shoal facies. Good correlation between porosity and permeability is the result of extensive dolomitization, late stage dissolution, and fracturing that combined to connect isolated moldic and vuggy pores to produce an effective pore system.

The shoal complex reservoirs are dolomitized ooid-oncoidal grainstone and packstone with primary intergranular porosity and secondary intercrystalline, moldic and vuggy pores. In this lithofacies, dolomitization improved connectivity among moldic pores and also generated new intercrystalline pores. Early marine cementation contributed in the preservation of primary porosity, while anhydrite and dolomite cementation are the main processes that occluded pores in the shoal facies. Total porosity is commonly between 4 and 15% with an average of 10% and permeability varies between 3 and 160 md with an average of 66 md. The thickness of the reservoir interval is normally between 20 and 40 feet, reaching 90 feet. The shoal facies is widespread in the field, but probably the high-quality reservoir intervals are not connected along the entire length of the field due to pinch-outs and facies changes that are common in this depositional setting.

The potential reef reservoir intervals are characterized by chaotic and layered thrombolite fabrics commonly with primary shelter and intergranular porosity and secondary moldic, solution enlarged and fracture porosity. This potential reservoir is petrophysically heterogeneous due to the characteristic patchy texture of these deposits, and the presence of impermeable wackestone-mudstone levels and insoluble residual laminae. In this lithofacies, dolomitization, the nonselective dissolution episode, and fracturing substantially improved the amount of porosity and the connectivity of isolated shelter and vuggy pores. The normal thickness for the microbial reef intervals is between 100 and 150 feet, approximating a thickness of 200 feet (Well Permit #3739). Core and well-log analyses suggest that these thick sequences are limited spatially to the northeastern part of the structure. Porosity ranges between 8 and 20% with an average of 13%, while permeability is in the order of 30 and 410 md with an average of 175 md.

Unfortunately, in Vocation Field significant accumulations of these facies are normally located below the oil-water contact.

The Smackover Formation at Vocation Field has undergone a long history of diagenetic events that document a paragenetic sequence similar to the ones described by other authors for nearby areas. Average values of porosity (10 % and 13 %, respectively) in Vocation Field for the shoal and microbial reef facies, which are commonly buried at depths greater than 14,000 feet, indicate that diagenesis has been critical for the preservation and generation of significant amounts of pore space. The most important diagenetic event for the preservation and improvement of the reservoir properties is dolomitization that not only generated new porosity but improved the connectivity among the existing pore space. Dissolution (i.e. leaching of aragonite allochems and the deep non-fabric selective event) and fracturing were also important in the generation of secondary porosity. Diagenesis began soon after deposition and evolved through time due to progressively deeper burial conditions modifying the primary depositional texture of the rock. Despite all the diagenetic overprints, the depositional textures still define the best reservoirs.

3-D Geologic Model.--This task involves using the integrated database which includes the information from the reservoir characterization tasks to build a 3-D stratigraphic and structural model for Appleton Field and for Vocation Field. The resulting two geologic models represent, one for reef-shoal reservoirs associated with low-relief paleohighs and one for reef-shoal reservoirs associated with high-relief paleohighs. This task also provides the framework for the reservoir simulation modeling in these fields. Geologic modeling sets the stage for reservoir simulation and for the recognition of flow units, barriers to flow and flow patterns in the respective fields. Sequence stratigraphy in association with structural interpretation forms the

framework for the model(s). The model(s) incorporate data and interpretations from sequence stratigraphic, depositional history and structural studies, core and well log analysis, petrographic and diagenetic studies, and pore system and petrophysical analysis. The model(s) incorporate the geologic observations and interpretations made from studying stratigraphic and spatial lithofacies relationships observed in Late Jurassic microbial reefs in outcrops. The purpose of the 3-D geologic model(s) is to provide an interpretation for the interwell distribution of systems tracts, lithofacies, and reservoir-grade rock. This work is designed to improve well-to-well predictability with regard to reservoir parameters, such as lithofacies, diagenetic rock-fluid alterations, pore types and systems, and heterogeneity. The geologic model(s) and integrated database become effective tools for cost-effective reservoir management for making decisions regarding operations in these fields. Accepted industry software, Stratamodel, was used to build the 3-D geologic model(s). This research task was conducted by Mancini, Llinas and Panetta at the University of Alabama.

Appleton Field. The 3-D geologic (structure and stratigraphic) model for Appleton Field included advanced carbonate reservoir characterization (structural, sequence and seismic stratigraphy, outcrop analog, depositional lithofacies, diagenesis and pore systems studies), three-dimensional geologic visualization modeling, seismic forward modeling, and porosity and permeability distribution analysis (seismic attribute and three-dimensional stratigraphic studies). The structure at Appleton Field is a low relief composite paleotopographic high (Figures 252-255). The well production differences in the field are related to the heterogeneous nature of the reservoir (Figure 256). The quality of the reef reservoir is greater than that of the shoal reservoir due to higher permeabilities (Figure 257) and better connected pore systems inherent to the

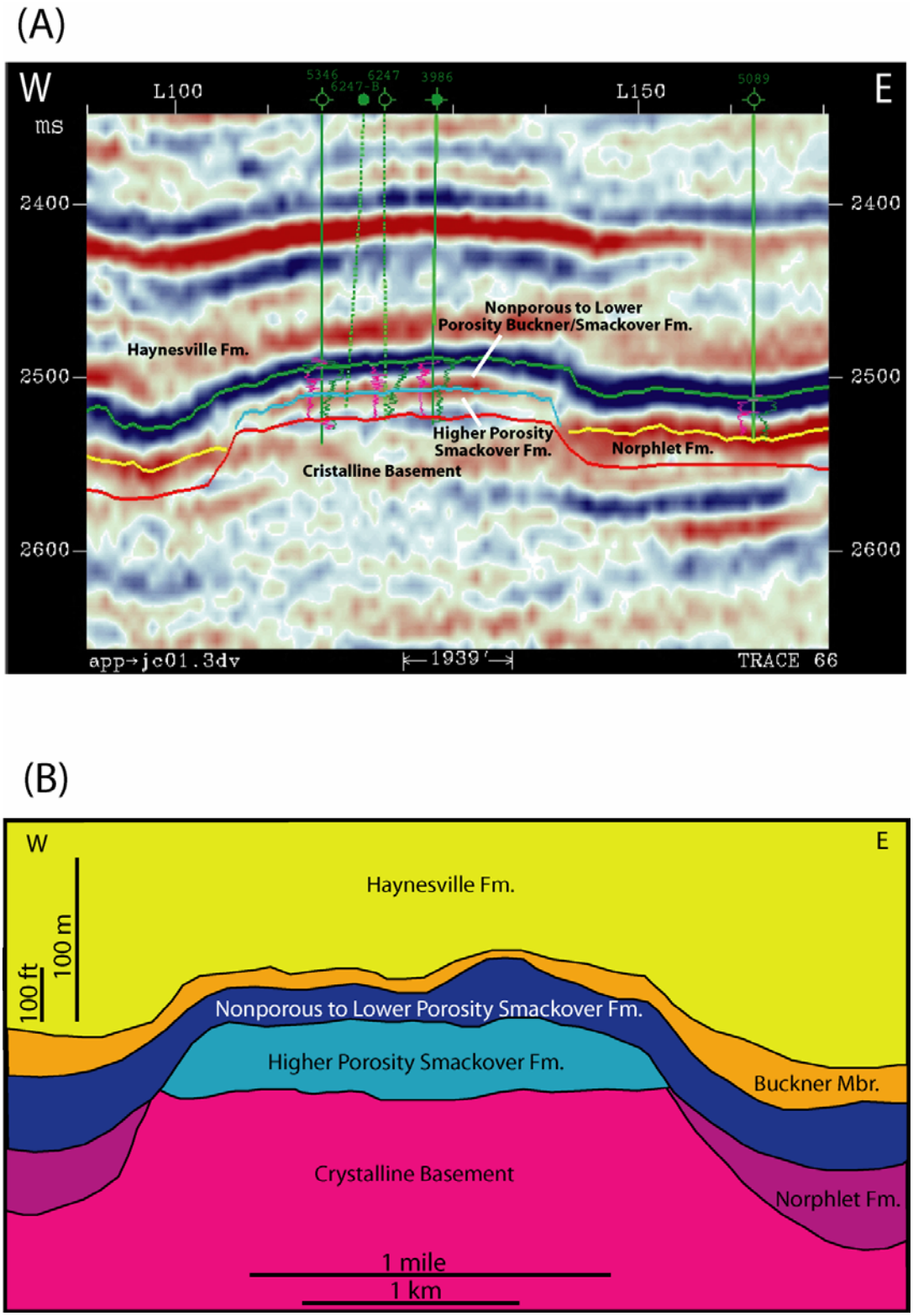

Figure 252. (A) Interpreted seismic project in the Appleton Field area, and (B) geologic model based on the seismic interpretation of Appleton Field. The seismic data show the distribution of the thrombolite buildup on the crystalline basement paleohigh in the Appleton Field area.

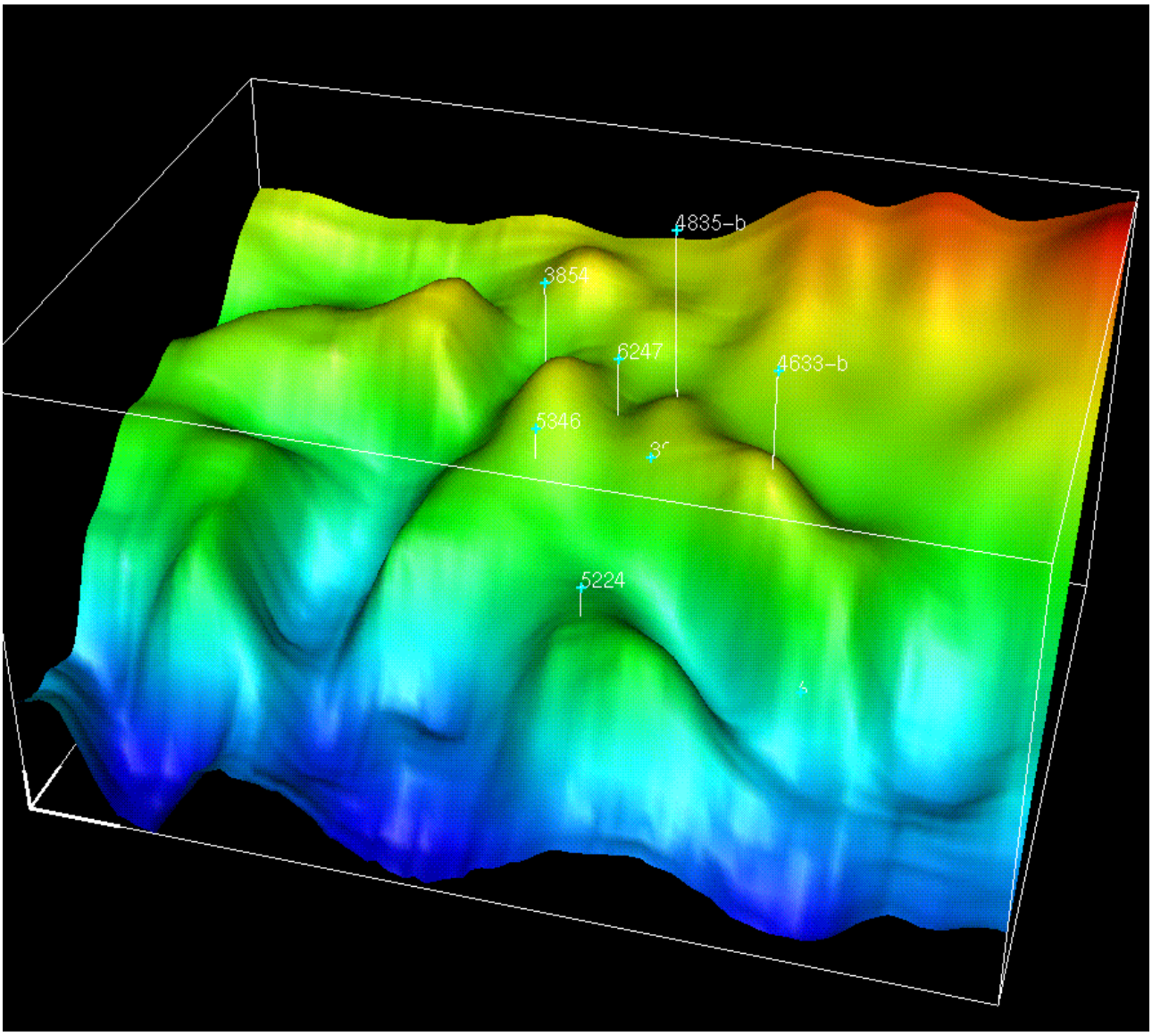

Figure 253 – 3-D model of Appleton Field structure on top of the Smackover/Buckner.

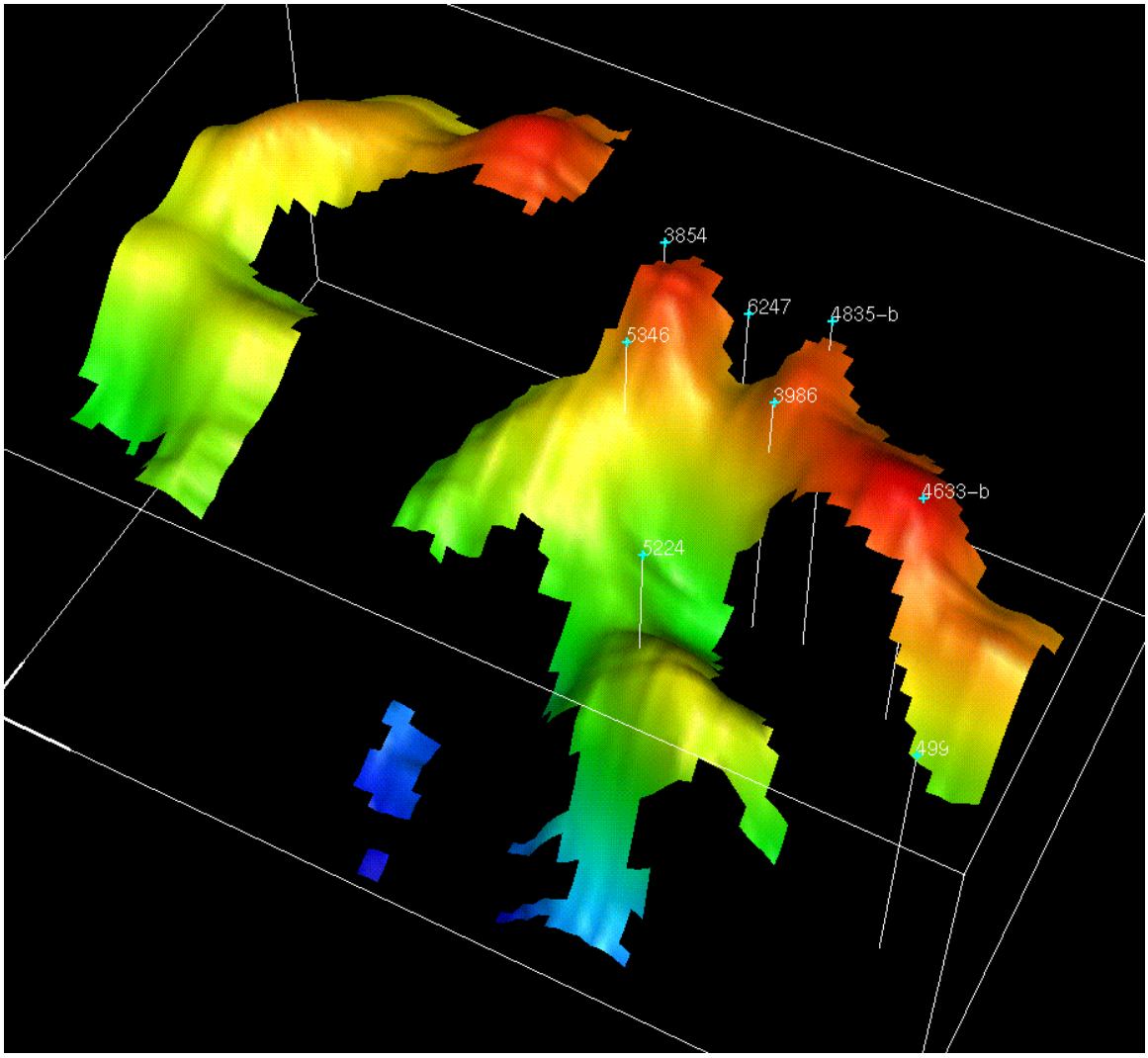

Figure 254. 3-D model of Appleton Field structure on top of the reef interval.

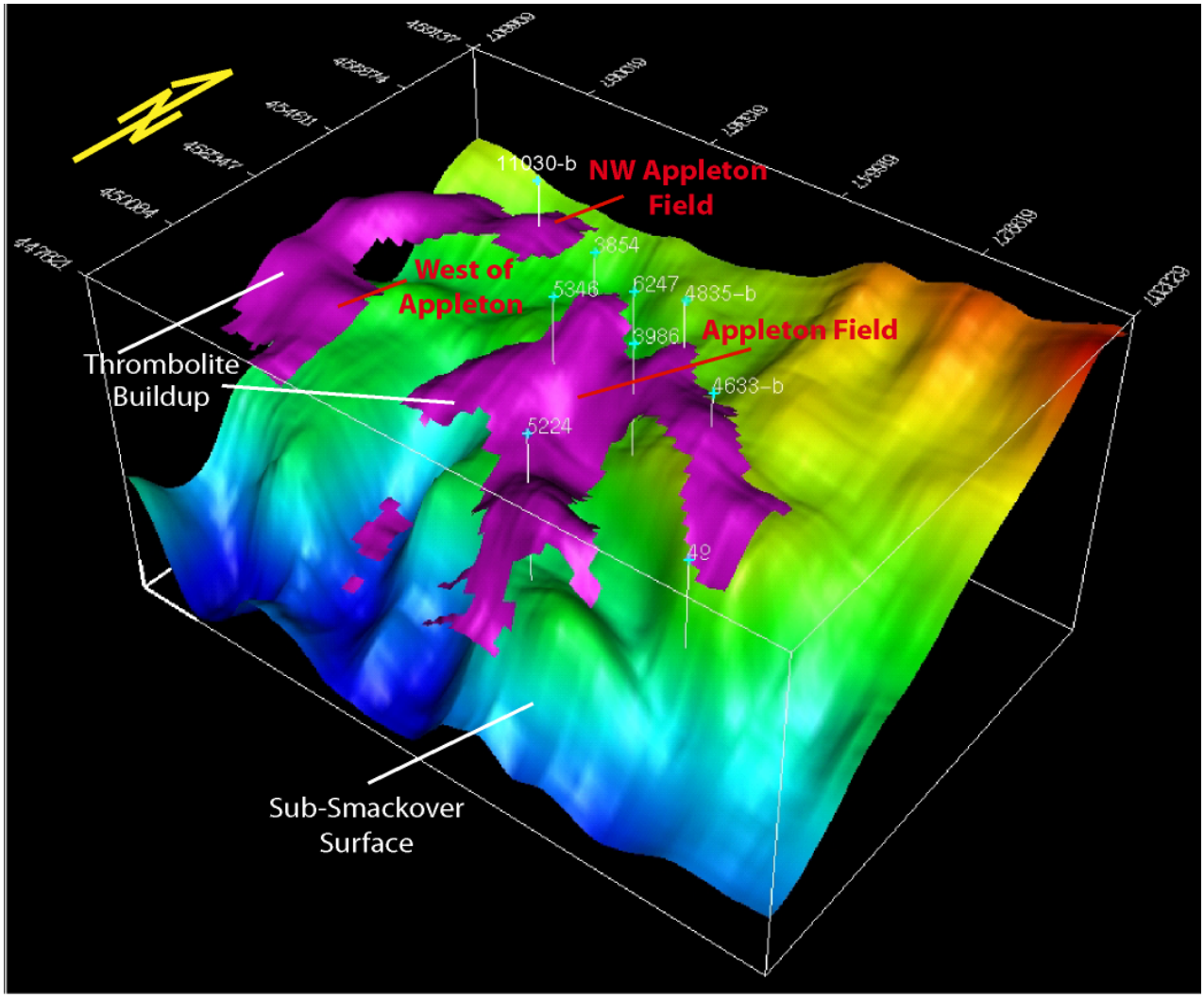

Figure 255. Three dimensional view of the Appleton composite paleohigh, including Appleton Field, Northwest Appleton Field, and an area west of Appleton Field, showing the spatial distribution of the thrombolite buildups on the crest and flanks of the crystalline basement high.

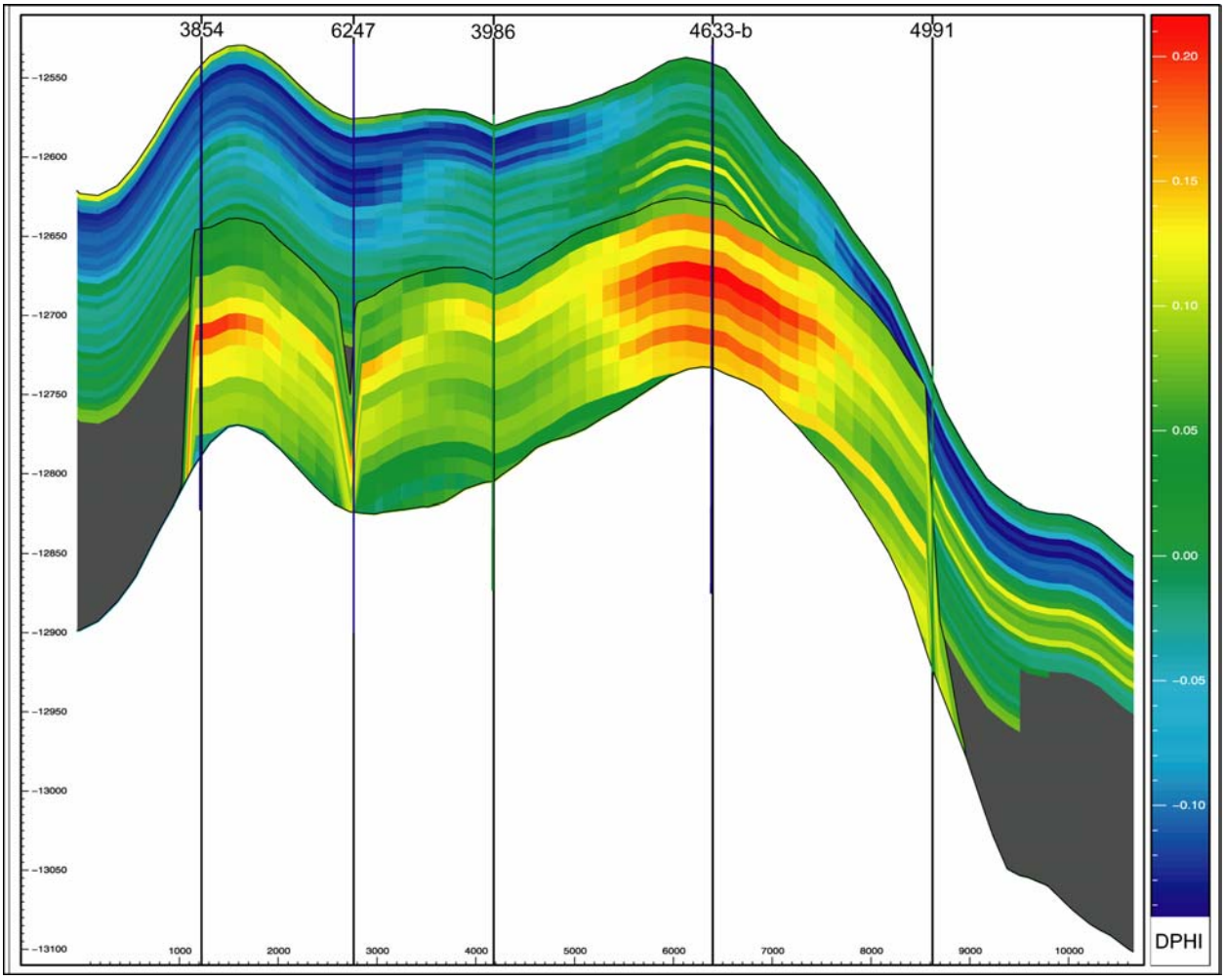

Figure 256 –Cross section showing reservoir porosity at Appleton Field.

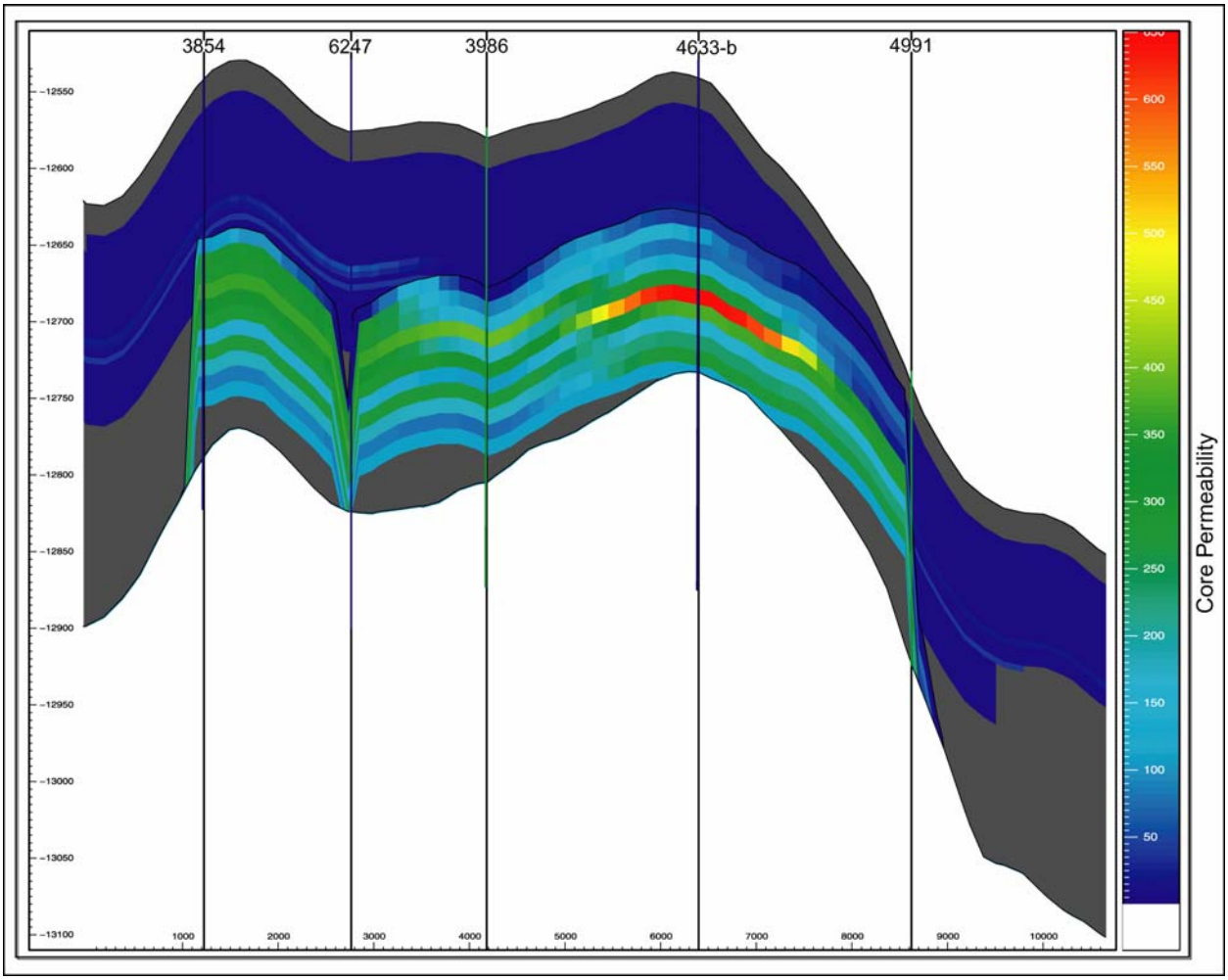

Figure 257 –Cross section showing permeability at Appleton Field.

depositional architecture and diagenetic fabric of the reef facies. Another significant factor controlling reservoir productivity is related to the variation in the size of individual reservoir compartments associated with the eastern and western paleohighs. The greater production from the eastern paleohigh is a reflection of the greater relief of the paleohigh, which places more reef reservoir above the oil – water contact. Production from the western paleohigh is limited by the lower relief of the structure, which places much of the reef reservoir below the oil – water contact. Thus, at Appleton Field, because the shoal and reef facies are continuous over this low relief composite paleohigh, reservoir producibility is principally controlled by reservoir quality, in combination, with structural relief.

Vocation Field. The 3-D geologic model for Vocation Field included advanced carbonate reservoir characterization (structural, sequence and seismic stratigraphy, outcrop analog, depositional lithofacies, diagenesis and pore systems studies), three-dimensional geologic visualization modeling, and porosity and permeability distribution analyses. The structure at Vocation Field is a high relief composite paleotopographic feature with multiple water levels. This composite feature consists of one main north-south elongated paleohigh with three crests that remained subaerially exposed until the end of Smackover time (Figure 258), and a smaller and lower elevated feature to the northeast, which was completely inundated during that time. These paleohighs are bounded to the east and north by high angle normal faults (Figures 258 and 259) that formed prior to Smackover accumulation and continued to be active during Smackover time. Figure 259 is an interpreted W-E seismic line showing the main and smaller basement features and the onlap and pinchout of the Norphlet and Smackover formations on the flanks of the paleohighs. The transition from the low velocity siltstone beds of the

Haynesville Formation the dense anhydrite layers of the Buckner is expressed by a peak (positive reflection coefficient)

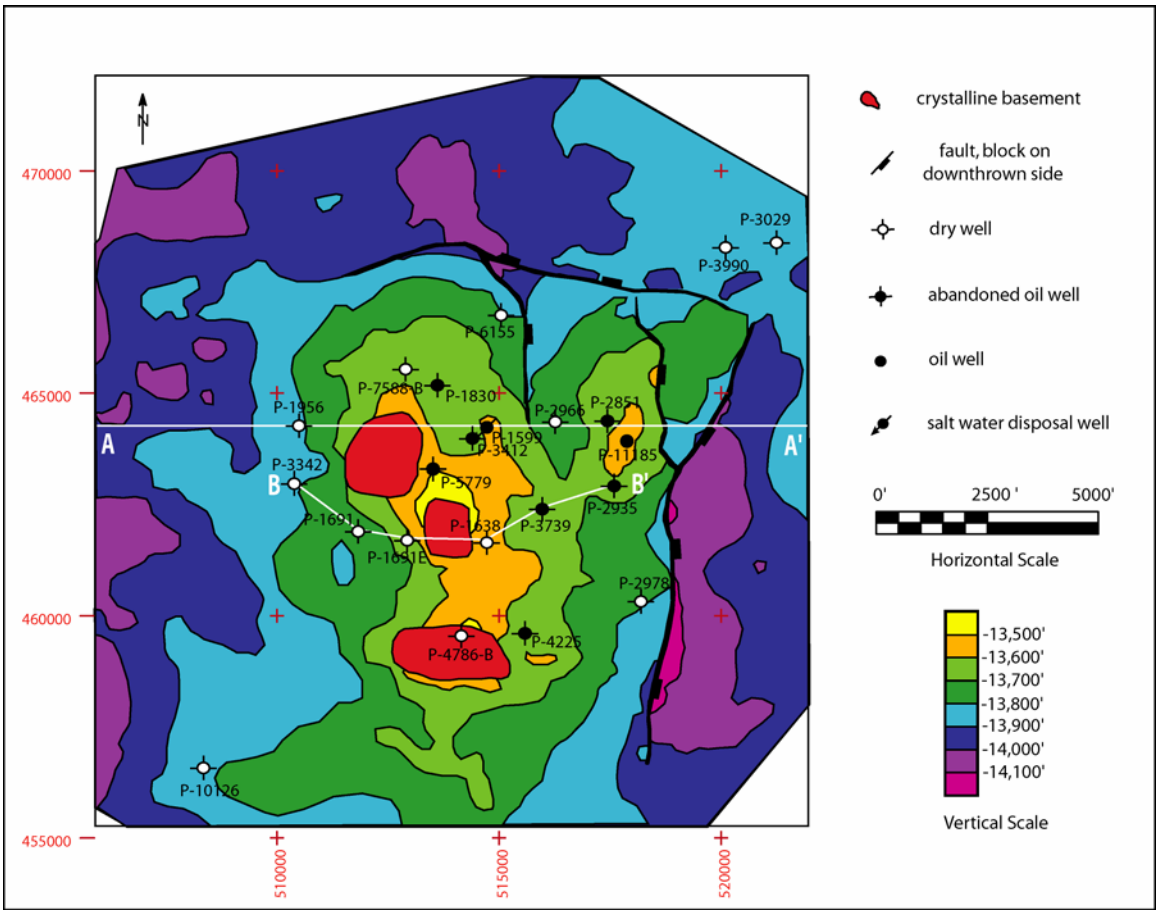

Figure 258: Structure contour map in depth based on 3-D seismic interpretation of the top of the Buckner-Smackover Formation at Vocation Field.

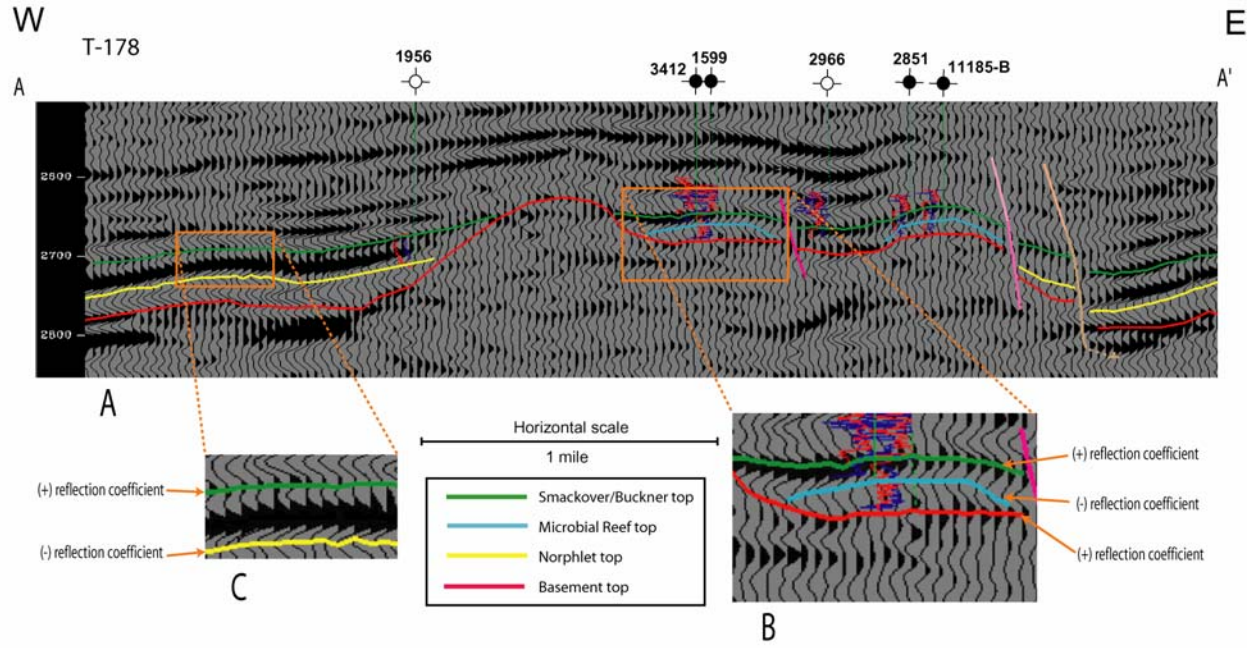

Figure 259: (A) W-E interpreted seismic line along Vocation Field (see Figure 6 for its location), (B) Close-up of the Smackover microbial reefal buildup on top of crystalline rocks, and (C) Close-up of the Smackover Formation on top of the Norphlet Formation.

in the seismic trace. The reefal facies was detected as subtle mounded geometries (Figure 259) formed by a trough in the seismic trace (negative reflection coefficient) generated as the seismic signal enters into this more porous medium. The lower contact of the Smackover Formation is manifested as a trough when it rests directly upon the more dense rocks of the crystalline basement or as a peak when it overlies the Norphlet Formation (Figure 259). This seismic interpretation confirmed that the presence of microbial buildups is limited to the eastern and northern flanks of the structure as illustrated in Figure 260-261. The crest of the lower elevated feature to the northeast was completely colonized by these organisms as predicted in the low relief paleotopographic conceptual model. Figure 262 is a cross section showing the distribution of the reservoir facies based on porosity data. The Appleton low-relief paleohigh and Vocation high-relief paleohigh are represented as conceptual models in Figure 263.

The well production differences in the field are related to the variable relief of the individual paleohighs and associated oil – water contact. The shoal and reef facies and resulting reservoir distribution is directly related to the individual paleohighs. The reef facies, which has higher reservoir quality than the shoal facies, is limited to the northern and eastern portions of the field. This distribution in reef facies is believed to be attributed to the microbial buildups occurring only on the leeward side of the Vocation composite feature. On the leeward side, the microbes could grow in a restricted environment not affected by ocean currents and circulation patterns. Another major factor controlling reservoir occurrence and producibility is related to the presence and variation in the size of the individual reservoir compartments associated with the elevation of the individual paleohighs. If the paleohigh remained above sea level during Smackover deposition, no marine shoal or reef facies could be deposited. Thus, too high a relief precludes reservoir occurrence. However, greater production from certain paleohighs is a reflection of their

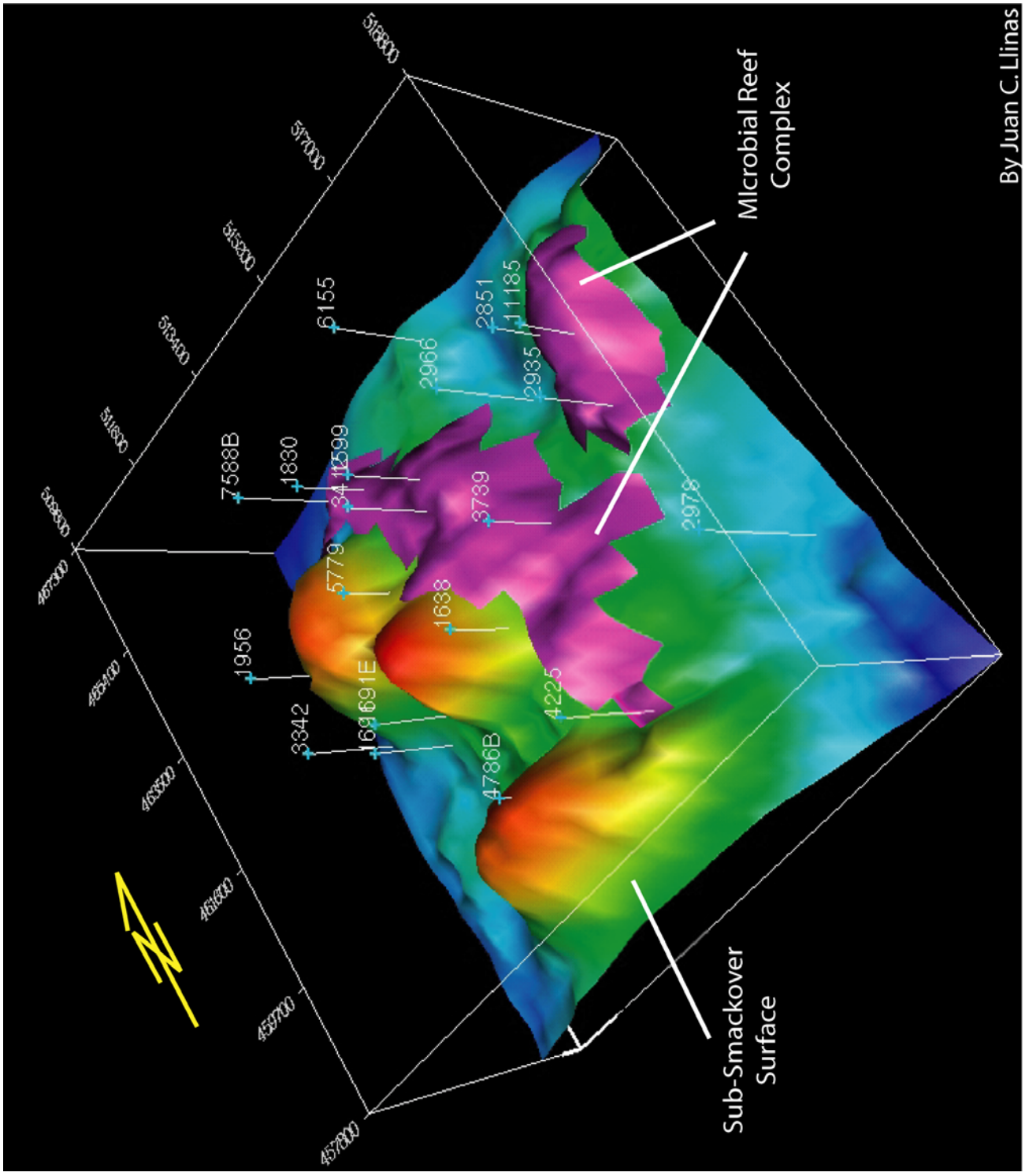

Figure 260. Distribution of microbial reef complex facies in Vocation Field.

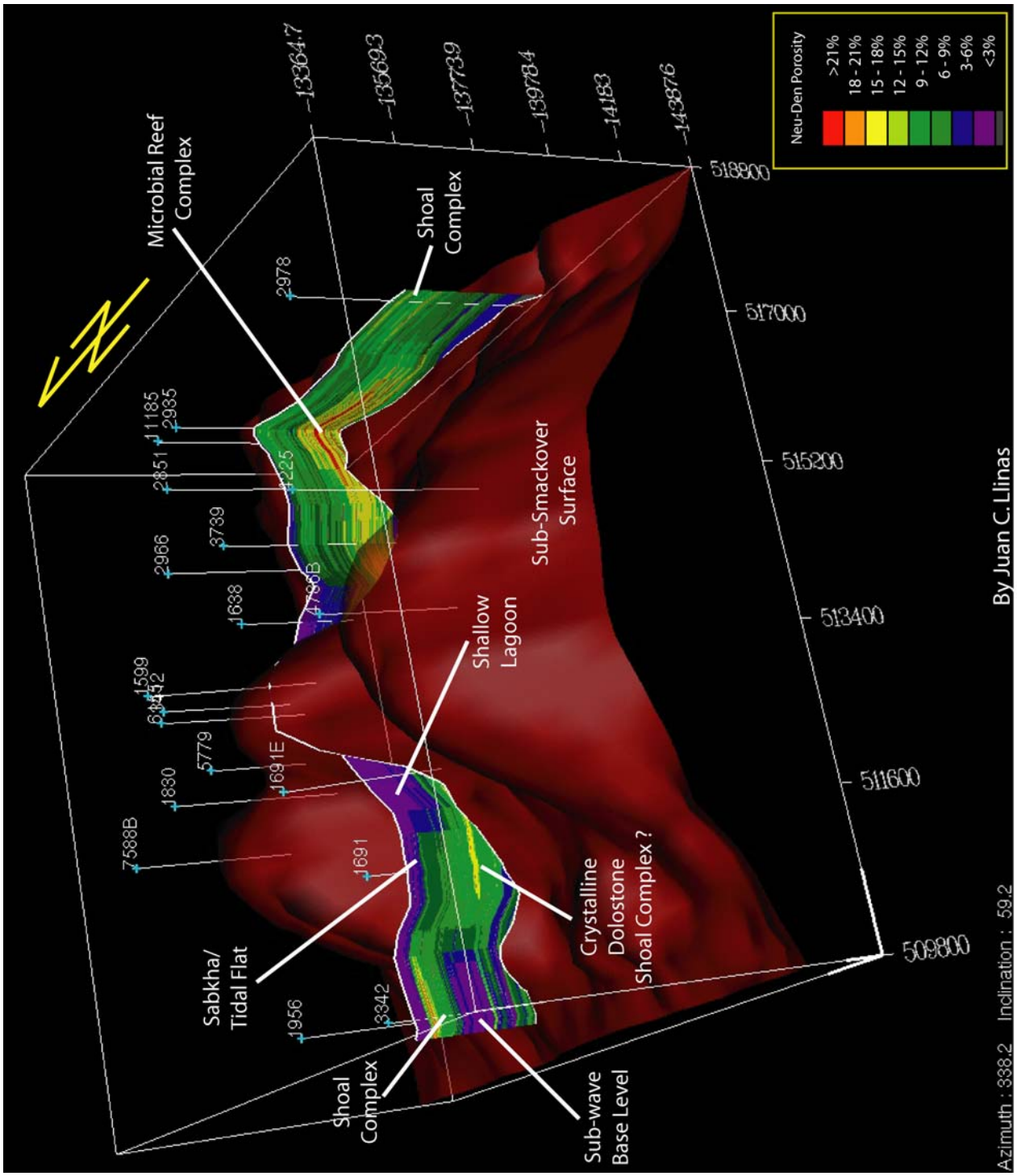

Figure 261. Depositional facies of the Smackover Formation in Vocation Field.

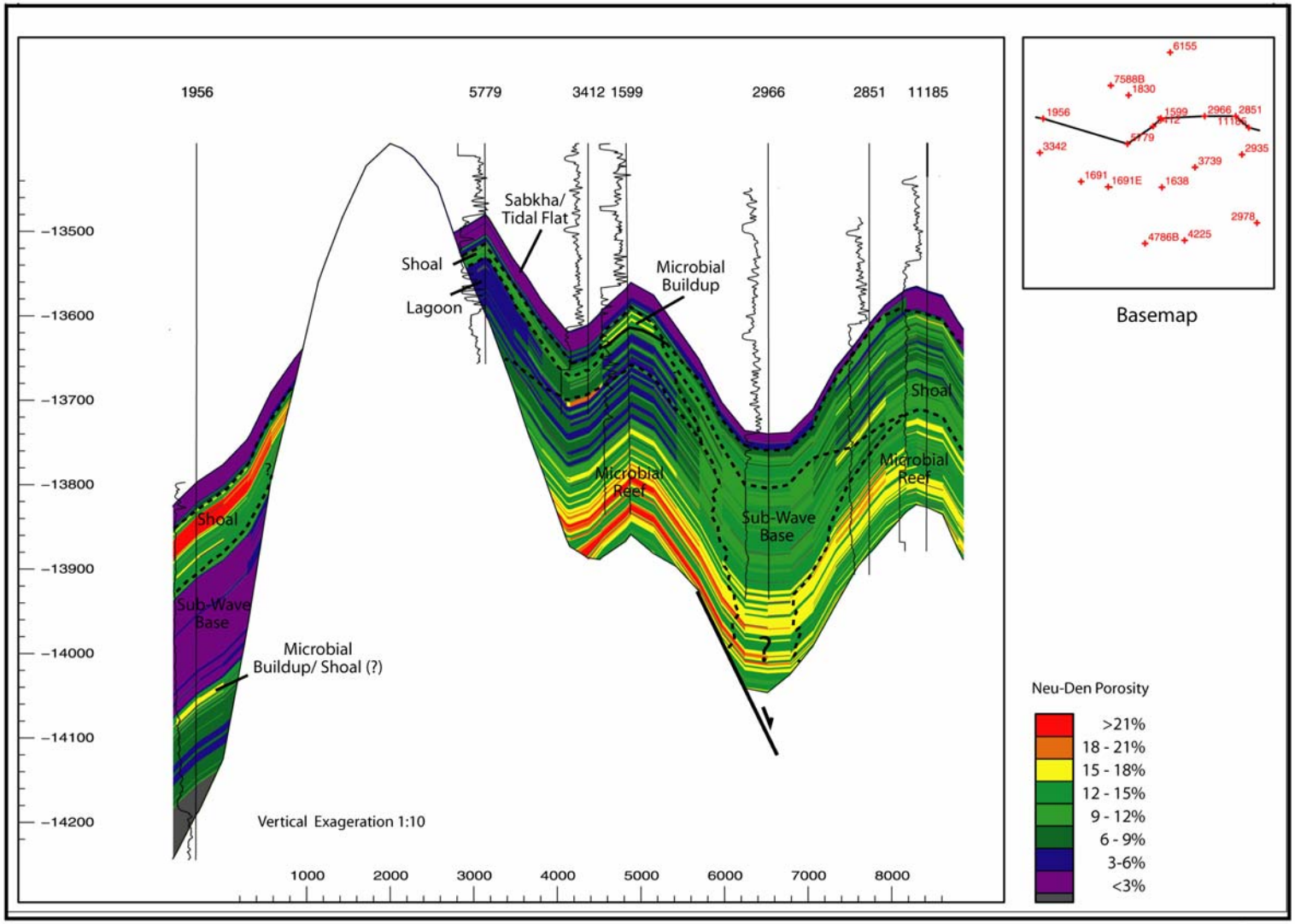

Figure 262. Cross section in Vocation Field showing the distribution of depositional facies based on density-neutron porosity data.

By Juan C. Llinas

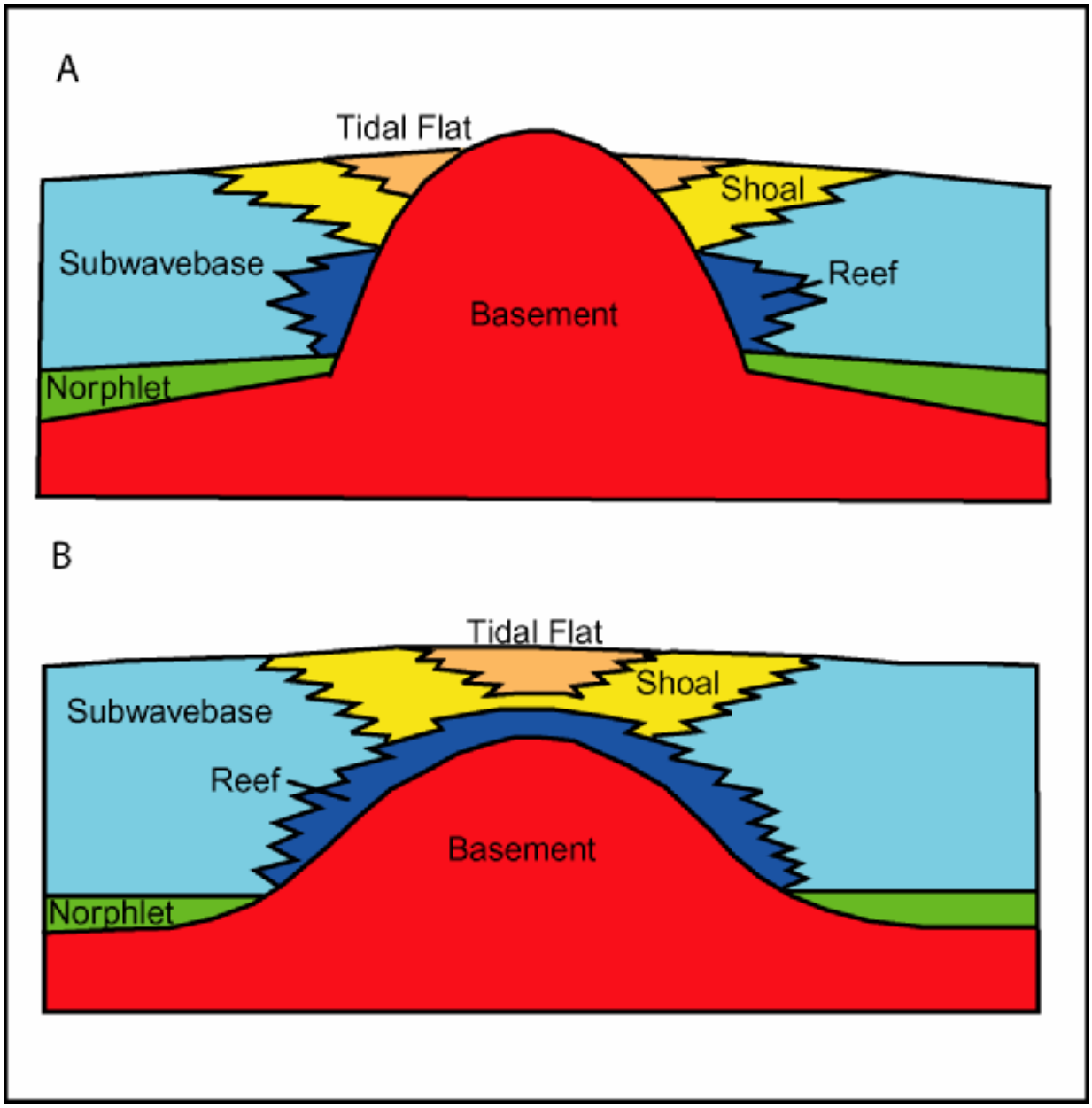

Figure 263. Conceptual model of Smackover plays in updip basement ridge play. High relief (A) and low relief (B) paleotopographic features (modified from Mancini *et al.,* 1998).

greater relief, which places more of the shoal or reef facies above the oil – water contact. Thus, at Vocation Field because of the discontinuity of the shoal and reef facies due to the high relief of the composite paleotopographic high and because of the differential relief on the individual paleohighs, reservoir producibility is principally controlled by the degree of structural relief, in combination with reservoir quality.

3-D Reservoir Simulation Model.--This task focuses on the construction, implementation and validation of a numerical simulation model(s) for Appleton and Vocation Fields that is based on the 3-D geologic model(s), petrophysical properties, fluid (PVT) properties, rock-fluid properties, and the results of the well performance analysis. The geologic model(s) are coupled with the results of the well performance analysis to determine flow units, as well as reservoir-scale barriers to flow. Reservoir simulation is performed separately for cases of the Appleton and Vocation Fields. However, because these reservoirs are associated with basement paleohighs of varying degrees of relief, two simulation models are required—one for reef-shoal reservoirs associated with low-relief paleohighs (Appleton) and one for reef-shoal reservoirs associated with high-relief paleohighs (Vocation). The purpose of this work is to validate the reservoir model with history-matching and then build forecasts. The purposes of reservoir simulation are to forecast expected reservoir performance, to forecast ultimate recovery, and to evaluate different production development scenarios. Probably the most important aspect of the simulation work will be the setup phase. The Smackover is well known as a geologically complex system, and the ability to develop a representative numerical model for both the Appleton and Vocation Fields is linked not only to the engineering data, but also to the geological, petrophysical, and geophysical data. Researchers at Texas A&M University conducted the reservoir simulation. These researchers included Archer and students.

Appleton Field. 3-D reservoir simulation of the reservoir at Appleton Field has been completed. The 3-D geologic model formed the foundation for the reservoir simulation. Fluid data (Figure 264 and Tables 27-30), rock properties (Figures 265-266), historical production (Table 31 and Figures 267-268), phase flowrates (Figures 269-270), cumulative production (Figure 271), gas-oil ratio profile (Figure 272), watercut profile (Figure 273), oil production rate history match (Figure 274), water production rate history match (Figure 275), gas production history match (Figure 276) and water production rate history match per well (Figures 277-281) were used in the simulation model for Appleton Field. The results of the simulation for Appleton Field are illustrated in Figures 282-285 and Tables 32 and 33.

The volume of oil initially in-place in this model is 5,391 MSTB (with the water-oil contact at 12,766 ft and a connate water saturation of 0.3). As in our other simulation models for this field, the estimate of original-oil-in-place is dependent on the location of the water-oil contact and the connate water saturation. The historical oil recovery of 2,691 MSTB (to September 2003) implies a recovery factor of 50 percent.

Figures 265 and 266 show the relative permeability and capillary pressure curves used in the history matched model. These data are reasonable and should provide a representative behavior in the reservoir simulation.

Figures 277 to 281 show the history matched watercut in each of the five producing wells in the Appleton Field. The same data are shown in Figs. 275 and 273 in terms of fieldwide water production rate and fieldwide watercut. Note that, for simulation purposes, wells 3986 and 3986B were combined and treated as one well. In general these figures show that the simulation model can reproduce the historical water production quite well. There are some differences in actual and predicted water breakthrough times for well permits #4633B and #4835B. Well

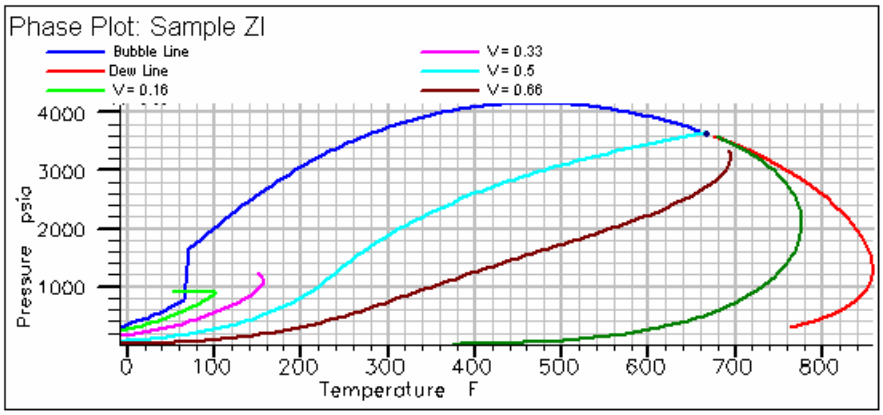

Figure 264 – Phase Envelope, Appleton Oil Field.

Table 27 — Pseudocomponent Grouping, Appleton Field.

Pseudocomponent	Components
Group 1	H_2S
Group 2	$C_1 + N_2$
Group 3	$C_2 + CO_2$
Group 4	$C_3+C_4+C_5$
Group 5	$C_6 + C_7$

Table 28 — Pseudocomponent Properties, Appleton Field.

Component	Molecular Weight (dim-less)	Critical Temperature (deg R)	Critical Pressure, (psia)	Critical z-Factor (dim-less)	Acentric Factor (dim-less)
Group 1	34.07	672.48	1296.18	0.2820	0.0642
Group 2	16.42	339.39	662.20	0.2847	0.0089
Group 3	35.11	549.29	839.63	0.2931	0.0927
Group 4	56.71	744.35	555.77	0.2790	0.1232
Group 5	179.62	1216.73	289.19	0.2524	0.3783

Table 29 — Pseudocomponent Properties, Appleton Field (continued).

Component	Ω_a (dim-less)	Ω_b (dim-less)	V_s (dim-less)
Group 1	0.4898	0.0749	-0.000642
Group 2	1.0288	0.1109	-0.000887
Group 3	0.9591	0.1235	-0.000501
Group 4	0.6951	0.0965	-0.000362
Group 5	0.6951	0.0717	0.000663

Table 30 — Binary Interaction Coefficients, Appleton Field.

	Group 1	Group 2	Group 3	Group 4	Group 5
Group 1	0.0	-	-	-	-
Group 2	0.0540	0.0	-	-	-
Group 3	0.0622	0.0369	0.0	-	-
Group 4	0.0684	0.0011	0.0332	0.0	-
Group 5	0.0684	0.016	0.0044	0.0062	0.0

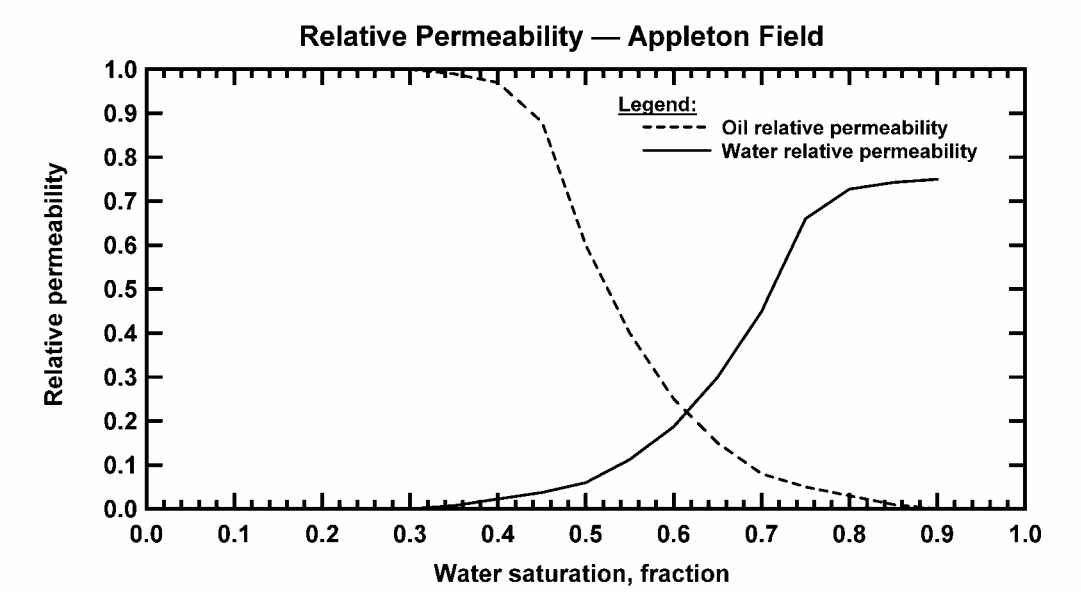

Figure 265 — History matched relative permeability curves, Appleton Field.

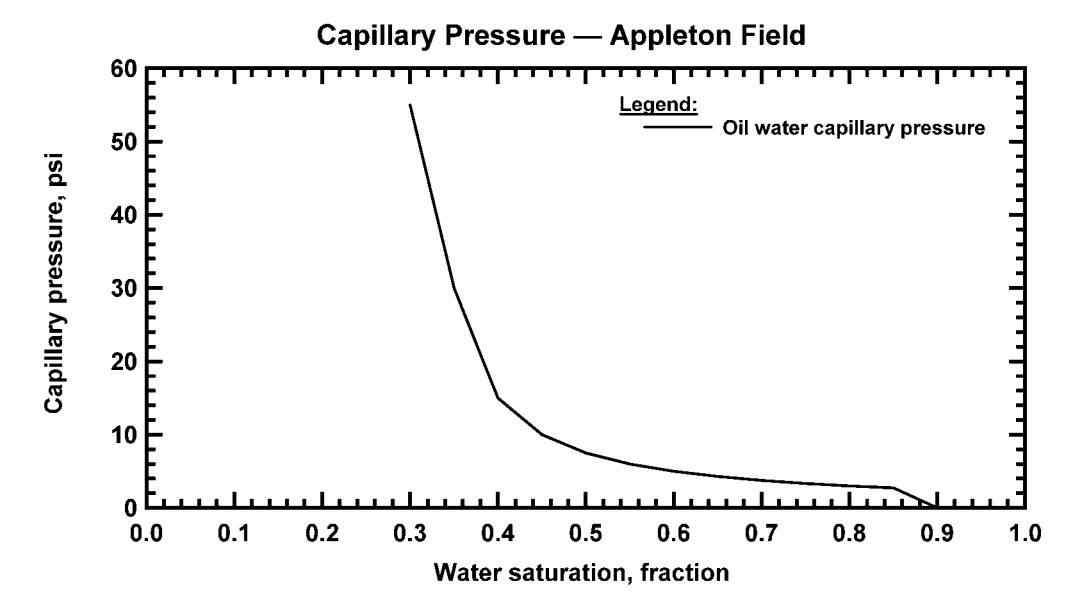

Figure 266 — History matched capillary pressure curve, Appleton Field.

Table 31 – Reported Cumulative Production per Well, Appleton Oil Field.

Well	Oil Production (MSTB)	Water Production (MSTB)	Gas Production (MMSCF)
3854	405	1,246	850
3986	158	141	309
3986B	41	32	86
4633B	1,149	1,618	1,781
4835B	778	738	1,468
6247B	184	334	280

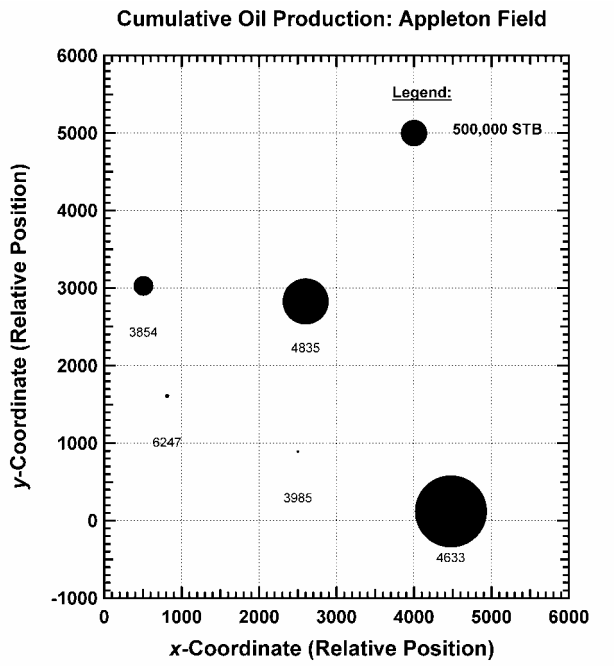

Figure 267 — Oil Production as a Function of Well Location, Appleton Field.

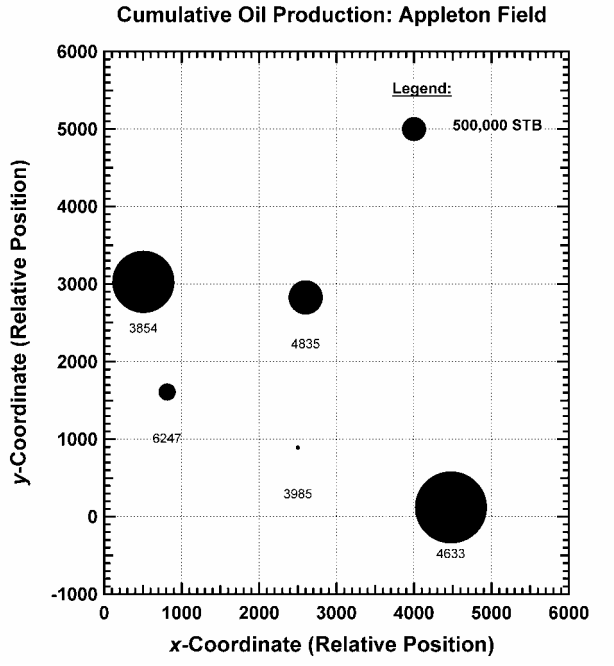

Figure 268 — Water Production as a Function of Well Location, Appleton Field.

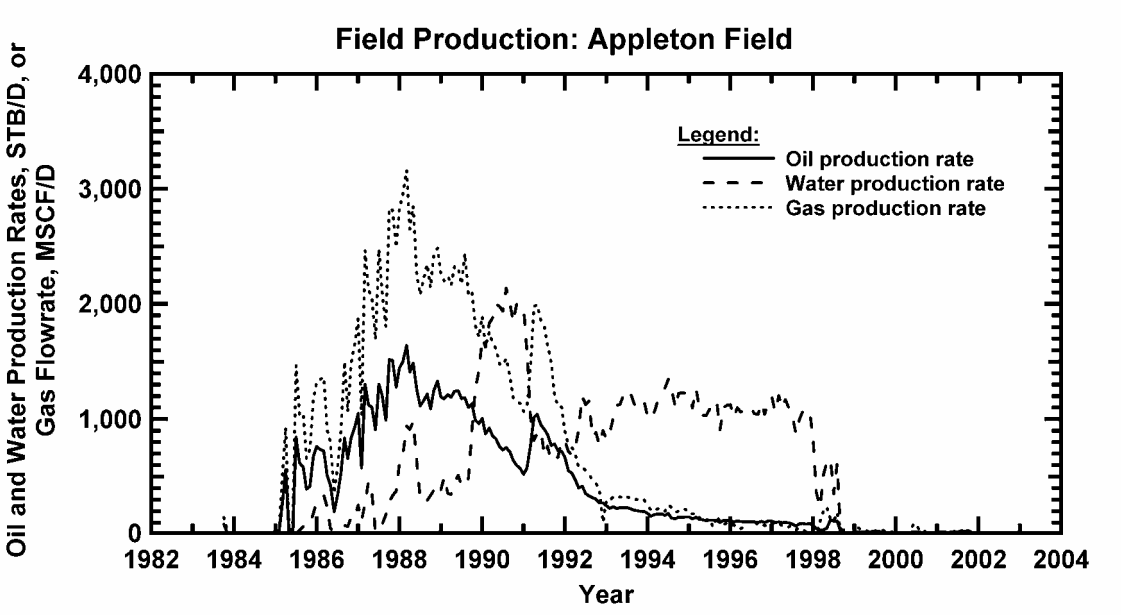

Figure 269 — Individual Phase Flowrates, Appleton Field (Cartesian Format).

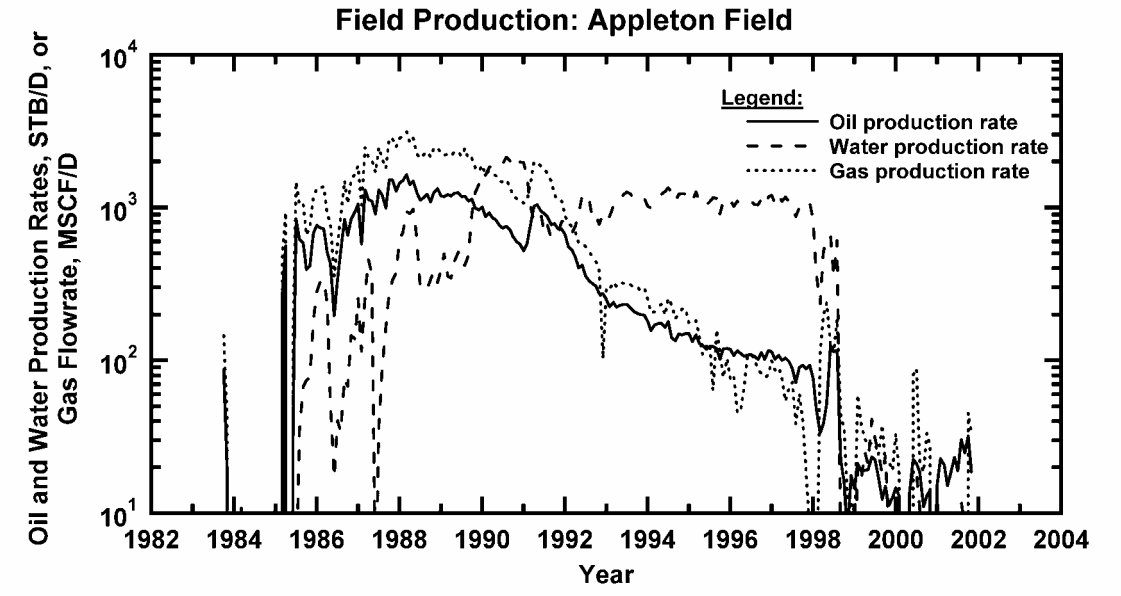

Figure 270 — Individual Phase Flowrates, Appleton Field (Semilog Format).

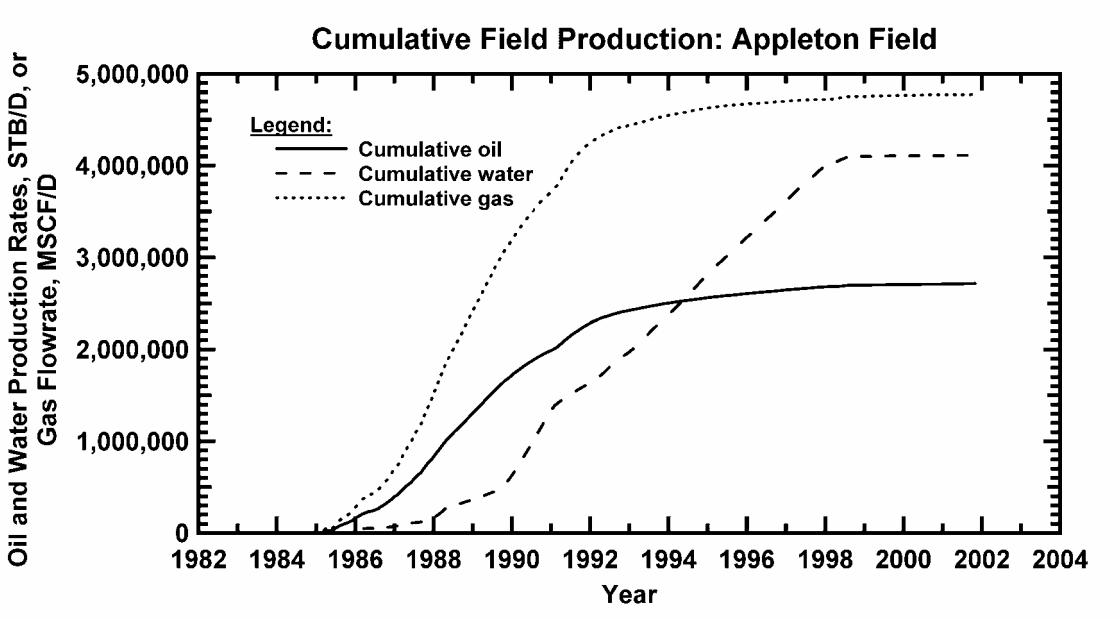

Figure 271 — Cumulative Production Profiles, Appleton Field.

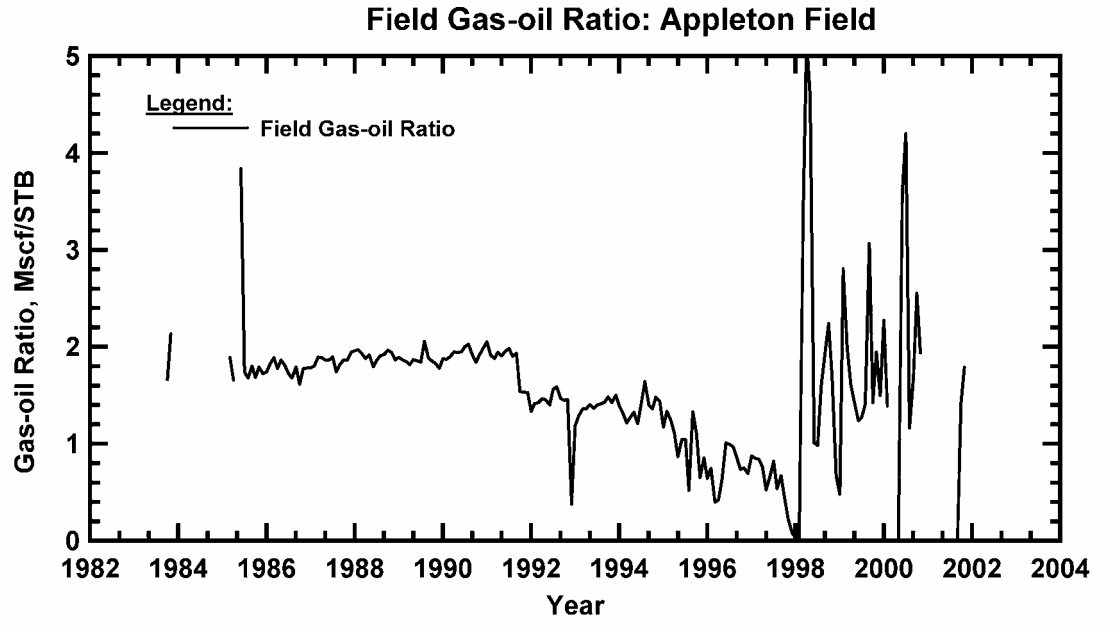

Figure 272 — Gas-Oil Ratio Profile, Appleton Field.

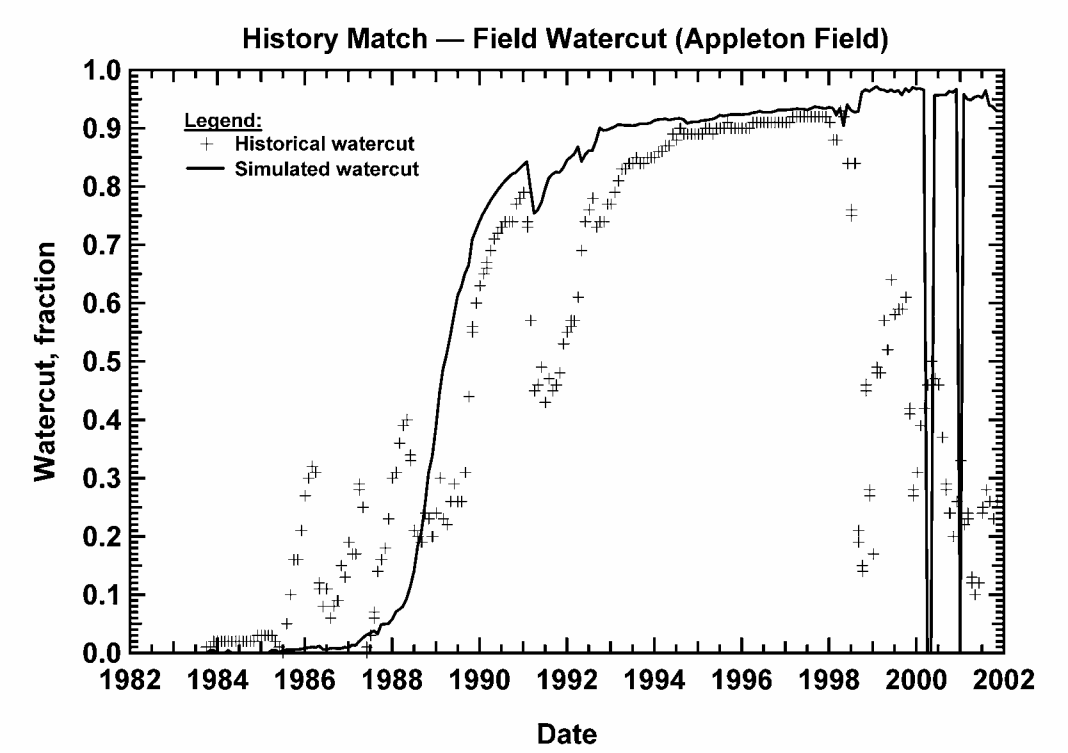

Figure 273 — Fieldwide watercut history match, Appleton Field

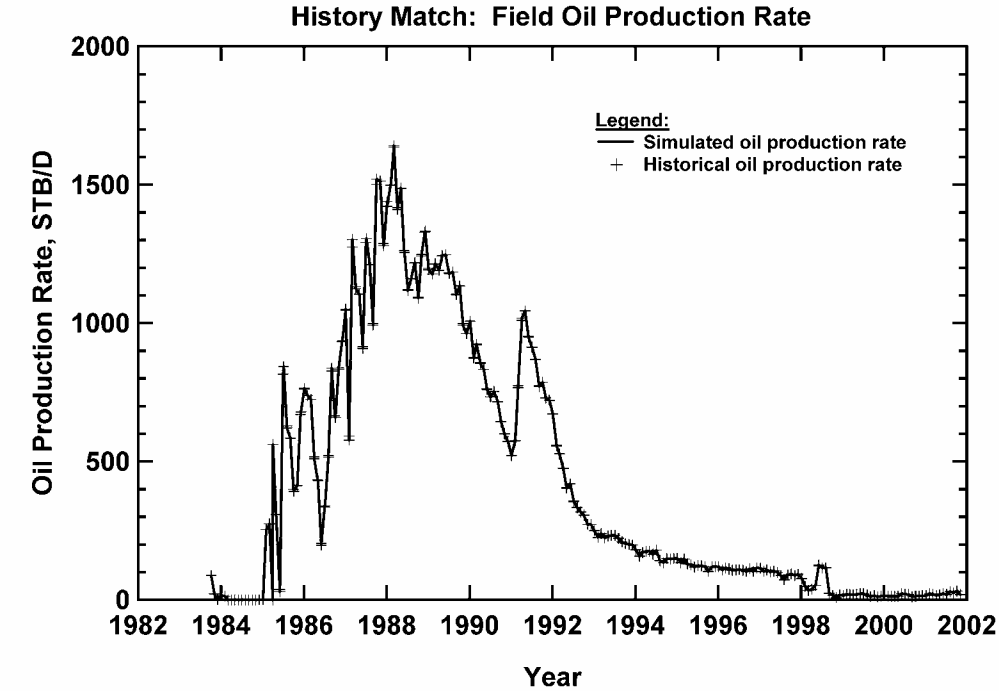

Figure 274 — Oil Production Rate History Match, Appleton Field.

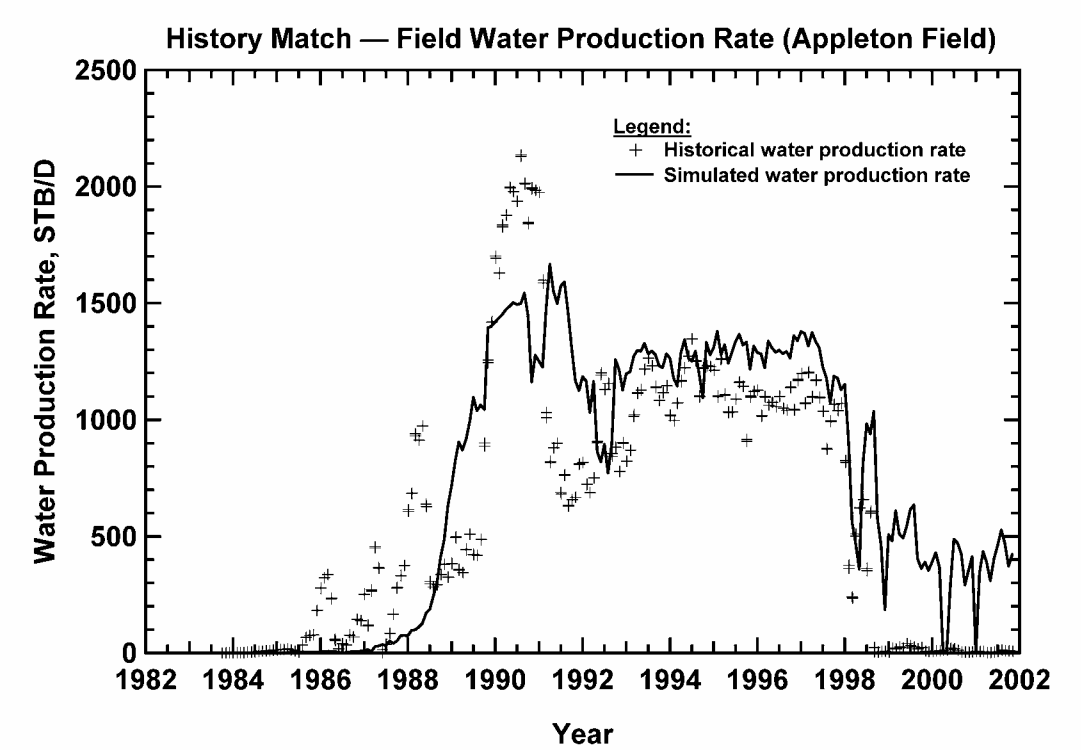

Figure 275 — Fieldwide water production rate history match, Appleton Field.

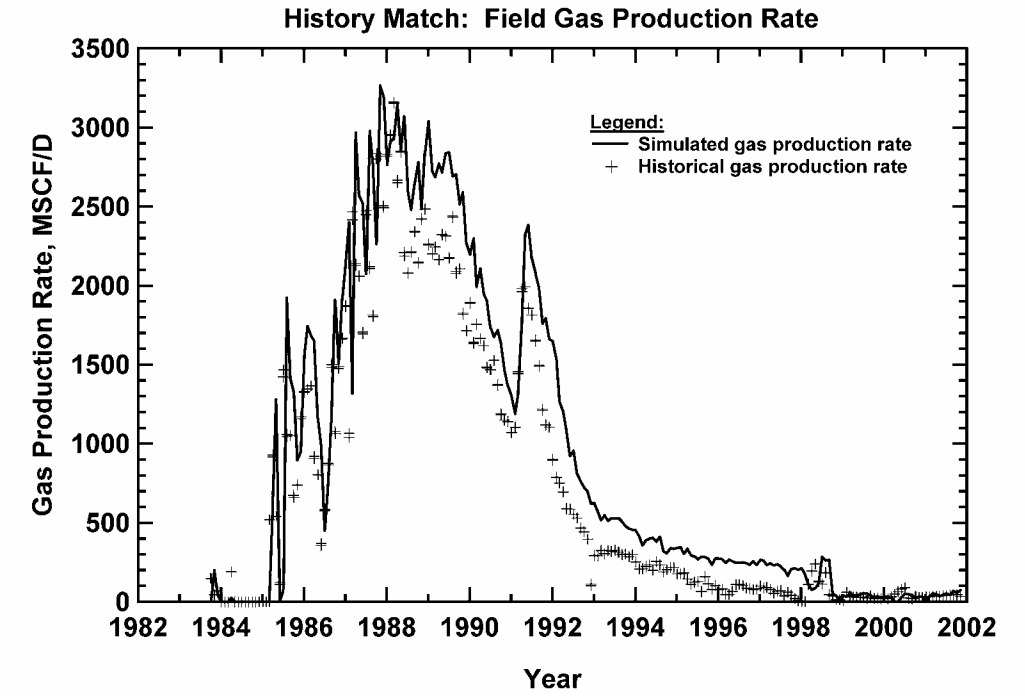

Figure 276 — Gas Production Rate History Match, Appleton Field.

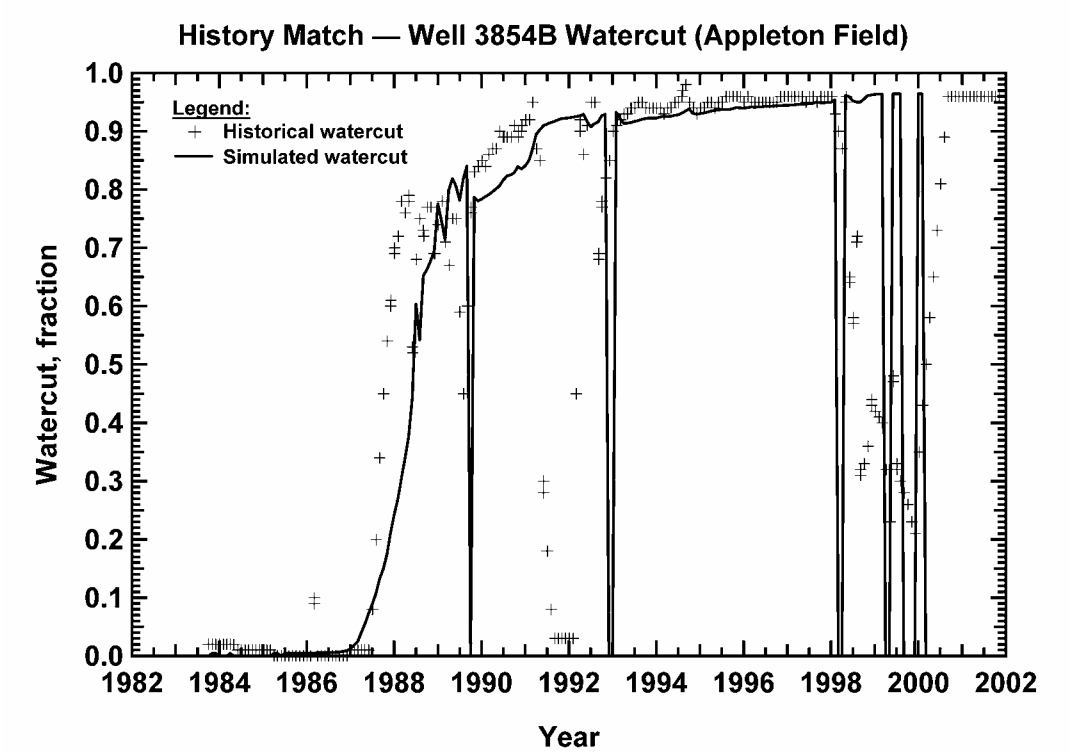

Figure 277 — Watercut history match, Well 3854B (Appleton Field).

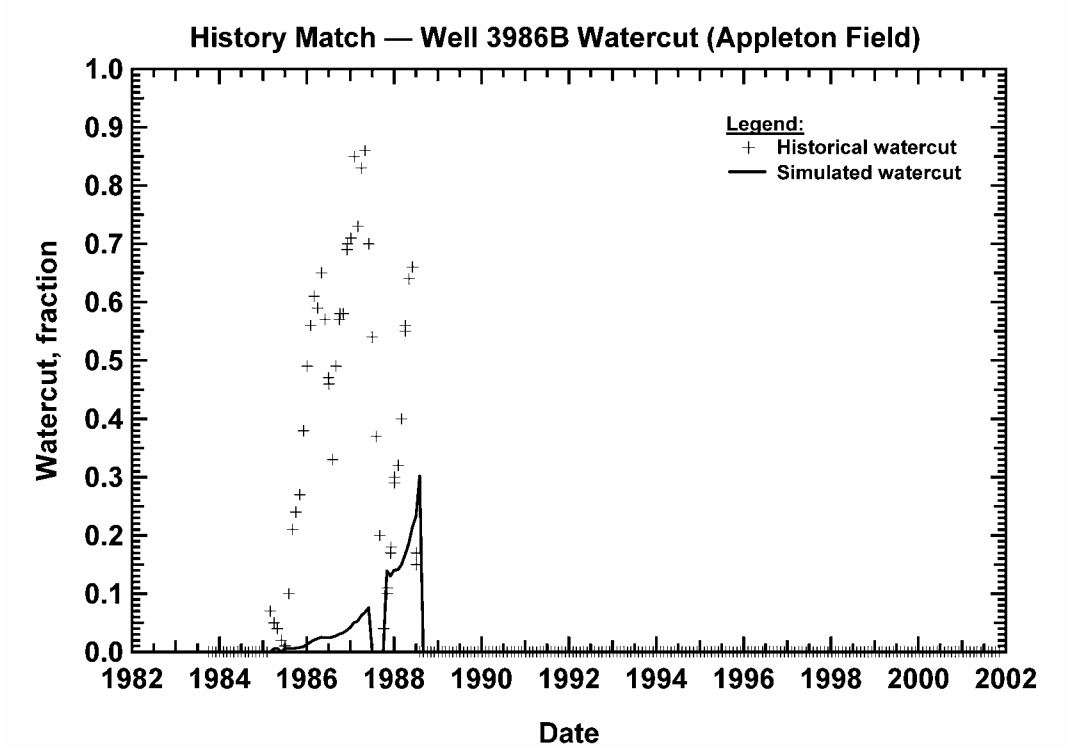

Figure 278 — Watercut history match, Well 3986B (Appleton Field).

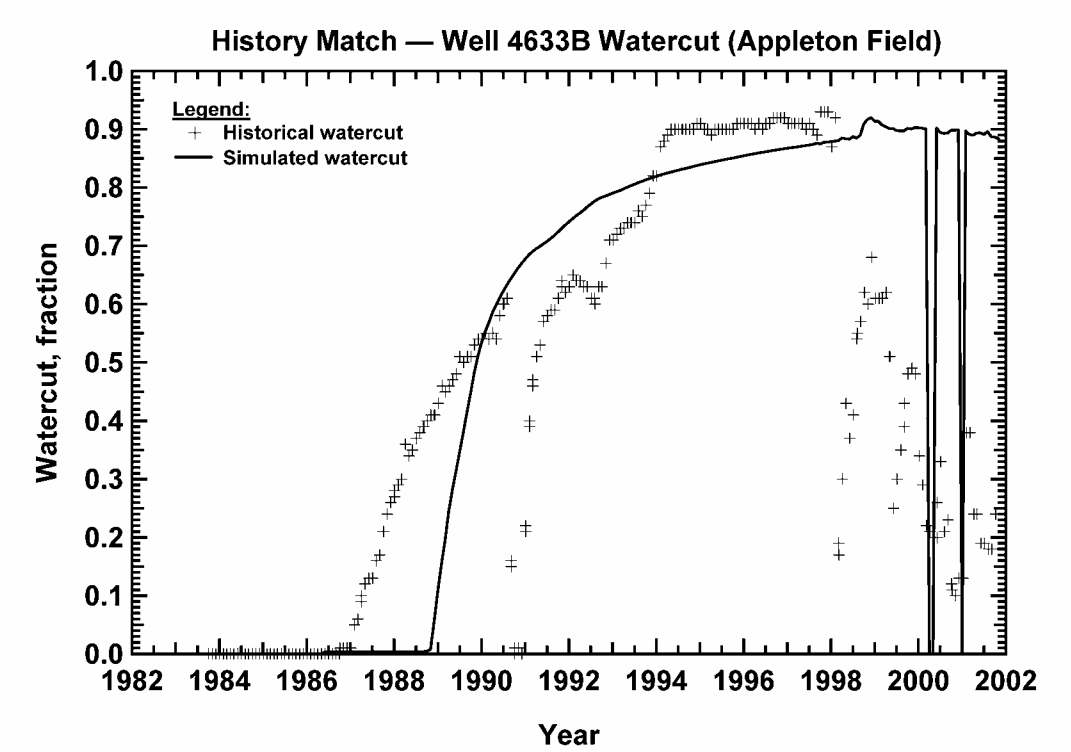

Figure 279 — Watercut history match, Well 4633B (Appleton Field).

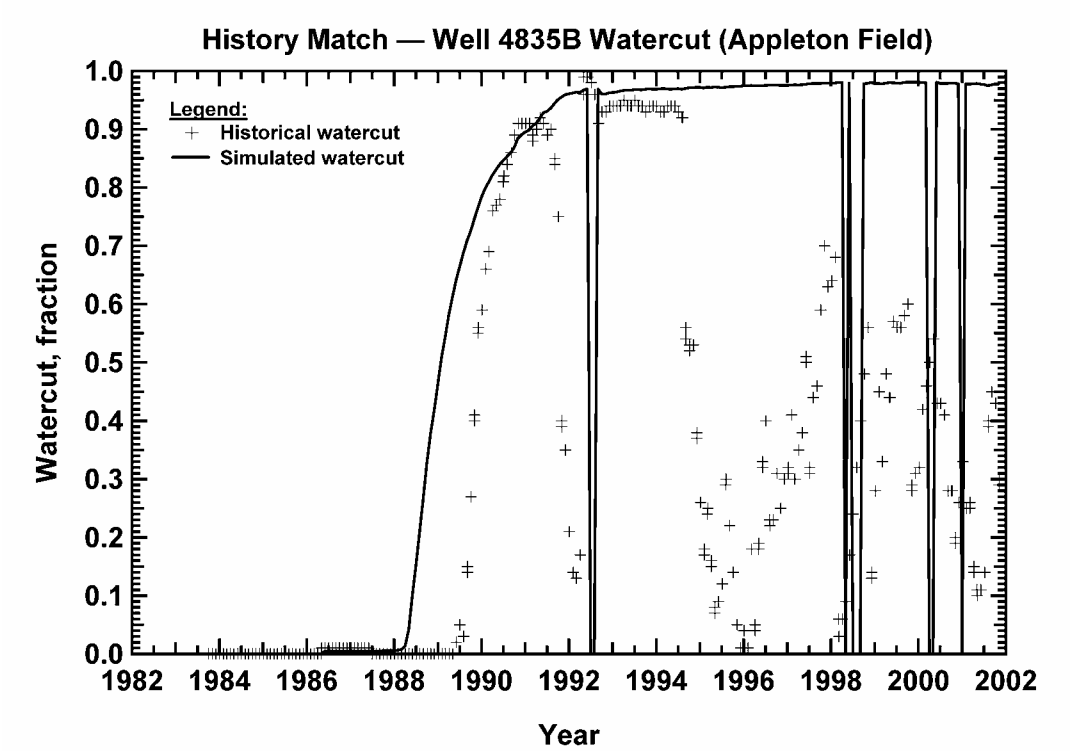

Figure 280 — Watercut history match, Well 4835B (Appleton Field).

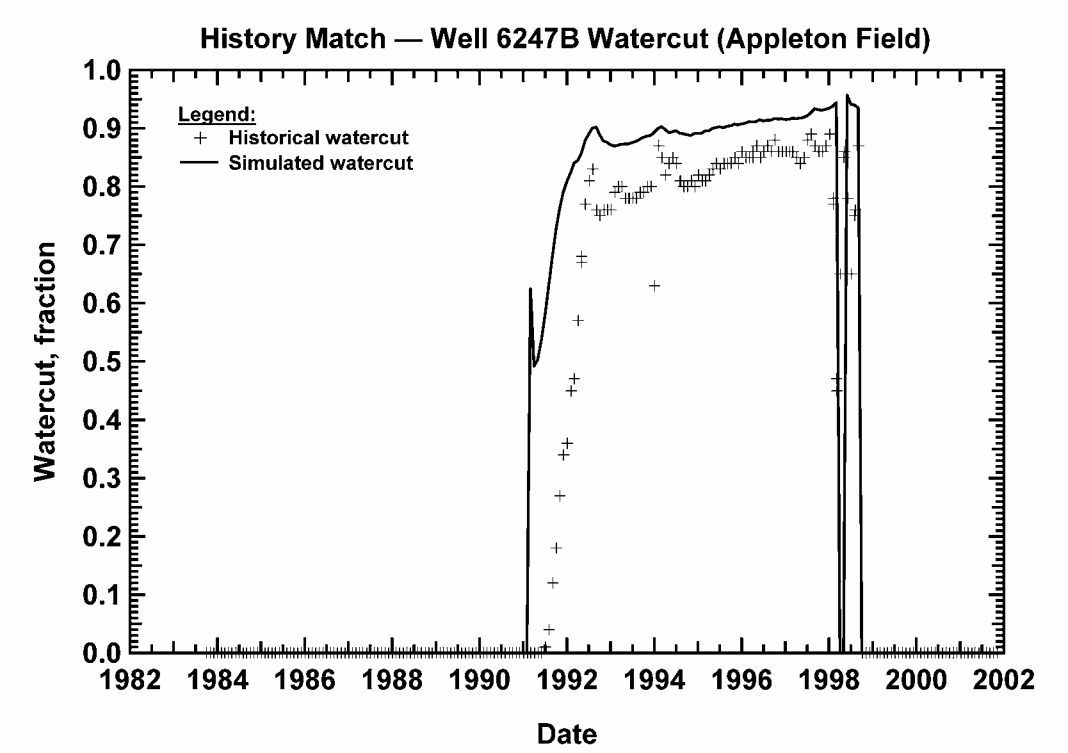

Figure 281 — Watercut history match, Well 6247B (Appleton Field).

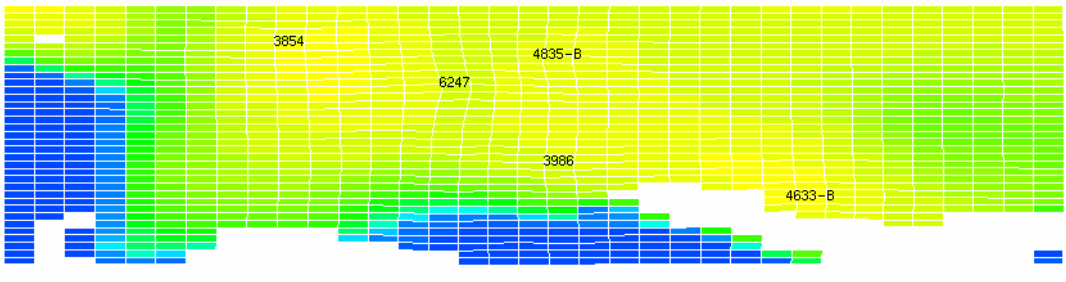

Figure 282 — Water saturations in 1983 at the top of the reef

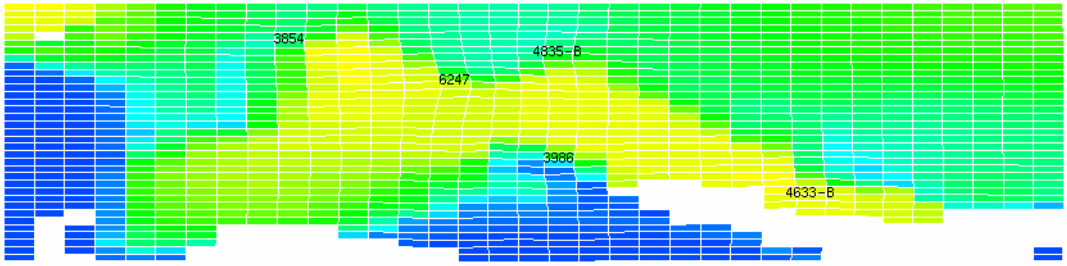

Figure 283 — Water saturations in 1988 at the top of the reef

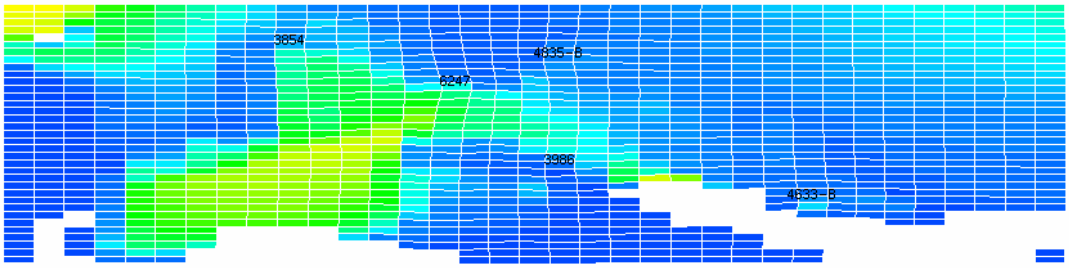

Figure 284— Water saturations in 1993 at the top of the reef

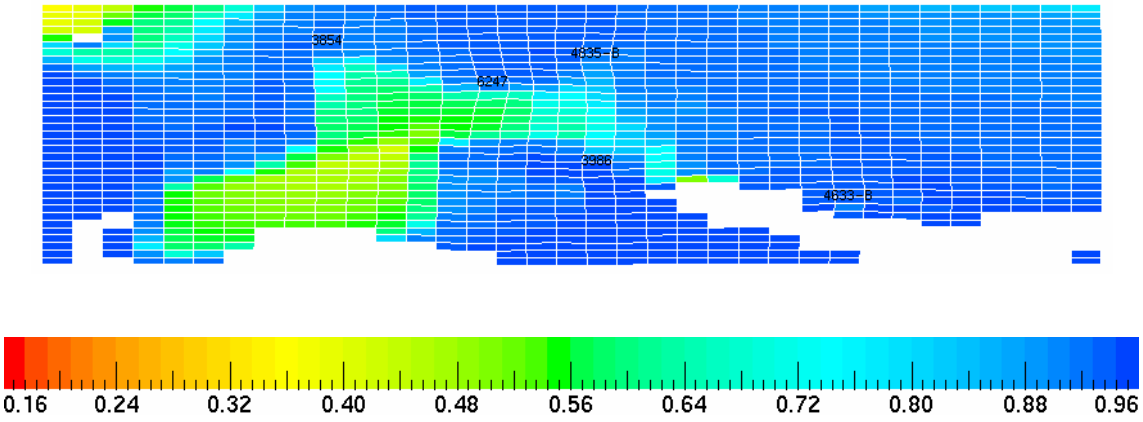

Figure 285 — Water saturations in 2001 at the top of the reef

Table 32 — Oil production (historical and simulated to February 2001), Appleton Field.

Well	Historical Oil Production, MSTB	Simulated Oil Production, MSTB
3854B	405	397
3986	158	152
4633B	1,149	646
4835B	778	677
6247B	184	146
Total	2,674	2,018

Table 33 — Water production (historical and simulated to February 2001), Appletonn Field.

Well	Historical Water Production, MSTB	Simulated Water Production, MSTB
3854B	1,246	907
3986	141	9.6
4633B	1,618	901
4835B	738	2268
6247B	334	814
Total	4,077	4,900

permit #3986 is the only well which is poorly matched. No explanation was found for the sudden change in the watercut in well permits #4633B and #4835B. In 1998 and 1994, respectively, these wells suddenly changed from producing at watercuts on the order of 90 percent to significantly lower watercuts (60 percent or less). A recompletion, or shutting-off of lower perforations probably occurred.

Cumulative recovery of water and oil for each well (both historical and simulated) are shown in Tables 32 and 33. There are differences in the data between the historical and simulated oil production for well permits #3986 and #4633B. In the case of well permit #3986, we believe that this mismatch is due to the low permeability of the reservoir in the region of well permit #3986. In fact, to achieve any oil production at all the permeability around well permit #3986 had to be adjusted (multiplied by ten) from the values determined from the geologic model. In the case of well permit #4633B the permeability values determined from the geologic model did not provide the high productivity observed historically in this well. When permeability around the well was increased oil production improved somewhat; however, water production became excessive.

The history matched model placed the water-oil contact at depth of 12,766 ft (TVDSS). A strong aquifer was placed below the reservoir. Simulated water saturation profiles at several times during the life of the field are shown in Figures 282 to 285. In each profile the view is an areal view of the layer corresponding to the top of the reef. These water saturation profiles show the impact of the strong bottom water drive mechanism.

High water saturations are predicted throughout the entire reef zone which implies there is little potential for economic production in the field via infill drilling. Remaining oil production from the existing wells is expected to be accompanied by high water production. In

Figure 285, the areas of the field which indicate remaining oil saturation can not be considered a drilling target. This area is low permeability (2 md or less) and very low pore volume in the geologic model.

Vocation Field. 3-D reservoir simulation at Vocation Field has been completed. The 3-D geologic model formed the foundation for the reservoir simulation. Fluid data (Figure 286 and Tables 34-37), rock properties (Figures 287-288), historical production (Table 38 and Figures 289-290), phase flowrates (Figures 291-292), cumulative production (Figure 293), gas-oil ratio profile (Figure 294), watercut profile (Figure 295), oil production rate history match (Figure 296), water production rate history match (Figure 297), gas production rate history match (Figure 298) and water production history match per well (Figures 299-308) were used in the simulation for Vocation Field. The results of the simulation for the field are illustrated in Figures 309-314 and Tables 39 and 40.

The volume of oil initially in place in this model is 26,564 MSTB (with the water-oil contact at 13,693 ft and a connate water saturation of 0.3). The estimate of original oil-in-place is dependent on the assumed water-oil contact location as well as the connate water saturation. The historical oil recovery of 2,261 MSTB (to August 2003) implies a recovery factor of 8.5 percent. There is significant structural relief in the geologic structure of the Vocation Field. In the geologic model much of this is uncontrolled by well data. The model has points on the top of the reservoir structure at depths of as shallow as 13,490 ft. This leads to the interpretation that there is a significant volume of oil being predicted to be (though not proven to be) in these areas. However, we note that the pore volume for the geologic model is in general agreement with that predicted via production data analysis. Figures 287 and 288 show the relative permeability and capillary pressure curves used in the final version of the history matched model.

.

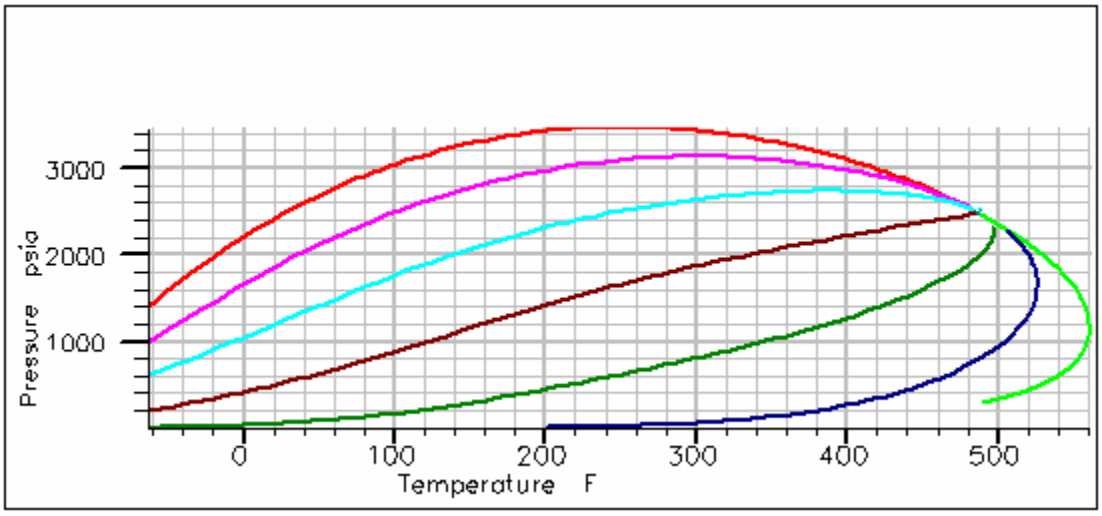

Figure 286 – Phase Envelope, Vocation Field.

Table 34 — Pseudocomponent Grouping, Vocation Field.

Pseudocomponent	Components
Group 1	$C_1 + N_2$
Group 2	$C_2 + CO_2$
Group 3	C_3
Group 4	$C_4 + C_5$
Group 5	$C_6 + C_7$

Table 35 — Pseudocomponent Properties, Vocation Field.

Component	Molecular Weight (dim-less)	Critical Temperature (deg R)	Critical Pressure, (psia)	Critical z-Factor (dim-less)	Acentric Factor (dim-less)
Group 1	17.64	327.89	644.28	0.2845	0.0166
Group 2	31.26	549.99	739.41	0.2878	0.1094
Group 3	44.10	665.97	615.75	0.2762	0.1524
Group 4	63.85	789.93	521.87	0.2751	0.2145
Group 5	160.13	1169.96	293.41	0.2629	0.4918

Table 36 — Pseudocomponent Properties, Vocation Field (continued).

Component	Ω_a (dim-less)	Ω_b (dim-less)	V_s (dim-less)
Group 1	0.6951	0.0717	-0.1425
Group 2	0.4898	0.0749	-0.0981
Group 3	1.0288	0.1109	-0.0775
Group 4	0.9591	0.1235	-0.0477
Group 5	0.6951	0.0965	0.2561

Table 37 — Binary Interaction Coefficients, Vocation Oil Field.

	Group 1	Group 2	Group 3	Group 4	Group 5
Group 1	0.0	-	-	-	-
Group 2	0.019519	0.0	-	-	-
Group 3	0.013889	0.008559	0.0	-	-
Group 4	0.013889	0.008559	0.0	0.0	-
Group 5	0.049655	0.017704	0.013889	0.0	0.0

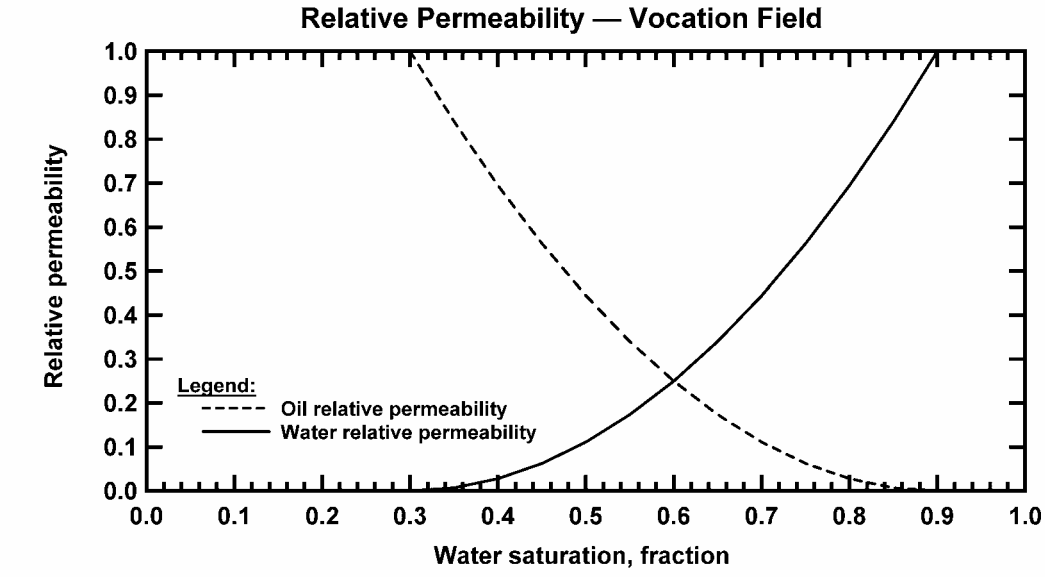

Figure 287 — History matched relative permeability curves, Vocation Field.

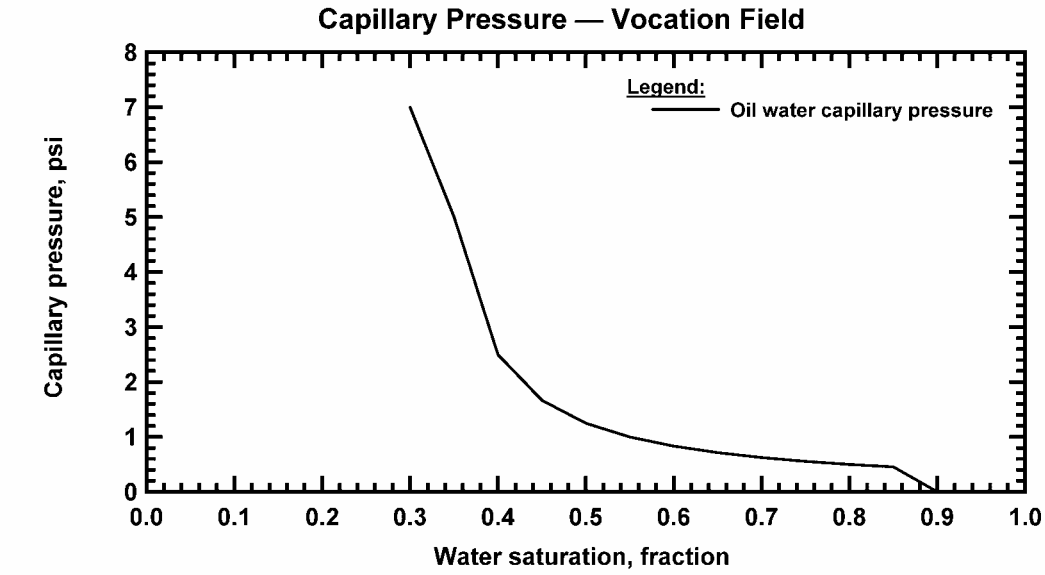

Figure 288 — History matched capillary pressure, Vocation Field.

Table 38 – Reported Cumulative Production per Well, Vocation Oil Field.

Well	Oil Production (MSTB)	Water Production (MSTB)	Gas Production (MMSCF)
1599	168	0	532
1830	733	332	1750
2851	388	1810	530
2935	165	817	284
3412	36	84	60
3739	529	163	1286
4225A	47	28	79
4225B	29	50	71
5779	102	50	226
11185	120	0.6	194

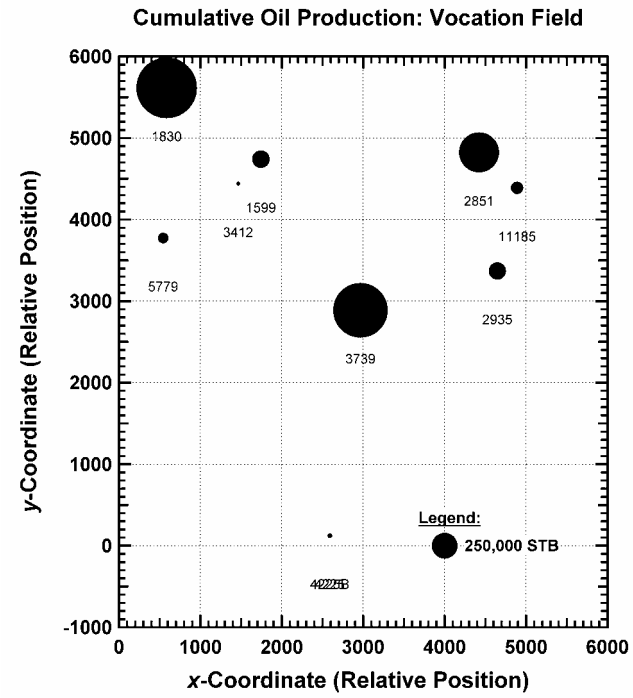

Figure 289 — Oil Production as a Function of Well Location, Vocation Field.

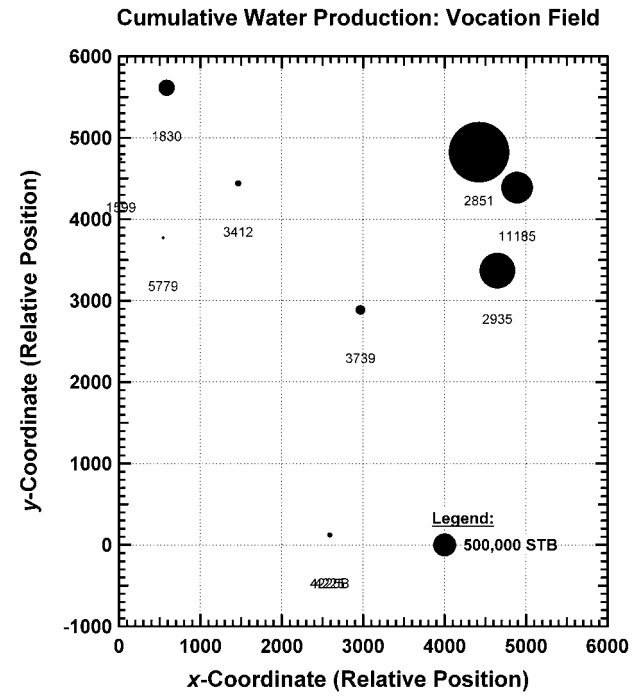

Figure 290 — Water Production as a Function of Well Location, Vocation Field.

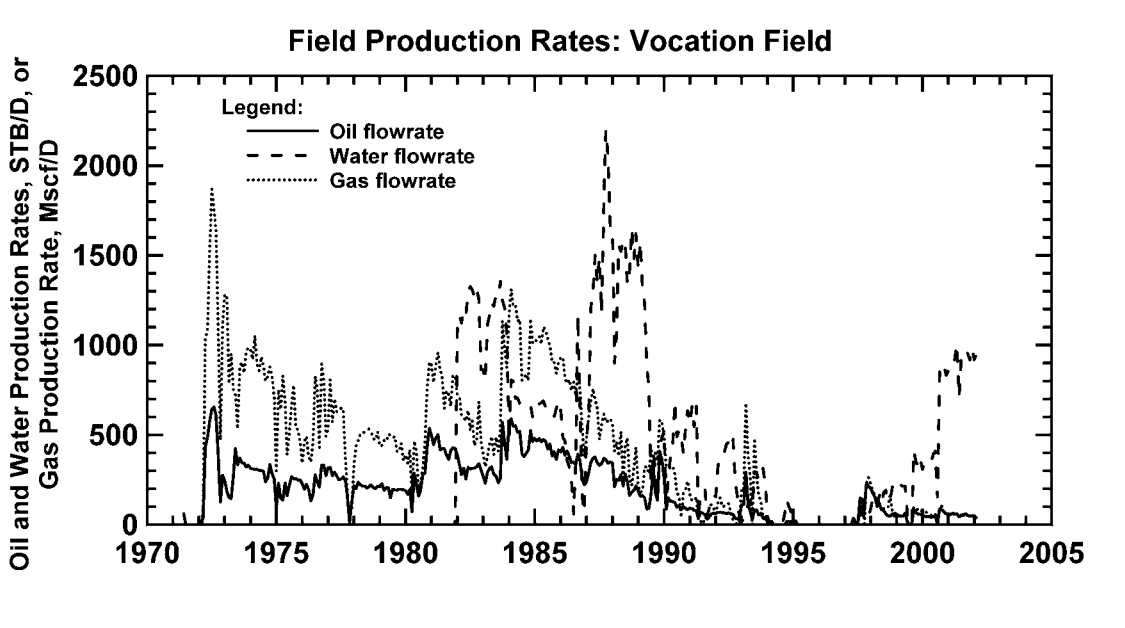

Figure 291 — Individual Phase Flowrates, Vocation Field (Cartesian Format).

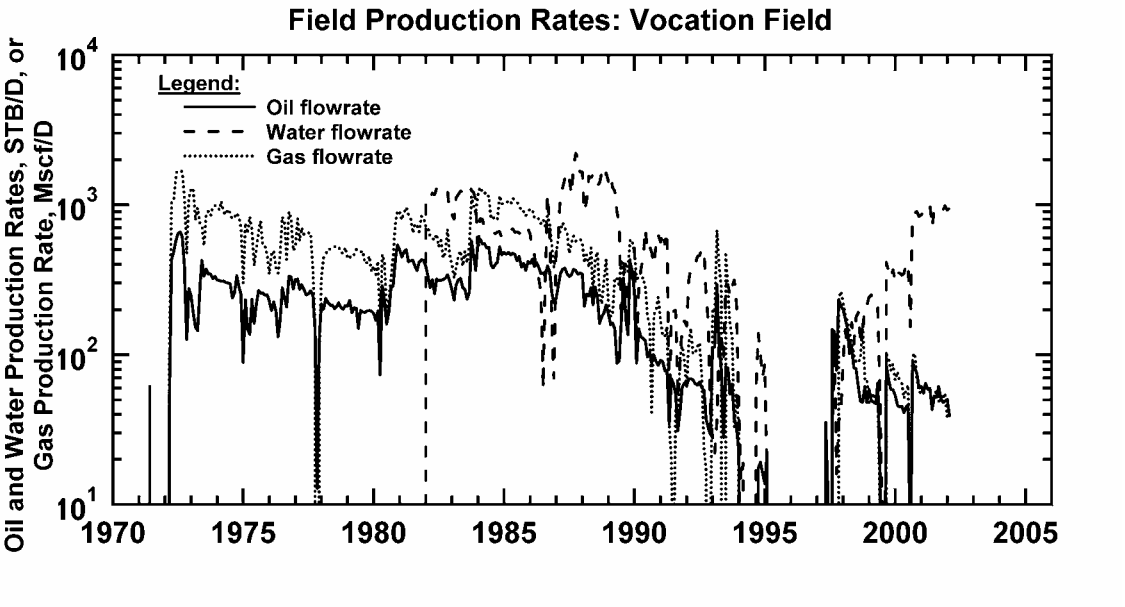

Figure 292 — Individual Phase Flowrates, Vocation Field (Semilog Format).

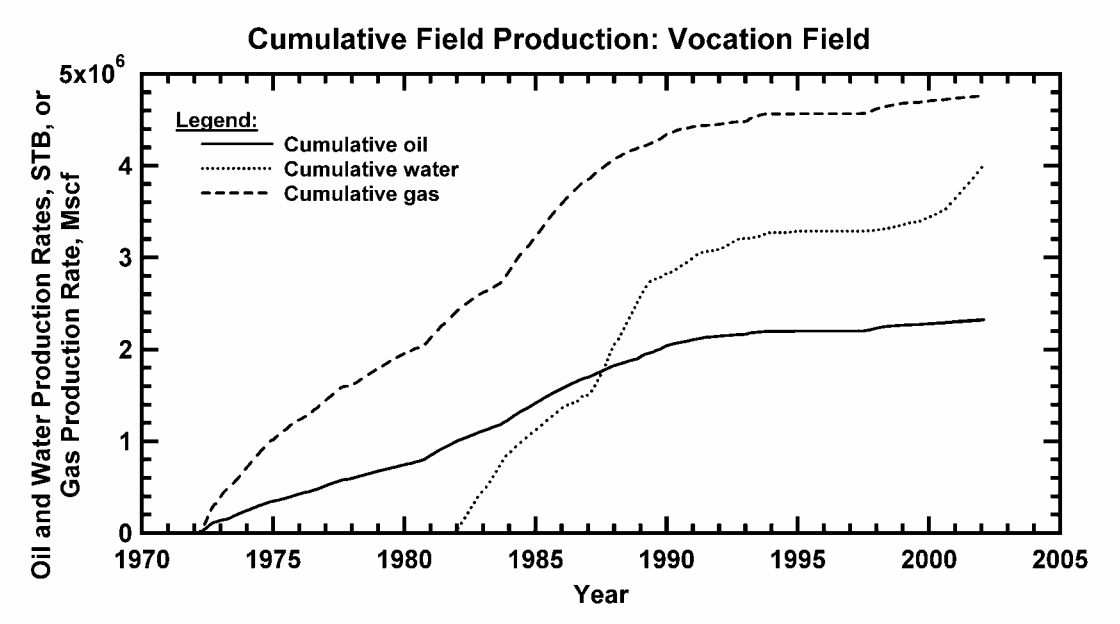

Figure 293 — Cumulative Production Profiles, Vocation Field.

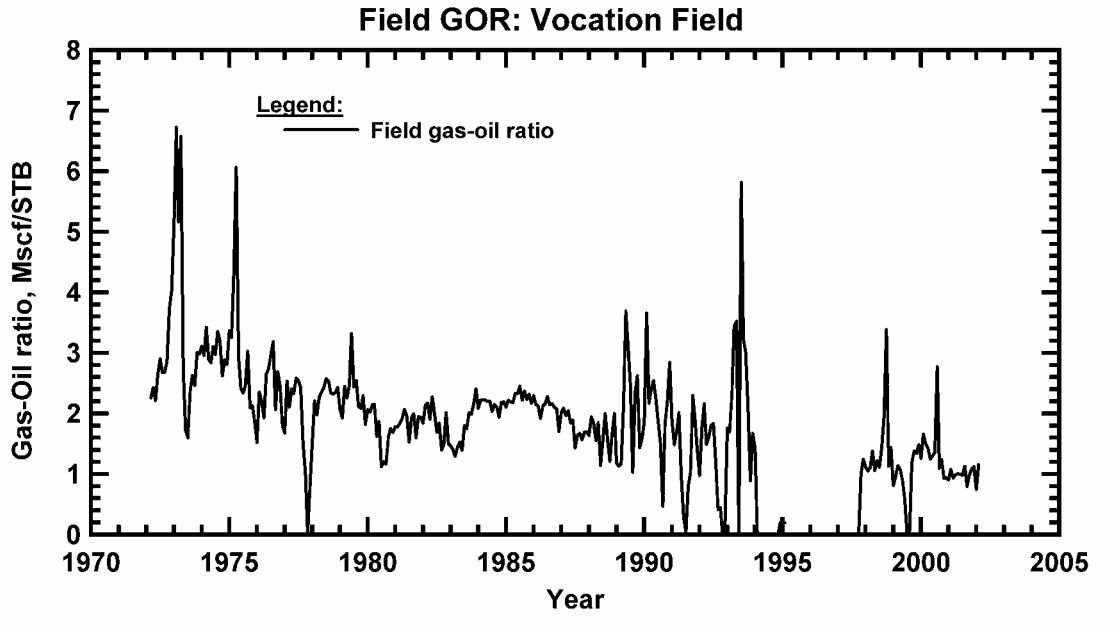

Figure 294 — Gas-Oil Ratio Profile, Vocation Field.

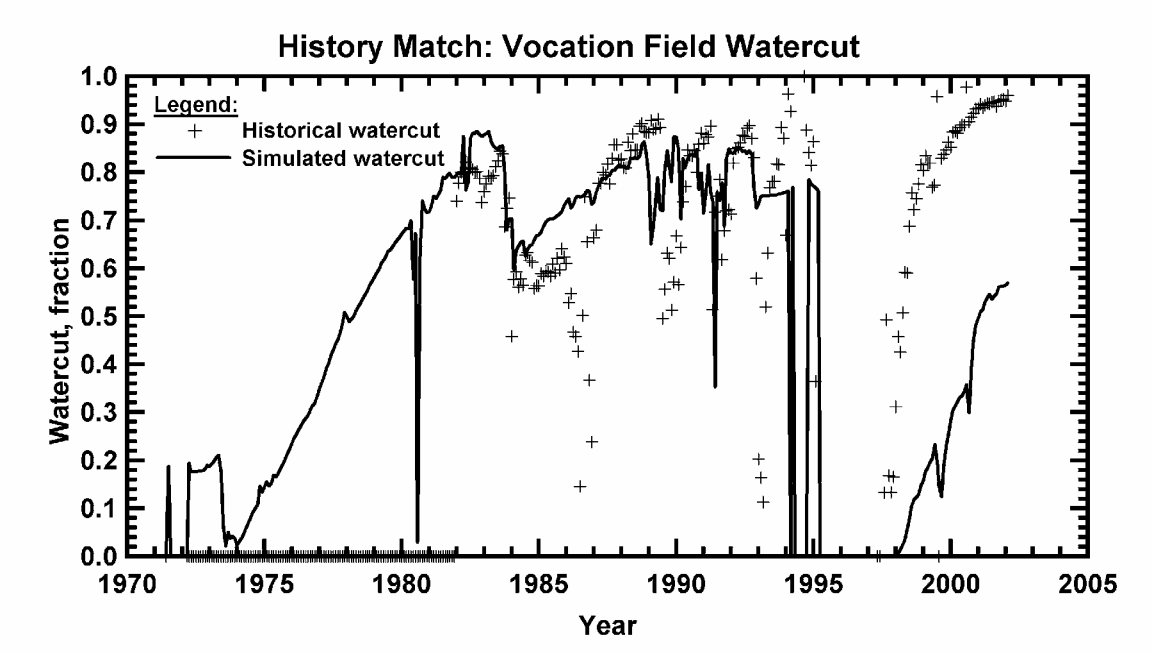

Figure 295 — Watercut history match, Vocation Field.

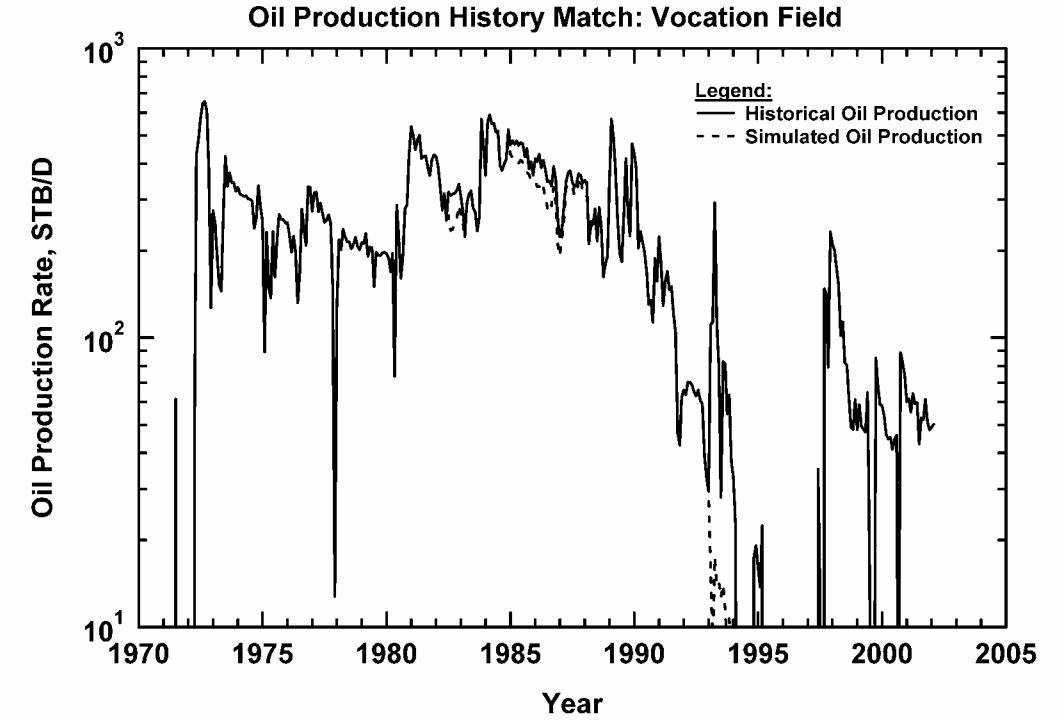

Figure 296 — Oil Production Rate History Match, Vocation Field.

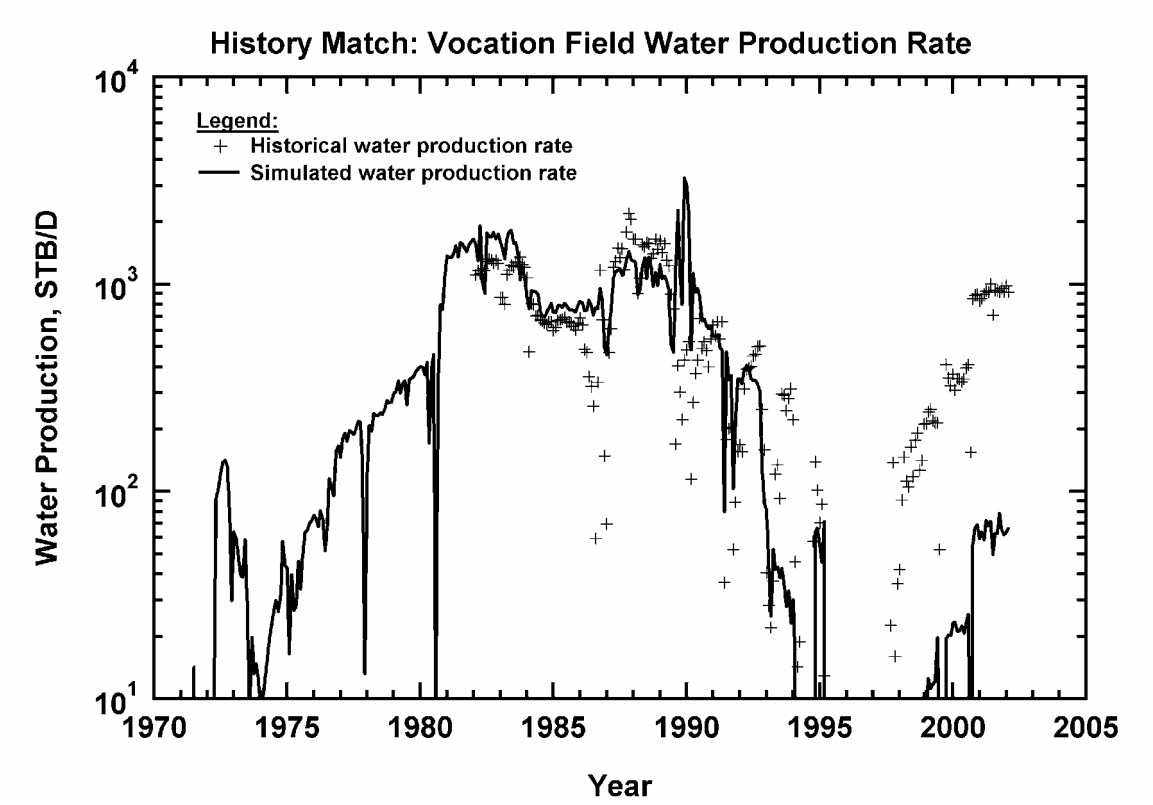

Figure 297 — Water production rate history match, Vocation Field.

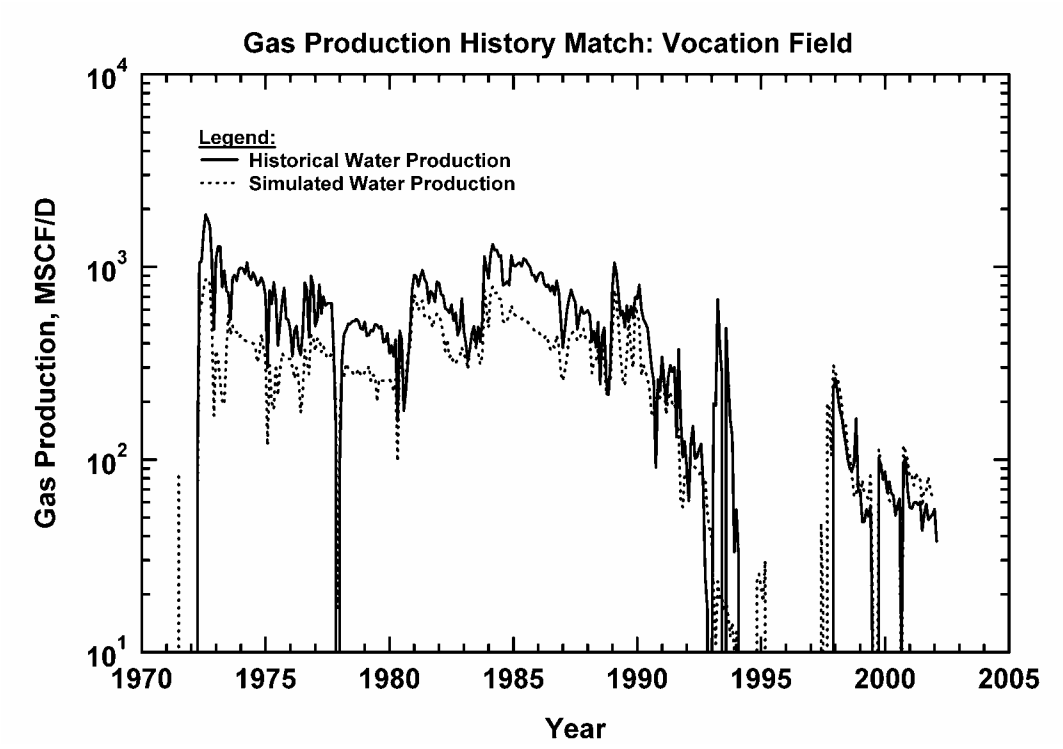

Figure 298 — Gas Production Rate History Match, Vocation Field.

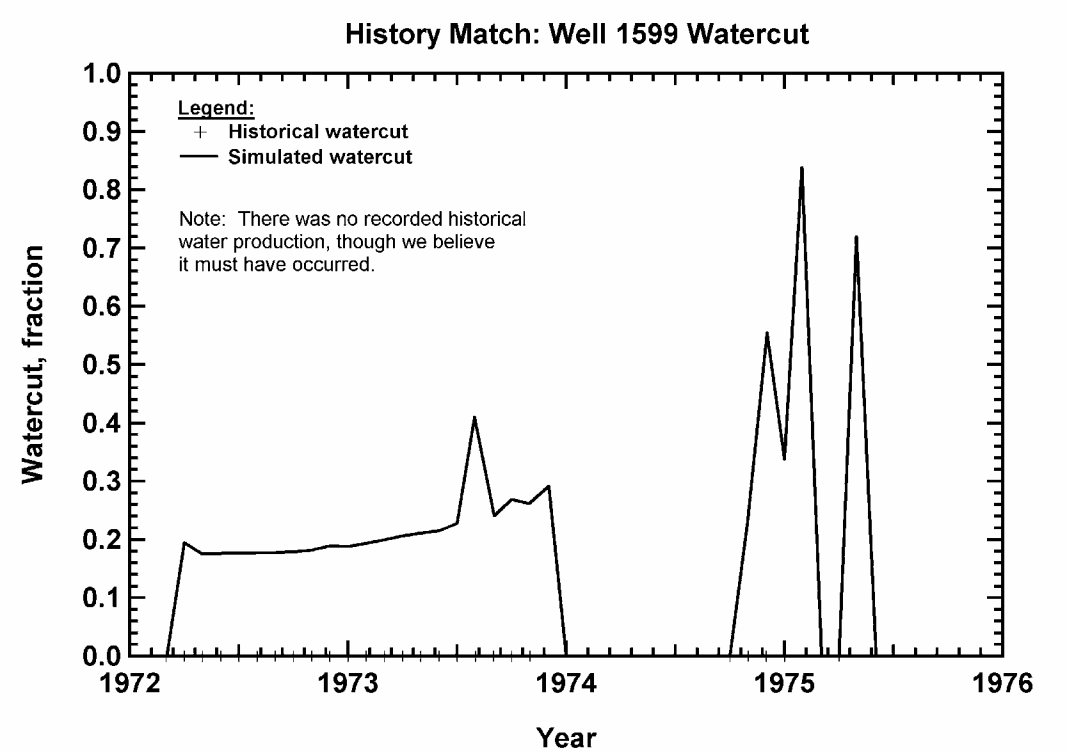

Figure 299 — Watercut history match, Vocation Well 1599.

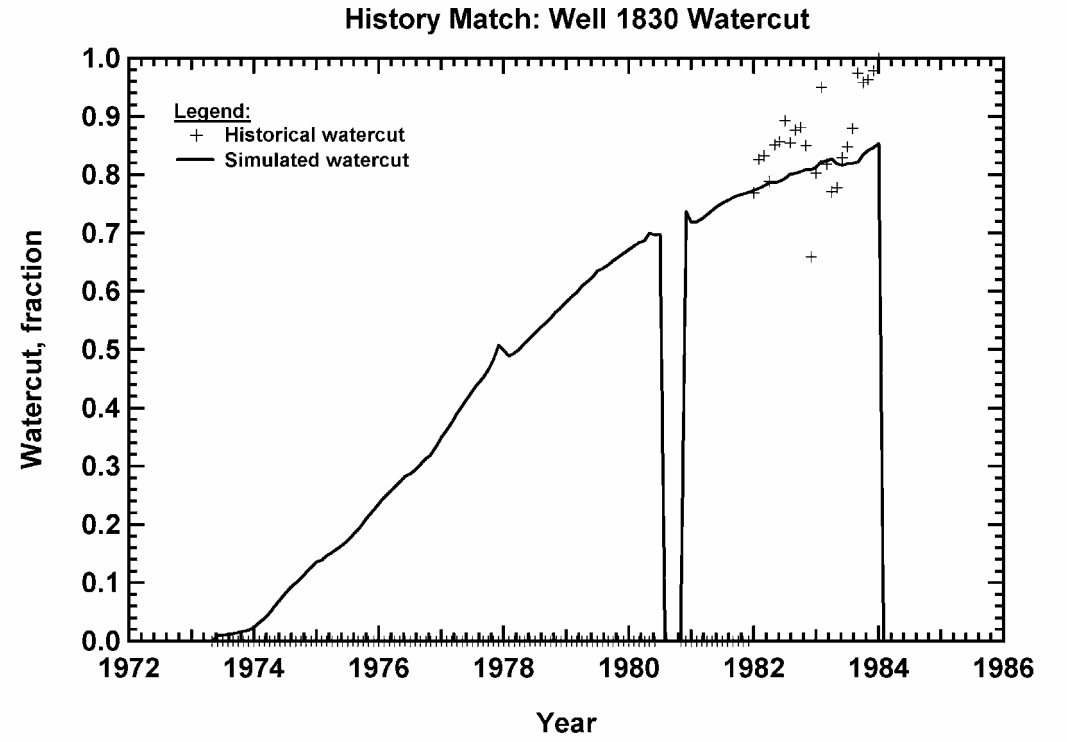

Figure 300— Watercut history match, Vocation Well 1830.

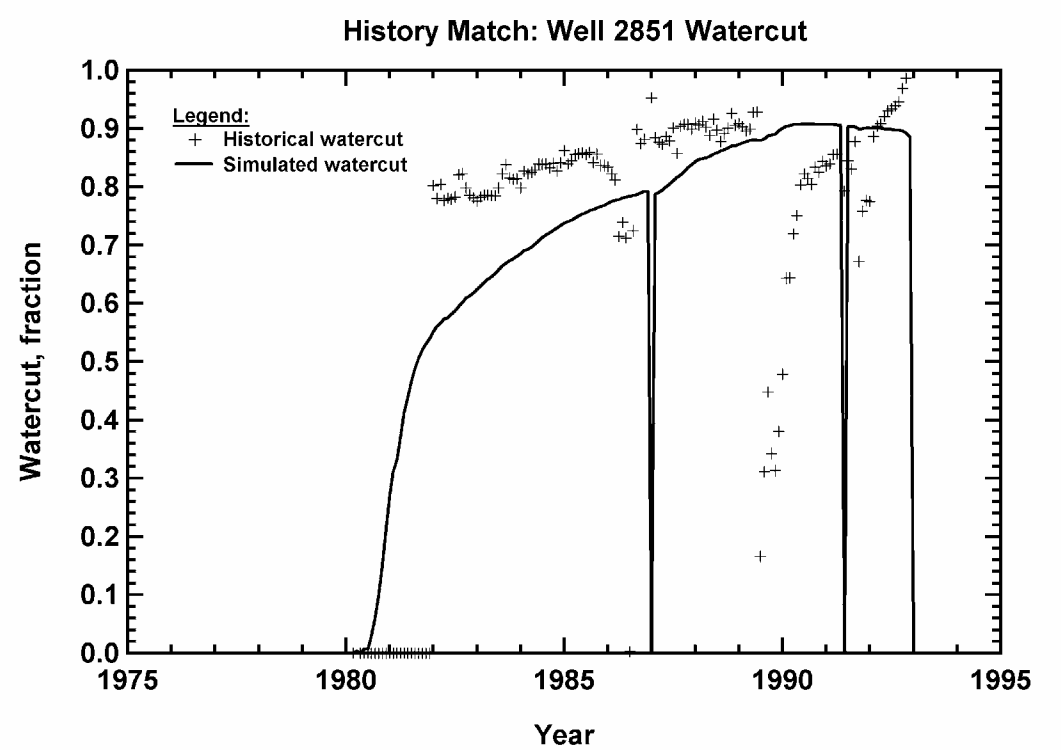

Figure 301 — Watercut history match, Vocation Well 2851.

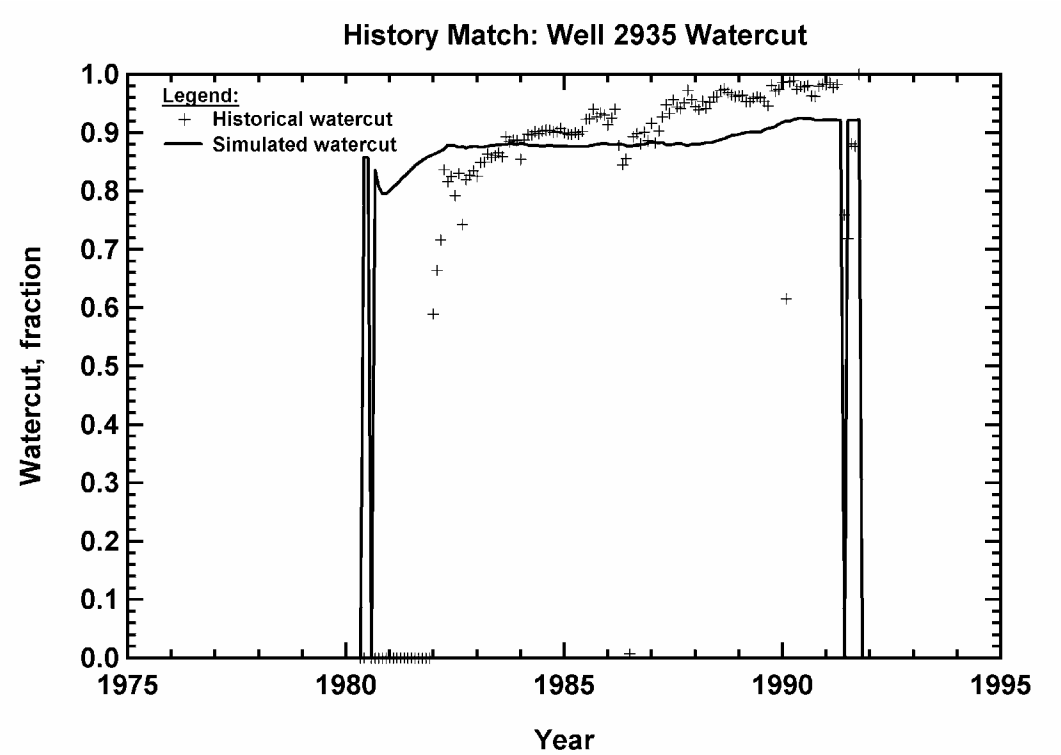

Figure 302 — Watercut history match, Vocation Well 2935.

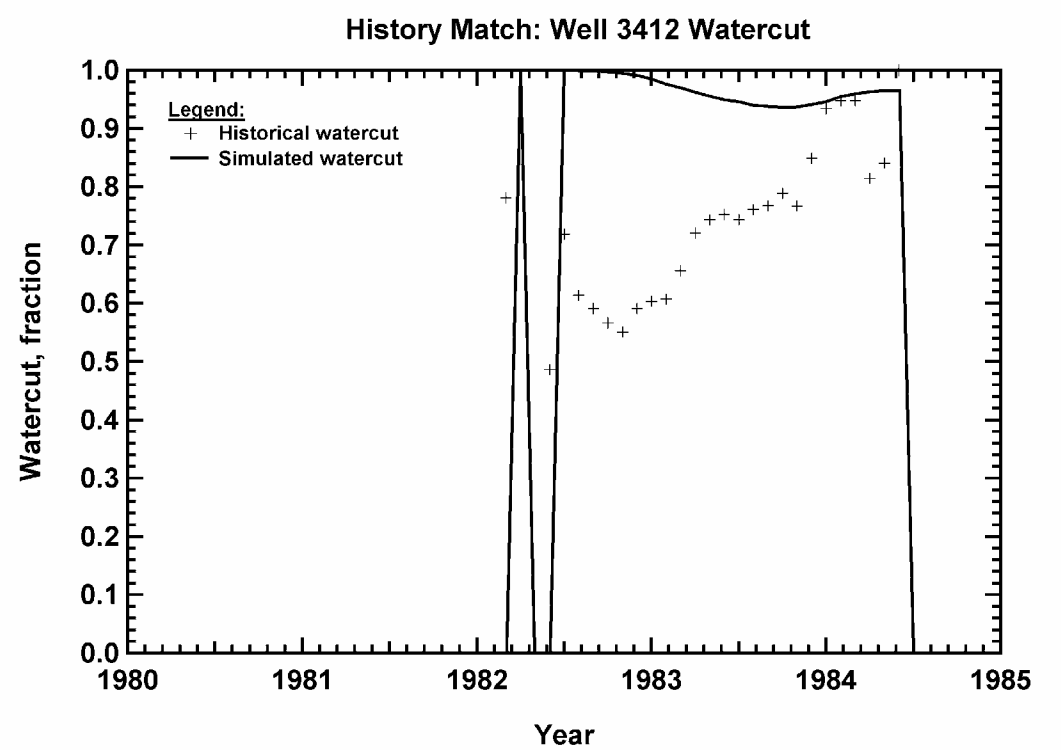

Figure 303 — Watercut history match, Vocation Well 3412.

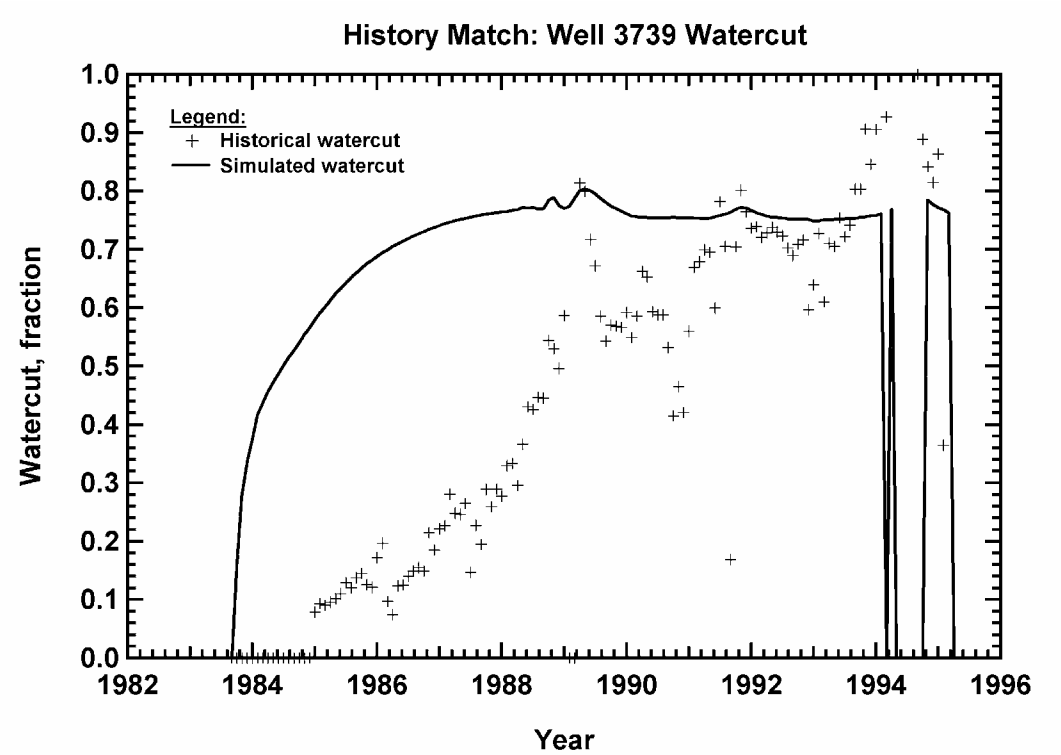

Figure 304 — Watercut history match, Vocation Well 3739.

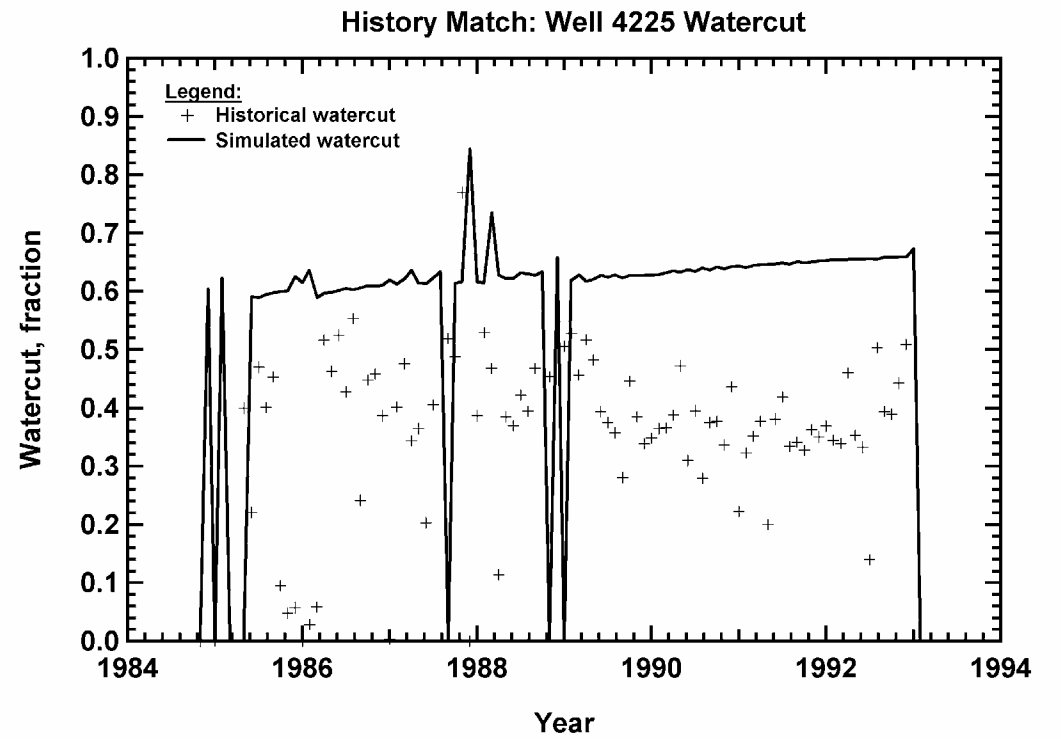

Figure 305 — Watercut history match, Vocation Well 4225.

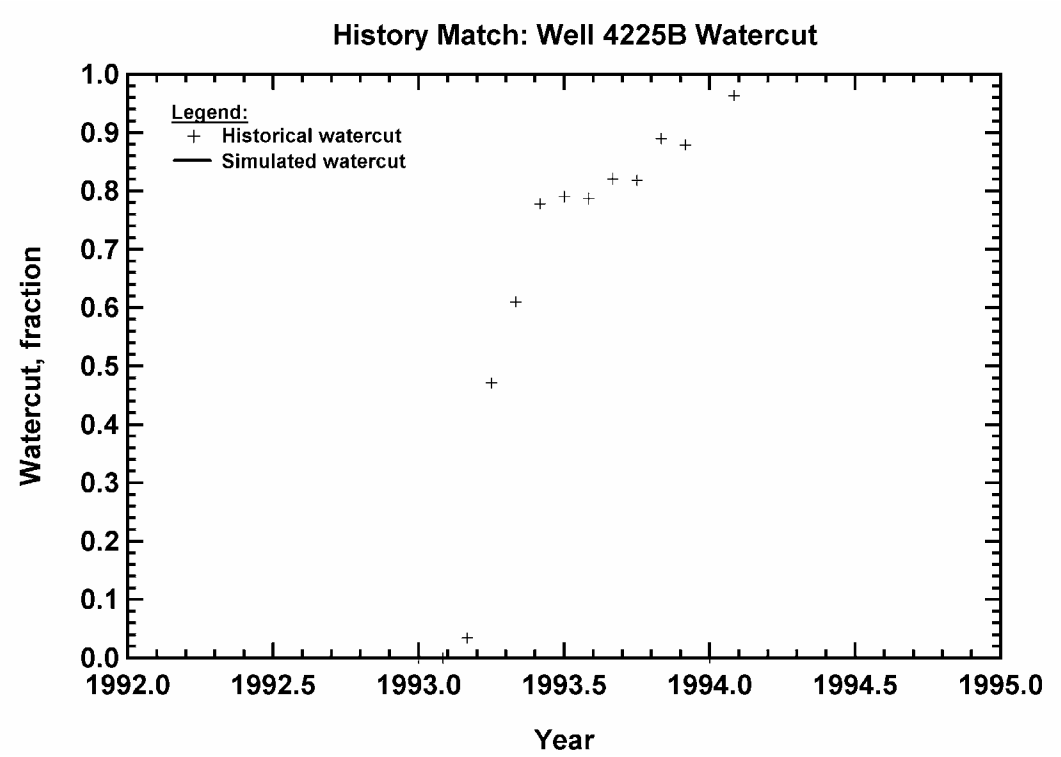

Figure 306 — Watercut history match, Vocation Well 4225B.

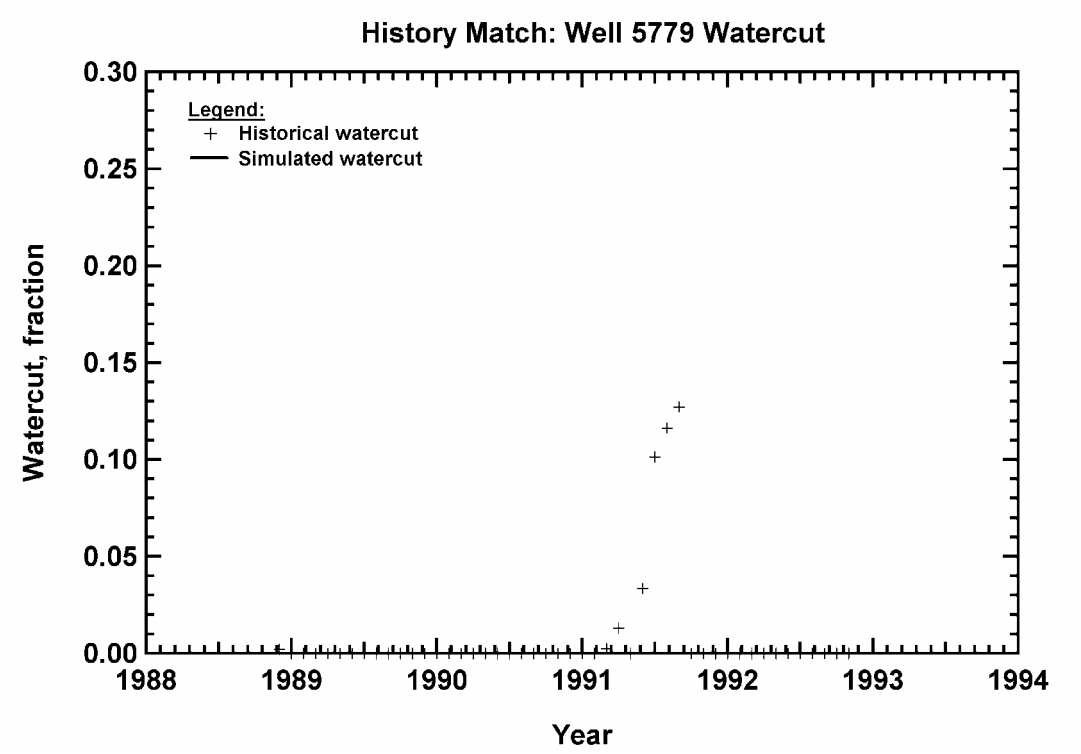

Figure 307 — Watercut history match, Vocation Well 5779.

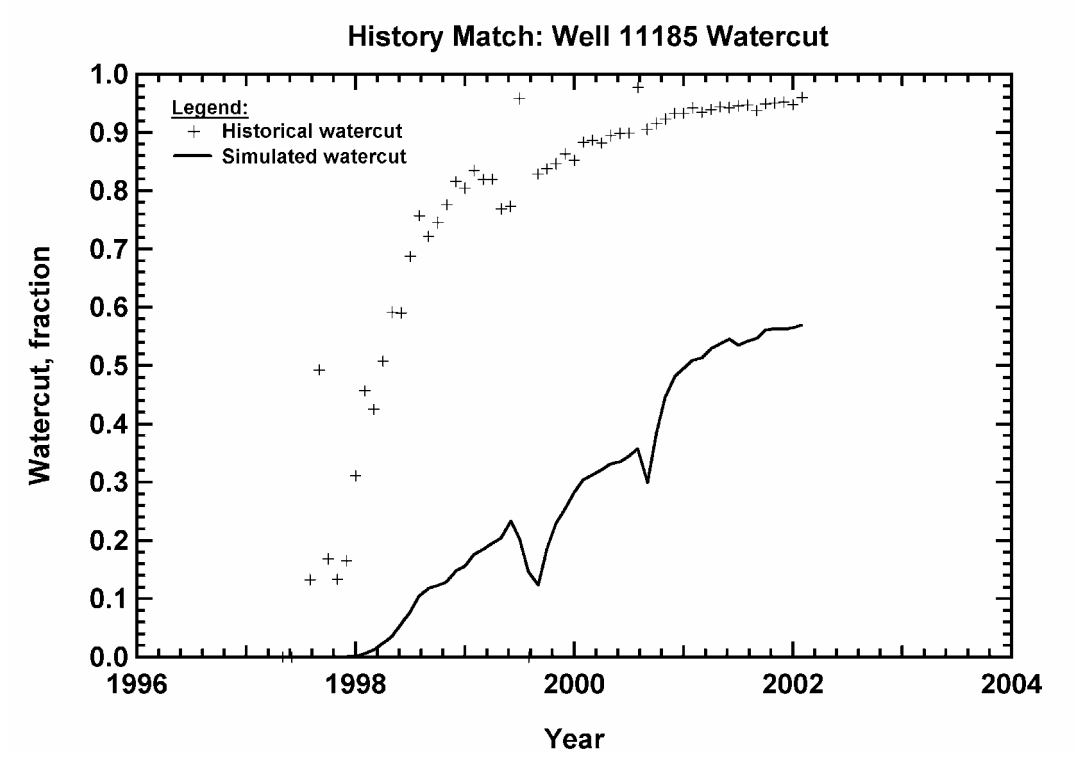

Figure 308 — Watercut history match, Vocation Well 11185.

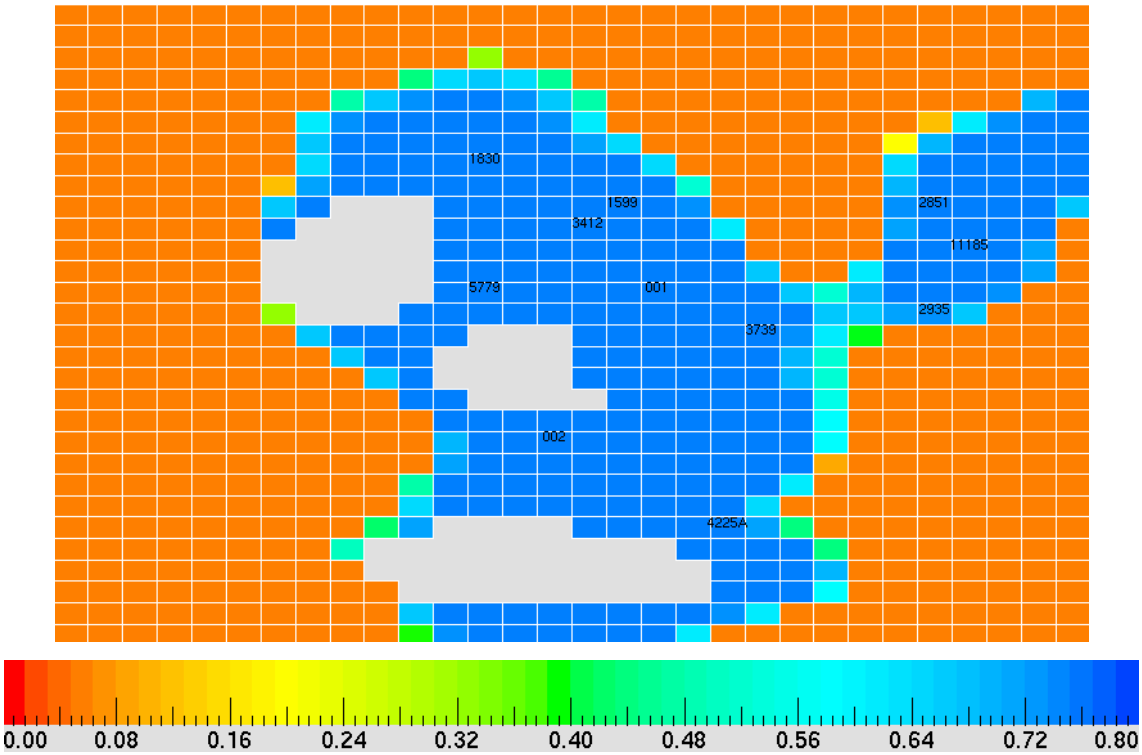

Figure 309 — Oil saturation in top simulation layer 1971, Vocation Field.

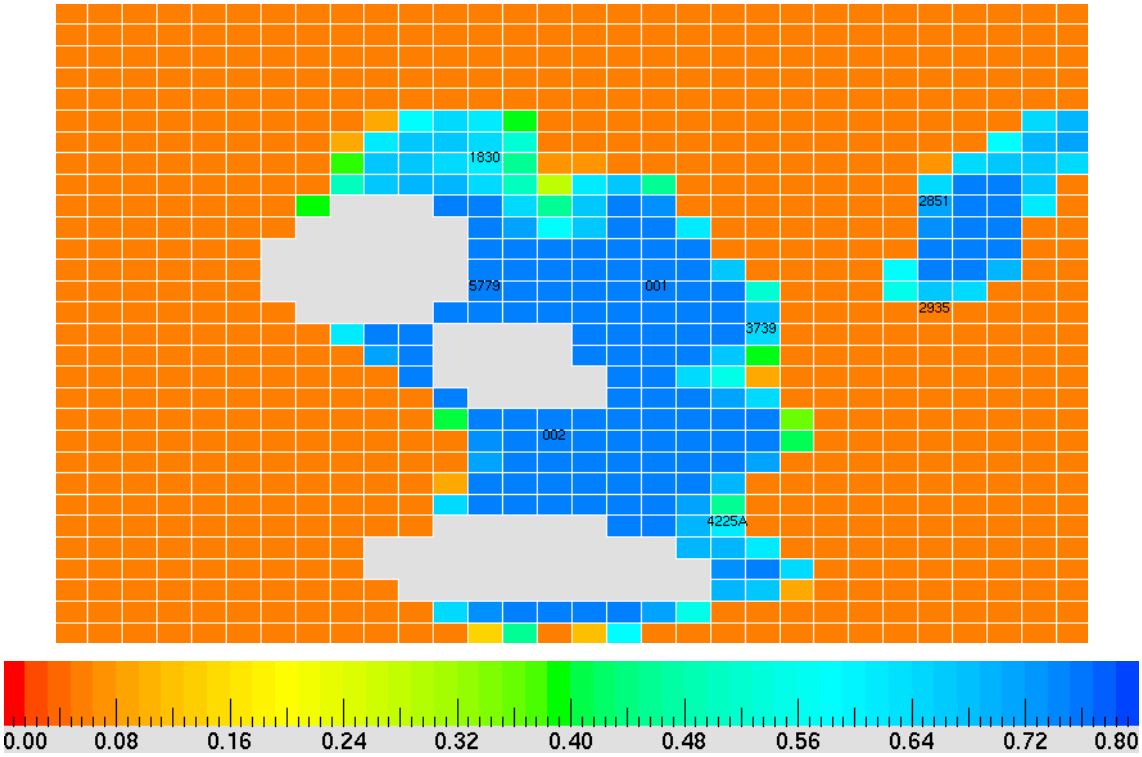

Figure 310 — Oil saturation in intermediate simulation layer (50ft from reservoir top) 1971, Vocation Field.

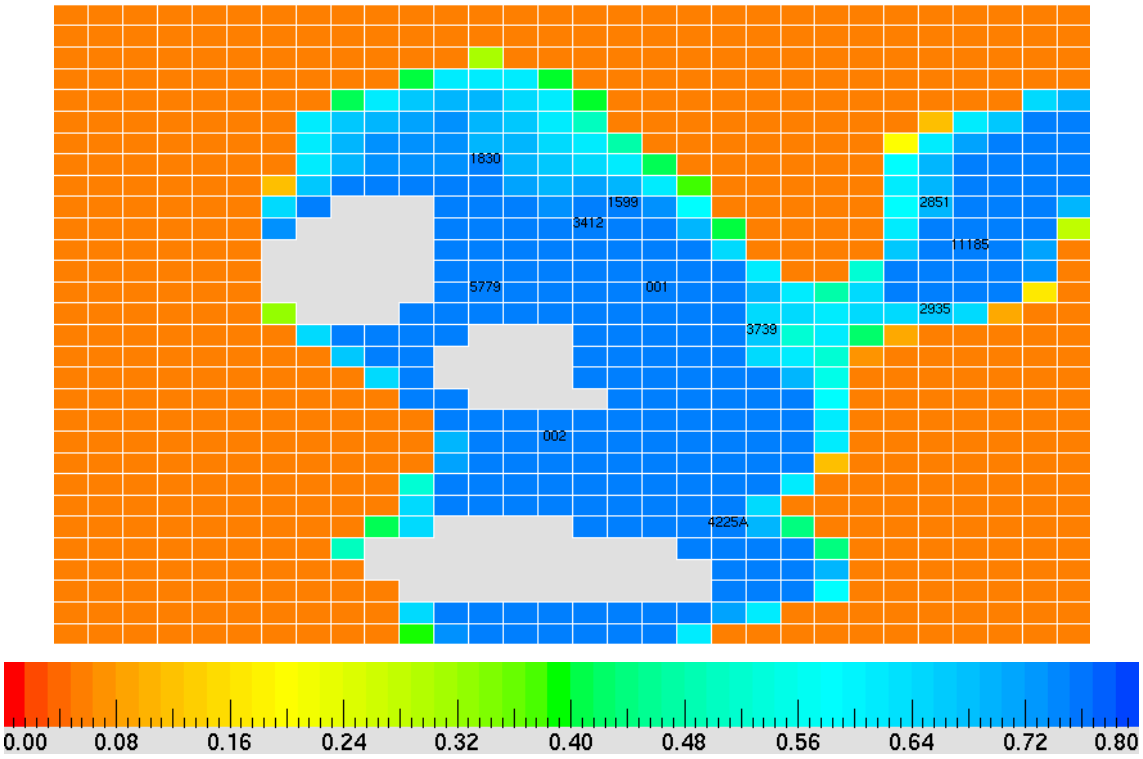

Figure 311 — Oil saturation in top simulation layer 1986, Vocation Field.

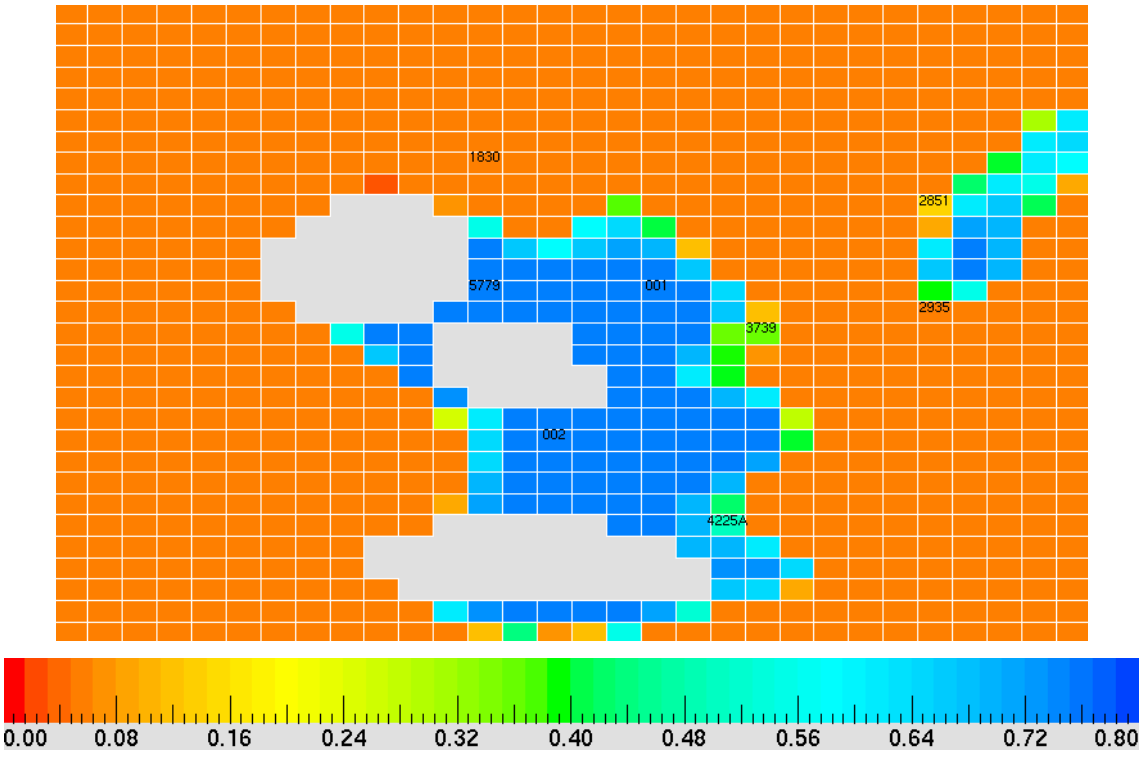

Figure 312 — Oil saturation in intermediate simulation layer (50ft from reservoir top) 1986, Vocation Field.

Table 39 — Oil production (historical and simulated to February 2002), Vocation Field.

Well	Historical Oil Production, MSTB	Simulated Oil Production, MSTB
1599	169	169
1830	733	733
2851	388	388
2935	166	166
3412	37	13
3739	529	411
4225	47	47
4225B	29	0
5779	102	102
11185	138	119
Total	2,338	2,148

Table 40 — Water production (historical and simulated to February 2002), Vocation Field.

Well	Historical Water Production, MSTB	Simulated Water Production, MSTB
1599	0	39
1830	332	866
2851	1,810	1,685
2935	817	1016
3412	85	459
3739	163	818
4225	28	81
4225B	50	0
5779	0.6	0
11185	1,123	45
Total	4,408	5,009

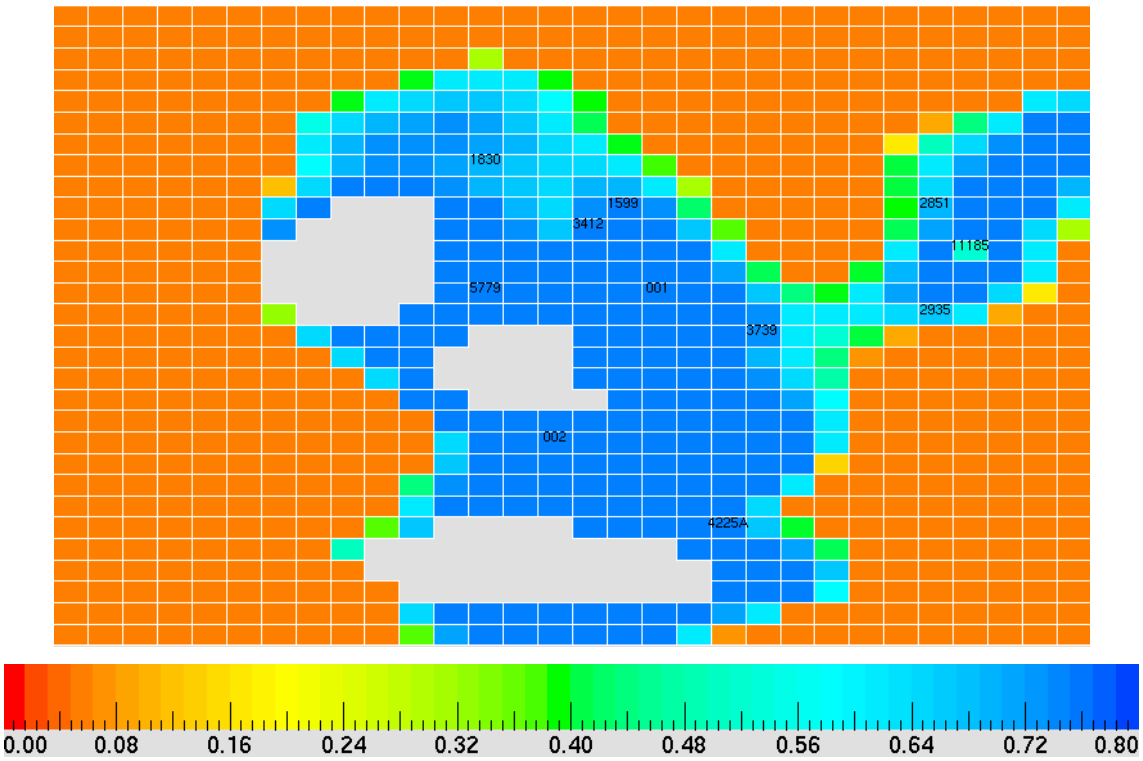

Figure 313— Oil saturation in top simulation layer 2001, Vocation Field.

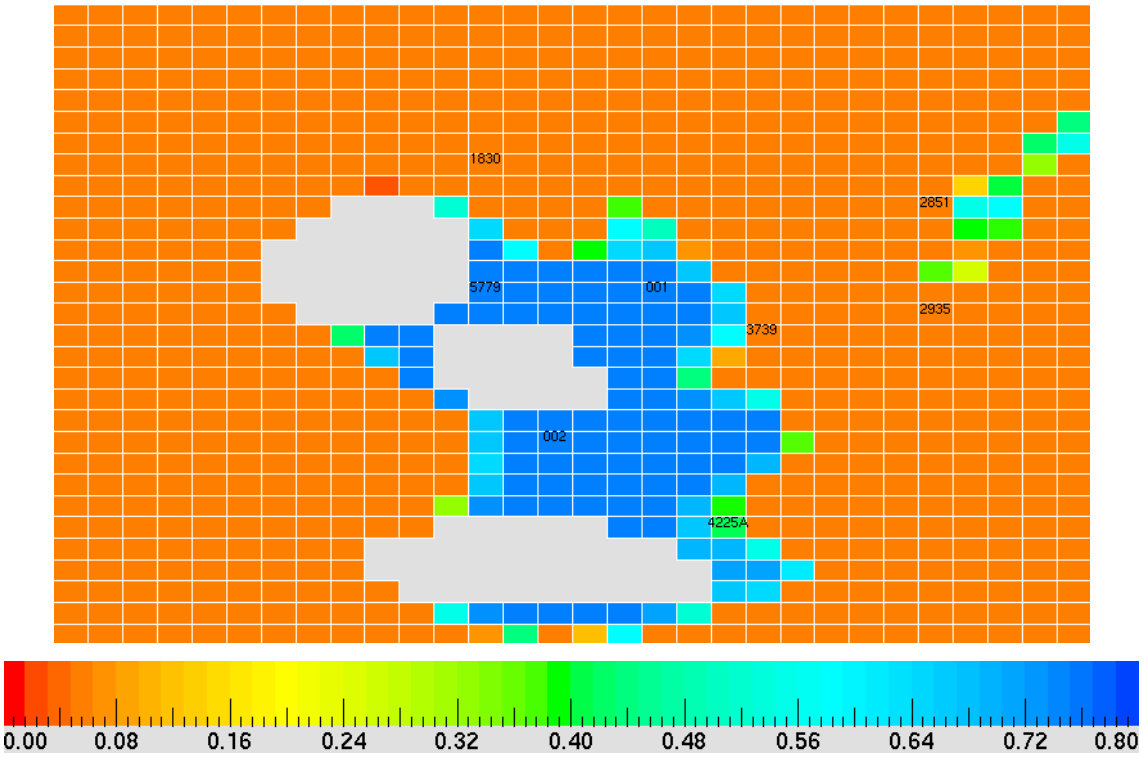

Figure 314 — Oil saturation in intermediate simulation layer (50ft from reservoir top) 2001, Vocation Field.

Figures 299 to 308 show the history-matched watercut for each of the producing wells in the Vocation field. In Figures 297 and 295 we present the fieldwide water production rate and fieldwide watercut. Before 1995 the fieldwide matches shown in Figures 297 and 295 are quite good. The behavior of the reservoir after 1995 is not well captured. The quality of the individual well matches in Figures 299 to 308 is not as good as the overall fieldwide data matches. However, these matches are considered acceptable in light of the poor data availability discussed above.

Cumulative recovery of water and oil for each well (both historical and simulated) is shown in Tables 39 and 40. In a few cases (Well permits #3412, #3729, #4225B and #11185) the wells did have sufficient productivity to meet the historically produced oil volumes. When considering the cumulative water production data (Table 40) the problem of unrecorded water production should be kept in mind. Water production in the field is believed to be due to a bottomwater drive/water coning.

Figures 309 to 314 provide areal maps of the oil saturation in the reservoir (note that blue colors denote high oil saturations). For reference, the modeling cells are approximately 300 ft by 300 ft and up to 10 ft thick. These maps illustrate the impact of water influx into the reservoir.

Reperforation of existing wells may provide a cost-effective mechanism to produce additional oil from Vocation Field. We recommend that the well logs and well completion histories of existing wells be reviewed to determine if there is any possibility to enhance production by reperforating wells higher in the oil column. Note that the simulation model assumes that all pore volume above the oil-water contact (and capillary transition zone) is oil saturated.

Infill drilling is also a possibility, especially if the high structural relief of the reservoir can be confirmed. Figure 315 shows two possible target areas for infill wells. The infill wells are denoted 001 and 002. Production profiles for these wells are shown in Figures 316 and 317. When considering infill however it should be remembered that this simulation model did not accurately capture water production behavior after 1995 — suggesting that water movement may negate infill drilling opportunities..

Several infill locations were evaluated. The results of this evaluation are shown in Figures 318 and 319 in the form of bubble maps of incremental oil and water production as a result of a single infill well placed at the location of the bubble. The incremental volumes depicted are based on simulations that run until the end of 2005. The maps can be used to guide possible drilling locations in relative terms. The best locations are in the area of the reservoir that is structurally high (and assumed to be oil saturated).

Testing and Applying Integrated Geologic-Engineering Models--This task is designed to test and apply the integrated geologic-engineering models for reef and shoal reservoirs associated with petroleum traps in Smackover fields represented by varying degrees of relief on pre-Mesozoic basement paleohighs (Figure 263). The Appleton case study (low-relief) and the Vocation case study (high-relief) are the basis for the models. The integrated geologic models have been constructed utilizing the geological and geophysical characterization data for the reef-shoal reservoir and structure at Appleton and Vocation Fields. Although these data have served as the basis for the integrated geologic models, petrophysical and engineering data have been utilized to construct the models as well.

This task also focuses on the use of the integrated geologic model for a low relief paleohigh (Appleton Field example, Figure 252) as a predictive methodology to evaluate the

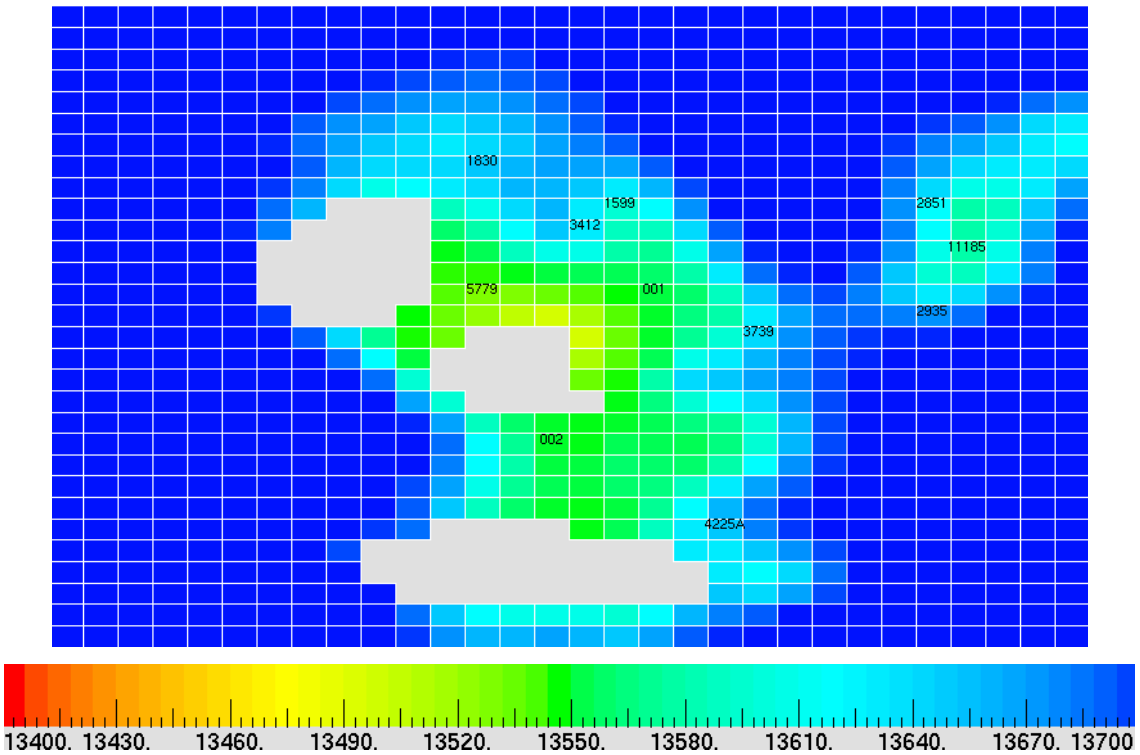

Figure 315 — Map showing well locations and depth to reservoir top, Vocation Field.

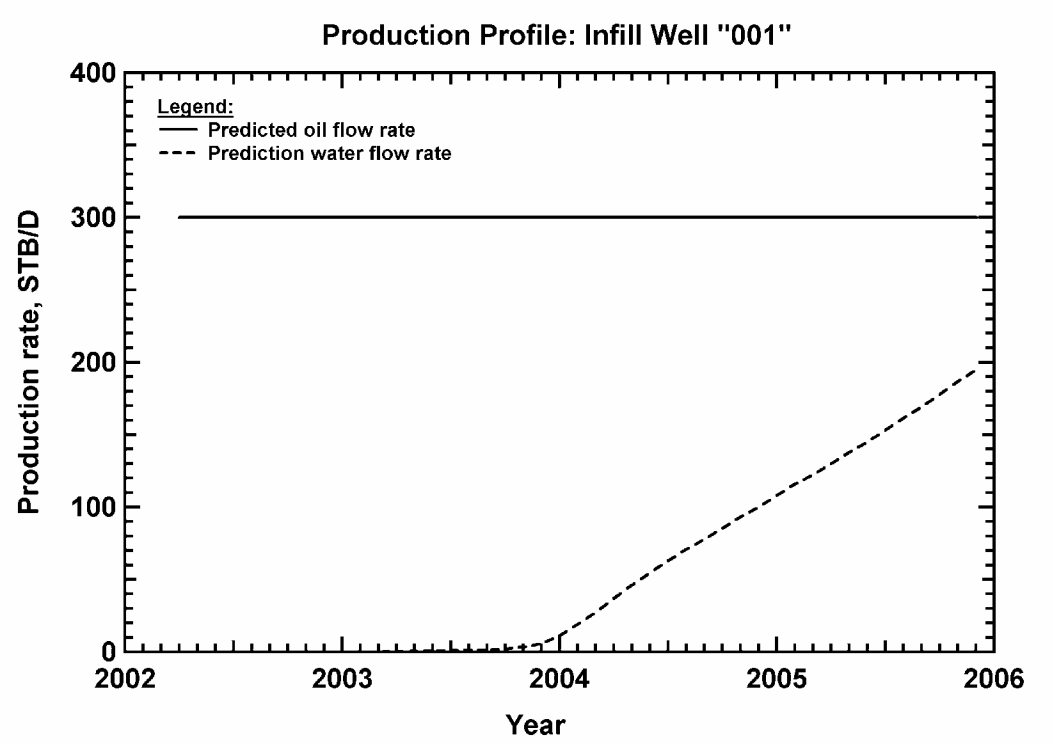

Figure 316 — Oil and water production rates, proposed infill well 001, Vocation Field.

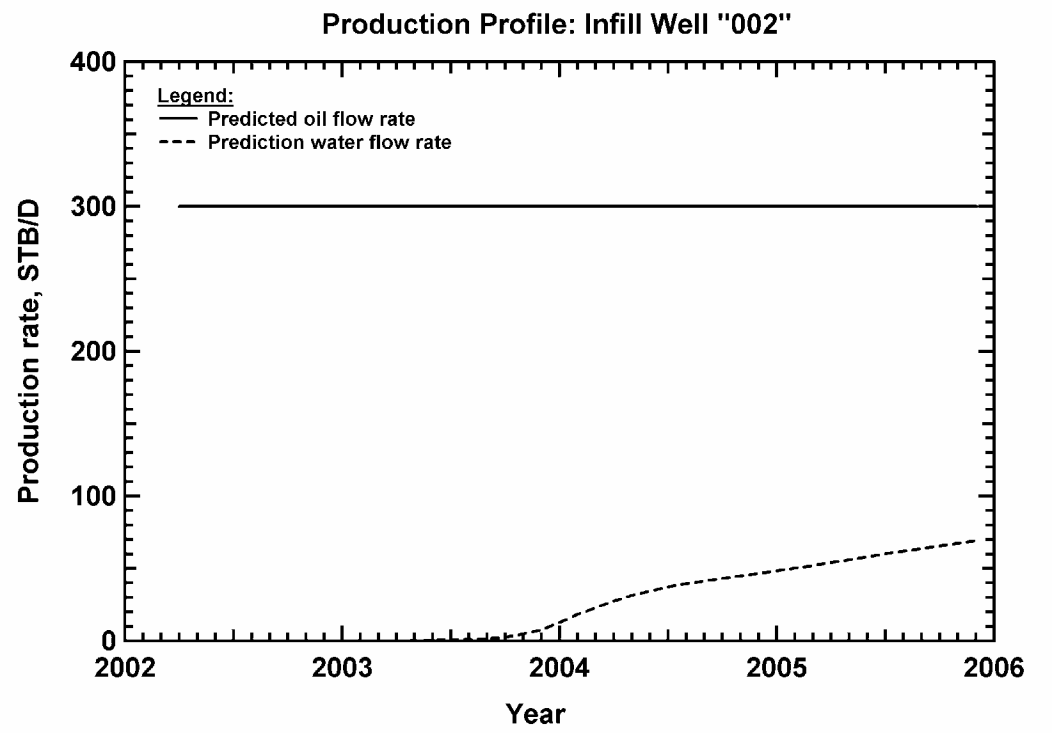

Figure 317 — Oil and water production rates, proposed infill well 002, Vocation Field.

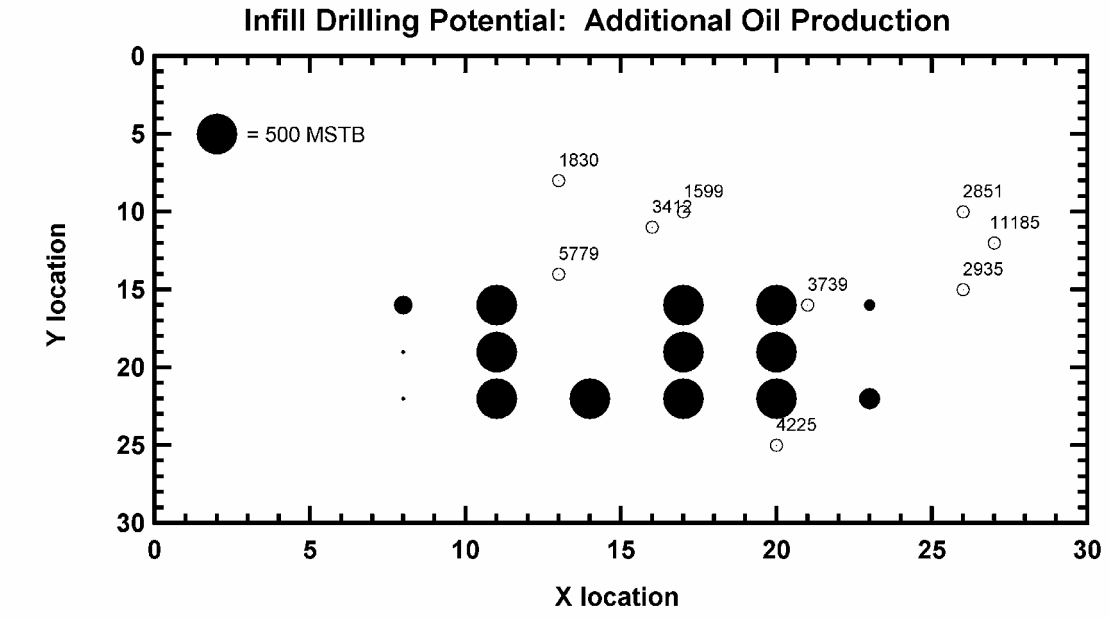

Figure 318 **— Incremental *oil* production via an infill well at various locations, Vocation Field.**

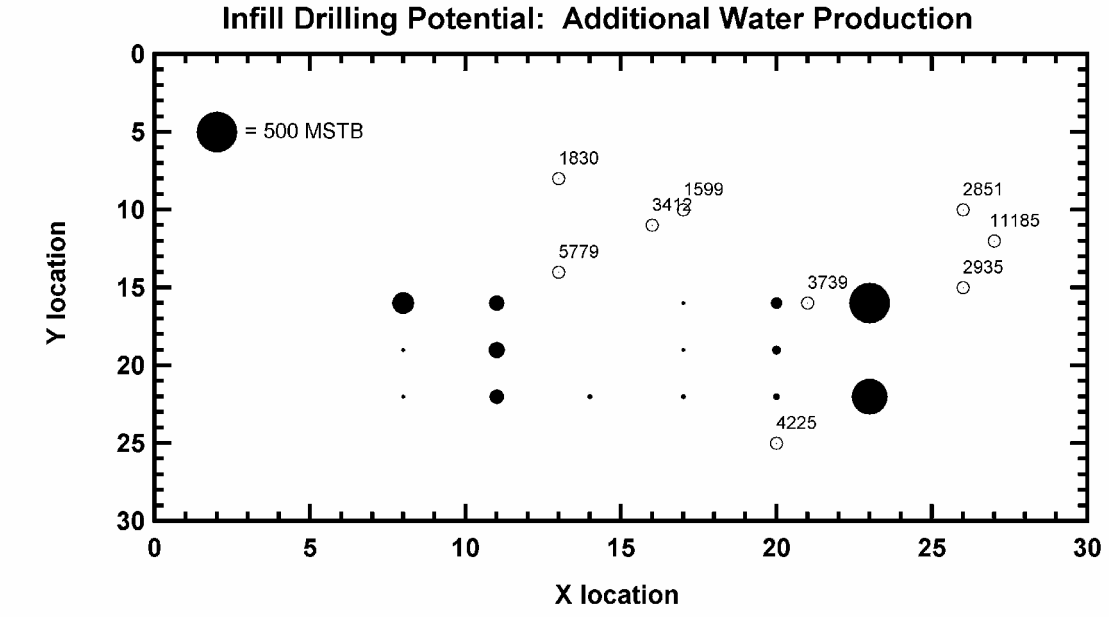

Figure 319 **— Incremental *water* production via an infill well at various locations, Vocation Field.**

potential of a prospective reef-shoal reservoir associated with a basement low-relief paleohigh. Seismic data from the prospective structure and reservoir have been evaluated based upon the model. The model has been used in the interpretation of the seismic data to improve the detection, characterization and imaging of the reservoir and to improve the prediction of reservoir quality in the potential reef-shoal reservoir. The knowledge gained from studying the Appleton reservoir and structure has facilitated this model integration approach. The model has been used to determine whether reef-shoal lithofacies are present on the crest, flanks, or both crest and flanks of this paleohigh. The model has been used to assess whether reef-shoal reservoir porosity is expected on the crest, flank, or crest and flanks of this paleohigh.

This task also applies the integrated geologic models (Figure 263) to the Appleton reservoir and the Vocation reservoir to evaluate the potential for new improved or enhanced oil recovery operations, such as a strategic infill drilling program and/or a waterflood or enhanced oil recovery project in these fields. The geologic models have been applied with emphasis for additional oil recovery from these fields, and the recommendations include the results from the reservoir simulation modeling. The benefits of each modeling approach (the geologic and the reservoir simulation) have been evaluated. Researchers Mancini and Llinas at the University of Alabama have performed these project tasks.

In using the data and analysis from the case study of the Appleton paleohigh and associated Smackover facies as a stratigraphic and structural model for the development of potential thrombolite reservoirs on the crest and flanks of a low-relief paleohigh (Figure 252), predictions as to the hydrocarbon potential of other paleohighs in the thrombolite reservoir play can be made. Figures 320, 321 and 322 were prepared to demonstrate three scenarios involving

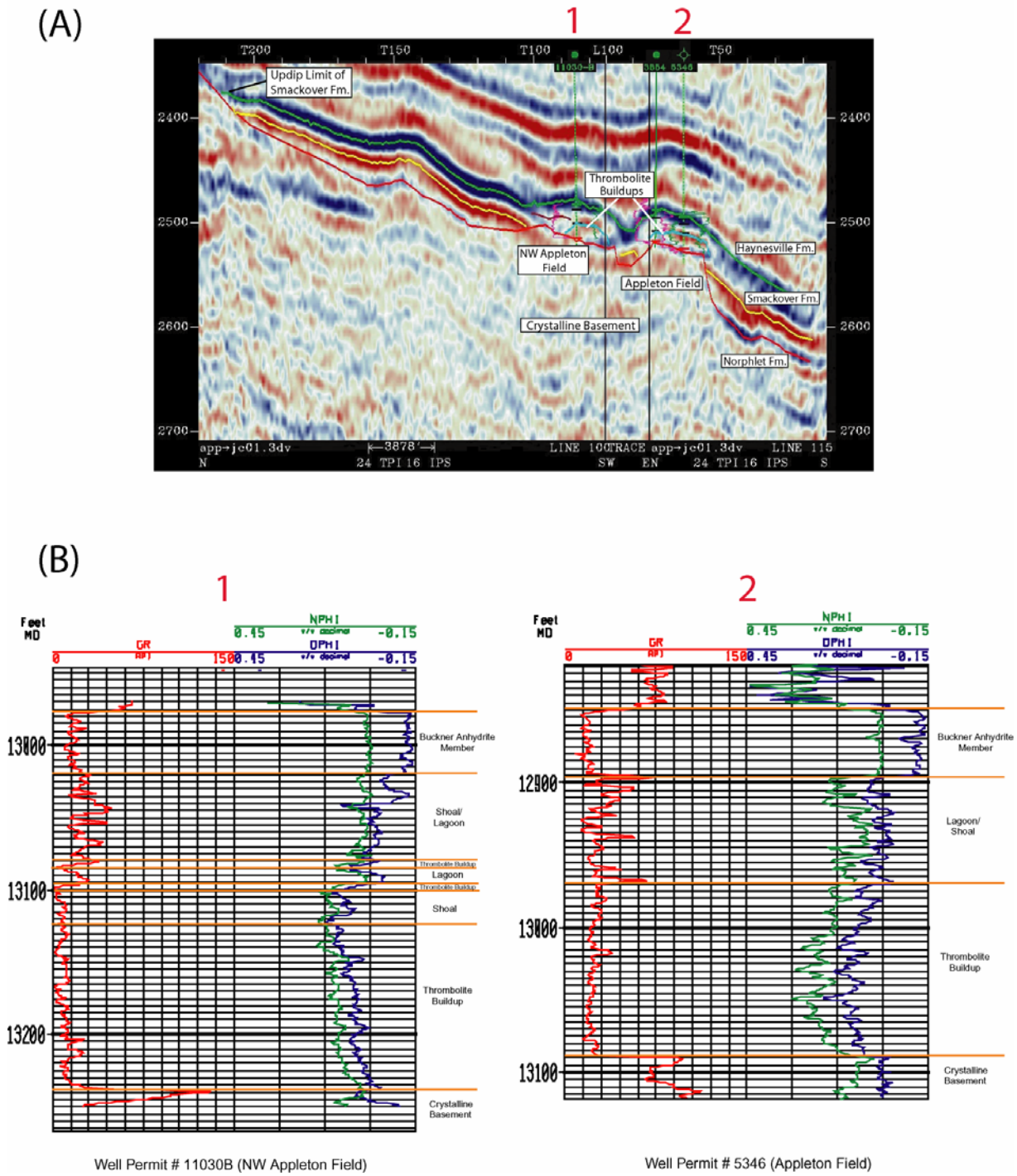

Figure 320. (A) Seismic profile oriented in an approximate dip direction showing the thrombolite buildups on the Appleton and Northwest Appleton paleohighs. Note the termination of Smackover and the underlying Norphlet strata against basement (updip depositional limit of these formations). (B) representative well logs from wells in these fields illustrating the characteristic regular pattern of lower gamma ray (GR) values coupled with relative high neutron (NPHI) and density (DPHI) porosity values for the thrombolite facies (well Permits #11030B and #5346).

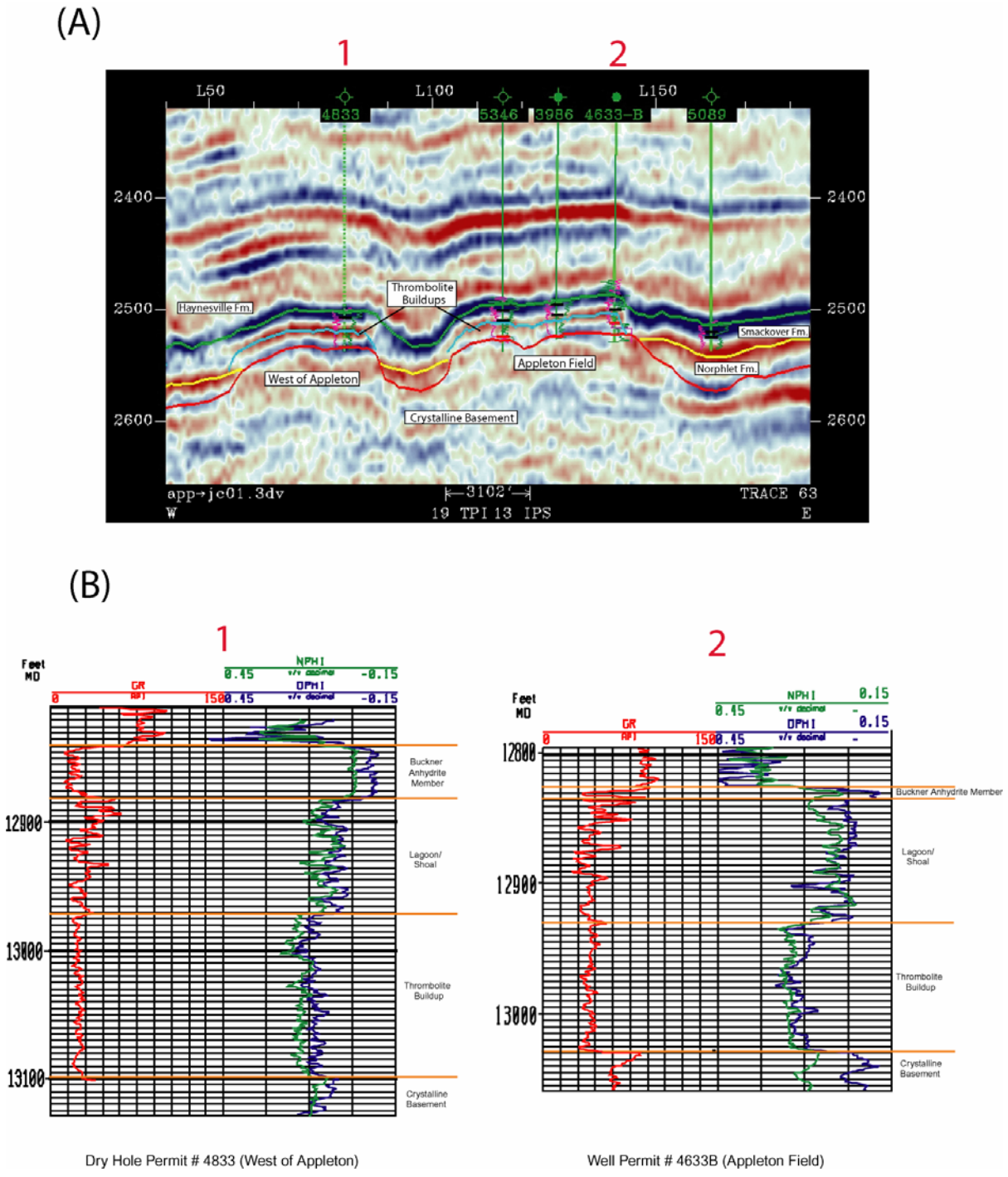

Figure 321. (A) Seismic profile oriented in an approximate strike direction showing the thrombolite buildups on the Appleton paleohigh and on a paleohigh west of Appleton Field, and (B) representative logs from wells for these areas illustrating the characteristic regular pattern of lower gamma ray (GR) values coupled with relative high density (DPHI) and neutron (NPHI) porosity values for the thrombolite facies (dry hole Permit #4833 and well Permit #4633B).

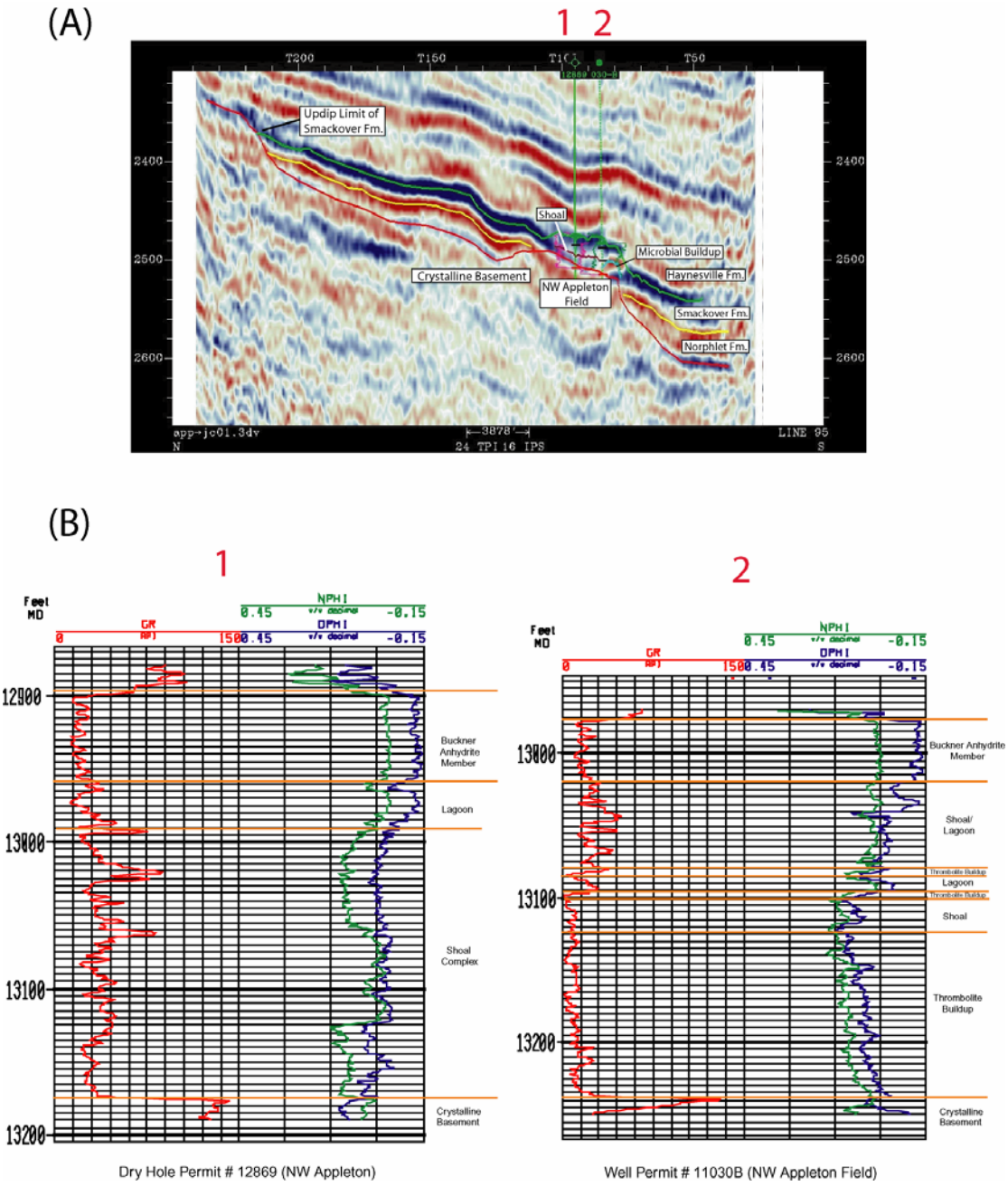

Figure 322. (A) Seismic profile oriented in an approximate dip direction showing the Northwest Appleton paleohigh where thrombolite facies developed on the southern part of this basement high. To the north of Northwest Appleton Field on this paleohigh, the strong reflector that identifies the thrombolite buildup is replaced by a fuzzy low amplitude reflector.
(B) representative logs from wells for these areas. Notice that the dry hole (Permit #12869), located in the area north of Northwest Appleton, shows an irregular pattern of relatively high gamma ray (GR) values and lower density (DPHI) and neutron (NPHI) porosities which may indicate the presence of shoal/lagoon facies.

the variables of present-day structural elevation, and presence or absence of potential thrombolite facies.

The 3-D seismic interpretation for the paleohighs studied uses the criteria for seismic reflection horizon identification and mapping described by Hart and Balch (2000). The top of the Buckner/Smackover interval is identified as a high amplitude peak or positive reflector (Figures 252, 320) formed as the wavelet travels from shaly and sandy deposits of the middle part of the Haynesville Formation to the denser layers of anhydrite of the Buckner Anhydrite Member of the Haynesville Formation and of nonporous and lower porosity carbonate facies of the upper Smackover Formation. The acoustic impedance contrast between the upper nonporous and lower porosity Smackover facies and the underlying higher porosity Smackover thrombolite facies is great enough for a distinct seismic event (a trough, corresponding to a negative reflection coefficient) to be generated across this intraformational contact. On-structure, the thrombolite facies overlies Paleozoic crystalline basement rocks. This unconformity corresponds to a transition from slow velocity (porous, less dense) rocks to fast velocity (nonporous, more dense) rocks that results in a positive reflection coefficient and is manifested as a peak in the seismic reflection data. Variations in amplitude for this reflector are the result of changes in thickness and lateral variations in the thrombolite facies.

Figure 320 compares the Appleton thrombolite buildup over a low-relief paleohigh to a potential thrombolite buildup over a low-relief paleohigh to the northwest of the Appleton feature. Figure 320 shows a mounded geometry configuration for the top of the thrombolite reflector at Appleton Field, and this geometry is also characteristic of this reflector over the crest of the paleohigh northwest of Appleton Field. This feature was drilled in 1996 and penetrated a

total of 38.4 m of thrombolite facies (Figure 320). The discovery well tested 264 BOPD, and led to the establishment of the Northwest Appleton Field, which has produced 592,924 barrels of oil. The presence of the thrombolite boundstone reservoir at Northwest Appleton Field is confirmed by core study. The well log curves from the depth of 13,124 ft (4,000 m) to the depth of 13,238 ft (4,035 m) (and thin intervals above this section) for the discovery well also are consistent with a thrombolite facies. These well log signatures are characterized by a regular pattern of lower gamma ray values, and higher porosity values as determined by density and neutron porosity curves (Figure 320).

Figure 321 compares the Appleton thrombolite buildup to a potential thrombolite buildup over a low-relief paleohigh to the west of the Appleton feature. Figure 321 shows a mounded geometry configuration for the top of the thrombolite reflector for this area. This feature was drilled in 1986 and penetrated 39 m of the thrombolite facies as determined from the well log signature and core study from dry hole Permit #4833. The gamma ray log curve, characterized by a regular pattern of lower values, from the depth of 12,972 ft (3,954 m) to the depth of 13,100 ft (3,993 m) for this dry hole is consistent with a thrombolite facies (Figure 321). The high porosity values as determined by density and neutron porosity curves indicate that the thrombolite facies has reservoir potential in this area. However, as seen from the seismic data (Figure 321), the basement paleohigh is structurally lower today than the Appleton paleohigh, thus resulting in the drilling of a dry hole. The top of the thrombolite buildup is 34.4 m higher in well Permit #4633-B (Appleton Field) than in dry hole Permit #4833 (structure to the west of Appleton). Well Permit #4633-B from Appleton Field has produced 1.16 million barrels of oil.

Figure 322 compares the Northwest Appleton thrombolite buildup to a potential buildup north of the Northwest Appleton Field. The seismic data indicate that the high amplitude trough,

as seen in the seismic data from Northwest Appleton Field, is replaced by a fuzzy low amplitude reflector in this area suggesting that the thrombolite facies is absent (Figure 322). The apparent absence of the thrombolite facies in this area is confirmed by the gamma ray log curve for dry hole Permit #12869 (Figure 322). The gamma ray pattern in this well from the depth of 12,990 ft (3,959 m) to the depth of 13,175 ft (4,016 m) suggests that shoal/lagoon facies instead of thrombolite facies, overlie the Northwest Appleton paleohigh to the north. The gamma ray curve for this interval is irregular rather than regular, and it has higher values than the pattern for the thrombolite facies in this area. The porosity values, as indicated from the density and neutron porosity curves, are relatively lower indicating that the Smackover shoal/lagoon facies has little reservoir potential in this area. Wave and/or current activity and/or sediment influx were probably too high in this area to support thrombolite development. Although, no core data are available to confirm this interpretation, well cuttings from dry hole Permit #12869 support this conclusion.

The results from the geologic modeling and reservoir simulation indicated that additional oil has the potential to be recovered from a strategic infill drilling program in Vocation Field. Potential drill sites are located (1) north of well Permit #4786-B and south of well Permits #1638 and #1691 and (2) southeast of well Permits #1599 and #3412 and northwest of well Permit #3739 (Figures 5, 39, 40, and 315). The strong combination drive of depletion and water in this field suggests that a waterflood program and/or enhanced oil recovery project are not required at this time. Reservoir simulation indicates that 50% of the oil has been recovered at Appleton Field. These results suggest that little oil remains to be recovered from this field. This field benefits from a strong bottom up water drive. Geologic modeling indicates that potential drill sites for the recovery of additional oil at Appleton Field are (1) in the vicinity of well Permits

#3854B, #6247, and #4835B and (2) northwest of well Permit #3854B and south of well Permit #11030B (Figures 4, 19, 20 and 285). Reservoir simulation results support these potential drill sites.

Technology Transfer.--During this project, two technology workshops have been held in Jackson, Mississippi, to transfer the results of this project. These workshops included results from the carbonate reservoir characterization, data integration, carbonate reservoir and structural modeling, and microbial reef detection tasks. Also, the results of this work have been presented at the annual meetings of GCAGS, GCS-SEPM, and AAPG and have been published in the GCAGS Transactions, GCS-SEPM Proceedings, and the AAPG Bulletin. A third workshop will be held to present the results from the application of the integrated geologic model

1. Technology Workshops (2)

Smackover Microbial Reef Detection and Characterization, July 18, 2001, Jackson, Mississippi (conducted by the Eastern Gulf Region of the Petroleum Technology Transfer Council).

Appleton and Vocation Fields Technology Workshop on Reservoir Characterization and Modeling (also included Womack Hill and North Blowhorn Creek Fields), August 14, 2002, Jackson, Mississippi (conducted by the Eastern Gulf Region of the Petroleum Technology Transfer Council).

2. Technical Presentations (31)

Mancini, E.A., 2000, Integrated geoscientific study of Upper Jurassic Smackover reef and carbonate shoal reservoirs associated with a paleotopographic basement structure: Appleton Field, south Alabama, AAPG/EAGE International Research Conference, El Paso, Texas, October 3, 2000.

Parcell, W.C., 2000, Classification of microbial growth forms and fabric in the Smackover Formation, southwest Alabama and implications for reservoir quality, AAPG/EAGE International Research Conference, El Paso, Texas, October 3, 2000.

Parcell, W.C., 2000, Documenting early highstand development of microbial bioherms in the Upper Oxfordian Smackover Formation with a 3-D fuzzy logic stratigraphic simulator, GSA Annual Meeting, Reno, Nevada, November 14, 2000.

Parcell, W.C., 2000, 3-D computer simulation of carbonate depositional facies distribution and productivity rates using continuous set theory to mimic geologists' reasoning, GCAGS Annual Meeting, Houston, Texas, October 26, 2000.

Mancini, E.A., 2001, Application of research to reef detection and exploration, EGR-PTTC Technology Workshop, Jackson, Mississippi, July 18, 2001.

Mancini, E.A., 2001, Integrated carbonate exploration approach for Upper Jurassic Smackover reef and shoal reservoirs, northeastern Gulf of Mexico, AAPG Annual Meeting, Denver, Colorado, June 4, 2001.

Mancini, E.A., 2001, Outcrop analogs for reservoir characterization and modeling of Smackover microbial reefs in the northeastern Gulf of Mexico, Shreveport, Louisiana, October 18, 2001.

Mancini, E.A., 2001, Smackover reef outcrop analogs, EGR-PTTC Technology Workshop, Jackson, Mississippi, July 18, 2001.

Parcell, W.C., 2001, Modeling controls on microbial reefs, EGR-PTTC Technology Workshop, Jackson, Mississippi, July 18, 2001.

Parcell, W.C., 2001, Microbial reef fabric and growth classification, EGR-PTTC Technology Workshop, Jackson, Mississippi, July 18, 2001.

Llinas, J.C., 2002, Influence of paleotopography, eustasy and tectonic subsidence: Upper Jurassic Smackover Formation, Vocation Field, Manila Sub-basin (eastern Gulf Coastal Plain), GCS–SEPM Research Conference, Houston, Texas, December 10, 2002.

Llinas, J.C. 2002, Diagenetic history of the Upper Jurassic Smackover Formation and its effects on reservoir properties: Manila Sub-basin, eastern Gulf Coastal Plain, GCAGS Annual Meeting, Austin, Texas, October 31, 2002.

Llinas, J.C., 2002, Reservoir characterization and modeling, Vocation and Appleton Fields, EGR-PTTC Technology Workshop, Jackson, Mississippi, August 13, 2002.

Llinas, J.C., 2002, New perspectives in the geological interpretation and reservoir characterization of Vocation Field, Alabama, USA, AAPG Annual Meeting, Houston, Texas, March 12, 2002.

Mancini, E.A., 2002, Thrombolitic reef play, northeastern Gulf of Mexico, East Texas Geological Society, Tyler, Texas, July 29, 2002.

Mancini, E.A., 2002, Mesozoic thrombolitic reef play, northeastern Gulf of Mexico, AAPG Annual Meeting, Houston, Texas, March 13, 2002.

Mancini, E.A., 2002, Upper Jurassic Smackover carbonate shoal and reef reservoirs of the eastern Gulf Coastal Plain and outcrop analogs from Western Europe, AAPG Annual Meeting, Houston, Texas, March 14, 2002.

Parcell, W.C., 2002, Correlation of Upper Jurassic carbonate and reef facies across Burgundy and Ardennes platforms, eastern Paris Basin, France, AAPG Annual Meeting, Houston, Texas, March 12, 2002.

Aurell, M., 2003, Use of Upper Jurassic Coral-microbial and thrombolitic reefal buildups of northeast Spain as outcrop analogs for Upper Jurassic coral-microbial and microbial petroleum reservoirs in the U.S. Gulf of Mexico, AAPG International Meeting, Barcelonia, Spain, September 24, 2003.

Llinas, J.C. 2003, Carbonate reservoir facies associated with paleotopographic features: examples from the Upper Jurassic (Oxfordian) Smackover Formation, U.S. Gulf Coastal Plain, AAPG International Meeting, Barcelona, Spain, September 22, 2003.

Llinas, J.C., 2003, Reservoir facies in the Upper Jurassic Smackover Formation and identification of factors that control their distribution in the Vocation Field structure, Manila Sub-basin, eastern Gulf Coastal Plain, AAPG Annual Meeting, Salt Lake City, Utah, May 13, 2003.

Llinas, J.C., 2003, Petroleum exploration for Upper Jurassic Smackover carbonate shoal and microbial reefal lithofacies associated with paleohighs, southwest Alabama, GCAGS Annual Meeting, Baton Rouge, Louisiana, October 23, 2003.

Mancini, E.A., 2003, Upper Jurassic microbial outcrop analogs for characterization of thrombolitic reservoirs in the northern Gulf of Mexico, AAPG Annual Meeting, Salt Lake City, Utah, May 12, 2003.

Mancini, E.A. 2003, Mesozoic thrombolitic reef play, northeastern Gulf of Mexico, AAPG-SPE Eastern Section Meeting, Pittsburgh, Pennsylvania, September 8, 2003.

Morgan, D., 2003, Characterization of complex grainstone-microbial reef reservoirs, Vocation and Appleton Fields, Escambia County, Alabama, AAPG Annual Meeting, Salt Lake City, Utah, May 12, 2003.

Ahr, W., 2004, Microbial buildups as hydrocarbon reservoirs, AAPG Annual Meeting, Dallas, Texas, April 19, 2004.

Aurell, M., 2004, Use of Upper Jurassic coral-microbial and thrombolite reef buildups of northeast Spain as outcrop analogs for Upper Jurassic microbial reef petroleum reservoirs, AAPG Annual Meeting, Dallas, Texas, April 19, 2004.

Badali, M., 2004, Lower Cretaceous microbial deposits, northeastern Gulf of Mexico, AAPG Annual Meeting, Dallas, Texas, April 19, 2004.

Llinas, J.C. 2004, Controlling factors on the occurrence of microbial buildups in the Upper Jurassic Smackover, eastern Gulf Coastal Plain, AAPG Annual Meeting, Dallas, Texas, April 19, 2004.

Mancini, E.A., 2004, Upper Jurassic shallow water thrombolites from the northeastern Gulf of Mexico, AAPG Annual Meeting, Dallas, Texas, April 19, 2004.

Tebo, J., 2004, 3-D seismic imaging of porosity in Jurassic carbonates: Smackover Formation, southern Alabama, AAPG Annual Meeting, Dallas, Texas, April 19 2004.

3. Technical Publications (40)

Mancini, E.A., Benson, D.J. and Hart, B.S., 2000, Integrated geoscientific study of Upper Jurassic Smackover reef and carbonate shoal reservoirs associated with a paleotopographic basement structure: Appleton Field, south Alabama, AAPG/EAGE International Research Conference, Program and Abstracts Volume, p. 43.

Parcell, W.C., 2000, Classification of microbial growth forms and fabric in the Smackover Formation, southwest Alabama and implications for reservoir quality, AAPG/EAGE International Research Conference, Program and Abstracts, Volume, p. 49.

Parcell, W.C., 2000, Documenting early highstand development of microbial bioherms in the Upper Oxfordian Smackover Formation with a 3-D fuzzy logic stratigraphic simulator, GSA Annual Meeting, Reno, Abstracts with Programs, p. A-176.

Parcell, W.C., 2000, 3-D computer simulation of carbonate depositional facies distribution and productivity rates using continuous set theory to mimic geologists' reasoning, AAPG Bulletin, Volume 84, p. 1688.

Parcell, W.C., 2000, 3-D computer simulation of carbonate depositional facies distribution and productivity rates using continuous set theory to mimic geologists' reasoning, GCAGS Transactions, Volume 50, p. 439-450.

Mancini, E.A. and Parcell, W.C., 2001, Smackover reef detection and exploration, EGR-PTTC Technology Workshop, Book, 206p.

Mancini, E.A. and Parcell, W.C., 2001, Integrated carbonate exploration approach for Upper Jurassic Smackover reef and shoal reservoirs, northeastern Gulf of Mexico, AAPG 2001 Abstract Volume, p. A124.

Mancini, E.A., and Parcell, W.C. 2001, Outcrop analogs for reservoir characterization and modeling of Smackover microbial reefs in the northeastern Gulf of Mexico area, GCAGS Transactions Volume 51, 207-228.

Mancini, E. A. and others, 2001, Integrated geologic-engineering model for reef and carbonate shoal reservoirs associated with paleohighs: Upper Jurassic Smackover Formation, northeastern Gulf of Mexico, DOE Project Technical Report, Year 1, 92 p.

Llinas, J.C. 2002, Influence of paleotopography, eustasy and tectonic subsidence: Upper Jurassic Smackover Formation, Vocation Field, Manila Sub-basin (eastern Gulf coastal Plain), GCS-SEPM 2002 Research Conference Proceedings Volume, p. 383-401.

Llinas, J.C. 2002, Diagenetic history of the Upper Jurassic Smackover Formation and its effects on reservoir properties: Manila Sub-basin, eastern Gulf Coastal Plain, GCAGS Transactions, Volume 52, p. 631-644.

Llinas, J.C., 2002, Influence of paleotopography, eustasy and tectonic subsidence: Upper Jurassic Smackover Formation, Vocation Field, Manila Sub-basin (eastern Gulf Coastal Plain), GCS–SEPM Research Conference, Program and Abstracts, p. 27.

Llinas, J.C. 2002, Diagenetic history of the Upper Jurassic Smackover Formation and its effects on reservoir properties: Manila Sub-basin, eastern Gulf Coastal Plain, GCAGS Annual Meeting, Program and Abstracts, p. 92.

Mancini, E.A. and others, 2002, Integrated geologic-engineering model for reef and carbonate shoal reservoirs associated with paleohighs: Upper Jurassic Smackover Formation, northeastern Gulf of Mexico, DOE Project Technical Report, Year 2, 229 p.

Parcell, W.C. 2002, Sequence stratigraphic controls on development of microbial fabrics and growth forms-implications for reservoir quality in the Upper Jurassic (Oxfordian) Smackover Formation, eastern Gulf Coast, U.S.A., Carbonates and Evaporites, Volume 17, p. 166-181.

Llinas, J.C., 2002, Reservoir characterization and modeling, Vocation and Appleton Fields, EGR-PTTC Technology Workshop Book, 31p.

Llinas, J.C., 2002, New perspectives in the geological interpretation and reservoir characterization of Vocation Field, Alabama, USA, AAPG 2002 Abstract Volume, p. A105.

Mancini, E.A., 2002, Thrombolitic reef play, northeastern Gulf of Mexico, East Texas Geological Society Publication, p.2.

Mancini, E.A., Parcell, W.C., Badali, M., and Llinas, J.C., 2002, Mesozoic thrombolitic reef play, northeastern Gulf of Mexico, AAPG 2002 Abstract Volume, p. A111.

Mancini, E.A., and Parcell, W.C., 2002, Upper Jurassic Smackover carbonate shoal and reef reservoirs of the eastern Gulf Coastal Plain and outcrop analogs from Western Europe, AAPG 2002 Abstract Volume, p. A110.

Parcell, W.C., 2002, Correlation of Upper Jurassic carbonate and reef facies across Burgundy and Ardennes platforms, eastern Paris Basin, France, AAPG 2002 Abstract Volume, p. A136.

Aurell, M., Badenas, B., Mancini, E A., Parcell, W.C., and Llinas, J.C., 2003, Use of Upper Jurassic Coral-microbial and thrombolitic reefal buildups of northeast Spain as outcrop analogs for Upper Jurassic coral-microbial and microbial petroleum reservoirs in the U.S. Gulf of Mexico, AAPG International 2002 Abstract Volume, p. A5.

Llinas, J.C., 2003, Carbonate reservoir facies associated with paleotopographic features: examples from the Upper Jurassic (Oxfordian) Smackover Formation, U.S. Gulf Coastal Plain, AAPG International 2002 Abstract Volume, p. A55.

Llinas, J.C., 2003, Reservoir facies in the Upper Jurassic Smackover Formation and identification of factors that control their distribution in the Vocation Field structure, Manila Sub-basin, eastern Gulf Coastal Plain, AAPG 2003 Abstract Volume, p. A106.

Llinas, J.C., 2003, Petroleum exploration for Upper Jurassic Smackover carbonate shoal and microbial reefal lithofacies associated with paleohighs, southwest Alabama, GCAGS Transactions Volume. 53, p. 462-474.

Llinas, J.C., 2003, Petroleum exploration for Upper Jurassic Smackover carbonate shoal and microbial reefal lithofacies associated with paleohighs, southwest Alabama, GCAGS Annual Meeting, Program and Abstracts, p. 14-15.

Mancini, E.A., 2003, Upper Jurassic microbial outcrop analogs for characterization of thrombolitic reservoirs in the northern Gulf of Mexico, AAPG 2003 Abstract Volume, p. A112.

Mancini, E.A. and others, 2003, Integrated geological-engineering model for reef and carbonate shoal reservoirs associated with paleohighs: Upper Jurassic Smackover Formation, northeastern Gulf of Mexico, DOE Project Technical Report Year 3, 121p.

Mancini, E.A. 2003, Mesozoic thrombolitic reef play, northeastern Gulf of Mexico, AAPG-SPE Eastern Section Meeting, Program and Abstracts, p. 8.

Morgan, D., and Ahr, W., 2003, Characterization of complex grainstone-microbial reef reservoirs, Vocation and Appleton Fields, Escambia County, Alabama, AAPG 2003 Abstract Volume, p. A123.

Morgan, D., 2003, Mapping and ranking flow units in reef and shoal reservoirs associated with paleohighs: Upper Jurassic (Oxfordian) Smackover Formation, Appleton and Vocation Fields, Escambia and Monroe Counties, Alabama, M.S. thesis, Texas A&M University, 157 p.

Parcell, W.C., 2003, Evaluating the development of Upper Jurassic reefs in the Smackover Formation, eastern Gulf Coast, U.S.A. through fuzzy logic computer modeling, JSR, Volume 72, p. 498-515.

Tebo, J.M., 2003, Use of volume-based 3-D seismic attribute analysis to characterize physical property distribution: a case study to delineate reservoir heterogeneity at the Appleton Field, S.W. Alabama, M.S. thesis, McGill University, 169 p.

Ahr, W., and Morgan, D., 2004, Microbial buildups as hydrocarbon reservoirs, AAPG 2004 Abstract Volume, in press.

Aurell, M., Badenas B., Mancini, E.A. Parcell, W.C. and Llinas, J.C. 2004, Use of Upper Jurassic coral-microbial and thrombolite reef buildups of northeast Spain as outcrop analogs for Upper Jurassic microbial reef petroleum reservoirs, AAPG 2004 Abstract Volume, in press.

Badali, M., 2004, Lower Cretaceous microbial deposits, northeastern Gulf of Mexico, AAPG Volume, in press.

Llinas, J.C. 2004, Controlling factors on the occurrence of microbial buildups in the Upper Jurassic Smackover, eastern Gulf Coastal Plain, AAPG Abstract Volume, in press.

Mancini, E.A., Llinas, J.C. and Parcell, W.C. 2004, Upper Jurassic shallow water thrombolites from the northeastern Gulf of Mexico, AAPG Abstract Volume, in press.

Tebo, J., and Hart, B.S., 2004, 3-D seismic imaging of porosity in Jurassic carbonates: Smackover Formation, southern Alabama, AAPG Abstract Volume, in press.

Llinas, J.C., 2004, Identification, characterization and modeling of Upper Jurassic Smackover carbonate deposits and facies and reservoirs associated with basement paleohighs: Vocation Field, Appleton Field, Northwest Appleton Field areas, Alabama, Ph.D. dissertation, University of Alabama, in progress.

DISCUSSION AND RESULTS

Upper Jurassic microbial (formerly called “blue-green algae” or cyanobacteria) mounds in the northeastern Gulf of Mexico have been documented by numerous researchers (Baria et al., 1982; Crevello and Harris, 1984; Powers, 1990; Markland, 1992; Benson et al., 1996; Kopaska-Merkel, 1998, 2002; Parcell, 1999, 2000, 2002; Hart and Balch, 2000; Mancini et al., 2000; Mancini and Parcell, 2001; Llinás, 2002a,b). The thrombolite facies associated with these buildups are hydrocarbon productive from the Oxfordian Smackover Formation in numerous fields in the eastern Gulf Coastal Plain (Figure 323). The most studied of these fields are Melvin Field (Baria et al., 1982), Vocation Field (Baria et al., 1982; Powers, 1990; Parcell, 2000; Llinás, 2002a,b) and Appleton Field (Markland, 1992; Benson et al., 1996; Mancini and Benson, 1998; Parcell, 2000; Hart and Balch, 2000; Mancini et al., 2000). The reservoir facies at Appleton Field consists essentially of microbial (thrombolite) boundstone (Benson et al., 1996; Mancini et al., 2000). Crevello and Harris (1984) reported that Smackover stromatolite (microbolite) mounds are primarily restricted to the eastern Gulf Coastal Plain. Also, Dobson and Buffler (1997) recognized Smackover mounds on seismic profiles for the northeastern Gulf of Mexico area. The basis for the restriction of microbial mound development to the northeastern Gulf of Mexico was postulated by Parcell (2003) to be the result of a combination of local substrate and basement relief elements, regional sedimentologic and water depth, energy and chemistry conditions and global oceanographic, climatic and latitude factors prevalent in this area during the Late Jurassic.

Although Upper Jurassic Smackover microbial buildups (Figure 324A) have been an exploration target in the northeastern Gulf of Mexico for over 30 years, new field discoveries continue to be made in this area indicating that the development of these buildups is not completely understood and that the organosedimentary aspects of these deposits have not been

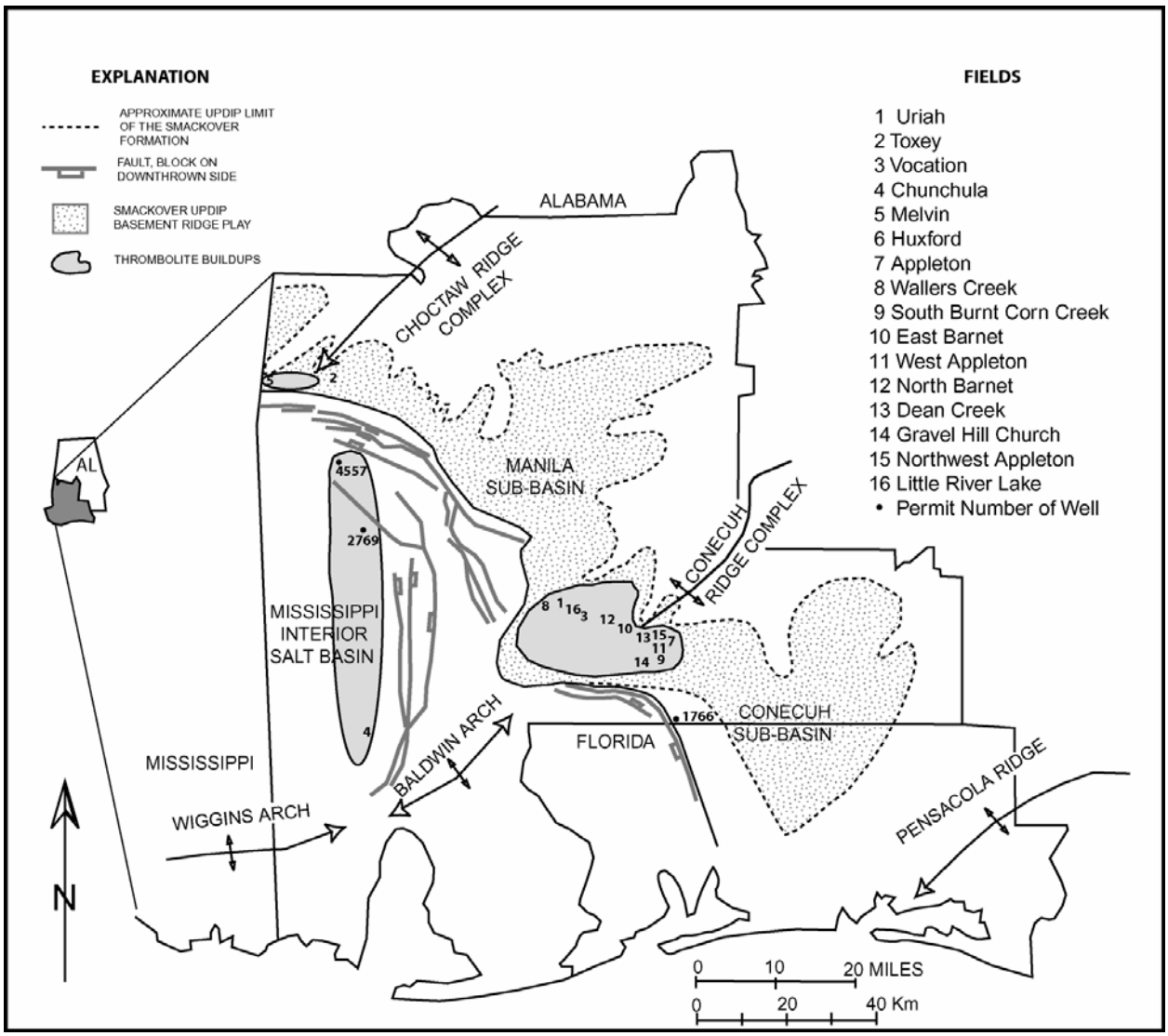

Figure 323. Location map showing major structural features, trend of the Smackover updip basement ridge play, distribution of major thrombolite buildups, and key oil fields with thrombolite facies in southwest Alabama.

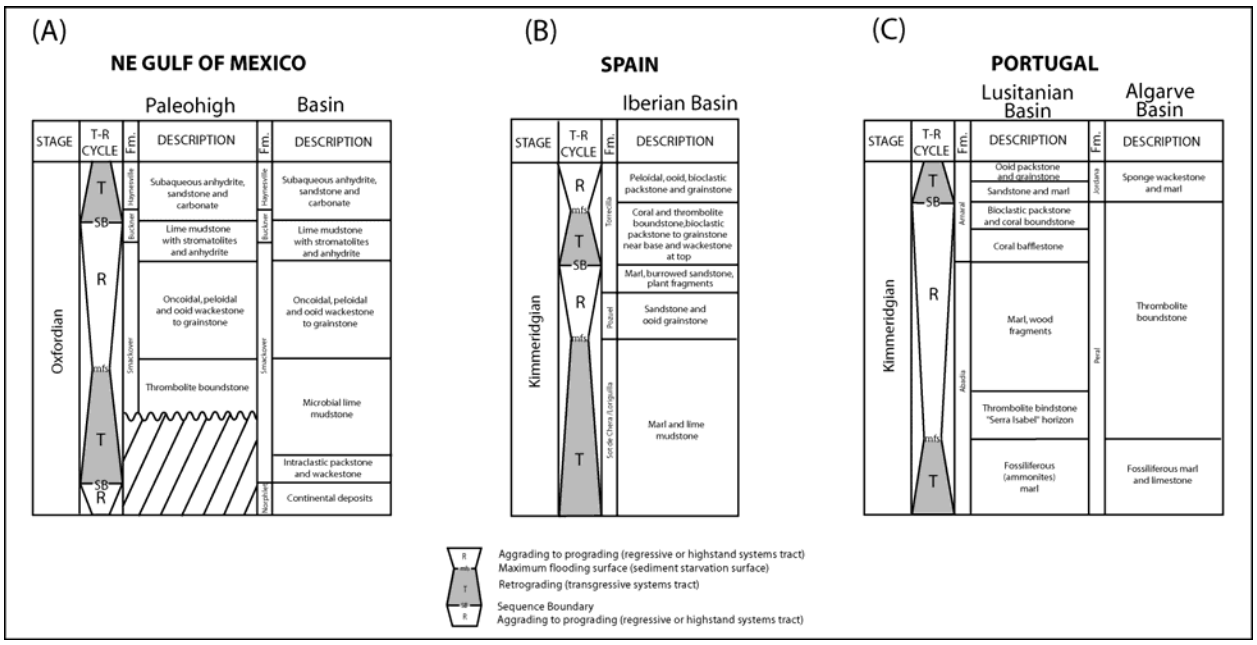

Figure. 324. Comparison of Upper Jurassic stratigraphy for: (A) the northeastern Gulf of Mexico, (B) Iberian Basin, Spain, and (C) Lusitanian and Algarve Basins, Portugal (modified from Leinfelder et al., 1993a; Aurell and Bádenas, 1997; Mancini and Parcell, 2001).

adequately studied. On the other hand, the characteristics of Upper Jurassic thrombolite bioherms and reefs have been studied extensively in outcrop, especially in Portugal and Spain, by Leinfelder (1986), Ramalho (1988), Fezer (1988), Leinfelder (1993), Leinfelder et al. (1993a,b), Leinfelder et al. (1994), Nose (1995), Aurell and Bádenas (1997) and Bádenas (1999), and the results of these outcrop studies, which included such topics as the origin, composition, geometries, areal extent, and facies relationships affecting thrombolite bioherms and reefs, have not been widely applied to the Upper Jurassic thrombolite buildups in the Gulf of Mexico area, nor have the results of these outcrop studies been used effectively in the design of exploration strategies to identify and delineate potentially new hydrocarbon-bearing thrombolite buildups in the updip basement ridge play.

The updip basement ridge play is defined as the area between the updip limit of Smackover deposition and the regional peripheral fault trend (Mancini et al., 1991). The play is characterized by thin or absent Jurassic salt, and the hydrocarbon structures are related to pre-Jurassic paleotopographic features. Petroleum traps are structural anticlines and faulted anticlines that are developed in association with Paleozoic crystalline basement paleohighs. Reservoir facies are shoreface and shoal grainstone and thrombolite boundstone. The source of the hydrocarbons found in these reservoirs is Smackover basinal lime mudstone, and the migration pathway of the oil is from the basin centers of the Manila and Conecuh subbasins updip, with entrapment in the paleohighs. The petroleum seal rocks are generally Kimmeridgian Buckner anhydrite beds that overlie the Smackover Formation. The thrombolite reservoir play consists of those paleohighs on which thrombolite reservoir facies developed.

According to Riding and Awramik (2000), microbes are abundant and widespread in sediments, carbonate and siliciclastic. They are microscopic and include bacteria, algae, fungi

and protozoans. These organisms stabilize grains and provide for mineral nucleation; thus, they modify and create sediment. They range in geologic age from the Proterozoic to today (Riding, 1991).

Microbolites are organosedimentary deposits that are a result of the activity of microbes. Microbes can stabilize loose sediment, and microbial coatings on sediment surfaces can serve to protect the sediment from erosion. Microbial mats and biofilms consist of microbial communities, primarily cyanobacteria (which are photosynthetic), other microbes (which can be chemosynthetic and anaerobic), and foraminifera that colonize a surface (Stolz, 2000). There is interaction between the microbes, the colonized surface, and the surrounding environment.

Stolz (2000) considered the microbial mats as complex biofilms and described the biofilms as consisting of micro-organisms and their intracellular products that are bound to a solid surface. Biofilms are recognized from microbial mats in that they form on solid substrates such as rock. Beneath the surface layer of a microbial mat, a layer composed of cyanobacteria is found (Stolz, 2000). This layer is where photosynthesis occurs. Underlying this layer, a transition of anoxic conditions occurs. Anoxygenic phototrophs occur in this layer. Heterogeneity is common within these distinct layers. Thus, Stolz (2000) views a biofilm as a mass of microcolonies surrounded by a matrix of extracellular polymeric molecules, which is honeycombed with water channels. The water channels and the associated convective flow facilitate nutrient delivery and waste removal.

Microbial structures characterized by a mesoscopic clotted internal fabric are called thrombolites (Aitken, 1967; Kennard and James, 1986). The clots are interpreted as primary features produced by calcified microbes. Thrombolites are interpreted as microcolonies of coccoid-dominated calcimicrobes, such as *Girvanella* and *Renalcis*, (Kennard and James, 1986).

The clotted fabric is primarily a microbial feature and not a disrupted or modified laminated fabric; however, the clotted fabric can be enhanced by physical damage in high-energy conditions and by bioerosion. Calcium carbonate precipitation can be facilitated by an increase in carbonate alkalinity according to Knorre and Krumbein (2000). Increased carbonate alkalinity can be induced by microbes as a by-product of physiological activities (Knorre and Krumbein, 2000). Cyanobacterial photosynthesis, thus, can promote carbonate precipitation of micrite (Golubic et al., 2000). In situ, microbial calcification has been associated commonly with thrombolites, while agglutination of allochthonous grains has been associated with stromatolites (Kennard and James, 1986). However, both organosedimentary deposits can be produced by either process (Braga et al., 1995). Sediment trapping can be accomplished by thrombolites and calcification can be achieved by stromatolites. Episodic sediment trapping has been shown to produce either fabric with an uneven pattern of accretion favoring a clotted fabric and an even pattern of accretion favoring a laminated fabric (Braga et al., 1995). Leiolites (microbial structureless or dense macrofabric) formed where a steady uniform supply of well-sorted sediment was provided to the area colonized by the microbes (Braga et al., 1995).

Key papers in the development of a classification for microbial and thrombolite structures are as follows. Aitken (1967) proposed a field classification for cryptalgal biolithites, which included oncolites, stromatolites, thrombolites and crytalgalaminates. Cryptalgal was defined as sedimentary rocks or structures originating through sediment-binding and/or carbonate-precipitating activities of non-skeletal algae. Aitken (1967) used the term thrombolite to describe cyptalgal structures related to stromatolites (as defined by Kalkowsky, 1908) that lacked lamination and were characterized by a macroscopic clotted fabric.

Kennard and James (1986) proposed a tripartite field classification of lower Paleozoic microbial structures based on the dominant type of constructive mesoscopic constituent. The three end members were stromatolites, thrombolites and undifferentiated microbial boundstones. Stromatolites were described as laminated organosedimentary structures built by episodic sediment-trapping, sediment-binding and/or carbonate-precipitating activity of microbial communities. Thrombolites were described by Kennard and James (1986) as lacking lamination and characterized by a mesoscopic clotted fabric. Thrombolites were recognized to have a distinct internal structure consisting of clots separated by patches of mud and sand-size sediment or calcite cement. The individual clots or mesoclots were described as typically dark in color and having a micritic, microcrystalline structure.

Braga et al. (1995) used a classification of laminated (stromatolite), clotted (thrombolite) and structureless and dense (leiolite) to describe the macrofabric of late Miocene microbial biostromes and bioherms. They recognized that stromatolitic lamination can form by regular episodic accretion, involving particle trapping, microbial growth and/or precipitation. The lamination was described as the primary feature. Thrombolites can form by microbial calcification and/or agglutination of particles (Braga et al., 1995). The clots of the thrombolites were recognized as the primary features produced by calcified microbes or the clots can be a result of an alteration or disturbance of stromatolite fabrics. Thus, Braga et al. (1995) believed that stromatolites and thrombolites in the late Miocene were basically formed by similar combined processes of agglutination of sediment grains together with microbial calcification.

Schmid (1996) and Leinfelder and Schmid (2000) recognized three basic fabrics of Jurassic microbolites. Schmid (1996) uses the term microbolite rather than microbialite as per the recommendation of Riding (1991). The fabrics included stromatolites (laminated), thrombolites

(clotted) and leiolites (unstructured). Using these basic fabric types, a tripartite classification of Upper Jurassic microbolites at the microscopic scale (millimeters) based on the end members of peloidal microstructure, laminated particle microstructure, and dense microstructure was proposed by Schmid (1996) and Leinfelder et al. (1996). Schmid (1996) published a compilation of growth forms at the macroscopic scale (centimeters to kilometers), which included bioherms, patch reefs, conical patch reefs, biostromes, isolated crusts, and oncoids, and at the mesoscopic scale (centimeters), which included massive, columnar, dendroid, flat, platy, reticulate, hemispheroid, and basal cover crust.

Parcell (2000, 2002) used a classification of microbial facies to study Upper Jurassic microbolites in the subsurface. He used the following end members thrombolite, stromatolite and leiolite after Braga et al. (1995) and Schmid (1996). A calcimicrobe growth form classification at the centimeter scale was used to recognize five dominant forms: laminated (layered) thrombolite, reticulate (chaotic) thrombolite, dendritic (dendroidal or branching) thrombolite, encrusting stromatolite, and oncoidal cortexes after Schmid (1996). The layered thrombolites were characterized by a clotted fabric that consists of dark-colored horizontal microbial laminae with abundant crypts (millimeter to centimeter scale) and were usually bioturbated. The chaotic and dendroidal thrombolites were described as having a clotted fabric and a vertical growth component (stronger in the dendroidal form) and much interstitial sediment associated with these forms. The encrusting stromatolite form was recognized to lack a clotted fabric and represented essentially horizontal growth. Oncoids served as stable nucleation points for the development of the microbial oncoidal cortexes.

This study utilizes the classification of Upper Jurassic thrombolite fabrics (peloidal and micritic or dense) and growth forms (layered, chaotic, and dendroidal or branching) of Parcell

(2000, 2002), which builds on the classifications of Aitken (1967), Kennard and James (1986), Braga et al. (1995), and Schmid (1996).

As described in this report, Upper Jurassic (Oxfordian) Smackover thrombolite buildups developed on paleotopographic features (Paleozoic basement paleohighs or Jurassic salt anticlines and ridges) in the northern Gulf of Mexico. Major basement ridges include the Choctaw Ridge Complex (Melvin Field), Conecuh Ridge Complex (Vocation and Appleton Fields), and the Wiggins Arch (Mancini and Benson, 1980) (Figure 323). These paleotopographic highs interrupted the depositional surface of the inner portion of a Smackover distally steepened ramp setting. The Smackover carbonates accumulated during an overall eustatic rise in Jurassic sea level. Lower Smackover intertidal oncoidal and peloidal packstone and wackestone were deposited during the initial rise in sea level (Figure 324). Middle Smackover subtidal microbial lime mudstone and peloidal wackestone accumulated as the rate of sea level rise and amount of accommodation space increased. Upper Smackover shoal ooid, peloidal, and oncoidal grainstone and peloidal packstone and intertidal lime mudstone were deposited as the rate of sea level rise and the amount of accommodation space decreased.

Early descriptions of Smackover buildups in the Gulf Coastal Plain (Arkansas to Florida) were by Baria et al. (1982). These authors report that nearly all the buildups found in the eastern part (Alabama and Florida) of the trend have been at the base of the upper Smackover interval (in association with the maximum flooding surface) and in the western part (Arkansas and Louisiana) of the trend the buildups occur within the upper Smackover interval. The organosedimentary buildups in the eastern Gulf have depositional relief and are elongate features, 3 to 40 m in thickness, covering an area of some 8 km^2 (1.6 km in width and 5 km in length) (Crevello and Harris, 1984). The buildups have been described as stromatolitic algal

mounds dominated by laminated stromatolites with pelleted thrombolite growth forms (Crevello and Harris, 1984). These mounds in the eastern Gulf consist of digitate and branching blue-green algae (cyanobacteria), *Tubiphytes* and marine cements, and the reefal buildups to the west have a more diverse coral-algal assemblage of corals (*Actinostrea*), skeletal algae (*Parachaetetes* and *Cayeuxia*), lithistid and hexactinellid sponges, bryozoans and hydrozoans (Baria et al., 1982).

Our work has focused on the microbolites, mainly thrombolites, in the eastern Gulf Coastal Plain. This effort builds on the initial work of Powers (1990), Markland (1992), and Benson et al. (1996). In this area, microbolites include basinal microbial laminates that occur in the middle Smackover section, lagoonal stromatolites and oncoidal cortexes that generally are found in the upper part of the upper Smackover, and shallow water (less than 10 m in water depth) thrombolites that occur in the upper part of the middle Smackover section and the lower part of the upper Smackover section (Figure 324A). The basinal microbial laminates are the petroleum source rocks for Smackover hydrocarbons, including the Smackover oil discovered in the Upper Jurassic thrombolite reservoir play of the northeastern Gulf of Mexico (Claypool and Mancini, 1989). The thrombolites include layered (Figure 325A), dendroidal (Figure 325B), chaotic (Figures 325C, 325D, and 326A) growth forms. The microstructure of the thrombolite boundstone is peloidal and dense micrite. Encrusting stromatolites are also present (Figure 326B).

Geographically, we have studied thrombolites occurring in the eastern part of the Mississippi Interior Salt Basin, the Manila Subbasin and the Conecuh Subbasin (Figure 323). In the Mississippi Interior Salt Basin, thrombolite buildups developed on faulted Paleozoic basement blocks (Melvin Field) (Baria et al., 1982) and on salt features (ridges, anticlines) along the eastern margin of the Mississippi Interior Salt Basin (Kopaska-Merkel and Mann, 2000;

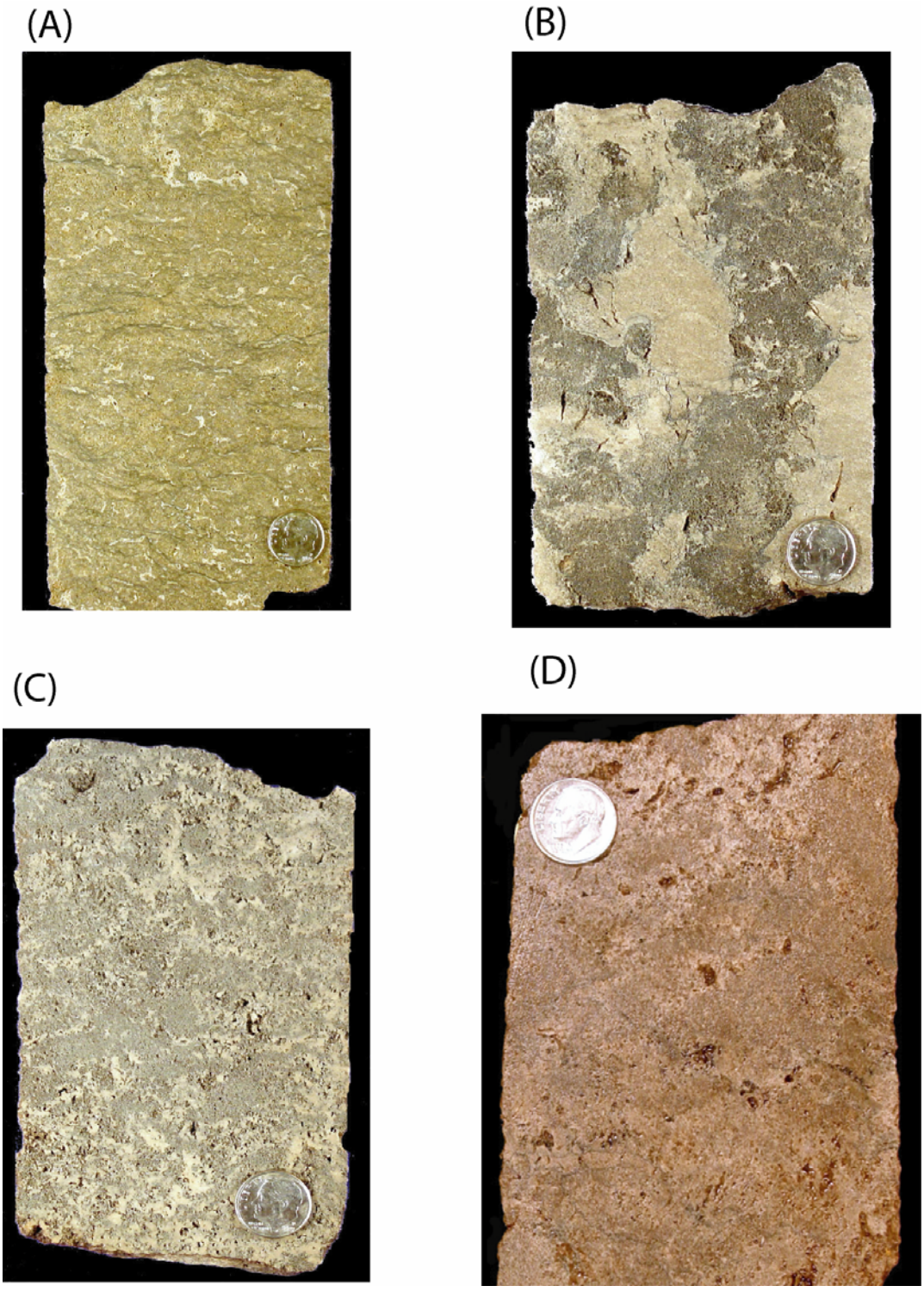

Figure 325. Core photographs of Smackover microbolite mesostructure: (A) layered thrombolite, well Permit #3986, depth 3,969 m (13,021 ft), Appleton Field, (B) dendroidal thrombolite, well Permit #3986, depth 3,954 m (12,971 ft), Appleton Field, (C) chaotic thrombolite, well Permit #4633-B, depth 3,683 m (12,083 ft), Appleton Field, (D) chaotic thrombolite, well Permit 11030-B, depth 4,006 m (13.144 ft), Northwest Appleton Field.

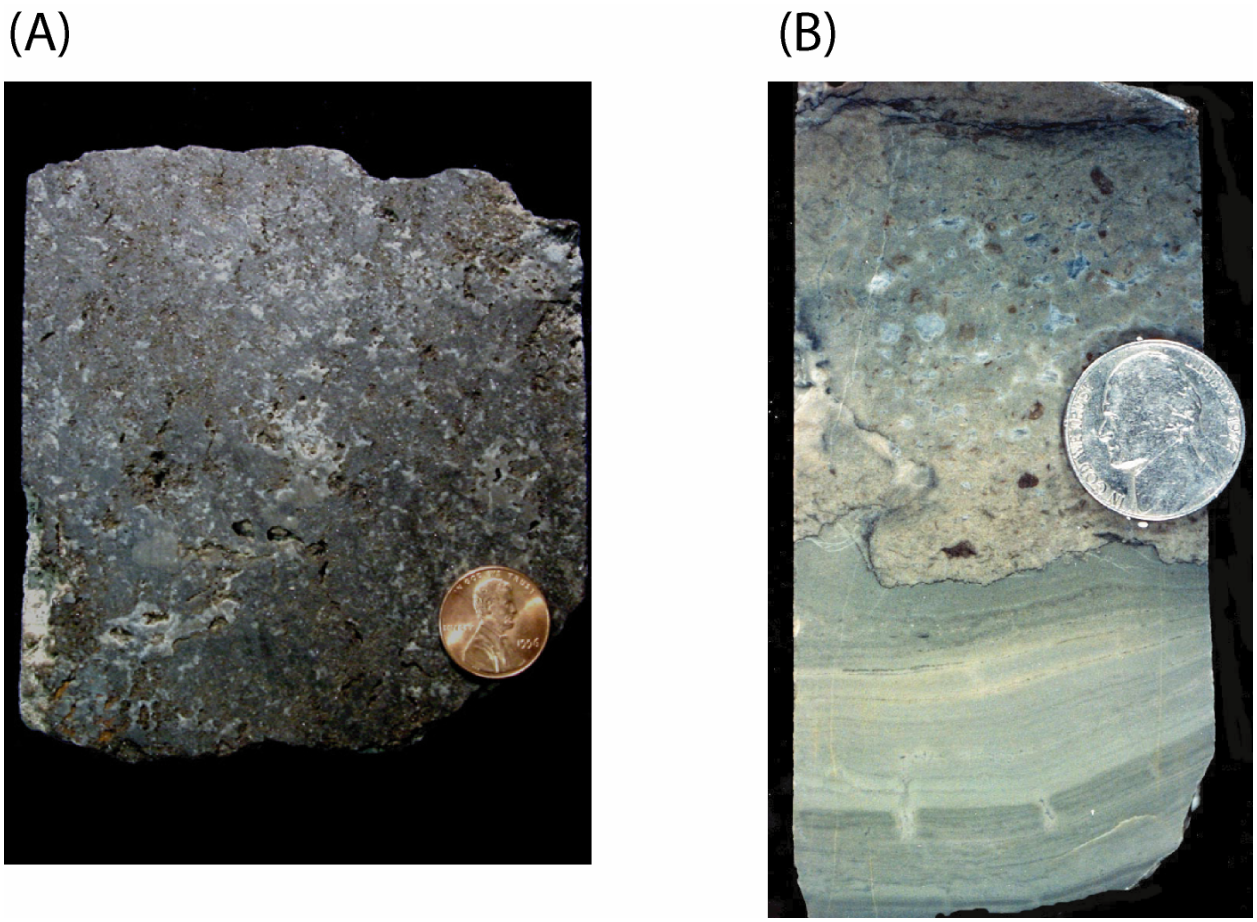

Figure 326. Core photographs of Smackover microbolite mesostructure: (A) chaotic thrombolite, well Permit #2935, depth 4.308 m (14,135 ft), Vocation Field, (B) stromatolite, well Permit #3739, depth 4,287 m (14,066 ft), Vocation Field.

Kopaska-Merkel, 2002). The 6 m thrombolite buildup at Melvin Field (Figure 323) is elongate and is about 1.6 km in length and 0.5 km in width. Serpulids, foraminifera, lithistid sponges and red algae are common in the thrombolite dominated boundstone (Baria et al., 1982). The boundstone has been highly leached and dolomitized and is underlain and overlain by lime mudstone. The microbial buildups associated with salt anticlines, such as that at Chunchula Field and the salt ridge along the eastern margin of the Mississippi Interior Salt Basin (well Permits #2769 and #4557), consist of renalcids and other calcimicrobes, foraminifera, ostracods, bivalves, gastropods, echinoderms and thalassinidean trace fossils in thrombolite dominated doloboundstone and dolograinstone (Kopaska-Merkel, 2002). These microbial buildups attain a thickness of up to 9 m and occur over a distance of 75 km on an elongate salt ridge (Figure 323) (Kopaska-Merkel, 2002). These buildups overlie subtidal peloidal wackestone and are overlain by lagoonal peloidal wackestone.

The thrombolite buildups in the Manila and Conecuh subbasins occur along the northwestern and southeastern flanks of the Conecuh Ridge (Figure 323). In the Manila Subbasin, thrombolite dominated buildups developed on the flanks of Paleozoic basement paleohighs (Vocation Field) (Baria et al., 1982; Llinás, 2002a,b, 2003). The 58 m thrombolite buildup at Vocation Field covers an area of 2 km^2 (Figure 260). The thrombolite facies is characterized by a regular pattern of lower gamma ray values, and higher porosity values as determined from density and neutron porosity curves (Figure 327). Calcimicrobes, red algae, foraminifera, sponges, echinoids, and bivalves are common in the thrombolite boundstone (Baria et al., 1982). The Vocation thrombolite buildup overlies Paleozoic igneous/metamorphic rocks and is overlain by shoreface and shoal ooid grainstone and lagoonal peloidal wackestone (Figure 42). Lateral facies are subtidal lime mudstone (Table 41). The buildup is only developed on the

Table 41. Characteristics of Thrombolite Buildups.

Parameter	Smackover Formation	Outcrop
Thickness	Up to 58 m	Up to 30 m
Areal Extent	Up to 12 km^2	Up to 7 km^2
Sequence Stratigraphy	Upper Transgressive and Regressive or Lower Highstand Systems Tracts	Upper Transgressive and Regressive or Lower Highstand Systems Tracts
Underlying Facies	Paleozoic Basement, Localized Cemented Packstone-Grainstone	Localized Cemented Packstone-Grainstone
Overlying Facies	Grainstone, Packstone, Wackestone	Grainstone, Packstone
Lateral Facies	Lime Mudstone	Wackestone, Packstone
Origin	Shallow Water, Inner Ramp	Deeper Water, Middle to Outer Ramp
Environmental Conditions	Hard Substrate Low Background Sedimentation Sea-Level Rise Low Energy Restricted Circulation and Fluctuating Salinities, Oxygen Levels?, Nutrient Supply?	Hard Substrate Low Background Sedimentation Sea-Level Rise Low-Moderate Energy Fluctuating Oxygen and Nutrient Contents

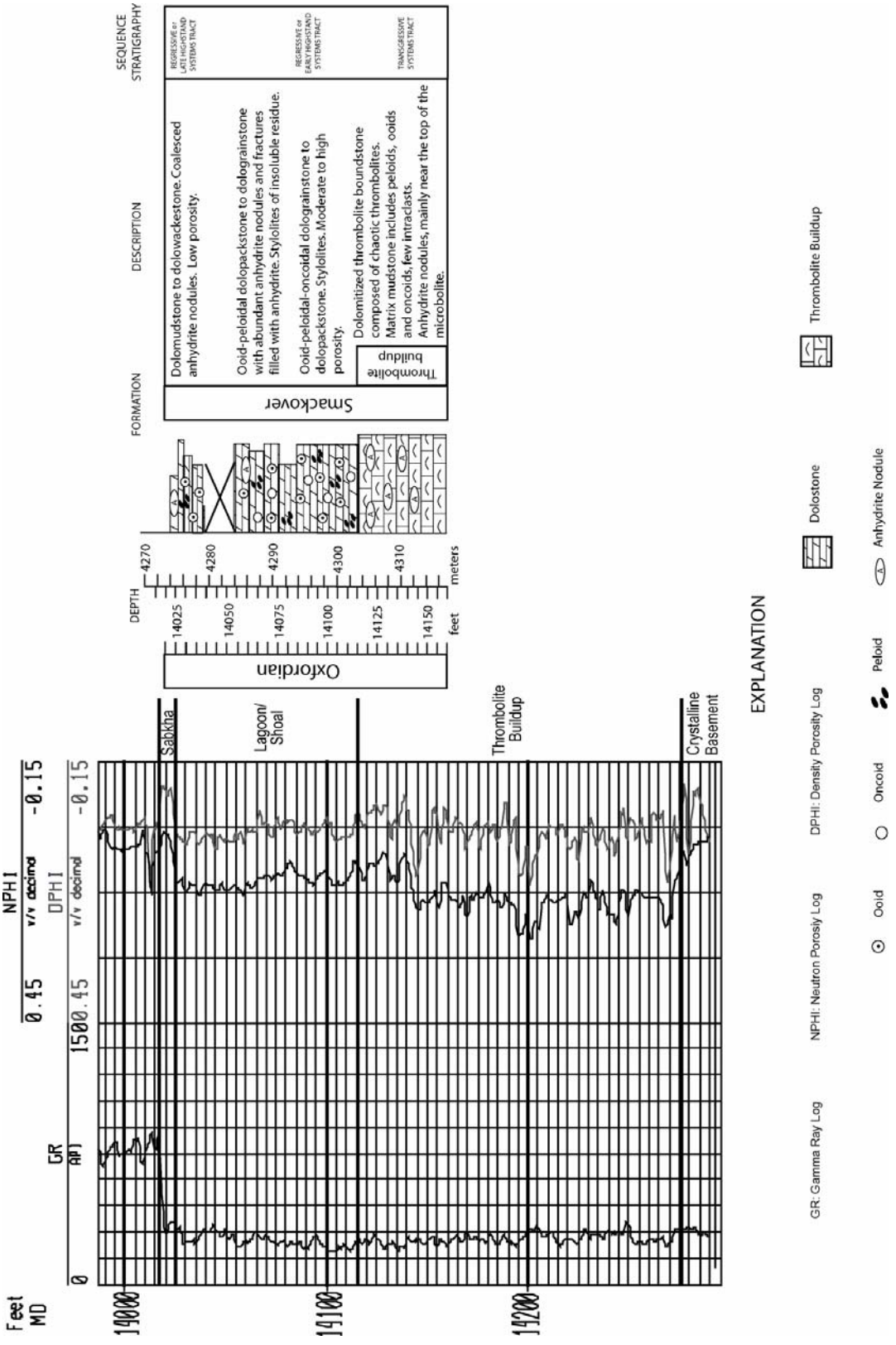

Figure 327. Correlation between core description and well log response in well Permit #2935, Vocation Field. The cored interval includes the upper 13.7 m of the thrombolite buildup.

northeastern flank or leeward side of the Vocation paleohigh (Figure 261). In the Conecuh Subbasin, thrombolite buildups developed on the crests and flanks of Paleozoic crystalline basement paleohighs (Appleton Field, Figure 252), Northwest Appleton Field, West Appleton Field, and Dean Creek Field) (Benson et al., 1996; Kopaska-Merkel, 1998; Mancini et al., 2000). The 45 m thrombolite buildup in the Appleton Field-Northwest Appleton Field area occurs over a 12 km^2 area (Figure 255). The thrombolite facies is characterized by gamma ray, density porosity and neutron porosity well log signatures (Figure 328) similar to the thrombolite facies at Vocation Field. Renalcids and other calcimicrobes, foraminifera, sponges, skeletal algae, bivalves, gastropods, and echinoids are common in the thrombolite boundstone (Benson et al., 1996; Kopaska-Merkel, 1998). The Appleton buildup overlies Paleozoic igneous/metamorphic rocks and is overlain by shoal/shoreface oncoidal and ooid grainstone (Figure 26). Lateral facies are subtidal lime mudstone.

In studying microbial buildups in outcrop in France, Portugal, Spain and Italy, the surface exposures in Portugal and Spain were found to be the best analogs for the thrombolite buildups in the Gulf of Mexico.

The Upper Jurassic (Kimmeridgian to Lower Tithonian) outcrops of the Jabaloyas, Tormón and Arroyo Cerezo areas (Figure 329) are located southeast of Teruel in northeastern Spain (Fezer, 1988; Leinfelder et al., 1993b; Leinfelder et al., 1994; Nose, 1995; Aurell and Bádenas, 1997; Bádenas, 1999). They occur around the Sierra de Abarracín in the southeastern part of the Iberian Chain, and the pinnacle reefs observed in these outcrops were developed in marginal areas of the Iberian Basin (Aurell and Bádenas, 1997). Late Jurassic marine sedimentation in this basin occurred in a carbonate ramp setting (Bádenas, 1999). The carbonate ramp was open to the

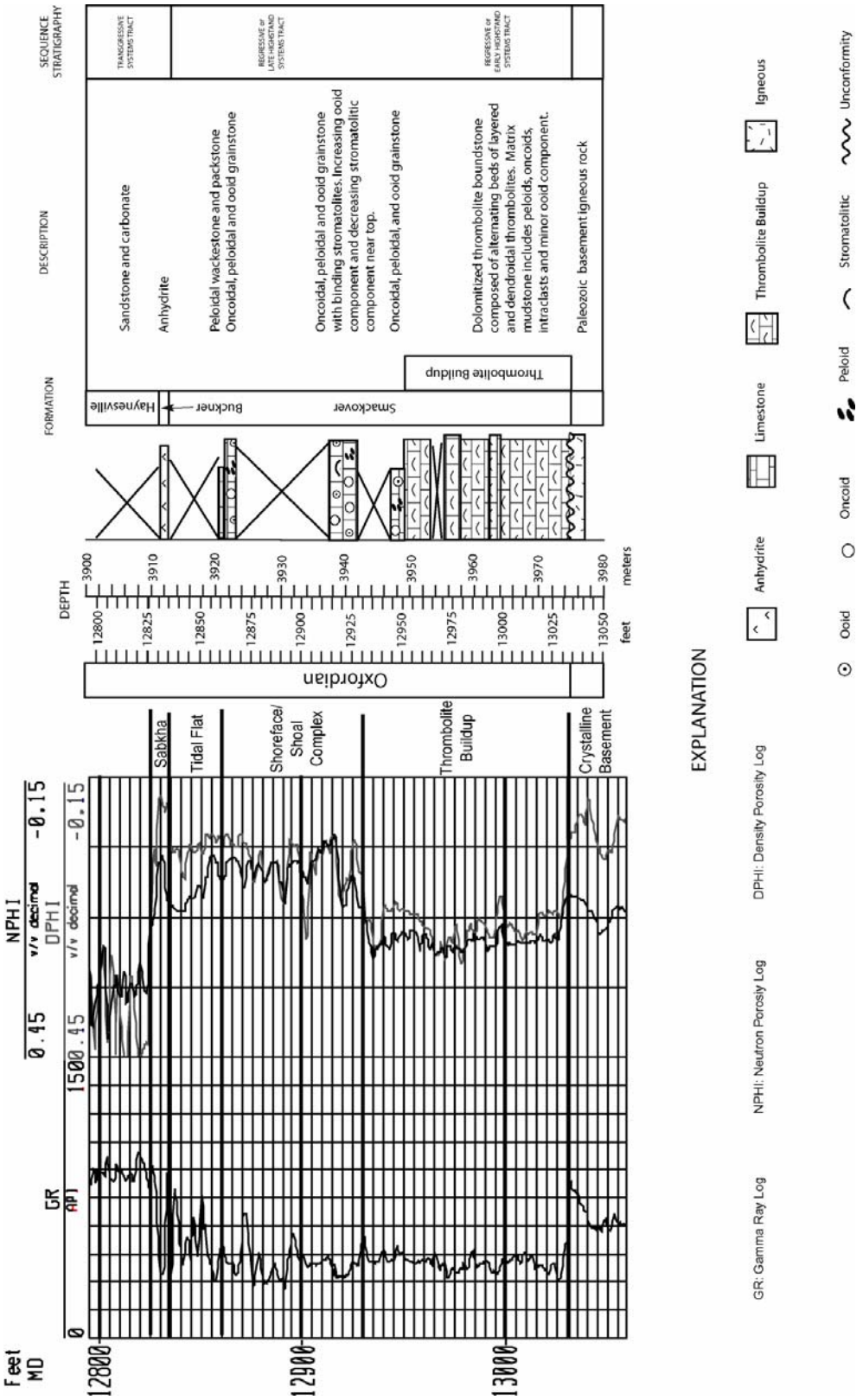

Figure 328. Correlation between core description and well log response in well Permit #4633-B, Appleton Field. The cored interval includes the entire thrombolite buildup.

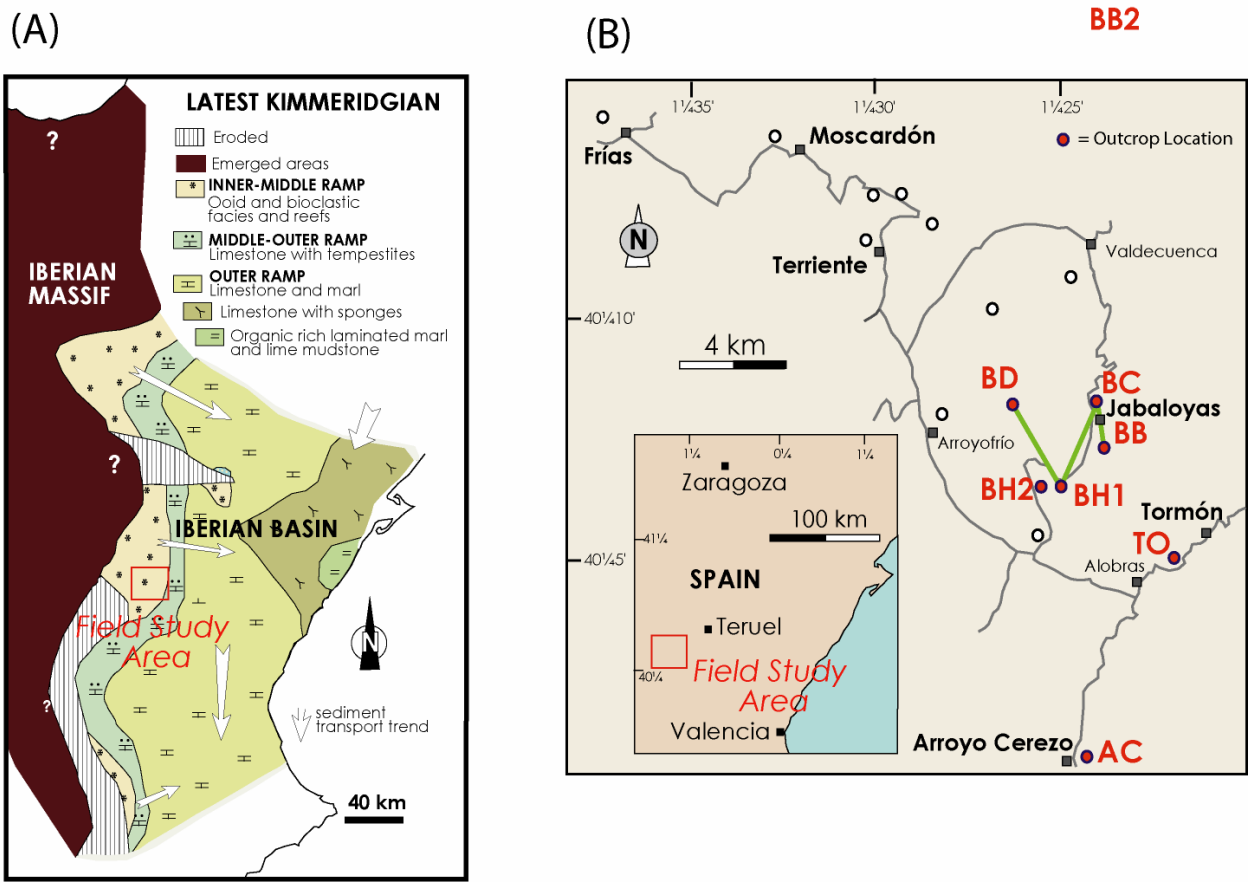

Figure 329. (A) Paleographic map of the Iberian Basin during the latest Kimmeridgian, and location of the field study area, and (B) location of the key pinnacle reef outcrops studied in the Sierra de Albarracin. BD=Barranco del Diablo, BC=Barranco del la Canaleja, BB=Barranco de las Balsillas, BH1 and BH2=Barranco de la Hoz, TO=Tormón, AC=Arroyo Cerezo (modified from Aurell and Bádenas, 1997).

Tethys Sea to the east, but during major flooding episodes connection with the Boreal Realm was possible (Aurell and Bádenas, 1997).

The stratigraphic section for the area, as summarized from Aurell and Bádenas (1997), is as follows (Figure 324B). The Upper Oxfordian to Lower Kimmeridgian Sot de Chera Formation (20 to 130 m) is a marly unit, which grades offshore into rhythmic bedded mudstone and marl of the Loriguilla Formation (20 to 118 m). The Kimmeridgian sandstone and ooid grainstone of the Pozuel Formation (8 to 55 m) prograde over these units. The Upper Kimmeridgian Torrecilla Formation (80 m), which contains reefal deposits, overlies the Pozuel Formation. The Tithonian Higueruelas Formation (80 m) overlies the Torrecilla Formation to the southeast. To the west, the upper part of this formation is partly eroded and is unconformably overlain by Albian fluvial sandstone of the Utrillas Formation. The lower part of the Torrecilla Formation consists of marl and burrowed sandstone containing plant remains. These deposits probably accumulated in lagoonal environments. Two cyclic parasequences have been identified in this formation. The lower parasequence, including pinnacle reefs, is exposed in the Jabaloyas and Arroyo Cerezo area, and the upper parasequence, including pinnacle reefs, is exposed around Tormón.

The thrombolite and coral buildups in Spain have been described as pinnacle reefs by Aurell and Bádenas (1997) and Bádenas (1999). They described and we observed these deposits in the field to be as follows. The pinnacle reefs have a height/width ratio of approximately one (1) and have very steep slopes, greater than 45 degrees. They can attain a thickness of 16 m. These coral-thrombolite and thrombolite-coral reefs occur as irregularly spaced, cylindrical to conical shaped buildups on a continuous ramp gradient of 15 km in a middle carbonate ramp setting (10 to 50 m in water depth) (Figure 330). The reefs are classified as coral-thrombolite (where the thrombolite content is less than 45% (Figures 331A,B) and thrombolite-coral (where the thrombolite content

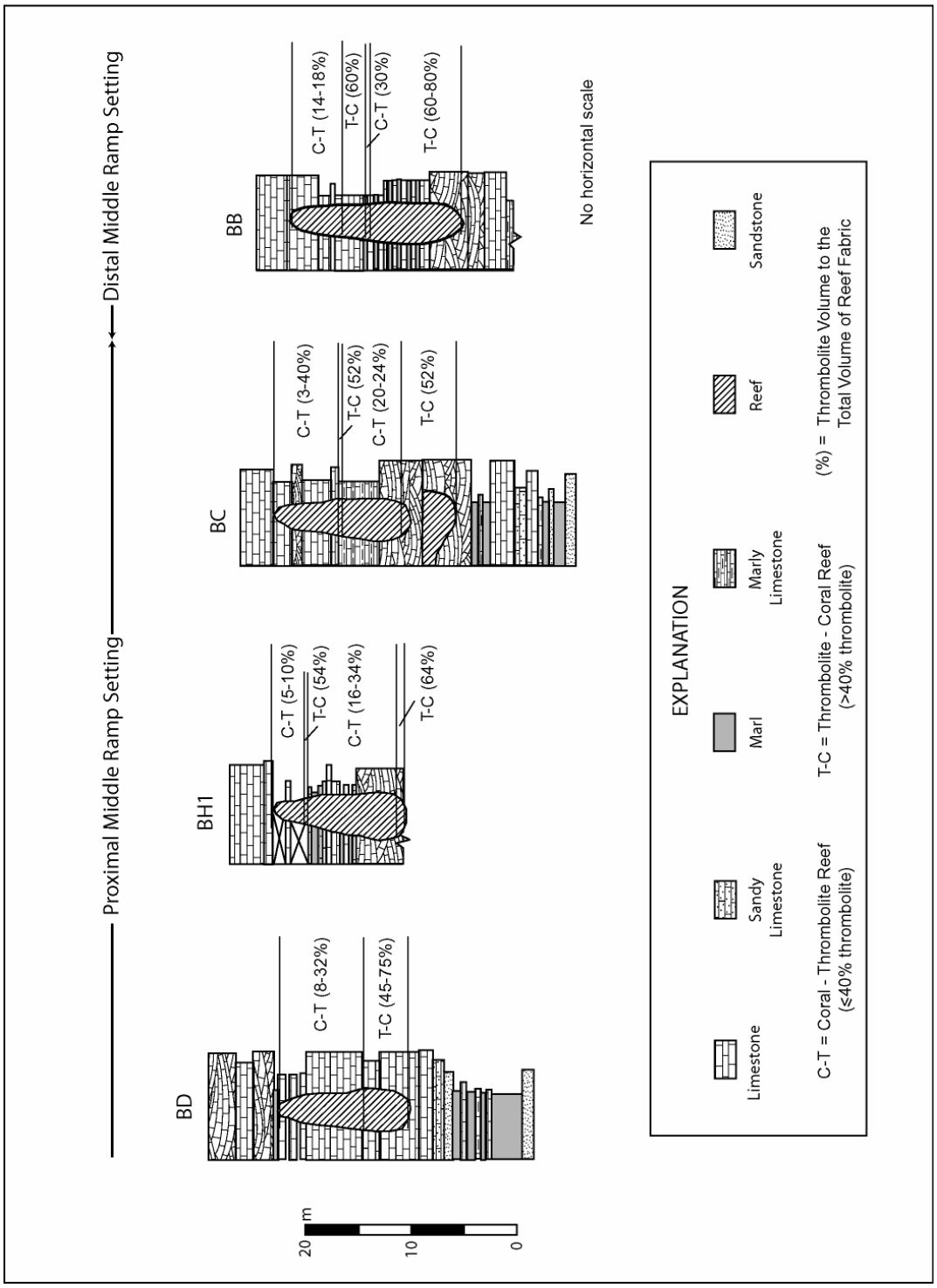

Figure 330. Stratigraphic cross section illustration the lateral and vertical variation of depositional facies, including faunal changes, in the pinnacle reefs in the Upper Jurassic Torrecilla Formation in the Jabaloyas area, northeastern Spain (modified from Aurell and Bádenas, 1997). The percentage of thrombolites in the pinnacle reefs was calculated based on thin section point-counting by Bádenas (1999).

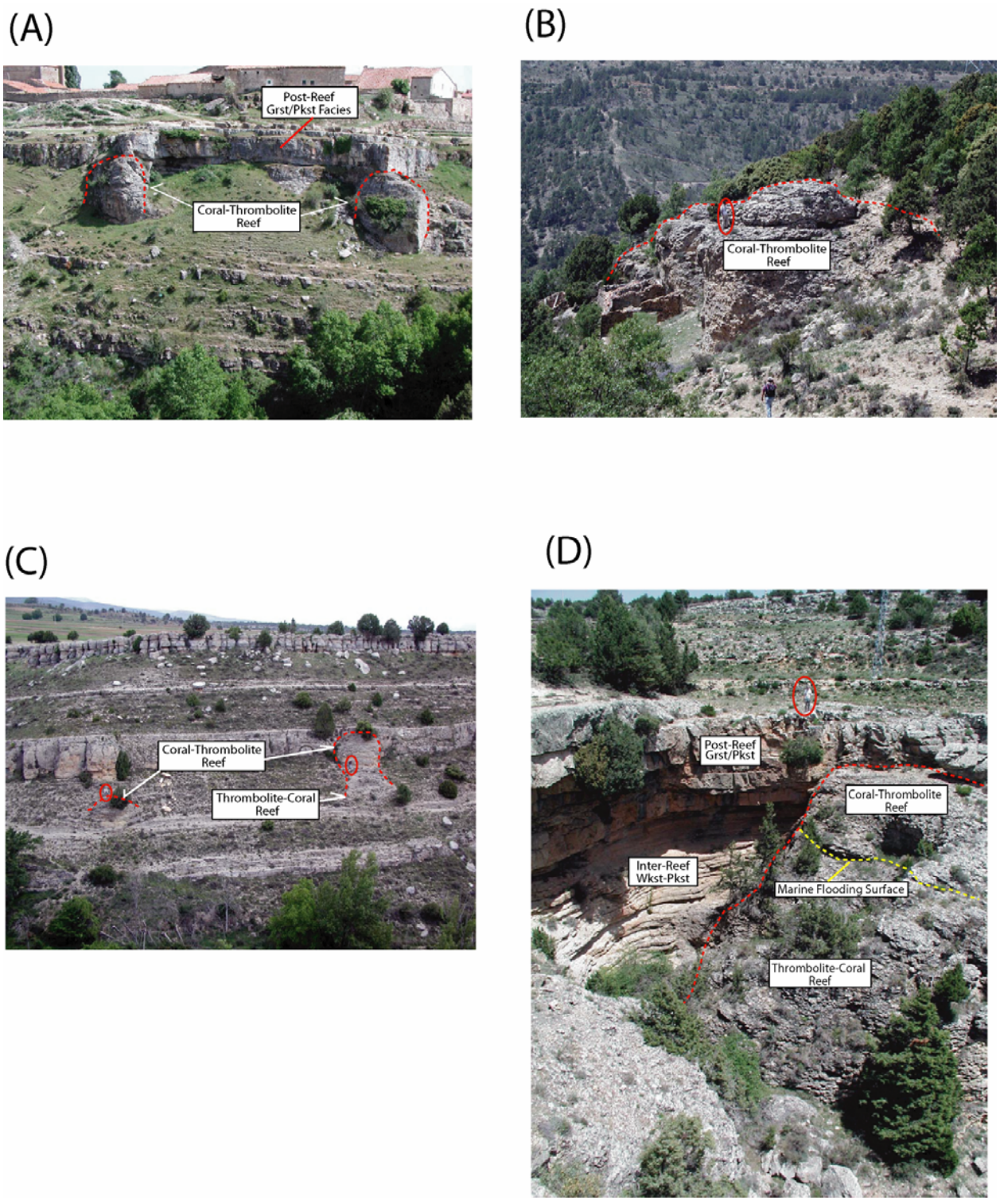

Figure 331. Outcrop photographs of middle ramp pinnacle reefs and associated facies of the Torrecilla Formation at: (A) Jabaloyas, (B) Barranco de la Hoz (BH1), (C) Arroyo Cerezo (AC), and (D) Barranco de las Balsillas (BB).

is equal to or greater than 45% (Figures 331C, D). Two types of internal cavities occur: cavities resulting from the growth of colonial corals and microbial crusts and cavities originating from bioerosion and boring. The internal sediment filling the cavities consists mostly of silty mudstone and wackestone. Bivalves, gastropods and echinoids are common in the reef facies.

The coral-thrombolite reefs have been described as coral-chaetetid-stromatoporoid-microbial reefs (Leinfelder et al. 1994; Nose, 1995). Solenoporarean algae and sponges are present and corals include massive, hemispherical (Figure 332A) and branching forms (Nose, 1995). The dominant taxa are *Thamnasteria* and *Microsolena* (Fezer, 1988; Nose, 1995).

The microbial crusts consist of a dense micrite to peloidal composition (Aurell and Bádenas, 1997). The fabric is primarily clotted with a domal morphology. *Tubiphytes*, serpulids and bryozoans are common (Bádenas, 1999).

Associated reef facies include pre-reef ooid, peloidal and bioclastic packstone and grainstone (Figure 332B), inter-reef skeletal wackestone and peloidal packstone (Figures 332C) and post-reef ooid and bioclastic grainstone and packstone (Figures 333C) in middle ramp areas (Aurell and Bádenas, 1997). Beds comprised chiefly of oncoids (Figure 333D) are part of the post-reef facies. The facies distribution overall shows a retrogradational stacking pattern in the lower part of the section and a progradational stacking pattern in the upper part (Bádenas, 1999).

Reef growth is initiated on a cemented and encrusted surface (sediment starvation surface) (Figure 333A, B). Reef growth occurred chiefly during a time of sea-level rise (Aurell and Bádenas, 1997). A marine flooding surface separates the transgressive deposits from the regressive or highstand deposits in the pinnacle reefs (Figure 332D). During sea level highstand conditions, the relative proportion of thrombolites to corals decreased (Figure 330), and the

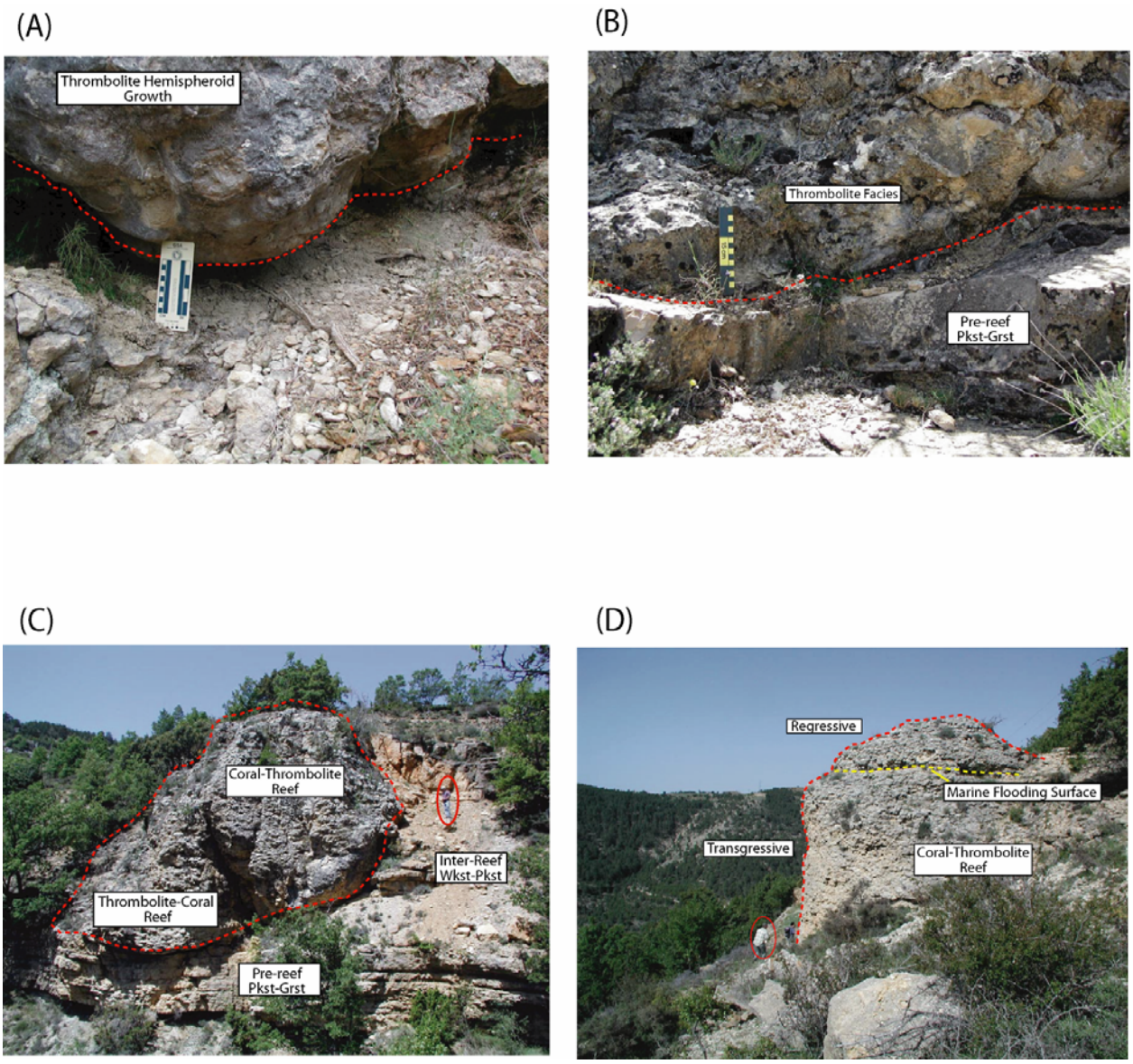

Figure 332. Outcrop photographs of pinnacle reefs and associated facies of the Torrecilla Formation : (A) thrombolite hemispheroid growth form of Leinfelder et al. (1993b), Tormón (TO), (B) pre-reef facies of packstone and grainstone, Barranco de Diablo (BD), (C) inter-reef facies of wackestone and packstone, Barranco de la Hoz (BH2), and (D) marine flooding surface affecting pinnacle reef faunal composition and growth, Barranco de la Hoz (BH1).

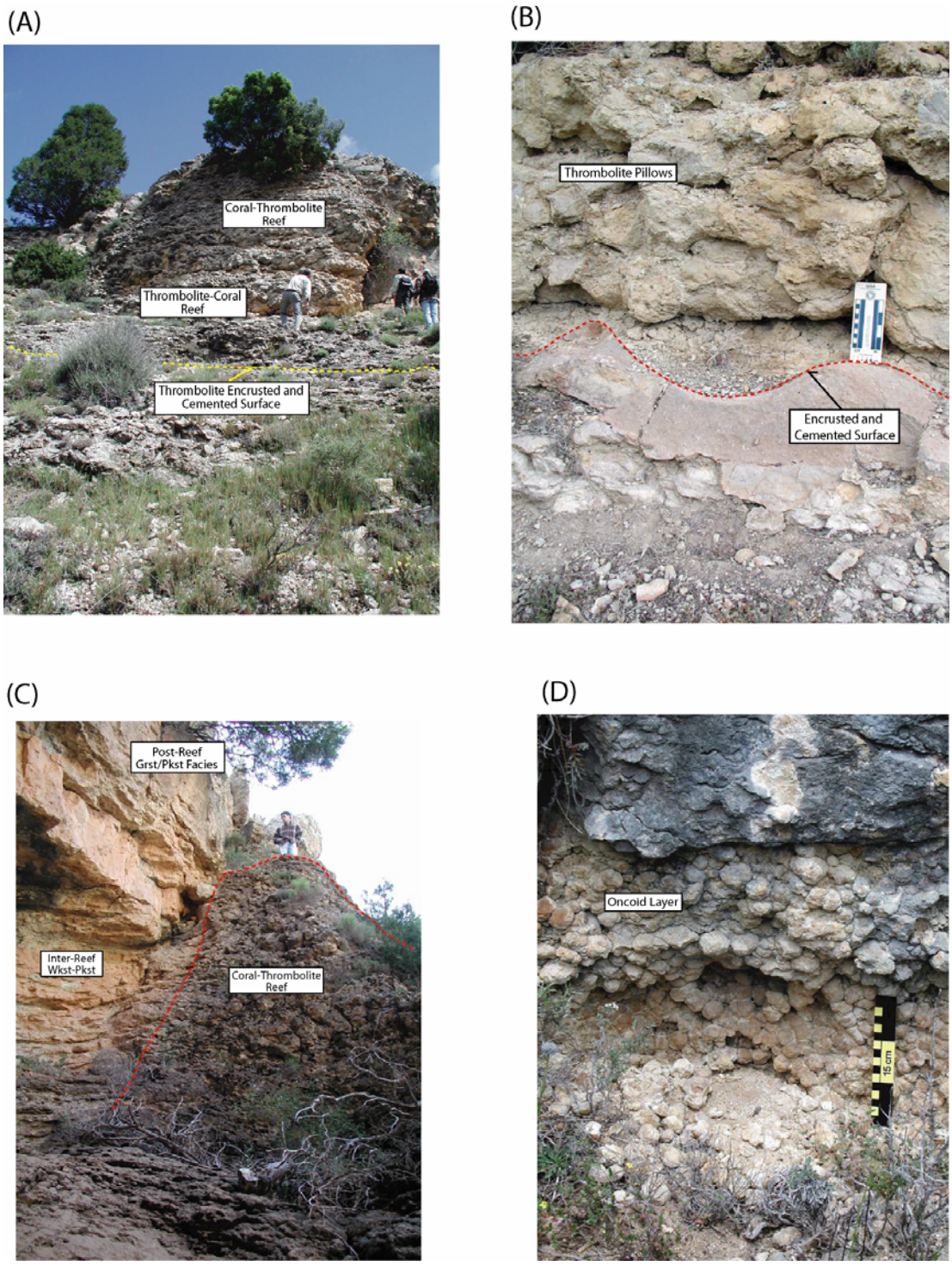

Figure 333. Outcrop photographs showing: (A) encrusted and cemented surface on which reef growth initiated, Arroyo Cerezo (AC), (B) close-up of the encrusted and cemented surface, Arroyo Cerezo (AC), (C) post-reef facies of grainstone and packstone, Barranco de las Balsillas (BB), and (D) oncoid layer, part of the post-reef facies, Tormón (TO).

growth of the reef eventually was diminished (Bádenas, 1999). Coral-thrombolite reefs are more common in the proximal portion of the middle ramp setting (Figure 331A, B), while thrombolite-coral reefs of up to 12 m in height developed in the distal portion of this middle ramp setting (Figures 331C, D) (Aurell and Bádenas, 1997).

The thrombolite buildups in Portugal occur in the Algarve Basin and Lusitanian Basin (Figure 334). The discussion regarding outcrops in Portugal is from the following publications: Ramalho, 1988; Leinfelder, 1993; Leinfelder et al., 1993a,b; Leinfelder and Wilson, 1998; Mancini and Parcell, 2001.

The eastern part of the Algarve Basin of Portugal has been interpreted as the northern shelf of the western Tethyan Ocean (Leinfelder et al., 1993a). The western part of the Algarve Basin is a transition area between the Tethys shelf and the central Portuguese Lusitanian Basin, which is a marginal basin associated with the opening of the North Atlantic Ocean (Leinfelder and Wilson, 1989). Tectonic events, as described by Wilson (1989) and Leinfelder (1993a), are as follows: Triassic to Callovian rifting and thermal subsidence, Middle Oxfordian to Early Berriasian ocean rifting and ocean spreading, Valanginian to Early Aptian rifting, and Late Aptian to Campanian ocean spreading. Sedimentation in the Algarve and Lusitanian Basins began with an initial graben rift phase that resulted in the deposition of upper Triassic and lower Jurassic red beds, volcanics and evaporites. Shallow water and hemipelgic carbonates and muds accumulated in the early to middle Jurassic. The Callovian to Oxfordian transition is marked by a subaerial unconformity in these basins. Upper Jurassic sediments in the eastern part of the Algarve Basin and the central part of the Lusitanian Basin consist of a mixed carbonate and siliciclastic shallowing upwards succession.

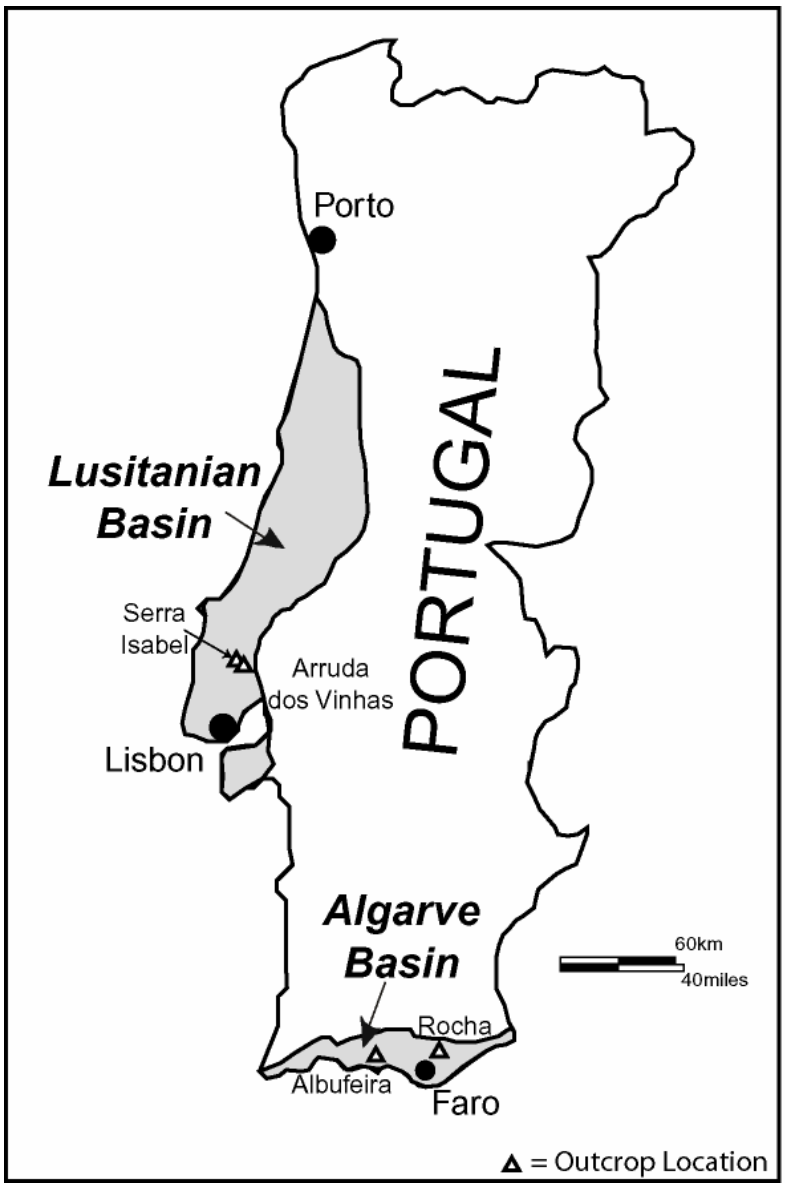

Figure 334. Map showing the location of key thrombolite outcrops studied in western Portugal, near Arruda dos Vinhas, Lusitanian Basin, and in southern Portugal, near Albufeira and Rocha, Algarve Basin.

In the eastern Algarve Basin, a shallowing upward succession is developed. The stratigraphic section (Figure 324C) for the area is summarized from Leinfelder et al. (1993a). The Kimmeridgian Peral deposits (200 m) represent a shallowing upward section of ammonite-rich marl and bedded marly limestone. The Jordanna beds (20 to 160 m) typically include intraclastic and bioclastic grainstone, packstone and wackestone, but at the Rocha section in southern Portugal this unit consists of sponge wackestone and marl.

At Rocha, Portugal, a thrombolite bioherm with a thickness of 30 m (Table 41) occurs between the Peral and Jordanna units (Figure 335A). This bioherm is described by Ramalho (1988) and Leinfelder et al. (1993a) as follows and has been interpreted by Leinfelder (1993b) to have formed in an outer ramp setting at a water depth of approximately 70 m (Figure 336). From our observations in the field, we concur with the description of this deeper water thrombolite buildup. The bioherm (Figure 337A) is underlain by the marly to micritic Peral unit that contains abundant ammonites (transgressive systems tract deposits). The top of these beds (Peral) is characterized by a marly, encrusted limestone bed, rich in glauconite, bioclastic debris, and highly bioturbated with *Planolites* burrows (sediment starvation surface). Cauliflower and pillow thrombolites (Figure 335B) containing glauconite constitute the majority of the bioherm (regression or highstand systems tract deposits). *Tubiphytes*, serpulids and siliceous sponges occur throughout the bioherm with an interval rich in cup-shaped dictyid sponges in the middle part of the bioherm section. Layered thrombolite is common in the middle and near the lower part of the top of the section, reflecting changes in rates of sea-level rise and water energy. The bioherm encompasses an area of 7 km^2 (Figure 337B). Transgressive systems tract sponge spicule packstone and wackestone of the Jordanna beds overlie the bioherm. Typically, the

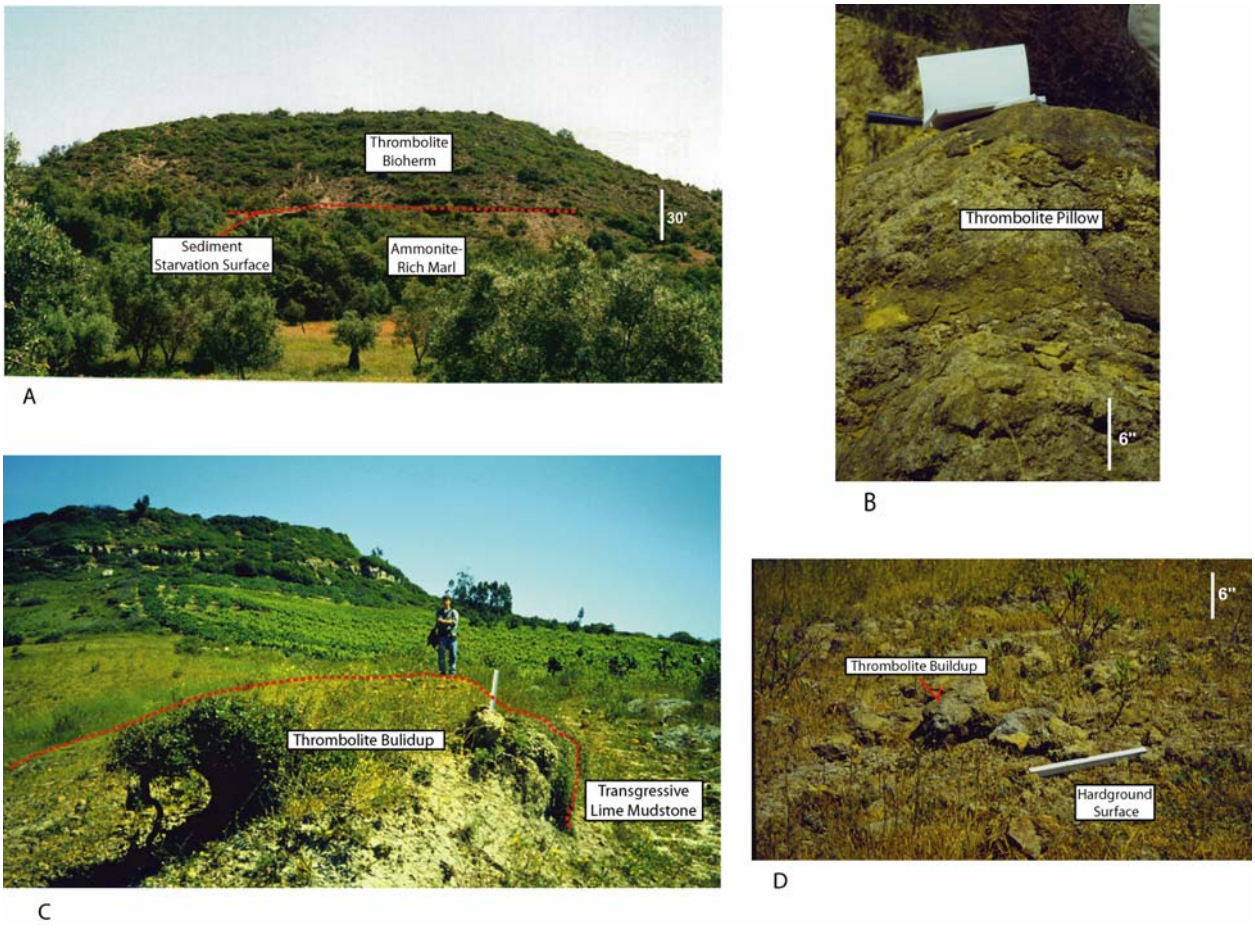

Figure 335. Outcrop photographs of thrombolite buildups: (A) deeper water thrombolite bioherm, Rocha, Algarve Basin, (B) close-up of deeper water thrombolite illustrating a pillow feature, Albufeira, Algarve Basin, (C) thrombolite buildup developed over a sediment starvation surface and hardground, Arruda dos Vinhas, Lusitanian Basin, and (D) close-up of the thrombolite buildup and encrusted hardground surface, Arruda dos Vinhas, Lusitanian Basin.

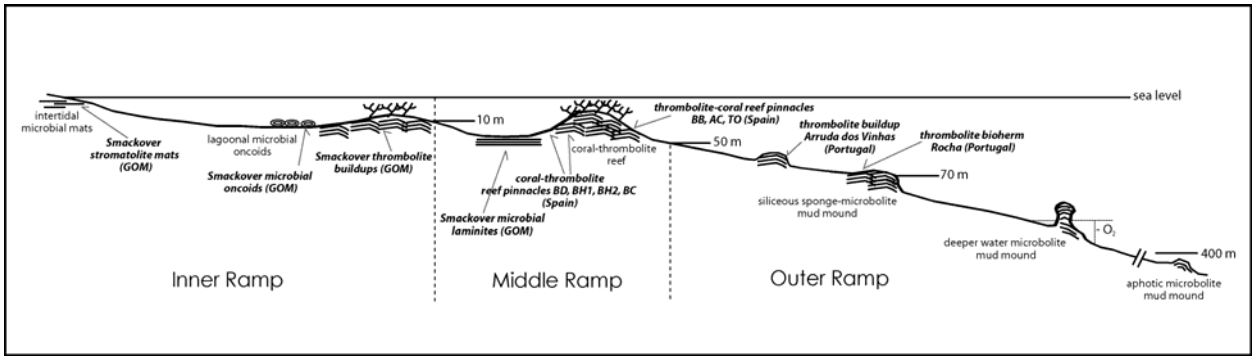

Figure 336. Generalized diagram illustrating the distribution of microbial buildups on a carbonate ramp (modified from Leinfelder, 1993b and Leinfelder and Schmid, 2000). Note inner to middle ramp settings for Upper Jurassic Smackover microbial growth in the northeastern Gulf of Mexico (GOM), middle ramp setting for the Upper Jurassic pinnacle reef development in northeastern Spain, and outer ramp setting for Upper Jurassic thrombolite buildups in Portugal.

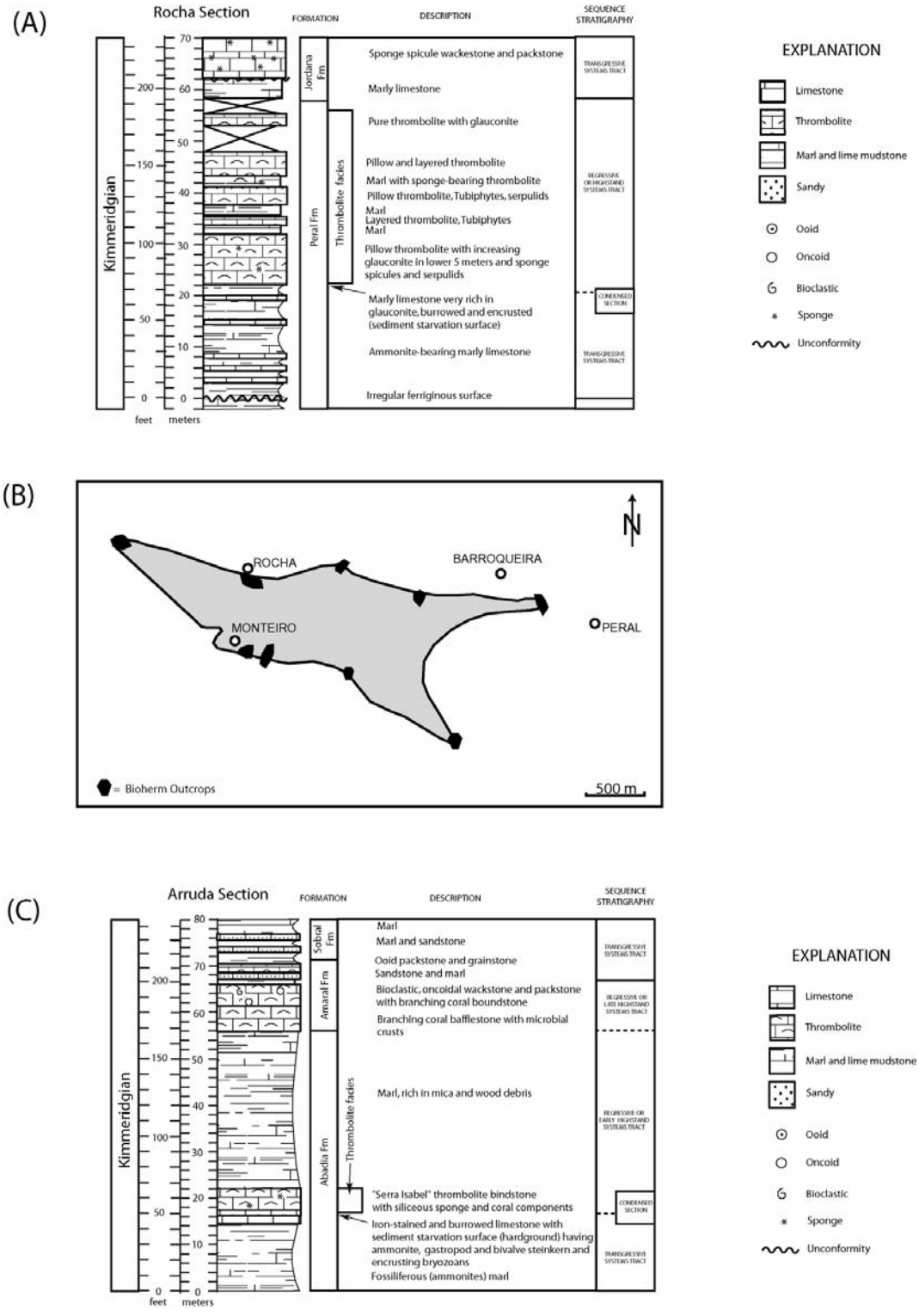

Figure 337. (A) Measured stratigraphic section of the Rocha thrombolite bioherm, Algarve Basin, (B) areal coverage of the thrombolite bioherm at Rocha, and (C) measured stratigraphic section of the Arruda dos Vinhas thrombolite buildup, Lusitanian Basin.

Jordanna deposits consist of intraclastic and bioclastic grainstone. The intraclasts include reworked thrombolitic limestone.

The stratigraphic succession in the central part of the Lusitanian Basin (Arruda Subbasin) is similar to the section in the eastern part of the Algarve Basin (Figure 324C). The stratigraphic section for the Arruda Subbasin area is summarized from Leinfelder (1993), Leinfelder et al. (1993a) and Leinfelder and Wilson (1998). Synsedimentary tectonics and sea-level fluctuations played a major role in the development of the stratigraphic succession in the overall shallowing upward section of the Arruda Subbasin. The Upper Oxfordian to Lower Kimmeridgian Abadia deposits are associated with a rifting phase that resulted in siliciclastic sediments being deposited in the Lusitanian Basin. The Abadia beds (800 m) include clay and marl locally rich in ammonites. The Abadia section shallows upwards to thrombolite bindstone (Serra Isabel unit). The thrombolite boundstone is overlain by marl containing wood fragments. The overlying Amaral beds (30 to 40 m) consist of a lower unit of coral bafflestone and bioclastic packstone and coral boundstone, and an upper marine sandstone and marl and ooid packstone and grainstone. The overlying Upper Kimmeridgian Sobral beds include prodelta and delta marl and clay.

In the Arruda area of the Arruda Subbasin, north of Arruda dos Vinhas, a condensed section (sediment starvation surface) in the Abadia beds is exposed at Serra Isabel (Figure 335C). The Serra Isabel horizon (Figure 337C), which occurs 30 to 40 m below the Abadia-Amaral Formation contact, has been described by Leinfelder (1993), Leinfelder et et. (1993a) and Leinfelder and Wilson (1998) as follows. From our field observations, we concur with this description. The Serra Isabel marly limestone and bindstone are up to 10 m thick and consist of a basal iron-stained, burrowed sediment starvation surface, which includes numerous steinkern of

ammonites, gastropods and bivalves and encrusting bryozoans (Figure 335D). This marly limestone is overlain by up to 7 m of thrombolite bindstone containing corals, siliceous sponges and *Tubiphytes*. These thrombolites have been interpreted by Werner et al. (1994) to have formed in a ramp setting (50-60 m in water depth). The marl beds in the Abadia Formation, which are locally rich in ammonites (transgressive systems tract), underlie the Serra Isabel unit. Marl beds of the Abadia Formation locally containing wood debris (regressive or early highstand systems tract) overlie the Serra Isabel unit. The Amaral beds, coral/microbial bafflestone and bioclastic wackestone/packstone with coral boundstone, and ooid grainstone/packstone with sandstone, have been interpreted as regressive or late highstand systems tract deposits (Mancini and Parcell, 2001), or as parts of two overlying depositional sequences (Leinfelder and Wilson, 1998).

Although microbial buildups occur throughout the geologic record (Riding, 1991), microbolites were particularly abundant in the Late Jurassic in the northern Tethyan Realm, where they occur in shallow to deep water settings (Leinfelder et al., 2002). The increase in the abundance of thrombolite mounds in the Mesozoic shows correspondence with rises in global and regional sea level during this time (Leinfelder and Schmid, 2000). Such is the case with the Smackover buildups which accumulated in the northern Tethyan Realm in the Oxfordian during a rise in global sea level.

In Western Europe, pure thrombolite bioherms are restricted to outer ramp, deep water settings (Figure 336) of greater than 70 m and as deep as 400 m (Leinfelder and Schmid, 2000). This is not the case with Smackover buildups which developed in inner ramp, shallow water settings (below wave base in settings of less than 10 m). Clearly, bathymetry is not a limiting factor for thrombolite growth. In fact, Leinfelder et al. (1993b) have concluded that microbolites

are eurytopic. That is, they are not restricted by water depth, salinity, light penetration, oxygen content or nutrient supply. However, in addition to being abundant in the northern Tethyan Realm and during a rise in sea level, these opportunistic species require a hard substrate for nucleation, zero to low background sedimentation rate for initial growth, and low to moderate sedimentation rate for continued growth to support the calcification process (Leinfelder et al., 1993b). Smackover thrombolites nucleated on rockgrounds associated with Paleozoic basement paleohighs (Figure 338), or sediment starvation surfaces (cemented shells and/or an encrusted substrate or hardground) associated with salt features. Although the rockgrounds are located near the Late Jurassic shoreline, the siliciclastic sediment influx essentially had ceased at this time. The initial growth of the thrombolites occurred at the point where the rate of sea level rise is the greatest and the accommodation space available is also the greatest (time of maximum sediment starvation).

Thrombolite buildups were dominated by calcimicrobes (cyanobacteria and other heterotrophic bacteria) with encrusters (foraminifera-*Tubiphytes*, algae and metazoans (Leinfelder et al., 1993b). Normal marine (stenotopic) grazing mollusks (gastropods) were present, but their numbers are limited probably due to fluctuations in paleoenvironmental conditions, particularly the periodic occurrence of low oxygen concentrations (Leinfelder et al., 1993b). Microbes, on the other hand, were capable of surviving dysaerobic conditions and were at least partly light independent with some forms being aphotic (Dromart et al., 1994; Leinfelder and Schmid, 2000). Leinfelder et al. (1996) has postulated that the fluctuation in oxygen content was the main limiting factor that favored the development of thrombolite mounds as opposed to the growth of coral or sponge reefs. Typically, microbial mats and their associated biofilms form on a hard substrate, form relief above the sea floor, and grow laterally over soft areas of the

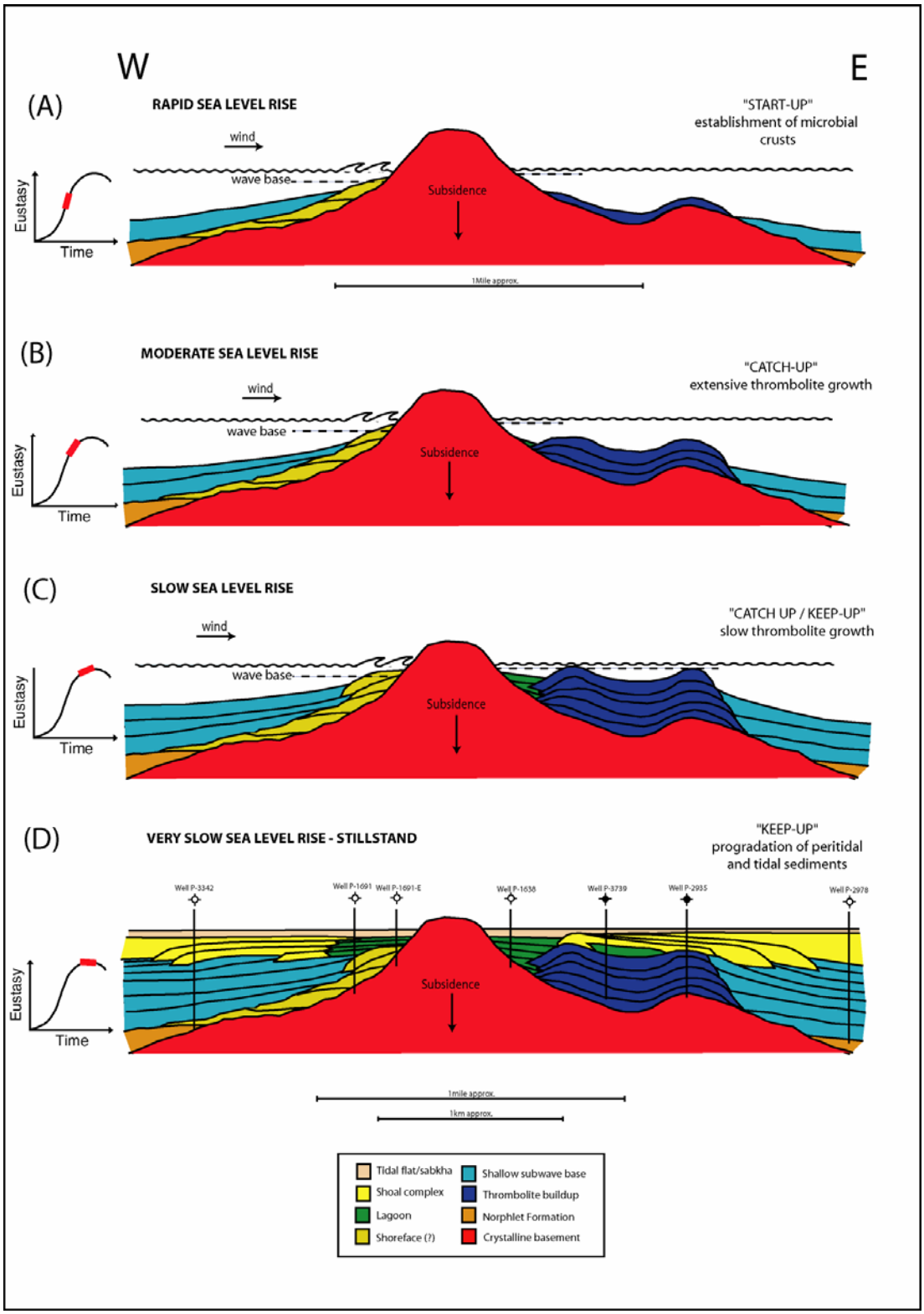

Figure 338. Evolution of thrombolite growth and associated facies on the high-relief structure at Vocation Field (modified from Llinás, 2002b).

substrate by producing an extracellular polymeric matrix, which is then calcified and produces a bridge over the previous substrate surface (Leinfelder et al., 1993b; Mancini and Parcell, 2001; Parcell, 2003). Generally, with a reduction in the rate of sea level rise and resulting stabilization of paleoenvironmental conditions, metazoans, such as corals, colonized the area of thrombolite development, and the growth of the thrombolites is reduced (Leinfelder et al., 1993b). In the case with the Smackover buildups, the nearshore and shallow water setting precluded coral reef growth, but rather, resulted in the development of ooid shoals and upper shoreface deposits (Figure 338). The relief and geographic location of the paleohighs had an effect on thrombolite growth and distribution. On low-relief paleohighs (submerged by the Smackover transgression), microbial crusts colonized the crests of these paleotopographic features as well as the flanks. On high-relief paleohighs (partially emergent throughout the Oxfordian), microbial crusts colonized only the flanks of these features. Thrombolites only developed on the leeward or northeastern side of the Vocation paleohigh due to the higher energy conditions on the windward side of this feature (Figure 338). Ooid upper shoreface deposits accumulated on this flank of the paleohigh.

Smackover oil was first discovered in 1967 in southwestern Alabama at Toxey Field in shoal/shoreface grainstone facies deposited in association with a Paleozoic basement paleohigh related to the Choctaw Ridge Complex (Figure 323). In 1970, Smackover oil was discovered at Uriah Field in Smackover shoal/shoreface grainstone facies on a Paleozoic basement paleohigh related to the Conecuh Ridge Complex. Microbial boundstone was penetrated in this field. Vocation Field, which produces oil from thrombolite boundstone (Figure 326A) and shoal/shoreface grainstone facies, was discovered in 1971 on a basement paleohigh (Figure 260) related to the Conecuh Ridge Complex. Significant (total oil production greater than 1 million barrels) Smackover discoveries associated with basement paleohighs, in addition to Toxey Field,

Uriah Field and Vocation Field, followed and included Huxford Field (1982), Appleton Field (1983), Wallers Creek Field (1985), South Burnt Corn Creek Field (1987), East Barnett Field (1988), West Appleton Field (1988), North Barnett Field (1991), Gravel Hill Church Field (1995), and Little River Lake Field (1998) (Figure 323). To date, some 54 Smackover oil fields (Table 42) have been discovered in the updip basement ridge play. The most recent Smackover paleohigh discovery was Juniper Creek Field in 2001.

Delineation of a paleotopographic anomaly utilizing seismic reflection data was the key to detecting these paleohighs. However, because paleohighs were both emergent (high relief, Figure 260) and submergent (low relief, Figure 255) during Smackover carbonate accumulation, a critical element to the exploration strategy was the determination as to whether reservoir facies were developed on the crest and flanks of a particular paleohigh or restricted to the flanks of the feature.

With the advent of three-dimensional seismic reflection technology, the prediction as to whether Smackover facies were present on the crest and flanks or restricted to the flanks of a particular paleohigh has been highly improved. The current issue is the prediction of the type of facies present; that is, whether shoal/shoreface grainstone and/or thrombolite boundstone reservoir facies accumulated on a given targeted paleohigh (Figures 255, 260).

Although the primary control on reservoir architecture and geographic distribution of Smackover reservoirs is the fabric and texture of the depositional facies, diagenesis (chiefly dolomitization) is a significant factor that preserves and enhances reservoir quality. At Appleton Field, the shoal grainstone and thrombolite boundstone are the reservoir facies, while tidal packstone and lagoonal wackestone are non-reservoir facies. The reservoir quality of the thrombolite boundstone facies is greater than the quality of the shoal grainstone facies (Mancini

Table 2. Field Discoveries in the Smackover Updip Basement Ridge Play.

Field	Discovery Date	Location (County)	No. of Wells	Total Production
Toxey	1967	Choctaw	7	2,004,390
Uriah	1970	Monroe	4	306,052
Vocation	1971	Monroe	8	2,260,179
Barnett	1975	Conecuh & Escambia	4	576,366
Melvin	1977	Choctaw	2	324,318
Blacksher	1980	Baldwin	5	2,386,343
Little River	1981	Baldwin & Monroe	2	127,958
Huxford	1982	Escambia	6	2,016,050
Appleton	1983	Escambia	6	2,689,489
South Vocation	1984	Monroe	2	76,739
Wallers Creek	1985	Monroe	2	987,247
Burnt Corn Creek	1986	Escambia	1	10,911
Hanberry Church	1987	Escambia	1	99,844
Wallace	1987	Escambia	2	11,164
South Burnt Corn Creek	1987	Escambia	3	997,050
Wild Fork Creek	1988	Escambia	2	963,079
East Barnett	1988	Conecuh & Escambia	4	1,600,250
Smiths Church	1988	Escambia	1	102,153
Palmers Crossroads	1988	Monroe	1	412,908
Broken Leg Creek	1988	Escambia	2	376,029
West Okatuppa Creek	1988	Choctaw	1	6,961
South Wild Fork Creek	1988	Escambia	1	22,836
West Appleton	1988	Escambia	3	1,293,890
Northwest Range	1988	Conecuh	2	230,290
East Huxford	1989	Escambia	1	246,433
Northeast Barnett	1989	Conecuh	2	510,973
North Smiths Church	1990	Escambia	1	15,212
North Wallers Creek	1990	Monroe	1	55,247
Robinson Creek	1990	Escambia	1	476,742
Mineola	1990	Monroe	1	610,896
East Corley Creek	1990	Conecuh	3	204,493
South Uriah	1990	Monroe	1	50,842
North Barnett	1991	Conecuh	2	1,134,953
South Dean Creek	1991	Escambia	1	212,352
Southwest Range	1992	Conecuh	2	71,374
Dean Creek	1992	Escambia	2	149,942

Big Spring Creek	1992	Escambia	1	372,325
Northwest Smiths Church	1992	Escambia	1	410,361
Canaan Church	1992	Escambia	2	820,433
Chitterling Creek	1992	Escambia	1	204,668
Baileys Creek	1994	Escambia	1	76,630
East Robinson Creek	1994	Escambia	1	24,900
Horseneck Creek	1994	Baldwin	1	154,148
Little Cedar Creek	1994	Conecuh	3	188,443
Northeast Melvin	1995	Choctaw	2	172,165
Gravel Hill Church	1995	Escambia	2	1,040,024
Narrow Gap Creek	1996	Escambia	1	196,574
West Canaan Church	1996	Escambia	2	697,520
Northwest Appleton	1996	Escambia	1	592,924
South Gravel Hill Church	1996	Escambia	1	21,662
Southwest Canaan Church	1997	Escambia	2	608,552
Little River Lake	1998	Monroe	1	1,056,862
Juniper Creek	2001	Conecuh	1	20,547
North Robinson Creek	2001	Escambia	1	117,085

et al., 2000). Also, the reservoir quality of the dendroidal (Figure 325B) and chaotic (Figures 325C, D, 326A) thrombolite boundstone is greater than the layered thrombolite bindstone (Figure 325A) because the dendroidal and chaotic thrombolites produce high lateral and vertical pore interconnectivity due to their vertical and horizontal branching growth pattern (Mancini and Parcell, 2001).

Porosity in the thrombolite boundstone facies is a mixture of primary shelter and fenestral porosity overprinted by secondary dolomite intercrystalline and vuggy porosity (Figure 339). The higher reservoir quality of the dendroidal (Figure 339B) and chaotic (Figure 339C, D) thrombolite boundstone is attributed to the higher permeability and greater interconnectivity of this facies due to the nature of the pore system (pore topology and geometry and pore throat size distribution), rather than the amount of porosity. Pore throat size distribution is one of the important factors determining permeability because the smallest pore throats are the bottlenecks that determine the rate at which fluids pass through a rock (Kopaska-Merkel, 1991; Ahr and Hammel, 1999). The intercrystalline- and vuggy- dominated pore system of the dolomitized and leached boundstone is characterized by a higher percentage of large-sized pores (>10,000 μm^2 in size) having larger pore throats.

The exploration challenge, therefore, in drilling a successful wildcat well in the Upper Jurassic thrombolite reservoir play in the northeastern Gulf of Mexico is to identify and delineate low-relief basement paleohighs associated with dendroidal thrombolite boundstone that has been dolomitized and occurs above the oil-water contact. As mentioned previously, the use of three-dimensional seismic data provide for the imaging of low-relief structures that are characterized by thrombolite development on their crest and flanks and that have sufficient present-day structural relief so the thrombolite buildup rests above the oil-water contact. Utilization of the

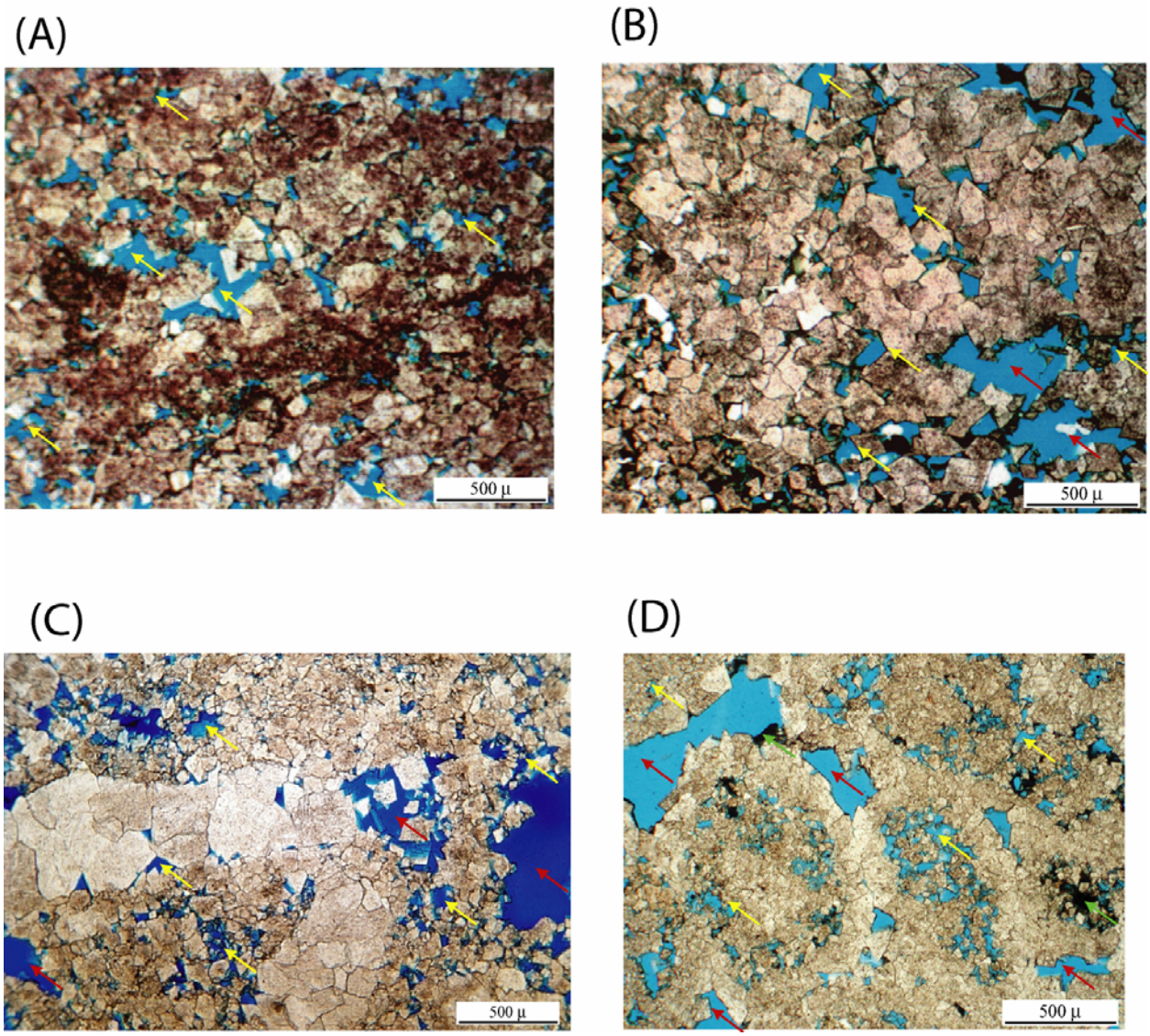

Figure 339. Photomicrographs of Smackover thrombolite facies from Appleton, Vocation and Northwest Appleton Fields showing the intense degree of dolomitization and the resulting development of effective dolomite intercrystalline (yellow arrows) and vuggy (red arrows) porosity, that acted to improve reservoir connectivity of: (A) layered thrombolite, well Permit #4633-B, depth 3,969 m (13,022 ft), Appleton Field, (B) dendroidal thrombolite, well Permit #3986, depth 3,953 m (12,970 ft), Appleton Field, (C) chaotic thrombolite, well Permit #2935, depth 4,305 m (14,124 ft), Vocation Field, and (D) chaotic thrombolite, well Permit #11030-B, depth 4,005 m (13,139 ft), Northwest Appleton Field. Notice in the last photomicrograph the presence of dead oil residue that is partially filling pore space (green arrows).

characteristics of thrombolites, as observed in outcrop and as seen from past subsurface studies, has the potential to facilitate the formulation of an effective exploration strategy for determining whether dendroidal thrombolite facies are associated with the structure. Low-relief basement paleohighs geographically located updip or near the Jurassic paleoshoreline have been shown to be features that are conducive for thrombolite colonization and growth. These paleohighs were submergent during Smackover deposition, and they provided the hard substrate required for microbial crust nucleation. Because the leeward side of these features provided protection from ocean currents and waves and acted as barriers producing paleoenvironments characterized by abnormal marine conditions (low or fluctuating oxygen; low, high, or fluctuating salinities; and/or fluctuating nutrient supplies), which acted to exclude stenotopic marine metazoans (corals) and to support the growth of the eurytopic and opportunistic thrombolites. Stratigraphically, thrombolite development was optimal during maximum transgression of the Smackover seas. The Smackover maximum transgression event approximates the greatest rate of sea level rise during the Oxfordian, the maximum sediment starvation in the basin, which corresponds to zero to minimum terrigenous sediment influx from Jurassic highlands into the basin, and the creation of the greatest accommodation space. These factors all contributed to optimal shallow water thrombolite development. After microbial crust colonization in a low energy paleoenvironment, an elevated background sedimentation rate would favor dendroidal thrombolite growth in that area. Schmid (1996) reported that Upper Jurassic microbolites developed dendroidal growth forms as a reaction to slightly elevated sedimentation rates in low energy paleoenvironments.

With three-dimensional seismic and three-dimensional geologic modeling technologies available for the reliable prediction of petroleum trap development and of reservoir depositional

facies, the major exploration uncertainty remaining is how to determine whether the thrombolite boundstone has been dolomitized. Fortunately, as reported by Benson and Mancini (1999), Mancini et al. (2000) and Llinás (2002b), dolomitization is a very common agent of diagenesis in the onshore areas of the northeastern Gulf of Mexico. Dolomitization in this area has been interpreted as a relatively early diagenetic event with paleotopography, fluctuations in sea level, and climate being critical factors to this diagenetic process (Benson and Mancini, 1999). The arid climate, the elevation of paleotopographic features, the restrictive nature of ocean circulation due to barriers, the decrease in the rate of sea level rise, and the overall paleoenvironmental conditions in the nearshore areas of the northeastern Gulf of Mexico during the latest Oxfordian into the Kimmeridgian were conducive for dolomitization. Although seepage reflux and mixing zone diagenetic processes are mechanisms for the formation of Smackover dolostone, Benson and Mancini (1999) favored the evaporative pumping mechanism of Saller and Moore (1986) to explain the movement of hypersaline, marine-derived waters through Smackover lime sediments soon after deposition in updip areas of the eastern Gulf Coastal Plain (Figure 340). This mechanism is attractive because it explains very early perhaps even syndepositional dolomitization and would predict dolomitization of thrombolite facies on any paleohigh having sufficient depositional relief to stand above sea level for a period during sediment deposition. However, due to the intense and extensive dolomitization of Smackover carbonates in the northeastern Gulf of Mexico, several processes, including seepage (brine) reflux, mixing zone (shallow burial mixed water), and evaporative pumping, probably have altered Smackover deposits in this area (Prather, 1992).

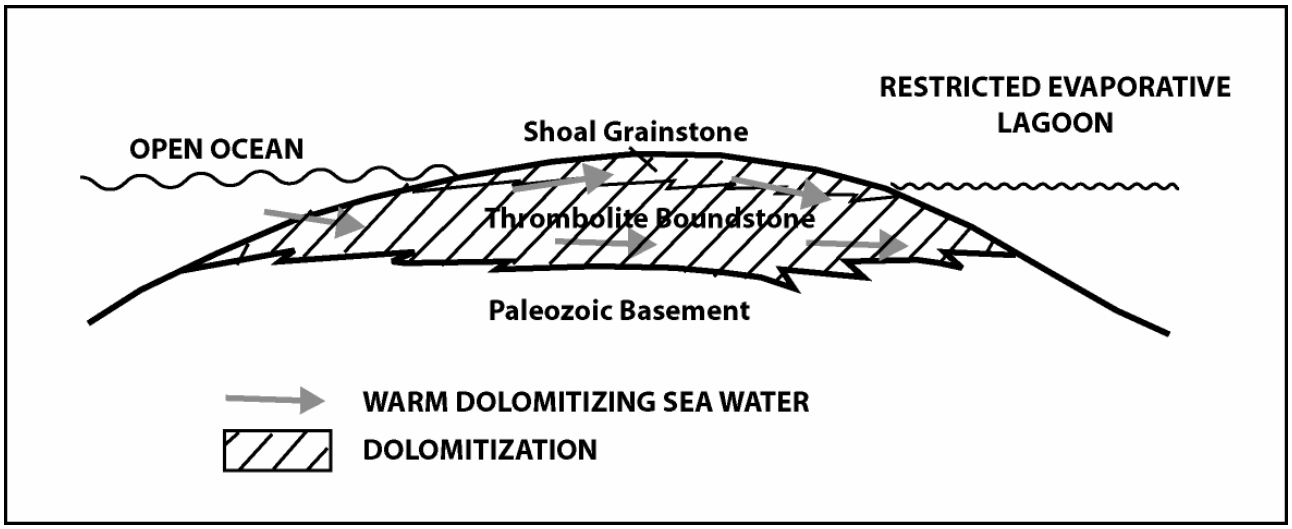

Figure 340. Generalized diagram of evaporative pumping mechanism of Saller and Moore (1986) as a means of explaining dolomitization of boundstone facies associated with basement paleohighs in the northeastern Gulf of Mexico.

CONCLUSIONS

The University of Alabama, in cooperation with Texas A&M University, McGill University, Longleaf Energy Group, Strago Petroleum Corporation, and Paramount Petroleum Company, has undertaken an integrated, interdisciplinary geoscientific and engineering research project. The project is designed to characterize and model reservoir architecture, pore systems and rock-fluid interactions at the pore to field scale in Upper Jurassic Smackover reef and carbonate shoal reservoirs associated with varying degrees of relief on pre-Mesozoic basement paleohighs in the northeastern Gulf of Mexico. The project effort includes the prediction of fluid flow in carbonate reservoirs through reservoir simulation modeling which utilizes geologic reservoir characterization and modeling and the prediction of carbonate reservoir architecture, heterogeneity and quality through seismic imaging.

The project has direct and significant economic benefits because the Smackover is a prolific hydrocarbon reservoir in the northeastern Gulf of Mexico. To date, 30 million barrels of oil have been produced from 54 fields that have been discovered and developed in the basement ridge play. Smackover reef and carbonate facies associated with paleohighs in this play represent underdeveloped reservoirs. The combined oil production from the Smackover fields (Appleton and Vocation Fields) studied in this project total 5 million barrels of oil. The results from this project should lead to increased oil producibility from existing and newly discovered fields similar to Appleton and Vocation Fields.

The primary goal of the project is to increase the profitability, producibility and efficiency of recovery of oil from existing and undiscovered Upper Jurassic fields characterized by reef and carbonate shoals associated with pre-Mesozoic basement paleohighs.

The objectives of the project are: (1) to evaluate the geological, geophysical, petrophysical and engineering properties of reef-shoal reservoirs using Appleton and Vocation Fields as case studies; (2) construct a digital database of integrated geoscience and engineering data for reef-shoal reservoirs associated with basement paleohighs; (3) develop integrated geologic models, based on geological, geophysical, petrophysical, and engineering data and analysis, for improving reservoir detection, characterization, imaging, flow simulation and performance prediction for reef-shoal reservoirs using the case studies of Appleton and Vocation Fields; and (4) test and apply the integrated geologic models to prospective Smackover reef-shoal reservoirs associated with basement paleohighs.

The objectives have been achieved through the accomplishments resulting from the following research tasks: geoscientific reservoir property characterization, geophysical seismic attribute characterization, petrophysical property characterization, engineering property characterization, rock-fluid interactions (diagenesis), geologic modeling, reservoir simulation, testing and applying the integrated geologic–engineering models, and technology transfer.

Geoscientific reservoir property characterization has shown that the main Smackover lithofacies are subtidal, reef flank, reef crest, shoal flank, shoal crest, lagoon, tidal flat and sabkha. The reef lithofacies consist of thrombolite layered, chaotic and dendroidal subfacies. The shoal complex consists of the lagoon/subtidal and shoal flank and crest lithofacies. These reef and shoal reservoir lithofacies are developed on the flanks of high-relief crystalline basement paleohighs (Vocation Field example) and on the crest and flanks of low-relief crystalline basement paleohighs (Appleton Field example).

Seismic attribute characterization has shown that seismic attributes can be used to predict subsurface rock properties, such as the presence/absence of porosity and porosity thickness in the

Smackover reservoir lithofacies, associated with basement paleohighs. Porous intervals were generally greater and thicker on the flanks of the paleohighs, rather than the crests of these features, due to greater accommodation space and improved growth conditions for reef organisms. This volume-based seismic attribute study was also used to determine lithofacies distribution and thickness and to define the vertical and lateral heterogeneity in Smackover reservoirs.

Petrophysical property characterization has shown that the shoal and reef thrombolite lithofacies are the main reservoir lithofacies. The reservoir quality of the thrombolite lithofacies is greater than the shoal lithofacies because the thrombolite reservoir consists of a pore system comprised of a higher percentage of large-sized pores and larger pore throats. The shoal pore system is dominated by moldic and dolomite intercrystalline pores. The dendroidal and chaotic thrombolite reservoirs have higher producibility than the layered thrombolite reservoirs because they have overall higher permeabilities and greater interconnectivity due to their vertical and horizontal branching growth pattern. Thrombolite flow units are characterized by dolomite intercrystalline and vuggy pores.

Engineering property characterization has shown that reservoirs at Appleton and Vocation Fields have a heterogeneous nature. Porosity and permeability data show that the reef reservoirs are of higher quality than the shoal reservoirs. The primary production mechanism in Vocation Field is a combination drive consisting of fluid/rock/gas expansion and water from an underlying and/or adjoining aquifer. The primary production mechanism in Appleton Field is a strong bottom up water drive. New well pressure test data acquired for Appleton Field show that the reservoir pressures at Appleton Field currently range from 4423 to 5125 psia.

Rock-fluid interactions (diagenesis) studies show that although the primary control on reservoir architecture and geographic distribution of Smackover reservoirs is the fabric and texture of the depositional lithofacies, diagenesis (chiefly dolomitization) is a significant factor that preserves and enhances reservoir quality. Porosity in the thrombolite doloboundstone lithofacies is a mixture of primary shelter and fenestral porosity overprinted by secondary dolomite intercrystalline and vuggy porosity. Porosity in the shoal dolograinstone lithofacies is primary interparticle porosity overprinted by secondary moldic and dolomite intercrystalline. Although seepage reflux and mixing zone diagenetic processes are mechanisms for the formation of Smackover dolostone, the evaporative pumping mechanism is favored to explain the intense and extensive dolomitization of the Appleton and Vocation reservoir flow units.

Geologic modeling of the Appleton and Vocation paleohighs and associated lithofacies has shown that these features are complex structures. The structure at Appleton Field is a northwest-southeast trending, low-relief composite paleotopographic high with two water levels. The well production differences in the field are related to the heterogenous nature of the reservoirs. The greater production from the eastern part of the composite paleohigh is attributed to the higher relief, which results in the placement of more thrombolite dolostone above the oil-water contact. The structure at Vocation Field is a high-relief composite paleotopographic high with multiple water levels. This composite feature consists of one main north-south oriented elongated feature with three crests that remained subaerially exposed throughout the time of Smackover deposition. The Vocation structure is bounded to the east and north by high-angle normal faults. Reef growth was limited to the eastern and northern flanks (leeward side) of the structure due to Smackover paleoenvironmental conditions.

Reservoir simulation of the reservoirs at Appleton and Vocation Fields used the 3-D geologic models for these reservoirs as a foundation for the simulation modeling. Reservoir simulation at Appleton Field shows that 50% of the recoverable oil in this field has been produced; thus, little oil remains to be recovered. Of the oil remaining, the areas around well Permits #3854B, #6247 and #4735B (western part of the structure) have the most potential to recover additional oil. Reservoir simulation at Vocation Field shows that a significant amount of oil remains to be recovered in this field through infill drilling. The area north of well Permit #4786B and south of well Permits #1638 and #1691 and the area southeast of well Permits #1599 and #3412 and northwest of well Permit #3739 have high potential for recovering additional oil from this field.

The integrated geologic-engineering model developed for a low-relief paleohigh (Appleton Field) was tested using three scenarios involving the variables of present-day structural elevation and the presence or absence of potential reef thrombolite lithofacies. In each case, the predictions based upon the model were correct. The integrated model was also used to evaluate existing reservoir management strategies at Appleton and Vocation Fields. It was concluded that the drive mechanisms for primary production in these fields remain effective; and therefore, no recommendations for the initiation of a pressure maintenance program or an enhanced recovery project were justified at this time. It was determined that these fields would benefit from additional infill drilling, particularly Vocation Field, at the strategic drill sites identified from the reservoir simulation modeling. From the integrated geologic model, a drill site northwest of well Permit #3854B (Appleton Field) and south of well Permit #11030B (Northwest Appleton Field) was identified as a location with high potential to encounter thrombolite doloboundstone and dolostone on a low-relief paleohigh.

To date, technology transfer activities have included conducting two technology workshops in Jackson, Mississippi, making 31 technical presentations at regional and national meetings, and publishing 40 technical publications on the research results from this project.

REFERENCES

Ahr, W. M., 1973, The carbonate ramp: an alternative to the shelf model: Gulf Coast Association of Geological Societies Transactions, v. 23, p. 221-225.

Ahr, W. M., and B. Hammel, 1999, Identification and mapping of flow units in carbonate reservoirs: an example from Happy Spraberry (Permian) field, Garza County, Texas USA: Energy Exploration and Exploitation, v. 17, p. 311-334.

Aitken, J. D., 1967, Classification and environmental significance of cryptalgal limestones and dolomites, with illustrations from the Cambrian and Ordovician of southwestern Alberta: Journal of Sedimentary Petrology, v. 37, p. 1163-1178.

Aurell, M., and B. Bádenas, 1997, The pinnacle reefs of Jabaloyas (Late Kimmeridgian, NE Spain): vertical zonation and associated facies related to sea level changes: Cuadernos de Geología Ibérica, no. 22, p. 37-64.

Bádenas, B., 1999, La sedimentación en las rampas carbonatadas de Kimmeridgiense en las cuencas del este de la placa Iberica: Ph.D. dissertation, University of Zaragoza, Zaragoza, Spain, 189 p.

Baria, L. R., D. L. Stoudt, P. M. Harris, and P. D. Crevello, 1982, Upper Jurassic reefs of Smackover Formation, United States Gulf Coast: AAPG Bulletin, v. 66, p. 1449-1482.

Benson, D. J., 1985, Diagenetic controls on reservoir development and quality, Smackover Formation of southwest Alabama: Gulf Coast Association of Geological Societies Transactions, v. 35, p. 317-326.

Benson, D. J., 1988, Depositional history of the Smackover Formation in southwest Alabama: Gulf Coast Association of Geological Societies Transactions, v. 38, p. 197-205.

Benson, D. J., and E. A. Mancini, 1999, Diagenetic influence on reservoir development and quality in the Smackover updip basement ridge play, southwest Alabama: Gulf Coast Association of Geological Societies Transactions, v. 49, p. 96-101.

Benson, D. J., E. A. Mancini, R. H. Groshong, J. H. Fang, L. M. Pultz, and E. S. Carlson, 1997, Petroleum Geology of Appleton Field, Escambia County, Alabama: Transactions, Gulf Coast Association of Geological Societies, v. 47, p. 35-42.

Benson, D. J., L. A. Markland, and T. H. Powers, 1991, Paleotopographic control on Smackover reservoir evolution: southwest Alabama. (Abstract): American Association of Petroleum Geologists, v. 75, p. 540-541.

Braga, J. C., J. M. Martín, and R. Riding, 1995, Controls on microbial dome fabric development along a carbonate-siliciclastic shelf-basin transect, Miocene, SE Spain: Palaios, v. 10, p. 347-361.

Benson, D. J., L. M. Pultz, and D. D. Bruner, 1996, The influence of paleotopography, sea level fluctuation, and carbonate productivity on deposition of the Smackover and Buckner formations, Appleton field, Escambia County, Alabama: Gulf Coast Association of Geological Societies Transactions, v. 46, p. 15-23.

Brown, A. R., 1996, Interpretation of Three-Dimensional Seismic Data, 4th ed.: American Association of Petroleum Geologists Memoir 42, 424p.

Carr, M., R. Cooper, M. Smith, M. T. Taner, and G. Taylor, 2001, The generation of rock and fluid properties volume via the integration of multiple seismic attributes and log data: First Break, v. 19, no. 10, p. 567-571.Claypool, G. E., and E. A. Mancini, 1989, Geochemical

relationships of petroleum in Mesozoic reservoirs to carbonate source rocks of Jurassic Smackover Formation, southwestern Alabama: AAPG Bulletin, v. 73, p. 904-924.

Chen, Q., and S. Sidney, 1997, Seismic attribute technology for reservoir forecasting and monitoring: The Leading Edge, v. 16, no. 5, p 445-456.

Crevello, P. D., and P. M. Harris, 1984, Depositional models for Jurassic reefal buildups: *in* W. P. S. Ventress, D. G. Bebout, B. F. Perkins, and C. H. Moore, eds., The Jurassic of the Gulf Rim: Proceedings of the Third Annual Research Conference, Gulf Coast Section, SEPM Foundation, p. 57-102.

Dobson, L. M., and R. T. Buffler, 1997, Seismic stratigraphy and geologic history of Jurassic rocks, northeastern Gulf of Mexico: AAPG Bulletin, v. 81, p. 100-120.

Dromart, G., C. Gaillard, and L. F. Jansa, 1994, Deep-marine microbial structures in the Upper Jurassic of western Tethys, *in* J. Bertrand-Sarfati and C. Monty, eds., Phanerozoic Stromatolites II: Kluwer Academic Publishers, Boston, p. 295-318.

Dubrule, O., 1998, Geostatistics in petroleum Geology: American Association of Petroleum Geologists Continuing Education Course Note Series, no. 38, 52p.

Fezer, R., 1988, Die oberjurassische karbonatische regressionsfazies im sudwestlichen Keltiberikum zwischen Griegos und Aras de Alpuente (Prov. Teruel, Cuenca, Velencia; Spanien): Arb. Inst. Geol. Palaont., University of Stuttgart, 84, 119 p.

Gastaldi, C., J-P. Biguenet, and L. DePazzis, 1997, Reservoir characterization from seismic attributes: An example from the Peciko Field (Indonesia): The Leading Edge, v. 16, no. 3, p. 263-266.

Golubic, S., L. Seong-Joo, and K. M. Browne, 2000, Cyanobacteria: architects of sedimentary structures, *in* R. R. Riding and S. M. Awramik, eds., Microbial Sediments: Springer-Verlag, Berlin, p. 57-67.

Hampson, B., J. Schuelke, and J. Quirein, 2001, Use of Multi-attribute Transforms to Predict Log Properties from Seismic data: Geophysics, v. 66, no. 1, p. 3-46.

Hart, B. S., 1999, Geology plays key role in seismic attribute studies: Oil & Gas Journal, p. 76-80.

Hart, B. S., 2000, 3-D seismic interpretation: A primer for geologists. SEPM Short Course Notes #48, Tulsa, OK, 124p.

Hart, B. S., 2002, Validating seismic attribute studies: Beyond statistics: The Leading Edge, 21, no. 10, p. 1016-1021.

Hart, B. S., and R. S. Balch, 2000, Approaches to defining reservoir physical properties from 3-D seismic attributes with limited well control: an example from the Jurassic Smackover Formation, Alabama: Geophysics, v. 65, p. 368-376.

Haywick, W. D., M. B. Brown, and L. Pfeiffer, 2000, Smackover Reservoir diagenesis in the Appleton Field, Escambia County, Alabama (Extended Abstract): American Association of Petroleum Geologists Bulletin, v. 84, no. 10, p. 1680.

Hirsche, K., S. Boerner, C. Kalkomey, and C. Gastaldi, 1998, Avoiding pitfalls in geostatistical reservoir characterization: A survival guide: The Leading Edge, v. 17, no. 4, p. 493-504.

Jansa, L. F., B. R. Pratt, and G. Dromart, 1989, Deepwater thrombolite mounds from Upper Jurassic of Offshore Nova Scotia, *in* Geldsetzer, H.H., James, N.P., and Febbutt, G.E. (eds.), Reefs, Canada and Adjacent Areas: Canadian Society of Petroleum Geologists Memoir, no. 13, 1989, p. 725-735.

Kalkomey, C. T., 1997, Potential risks when using seismic attributes as predictors of reservoir properties: The Leading Edge, v. 16, no. 3, p. 247-251.

Kalkowsky, E., 1908, Oolith and stromatolith im norddeutschen Bundsandstein: Deutschen Geologischen Gesellschaft, v. 60, p. 68-125.

Kennard, J. M., and N. P. James, 1986, Thrombolites and stromatolites: two distinct types of microbial structure: Palaios, v. 1, p. 492-503.

Kerans, C., and S. W. Tinker, 1997, Sequence stratigraphy and characterization of carbonate reservoirs: SEPM Short Course No. 40, 130 p.

Knorre, H. V., and W. E. Krumbein, 2000, Bacterial calcification, *in* R. R. Riding and S. M. Awramik, eds., Microbial Sediments: Springer-Verlag, Berlin, p. 25-31.

Kopaska-Merkel, D. C., S. D. Mann, and J. W. Schmoker, 1994, Controls on reservoir development in a shelf carbonate: Upper Jurassic Smackover Formation of Alabama: American Association of Petroleum Geologists Bulletin, v. 78, no. 6, p. 938-959.

Kopaska-Merkel, D. C., 1991, Analytical procedure and experimental design for geological analysis of reservoir heterogeneity using mercury porosimetry: Geological Survey of Alabama Circular 153, 29 p.

Kopaska-Merkel, D. C., 1998, Jurassic reefs of the Smackover Formation in south Alabama: Geological Survey of Alabama Circular 195, 28 p.

Kopaska-Merkel, D. C., and S. D. Mann, 2000, Diagenetic control of reservoir quality in Chunchula Field (Smackover Formation), Mobile County, Alabama: Geological Survey of Alabama Circular 198, 27 p.

Kopaska-Merkel, D. C., 2002, Jurassic cores from the Mississippi Interior Salt Basin, Alabama: Geological Survey of Alabama Circular 200, 83 p.

Leinfelder, R. R., 1986, Facies, stratigraphy and paleogeographic analysis of Upper? Kimmeridgian to Upper Portlandian sediments in the environs of Arruda dos Vinhos, Estremadura, Portugal: Münchner Geowissenschaftliche Abhandlungen (A), v. 7, p. 1-216.

Leinfelder, R. R., 1993, A sequence stratigraphic approach to the Upper Jurassic mixed carbonate-siliciclastic succession of the central Lusitanian Basin, Portugal: Profil 5, p. 119-140.

Leinfelder, R. R., M. Krautter, R. Laternser, M. Nose, D. Schmid, G. Scheigert, R. Werner, U. Rehfeld-Kiefer, R. Schroeder, C. Reinhold, R. Kock, A. Zeiss, V. Schweizer, H. Christmann, G. Menger, and H. Luterbacher, 1994, The origin of Jurassic reefs: Current research and development results: Facies, v. 31, p. 1-56.

Leinfelder, R. R., M. Krautter, M. Nose, M. M. Ramaho, and W. Werner, 1993a, Siliceous sponge facies from the Upper Jurassic of Portugal: Neus Jahrbuch fur Geologie and Palaontologie, Abhandlugen 189, p. 199-254.

Leinfelder, R. R., M. Nose, D. U. Schmid, and W. Werner, 1993b, Microbial crusts of the Late Jurassic: composition, paleoecological significance and importance in reef construction: Facies, v. 29, p. 195-230.

Leinfelder, R. R., and D. U. Schmid, 2000, Mesozoic reefal thrombolites and other microbolites, *in* R. R. Riding and S. M. Awramik, eds., Microbial Sediments: Berlin, Springer-Verlag, p. 289-294.

Leinfelder, R. R., D. U. Schmid, M. Nose, and W. Werner, 2002, Jurassic reef patterns—the expression of a changing globe, *in* W. Kiessling, E. Flugel, and J. Golonka, eds., Phanerozoic Reef Patterns: SEPM (Society for Sedimentary Geology) Special Publication No. 72, Tulsa, Oklahoma, p. 465-520.

Leinfelder, R. R., W. Werner, M. Nose, D. U. Schmid, M. Krautter, R. Laternser, M. Takacs, and D. Hartman, 1996, Paleoecology, growth parameters and dynamics of coral, sponge and microbolite reefs from the Late Jurassic, *in* J. Reitner, F. Neuweiler, and F. Gunkel, eds., Global and Regional Controls on Biogenic Sedimentation, I, Reef Evolution, Research Reports: Göttinger Arbeiten zur Geologie und Paläontologie, Sb 2, p. 227-248.

Leinfelder, R. R., and R. C. L. Wilson, 1998, Third-order sequences in an Upper Jurassic rift-related second order sequence, central Lusitanian Basin, Portugal, *in* P-C. de Graciansky, J. Hardenbol, T. Jacquin, and P. R. Vail, eds., Mesozoic and Cenozoic Sequence Stratigraphy of European Basins: SEPM (Society of Sedimentary Geology) Special Publication 60, p. 507-525.

Leiphart, D. J., and B. S. Hart, 2001, Comparison of linear regression and probabilistic neural network to predict porosity from 3-D seismic attributes in Lower Brushy Canyon channeled sandstones, southeast New Mexico: Geophysics, v. 66, no. 5, p. 1349-1358.

Llinás, J. C., 2002a, Diagenetic history of the Upper Jurassic Smackover Formation and its affect on reservoir properties, Vocation field, Manila Sub-basin, Eastern Gulf Coastal Plain: Gulf Coast Association of Geological Societies Transactions, v. 52, p. 631-644.

Llinás, J. C., 2002b, Carbonate sequence stratigraphy, influence of paleotopography, eustasy, and tectonic subsidence: Upper Jurassic Smackover Formation, Vocation field, Manila Sub-basin (Eastern Gulf Coastal Plain): *in* J. M. Armentrout and N. C. Rosen, eds., Sequence Stratigraphic Models for Exploration and Production: Evolving Methodology, Emerging Models and Application Histories: Proceedings of the 22nd Annual Research Conference, Gulf Coast Section, SEPM Foundation, p. 383-401.

Llinás, J. C., 2003, Petroleum exploration for Upper Jurassic Smackover carbonate shoal and microbial reef lithofacies associated with paleohighs, southwest Alabama: Gulf Coast Association of Geological Societies Transactions, v. 53, p. 462-474.

Mancini, E. A., M. Badali, T. M. Puckett, W. C. Parcell, and J. C. Llinas, 2001, Mesozoic carbonate petroleum systems in the northeastern Gulf of Mexico, Petroleum Systems of Deep-Water Basins: Global and Gulf of Mexico Experience, Proceedings of the 21st Annual Research Conference, Gulf Coast Section, SEPM Foundation, p. 423-451.

Mancini, E. A., and D. J. Benson, 1980, Regional stratigraphy of Upper Jurassic Smackover carbonates of southwest Alabama: Gulf Coast Association of Geological Societies Transactions, v. 30, p. 151-165.

Mancini, E. A., and D. J. Benson, 1998, Upper Jurassic Smackover carbonate reservoir, Appleton field, Escambia County, Alabama: 3-D case history, *in* J. L. Allen, T. S. Brown, C. J. John, and C. F. Lobo, eds., 3-D Case Histories from the Gulf Coast Basin: Gulf Coast Association of Geological Societies Special Publication, p. 1-14.

Mancini, E. A., D. J. Benson, B. S. Hart, R. S. Balch, W. C. Parcell, and B. J. Panetta, 2000, Appleton field case study (eastern Gulf Coastal Plain): field development model for Upper Jurassic microbial reef reservoirs associated with paleotopographic basement structures: AAPG Bulletin, v. 84, p. 1699-1717.

Mancini, E. A., D. J. Benson, B. S. Hart, H. Chen, R. S. Balch, W. C. Parcell, W-T. Yang, and B. J. Panetta, 1999, Integrated geological, geophysical and computer modeling approach for predicting reef lithofacies and reservoirs: Upper Jurassic Smackover Formation, Appleton Field, Alabama, Advanced Reservoir Characterization for the Twenty-First Century,

Proceedings of the 19th Annual Research Conference, Gulf Coast Section, SEPM Foundation, p. 235-247.

Mancini, E. A., R. M. Mink, B. H. Tew, D. C. Kopaska-Merkel, and S. D. Mann, 1991, Upper Jurassic oil plays in Alabama, Mississippi and the Florida panhandle: Gulf Coast Association of Geological Societies Transactions, v. 41, p. 475-480.

Mancini, E. A., and W. C. Parcell, 2001, Outcrop analogs for reservoir characterization and modeling of Smackover microbial reefs in the northeastern Gulf of Mexico area: Gulf Coast Association of Geological Societies Transactions, v. 51, p. 207-218.

Mancini, E. A., W. C. Parcell, D. J. Benson, H. Chen, and W-T. Yang, 1998, Geological and computer modeling of Upper Jurassic Smackover reef and carbonate shoal lithofacies, Eastern Gulf Coastal Plain: Gulf Coast Association of Geological Societies Transactions, v. 48, p. 225-233.

Mancini, E. A., T. M. Puckett, and W. C. Parcell, (eds.), 2000, Carbonate Reservoir Characterization and Modeling for Enhanced Hydrocarbon Discovery and Recovery, AAPG/EAGE International Research Conference, Program and Abstracts Volume, 68 p.

Mancini, E.A., B. H. Tew, and R. M. Mink, 1990, Jurassic sequence stratigraphy in the Mississippi Interior Salt Basin: Gulf Coast Association of Geological Societies Transactions, v. 40, p. 521-529.

Marhaendrajana, T., and T. A. Blasingame, 1997, Rigorous and semi-rigorous approaches for the evaluation of average reservoir pressure from pressure transient tests: Paper 38725 presented at the 1997 Annual SPE Technical Conference and Exhibition, San Antonio, TX, October 6-8.

Markland, L. A., 1992, Depositional history of the Smackover Formation, Appleton field, Escambia County, Alabama: Master's thesis, University of Alabama, Tuscaloosa, Alabama, 156 p.

Masters, T., 1994, Signal and image processing with neural networks: John Wiley and Sons (publ.)

Mukerji, T., P. Avseth, G. Mavko, I. Takahashi, and W. S. Goree, 2001, Statistical rock physics: Combining rock physics, information theory, and Geostatistics to reduce uncertainty in seismic reservoir characterization: The Leading Edge, v., 20, no. 3, p. 313-319.

Nose, M., 1995, Vergleichende faziesanalyse und palokologie korallenreicher verflachungsabfolgen des Iberischen Objerjura: Profil 8, University of Stuttgart, 237 p.

Parcell, W. C., 1999, Stratigraphic architecture of Upper Jurassic (Oxfordian) reefs in the northeastern Gulf Coast, U.S. and the eastern Paris Basin, France: Gulf Coast Association of Geological Societies Transactions, v. 49, p. 412-417.

Parcell, W. C., 2000, Controls on the development and distribution of reefs and carbonate facies in the Late Jurassic (Oxfordian) of the eastern Gulf Coast, United States and eastern Paris Basin, France: Ph.D. dissertation, University of Alabama, Tuscaloosa, 226 p.

Parcell, W. C., 2002, Sequence stratigraphic controls on the development of microbial fabrics and growth forms—implications for reservoir quality in the Upper Jurassic (Oxfordian) Smackover Formation, eastern Gulf Coast, U.S.A.: Carbonates and Evaporites, v. 17, p. 166-181.

Parcell, W. C., 2003, Evaluating the development of Upper Jurassic reefs in the Smackover Formation, eastern Gulf Coast, U.S.A. through fuzzy logic computer modeling: Journal of Sedimentary Research, v. 73, p. 498-515.

Partyka, G., J. Gridley, and J. Lopez, 1999, Interpretational applications of spectral decomposition in reservoir characterization: The Leading Edge, v. 18, no. 3, 353-360.

Pearson, R. A., and B. S. Hart, *in press*, 3-D seismic attributes help define controls on reservoir development: case study from the Red River Formation, Williston Basin. *In:* G.P. Eberli, J.L. Masaferro, and J.F. Sarg (eds.), Seismic Imaging of Carbonate Reservoirs and Systems: American Association of Petroleum Geologists Memoir.

Petyon, L., R. Bottjer, and G. Partyka, 1998, Interpretation of incised valleys using new 3-D seismic techniques: A case history using spectral decomposition and coherency: The Leading Edge, v. 17, no. 9, 1294-1298.

Powers, T. J., 1990, Structural and depositional controls on petroleum occurrence in the Upper Jurassic Smackover Formation, Vocation field, Monroe County: Master's thesis, University of Alabama, Tuscaloosa, Alabama, 171 p.

Prather, B. E., 1992, Origin of dolostone reservoir rocks, Smackover Formation (Oxfordian), northeastern Gulf Coast, U.S.A: American Association of Petroleum Geologists Bulletin, v. 76, p.133-163.

Pratt, B. R., 1995, The origin, biota, and evolution of deep-water mud-mounds, *in* Monty, C.L.V., Bosence, D.W.J., Bridges, P.H., and Pratt, B.R. (eds.) Carbonate Mud Mounds: Their Origin and Evolution: International Association of Sedimentologists Special Publications, v. 23, p. 49-123.

Pratt, B. R., N. P. James, and P. Bourque, 1992, Reefs and Mounds, *in* Walker, R.G and N.P. James (eds.), Facies Models - Response to Sea Level Change: Geological Association of Canada, p. 323-348.

Raeuchle, S. K., D. S. Hamilton, and M. Uzcátegui, 1997, Case history: Integrating 3-D seismic mapping and seismic attribute analysis with genetic stratigraphy: Implications for infield reserve growth and field extension, Budare Field, Venezuela: Geophysics, v. 62, no. 5, p. 1510-1523.

Ramalho, M., 1988, Sur la decouverte de biomermes stromatolithiques a spongiaires siliceux dans le Kimmeridgien de l'Algarve (Portugal): Communicoes dos Servicos Geologicos de Portugal, 74, p. 41-55.

Riding, R., 1991, Classification of microbial carbonates, *in* R. Riding, ed., Calcareous Algae and Stromatolites: Springer-Verlag, Berlin, p. 21-51.

Riding, R. R., and S. M. Awramik, 2000, Preface, *in* R. R. Riding and S. M. Awramik, eds., Microbial Sediments: Springer-Verlag, Berlin, p. i.

Robertson, J. D., and H. H. Nogami, 1984, Complex seismic trace analysis of thin beds: Geophysics, v. 49, no. 4 (April 1984), p. 344-352.

Russell, B., D. Hampson, J. Schuelke, and J. Quirein, 1997, Multi-attribute Seismic Analysis: The Leading Edge, v. 16, no. 10, p. 1439-1443.

Saller, A. H., and B. R. Moore, 1986, Dolomitization in the Smackover Formation, Escambia County, Alabama: Gulf Coast Association of Geological Societies Transactions, v. 36, p. 275-282.

Schmid, D. U., 1996, Marine mikrobolithe und mikroinkrustierer aus dem Oberjura: Profil, v. 9, p. 101-251.

Schultz, P. S, S. Ronen, M. Hattori, and C. Corbett, 1994a, Seismic-guided estimation of log properties: Part 1: A data-driven interpretation methodology: The Leading Edge, v. 13, no. 5, p. 305-315.

Schultz, P. S., S. Ronen, M. Hattori, and C. Corbett, 1994b, Seismic-guided estimation of log properties: Part 2: Using artificial neural networks for nonlinear attribute calibration: The Leading Edge, v. 13, no. 6, p. 674-678.

Stolz, J. F., 2000, Structure of microbial mats and biofilms, *in* R. R. Riding and S. M. Awramik, eds., Microbial Sediments: Springer-Verlag, Berlin, p. 1-8.

Taner, M. T., 2001, Seismic attributes: CSEG Recorder, September 2001, 49-56.

Taner, M. T., F. Koehler, and R. E. Sheriff, 1979, Complex seismic trace analysis: Geophysics, v. 44, no. 6 (June 1979), p. 1041-1063.

Tebo, J. M., 2003, Use of volume-based 3-D seismic attribute analysis to characterize physical property distribution: A case study to delineate reservoir heterogeneity at the Appleton Field, SW Alabama (M.Sc Thesis): McGill University, 181p.

Tew, B. H., R. M. Mink, E. A. Mancini, S. D. Mann, and D. C. Kopaska-Merkel, 1993, Geologic framework of the Jurassic (Oxfordian) Smackover Formation, Alabama and Panhandle Florida coastal waters area and adjacent federal waters area: Gulf Coast Association of Geological Societies Transactions, v. 43, p. 399-411.

Vail, P. R., J. Hardenbol, and M. G. Todd, 1984, Jurassic unconformities, chronostratigraphy and sea-level changes from seismic stratigraphy and biostratigraphy; in W.P.S. Ventress, D.G. Bebout, B.F. Perkins and C.H. Moore, eds., The Jurassic of the Gulf Rim: Proceedings of the Third Annual Research Conference Gulf Coast Section. Society of Economic Paleontologists and Mineralogists Foundation, p. 347-364.

Werner, W., R. R. Leinfelder, F. T. Fürsich, and M. Krautter, 1994, Comparative palaeoecology of marly coralline sponge-bearing reefal associations from the Kimmeridgian (Upper

Jurassic) of Portugal and Southwestern Germany: Courier Forschungsinstitut Senckenberg, v. 172, p. 381-397.

Wilson, R. C. L., 1989, Mesozoic development of the Luisitanian Basin, Portugal: Revista de la Sociedad Geologica de Espana, v. 1, p. 393-407.